NOMENCLATURE FOR PYROLYSIS EXPERIMENTS INVOLVING H_2O

M. D. Lewan
U.S. Geological Survey
Box 25046, MS 977
Denver Federal Center
Denver, CO 80225

The importance of H_2O in laboratory pyrolysis experiments designed to simulate natural processes is well documented in studies of coalification (Berl and Schmidt, 1932; Schuhmacher et al., 1960) and petroleum formation (Jurg and Eisma, 1964; Lewan et al., 1979). Industrial pyrolysis processes also benefit from the presence of H_2O as demonstrated in oil-shale retorting (Gavin, 1922, p. 181), conversion of coal to oil (Fischer, 1925, p. 180), heavy oil upgrading (McCollum and Quick, 1976a and b), and conversion of organic refuse to oil (Appell et al., 1971 and 1975). As experimental work continues to indicate that the phase as well as the presence of H_2O are important in natural and industrial processes, a nomenclature for pyrolysis experiments involving different H_2O phases is needed to improve interlaboratory communication and comparison of results. The following nomenclature is proposed to meet this need.

Hydrous pyrolysis as originally defined by Lewan and others (1979) denotes experiments in which a sample is pyrolyzed in contact with H_2O liquid. This condition best represents subsiding sedimentary basins in which the pores and fractures in sedimentary rocks are usually filled with water. As shown in Figure 1, the upper temperature limit for pure H_2O in this type of pyrolysis is 374°C, but higher temperature limits in excess of 600°C may be obtained by the addition of soluble salts (i.e., NaCl). H_2O in hydrous pyrolysis experiments typically occurs as both liquid and vapor, unless pressure regulators are employed to maintain only a liquid phase. It is important in the vapor/liquid H_2O system to optimize the amount of water used for specific reactor and sample volumes to insure that the sample is completely submerged in the liquid phase during pyrolysis (Lewan, 1993).

Supercritical H_2O pyrolysis denotes experiments in which a sample is pyrolyzed in contact with a supercritical fluid containing more than 50 mole % H_2O. Although the lower temperature limit for pure water in this type of pyrolysis is 374°C, this critical temperature may be lowered below 300°C with the addition of CO_2 to the system (Figure 1). Supercritical H_2O pyrolysis represents deep crustal regimes where metamorphic grades in excess of greenschist facies occur.

Steam pyrolysis is more difficult to define because sedimentary organic matter and its accompanying rock usually generate or liberate minor amounts of H_2O during experiments commonly referred to as **dry** or **anhydrous pyrolysis**. The headspace in these experiments is typically sufficient for the minor amounts of

evolved H_2O to occur as vapor at a partial pressure dictated by the available volume and experimental temperature. As an operational definition, it is suggested that steam pyrolysis denotes experiments in which a sample is pyrolyzed in contact with H_2O vapor at partial pressures in excess of 20 percent of its saturated vapor pressure at experimental temperatures. Steam pyrolysis represents localized near-surface conditions where geothermal vents or subaerial volcanoes are active.

Hydrous, supercritical H_2O, and steam pyrolysis may be collectively referred to as **hydrothermal pyrolysis** or **aquathermolysis** (e.g. Siskin et al., 1990). These collective names are particularly useful for referring to pyrolysis experiments in which insufficient information is given to assess the H_2O phases present or the phase in which a reaction has occurred at experimental conditions.

REFERENCES

Appell, H. R., Fu, Y. C., Illig, E. G., Steffgen, F. W., and Miller, R. D., 1975, Conversion of cellulosic wastes to oil: U.S. Dept. of Interior, Bur. Mines Rept. Invest. 8013.

Appell, H. R., Fu, Y. C., Friedman, S., Yavorsky, P. M., and Wender, I., 1971, Converting organic wastes to oil: A replenishable energy source: U.S. Dept. of Interior, Bur. Mines Rept. Invest. 7560.

Berl, E., and Schmidt, A., 1932, Über die Entstehung der Kohlen, II. Die Inkohlung von Cellulose and Lignin in neutralem Medium: A. der Chemie 493:97.

Fischer, F., 1925, The Conversion of Coal into Oils, Ernest Benn Ltd., London.

Gavin, M. J., 1922, Oil-Shale: An historical, technical, and economic study: Dept. of Interior, Bur. Mines Bulletin 210, Bradford-Robinson, Denver.

Haas, J. L, Jr., 1976, Thermodynamical properties of the coexisting phases and thermochemical properties of the NaCl component in boiling NaCl solutions: U.S. Geol. Surv. Bull. 1421-B.

Jurg, J. W., and Eisma, E., 1964, Petroleum Hydrocarbons: Generation from fatty acid: *Science* 144:1451.

Lewan, M. D., 1993, Labortory simultion of petroleum formation: Hydrous pyrolysis, in *Organic Geochemistry* (M. H. Engel and S. A. Macko, eds.), Plenum, New York (in press).

Lewan, M. D., Winters, J. C., and McDonald, J. H., 1979, Generation of oil-like pyrolyzates from organic-rich shales. *Science* 203:897.

McCollum, J. D., and Quick, L. M., 1976a, Process for upgrading a hydrocarbon fraction: U.S. Patent 3, 960:708.

McCollum, J. D., and Quick, L. M., 1976b, Process for upgrading a hydrocarbon fraction: U.S. Patent 3, 989, 618.

Schuhmacher, J. P., Huntjens, F. J., and van Krevelen, D. W., 1960, Chemical structure and properties of coal XXVI. Studies on artificial coalification: *Fuel* 39:223.

Siskin, M., Brons, G., Katritzky, A. R., and Balasubramanian, 1990, Aqueous Organic Chemistry 1. Aquathermolysis: Comparison with thermolysis in the reactivity of aliphatic compounds: *Energy & Fuels* 4:475.

Sourirajan, S., and Kennedy, G. C., 1962, The system H_2O-NaCl at elevated temperatures and pressures: *Am. Jour. Sci.*, 260:115.
Takenouchi, S., and Kennedy, G. C., 1964, The binary system H_2O-CO_2 at high temperatures and pressures: *Am. Jour. Sci.* 262:1055.

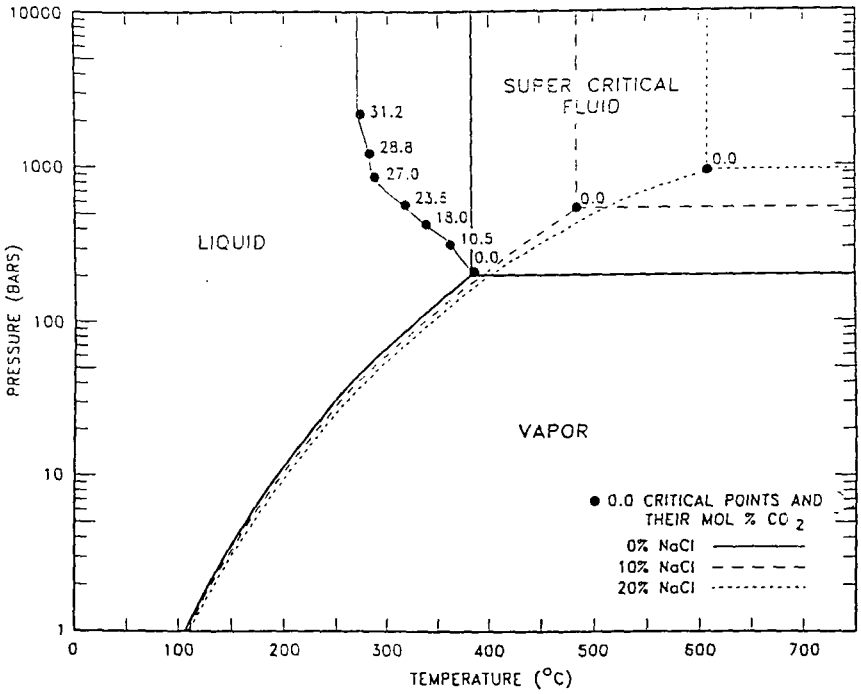

Figure 1. Pressure-temperature diagram showing phase relations and critical points for pure H_2O (heavy solid lines), CO_2 in solution with H_2O (solid circles on light solid line refer to critical points at denoted CO_2 mole fractions), 10 wt% NaCl solution with H_2O (dashed lines), and 20 wt% NaCl solution with H_2O (dotted lines). Diagram is based on experimental data reported by Haas (1976), Sourirajan and Kennedy (1962), and Takenouchi and Kennedy (1964).

LASER MICROPYROLYSIS/GAS CHROMATOGRAPHY MASS SPECTROMETRY: A USEFUL TECHNIQUE FOR THE STUDY OF COAL MACERALS?

Paul E. Greenwood, Etuan Zhang, Patrick G. Hatcher, Frank Vastola and Alan Davis,
The Pennsylvania State University, University Park, PA 16802

INTRODUCTION

Structural information regarding the microscopic composition of heterocyclic, polymaceralic materials such as coal and kerogens has proved elusive. The primary reason for this is the limited number of techniques which can analytically probe involatile, thermally labile materials.

Pyrolysis (i.e., thermal degradation) of coal and other organic materials is one technique to show much promise.[1,2] Conventional methods of coal pyrolysis include slow pyrolysis (heating rate between 25 °C/sec) and flash/fast pyrolysis (10,000 °C/sec). The pyrolysis of coal produces many gaseous fragments which can be analysed by mass spectrometry. The detected pyrolysates often reveal much structural information which can be related to the macroscopic composition of the parent coal.

The rapid heating from lasers has also been used to effectively induce coal pyrolysis.[3,4] Laser pyrolysis offers the unique advantage of micro-selective *in situ* sampling. Since readily available optics can focus the laser output to very small areas, it is possible to analyse very small components within complex mixtures such as coal. Several independent groups, some using the commercially available LAMMA instrument,[5] have demonstrated how individual components of coals and oil shales can be selectively irradiated with microscopic optics.[6-16]

Previous efforts to study individual maceral types involved the physical isolation of the selected macerals. This was performed either via hand-picked techniques[17] or density-gradient centrifugation.[18-20] The severe and time consuming sample pre-treatment requirements associated with these techniques is not present with the *in situ* analysis of the micropyrolysis technique.

The majority of the coal micro-pyrolysis studies to date have been concerned only with the laser techniques which produce charged particles. Many more neutrals than ions are produced during any laser ablation process so the detection sensitivity of pyrolysis products will be significantly reduced when limiting the analysis to ionic species. Other studies, by one of us, have revealed that carbon clusters tend to dominate the charged population produced from the laser ablation of coals.[21] This suggests analysis of directly produced ionic pyrolysates may not be an appropriate method to study the structural fragments from coal macerals.

In this paper we present a novel laser pyrolysis/GC-MS study using an instrument recently assembled in our laboratory. This apparatus includes a microscope to selectively pyrolyse individual coal macerals. The entire pyrolysate population, including neutrals, is subjected to the process of trapping (with a N_2 cold trap), separated by gas chromatography and analysed by electron impact mass spectrometry. In general, the product distribution from laser pyrolysis closely resembles that observed for flash pyrolysis. This exceptionally encouraging result suggests that laser micro-pyrolysis has

tremendous potential for the study of individual components not only within coals, but also other heterogeneous solids.

INSTRUMENTATION

The main components of the micropyrolysis apparatus used in this study include a laser, microscope, pyrolysis chamber and Kratos MS-80 GC-MS. A schematic illustration of the assembled system is shown in Figure 1.

Details of the laser (a pulsed ruby variety) and microscope can be found elsewhere.[3] In brief, the visible output of the laser has a wavelength of 694.3 nm and a maximum energy of 0.1 Joule. The microscope is equipped for reflected light illumination and long working distance objectives to enable the sample chamber to be mounted directly on the microscope substage. The laser beam is focused by the 4x objective of the microscope onto the surface of a polished coal sample mounted in the pyrolysis chamber. Focussing the laser pulse to very small sizes ensures that the very high irradiances necessary for pyrolysis are reached. The microscope also allows close visual examination of the coal sample so that particular macerals can be selected.

The pyrolysis chamber, developed in this laboratory, was designed to meet the requirements of the pyrolysis/GC-MS experiment. The sample port was kept to a small size (ID 7 mm, depth 10 mm) to reduce the amount of dead volume. A silica glass window on the the top allowed microscopic observation and laser penetration. The chamber was constructed of stainless steel and included a bore into which a thermocouple and heating element could be placed so as to heat the chamber (typically to 180 - 220 °C). Inlet and outlet carrier gas ports were also included. The pyrolysis chamber was connected to the column of the GC via (1/16") metal lined tubing (ID = 0.5 mm). A cold trap consisting simply of a loop of the column submerged in a liquid nitrogen bath is located in the oven of the GC. Heating ribbons were used to heat the transfer tubing as well as to pre-heat the helium carrier gas.

The Kratos MS-80 interfaces a Carlo-Erba GC with a scanning magnetic sector mass spectrometer. The GC is fitted with a fused-silica capillary column (30m x 0.25 mm ID) with stationary phase consisting of 50% phenylmethyl polysiloxane (J&W, DB-17). The column was temperature programmed from 40 to 280 °C at 4 °C/min. Mass spectra were obtained under EI conditions at 70 eV, a scan rate of 1500 m/z s^{-1} and an m/z 40 to 500 mass range. The individual peaks were identified by comparison of mass spectra to published spectra.

EXPERIMENTAL

Two coal samples were selected for analysis from the Penn. State Coal Sample Bank. These comprised a subbituminous humic coal (PSOC-1532) with a maximum vitrinite reflectance of 0.33% and a high volatile C bituminous cannel coal (PSOC-1109) with a vitrinite reflectance value of 0.44%. These particular coals were selected to examine the ability of this technique to differentiate the different types of macerals.

Sample pretreatment included: cutting the sample to small block sizes which could be accommodated by the sample port of the pyrolysis chamber; polishing by hand with grinding and polishing wheels according to conventional methods; and heating for considerable time (i.e., > 24 hrs) in an inert atmosphere (i.e., He) to remove absorbed volatiles.

The procedure for the pyrolysis experiments of this study is briefly as follows. Pyrolysis is induced by the focussed laser output. The microscope used to focus the laser

also allows particular coal surface sites to be selectively irradiated. The pyrolysed craters from the laser beam can be varied by altering the degree of focussing to between 10 to 250 μm in diameter. These craters can be 5 to 10 μm in depth. The actual depth is also dependent upon the size of the irradiated area as well as the energy setting of the laser. Throughout pyrolysis the volatile products are swept by He gas through the heated transfer line to the column and trapped in the liquid N_2 bath. The transfer efficiency of the volatiles being dependent on the temperature of the transfer line. This relationship between transfer efficiency and temperature is also observed to be mass discriminate with higher molecular weight species being filtered out by lower temperatures. Once the volatiles from a number of laser pulses (typically 10 - 20) have been collected, the oven of the GC is heated (at 4 ^{o}C/min from 40 ^{o}C to 280 ^{o}C) effectively releasing and separating them according to size as they pass through the column.

The separated samples are continually analysed by electron impact mass spectrometry as they emerge from the column.

RESULTS

Laser parameters such as duration of irradiation, wavelength, power density, and size of the irradiated area have been identified from the previous laser pyrolysis studies of coal[3]. Optimum spectral conditions are also investigated for the present experiments. A sufficient number of volatiles were produced from 20 laser shots at different surface sites. It was necessary to investigate fresh surfaces with each pulse so that char produced from a previous pulse is not subsequently analysed. The coal samples were successfully pyrolysed with tightly focussed (i.e., high energy) pulses. Different products were obtained by varying the laser power either through defocusing the microscope or using a neutral density filter control.

The volume of volatiles produced by the laser proved insufficient in itself to facilitate continual signal detection by the Kratos MS-80 mass spectrometer. Because of this it was necessary to extend the mass range to m/z 40 - 600 so that CO_2 (i.e., m/z = 44) contributes to the background ion signal. The signal from CO_2 is much larger than the signal from the pyrolysis volatiles which often remain hidden in the baseline (i.e., CO_2 signal) of the total ion chromatogram (TIC). A large signal present in all laser pyrolysis TIC's at a retention time of ~ 3 - 4 minutes can also be assigned to CO_2. This result is consistent with many of the earlier studies in which CO_2 was observed to be the most dominant pyrolysis product. Other low abundant pyrolysis products may only be successfully revealed by individual and summed ion chromatograms.

Summed ion chromatograms for the subbituminous coal and high volatile C bituminous cannel coal are shown in Figures 2 and 3, respectively. Ions of mass 108, 122 and 136 are summed in the case of the subbituminous coal to reveal the pyrolysis production of alkyl phenols. The 108 ion identifies cresol (i.e. C_1-phenol), the 122 ion C_2-phenol and the 136 ion C_3-phenol. Such products, previously observed from flash pyrolysis,[22] are thought to dominate the vitrinite component of these coals. The resolution of ortho-Cresol isomer from the para and meta isomers was also observed from flash pyrolysis. The detection of these known pyrolysis products highlights the suitability of the laser as a pyrolysis source. Other species identified from the laser pyrolysis TIC include C_n-benzenes ($n \leq 2$), phenol, indene and naphthalene. Although low molecular weight alkyl - aromatics such as these are typically produced from coal pyrolysis some of these products may arise from simple evaporation from the coal surface at the high temperatures (180 - 220) of the pyrolysis chamber. Studies are presently under way to determine which species do arise from simple evaporation.

All ions from 46 - 600 contribute to the summed chromatogram associated with the high volatile coal (i.e., Fig. 3) This trace effectively reflects the CO_2 subtracted TIC. Low molecular weight products such as alkyl benzenes, toluene, indene and naphthalene are again observed. In addition, a prominent homologous series of dominant n-alkanes which range to above n-C_{29} are observed. This distribution of n-aliphatic hydrocarbons is typical of immature, lignite-rich terrestrial organic matter.[23] The biomarker 17β(H)-22,29,30-trisnorhopane is also detected at a retention time of ~ 70 minutes. The production and detection of this species is particularly encouraging since pentacyclic triterpenoids with the hopane type skeleton are a widely utilized group of biomarkers found in organic geochemical materials.[24] The detection of these large molecular weight products indicates the successful transfer, trapping and column separation of high molecular weight species by this technique. It is likely that these alkanes and biomarkers are released from the coal not as pyrolysis fragments but as trapped molecules released during laser heating.

Interpretation of the different mass spectra does suggest that there exists a fundamental difference between the chemical and structural compositions of the two coals.

CONCLUSIONS

The initial results presented in this paper demonstrate that coal macerals can be successfully investigated by laser micropyrolysis. The energy from the focussed laser beam was sufficient to induce coal pyrolysis and the microscope offers the added advantage of irradiating specific areas of the coal surface. Heating the pyrolysis chamber and transfer line prevents condensation of the laser emitted volatiles which are successfully flushed into the column of the GC by the pre-heated He carrier gas.

Products typical of coal pyrolysis were detected from the two samples. The different results for the respective samples reflects the contrasting maceral components of the coals and the ability of this technique to differentiate these differences is established The investigation of individual components within a whole range of heterogeneous geochemical materials should now be possible with this technique.

REFERENCES

1 T. I. Elington, S. R. Larter and J. J. Boon, J. Anal. Appl. Pyrolysis, 20, 20 (1991).

2. B. Horsfield, Geochimica. et. cosmochimica. acta, 53, 891 (1989).

3. a) F. J. Vastola and L. J. McGahon, Fuel, 66, 886 (1987).

   b) F. J. Vastola and A. J. Parone, Am. Chem. Soc. Div. Fuel Chem., Prepr., 10, 53 (1966).

   c) F. J. Vastola, A. J. Parone, P. H. Given and R. R. Dutcher, "Spectrometry of Fuels", Plenum Press, N. Y., (1970), p29.6.

4. a) S. A. Stout and K. Hall, J. Anal. Appl. Pyrolysis, 21, 195 (1991).

   b) S. A. Stout and R. Lui, Org. Geochem., In Press (1992).

5. D. M. Hercules, R. J. Day, K. Balasanmugam, T. A. Dang and C. P. Li, Anal. Chem., 54, 280A (1982).

6. J. J. Morelli, D. M. Hercules, P. C. Lyons, C. A. Palmer and J. D. Fletcher, Mikrochim. Acta [Wien], 111, 105 (1988)

7. A. F. Gaines and F. M. Page, Fuel, 62, 1041 (1983).
8. P. K. Dutta and Y. Talmi, Fuel, 61, 1241 (1982).
9. F. S. Karn, R. A. Friedal and A. G. Sharkey, Carbon, 5, 25 (1967).
10. F. S. Karn, A. G. Sharkey, A. F. Logar and R. A. Friedal, US Bur. Mines Rep. Invest. 7328, 32 (1970).
11. W. H. Joy, W. R. Ladner, and E. Pritchard, Fuel, 19, 26 (1968).
12. J. P. Biscar, J. Chromatogr., 56, 348 (1971).
13. R. L. Hanson, N. E. Vanderborgh and D. G. Brookins, Anal. Chem., 47, 335, (1975).
14. R. L. Hanson, D. G. Brookins and N. E. Vanderborgh, Anal. Chem., 48, 2210, (1976).
15. R. L. Hanson, N. E. Vanderborgh and D. G. Brookins, Anal. Chem., 49, 390, (1977).
16. N. E. Vanderborgh, W. J. Verzino, M. A. Fletcher and B. A. Nichols, J. Anal. Appl. Pyrolysis, 4, 21 (1982).
17. D. R. Dyrkacz, C. A. A. Bloomquist and L. Rusic, Fuel, 63, 1367 (1984).
18. N. Bostick and B. Alpern, J. Microscopy, 109, 41 (1971).
19. P. Robert in "Organic Metamorphism and Geothermal History: Microscopic Study Organic Matter and Thermal Evolution of sedimentary basins", D. Reidel Publishing Comp., Boston, 1988, p311
20. M. Nip, J. W. deLeeuw, and J. C. Crelling, Energy and Fuels, 6, 125 (1991).
21. P. F. Greenwood, M. G. Strachan, G. D. Willett and M. A. Wilson, Org. Mass Spectrom., (1991).
22. P. G. Hatcher, H. E. Lerch, III, R. K. Kotra and V. T. Vincent, Fuel, 67, 1069 (1988).
23. S. R. Larter in "Analytical Pyrolysis, Techniques and Applications", Ed. K. J. Voorhees, Butterworths, Boston, 1984, pp 212 - 275.
24. G. Ourisson, P. Albrecht and M. Rohmer, Sci. American, 251, 44 (1984).

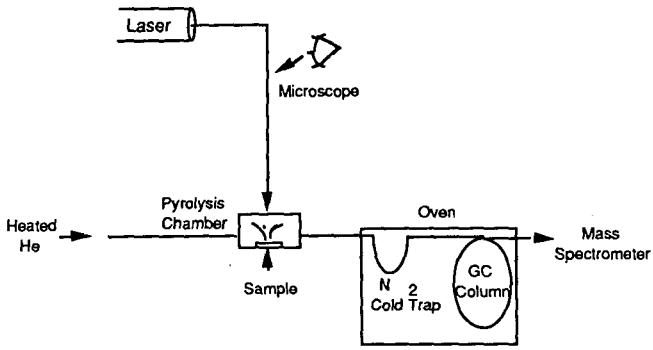

Figure 1 Assembly of Apparatus Used in the Micropyrolysis Experiment.

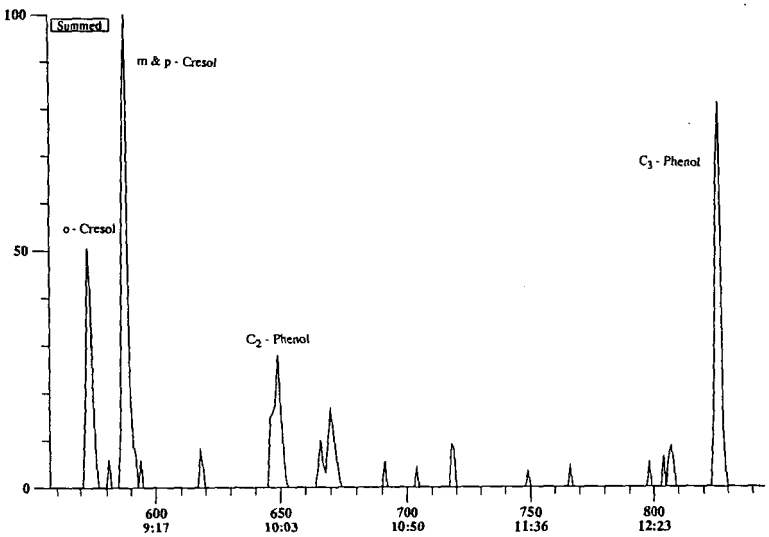

Figure 2 Summed chromatogram of the m/z 108, 122, 136 ions from the laser pyrolysis of a subbituminous coal.

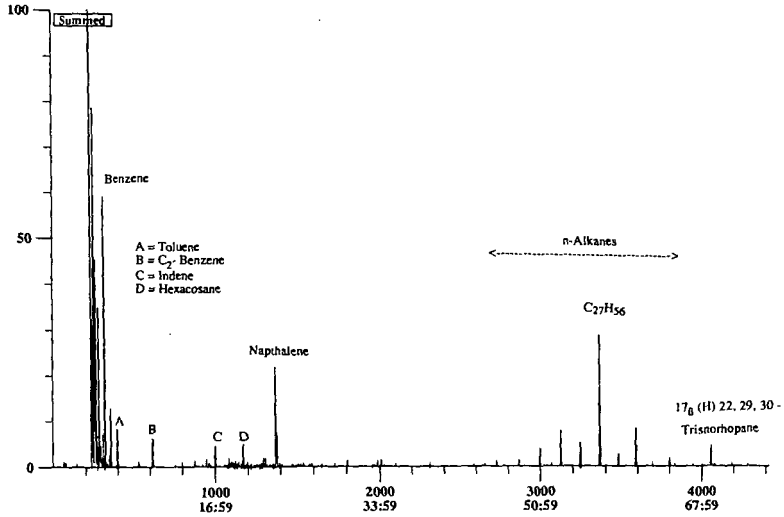

Figure 3 Summed chromatogram of all m/z 46 - 600 ions from the laser pyrolysis of a high volatile C bituminous cannel coal.

HYDROTHERMAL MEDIA, OIL SHALE, AND COAL

David S. Ross
SRI International
Menlo Park, CA 94025 USA

Keywords: hydrous pyrolysis, Wyodak, hydrothermal

INTRODUCTION

Hydrous pyrolysis has proved to be useful tool for the study of accelerated petroleum generation in source rocks. The techniques uses liquid water as a medium at thermolytic conditions in the 290°-360°C range (Lewan et al., 1979; 1981). Dry pyrolysis provides olefins in the pyrolysate, but with the addition of water the olefin yield is reduced and n-alkanes resembling those in petroleum emerge. Hoering (1984) extended the work using D_2O, developing results discussed below. The claim that hydrous pyrolysis mimics the natural process has been questioned recently (Monthioux et al., 1985; Tannenbaum and Kaplan, 1985; Comet et al., 1986). Nonetheless there is little question that the chemistry operating at hydropyrolysis conditions generates alkanes and other hydrocarbons from the immature source material.

The lack of understanding of the chemistry at hydrothermal conditions is underscored by a several observations. For example highly condensed polynuclear aromatic hydrocarbons (PAHs) including pyrene, benzpyrenes, and coronene are found in hydrothermal vent petroleums (Simoneit, 1985a; 1988). These compounds are commonly observed as products of hydrocarbon pyrolysis above 550°C, and coronene itself is not generated in pyrolyses at temperatures below 650°C (Commins, 1969). However it is difficult to explain their presence in the vent zones where temperatures are considerably lower.

Another curious point is the unusually high rate of epimerization of biological markers in hydrous pryolysis. Although cationic centers generated on highly acidic clay surfaces could be responsible (Alexander et al., 1984), the acidity of the clay sites is substantially reduced in an aqueous environment (Tannenbaum and Kaplan, 1985), and the high acidities required for epimerization at the rates observed cannot be present. The activity of acid clay sites can be questioned further because of the presence of normal alkanes, whereas acid-promoted cationic chemistry should produce highly branched alkanes. Calcium carbonate has also been suggested as significant to the isomerization (Eglinton et al., 1986), but the mechanistic aspects of that process are not apparent.

The role of water in the maturation process has not been clearly defined. It has been suggested that water transfers hydrogen to organic free radicals in the reaction mixture (Monthioux et al., 1985: Hoering, 1984; Comet et al., 1986).

$$R\cdot + H_2O \longrightarrow HO\cdot + R\text{-}H$$

However this reaction is endothermic by 25-30 kcal/mol and should not be significant at hydrous pyrolysis temperatures.

In the discussion here we seek to develop some understanding of the chemical processes in hydrous pyrolysis by first modeling the results of Hoering in D_2O. Some of that work has been recently reviewed (Ross, 1992), and the results are summarized here. We then seek to extend this view to the chemistry of coal, discussing our findings in studies of Argonne samples of

Wyodak coal in hydrothermal media (Ross, et al., 1990a,b). We begin with a summary of the nature of the medium at hydrous pyrolysis conditions.

RESULTS AND DISCUSSION

The Nature of the Hydrothermal Medium

Under common conditions, water is a highly polar, fluid medium accommodating ionic salts and having a modest capacity for dissolving some gases and polar organic compounds. However, liquid water near its critical point (374°C/220 atm) becomes a very different medium. The shifts in the key physical properties of liquid water up to its critical temperature are presented in Figure 1, with the shaded portion representing the region where hydrous pyrolysis is commonly conducted. The figure shows that while the density of the medium stays in the liquid-like region (> 0.3 g/mL) over most of the subcritical regime, the viscosity falls early to very low, almost gas-like, values. The net result is an interesting region where the medium has a liquid-like solvent capacity combined with a very high gas-like diffusivity. The mobilities of both neutral and charged solutes are much higher than they are in normal liquids, overcoming what could be mass transfer limitations at more conventional conditions.

The dielectric constant falls to levels like that of organic solvents, dramatically affecting the solubilities of organic materials. Thus naphthalene, virtually insoluble in water at ambient conditions, it is miscible in all proportions in liquid water at temperatures as low as 300°C (Jockers and Schneider 1978). Fully homogeneous combinations of ionic salts and nonpolar organics, which might not be feasible at common conditions, can easily be established at these conditions (Alwani and Schneider, 1969).

Hydrous Pyrolysis with D_2O -- The Results of Hoering

Hoering's data on the D-content in the n-alkanes from the treatment of preextracted Messel shale with D_2O at 330°C/3 days (1984) have been used to model the process (Ross, 1992). The profiles for the heptadecane recovered from the treatment are shown in Figure 2. The figure also shows the results of control experiments in which heptadecane was purposely added to the treatment mixture, and for heptadecane recovered from work in which heptadecene was initially added. In the latter, 60% of the added olefin was recovered as alkane, a remarkable result reflecting a considerable reducing potential in the reaction mixture, and requiring an explanation.

The added alkane does not undergo much exchange, and the fact that the kerogen-generated alkane is very highly exchanged rules out preexisting alkane as the source. The olefin-generated alkane contains considerable deuterium, but the distribution pattern is very different from that for the kerogen-derived material.

A process reconciling these facts is shown as Scheme I. The scheme features the view that water is significant to the reduction of olefins generated pyrolytically from the kerogen. The general arrangement was confirmed in modeling work done employing an integration routine based on the Gear algorithm (Moore and Pearson, 1981) and operated on a VAX 11/750 computer. The fit, shown in Figure 3, was generated for a reaction rates alignment in which reduction >> pyrolysis and exchange ≈ 2 x pyrolysis. It is emphasized that for the fit, it is necessary that reduction requires water, but produces *protio* alkane. The alkane then exchanges with the medium, presumably likely on the mineral surface.

A key question concerns the reduction step; there are no obvious reducing species introduced into the reaction. A clue to that chemistry may lie in the results of Amin, who studied the

pyrolysis of glucose in water at its critical point (1975). Data from the study in Table I show that the pyrolysis yields char, an oil, and gases including CO, CO_2, H_2, and CH_4.

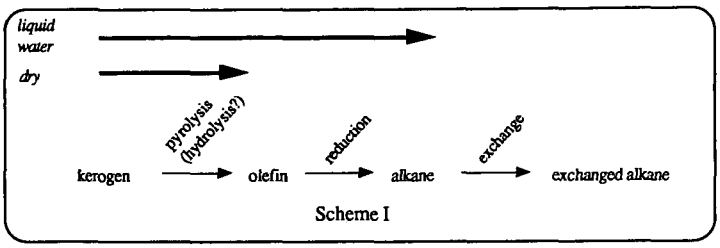

Scheme I

Significantly, however, as the density of the medium is increased from a gas-like value to one more liquid-like, the quantity of gas and oil increase substantially with a corresponding decrease in the char yield. Factors associated with the increased density that appear to promote reduction of the starting glucose and formation of simple gases.

Hoogwater reports similar findings in the pyrolysis a series of haloorganic compounds in supercritical water at liquid densities (1991). The results for trichloroethane are shown in Figure 4. These experiments, conducted in sealed quartz tubes and therefore eliminating metal wall-promoted reactions, yielded surprisingly large quantities of CO, CO_2, H_2, and a collection of hydrocarbons including alkanes and benzene.

These data suggest that liquid water in the near critical region or supercritical water at liquid densities promotes gasification reactions. Such conversions are essentially the water-promoted disproportionation of carbon, i.e.

modestly oxidized organics	➤	**highly reduced products**	+	**highly oxidized products**
e.g. olefins, phenols		alkanes, H_2		PAHs, CO, CO_2

They could be the basis of alkane production in petroleum genesis. We are unaware of studies confirming such chemistry, and submit that this area is an important one for development.

Hydrous Pyrolysis of Wyodak Coal

Our earlier accounts of this work described the effects of the treatment of Argonne samples of Wyodak coal with liquid water (hydrothermal) and with no medium (under N_2/thermal) at 250°-350°C for periods of 30 min and 5 hr (Ross, et al, 1990a). Much of the data were developed using thermal gravimetric analysis (TGA) and SRI's field ionization mass spectrometer (FIMS), both operating from ambient to 500°C at 2.5°C/min. A later report included additional results from studies in which water was replaced by n-undecane, a hydrocarbon with a critical temperature (363°C, estimated by the method of Lydersen, 1955) near that of water (374°C), and expected to be chemically unreactive over at least the 30-min heating period (Ross, et al., 1990b).

A tar representing 5-7% of the starting coal was consistently deposited on the quartz insert walls solely at the hydrothermal conditions. There was no evidence of tar in the thermal and undecane runs. In all cases the coal lost oxygen, with O-losses falling in the order:

hydrothermal (5 hr) > [hydrothermal (30 min) ≈ thermal (30 min) ≈ thermal (5 hr)] > undecane (30 min)

Some properties of the recovered coal and the tars are presented in Table II.

Our earlier accounts discussed these data; however there are two features of specific interest here. The first is the fact that the hydrothermally-promoted tars are at the same time more volatile and of a greater molecular weight than the FIMS-volatile products from the recovered coals. They are also considerably richer in hydrogen. They are thus substantially less polar, and it is tempting to view these results as parallel to those for hydrocarbon production in the hydrous pyrolysis of petroleum source rock and due to water-promoted reduction chemistry.

The second are the volatility changes shown in Figure 5, which displays the total FIMS ion count *vs* evaporation temperature for samples for both 30 min and 5 hr treatments. The profile for the untreated coal is also presented for comparison. (FIMS mass analysis begins at m/e 48, and so the profiles are independent of the evolution of water and carbon dioxide. They reflect solely organic volatiles.) For the 30 min treatment the undecane result is little different from that for the untreated coals. The thermally pretreated sample shows the presence of volatiles beginning to emerge at around 100°C; however these materials must be the thermolytically volatiles generated during the pretreatment. They are deposited on the coal, and then evaporated into the instrument during the FIMS heating.

The aqueous pretreatment, however, clearly has produced new material. It is emphasized that the ordinate in the figure is logarithmic and thus the absolute quantities of product are significantly greater than for the thermal case. This new material would seem to be the portion of the tar that condensed on the coal rather than on the insert walls.

For the 5-hr treatment little of the tar remains on the coal, and the hydrothermal and thermal results are similar. It is notable from Table II that the tar has become considerably more volatile with little change in the molecular weight. We found in addition by FIMS that the arenol content of the 30 min tar was less than 30% that of the treated coals. The arenols in the 5 hr tar were reduced yet further by another factor of 3.* Continued hydrothermal treatment appears to provide extended reduction and convert phenols to less polar material.

Remarkably, the undecane treatment has drastically reduced the volatility of the coal, essentially converting it to a char. The shaded portion of the figure reflects the loss in volatile material, those fractions becoming irreversibly reincorporated into the coal matrix.

CONCLUSIONS

The effects of water on the thermolysis of coal suggest a process similar to that in Scheme I for petroleum source rock (Scheme II). As in I, water promotes reduction of the initial pyrolytic products, and tar is the result. The scheme shows that extended hydrothermal treatment substantially increases the volatility of the tar.

In the absence of added water there is a pyrolytic release of material, including olefins and large quantities of phenolic material. These fragments will migrate to other regions of the coal and will probably tend to concentrate at the mineral sites due to acid/base interactions. At this point the recent results of Stein et al. can apply (1989). Their work showed that at 400°C dihydroxyben-zenes are very reactive and undergo acid catalyzed dehydroxylation and condensation. For coal, with distributions of clay and silica particles throughout the organic phase in sizes down perhaps to the nanometer level (Allen and VanderSande, 1984), we can expect significant degrees of such retrogressive chemistry.

For undecane the process is even more retrogressive. Neither water nor alkanes are good coal swelling media at ambient temperatures, the former because it is too polar, and the latter because

* The arenol content is the sum of the FIMS signals for phenol, dihydroxybenzene, and their respective C_1-, C_2-, and C_3- derivatives.

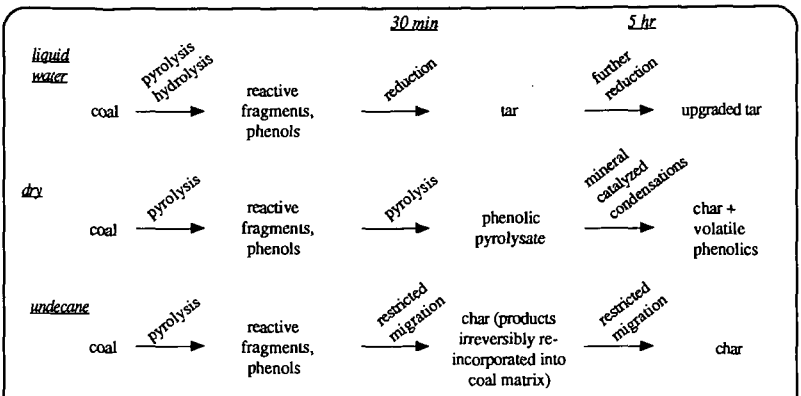

Scheme II

it is not polar enough. However water becomes increasingly more coal-accommodating in the hydrothermal region because its dielectric constant decreases to values like those for polar organic liquids (Schneider and Jockers, 1978). Undecane in contrast likely becomes an even poorer solvent, or in effect an antisolvent. In that medium coal should thus not swell but possibly collapse, a negative solvent action discussed for polymers by Magda et al. (1988). Such a tendency for the coal would trap otherwise volatile fractions, resulting ultimately in their irreversible reincorporation into the coal matrix, and the formation of char. As a consequence, the arenols will increasingly react within the cage.

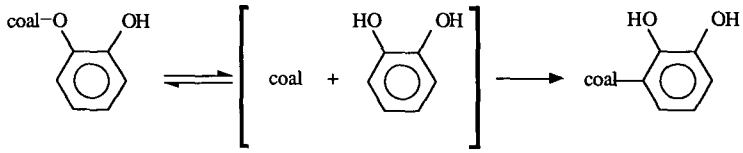

The essential component of this process is the replacement of labile, aryl ether links by stable, C-aryl bonds. That activity ultimately leads to the accumulation of structures that will tend to condense with further heating, and proceed to char. Such alkane-promoted condensation chemistry is clearly an undesirable component in conversion generally. Its regressive action, however, could be most seriously encountered in coprocessing, and additional studies in this area could prove profitable.

ACKNOWLEDGMENT

We acknowledge support of the US DOE for the coal-related portion of this work.

REFERENCES

Alexander, R, Kagi, R. I., and Larcher, A. V. (1984). Clay catalysis of alkyl hydrogen exchange reactions-reaction mechanisms. *Organic Geochemistry*, **6**, 755-760.

Allen, R. M., and VanderSande, J. B. (1984). Analysis of sub-micron mineral matter in coal via scanning transmission electron microscopy. *Fuel*, **63**, 24-29.

Alwani, Z. and Schneider, G. M. (1969). Phasengleichgewichte, kritische Erscheinungen und PVT-Daten in binären Mischungen von Wasser mit aromatischen Kohlenwasserstoffen bis 420°C und 2200 Bar. *Ber. Bunsenges.*, **73**, 294-301.

Amin, S. I. (1975). Reforming and decomposition of organics in water. Thesis prepared for M. Modell, MIT.

Comet, P. A., McEvoy, J., Giger, W., and Douglas, A. G. (1986). Hydrous and anhydrous pyrolysis of DSDP Leg 75 kerogens--a comparative study using a biological marker approach. *Organic Geochemistry*, **9**, 171-182.

Commins, B. T. (1969). Formation of polycyclic aromatic hydrocarbons during pyrolysis and combustion of hydrocarbons. *Atm. Env.* **3**, 565-572.

Eglinton, T. I., Rowland, S. J., Curtis C. D., and Douglas, A. G. (1986). Kerogen-mineral reactions at raised temperatures in the presence of water. *Organic Geochemistry*, **10**, 1041-1052.

Hoering, T. C. (1984). Thermal reactions of kerogen with added water, heavy water and pure organic substances, *Org. Geochem.* **5**, 267-278.

Hoogwater, S. (1991). High pressure hydrothermolysis of chlorinated hydrocarbons. Thesis prepared for J. M. L. Penninger, Eindhoven University of Technology.

Jockers, R. and Schneider, G. M. (1978). Fluid mixtures at high pressures--fluid phase equilibria in the systems fluorobenzene + water, 1,4-difluorobenzene + water, and 1,2,3,4-tetrahydronaphthalene + decahydronaphthalene (trans) + water up to 360 MPa. *Ber. Bunsenges. Phys. Chem.*, **82**, 576-582.

Lewan, M. D., Winters, J. C., and McDonald, J. H. (1979). Generation of oil-like pyrolysates from organic-rich shales, *Science*, **203**, 897-899.

Lewan, M. D., Winters, J. C., and Williams, J. A. (1981). A laboratory study of petroleum generation by hydrous pyrolysis, *Adv. in Organic Geochemistry 1979*, M. Bjorøy et al., eds., John Wiley and Sons, Ltd., Chichester, p. 524-533

Lydersen, A. L. (1955). Estimation of critical properties of organic compounds, College of Engineering, University of Wisconsin, *Eng. Expt. Sta. Rept.* **3**, Madison, WI.

Magda, J. J., Fredrickson, G. H., Larson, R., and Helfand, E. (1988). Dimensions of a polymer chain in a mixed solvent. *Macromolecules*, **21**, 726-732.

Monthioux, M., Laniais, P., and Monin, J-C. (1985). Comparison between natural and artificial maturation series of humic coals from the Mahakam delta, Indonesia. *Organic Geochemistry*, **8**, 275-292.

Moore, J., and Pearson, R. (1981). *Kinetics and Mechanism*, Third Edition, John Wiley and Sons, New York, 318-324.

Ross, D. S., Hirschon, A. S., Tse, D. S., and Loo, B. H. (1990a). The effects of hydrothermal treatment on Wyodak coal, *American Chemical Society Division of Fuel Chemistry Preprints* **35**, 352-363.

Ross, D. S., Loo, B. H., Tse, D. S., and Hirschon, A. S. (1990b). Hydrothermal treatment and the oxygen functionalities in Wyodak coal, *Fuel* **70**, 289-295.

Ross, D. S. (1992). Autoradiographic and hydrothermal probes of interfacial chemistry in oil shale and coal, *American Chemical Society Division of Fuel Chemistry Preprints* **37**, 375-384.

Simoneit, B.R.T. (1985a). Hydrothermal petroleum: Genesis, migration, and deposition in Guaymas Basin, Gulf of California. *Can. J. Earth Sci.* **22**, 1919-1929.

Simoneit, B.R.T. (1988). Petroleum generation in submarine hydrothermal systems: An update. *Can. Mineralogist* **26**, 827-840.

Stein, S. E., Wang, F., and Senthilnathan, V. P., 1989. Chemical Models for Regressive Reactions: I. Thermolysis of Dihydroxybenzenes, Proceedings of the 1989 International Conference of Coal Science, *International Energy Agency*, 165-168.

Tannenbaum, E. and Kaplan, I. R. (1985). Low-M_r hydrocarbons generated during hydrous pyrolysis and dry pryolysis of kerogen. *Nature*, **317**, 708-709.

Table I

PRODUCTS FROM THE PYROLYSIS OF GLUCOSE IN WATER (374°C/30 MIN)

Pressure (atm)	Density (g/Ml)	Fraction of Starting C (%)		
		Oil	Solid	Gas
152	0.07	27.8	68.9	3.4
220	0.32	60.4	8.5	9.5

Table II

Some Properties of the Recovered Coals and Tars

	Treatment Period	Starting coal	Hydrothermal	Thermal	Undecane
H/C					
		0.90			
	30 min	–	0.82	0.83	0.81
	5 hr	–	0.72 1.13 (tar)	0.76	0.75
O/C[a]					
		0.24			
	30 min	–	0.16	0.15	0.18
	5 hr	–	0.12 0.18 (tar)	0.16	–
$T_{1/2}$(°C)[b]					
	–	395-400	–	–	–
	30 min	–	340-350 200 (tar)	377-395	405
	5 hr	–	410 140 (tar)	425	465
$\bar{M}_w$[c]					
	–	403-411	–	–	–
	30 min	–	410-421 393 (tar)	329-380	373
	5 hr	–	332	308 432 (tar)	201

a. Oxygen determined by direct O-analysis.
b. The temperature at which one-half of the FIMS volatiles has passed into the instrument.
c. Weight average molecular weight.

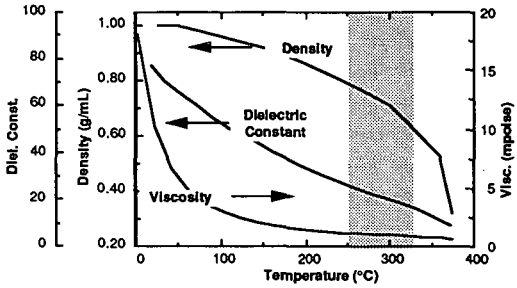

Figure 1. Some key properties of liquid water.

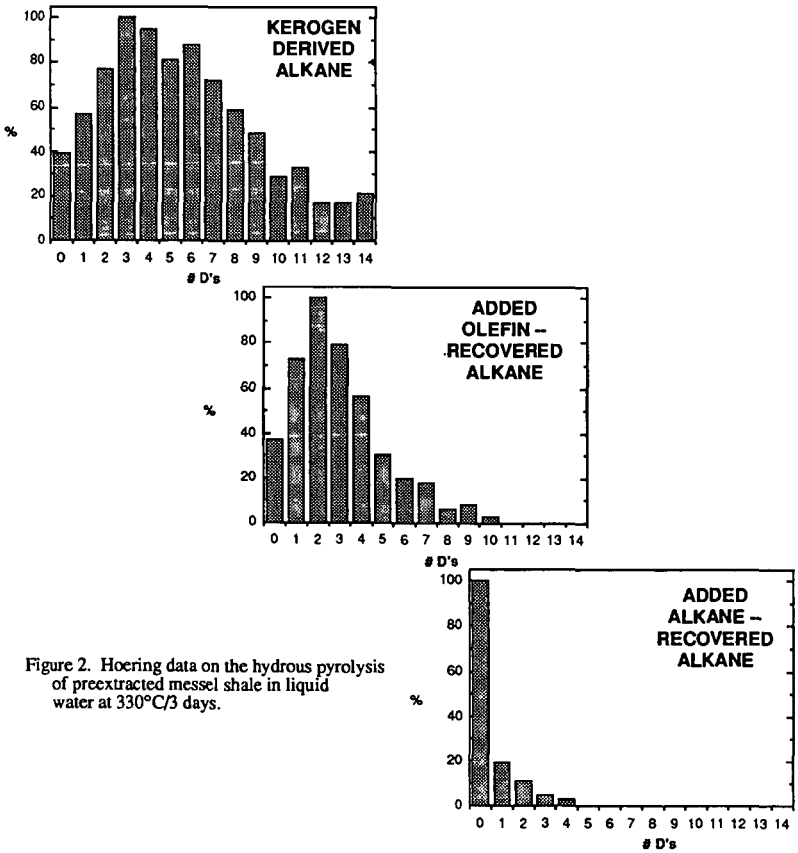

Figure 2. Hoering data on the hydrous pyrolysis of preextracted messel shale in liquid water at 330°C/3 days.

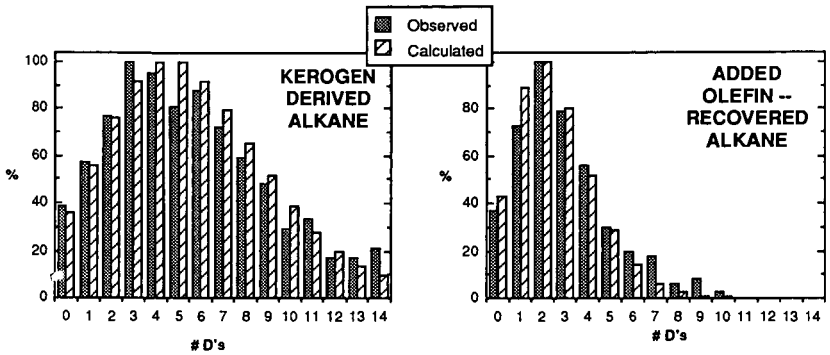

Figure 3. Hoering data and calculated profiles. The kinetic factors are reduction >> pyrolysis and exchange ≈ 2 x pyrolysis.

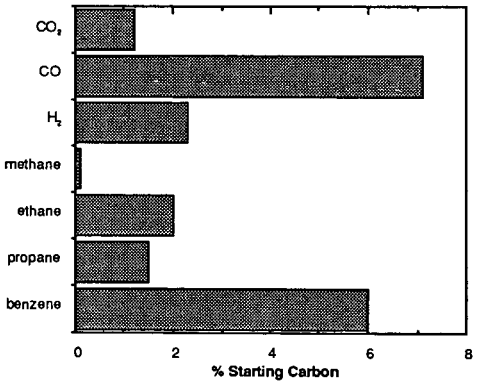

Figure 4. 1,1,2-trichloroethane conversion 428°C/ρ = 0.32mL/50 min.

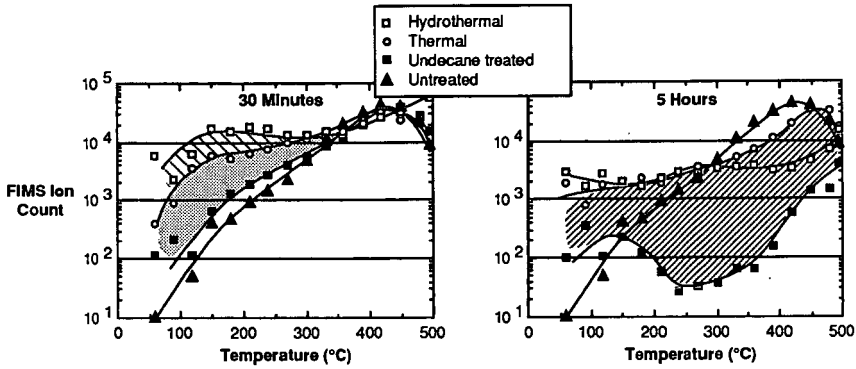

Figure 5. FIMS ion count values vs evaporation temperature for 30-min and 5-hr runs at 350°C.

Effects Of Transport Limitations On Pyrolysis Of Cellulosics

Ivan Milosavljevic and Eric M. Suuberg
Division of Engineering, Brown University
Providence, RI 02912

Keywords: Pyrolysis, Cellulosics, Heat Transfer, Mass Transfer

Introduction

The tendency of cellulosic materials to form chars during pyrolysis is well established. However the effects of sample density, size and grain orientation on char formation are not yet well established. In this work, the data obtained from different experimental systems are compared in order to deduce the effects of sample density, size and grain orientation on pyrolysis of cellulosics. It was noted that the overall pyrolysis process appears to be similar for a wide range of materials, sample densities and grain orientations, at least under high (fire-level) heat flux conditions.

Experimental

The pyrolysis behavior of purified cellulose (pressed to three different densities), white pine and oak were investigated in a large scale pyrolysis apparatus (designed to simulate fire conditions), a standard TGA, a standard tube furnace and a heated wire gauze reactor. This work was motivated by a desire to establish whether the kinetics of pyrolysis, measured in TGA-type devices can apply to room fire-type situations.

The large scale pyrolysis apparatus is shown schematically in Figure 1. A sample is heated by radiative heaters as it is positioned atop an electronic balance. The heat flux from the radiative heaters was 40 kW/m^2 in all tests reported here and all the tests were performed under nitrogen purge. It should be noted that not all of the incident heat flux was absorbed due to the heat losses from the surface (i.e. reflection, re-radiation and convection). Mass changes and/or temperatures within the sample were monitored continuously. Samples used in the large scale pyrolysis apparatus were cylindrical with diameter 38 mm and various thicknesses (typically about 10mm). Pressed cellulose samples had densities of 0.475 ± 0.025 g/cm^3, 0.725 ± 0.025 g/cm^3 and 1.000 ± 0.090 g/cm^3, white pine a density of 0.377 g/cm^3 and oak a density of 0.734 g/cm^3. For tests with cellulose and white pine there were two different grain orientations with respect to the axis of incident radiative flux: parallel and perpendicular. For tests with oak only a "tangential" (with respect to growth rings) orientation was used.

In order to establish the difference in behavior between large samples (as used in a large scale pyrolysis apparatus) and small samples of purified cellulose, some tests were performed in a TGA/FTIR system using 3x3x3 mm cellulose samples of same densities as in a large scale pyrolysis apparatus. The atmosphere was helium and the heating rate was 60°C/min.
The wire gauze reactor was used in order to investigate the effect of grain orientation on the ultimate char yield. Samples for the wire gauze reactor were of 1.0 g/cm^3 density, 2.7x27 mm and different widths. The atmosphere was helium and the heating rate was 60°C/min.

Results and Discussion

Figures 2a and 2b show mass loss as a function of time for different initial sample densities for perpendicular (tangential for oak) and parallel grain orientation recorded in the large scale pyrolysis apparatus, respectively. Despite the diversity of materials and their densities, the behavior, with respect to mass loss, appears similar. There is some small amount of mass loss observed before the actual heating started. This is probably due to the sample drying, since the samples were handled in air without any drying prior to a run, and the atmosphere in the apparatus was dry nitrogen from the moment the sample was placed in the apparatus.

It can be seen from Figures 2a and 2b that the point of first significant mass loss is a function of density. Higher density samples tend to start to pyrolyze later than the lower density samples, independent of the grain orientation. The reason for such behavior is a difference in heat transport. The higher the density of the sample, the more efficiently it serves as a heat sink (since thermal conductivity varies with density), and the more slowly the temperature of the surface rises. Since it is the surface layer that begins the process of pyrolysis, it is the temperature of the surface that matters. This hypothesis is supported by the data of Figure 3, which shows the behavior of small samples of cellulose in a TGA device. In this case, the samples are uniformly heated over their surface and the gas phase temperature histories are identical, but there is a trend, again, towards "earlier" pyrolysis in the lower density samples. The process is undoubtedly external heat transfer controlled, since there is absolutely no reason to believe that pressing density affects kinetics (all samples were pressed from the same powder).

The pine samples of Figures 2a and 2b behave in a manner quite similar to that of pure cellulose. This cannot be said for the oak sample, perhaps because the pine is much more homogenous than the oak (there are clearly observable inhomogenities in the oak sample). The nature of sample inhomogeneity and its importance will be further discussed below.

It can be seen from Figures 2a and 2b that during the middle stage of pyrolysis mass loss is linear in time, as is often seen in the literature for this type of material [1, 2, 3, 4, 5]. The reason for such a behavior is that the process is heat conduction limited, with surface flux prescribed. The pyrolysis wave is "pushed" at constant velocity by the heat deposited on the surface at constant rate (vide infra).

Figure 2c depicts the temperature at the surface and at 10 mm from the surface for a 12.25 mm thick cellulose sample of 1.078 g/cm^3 density with perpendicular grain orientation, recorded in the large scale pyrolysis apparatus. The temperature profiles clearly establish that the pyrolysis process is heat transfer limited, in such a system. Note that the "kinks" in the profiles at between 300°C and 400°C are reproducible, and we believe indicate an endothermic step in the overall process (though not necessarily the main reaction process). This will be discussed elsewhere.

Figures 4a, 4b and 4c show cumulative amounts of carbon monoxide, carbon dioxide and methane, respectively from the TGA experiments of Figure 3. It is obvious that there is an effect of sample density. There is more gas evolved from higher density samples. This is probably due to the higher residence times of tars, such that there is a higher probability for their cracking to lighter gases prior to escape from the particles. By examining the starting point of gas evolution in these figures, it can be concluded that both carbon monoxide and carbon dioxide are the products of primary pyrolysis as well as of secondary cracking reactions whereas methane appears as a product of the secondary reactions alone (otherwise it should start to evolve immediately with the other gases).

Figure 5 shows the final char yield for the three different sample densities, examined in the TGA and large scale pyrolysis apparatus. Obviously the TGA data support the notion that with increasing density, there is an increasing tendency towards cracking reactions of tars, which leave behind a char product as well. The effect, while measurable, certainly cannot be termed large, over the range of densities explored. Thus for pyrolysis of cellulose in woody materials, there is a suggestion that density alone is not a key factor in determining pyrolysis char yields. The data from the large scale apparatus requires consideration of other factors, discussed below.

Figure 6 presents mass loss rates (averaged over the linear portions of mass loss curves only) as a function of initial sample density for cellulose samples with perpendicular and parallel grain orientation from experiments in the large scale pyrolysis apparatus and from the experiments in the TGA. The samples used for a TGA should not be affected by a grain orientation due to the uniform heating of the samples from all sides. The mass loss rate follows the same trend for both grain orientations used in the large pyrolysis apparatus. The rate of mass loss is linear in density. The actual mass loss rates are shown in Table I as the parameter B, where the relationship between sample mass M and time t is roughly:

$$M = M_0 - Bt$$

Again, this holds approximately over a large fraction of the sample's pyrolysis history. The fact that Figure 6 shows B to be linear in density (ρ) suggests that the ratio (B/ρ) is constant, and these values are also shown in Table I. For a sample of constant cross-sectional area, (B/ρ) is proportional to the linear propagation velocity of a pyrolysis wave through the sample, viz:

$$(B/\rho) = V\,A$$

where V is the velocity and A is the cross-sectional (1134 mm^2). Thus it may be seen that the average propagation velocity is $9.8 \times 10^{-3}/1.134 = 8.6 \times 10^{-3}$ cm/s or about 0.5 cm/min. It can be seen from Table I that the pyrolysis wave speed is fairly independent of density. All (B/ρ) values fall within the standard deviation of the mean (i.e. $\pm 3 \times 10^{-3}$ cm^3/s). No clear trends are established by the limited data available. Again, the constancy of (B/ρ) is expected, if thermal conductivity is linear in density.

Mass loss rates (averaged over the linear portions of mass loss curves only), obtained in the TGA experiments are also shown in Figure 6. The effect of density is not pronounced but is certainly observable. These data show the opposite trend from the data recorded in the large scale pyrolysis apparatus. Of course there is a significant difference between the two situations. Consider the locus of resistance to heat transfer in the two cases. There is little doubt that in the large-scale pyrolysis system, the process is conduction-limited. A sample that is partially pyrolyzed and sectioned shows a sharp pyrolysis front separating a black char from a relatively white unpyrolyzed zone. In the case of the samples in the TGA, the process is <u>not</u> conduction limited within the sample. This may be easily shown by considering the Biot number for the sample $Bi = hr/k_s$, where h is the heat transfer coefficient, r is the radius of the sample (treated as an effective sphere) and k_s is its thermal conductivity. Taking h to be governed by the conduction limit, $Nu = hd/k_g = 2$, where d is the diameter of a particle and thus $Bi = k_g/k_s$. Since $k_g \cong 0.2 W/mK$ for helium near 500K, and since k_s for woods (cellulosics) is of the same order of magnitude, then clearly the influence of external heat transfer cannot be neglected since Bi is of order unity. With a few particles in a sample pan, the system is not as well-defined, but the conclusion that external heat transfer limitations can influence results still stands, and a clear relationship between density and rate should not be expected, as was seen in the conduction limited case.

Figures 5 and 6 clearly reveal effects of sample orientation in the bulk samples used in the large scale pyrolysis apparatus. The bulk samples all have a distinctly anisotropic appearance, despite the fact that they are produced by pressing from fine powder. Bands run across the entire diameter of the sample, in a direction perpendicular to the direction from which pressing force is exerted. The band structure reveals itself during pyrolysis as well. When samples are pyrolyzed in which the bands are perpendicular to the incident radiative flux, the samples tend to crack or split in a direction parallel to the bands. In the case in which incident flux is parallel to the bands the cracking is also in a direction parallel to the bands.

Given the anisotropy of the samples there is little surprise then that pyrolysis is affected to some extent by band orientation. As Figure 5 reveals, char yield correlates with band orientation as well as with density in the bulk samples. Care must be exercised in interpreting these results, because what is termed "char" in these experiments in fact includes partially pyrolyzed material, due to existence of heat losses at the back face of the sample. But for present purposes, it is significant that when the volatiles must cross the pressing bands to escape the front surface of the sample, a higher amount of secondary reactions occur than when the volatiles can move parallel to the bands (the secondary reactions, again, are believed to deposit extra char). Note that the volatiles must escape the front face of the sample because the back and sides are enclosed in a ceramic cup.

The effect of band orientation relative to a surface flux is probably somewhat analogous to wood grain orientation to a surface flux. The ultimate effect of such a choice of orientation does not

appear to be very large, in terms of char yield - a percent or two at most in Figure 5. Again, mass transfer effects are seen, but they are not large, just as in the case of the density effect seen with the small samples examined in the TGA. The density effect on char yield appears to be large in the case of the large samples of Figure 5, but again this is probably in large part an artifact induced by the differences in temperature profiles for samples of different density.

The mass loss rate data of Figure 6 suggest that the samples with band structures parallel and perpendicular to the incident flux have roughly comparable mass loss rates at low density (<0.5g/cm^3). Upon increasing the density above 0.7 g/cm^3, there begins to be apparent a slight tendency towards higher rates when the volatiles can move parallel the band structure. As was seen in Table I, the trend towards faster mass loss in parallel samples is not particularly pronounced, so that roughly comparable mass loss rates give rise to the conclusion of roughly comparable rates of thermal wave propagation, irrespective of orientation. The trend is nevertheless consistent with a slight retardation of volatiles escape from samples in which volatiles have to cross the bands.

The importance of with- and cross-band transport was explored in one further experiment. Figure 7 presents the variation of the ultimate char yield with sample width, obtained from thin samples pyrolyzed in a wire gauze reactor. These samples all had a thickness of 2.7 mm and a length of 27 mm, and all had a density of around 1 g/cm^3. The samples were heated at a rate of 60°C/min up to 600°C. The samples were thus thin rectangular parallelopipeds, and had been pressed in the direction of 2.7mm thickness. The pressing direction is again significant, as the work with the larger samples has revealed. There would be expected a slight difference in rates of escape of volatiles in a direction parallel to the main faces of the parallelopiped vs across the faces.

The results of Figure 7 were surprising in the magnitude of the effect they revealed. The work with the narrowest samples (2.3 mm) gave a char yield of just over 5.5%, perfectly consistent with the TGA results shown in Figure 5. Increasing the sample width (while keeping thickness constant at 2.7 mm and length constant at 27 mm) had a surprisingly large effect on char yield. These results strongly suggest that the volatiles in fact have a great deal of difficulty moving cross-band and must move parallel to the band to escape (otherwise the fact that the shortest dimension remained 2.7 mm should have dictated that there be little effect on yield). It should also be remembered that in these experiments the samples were heated from all sides, so a pathway to a cooler zone was not available, as it might be in larger samples.

Thus it must be concluded that the concept of "ultimate char yield" is somewhat meaningless, when applied to samples of characteristic dimensions more than a few millimeters, in view of the results of Figures 5 and 7.

Conclusions

The behaviors of three different materials (purified cellulose, white pine and oak) with different grain orientations and different densities were investigated using different experimental approaches. The behavior of white pine and oak are seen to be quite similar to pure high density cellulose under heat-transfer controlled, fire-like conditions. The role of density is seen in its effect on heat transfer; higher density samples conduct better, and if the process is conduction limited, will pyrolyze faster. The density also affects the ability of volatiles to escape pyrolyzing samples, and this affects both char yields and volatile yields. These effects are considerably less important than the effect of density on heat transfer.

Sample band, or grain, structure also has some small effect on volatiles escape, but again, the effect is small. Sample particle size is seen to be important in several respects, as it influences both heat and mass transfer measurably, even when particles are a few millimeters in size. Applications of TGA data to modeling of fire situations must involve cognizance of such issues.

Acknowledgments

The support from the Center for Fire Research of NIST under grant 60NANB0D1042 is gratefully

acknowledged. Authors deeply appreciate the contribution of Dr H. Teng who performed the TGA/FTIR experiments.

References

1. Lee, C. K., Chaiken, R. F. and Singer, J. M. XVI Symp. (Int) on Combustion, 1976
2. Julien, S., Chornet, E., Tiwari, P. K. and Overend, R. P. Journal of Analytical and Applied Pyrolysis, **19**, 81, 1991
3. Radlein, D., Piskorz, J. and Scott, D. S. Journal of Analytical and Applied Pyrolysis, **19**, 41, 1991
4. Lipowicz, P. J. and Rothenberg, S. J. Combustion and Flame, **75**, 217, 1989
5. Raissi, A. T., Mok, W. S. L. and Antal, M. J. Ind. Eng. Chem. Res., **28**, 856, 1989

Table I: Pyrolysis Wave Speed in Large Scale Apparatus, 40 kW/m^2 flux, as a function of sample density and orientation for Cellulose, Oak and Pine

Orientation	Density (g/cc)	B (g/s)x10^3	B/ρ (cc/s)x10^3
Perpendicular	0.47	5.0	10.6
Perpendicular	0.46	5.3	11.5
Perpendicular	0.70	6.5	9.8
Perpendicular	0.73	7.1	9.7
Perpendicular	1.06	8.0	7.5
Perpendicular	1.06	8.9	8.4
Parallel	0.49	4.7	9.6
Parallel	0.72	8.0	11.1
Parallel	0.72	7.8	10.8
Parallel	0.93	8.3	8.9
Parallel	0.97	9.2	9.5
Perpendicular (Oak)	0.73	7.2	9.9
Perpendicular (Pine)	0.38	2.9	7.6
Parallel (Pine)	0.38	4.9	12.9
			9.8

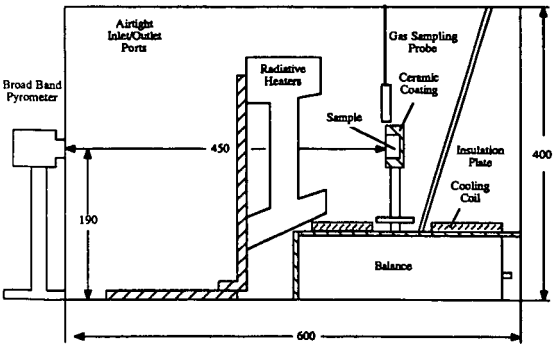

FIGURE 1: LARGE SCALE PYROLYSIS APPARATUS
(All measures in millimeters)

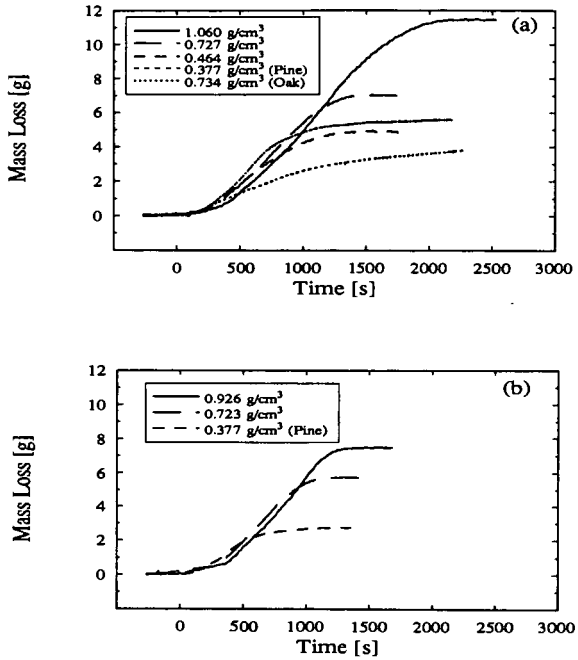

Figure 2: Mass loss as a function of time for (a)-perpendicular and (b)-parallel grain orientation from the large scale apparatus (flux was 40 kW/m^2)

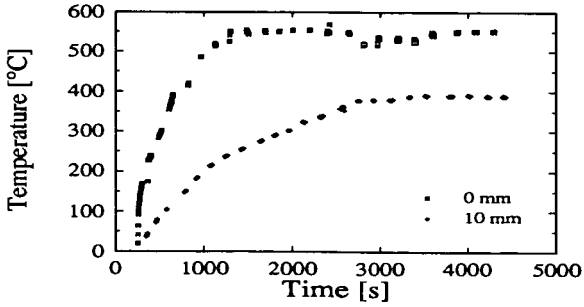

Figure 2c: Typical temperature profiles in a sample pyrolyzed in the large scale apparatus

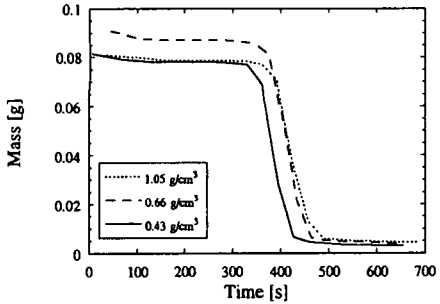

Figure 3: Mass loss as a function of time from the TGA (heating rate was 60°C/min)

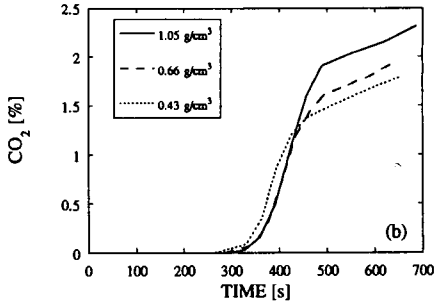

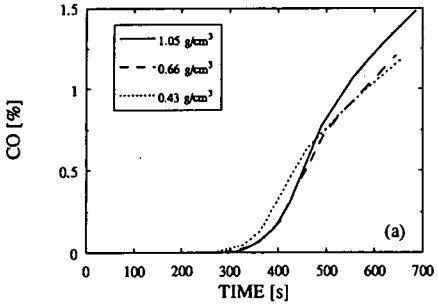

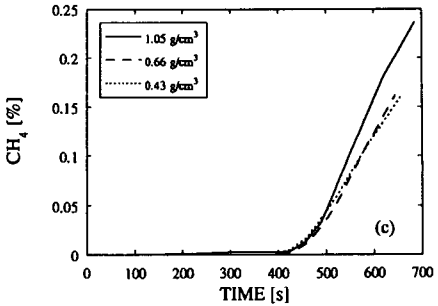

Figure 4: Cumulative amounts of a-CO, b-CO2 and c-CH4 as functions of time from the TGA (heating rate was 60°C/min)

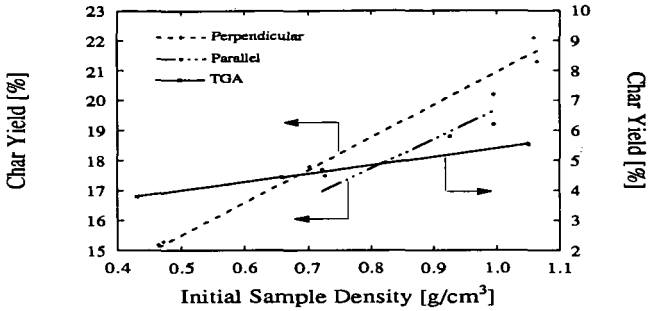

Figure 5: Cellulose char yield as a function of initial sample density for perpendicular and parallel grain orientation from the large scale apparatus and from the TGA

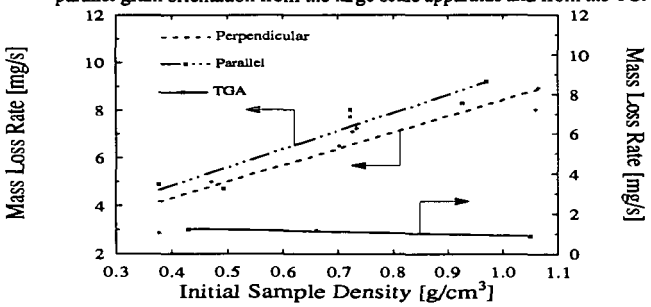

Figure 6: Mass loss rate as a function of initial sample density for perpendicular and parallel grain orientation from the large scale apparatus and from the TGA

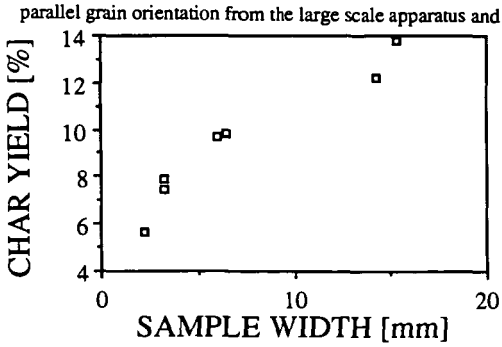

Figure 7: Cellulose char yield as a function of sample width from wire gauze reactor

FLASH HYDROPYROLYSIS OF THE COAL SUPPORTING A CATALYST THROUGH SOLVENT SWELLING

Kouichi Miura, Kazuhiro Mae, Hiroshi Morikawa and Kenji Hashimoto*
Research Laboratory of Carbonaceous Resources Conversion Technology
*)Department of Chemical Engineering
Kyoto University, Kyoto 606, Japan

Key words: Catalytic Hydropyrolysis, Solvent Swelling of Coal, Hydrogen Bonding

INTRODUCTION

Flash hydropyrolysis of coal is expected as a means to recover a large amount of liquid products under rather milder conditions than direct coal liquefaction. However, total coal conversion does not increase even under 10 MPa of H_2 as compared with the pyrolysis in an inert atmosphere. This is because hydrogen does not contribute to the primary coal devolatilization but to the secondary gas phase reaction of primary tar vapors, resulting in the increase in CH_4 yield. Several attempts to increase the coal conversion by use of catalysts such as Ni, Mo, Co, and Fe have not succeeded so far. The catalysts contributed only to the secondary gas phase reaction[1,2]. On the other hand, catalysts such as Zn, Sn and Mo are reported to be very effective to increase both the coal conversion and the liquid yield significantly under slow pyrolysis conditions when the catalysts are in sulfide forms[3-5]. Since Zn, for example, is supported as $ZnCl_2$, it is transformed to ZnS during the slow pyrolysis[6]. However, $ZnCl_2$ can not be sulfided in such a short time during which the primary devolatilization is finished. Summarizing these researches suggests that two conditions must be satisfied for the catalyst to be active during the primary devolatilization of the flash hydropyrolysis of coal: the first one is that the catalyst must be activated or presulfided, and the other is that the catalyst must be in close contact with the functional groups which will be cleaved during the flash pyrolysis.

In this paper a new catalyst supporting method which satisfies the above conditions was presented. The method consists of two steps: the first step is the impregnation of $ZnCl_2$ or $SnCl_2$ from a methanol solution into the micropores of coal by utilizing the swelling of coal induced by methanol, and the second step is the sulfidation of $ZnCl_2$ or $SnCl_2$ in a gas stream containing 5 % of H_2S at room temperature. The coal supporting the catalyst was pyrolyzed by use of a high pressure Curie-point pyrolyzer to examine the validity of the presented supporting method. The coal supporting catalyst was further treated by tetralin at 100 °C to prepare the coal containing both catalyst and tetralin in the swollen coal. The coal treated by tetralin by the above procedure was also prepared. These samples were pyrolyzed to examine the roles of the catalyst and tetralin during the pyrolysis.

EXPERIMENTAL

Catalyst supporting method

An Australian brown coal, Morwell (Ultimate analysis (daf basis): C; 67.1%, H;4.9%, S+O;27.40%) was used as a raw coal. It was ground into the particles less than 70 μm in diameter and dried in vacuo at 110°C for 24 h before use. The catalyst was supported on the coal by the following method:

1. 1.0 g of coal particles were immersed in 0.9 ml of methanol dissolving 0.123 g of $ZnCl_2$ or 0.094 g of $SnCl_2$ at room temperature, and kept for 24 h, by which all the methanol including the metal chloride was incorporated into the coal by swelling it by 32% by volume.

2. Methanol was removed by the vacuum drying almost completely, remaining the metal chloride within the coal. The coal incorporating the metal chloride is still swelling. The sample of this stage is abbreviated to Zn-Swell or Sn-Swell.
3. The Zn-Swell or the Sn-Swell was treated by a N_2 stream containing 5 % of H_2S by volume for 1 h, and was purged by a pure nitrogen stream for 30 min. The sample thus prepared was abbreviated to Zn-S-Swell or Sn-S-Swell.
4. The Zn-S-Swell was further treated by tetralin at 100°C under 1 MPa of N_2, by which the sample was swollen by 35% by volume, and tetralin was incorporated within the sample. This sample was abbreviated to Zn-S-Swell-Tet .

The coal sample supporting Zn by a conventional method was also prepared for comparison. Namely, $ZnCl_2$ was supported on the coal from an aqueous $ZnCl_2$ solution, then the sample was treated by the H_2S containing gas stream as stated above. The sample prepared by this method is abbreviated to Zn-S-Impreg. The amount of catalyst (as metal) in the coal was adjusted to be around 5 wt% on the daf basis for all the samples except for the Zn-S-Swell. The coal sample swollen by tetralin by the procedure 4 was also prepared. It was abbreviated to Tet.

Flash hydropyrolysis

Figure 1 shows a schematic of the experimental setup used for the flash hydropyrolysis. The detail of the high-pressure Curie-point pyrolyzer is shown in Figure 2. The quarts reactor (12 mm OD and 6.0 mm ID) was installed in the pressure vessel made of SUS-316. The inside of the reactor and the pressure vessel were pressurized using the same gas line, then experiments up to 10 MPa were possible in a flowing gas stream.

We have designed the apparatus so that the amount of hydrogen consumed (R_H) as well as each product yield can be measured during the pyrolysis. The procedure for the pyrolysis under 5 MPa of H_2, for example, is as follows: 2 to 3 mg of sample wrapped by a pyrofoil (an Ni-Fe alloy) which has a unique Curie-point temperature was placed in the reactor, and was pressurized up to 5 MPa by a He stream. Hydrogen containing 1 % of N_2 was stored at 5 MPa in a small gas holder (5.0 ml in volume), whose volume was adjusted to purge the reactor for 20 s. The hydrogen was pushed out by the He stream into the reactor by switching the 4-way valve 1. After the sample was exposed to the hydrogen for 5 s it was heated to the Curie-point temperature by the induction coil and kept there for 10 s to be pyrolyzed rapidly. The sample was exposed to the hydrogen for 5 more seconds. The primary tar vapors were all collected by the quarts wool placed just below the sample, because the vapors were cooled immediately by the gas stream. Gaseous products and the unreacted hydrogen were all stored in a product gas holder, and were analyzed to determine the amounts of inorganic gases (N_2, H_2, CO, CO_2 and H_2O) and hydrocarbon gases (CH_4, C_2H_4, C_2H_6, C_3H_6, C_3H_8, C_4H_8, C_4H_{10}, C_5, and C_6 gaseous compounds, benzene, toluene and xylene). The yields of char and tar were measured from the weight change of the sample in the pyrofoil and the reactor. From the analysis of N_2 and H_2 we can know both the hydrogen supplied and the amount of unreacted hydrogen, then we can calculate the amount of hydrogen consumed during the pyrolysis. The pyrolysis temperature was changed from 485 to 920°C by using the pyrofoils which have different Curie-point temperatures.

RESULTS AND DISCUSSION

Physical and chemical changes of coal through the catalyst support

Figure 3 shows the change in the volumetric swelling ratio and the micro pore volume of the Zn-Swell with the increase of the catalyst loading. The micrpore volume corresponding to

0.33 to 1.0 nm in pore diameter was calculated from the CO_2 adsorption isotherm measured at 25°C. Both the swelling ratio and the micropore volume increased with the increase of Zn loading. No such a change was observed for the Zn-S-Impreg. F.T.i.r. measurement of the Zn-Swell showed the increase in the intensity associated with free -OH groups as compared with the raw coal. Methanol is known to break the hydrogen bonds in the coal to produce free -OH groups and swell the coal. Therefore, $ZnCl_2$ in the Zn-Swell is probably retained between the free -OH functional groups which formed hydrogen bondings in the raw coal, which increased the micropore volume and the swelling ratio.

We are expecting that the Zn in the Zn-S-Swell or the Sn in the Sn-S-Swell is transformed into the sulfide by the treatment with H_2S at room temperature, but we could not prove it in spite of several chemical analyses performed. However, we can safely say ZnS is formed judging from the fact that $Zn(OH)_2$ is easily transformed into ZnS by the treatment with H_2S, because $ZnCl_2$ in the Zn-Swell is well expected to be less stable than $Zn(OH)_2$.

Effect of the catalyst supporting method on the pyrolysis yield

Figure 4 shows the product yields obtained by pyrolyzing the samples prepared above at 764°C under 5 MPa of H_2. Although each yield obtained from the Zn-Swell was almost similar as that obtained from the raw coal, the total volatile matter (TVM), the tar yield and the hydrocarbon gas yield of the Zn-S-Swell and Sn-S-Swell were significantly larger than those obtained from the raw coal. Significant decreases in the water yield were found for these two samples. The amount of hydrogen consumed, R_H, of the Zn-S-Swell and Sn-S-Swell were also larger than that of the raw coal. These results indicate clearly that Zn and Sn supported utilizing the solvent swelling and sulfided by H_2S at room temperature contribute to the primary devolatilization reaction. On the other hand, in case of the Zn-S-Impreg, where Zn is sulfided but the coal is not swelling, only the tar yield and the R_H value were slightly larger than those of the raw coal. Therefore, close contact of the catalyst with the coal matrix such as -OH functional groups, which is realized through the solvent swelling, is essential in addition to the sulfidation for the catalyst to contribute the primary devolatilization reaction.

Pyrolysis of the Zn-S-Swell

To examine how the catalyst contributes to the primary devolatilization reaction, the pyrolysis yields of the Zn-S-Swell obtained at different temperatures were compared with those of the raw coal in Figure 5. Within the temperature range where both samples were pyrolyzed, the total volatile matter, the tar yield, the hydrocarbon gas yield of the Zn-S-Swell were larger than those of the raw coal. On the other hand, the yield of water of the Zn-S-Swell was smaller than that of the raw coal. Significant difference was found in the R_H value as shown in the bottom figure. The gaseous hydrogen started to be utilized from around 600°C for the Zn-S-Swell, whereas from around 700°C for the raw coal. These results indicate that the total volatile matter of the Zn-S-Swell was increased by at least two mechanisms. The first mechanism is the acceleration of the hydrogen transfer from the gas phase as clearly shown in the R_H value, and the other is the suppression of the water forming cross-linking reaction, resulting in the increase of the tar yield through the suppression of the condensation reaction.

Roles of the catalyst, hydrogen and tetralin during the primary devolatilization

We have presented a novel flash pyrolysis method in which the coal swollen by a hydrogen donor such as tetralin was pyrolyzed in an atmospheric pressure of N_2[7,8]. Both the coal

conversion and the liquid yield were increased significantly by the method. This was because hydrogen radicals were effectively transferred from/via tetralin to coal fragments, and because the water forming cross-linking reaction was suppressed by the tetralin molecules retained within micropores. In this study we have clarified that hydrogen radicals were effectively transferred from gaseous hydrogen to coal fragments via catalyst if the catalyst was supported properly. Now, we have two hydrogen radical suppliers, hydrogen and tetralin, and two hydrogen radical transfer promoters, the catalyst and tetralin. Therefore, we can expect at least five hydrogen radical transfer paths as shown in Figure 6: (1) from gaseous hydrogen, (2) from tetralin, (3) from gaseous hydrogen via catalyst, (4) from gaseous hydrogen via tetralin, and (5) from tetralin via catalyst. Then we tried to examine the relative magnitude of the five hydrogen radical transfer paths.

Figure 7 shows the pyrolysis yields and the R_H values for 4 samples, the raw coal, the Tet, the Zn-S-Swell and the Zn-S-Tet, pyrolyzed at 764°C under 5MPa of H_2 or He. Helium was used as an inert carrier gas when gaseous hydrogen was not necessary. We will examine the relative magnitude of the 5 paths based on the value of the coal conversion (char yield) first. Three experiments from the left were performed to examine the separate effect of gaseous hydrogen and tetralin. These experiments showed that tetralin and gaseous hydrogen have similar effects. The next three experiments were related to the combined effect of the hydrogen radical supplier and the radical transfer promoter. The relative magnitudes of the paths (3), (4) and (5) are judged to be (5)>(4)>(3) from these experiments. It is interesting to note that the contribution of the path (4) is larger than that of the path (3). The last experiment was performed including the catalyst, tetralin and gaseous hydrogen. From the last four experiments we can judge the path (5) is the most effective to increase the coal conversion. Summarizing the above results, we can say that the order of the relative magnitudes of the 5 paths can be written as

$$(5) > (4) > (3) > (2) \cong (1)$$

Next, we focused our attention on the product distribution and the amount of hydrogen consumed. Hydrogen radicals supplied from tetralin tended to increase the tar yield preferentially, whereas those supplied from gaseous hydrogen increased the hydrocarbon gas yield also as clearly shown in the product distributions. This suggests that the rate and/or the mechanism of the hydrogen radical transfer is different among the gaseous hydrogen and tetralin. The R_H values could be measured for only the experiments performed in H_2 atmosphere. It is clearly shown that the amount of hydrogen consumed increases for the samples supporting the catalyst and/or incorporating tetralin within the coal, indicating that the increases in the coal conversion were realized through the increase in the amount of hydrogen transfer. However, we can not discuss the contribution of tetralin now from the view point of the amount of hydrogen transferred, since we could not measure the amount of radicals transferred from/via tetralin.

CONCLUSIONS

A new catalyst supporting method which enhances the primary reaction of the flash pyrolysis of coal was presented, in which $ZnCl_2$ or $SnCl_2$ was supported from a methanol solution and the chloride was sulfided (activated) by a gas containing H_2S. The catalyst thus prepared enhanced the hydrogen radical transfer from gaseous hydrogen and from tetralin incorporated within micropores of coal, resulting in the increase of the coal conversion and the liquid yield. The relative magnitude of the hydrogen radical transfer paths during the flash pyrolysis was also examined.

REFERENCES

1. Asami, K., Tani, H., Ohtsuka, Y. and Nishiyama, Y., Proceed. of the 26th Conf. on Coal Sci. (Japan), p.220(1989).

2. Yamashita, H., Jinoka, T., Shrotri, Y., Hajima, M., Xu, W.-C. and Tomita, A., Proceed. of the 26th Conf. on Coal Sci. (Japan), p.252(1989).

3. Sulimma, A., Leonhard, P., van Heek, K.H. and Juntgen, H., *Fuel*, **65**, 1457(1986).

4. Bolton, C., Riemer, C., Snape, C.E., Derburshire, F.J. and Terrer, M.T., *Fuel*, **67**, 901 (1988).

5. Snape, C.E., Bolton, C., Dosch, R.G. and Stephens, H.P., *Energy & Fuels*, **3**, 421(1989).

6. Jolly, R., Charcosset, H., Boudou, J.P. and Guet, J.M., *Fuel Process. Techn.*, **20**, 51(1988).

7. Miura, K., Mae, K., Asaoka, S., Yoshimura, T. and Hashimoto, K., *Energy & Fuels*, **5**, 340(1991).

8. Miura, K., Mae, K., Yoshimura, T., Masuda, K. and Hashimoto, K., *Energy & Fuels*, **5**, 803(1991).

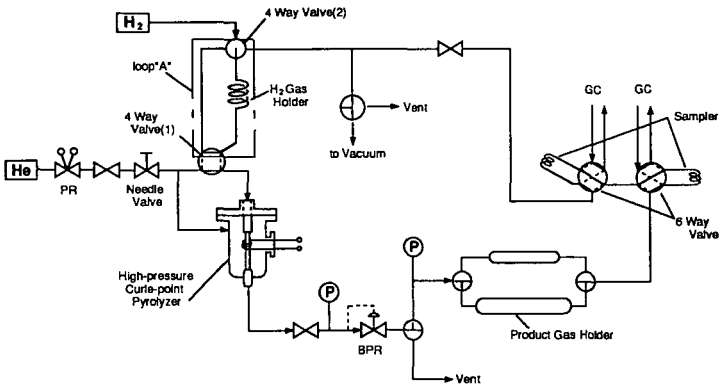

Figure 1 Schematic diagram of experimetnal apparatus

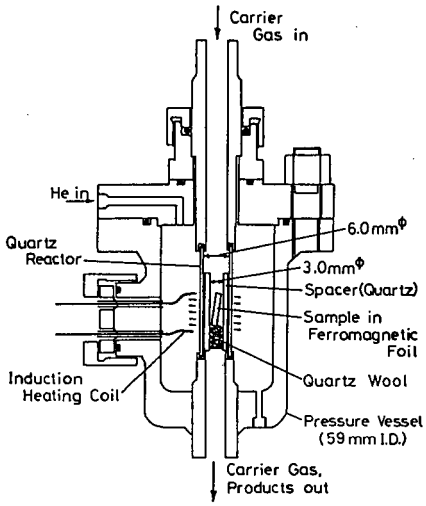

Figure 2 Detail of the high-pressure Curie-point pyrolyzer

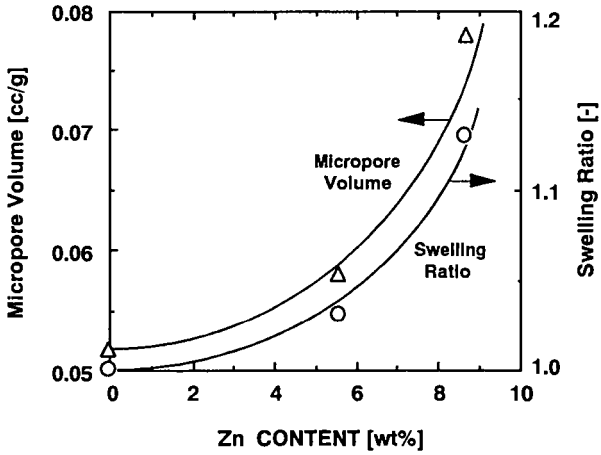

Figure 3 Change in the swelling ratio and the micropore volume with theincrease of the catalyst loading for the Zn-Swell

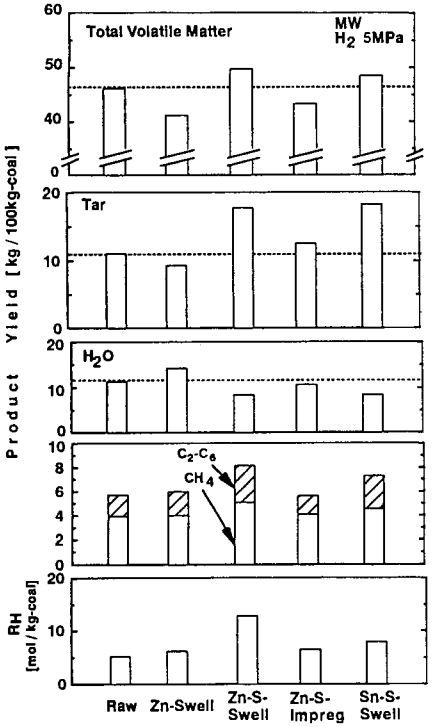

Figure 4 Effect of the catalyst supporting method on the product yield

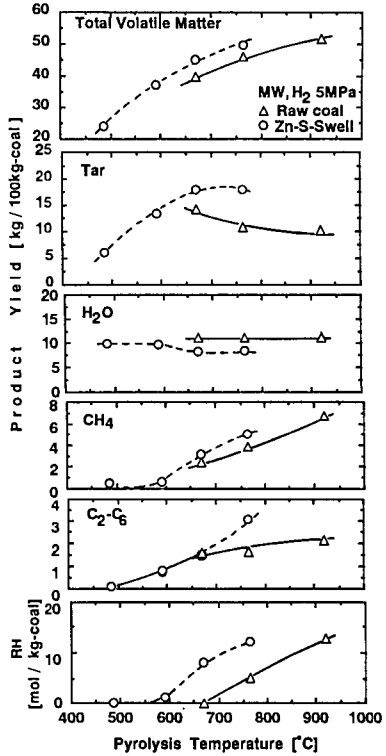

Figure 5 Comparison of the product yields between the raw coal and the Zn-S-Swell at different pyrolysis temperatures

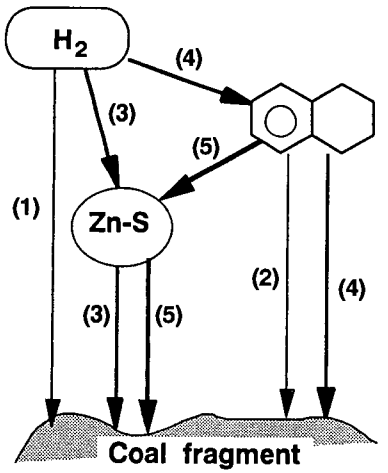

Contribution to increase the coal conv. and liquid yield

(5) > (4) > (3) > (2) ≈(1)

Figure 6 Possible hydrogen radical transfer paths during the flash pyrolysis

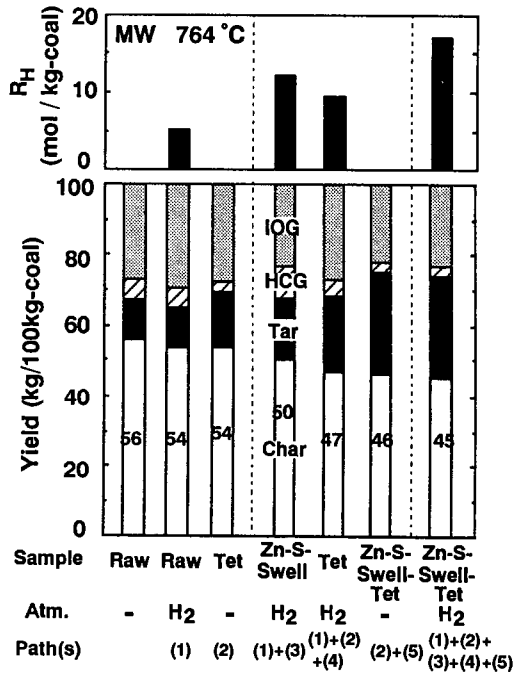

Figure 7 The product yields and the amount of hydrogen consumed for 7 experiments performed for examining relative importance of the gaseous hydrogen, tetralin and the catalyst

EVIDENCE FOR MACERAL SYNERGISM IN CATALYTIC HYDROPYROLYSIS AND HYDROGENATION OF A SUB-BITUMINOUS COAL

Stuart Mitchell[1], Carol McArthur[1], Colin E. Snape[1], Darrell Taulbee[2] and James C. Hower[2]

[1] University of Strathclyde, Dept. of Pure & Applied Chemistry, Glasgow G1 1XL, UK.
[2] University of Kentucky, Centre for Applied Energy Research, 3572 Iron Works Pike, Lexington, KY 40511-8433 ,USA.

Keywords: Maceral concentrates, liquefaction, hydropyrolysis, hydrogenation

ABSTRACT

In order to investigate the possible synergistic effect of exinite on vitrinite conversion in both hydropyrolysis and batchwise (solvent-free) hydrogenation, experiments with and without a sulphided molybdenum catalyst have been conducted on maceral concentrates separated by density gradient centrifugation (DGC) from an Indonesian sub-bituminous coal. As anticipated, the conversions achieved with virtually pure exinite in both catalytic hydropyrolysis (520°C, 150 bar) and hydrogenation (400°C, 70 bar) are close to 100% daf coal. Without catalyst, there is no evidence of synergism in hydropyrolysis. However, with catalyst, the conversions achieved in both regimes with the fractions and blends containing between 25 and 50% exinite are higher than the predicted values (both pyridine and dichloromethane-solubles in hydrogenation).

INTRODUCTION

Although it is now generally recognised that oil yields broadly increase with decreasing rank especially when retrogressive reactions for low-rank coals are avoided by having good contact between coal and solvent [1,2], these ideal circumstances are not realised under other conversion regimes. For example, in hydropyrolysis where there is no vehicle solvent to aid conversion, dispersed catalysts are much less effective for lignites and sub-bituminous coals [3] than for bituminous coals. In such instances, hydrogen transfer within the coal is going to be the crucial factor and, intuitively, this is going to be aided by having a high degree of fluidity and sufficient hydrogen-rich exinite. Indeed, it has been recognised that synergistic effects involving macerals may be evident in coal liquefaction and this has prompted a number of studies on maceral concentrates [4-6]. Care is required in interpreting results since fine grinding normally required to prepare high purity maceral concentrates may induce oxidation. Nonetheless, as anticipated, conversions for exinite concentrates are generally much higher than those for vitrinite [4-6], but appreciable conversions to pyridine and THF-soluble material have been found for inertinite fractions, especially those rich in semi-fusinite [4,5]. Further, conversions for whole coals have been found to be higher than those predicted from individual maceral yields suggesting that synergism occurs from the maceral associations within the coals [4,5]. Indeed, the liquefaction residue from the vitrinite of one of these coals comprised mainly vitroplast which was not evident for the whole coal [4].

Although the above evidence strongly suggests that synergism between macerals can occur at a microscopic scale within coals, there is little information thus far on the influence of liquefaction conditions on the extent to which this phenomenon occurs. However, hydropyrolysis tests on handpicked durain and fusain samples from a UK bituminous coal have indicated that exinite only promotes vitrinite conversion in the presence of catalyst [3]. In order to investigate this aspect further in both hydropyrolysis and batchwise (solvent-free) hydrogenation, experiments with and without a sulphided molybdenum (Mo) catalyst have been conducted on maceral concentrates separated by density gradient centrifugation (DGC) from an Eocene sub-bituminous coal from Indonesia. This coal has a high exinite and low inertinite content which facilitated the separation of relatively pure exinite and vitrinite fractions with + 400 mesh particles size required for hydropyrolysis to prevent the fixed-bed reactor plugging.

EXPERIMENTAL

The Indonesian sub-bituminous coal was obtained from the US Geological Survey. The coal was crushed to -100 mesh, demineralised with hydrofluoric and boric acids [7] and dry screened to + 400 mesh. Maceral separation was based on the density gradient centrifugation (DGC) method developed by Dyrkacz and co-workers [8] with certain modifications [7]. Briefly, the DGC separation involves forming forming a cesium chloride density gradient within a spinning, high capacity (2 dm^3) centrifuge rotor. A demineralised coal/surfactant slurry is then dispersed across this gradient at forces ranging from 7,000 to 25,000 gravity. The procedure can be repeated numerous times with the corresponding fractions from repeat runs being combined to provide sufficient sample. In this study, two preliminary DGC runs were carried out on 16.2 g of sample. This provided a density profile curve to design a more efficient larger scale separation which was conducted on 225.1 g of coal in a series of 15 DGC runs, the recovery being 98.5%. The rotor effluent was divided into 12 density fractions plus the remaining sink fraction. The results of chemical and petrographic analysis on the initial coal and the fractions actually used in the hydropyrolysis and hydrogenation experiments are listed in Table 1.

For the hydrogenation and hydropyrolysis experiments with the sulphided Mo catalyst, the maceral concentrates and their blends were impregnated with ammonium dioxydithiomolybdate in methanol solution to give a Mo loading of 1%. The fixed-bed hydropyrolysis apparatus in which the reactor tube is heated resistively has been described previously [3,9]. A temperature of 520°C and a pressure of 150 bar were chosen as the standard test conditions to optimise both the tar yield and selectivity (% tar/% gas) in catalytic hydropyrolysis [3,9]. To simplify the mass balances, dried coals were used (50°C *in vacuo* for 1 hr.). Tests were carried out on 2-5 g of sample which was mixed with of sand (1:2 mass ratio) to prevent blockages and to enable the reactor tube to be emptied easily. The reactor were heated at 5°C s^{-1} and held at 520°C for 10 minutes with a hydrogen flow rate of 10 dm^3 min^{-1} (measured at atmospheric pressure and ambient temperature) which was sufficient to overcome mass transfer. Char yields were determined from the weight loss of the reactor tube and tar yields from the weight gain of the dry-ice cooled trap. Tar was recovered for analysis by washing the trap thoroughly with dichloromethane (DCM).

The hydrogenation experiments were carried out in a 9/16" O.D. microautoclaves (*ca* 10 cm^3 internal volume) constructed of Autoclave Engineer high pressure fittings. 0.3 g of sample was loaded into the microautoclave which was pressurised to 70 bar with hydrogen. The sandbath at 400°C was raised to fully submerge the microautoclave for 60 min., the heat-up period being *ca* 5

min. After reaction, the microreactor was cooled in dry-ice before de-pressurising. The reactor contents were then recovered by filling the microreactor with dichloromethane (DCM) and placing it in an ultrasonic bath. The DCM washings were refluxed for *ca* 5 hours, filtered through phase separating paper and then the DCM-solubles were recovered by evaporating the filtrate to dryness. The DCM-insolubles were weighed after drying *in vacuo* and were then refluxed in pyridine for *ca* 5 hours and filtered to determine the yield of pyridine-insolubles.

RESULTS AND DISCUSSION

Hydropyrolysis

Figure 1 shows the effect of exinite concentration on conversion in hydropyrolysis with and without catalyst for the maceral concentrates and one of their blends. As anticipated, the conversion achieved with virtually pure exinite (fraction 1) in catalytic hydropyrolysis is close to 100% daf coal. Without catalyst, there is no evidence of synergism with the conversions lying close to the predicted values from those obtained with virtually pure exinite and the concentrates containing 90% vitrinite (fractions 5 and 6, Figure 1). However, with catalyst, the conversions achieved with the fractions containing between 25 and 50% exinite generally appear to be higher than the predicted values; above 50% exinite, the experimental error of ± 1-2% is greater than the differences anticipated making synergistic effects more difficult to identify. Since the two fractions, 5 and 6 which both contain *ca* 90% vitrinite give conversions differing by 5 % daf coal, it is difficult to deduce a baseline conversion for vitrinite. Further, synergism may be evident within these fractions as they contain 10% exinite (Table 1). However, the fact that the conversion with catalyst for the 50:50 blend of fractions 1 and 6 is higher by 5% daf coal than that predicted from the individual conversions confirms that the effect is real.

Hydrogenation

Figure 2 presents the yields of DCM-soluble product and pyridine-insolubles obtained in catalytic hydrogenation using essentially the same fractions and, again, there is clear evidence of synergism. The fact that it is evident in both the yields of DCM-soluble oil and pyridine-insolubles indicates that both the inital dissolution process and subsequent hydrocracking of the primary dissolution product are affected. Indeed, the synergistic effect is somewhat more pronouced than in catalytic hydropyrolysis possibly due to the longer residence time and the more effective contact between exinite and vitrinite in catalytic hydrogenation.

General discussion

The synergistic effects reported here are perhaps more evident than in hydroliquefaction where the presence of a vehicle solvent aids hydrogen transfer. Clearly, in both batchwise hydrogenation and hydropyrolysis, the exinite plays a crucial role in transferring hydrogen atoms from the catalyst sites to the depolymerising coal probably because it forms a fluid pyrobitumen in the early stages of conversion. For hydropyrolysis, the general trends found here are the same as those reported previously for a UK bituminous coal containing 87% dmmf C [3]. However, the reasons why lower conversions than anticipated are obtained in catalytic hydropyrolysis for the higher rank bituminous coals and most of the low-rank coals investigated thus far [3] are somewhat different. The low-rank coals do not soften to an appreciable extent and there is probably insufficient pyrobitumen generated in the early stages of conversion to prevent retrogressive reactions occurring which probably involve dihydric phenolic moieties. For the bituminous coals containing more than *ca* 84% dmmf C, the hydrogen requirement required for hydrogenating the aromatic structures is likely to be higher than for their lower rank counterparts and, despite the development

of plasticity at some stage during conversion, there is still insufficient hydrogen transfer capability to prevent retrogressive condensation reactions occurring.

ACKNOWLEDGEMENTS

The authors thank the European Community (Contract No. EN3V-0048-UK(H)), the US Department of Energy and Commonwealth of Kentucky for financial support.

REFERENCES

1. C.E. Snape, *Fuel Process. Technol.*, **15**, 257.(1987).
2. R.M. Baldwin, *Prepr. Am. Chem. Soc. Div. Fuel Chem.*, **34(3)**, 787.(1989).
3. C.E. Snape and C.J. Lafferty, *Prepr. Am. Chem. Soc. Div. Fuel Chem.*, **35(1)**, 1 (1990).
4. R.A. Keogh, B. Chawla, D. Taulbee and B.H. Davis, *Proc. 1989 Int. Conf. on Coal Sci.*, 683.
5. S. Parkash, K. Lali, M. Holuszko and M.P. Du Plessis, *Liquid Fuels Technol.*, **3(3)**, 345 (1985).
6. J. Pajek, *Fuel Process. Technol.*, **21**, 245 (1989).
7. D.N. Taulbee, S.H. Poe, T.L. Robl and B. Keogh, *Energy & Fuels*, **3(6)**, 662 (1989).
8. G.R. Dyrkacz and E.P. Horwitz, *Fuel*, **61**, 3 (1982).
9. C.E. Snape, C.J. Lafferty, S. Mitchell, F. Donald, C. A. McArthur, G. Eglinton, N. Robinson and R. Collier, *Final Report, EC Project EN3V-0048-UK(H)* (1991).

Table 1 Elemental, proximate and petrographic analysis of maceral concentrates

			Maceral fraction					
		Parent coal	1	2	3	4	5	6
Density range, g cm^{-3}			1.12-1.15	1.15-1.18	1.20-1.25	1.25-1.26	1.26-1.27	1.27-1.28
% moisture		1.5	0.6	0.9	1.5	1.8	2.3	1.9
% ash, dry basis		0.4	1.4	1.2	0.7	1.0	0.6	1.3
% V.M., daf basis		58.9	67.0	65.0	55.9	51.0	49.6	48.3
% dmmf	C	79.2	80.1	80.2	78.5	77.0	76.5	76.6
	H	7.2	8.2	7.9	6.8	6.4	6.1	6.0
	N	0.6	0.6	0.9	0.6	0.7	0.7	0.7
% dmmf	Exinite	39.8	97.8	95.2	52.6	22.4	10.0	9.8
	Vitrinite	54.4	1.8	3.4	46.8	77.2	89.4	89.0
	Inertinite	5.6	0.4	1.2	0.6	0.4	0.6	1.2

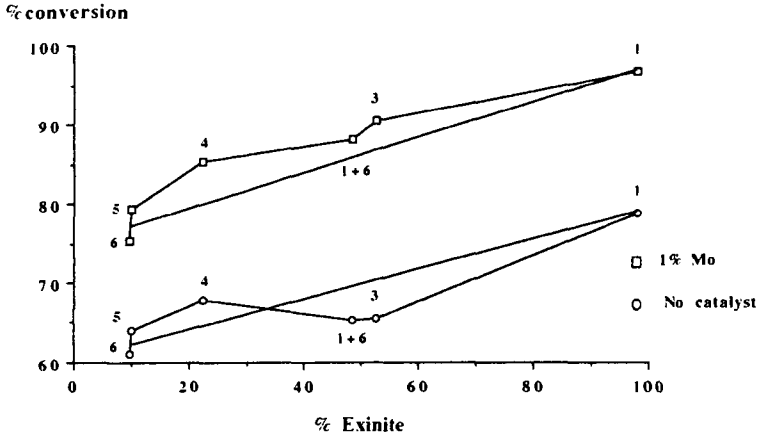

Figure 1. Effect of exinite concentration on hydropyrolysis conversions using maceral concentrates

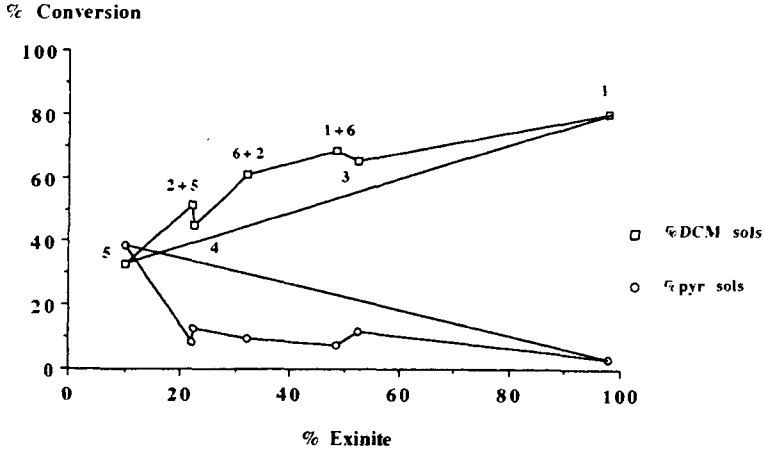

Figure 2. Effect of exinite on catalytic hydrogenation yields using maceral concentrates

EVALUATION OF FACTORS INFLUENCING THE THERMAL MATURATION OF ORGANIC MATTER DURING CONFINED PYROLYSIS EXPERIMENTS.

Raymond MICHELS, Patrick LANDAIS,
Marcel ELIE, Laurence GERARD and Laurence MANSUY.

CNRS-CREGU - BP 23, 54501 Vandoeuvre Cedex. FRANCE.

Key Words : Pyrolysis, Water, Pressure

INTRODUCTION

Pyrolysis of organic matter can be dedicated either to investigate its chemical structure or to mimic the transformations induced by subsidence in sedimentary basins i.e. thermal maturation. Reproducing natural geological conditions has been for a long time strictly considered as a matter of time and temperature. More recently, the roles of water, pressure, mineral content and type of autoclave have been investigated. However, few studies offered the opportunity to adjust and control these different parameters in order to evaluate their respective influence on the thermal maturation of kerogens and source-rocks. The present paper summarizes the results of confined and hydrous pyrolysis experiments dedicated to re-evaluate the validity of the technique and determine the influence of the experimental conditions.

EXPERIMENTAL

Confined Pyrolysis : 200 mg of kerogen or 1-1.5 g of source-rock are introduced in gold tubes (ø = 0.5 or 1 cm; L = 5 cm) under argon atmosphere. The sealed gold tubes are placed in stainless steel autoclaves and isothermally heated at temperatures ranging between 250 and 400 °C for 72 hours under pressures ranging between 300 and 1300 bars (1). At the end of each run, gold tubes are pierced and their organic content washed and extracted with chloroform.

Hydrous Pyrolysis : about 400 mg of rock are isothermally heated for 72 hours in a stainless steel autoclave in the presence of an excess of liquid water. The rock sample is covered by pure liquid water and the headspace is filled with helium (2). The pressure inside the autoclave is due to the expansion of water and to the generation of oil and gas but rarely exceeds 330 bars. The theoretical maximum pyrolysis temperature is limited by the supercritical temperature of pure water (374 °C) and generally set to 350 °C because of the generation of CO_2 and hydrocarbons. At the end of each run, the autoclave is cooled, gases are collected, floating oil (expelled oil) recovered and rock chips collected for subsequent extraction.

High Pressure Hydrous Pyrolysis : Because in conventional hydrous pyrolysis devices, internal pressure depends on the initial filling of the autoclave (water + rock) and on the temperature, high pressure hydrous pyrolysis runs were performed in order to test the effect of increasing pressures on the hydrocarbons expulsion and generation. The use of a high pressure system (pump + autoclave) allows water to be injected inside the autoclave as soon as the isothermal stage is reached and to adjust the pressure to the desired value (300, 700 and 1300 bars in the present work). The recovery of oil and gas is similar to that described for conventional hydrous pyrolysis.

TEMPERATURE CHOICE

Most of the artificial maturation series are generated using temperature steps of 30 to 50 °C. Nevertheless, in order to describe the complete thermal evolution of an immature organic matter, it can be necessary to perform more pyrolysis runs (3). For example, the different maturation stages of a Mahakam coal were fully evidenced only when using a 10 °C pyrolysis step. The maximum generation of polar compounds, aromatics and saturates occuring at 320, 330 and 340 °C respectively. Similarly, this was the only way to define the chronology of the transformations affecting both the solid residue and the soluble fraction.

CHOICE OF THE TIME-TEMPERATURE PAIR

In order to compensate geological times, pyrolysis experiments use higher temperatures than those noticed in natural environments. Several hours to several years experimentations have been carried out and generally show that long term experiments improve the quality of the simulation. On the other hand, comparison of the analytical data derived from 5 hours to 100 days experiments on an immature Mahakam coal has evidenced the influence of time-temperature pairs on the composition of both solid residues and $CHCl_3$ extracts. It is shown that saturates content increases with experimentation time (4). As far as $CHCl_3$ extract / TOC ratios are similar for a given Time Temperature Index (Arrhenius TTI), such evolution evidences the increasing effect of secondary cracking in long term experiments. Furthermore, the expulsion of oil from source-rock is enhanced in long term experiments (Paris Basin shale).

KEROGEN vs. WHOLE ROCK

Heating experiments can be performed either on whole rock or on kerogen concentrates. While kerogen pyrolysis allows more structural parameters to be investigated and catalytic effects to be ignored, whole rock pyrolysis takes into account the transformation of all the rock components

(organic + mineral) (5, 6). However, kinetics of clay minerals transformations cannot generally be extrapolated to temperatures higher than 300 °C and organo-mineral interactions are not easily duplicated. Then, the extent of the modifications of the maturation process related to the behaviour of the mineral matrix cannot be accurately determined. Results from confined-pyrolysis experiments on the Woodford shale have shown that the peak generation of hydrocarbons as well as the onset of the petroleum potential decrease always occur earlier for kerogen than for whole rock (Figure 1).

EFFECTS OF PRESSURE

The role of pressure in the simulation of organic matter thermal maturation has not been widely investigated. However, recent results have demonstrated that the rates of hydrocarbon cracking (7) as well as the activation energy (8) were pressure dependant. It is generally accepted that increasing pressures induce a delay in oil genesis and in kerogen transformation (9). In the present work the role of pressure has been studied in both confined and hydrous pyrolysis systems.

The effects of pressure on isolated kerogen or coal transformation are minor and necessitate a careful control of temperature (± 1°C) to be shown. No clear variations in the extract yield or in the Rock-Eval HI and Tmax have been noticed. However, a bimodal distribution of n-alcanes has been observed on GC traces for low pressure experiments (300 bars) on a type II kerogen. Furthermore the pristane/phytane ratios are systematically lower in high pressure experiments (1300 bars) whereas the evolutions of the Pr/nC17 and Ph/nC18 ratios are not pressure dependant. Similar results have been obtained when increasing the dead volume in gold tubes by decreasing the amount of kerogen (Mahakam coal) to be pyrolyzed from 200 mg to 50 mg. Spectroscopic studies of total extracts (^{1}H NMR, ^{13}C NMR, IR and synchronous UV fluorescence) also allowed pressure-dependant structural parameters to be recognized.

High pressure hydrous pyrolysis experiments on whole rock (Woodford shale) revealed that amounts of expelled oil and total yield (expelled + extracted) were highly dependant on pressure. Figure 2 confirms that high water pressure delays and hinders the genesis and expulsion of hydrocarbons. On the other hand, results from confined pyrolysis did not reveal an important control of pressure neither on the genesis nor on the expulsion of oil. The total yields maxima are similar but can be shifted of 50 °C (Figure 3) while expulsion maxima occur at the same temperature (330°C).

EFFECT OF WATER

The effect of water on the artificial maturation of organic matter is still a subject of controversy. Addition of water in confined experiments on Mahakam coals did not seem to give detectable effects (10). On the other hand, the role of water during organic compounds pyrolysis has been frequently emphasized (11).

Such situation can probably be related to the unavailability of analytical data derived from hydrous and confined pyrolysis experiments performed on the same rock and in the same P-T-t conditions. Furthermore the analytical procedures for oil and gas recovery as well as shale extraction cannot be identical for both types of pyrolysis. For example, the "expelled fractions" corresponding to floating oil and to cold chloroform washing in hydrous and confined pyrolysis respectively cannot be simply compared.

As far as pressure can be controled, experiments conducted in a high pressure hydrous pyrolysis system can be compared to those performed in confined pyrolysis. On Figure 4 are reported the expelled/washed as well as extracted fractions obtained on hydrous and confined Woodford shale pyrolyzates at 700 bars. Despite some discrepancies concerning the maximum temperature for extract yield, a general agreement can be noticed in the trends as well as in the amounts of generated and expelled hydrocarbons. Similarly, the addition of water in gold tubes (10, 50 and 100 wt % of shale) did not significantly modify the oil expulsion rate. However, when hydrous pyrolysis experiments are carried out in low pressure conditions (P<200 bars), the total oil yield is much more important than in confined and high pressure hydrous pyrolysis systems (see Figure 2, open circles).

SUMMARY

The examination of various sets of data deduced from organic matter pyrolysis in closed systems (confined and hydrous) revealed that experimental conditions must be carefully defined:

- A wide range of temperatures can be useful in order to determine the various stages of hydrocarbons generation and kerogen transformations.
- Long term experiments induce secondary cracking reactions that chiefly affect polar compounds.
- Pressure effects on oil generation and expulsion in confined pyrolysis system are not as determinative as in hydrous pyrolysis. However, variations of external pressure as well as effluents pressure can significantly modify the distribution of the generated hydrocarbons.
- In order to evaluate the role of water in organic matter maturation, hydrous and anhydrous pyrolysis must be conducted in the same experimental conditions (temperature, pressure, time).
- When performed in the same T-P-t conditions, confined and high pressure hydrous pyrolysis can generate and expell similar amonts of hydrocarbons.

These observations strongly suggest to take into account other experimental parameters than time and temperature when simulating organic matter thermal maturation. They also support further work on the comparison of the different pressurized pyrolysis systems used to reproduce the natural transformations of organic matter.

Anowledgements

The present work has benefited from the financial and technical supports of the Oklahoma University (USA), AMOCO (USA), CNRS (France) and DBT program 91/ATP/645.

REFERENCES

1. Landais P., Michels R., Poty B. and Monthioux M. J. Anal. Appl. Pyrol., 16, 1989, pp 103-115.
2. Lewan M.D., Winters J.C. and MCDonald J.H. Science, 203, 1979, pp 897-899.
3. Wenger L.M. and Price L.C. In "Organic geochemistry, advances and applications in the natural environment", 1991, D.A.C. Manning ed., Manchester University Press, pp 335-339.
4. Landais P. Org. Geochem., 17, 1991, pp 705-710.
5. Horsfield B. and Douglas A.G. Geochim. Cosmochim. Acta, 44, 1980, pp 1119-1131.
6. Huizinga B.J., Tannenbaum E. and Kaplan I.R. Org. Geochem., 50, 1987, pp 591-604.
7. Dominé F., Maquaire P., Muller C. and Côme G. Energy and Fuels, 4, pp 2-10.
8. Carr A.D. In "Organic geochemistry, advances and applications in the natural environment", 1991, D.A.C. Manning ed., Manchester University Press, pp 285-287.
9. McTavish R.A. Nature, 271, 1978, pp 648-650.
10. Monthioux M., Landais P. and Durand B. Org. Geochem., 10, 1985, pp 299-311.
11. Siskin M. and Katritzky A.R. Science, 254, 1991, pp 231-237.

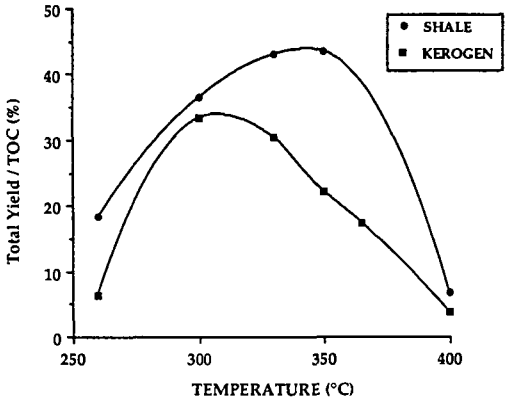

Figure 1: Comparison of the total yield evolution during the confined pyrolysis of type II shale and extracted kerogen

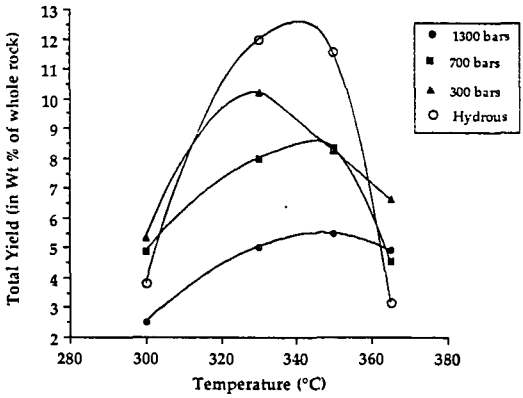

Figure 2: Effect of pressure on oil generation during hydrous and high pressure hydrous pyrolysis of a Woodford shale.

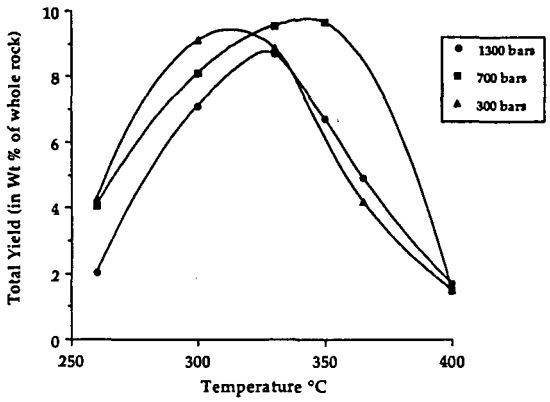

Figure 3 : Effect of pressure on the generation of hydrocarbons during the confined pyrolysis of a Woodford shale.

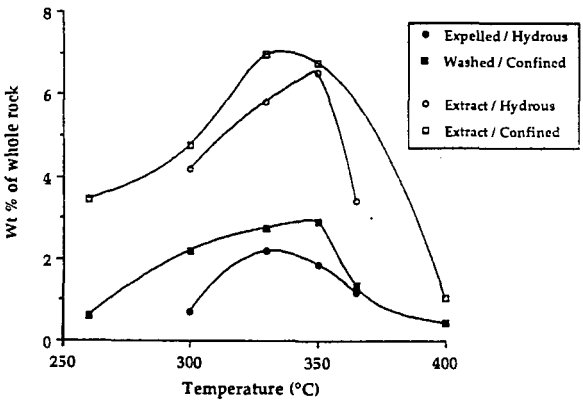

Figure 4: Comparison of the evolution of generated and expelled fractions during the high pressure hydrous and confined pyrolysis at 700 bars.

ARTIFICIAL MATURATION OF COAL AND MACERAL CONCENTRATES: SATURATE AND POLYAROMATIC MOLECULAR MARKERS

Michael A. Kruge[1] and Patrick Landais[2]

[1]Department of Geology, Southern Illinois University, Carbondale, IL 62901, USA
[2]GS CNRS-CREGU, BP 23, 54501 Vandoeuvre-lès-Nancy cedex, France

Keywords: Coal macerals, pyrolysis, polyaromatic hydrocarbons

ABSTRACT

A sample from the "Simon" coal bed (Lorraine Basin, France) was separated into its constituent macerals vitrinite, exinite and inertinite by density gradient centrifugation. Aliquots of the macerals and whole coal were sealed in gold tubes with no added water and pyrolyzed separately at 350, 375, 400 and 450 °C for 24 hr at 100 MPa. The distributions of *n*-alkanes in the pyrolyzates are profoundly affected by pyrolysis temperature and sample type, but hopane and sterane distributions show little variation. The classic maturity parameters based on sterane isomerization are particularly ineffective. In contrast, distributions of polyaromatic hydrocarbons (PAH) change dramatically as a function of pyrolysis temperature. A variety of maturity-sensitive ratios are shown to be efficacious, including those employing dimethylphenanthrenes and methylpyrenes. These PAH ratios work particularly well for vitrinite pyrolyzates. For exinite pyrolyzates, the PAH ratios consistently show little change between 350 and 375°, but by 400° the ratios operate effectively.

INTRODUCTION

Slow, confined pyrolysis is often called upon for laboratory simulation of the thermal maturation of organic matter. The chief variables in confined pyrolysis experiments include temperature, duration of heating, the use of isolated kerogen *vs.* a kerogen/mineral mixture (natural or artificial), hydrous *vs.* anhydrous conditions, and the use of metal *vs.* glass reactors[1-7]. Confined pyrolysis provides a better simulation of natural petroleum generation in that its products lack the *n*-alkenes characteristic of open pyrolysis methods. While several studies have used open pyrolysis techniques in the characterization of isolated coal macerals[8-10], the present work is an attempt at confined pyrolysis of macerals, with the objective of observing of the effects of temperature and starting material type on distributions of saturate and, especially, aromatic hydrocarbons.

METHODS

The sample employed in the study is from the "Simon" coal bed (Lorraine Basin, France), petrographically determined to be 74% vitrinite, 13.2% inertinite, 5.5% exinite and 7.3% mineral matter[11]. Maceral separation by density gradient centrifugation[12] was performed on hand-picked lithotype concentrates. The resulting isolated macerals were vitrinite, inertinite (predominantly semifusinite and fusinite), and exinite (mainly sporinite and resinite). The pyrolytic and liquid chromatographic techniques used in this study have been previously described[11,13]. In brief, isothermal confined pyrolysis experiments in sealed, thin-walled gold tubes were run on 150 mg aliquots of the raw coal and of each of the three isolated macerals at temperatures of 350, 375, 400 and 450 °C for 24 hours at 100 MPa. The saturate and aromatic fractions of the pyrolyzates were analyzed by a Hewlett Packard 5890A gas chromatograph, coupled to an HP 5970B Mass Selective Detector (GCMS). The GC was held

initially at 100° C for 10 min., then raised to 300° at 3°/min., where it was held for 21 min. (saturates) or 5 minutes (aromatics). A 25 m OV-1 column with 0.2 mm inside diameter and 0.33 μm film thickness was employed. The mass spectrometer, using an ionization energy of 70 eV, was run in selective ion monitoring mode, collecting data on the principal fragment ions of biological marker compounds and on the molecular ions of the polyaromatic compounds.

RESULTS AND DISCUSSION

The normal alkane distributions vary considerably as a function of starting material and pyrolysis temperature. The 350° pyrolyzate of the whole coal shows a broad maximum in the C_{22} to C_{27} region, with a slight odd carbon number preference. There is a increasingly severe depletion of higher molecular weight *n*-alkanes as one progresses to the 375° and on to the 400° runs. The *n*-alkane concentrations in the 450° pyrolyzate are extremely low. The exinite *n*-alkane distributions for both the 350 and 375° runs are essentially the same and are very similar to the 350° whole coal run, except that they lack the odd carbon number preference. By 400° however, the exinite pyrolyzate shows a marked shift towards lower carbon numbers, roughly comparable to the 375° coal. Normal alkane distributions in the 350 and 375° vitrinites are also very similar to one another, having a maximum at C_{19}. They bear a strong resemblance to the 375° coal. By 400°, the overall concentration of *n*-alkanes decreases. The *n*-alkane distributions in the 350 and 375° inertinite pyrolyzates are very similar to one another, with a maximum at C_{21} and a slight odd carbon predominance. When compared to other samples, they most closely resemble the 400° vitrinite. The high temperature destruction of *n*-alkanes sets in at 400° for the inertinite. The yields of the 450° inertinite experiment were too low for analysis. Overall, there is a loss of higher molecular weight *n*-alkanes as pyrolysis temperatures increase. As higher temperatures (≥ 400°) are reached, general destruction of *n*-alkanes occurs. 400° exinite resembles 375° coal and vitrinite. In turn, 400° vitrinite bears similarities to 350 and 375° inertinites. Thus, those samples richer in pyrolyzable and extractable organic matter lag behind the leaner in thermal alteration effects.

The hopane distributions show little variation among the samples, either as a function of temperature or starting material type. Lack of difference in hopane distributions in pyrolyzates of the macerals from a single coal is expected, because their bacterial precursors would have inhabited all macerals in the freshly deposited peat[14]. The steranes are a relatively minor component of the pyrolyzate saturate fractions. The sterane distributions within one sample vary even less than those of the hopanes as a function of organic matter type and level of thermal alteration. Consequently, the standard sterane maturation parameters[15] are ineffective, with the partial exception of the C_{29} ($\alpha\beta\beta/(\alpha\alpha\alpha + \alpha\beta\beta)$) ratio for exinite.

A wide variety of polyaromatic molecular marker compounds are readily detectable in the aromatic fractions of the pyrolyzates, by setting the GCMS to monitor their molecular ions, which are often the strongest peaks in their mass spectra. These compounds include homologues and isomers of naphthalene, phenanthrene, dibenzothiophene, pyrene, fluoranthene and chrysene, as well as several pentaaromatic hydrocarbons. The distributions of these compounds exhibit profound changes due to thermal alteration. Aromatic steroids are among the most frequently employed aromatic molecular markers[16]. However, in this study they are not discussed, as C_{26}-C_{28} triaromatic steroids were detected in only 4 samples and monoaromatics were not detected at all. For the sake of brevity, only two groups of compounds are covered in this paper — the dimethylphenanthrenes and methylpyrenes, along with their isomers. A fuller discussion will be presented elsewhere[17].

Figure 1a presents an example of a partial m/z 206 mass chromatogram showing the distribution of dimethylphenanthrenes, ethylphenanthrenes and dimethylanthracenes, identified and, for simplicity, labelled as peaks 206a through 206j. In figure 1b, the quantitation results from the m/z 206 data for each of the vitrinite and exinite experiments are presented.

Excluding the ethylphenanthrene and dimethylanthracene peaks 206a, b and e, it can be seen that dimethylphenanthrene peaks 206c and d increase with pyrolysis temperature, while peaks 206f, g, h and i decrease. This phenomenon is shown in ratio form (fig. 1c), in which the ratio increases smoothly with temperature for vitrinite. There is little increase in the exinite ratio between 350 and 375°, but by 400°, the exinite value has nearly overtaken the vitrinite. The exinite ratio shows little further increase at 450°. The behavior of this ratio is in strong contrast to the commonly employed methylphenanthrene index[18], which increases from 350 to 400° for these samples, but drops sharply by 450°. Similar dimethylphenanthrene ratios have previously been employed[19,20].

The data from the m/z 216 partial mass chromatograms, showing distributions of methylpyrenes and methylfluoranthenes, are presented in figure 2 in a fashion analogous to that of figure 1, except that specific isomer assignments were not possible, due to the lack of standards and published identifications. Peak 216b increases with pyrolysis temperature, while peaks 216e and f decrease markedly. The resulting ratio (fig. 2c) increases nicely for vitrinite over the entire 350 to 450° temperature range. In contrast, the increase in the exinite ratio is delayed until temperatures climb above 375°, giving a curve very similar to the dimethylphenanthrene ratio (fig. 1c). Methylpyrenes have been previously used as thermal alteration indicators, but employing Shpol'skii spectral data, rather than GCMS[21].

Among the differences between vitrinite and exinite, the most profound is the delay in maturation response of the exinite between 350 and 375°, corresponding to the temperatures at which it is generating the most pyrolyzate[11]. This phenomenon is consistently detected by both Rock Eval and molecular parameters. The recognition of maturity-independent molecular characteristics is also desirable, but difficult in this case, since the range of thermal alteration levels is so great, and the effects of temperature so all-pervasive. However, some success may be expected in differentiating exinite and vitrinite, since their macromolecular structures are so dissimilar. Very little difference is apparent among saturate biomarkers, either due to maturity or organic matter type. For polyaromatic compounds, subtle features which differentiate the vitrinite and exinite pyrolyzates are worthy of note. Peak 206h (1,7-dimethylphenanthrene, also known as pimanthrene) appears relatively stronger in exinite than in vitrinite (fig. 1b). Among methylpyrenes and methylfluoranthenes, peak 216c is also stronger in exinite than in vitrinite pyrolyzates (fig. 2b). Peaks 206h and 216c are minor features on their respective mass chromatograms and the differences tend to be lost by 450°. It would be of interest to examine a greater variety of maceral types from other coals and kerogens by the same methods, to determine if PAH distributions have greater potential for organic matter type differentiation than is apparent in this study.

CONCLUSIONS

1) The distributions of *n*-alkanes in the pyrolyzates are profoundly affected by pyrolysis temperature and sample type, but hopane and sterane distributions show little variation. The classic maturity parameters based on sterane isomerization are particularly ineffective.
2) Distributions of polyaromatic hydrocarbons change dramatically as a function of pyrolysis temperature. A variety of maturity-sensitive ratios are shown to be efficacious, including those employing dimethylphenanthrenes and methylpyrenes.
3) The aromatic ratios work particularly well for vitrinite pyrolyzates. For exinite pyrolyzates, these ratios consistently show little change between 350 and 375°, but by 400° the ratios operate effectively. For exinite, 350-375° is also the temperature range in which maximum generation of pyrolyzate occurs.
4) Vitrinite and exinite may be distinguished by subtle, temperature-independent features among the aromatic data.

REFERENCES

1. Comet P. A., McEvoy J., Giger W. and Douglas A.G., *Org. Geochem.* **9**, 171-182 (1986).
2. Rohrback B.G., Peters K.E. and Kaplan I.R., *AAPG Bull.* **68**, 961-970 (1984).
3. Lewan M.D., Winters J.C. and McDonald J.H., *Science* **203**, 897-899 (1979).
4. Lewan M.D., *Phil. Trans. R. Soc. Lond.* A **315**, 123-134 (1985).
5. Lewan M.D., Bjøroy M. and Dolcater D.L., *Geochim. Cosmochim. Acta* **50**, 1977-1987 (1986).
6. Tannenbaum E., Ruth E. and Kaplan I.R., *Geochim. Cosmochim. Acta* **50**, 805-812 (1986).
7. Saxby J.D., Bennett A.J.R., Corcoran J.F., Lambert D.E. and Riley K.W., *Org. Geochem.* **9**, 69-81 (1986).
8. Nip M., de Leeuw J.W. and Schenk P.A., *Geochim. Cosmochim. Acta* **52**, 637-648 (1988).
9. Nip M., de Leeuw J.W., Schenk P.A., Windig W., Meuzelaar H.L.C. and Crelling J.C., *Geochim. Cosmochim. Acta* **53**, 671-683 (1989).
10. Nip M., de Leeuw J.W. and Crelling J.C., *Energy & Fuels* **6**, 125-136 (1992).
11. Landais P., Zaugg P., Monin J.-C., Kister J. and Muller J.-F., *Bull. Soc. géol. France* **162**, 211-217 (1991).
12. Crelling J.C., *Am. Chem. Soc. Div. Fuel Chem. Prepr.* **34** (1), 249-255 (1989).
13. Monthioux M., Landais P. and Monin J.-C., *Org. Geochem.* **8**, 275-292 (1985).
14. Kruge M.A., Crelling J.C., Hippo E.J. and Palmer S.R., *Org. Geochem.* **17**, 193-204 (1991).
15. Mackenzie A.S., Patience R.L., Maxwell J.R., Vandenbroucke M. and Durand B., *Geochim. Cosmochim. Acta* **44**, 1709-1721 (1980).
16. Mackenzie A.S., Disko U. and Rullkötter J., *Org. Geochem.* **5**, 57-63 (1983).
17. Kruge M.A. and Landais P., in prep.
18. Radke M. and Welte D.H., *Adv. in Org. Geochem. 1981*, 504-512 (1983).
19. Radke M., *Advances in Petroleum Chemistry, Vol. 2* (eds. J. Brooks and D.H. Welte), 141-207, Academic Press, London (1987).
20. Garrigues P., Oudin J.L., Parlanti E., Monin J.C., Robcis S. and Bellocq J., *Adv. in Org. Geochem. 1989*, 167-173 (1990).
21. Garrigues P., De Sury R., Angelin M.L., Bellocq J., Oudin J.L. and Ewald M., *Geochim. Cosmochim. Acta* **52**, 375-384 (1988).
22. Budzinski H., Garrigues P., Connan J., Lee M.L., Andersson J. and Bellocq J., *Organic Geochemistry: Advances and Applications in the Natural Environment*, (ed. D.A.C. Manning) Manchester University Press, Manchester, p. 619-623 (1991).

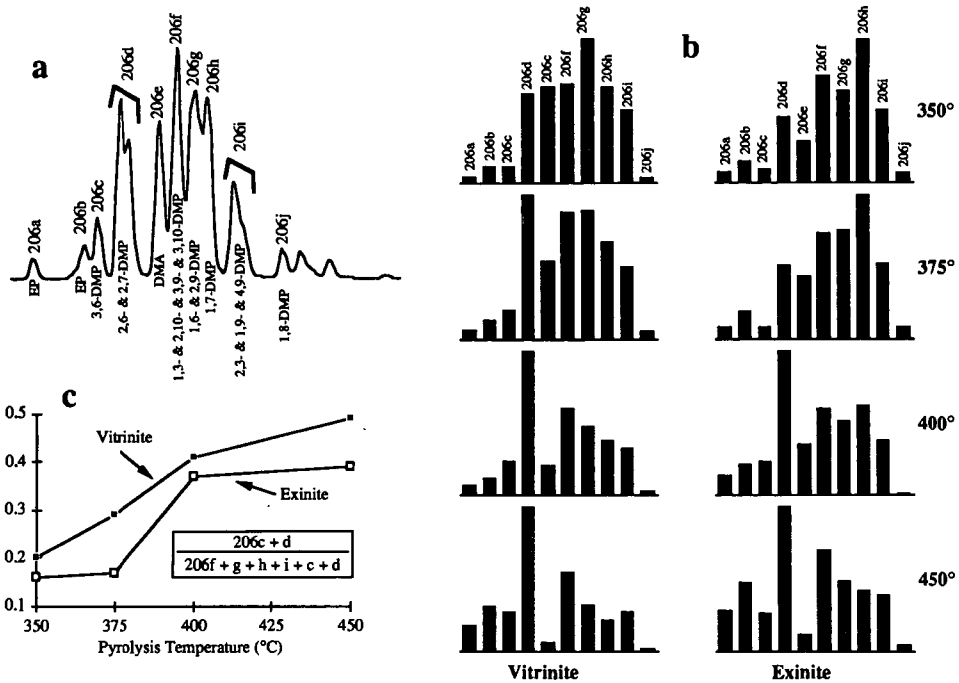

Figure 1 — Data from m/z 206 mass chromatograms of pyrolyzate aromatic fractions. 1a) Example of mass chromatogram (375° vitrinite). DMP peak identifications after Budzinski et al.[22]. EP: ethylphenanthrene, DMA: dimethylanthracene, DMP: dimethylphenanthrene. 1b) Peak distributions as a function of pyrolysis temperature and maceral type. 1c) Dimethylphenanthrene isomer ratio showing effects of thermal alteration.

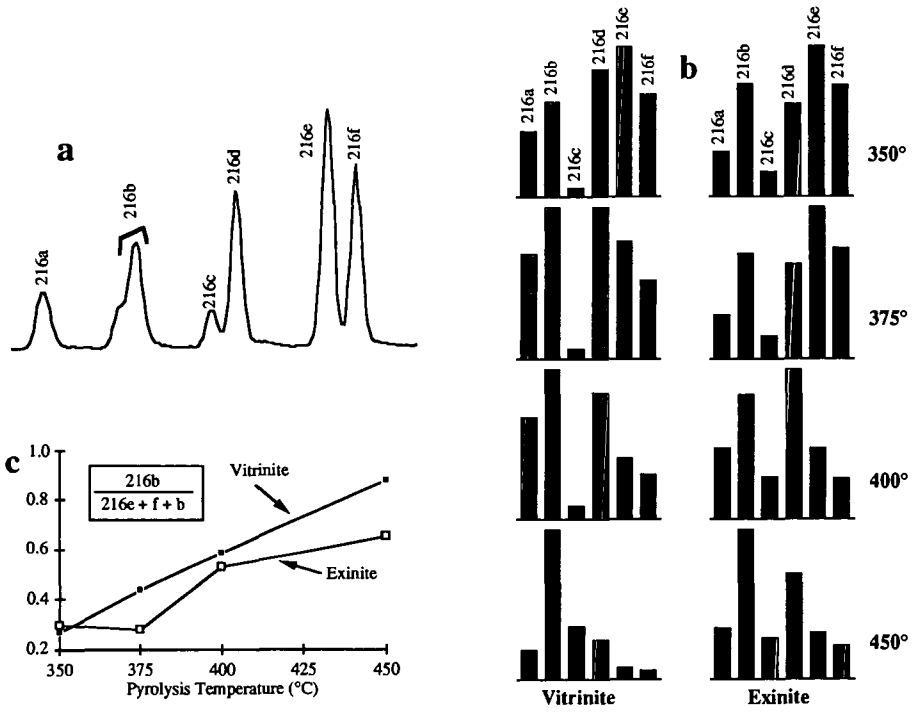

Figure 2 — Data from m/z 216 mass chromatograms of pyrolyzate aromatic fractions. 2a) Example of mass chromatogram (375° exinite), showing methylpyrene and methylfluoranthene isomers. 2b) Peak distributions as a function of pyrolysis temperature and maceral type. 2c) Isomer ratio showing effects of thermal alteration.

A comparison of maturity dependent chemical trends in samples from hydrous pyrolysis and naturally matured samples.

Tanja Barth*, Marit Seim and Kristin Skadsem
Department of Chemistry, University of Bergen
Allegt. 41, N-5007 Bergen, Norway

Keywords: Hydrous pyrolysis, asphaltenes, aromatic fraction

Introduction

Hydrous pyrolysis is the method most often used for simulated maturation of source rocks when the aim is to experimentally reproduce the chemical processes of organic matter maturation and petroleum generation as closely as possible. The procedure has been set up so the laboratory conditions correspond to the natural process within the limitations implicit in short-term experiments that do not require sophisticated equipment (1). However, the high temperature/short time procedure (e.g. 250-365°C for 72 hours) compared to the natural situation (80-120°C over millions of years) involve a risk of changes in reaction mechanisms or a decrease in importance of finely balanced energy relationships. The pyrolysis system has a high level of thermal energy which increases the probability of kinetic control of product composition, while thermodynamic control is more probable in the slow processes of the natural low-energy reaction systems.

A major part of petroleum generation consists of the irreversible breaking of carbon-carbon bonds during thermal decomposition of organic matter. Reproducing such processes at increased temperatures and short times should be possible with a reasonable correspondence to the naturally occurring chemical reactions. However, the detailed composition of the products, e.g. isomer composition, homolog distribution etc., should be more liable to be dependent on the reaction rates and temperature levels. Since hydrous pyrolysis is used as a method for chemical reproduction of the natural processes it is important to establish to what compositional levels the simulation is accurate. The molecular maturity markers are good test cases since they often are based on the relative amounts of isomeric forms of the same molecular skeleton. For such compounds there are only small variations in energy levels, and they can be expected to be especially sensitive to artificial effects.

We have compared the patterns of maturity induced change in the chemical composition of two sub-fractions of bitumen in samples from artificially matured source rocks and naturally matured coals. Asphalt fractions are analyzed by FT-IR (Fourier transform infrared) spectroscopy and the maturity related trends are extracted from the spectra by multivariate data analysis. The aromatic fractions of the same samples are analyzed by GC and phenanthrene isomer based maturity parameters are calculated. Multivariate analysis of a larger set of the aromatic components has also been performed.

Experimental

Hydrous pyrolysis: Samples from four immature source rock were artificially matured by hydrous pyrolysis in home-made stainless steel reactors by standard procedures (2). A fixed time of 72 hours and variable temperatures from 250°C to 365°C were used. This gave sets of samples covering the oil generation stage and the start of oil-to gas cracking. A summary of the source rock characteristics is given in Table 1.

The generated bitumen was Soxhlet extracted from the solid residue with dichloromethane (DCM). The extract was combined with the expelled oil collected from the water and reactor surfaces and deasphalted with 40 volumes of hexane. The deasphalted extract was separated into saturate, aromatic and polar fractions by MPLC on a silica column. The aromatic fractions were separated by ring size by HPLC. The maturity of the samples was measured on the residues as vitrinite reflectance, $\%R_o$, when possible and by Rock-Eval T_{max}.

Natural samples: A set of 56 coal samples from different sources with $\%R_o$ ranging from 0.38 to 2.62 (donated by Norsk Hydro, Bergen, Norway) were extracted and fractionated as described for the hydrous pyrolysis samples. The resulting fractions comprise the naturally matured reference set. Asphaltene spectra were recorded from all samples, and the aromatic fractions from 35 samples were also analyzed by GC.

Analytical procedures, asphalt fractions: Diffuse reflectance IR-spectra were recorded using a Perkin Elmer 1720x FTIR-spectrometer interfaced to a Vax computer. 10 µl of a 5 mg/ml solution of asphaltenes in DCM was deposited as a thin film on a KBr surface, and the solvent evaporated at room temperature. The spectra were analyzed in Kubelka-Munk form. The spectra initially had 3401 data points, but were reduced to 750 variables by a maximum entropy procedure (3). The resulting "condensed" spectra together with maturity measures or hydrous pyrolysis temperature comprise the matrices for multivariate data analysis of maturation trends.

Analytical procedures, aromatics: Aromatic fractions from Series I and II and the coal samples were analyzed. Both the whole aromatic fractions and the isolated three-ring fractions were analyzed by GC on a 50 m CP-Sil-5-CB column with FID-detection. The resulting chromatogram was directly registered in a VG Multichrom laboratory data system. The identification of specific components were based on retention times and comparisons with standards, and confirmed by GC-MS. As concentration measures, both peak heights and areas from the automatic integration were used together with manually measured peak heights. The methylphenanthrene parameters F_1 and F_2 (4) were calculated from the phenanthrene isomer ratios and used as maturity parameters. 30 peaks over the whole range of components were selected for multivariate analysis.

Data analysis: Multivariate analysis to establish patterns of chemical change calibrated to maturity measurements were performed by PLS (Projection to Latent Structures) using the Sirius program for chemometric multivariate analysis (5). Target rotated components were used to visualise the sum of maturity dependent changes in the spectra or chromatograms.

Results

FTIR of asphaltenes: Visual inspection of the IR-spectra to some degree shows the expected maturity trends in all sample sets, with increase in C-H and C=C aromatic stretching and decrease in C=O stretch, but the trends are difficult to quantify directly. However, the maturity components of the spectra extracted with multivariate analysis by PLS describe more than 90 % of the variation in all sample sets, and give well-fitted models. Fig.1 gives an overview of the results for source rock III, a Brent coal, with representative spectra after variable reduction, the target projected maturity component and the fit of the calibration model to the data points. Fig.2 gives an equivalent presentation of the naturally matured samples. Table 2 gives a qualitative summary of the maturity dependent changes for all the data sets. Clear similarities in the maturity dependent trends are observed. Series I shows most deviation. This can be caused by the initially very immature state of the brown coal sample, which gives a different range of maturation than the other series.

However, quantitative comparisons of the different series of hydrous pyrolysis samples and the naturally matured samples is not successful. The multivariate calibration models cannot be used to predict pyrolysis temperatures or maturity parameters for samples from other sets. The model based on the spectra of the naturally matured samples does not correctly predict maturity from the spectra of the artificially matured samples. The similarities in the asphaltene IR spectra thus reflect similar chemical trends with maturity, but the correspondence is not sufficient to be a basis for quantitative measurements or an universal calibration model.

GC of aromatics: The indices gave a reasonably good linearity with measured vitrinite reflectance for the naturally natured coals, as shown in Fig.3a. For the hydrous pyrolysis samples no trend was observed for either of the data sets analyzed. Series I is shown for comparison in Fig 3b. The multivariate analysis for maturity dependent trends is shown in Fig. 3c and d, where the naturally matured samples give inverse isomer loadings, i.e. negative correlations between the amounts of α and β isomers. The hydrous pyrolysis samples only give a negative correlation of the more volatile components with the less volatile components, and no isomer separation in either of the hydrous pyrolysis series.

Conclusion

The standard hydrous pyrolysis procedure which is used for simulating the chemical processes of organic matter maturation can reproduce overall chemical changes in a qualitative manner, as observed in IR-spectra of asphaltenes. The detailed isomer distributions between single components in the aromatic fraction is not reproduced. This indicates that hydrous pyrolysis should be used with caution as a method for simulating natural processes on a molecular level.

References

1: Winters, J.C; Williams, J.A.;Lewan, M.D. Adv. in Organic Geochemistry 1981, 1983, 524-533

2. Barth, T.; Borgund, A.E. and Hopland, A.L. Org. Geochem. 1989, 14, 69-76

3. Karstang, T.V. and Eastgate, R.J. Chemolab. 1987, 209-219

4. Kvalheim, O.M.; Christy, A.A.; Telnæs, N.; Bjørseth, A. Geochim.Cosmochim.Acta, 1987, 51, 1183-1888.

5. Kvalheim, O.M. Chemolab. 1988, 4, 11-25.

TABLES:

Table 1: Source rocks for hydrous pyrolysis.

Source rock	Initial maturity	TOC %	S_2 mg/g	Max.final maturity	No. of exp.
I: Brown coal	0.25 $\%R_o$	53.3	58.1	1.53 $\%R_o$	10
II: Kimmeridge	0.29 $\%R_o$	51.3	333	T_{max} 513	11
III: Brent	T_{max} 428	39.6	32.8	T_{Max} 525	8
IV: Heather	T_{max} 424	5.03	22.1	T_{Max} 536	7

Table 2: Maturity trends in IR-spectra of asphalt fractions.

Sample	O-H	C-H aro.	C-H ali.	C=O	C=C	C=O acid	C-H ali.	-O- eth.	C-H aro
	ca cm^{-1}								
	3700-3100	3100-3000	3000-2850	1765-1690	1630	1575-1520	1450-1380	1400-1050	880-700
I	-	+	+	-	+	-	+	-	
II	+	+	-	-	+				+
III		+	-		+				+
IV	+	+	-						+
V[1]		+	-	-	+		+		+

1: Naturally matured samples

Figure 1.
IR-spectra, target component and fit of model for series I Brent coal pyrolysis samples.

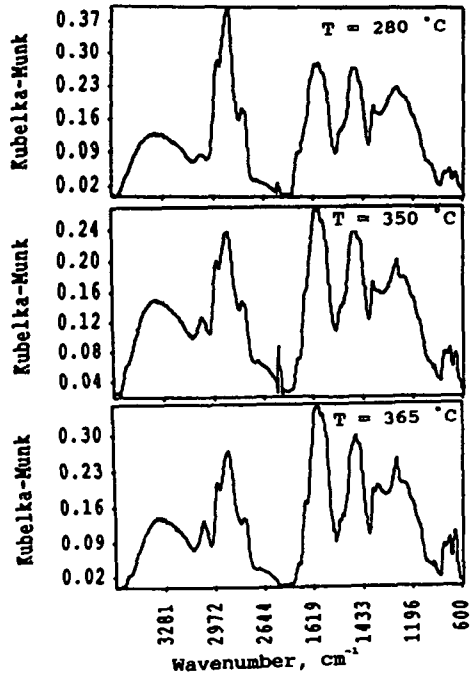

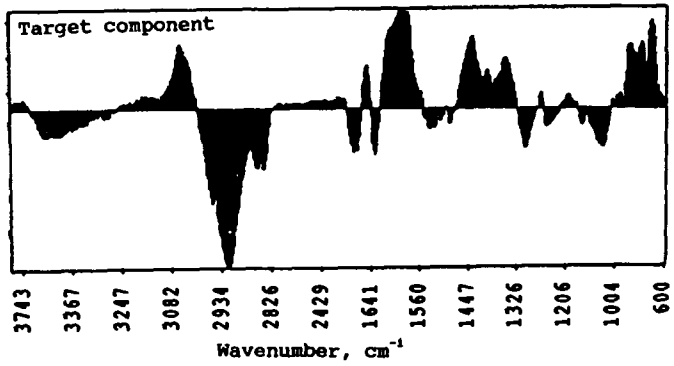

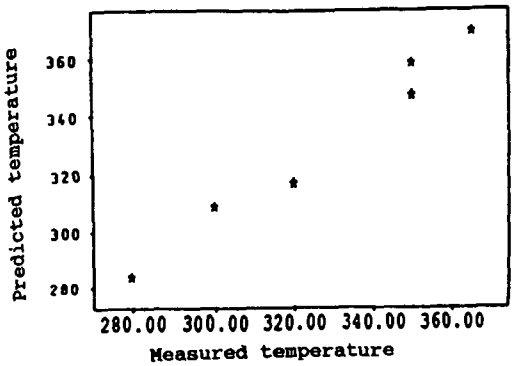

Figure 2.
IR-spectra, target component and fit of model for series V naturally matured coals.

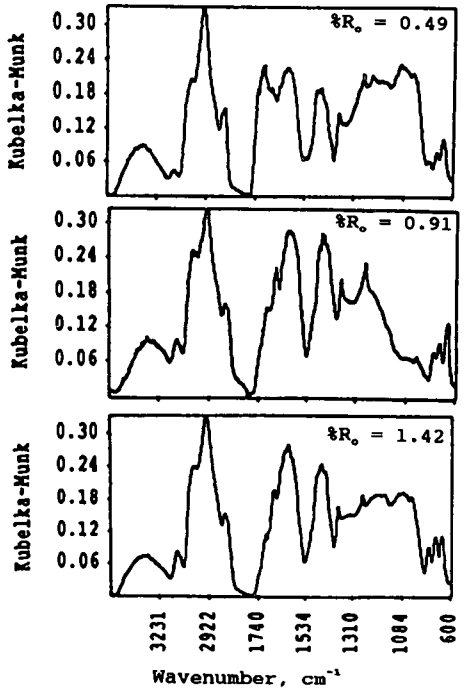

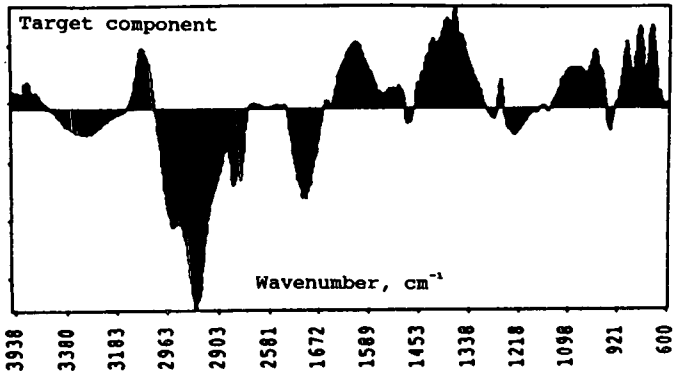

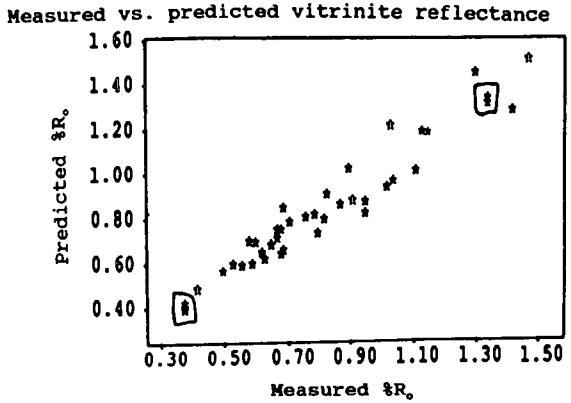

Figure 3.
Methylphenanthrene indices and maturity components for V - coal samples and I- pyrolyzed brown coal.

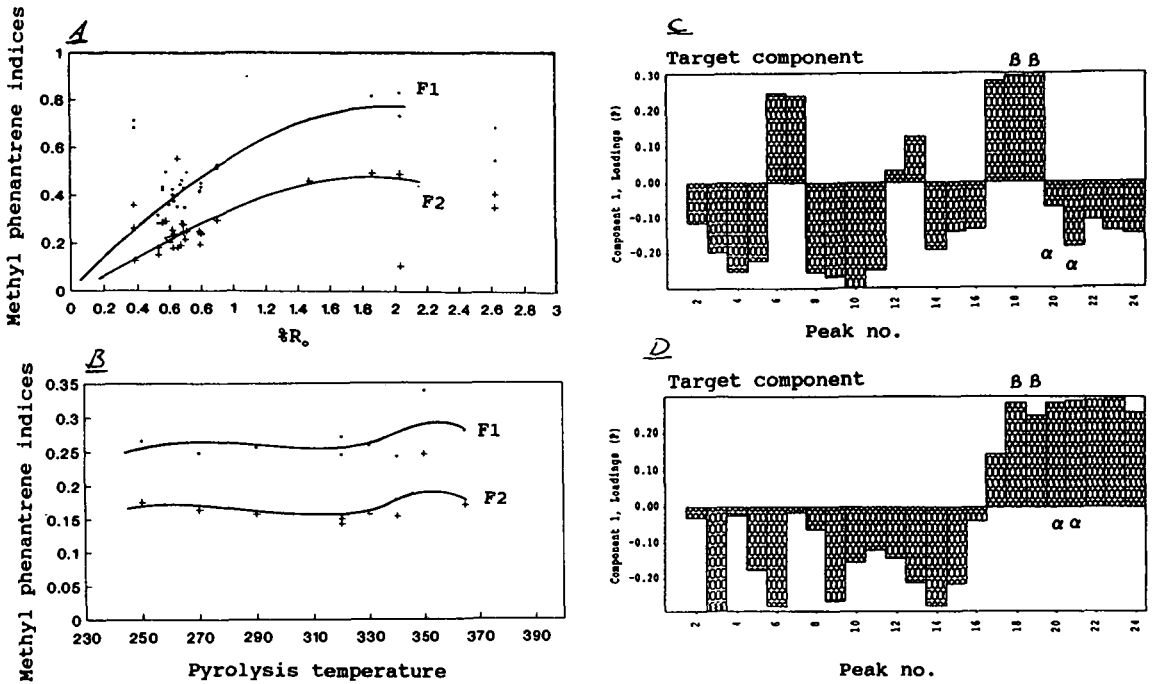

1607

THE OFF-LINE AND ON-LINE ANALYSIS OF EFFLUENTS GENERATED DURING CONFINED PYROLYSIS OF ORGANIC MATTER

Patrick LANDAIS
Laurence GERARD and Laurence MANSUY
CNRS-CREGU - BP 23 Vandoeuvre Cedex. FRANCE

Keywords: artificial maturation, confined pyrolysis, multidimensional GC.

INTRODUCTION

Confined system pyrolysis using gold tubes in cold-sealed pressurized autoclaves has proven his efficiency for simulating the main transformations of organic matter during thermal maturation (1), (2). However, these pressurized experimental systems are still poorly adapted to the quantitative analysis of effluents generated during pyrolysis. Indeed, until now, the acquisition of mass balances required fractionations of effluents into several classes and frequently induced the evaporation losses of volatile components.

In order to overcome such analytical problems, two new techniques have been designed and developped. The off-line analysis is a thermodesorption-multidimensional gas chromatograph which allows quantitative evaluation, in a single injection, of the amounts of CO_2, CO, N_2, H_2S, H_2O, C_1-C_{30} hydrocarbons after gold-tube piercing. The on-line technique couples confined pyrolysis and analytical devices by means of a dual-oven allowing effluents pressure recording and continuous analysis of effluents by GC or GC-IR-MS during thermal maturation.

Description and applications of these two techniques are presented in this paper.

THERMODESORPTION-MULTIDIMENSIONAL GAS CHROMATOGRAPHY

This analytical system is constituted by a thermodesorption oven connected to a multidimensional gas chromatograph (Figure 1). The thermodesorption system is composed of a specially designed piercing device connected to a high temperature Valco C6UWT gas sampling valve via a series of valves which allow the sampling system to be evacuated and calibration gases or calibration liquid hydrocarbons mixtures to be injected. This sampling part is placed into a thermostated oven providing a homogeneous temperature of 250°C. A pressure transducer connected to a -1/0 bar vacuummeter measures the vacuum level in the sampling zone before piercing. A high temperature pressure transducer connected to a 0/16 bar manometer measures the effluent pressure in the sampling zone after piercing and before injection. The 0.5 ml injection loop of the Valco valve is connected to the chromatograph by a capillary fused silica transfer line heated at 280°C (carrier gas: H_2).

The two ovens of the Siemens Sichromat 2-8 multidimensional GC have their own temperature control and program which facilitate the installation of two capillary columns (oven 1: OV1, 50 m • 0,32 mm; oven 2: paraplot Q, 23 m * 0,32 mm) connected together by a pneumatic live switching system. A selected portion of the column 1 effluent containing partially resolved components (Ar, CO_2, CO, H_2S, H_2O, N_2, C_1-C_6) is transferred to column 2 for a complete separation and detection by a TCD. Other components (C_7-C_{30}) are separated by column 1 and directly transferred to a FID. Chromatographic data are recorded and processed by a ChemStation HP3365 software running on a HP Vectra computer.

The 5 cm long gold tube in which the kerogen has been pyrolysed is introduced in the piercing device. The sampling system is closed, evacuated and heated to 250°C before the gold tube is pierced. The thermovaporizable content of the tube expands into the evacuated sampling system and fills the sample loop. After an equilibration time of 30 min, the pressure is recorded by the manometer and the sample is injected into the chromatograph system. After each run, the gold tube is collected and weighed in order to determine the total weight loss. Calibration of H_2O and C_7-C_{30} hydrocarbons is performed by injection of calibrated mixtures with a syringe. Gases are calibrated by direct injection of a calibration mixture into the sampling system.

Series of artificially matured kerogens from the Paris basin, the Mahakam Delta and the Woodford Shale have been obtained by confined pyrolysis at 250, 300, 350, 375, 400°C, 100M Pa in experiments lasting 24 and 72 hours. The pyrolyzates have been analyzed by TD-MDGC and subsequently $CHCl_3$ extracted.

On Figures 2a and 2b are represented the TD-MDGC FID and TCD traces of the 350°C pyrolyzate of an immature kerogen from Toarcian of the Paris Basin. The use of the selective transfer technique with columns of different polarity allows a good separation of the gases (TCD, b) and of the higher molecular weight hydrocarbons (FID, a).

Several results from TD-MDGC have been compared with data obtained by LC-GC of the high molecular weight components. Chromatographic distribution of *n*-alkanes as well as pristane/nC_{17} ratios are similar. However, more accurate quantitative information is obtained on the C_7-C_{12} and C_1-C_6 fractions. A complete mass balance for a series of artificially matured kerogens from the Toarcian of the Paris Basin is presented on Figure 3. The quantitative evolution of the different classes contribution relative to the initial organic matter weight clearly evidences the different phases of thermal maturation.

Comparison of TD-MDGC analysis of type II and type III series of maturation demonstrates their different behaviour especially when considering the amounts of CO_2, H_2O and gasolines generated during maturation. For example, late generation of CO_2 has been evidenced during the catagenetic phase of a type II kerogen.

Source-rocks pyrolyzates can also be directly analyzed by this technique.

PRESSURE RECORDING AND EFFLUENT SAMPLING DURING ARTIFICIAL MATURATION

Until now, the only pressure variations in the gold tube could be indirectly but continuously recorded. Preliminary results indicate a close correlation between effluents generation (gas + oil) and pressure variations. Furthermore, it is still impossible to differenciate the effects of secondary cracking from those of primary cracking.

So, a new pyrolysis system has been designed, allowing pressure recording and effluent sampling while preserving the characteristics of confined systems.

This device includes two separate ovens (Figure 4). The first one contains a 50 cc autoclave and a high temperature pressure transducer connected to a pressure recorder. The gold bag containing kerogen or source-rock (up to 10 g) is placed in the autoclave. An external pressure ranging between 0 to 100 MPa is applied on the bag through an argon pressurized line connected to an air-driven pump. A perfect gas-tight is assumed between the autoclave cell and the inside of the bag. This allows an absolute pressure record of the effluents released during pyrolysis. A micro-metering valve in the oven 1 and a pressure regulation valve in the oven 2 allows the transfer of an effluent aliquot toward the oven 2. In this second oven, a high temperature pressure transducer connected to a pressure recorder measures the effluent pressure in the 5 cc steel cell where the effluent are collected or in the sampling loop of the Valco C6UWT valve if the system is connected to a GC or a GC-IR-MS by a capillary fused silica transfer line heated at 360°C. In each oven, a blow-pipe valve connected to a vacuum pump allows the venting of the effluents at the beginning of the experiments and after each effluent sampling. The temperature is controled by four K-thermocouples located in each oven, in the autoclave and in the furnace. The temperatures in the two thermostated ovens and in the furnace are regulated independently with a precision of ± 1°C by an electronic system. The temperature is assumed to be homogeneous in the whole system. The effluent pressure variations are plotted against time by a graphic recorder.

The kerogen or the source-rock is placed in the gold bag and compacted. The bag is fixed to the autoclave and the external argon pressure is applied (0-100 MPa). The heating rate up to the isotherm temperature depends on the final temperature and range between 5 and 10 °C/mn. The generated effluents are released in the pipe of the oven 1 and the pressure evolution is recorded. Aliquots are sampled at different time intervals: each 2 hours during the first day of pyrolysis and then at longer time intervals. For each sampling, the aliquots are evacuated toward the oven 2 whose temperature is the same as oven 1 in order to avoid any condensation. A constant volume of effluents is injected toward a GC by the Valco valve after measuring the pressure. The chromatograph analyses H_2O, CO, CO_2, H_2S, N_2 and C_1-C_{40} hydrocarbons in one single injection. The connection with an IR-MS will allow the precise typing of oxygenated functions, cyclic and aromatic compounds. After each sampling, the

residual effluents of the oven 2 are vented by opening the blow-pipe valve connected to the vacuum pump.

This new technique makes possible new experiments in confined medium:

- the large volume of the gold bag (ø = 1,5 cm, L = 5 cm) facilitates source-rock pyrolysis and studies of organic/mineral interactions
- the sampling and venting facilities allow the studies of the expelled fraction in source-rock pyrolysis
- the differentiation between primary and secondary reactions can be done by venting the oven 1 after each sampling. So, the only effluents generated between two samplings are analysed and only primary cracking is considered. The secondary cracking can be studied by thermal maturation of the aliquot in the oven 2 (independant regulation) after each sampling.

Acknowledgements - This work has been supported by the CPM (France), SNEA(P) and INSU (n° 91/ATP/645).

REFERENCES

(1) Monthioux M., Landais P. and Monin J.C. (1985) Comparison between natural and artificial maturation series of humic coals from the Mahakam Delta, Indonesia. *Org. Geochem.*, 8, 275-292.

(2) Landais P., Michels R., Poty B. and Monthioux M. (1989) Pyrolysis of organic matter in cold-seal pressure autoclaves. Experimental approach and applications. *J. Appl. and Anal. Pyrol.*, 16, 103-115.

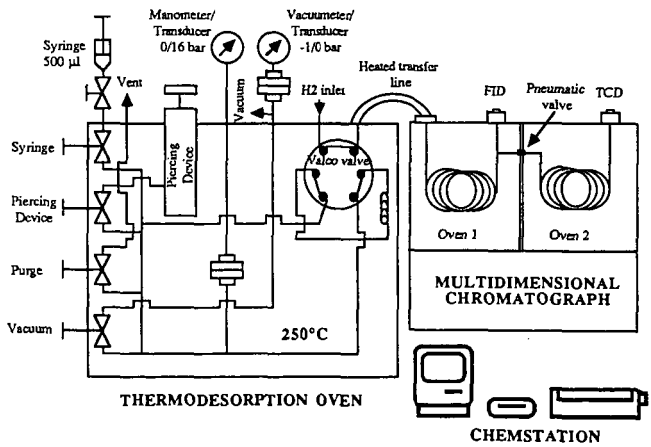

Fig.1. Scheme of the thermodesorption-multidimensional gas chromatography system

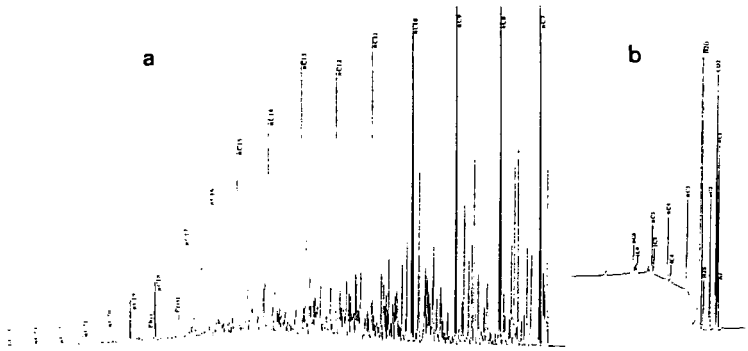

Fig. 2. TD-MDGC FID (a) and TCD (b) traces of the 350°C pyrolyzate of a Paris Basin kerogen.

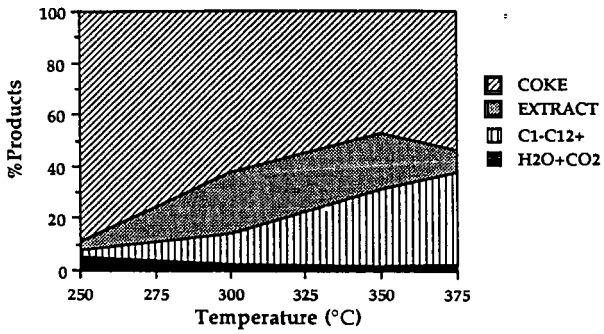

Fig. 3. Mass balance of a series of artificially maturated kerogens from the Paris Basin.

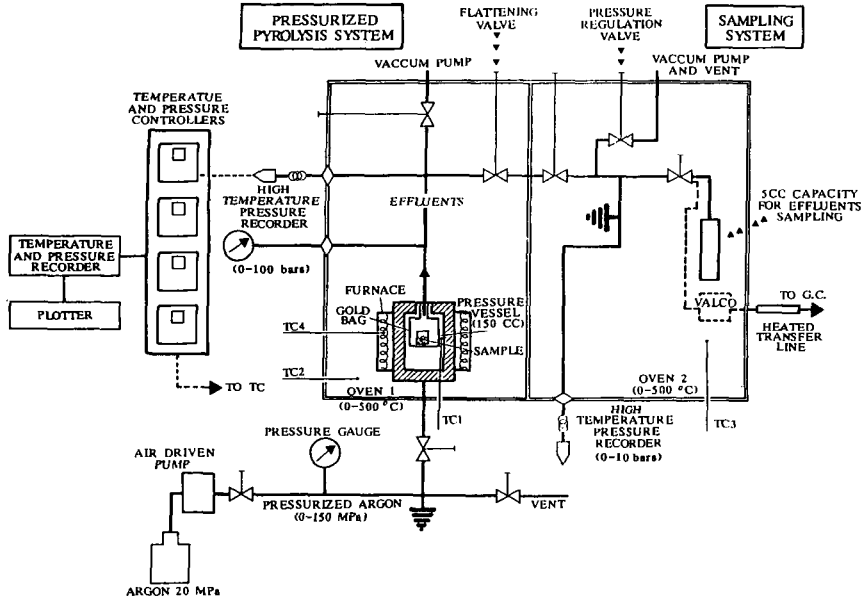

Fig. 4. Scheme of the pyrolysis and sampling systems in the new pressurized confined-pyrolysis device.

MEASUREMENT OF PRESSURE EFFECTS ON N-HEXADECANE CRACKING RATES

Kenneth J. Jackson, Alan K. Burnham, Robert L. Braun, and Kevin G. Knauss
L-202, Earth Sciences Dept.
Lawrence Livermore National Laboratory
Livermore, CA 94550

Keywords: Hexadecane, cracking rates, pressure effects

ABSTRACT

Experiments designed to determine the possible role of pressure in governing the kinetics of n-hexadecane (n-C_{16}) cracking reactions were conducted in Dickson-type autoclaves at temperatures from 300 to 370 °C and pressures from 150 to 600 bars. Good agreement with published reaction kinetics was obtained at temperatures ≥350 °C. Values determined at lower temperatures indicate slower rates than predicted from earlier experiments and show a distinct induction period at 300 °C. The activation energy determined for this reaction is about 60 kcal/mole at T > 330 °C, but it may exceed 70 kcal/mole at lower temperatures. Product hydrocarbon compounds lighter than n-C_{16} seem to follow the single, first order reaction kinetics shown by the disappearance of n-C_{16}. Hydrocarbons larger than n-C_{16}, however, seem to follow a serial reaction of generation and subsequent destruction (including conversion to solid products) at high percentage conversion. Limited data suggest that the cracking rate of n-C_{16} may have a small dependence on pressure.

EXPERIMENTAL PROCEDURES

The high temperature/pressure cracking experiments were run in Dickson-type, gold bag autoclaves (Seyfried et al., 1987). In this apparatus, the reaction vessel comprises an approximately 250 ml capacity gold bag which is capped with a commercially pure titanium head. The Ti head is fitted with a Ti or Au capillary-lined stainless steel sampling tube that allows the experiment to be sampled periodically during the course of a run at *in situ* conditions. During the runs, the samples contact only Au and carefully passivated Ti. The Au bag assembly is inserted into a stainless steel pressure cell filled with de-ionized water that serves as the pressure medium. In

turn, this assembly is fitted into a furnace assembly, as described by Seyfried et al. (1987).

Starting materials for all runs were 98.75 wt % n-C_{16} spiked with small amounts of naphthalene and phenanthrene (approximately 1.0 and 0.25 wt. %, respectively), which served as internal standards. Before the samples were loaded into the Au bags, high purity N_2 gas was bubbled through them for at least 30 minutes to remove any reactive gases (e.g., O_2) that might be dissolved in the starting materials. The Au bag was partially filled with about 70 g of the hexadecane solution. The remaining space was filled with N_2 gas after emplacing the Ti head assembly. After the vessel was loaded, pressure was gradually increased. This collapsed the Au bag and expelled the N_2 gas in the head space; leaving only the hexadecane solution in the reaction vessel.

SAMPLING PROCEDURES

During the course of the run, the solution was periodically sampled by bleeding off a small amount (usually 1-2 g) of the experimental charge into gas-tight glass syringes. The initial samples were a single liquid phase, but later samples yielded two phases because a gas phase separated from the liquid as the sample cooled. The gas was stripped from the liquid phase using a He gas extraction method, and the two fractions were analyzed separately. Liquid samples were diluted in CS_2 and analyzed by gas chromatography. Fig. 1 shows a sample analysis of the reaction products obtained from Run 1 at 353 ^{o}C and 300 bars after 169.3 hours of reaction. Gas samples were injected directly into a gas chromatograph, and checked for air contamination using mass spectrographic analyses.

RESULTS

The matrix of experimental conditions investigated in this work is shown in Table 1. Temperatures ranged from 300 to 370 ^{o}C and pressures ranged from 150 bars to 600 bars. Within this range of physical conditions, the disappearance of n-C_{16} was measured as a function of time (e.g., Fig. 2a). Exponential rates of disappearance of n-C_{16} are consistent with a single first order reaction and yield rate parameters consistent with published values (see below). An exception to this is the significant induction period exhibited by the 300 ^{o}C experiment (Fig. 2b). In addition to the disappearance of n-C_{16}, the rate of production of various classes of product phases was determined. For convenience in interpreting the data, the product

phases were separated into methane and four additional groups determined by their carbon numbers. These groups are arbitrarily defined as: C2-C4, C5-C9 C10-C15, and everything larger than C16. Fig. 3 shows that the rate of appearance of these products, when plotted as a function of the percent of hexadecane remaining in the solution, is essentially identical for all seven runs.

Rate constants for the reaction of hexadecane shown in Fig. 4 and 5 were determined using the KINETICS code of Braun and Burnham (1990). Based on results from these experiments, the cracking rate of n-C_{16} may have a small dependence on pressure (Fig. 5). It is not possible to quantitatively assess the size of this effect based on results from these experiments, because there are only a limited number of runs at a single temperature and different pressures. The activation energy for this reaction is 60 kcal/mole at T> 330 ^{o}C, but it appears to be increasing at lower T. However, this proposed decrease in activation energy is based on a single experiment at 300 ^{o}C in which there is some evidence of a distinct induction period, as shown in Fig. 2b. The significant induction period may influence interpretation of previous kinetic studies based on low-temperature, low-conversion data (e.g., Domine, 1991).

The kinetics of the production of the C1, C2-C4, C5-C9 and C10-C15 groups of product compounds seem to follow the same single, first order reaction kinetics exhibited by the disappearance of the hexadecane. However, the > C16 products follow a serial reaction of generation and subsequent destruction at high percent conversion.

REFERENCES

Braun, R. L. and A. K. Burnham (1990) KINETICS: A computer program to analyze chemical reaction data. UCID-21588 Rev. 1, Lawrence Livermore National Laboratory, Livermore, CA, 11 p.

Domine, F. (1991) *Organic Geochemistry* 17, 619-634.

Doue, F. and G. Guiochon (1968) *J. Chim. Phys -Chim. Biol.* 64, 395.

Doue, F. and G. Guiochon (1969) *Can. J. Chem.* 47, 3477.

Fabuss, B. M., J. O. Smith, R. I. Lait, A. S. Borsanyi, and C. N. Satterfield (1962) *Ind. Eng. Chem. Process Des. Dev.* 1, 293.

Fabuss, B. M., J. O. Smith, and C N. Satterfield, (1964) *Adv. Pet. Chem. Refin.* 9, 179.

Ford T. J. (1986) *Ind. Eng. Chem. Fundam.* 25, 240-243.

Groenendyk, H., E. J. Levy, and S. F. Sarner (1970) *J. Chromatogr. Sci.* 8, 115.

Panchenkov, G. M., V. Ya. Baranov (1958) *Izv. Vyssh. Uchebn. Zaved., Neft Gaz.* **1**, 703.
Tilcheev, M. D. and K. I. Zimina (1956) *Khim. Tekhnol. Topl.* **8**, 23.
Voge, H. H. and G. M. Good (1949) *J. Am. Chem. Soc.* **71**, 593.
Seyfried, W. E., D. R. Janecky and M. E. Berndt (1987) Rocking autoclaves for hydrothermal experiments II. The flexible reaction-cell system. In *Hydrothermal Experimental Techniques* (G. C. Ulmer and H. L. Barnes, eds.) Wiley-Interscience, 216-237.

Run Number	T (°C)	P (bars)	Maximum Conv. (%)	Duration (hr)
1	353	300	77.3	764
2	330	150	22.8	1052
3	300	300	1.1	5615
4	329	480	5.4	1027
5	333	600	28.1	2397
6	369	250*	89.3	433
7	371	300*	88.7	315

Table 1. Experimental conditions, extent of reaction, and run duration for the seven experiments described in this work. *Near the end of Runs 6 and 7, pressure increased to 283 and 343 bars, respectively.

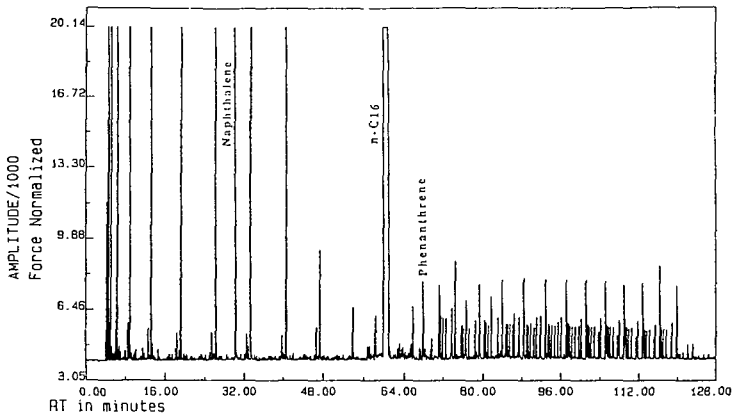

Figure 1. Sample gas chromatography trace showing the composition of the liquid phase in Run 1 (353 °C and 300 bars) at 169.3 hr elapsed time.

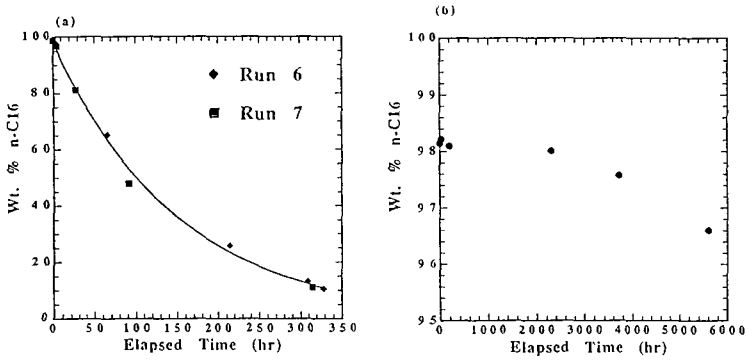

Figure 2. The disappearance of n-C_{16} as a function of elapsed time (a) in Runs 6 and 7 (370 °C) and (b) in Run 3 (300 °C). The symbols are experimental values, and the curve represents an exponential curve fit through the points.

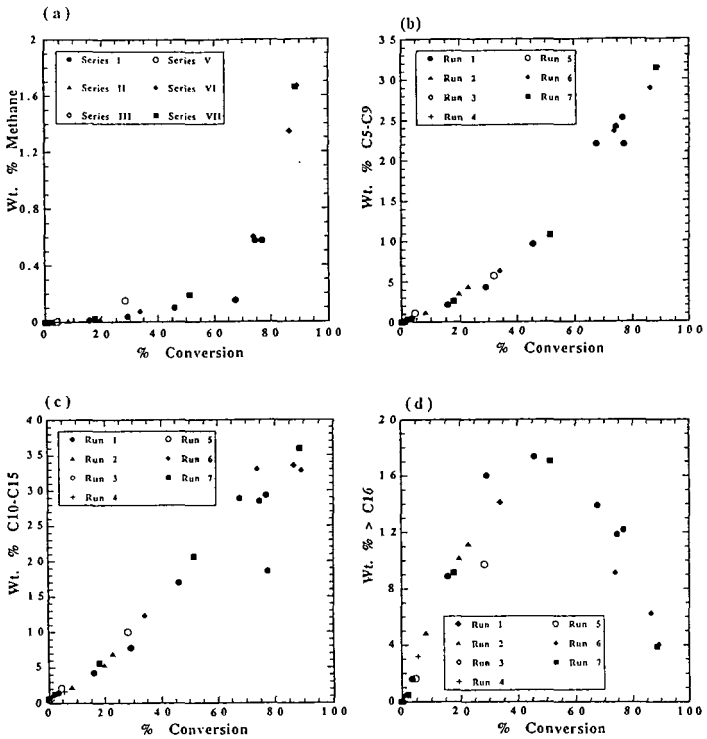

Figure 3. The appearance of product phases for all seven experiments as a function of % conversion of n-C_{16}: (a) the appearance of methane, (b) the appearance of the C5 to C9 fraction, (c) the appearance of the C10 to C15 fraction, and (d) the appearance and subsequent disappearance of the > C16 fraction.

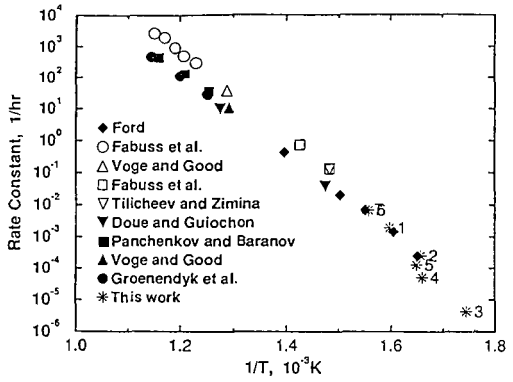

Figure 4. Comparison of hexadecane cracking rates compiled by Ford (1986) with values determined in this study. The numbered points correspond to run numbers listed in Table 1.

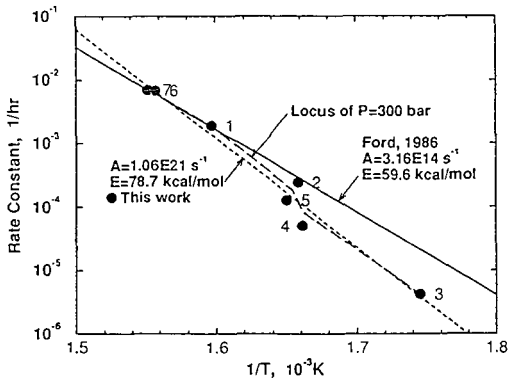

Figure 5. An enlargement of the lower right hand portion of Figure 4. The solid line shows an extrapolation of the activation energy and frequency factors determined by Ford (1986). The dotted line is a linear least squares fit through the rate constants determined in this work. The dashed line defines a locus of points consistent with the trace of a 300 bar isobar suggested by the data in this study.

HYDROUS PYROLYSIS OF NEW ALBANY AND PHOPHORIA SHALES: EFFECTS OF TEMPERATURE AND PRESSURE ON THE KINETICS OF PRODUCTION OF CARBOXYLIC ACIDS AND LIGHT HYDROCARBONS

Kevin G. Knauss, Sally A. Copenhaver, Robert L. Braun and Alan K. Burnham
Earth Sciences Department
Lawrence Livermore National Laboratory
Livermore, CA 94550

Keywords: Hydrous pyrolysis, Carboxylic acid, Kinetics

ABSTRACT

We used hydrous pyrolysis to determine the production kinetics of carboxylic acids and light hydrocarbons over the temperature interval 200° to 330°C at 300 and 600 bar pressure. We used Dickson-type, gold-bag autoclaves (1) allowing us to acquire multiple fluid and gas samples under *in situ* conditions throughout the runs, each lasting from 60 to 120 days, depending on temperature. During the runs and while sampling, fluids were exposed to only non-reactive materials (gold, passivated titanium and glass gas-tight syringes). Gases were extracted into He and analyzed using GC and MS. The aqueous samples were analyzed for carboxylic acids using IC, for inorganic cations using ICP-ES and for inorganic anions using IC. Carbon disulfide extractions were made on some aqueous fluids allowing GC analyses for heavier hydrocarbons.

The kerogen pyrolysis produced significant amounts of the monocarboxylic acids (acetic > propionic > butyric). Formic acid was present only briefly at the start of runs and little, if any, of the dicarboxylic acids were produced. The gases were dominated by CO_2 and methane, in that order, and progressively smaller amounts of the alkanes (ethane > propane > butane > pentane). Preliminary kinetic analyses of production rates suggest activation energies (E) ranging from 50 to 60 kcal/mol for both the light hydrocarbons and acids. Pressure had little effect on measured rates for the New Albany Shale.

INTRODUCTION

The potential importance of the carboxylic acids in generating reservoir porosity and controlling aqueous fluid chemistry (2) has resulted in considerable interest in knowing their rate of production and thermal stability (3), although not without some controversy (4). The recognition of the reactivity of organic compounds in aqueous solutions at high temperature (5) has argued for the use of hydrous pyrolysis as a particularly appropriate method of investigation (6). Unfortunately, experimental artifacts, like catalysis by the reaction vessel (6), and inappropriate kinetic analyses (7) have sometimes conspired to complicate progress in understanding the processes and rates.

We are studying the pyrolysis of oil shales and the generation of carboxylic acids and light hydrocarbons using chemically inert (Au and Ti) hydrothermal reaction vessels specifically designed to allow sampling of fluids under *in situ* condi-

tions. In this way we hope to avoid many of the complications noted by others. In addition, we are using a variety of approaches to kinetic analyses in determining kinetic parameters.

EXPERIMENTAL AND ANALYTICAL TECHNIQUES

The term hydrous pyrolysis has been used by some workers (8) to mean a relatively specific, restrictive experimental approach. Although useful for comparison between samples of the "potential for generating oil-like pyrolysate", this approach may not be ideally suited to studies aimed at mechanisms and kinetics of processes. We use the term more loosely to imply simply the pyrolysis (cracking) of kerogen in the presence of liquid water. Our lowest pressure (300 bar) was sufficiently high to keep the aqueous system single phase throughout each run. The use of a flexible gold bag allows us to control pressure (e.g., isobaric) through significant degrees of maturation. This approach has been used to advantage by others (9). Our apparatus differs from that of these earlier workers, however, in that we may withdraw multiple samples from each run while maturation continues uninterrupted. Concentration *vs.* time data are adjusted to compensate for the change in area/mass ratio caused by sampling.

Runs were isothermal (after a heating period lasting a few hours) and isobaric. All runs used 30 g of shale and an appropriate volume of de-oxygenated (purged using N_2 gas) distilled water to just fill the gold bag at run conditions. The headspace was further swept with N_2 gas prior to collapsing the gold bag before heating and pressurizing the vessel. Each run lasted from 2 to 4 months, depending on temperature. At the highest temperature, this allowed us to follow both the production and subsequent destruction (through decarboxylation) of the organic acids. A total of five runs were made with the New Albany Shale: 200°, 270° and 330°C at 300 bars pressure, 270° at 500 bars pressure, and 330°C at 600 bars pressure. Two runs are still in progress with the Phosphoria Shale at 330°C at 300 and 600 bars pressure. The Phosphoria Shale runs will not be dealt with here.

The shale samples were coarsely crushed (2 to 4 mm) and then washed ultrasonically in distilled water to remove adhering fine particles. We were faced with the usual conundrum of deciding whether or not to pre-extract the samples prior to hydrous pyrolysis. If we pre-extracted, we ran the risk of performing the hydrous pyrolysis on material unrepresentative of natural kerogen. If we didn't pre-extract, we would need to account for any light hydrocarbons or carboxylic acids released immediately upon heating that were the product of natural maturation and not the artificial maturation taking place as a result of the hydrous pyrolysis. We elected not to pre-extract, because we felt that the water washing would remove some of the acids already present, and because we could correct for the initial acid input, since we would take closely spaced samples early in each run.

During the runs and while sampling, fluids were exposed to only non-reactive materials (gold, passivated titanium and glass gas-tight syringes). Gases were extracted into He and analyzed using GC and MS. The aqueous samples were analyzed for carboxylic acids using IC, for inorganic cations using ICP-ES and for inorganic anions using IC. Carbon disulfide extractions were made on some aqueous fluids allowing GC analyses for heavier hydrocarbons. At the conclusion of each run the vessels were quenched to room temperature and pressure and the solids and remaining liquids recovered and sampled. Although the gas and liquid analyses are essentially complete for the five runs, the solid phase analyses continue. These will include XRD, SEM/electron microprobe, and pyrolysis-MS analyses.

Initial TOC analyses made post-run suggest that significant degrees of artificial maturation were achieved. For example, the 270°C and 300 bar run achieved 30% conversion (based on kerogen loss) during the two months of artificial maturation.

RESULTS

Carboxylic acids

The kerogen pyrolysis produced significant amounts of the monocarboxylic acids (acetic > propionic > butyric). Formic acid was present only briefly at the start of runs. No dicarboxylic acid anions were unequivocally identified in any samples, suggesting that if they are produced at all under any of the conditions that we investigated, their production rate is very small. Figure 1 illustrates typical results for the carboxylic acids produced at 270°C. Note that at all temperatures there was an initial rapid release of carboxylic acid anions to the aqueous phase upon heating. In the subsequent kinetic analyses we have corrected the results for this initial pulse of released carboxylic acid. At 270°C, following the initial pulse, carboxylic acid concentrations continue to increase throughout the runs.

Figure 2 illustrates typical results for the carboxylic acids produced at 330°C. At this temperature the production rate of the carboxylic acids is much higher than at 270°C, however, within a few days the rates of production and destruction *via* decarboxylation are about equal. Within two weeks the rate of decarboxylation exceeds the rate of production and there is a continuous decrease in carboxylic acid concentration throughout the remainder of the runs. It is very likely that both the processes of production and decarboxylation are catalyzed by the mineral phases in the shale and, although our experimental apparatus is unlikely to have catalyzed processes, any rates that we measure are specific to these shales.

Light hydrocarbons

Unlike the carboxylic acids, the light hydrocarbons (<C7) and CO_2 were not rapidly released upon initial heating in water, implying that such compounds produced as a result of natural maturation are rapidly lost from the kerogen. The gases were dominated by CO_2 and methane, in that order, and progressively smaller amounts of the alkanes (ethane > propane > butane > pentane). Figure 3 illustrates typical results for these compounds at 270°C. Gas concentration continues to increase throughout the runs.

Effect of pressure

Pressure (300 *vs.* 600 bars) had little effect on the production of either the carboxylic acids or the light hydrocarbons produced from the pyrolysis of kerogen contained in the New Albany Shale. As an illustration, Figure 4 compares the 330°C carboxylic acid results obtained at the two pressures.

KINETIC ANALYSES

The concentration data were used to calculate fraction reacted on an absolute scale, based on the maximum concentration measured for each compound during the period of production. We then used the KINETICS code (10) to analyze the data acquired from the hydrous pyrolysis experiments. Table 1 summarizes the kinetic analyses.

For the gases, the data acquired at all three temperatures were used in the kinetic analyses. At 200°C over a 4 month period, little if any carboxylic acid was

produced by the artificial maturation. All of the carboxylic acid present at this temperature was that produced naturally and rapidly released to the aqueous phase upon heating. For this reason, the kinetic analyses of the carboxylic acid data are based only on the results from the 270° and 330°C runs.

In order to test our assumption that the reactions producing the carboxylic acids and light hydrocarbons were first order, we first made a kinetic analysis based on a Gaussian distribution of activation energies with all terms (the pre-exponential (A), activation energy (E), Gaussian distribution parameter (S), and reaction order (N)) calculated by fit, rather than being fixed. The mean calculated N for the gases was 0.98 ± 0.12 and for the carboxylic acids was 0.87 ± 0.10. The results suggested that for all compounds the production reaction may be assumed to be approximately first order, although a spread in calculated activation energies resulted from the sparseness of the data. Pyrolysis kinetics determined using a Pyromat II instrument suggested that an appropriate pre-exponential factor, A, for the production of volatile hydrocarbons from the New Albany Shale was $2x10^{14}$ (11). The kinetics analyses summarized in Table 1 used this value.

The kinetic analyses suggest that the activation energies for the production of both the light hydrocarbons and the carboxylic acids from the hydrous pyrolysis of kerogen contained in the New Albany Shale are within the range of 50 to 60 kcal/mole.

CONCLUSION

We have demonstrated the use of a new type of hydrothermal apparatus in determining the production kinetics of light hydrocarbons and carboxylic acids from kerogen pyrolysis. It is ideally suited to determine the effects of temperature and pressure on production kinetics, free of the experimental artifacts frequently encountered using other types of apparatus.

In this paper we have only presented preliminary results from the organic analyses of fluids and gases. We are continuing to analyze the data from solid phase analyses and from the inorganic fluid chemistry analyses. We intend to try to understand the interaction between the inorganic and organic chemical systems. We are especially interested in the effectiveness of carboxylic acids in complexing the cations released as a result of mineral dissolution, i.e., the increase in "solubility", and the impact of the carboxylic acids on the solution pH. We are utilizing the geochemical modeling code EQ3/6 (12) in this effort.

REFERENCES

(1) Seyfried, W.E., Janecky, D.R. and Berndt, M.E., in Hydrothermal Experimental Techniques, edited by G.C. Ulmer and H.L. Barnes (John Wiley and Sons, N.Y., 1987), p. 216.

(2) Lundegard, P.D. and Kharaka, Y.K., in Chemical Modeling in Aqueous Systems II, edited by D.C. Melchior and R.L. Bassett (Amer. Chem. Soc. Symposium Series 416, 1990) p. 169.

(3) Crossey, L.J., Geochim Cosmochim. Acta 55, 1515 (1991).

(4) Stoessel, R.K. and Pittman, E.D., Am. Assoc. Petrol. Geol. 74, 1795 (1990).

(5) Sisken, M. and Katritzky, A.R., Science 254, 231 (1991).

(6) Lundegard, P.D. and Senftle, J.T., Appl. Geochem. 2, 605 (1987).

(7) Burnham, A.K., Braun, R.L. and Samoun, A.M., Org. Geochem. 13, 839 (1988).

(8) Lewan, M.D., Winters, J.C. and McDonald, J.H., Science 203, 897 (1979).
(9) Monthioux, M., Landais, P. and Monin, J.-C., Org. Geochem. 4, 275 (1985).
(10) Braun, R.L. and Burnham, A.K., Lawrence Livermore National Laboratory Report UCID-21588, Rev. 1 (1990).
(11) Braun, R.L., Burnham, A.K., Reynolds, J.G. and Clarkson, J.E., Ener. & Fuels 5, 192 (1991).
(12) Wolery, T.J., Jackson, K.J., Bourcier, W.L., Bruton, C.J., Viani, B.E., Knauss, K.G., and Delany, J.M., in Chemical Modeling in Aqueous Systems II, edited by D.C. Melchior and R.L. Bassett (Amer. Chem. Soc. Symposium Series 416, 1990) p. 104.

TABLE 1

KINETIC ANALYSES OF PRODUCTION RATE DATA

Compound	Pressure (bar)	E (kcal/mol)	A (s^{-1})	S (%E)	N
methane	300	55.3	2e14	3.46	1
	600	55.2	"	3.06	"
ethane	300	55.1	"	3.73	"
	600	54.9	"	1.71	"
propane	300	55.6	"	4.16	"
	600	54.9	"	0.57	"
butane	300	55.5	"	4.25	"
	600	55.7	"	1.49	"
acetate	300	52.6	"	0.77	"
	600	52.6	"	0.84	"
propionate	300	52.5	"	1.44	"
	600	51.6	"	2.49	"
butyrate	300	52.9	"	0.09	"

Figure 1. NA-1 (270°C, 300 bar)

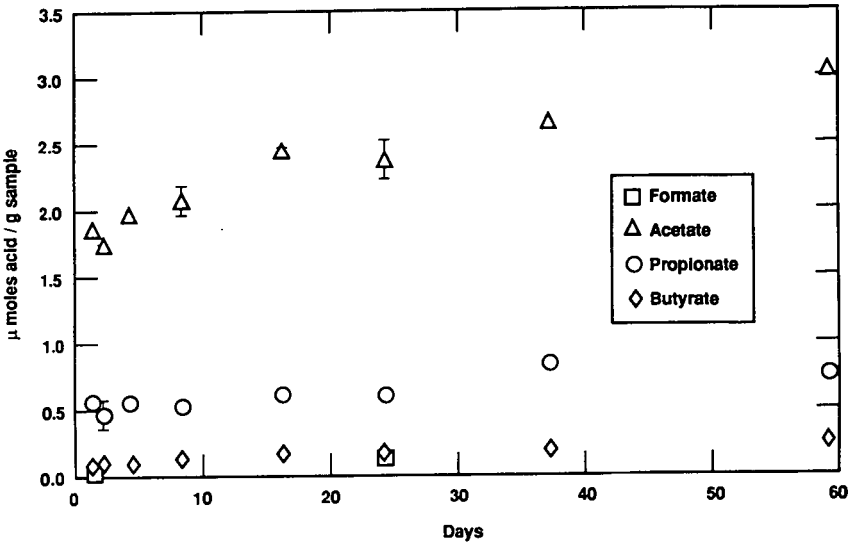

Figure 2. NA-7 (330°C, 600 bar)

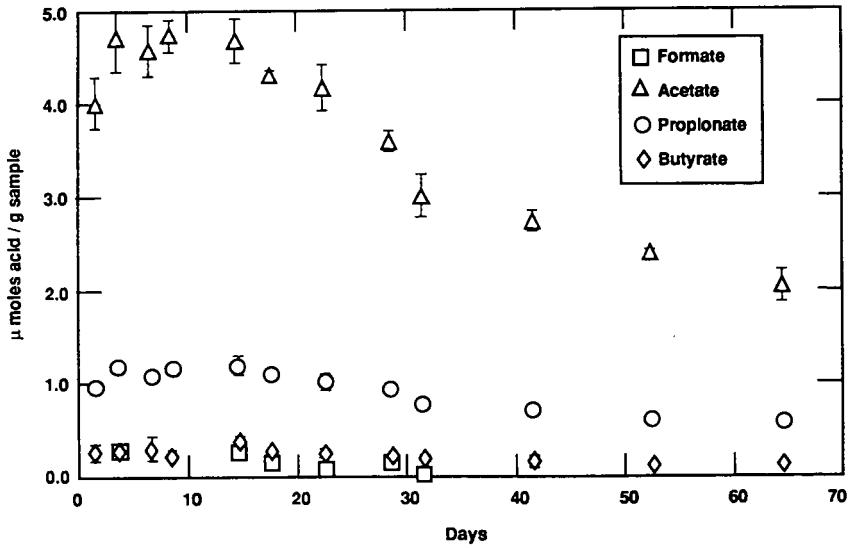

ES-05/28/92-KK#4-01 & 02

Figure 3. NA-4 gasses (270°C, 500 bar)

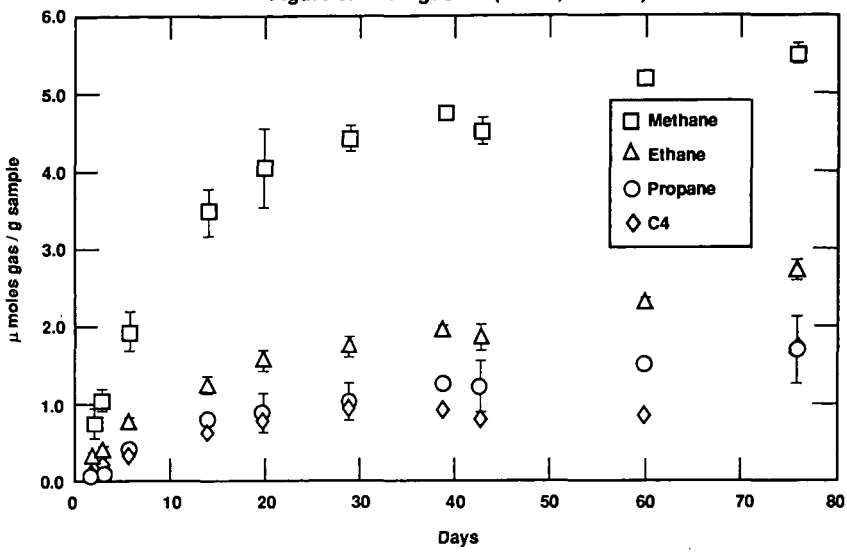

Figure 4. New Albany Shale at (330°C and 300 or 600 bar)

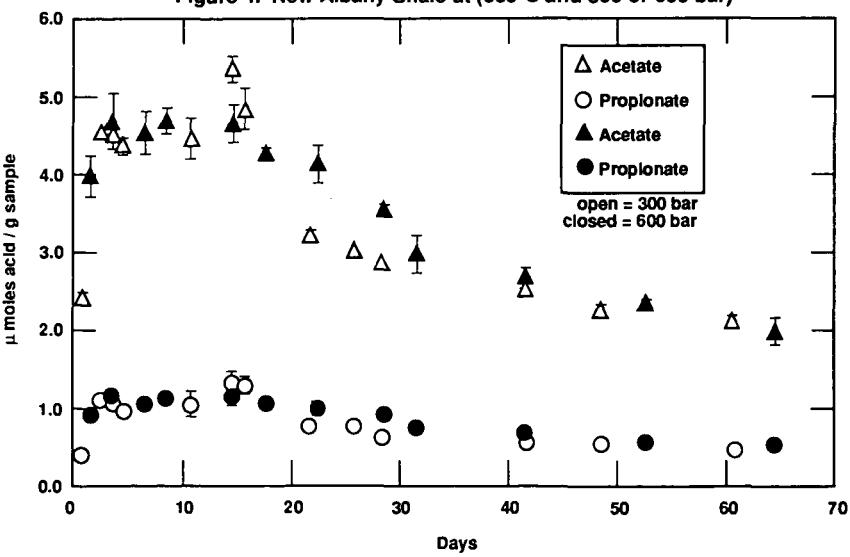

ES-05/28/92-KK#4-03 & 04

The Effect Of Pressure On The Kinetics Of Kerogen Pyrolysis

H. Freund, J. A. Clouse, G. A. Otten
Exxon Production Research Co.
P. O. Box 2189
Houston, TX 77252

Keywords: activated volume, pyrolysis kinetics, kerogen maturation,

Introduction

The determination of the kinetics of oil generation is usually done in the laboratory using shales of interest and subjecting the material to high temperatures to accelerate the conversion. Kinetics are determined at these high temperatures, low pressures and extrapolated back to the geological conditions believed to exist at the time of generation. The validity of the extrapolation of these rate constants over a wide range of temperatures[1,2] and pressures[2] has recently been studied.

Other authors have addressed the issue of pressure. Teichmuller and Teichmuller[3] have suggested that high pressure retards the coalification process based on field measurements of vitrinite reflectance. Also using vitrinite reflectance measurements from the offshore of northwestern Europe, McTavish developed a correlation quantitatively relating pressure to vitrinite reflectance.[4] More recently, Sajgo et al [5] compressed alginite and lignite into disks and determined the effect of pressure on their thermal alteration. They observed significant retardation at 1 kbar equivalent to about 50°C (i.e., the high pressure case had to be raised 50° to obtain the same extent of conversion). Price and Wenger have performed aqueous pyrolysis experiments on Phosphoria shale and report a similar retardation.[6]

The role of pressure in the generation of hydrocarbons has also been addressed theoretically by Perlovsky and Vinkovetsky[7] who presented a treatment involving an activated volume to suggest that increased pressure will retard the hydrocarbon generation reactions. In another theoretical paper, Neto[8] hypothesized that reactions only occur when reactants are within a critical distance between each other. He predicted a pressure dependence on the kinetics but did not quantify it.

Monthioux et al[9] studied the effect of reactor configuration, water, and pressure in the artificial maturation of coal. He found the effect of pressure (as well as water) to be minimal if the experiments were done in a confined system, with the pressure provided externally.

In an effort to elucidate the role of pressure in oil generation, we have done experiments to quantify the effect of pressure on the kinetics of maturation. Our approach was to quantify the pressure effect by determining an activated volume. We examined two shales: Bakken, a type II marine shale and Monterey, a type IIS

marine shale.

Experimental/Analytical

The samples to be heated were prepared in small gold tubes (~25mm long x 4mm O.D.) welded at one end before adding sample. Typically, 200 mg of ground shale were loaded into the tubes along with 25 mg sea water. The tubes were then welded shut under an argon atmosphere. The tubes were inserted into a pressure vessel and placed in a furnace. A thermocouple inserted in the end of the pressure vessel measured the temperature of the sample. It had been previously calibrated against a thermocouple inserted down the inside of the vessel. The vessel was then pressurized with argon causing the gold tube to collapse tightly around its contents. Experiments for a given shale were done varying the time, temperature, and pressure to which the sample was subjected. After heating, the samples were removed and the gold tubes punctured. The shale was removed and typically allowed to air dry, removing water and light hydrocarbons. The shale was then extracted using dichloromethane until the extract was visually colorless.

Conversion was defined based on Rock-Eval S_2 data:

$$\text{Conversion} = 1 - (S_2 \text{ (sample)} / S_2\text{(raw)})$$

The Rock-Eval parameters for the raw (initial, unheated) sample were also done on rock extracted by the above procedure.

Results

Bakken data

The results of a series of runs with the gold tubes at different pressures are shown in Figure 1, plotting S_2 and conversion versus pressure. The line is a quadratic best fit to the data.

In order to quantify the effect of pressure, we needed to put the data on a consistent kinetic basis. We chose to use a distributed, Gaussian activation energy functional form to fit the data. Data at 4000 psi were input to the Lawrence Livermore KINETICS[10] program. Figure 2 shows the fit obtained at 4000 psi allowing the program to optimize A, E, and s. Because we wanted to compare parameters as a function of pressure, the input values for the A factor and the breadth (standard deviation) of the distribution, s, were then fixed and not allowed to vary during subsequent optimizations at different pressures. Hence, we obtained as a function of pressure different activation energies. Figure 3 is a plot at high pressure showing an example of the fit obtained. Also included in Figure 3 is the sensitivity to a change in activation energy of 200 cal/mole. A total of more than 60 runs were made with the Bakken shale.

To quantify the effect of pressure for a reaction with rate constant k, one typically plots ln k versus PV_a/RT, where P is the system pressure, R the universal

gas constant and T is the absolute temperature.[11] The parameter V_a is the activated volume. It is the pressure analog to the Arrhenius activation energy and for simple or elementary reactions, represents the change in volume of the activated complex relative to the reactants. In more complex systems, as we have, the methodology is still valid but the activated volume is best thought of as a parameter which quantifies the pressure sensitivity of the system.

As we mentioned, we have reduced our kinetic data in the form of a distributed Gaussian activation energy. As the pressure is varied, we expect this distribution to shift, i.e., the center of the activation energy distribution, E, will vary with pressure. Because this activation energy tends to track ln k, we can relate E to the activated volume, V_a:

$$E = P V_a + E_o$$

where E is the center of the activation energy distribution determined from the kinetics program at a given pressure and E_o is the center of the distribution at very low pressures. Hence, we plot in Figure 4 the determined activation energy as a function of pressure. The solid line is a least squares fit through the Bakken data–the slope yields a value of 32.8 cc/mole for the activated volume of the Bakken.

What is conversion?

Conversion in these experiments is based on the S_2 peak in a Rock-Eval analysis after extraction. Hence, material which is very heavy yet soluble in methylene chloride is considered product and removed. This material would tend to increase S_2 if it weren't extracted. We did a series of experiments in which no extraction was done on the samples after reaction. In these experiments, we still define conversion as before, based on S_2, but now the reacted material contains those molecules (or pieces of kerogen) which have been released from the starting material but are very large, soluble molecules (as well as smaller product molecules which show up as S_1). During Rock-Eval, this material will decompose leading to a higher S_2 and hence lower calculated conversion. We constrain the data to have the same activation energy as the extracted case and determine a new A factor. The A factor for the unextracted runs at low pressure is 7.2×10^{15} sec^{-1} compared to the extracted case of 9.5×10^{16} sec^{-1}.

The effect of pressure for the unextracted case was examined at one high pressure (P = 25000 psi). Using the aforementioned methodology, we obtained an activated volume of 12.8 cc/mole.

Monterey data

To examine the dependence on kerogen type, we measured the pressure dependence of a high sulfur type IIS kerogen, a Monterey formation shale. The experiments were run as described earlier although only 14 runs were done and two

pressures were used. The KINETICS program determined the following parameters:

P= 2000 psi	P = 15000 psi
A =7.5 x 10^{15} sec^{-1}	
E = 54376 cal/mole	E = 54866 cal/mole
s = 3.46 %	

This led to an activated volume of 22.9 cc/mole as indicated in Figure 4.

Discussion

The activated volumes obtained in this work range from 13-33 cc/mole. Activated volumes are known for simple elementary free radical reactions, e.g., V_a for H-atom abstraction reactions range 10-20 cc/mole. For material as complex as kerogen, the authors are unaware of any measurements of activated volume for decomposition. Typical values for the activation volume in polymerization reactions are in the range – (15-25) cc/mole.[11] Because bonds are forming, the activation volumes are negative meaning the rates accelerate with increasing pressure. The polymerization reactions, however, are similar mechanistically in that they are free radical reactions involving initiation, propagation, and termination. It is reasonable to expect that the pyrolysis of kerogen (essentially a de-polymerization reaction) would have a similar, albeit positive, activation volume because of the similar kinds of reactions occurring. The activated volume we measured for the Bakken was 32.8 cc/mole and 22.8 cc/mole for the Monterey.

From Figure 4 for the Bakken, one can see that a pressure of 20000 psi would cause an activation energy increase of about 1 kcal/mole. If we assume that temperature would not effect the measured activated volume (determined around 300 °C) then it is valid to consider the effect of this on the maturation of kerogen at much lower temperatures. Figure 5 shows the effect a 1 kcal/mole difference between two kerogens would have under maturation conditions. We have taken the heating rate to be 1°/million years and have used the parameters obtained for the Bakken. At 50% conversion there is an offset of 7° between the two generation curves. This temperature offset is about the same as the extrapolation uncertainty from the determination of the high temperature rate constants. Hence the role of pressure is small. Note that Figure 1 indicates a significant change in S_2 as the pressure increases from 2000 to 30000psi. Although S_2, the amount of pyrolyzed volatiles expelled in Rock-Eval, increases over a factor of 2, the conversion only drops from around 80% to 58%. It is the conversion, not S_2, which is the important kinetic parameter. S_2 is a measure of what is still left behind unreacted and must be related to the initial or raw value to obtain the conversion.

The results of Sajgo et al and Price and Wenger would suggest an offset in

temperature of more than 35 ° when applied to a similar maturation situation. The discrepancy between these results and ours is disconcerting. We see a relatively minor effect with pressure whereas they see differences amounting to an increase of more than 5000 cal/mole in the activation energy at 15000 psi compared to 2000 psi. Sajgo et al examined lignite, a type III kerogen material whereas we have investigated types II and IIS. Price and Wenger examined the Phosphoria, a type IIS shale. We do not believe kerogen type is the cause of the differences. The reactor configuration used by Sajgo was quite different than our experimental apparatus. However, one set of our experiments was quite similar in configuration to that of Price and Wenger.

We have measured the activated volume for the pyrolysis of two shales We have done a large number of experiments in different configurations under a range of experimental conditions (in addition to those discussed here). Our results support our belief that pressures below 2 kbar (30000psi) play a minor role in kerogen pyrolysis.

References

1. Freund, H., Energy and Fuel, in press.
2. Dominé, F., Org. Geochem.,*1991*, v. 17, 619-634.
3. Teichmuller, M. and Teichmuller, R., in Coal and Coal-Bearing Strata, Murchison, D. and Westoll, T. S., editors, American Elsevier, New York, 1968.
4. McTavish, R. A., Nature, *1978*, v. 271,594-596.
5. Sajgo, C., McEvoy, J., Wolff, G. A., and Horvath, Z. A., Adv in Org. Geochem.,*1985*, v. 10, 331-337.
6. Price, L. C., and Wenger, L. M., Advances in Organic Geochemistry, *1991*, D. A. C. Manning, ed., 1992.
7. Perlovsky, L. I., and Vinkovetsky, Y. A., Bollettino di Geofisica Teorica ed Applicata, 1989, *v.* 31, 87-89.
8. Neto, C. C., Org. Geochem., *1991*, v. 17, 579-584.
9. Monthioux, M., Landais, P., and Monin, J., Org. Geochem., *1985*,, 275-292.
10. Braun, R. L. and Burnham, A.K., "Kinetics: A Computer Program to Analyze Chemical Reaction Data," Lawrence Livermore National Laboratory, Report UCID- 21588, Nov. 1988.
11. Isaacs, N. S., Liquid Phase High Pressure Chemistry, John Wiley & Sons, New York, 1981.

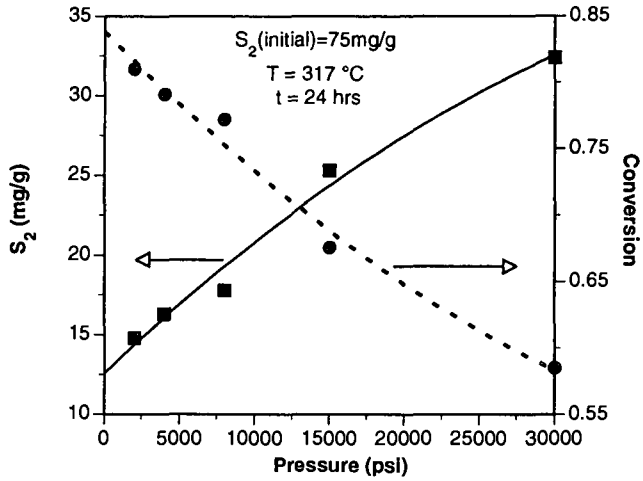

Figure 1. S_2 and conversion as a function of pressure.

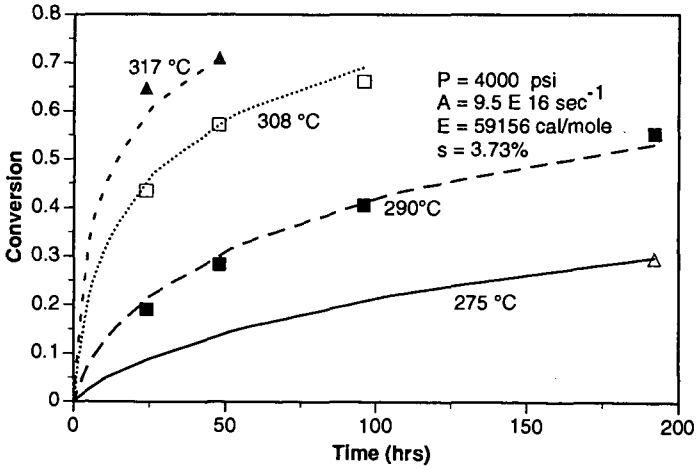

Figure 2. Determination of kinetic parameters using the KINETICS program. Curves are best fit to the experimental points by varying A, E, and s.

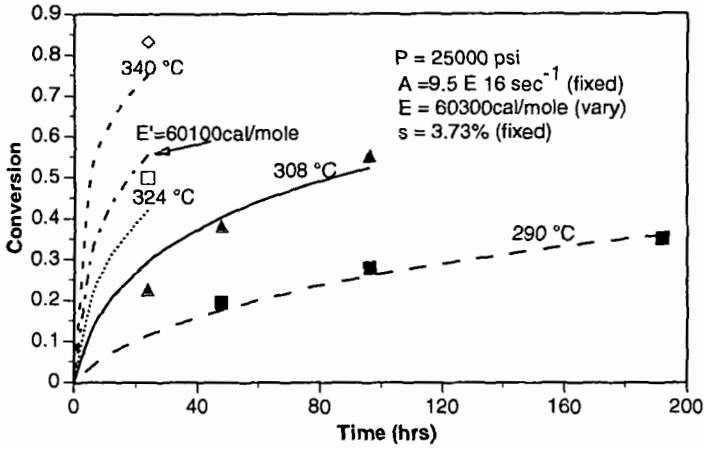

Figure 3. High pressure example of the fit obtained from the KINETICS program. Curves are fit to data varying only the activation energy. A and s are determined from the 4000 psi run. To get an idea of sensitivity, we also show for the 324°C case, a curve having the center of its activation energy distribution decreased by 200 cal/mole.

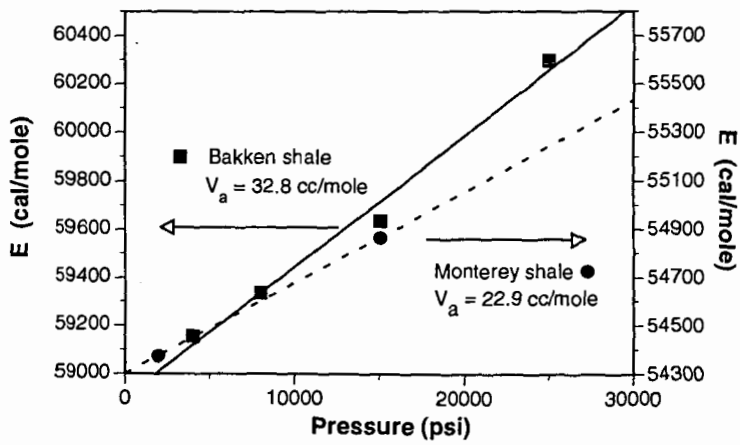

Figure 4. A plot of the center of the activation energy distribution, E, as a function of pressure. The temperature ranged from 250-360°C for the Bakken and from 270-300°C for the Monterey.

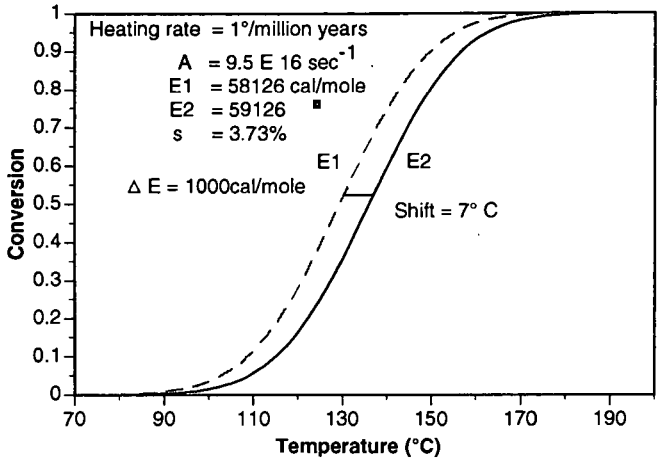

Figure 5. The effect of 1 kcal/mole on the kinetics of oil generation from kerogen.

BIARYL FORMATION AS A SOURCE OF HYDROGEN DURING PYROLYSIS OF RESID STRUCTURAL ELEMENTS

Donald F. McMillen, Jeffrey A. Manion, and Ripudaman Malhotra
Molecular Physics Laboratory, SRI International
333 Ravenswood Ave., Menlo Park, CA 94025-3493

Keywords: Coking, hydrous pyrolysis, PAH

ABSTRACT

The problems of formation of carbonaceous solids ("coke") during the processing of heavy petroleums and coal are clearly related to the formation of "excess" alkanes during hydrous or "confined" pyrolysis: in both cases the hydrogen needed to keep the ratio of alkanes/olefins high in the converted (i.e., volatile) aliphatic portions of the product streams must come primarily from the aromatic, or non-volatile, portions of the feed. In the first case, this transfer is undesirable because it forms coke; in the second case, it is (or "was") desirable because it increased the volatility and aliphatic nature of the petroleum pool during source rock maturation. In both cases, we have speculated that the formation of aryl-aryl coupling products is very likely a key step. In an effort to connect the dominant chemistry in these two contexts, we are performing experimental and mechanistic numerical model studies on selected structures as surrogates for the petroleum resid and kerogen components as well. One question of interest is how the presence of water in hydrous pyrolysis promotes the critical hydrogen transfer, particularly since the 118-kcal/mol O-H bond in water makes it very difficult for water to participate in any radical-chain hydrogen transfer pathways. Initial results are in accord with this reservation in that the presence of supercritical water, up to a fluid density of 0.4 g/cc, did not enhance the redistribution of hydrogen to produce more volatile alkanes.

INTRODUCTION

Hydrogen redistribution among feedstock components or structural elements is key to both the conversion of vacuum resids to distillate materials, and also to the formation of volatile fractions during hydrous pyrolysis. In the case of resid hydroprocessing, there is a well-appreciated tendency for some of the hydrogen required for bond scission and radical-capping to come from coke intermediates, thus propelling the formation of coke. This tendency toward disproportionation is well understood in thermodynamic terms, being due to the respective stabilities of methane and graphite. However, it is poorly understood in terms of the kinetic factors controlling its rate. The goal in catalytic hydroprocessing of resids is of course to ameliorate this tendency to the maximum extent practical through the use of catalysts and hydrogen pressure.

Hydrous pyrolysis of oil shale and other types of kerogen is presumably driven by a similar tendency for the kerogen structure to disproportionate into a hydrogen-rich volatile portion and a hydrogen-poor less-volatile portion. The presence of liquid phase (or dense supercritical fluid phase) water during the hydrous- or confined- pyrolysis is known to markedly increase the alkane/alkene ratio in the volatile products.[1-3] Since the evidence appears to indicate that water does not serve as the principal source of additional hydrogen in the volatile products, the additional hydrogen must be coming, as in the resid hydroprocessing case, from the organic matrix itself. Our basic premise is that the hydrogen-transfer chemistry in these two cases is closely related. Accepting that premise as a working hypothesis, the pertinent question then becomes, "From what structures and by what chemical mechanisms does this hydrogen come, and how might water influence that transfer?"

It is well known that petroleum residua consist basically of large polycyclic aromatic (PAH) clusters to which are attached a number of aliphatic chains. It is also generally appreciated that the problem of resid hydroprocessing is not primarily one of cracking off the alkyl chains, which occurs rather readily (even the absence of H_2 and a catalyst)[4-6], but one of doing so without having

the PAH form carbonaceous solids that foul the catalyst, coat reactor surfaces, and build aggregates that interfere with fluid bed operation. Nevertheless, prior to 1989, the open literature contained only one report[7] of the behavior of long-chain alkylaromatics other than of alkyl benzenes[8] or alkylpyridines.[9] On the basis of pyrolysis at high temperatures (ca. 800°C), Billaud et al. concluded that the pyrolysis pathways were independent of the number of rings in the PAH.[7] However, in work first reported in 1988, Savage and coworkers[10-12] showed that the conclusions of Billaud et al. definitely *do not* apply to pyrolysis at lower temperatures, particularly to the 350-450°C range relevant to resid hydroprocessing and hydrous- or confined- pyrolysis. Their experiments demonstrate very clearly that the ease of bond cleavage at the alkyl-aryl junction (i.e., ipso displacement) depends very markedly on the number and arrangement of rings in the PAH, ranging from extremely slow for alkylbenzenes to very fast for certain pyrenyl, anthryl, chrysyl, and perylenyl derivatives. For these PAH, the ispo displacement is so facile that it is often the dominant reaction in pyrolysis of the neat alkylaromatic (that is, even in the absence of a hydro-aromatic or other "intended" hydrogen-transfer agent). The relative ease of this ipso-displacement is also completely consistent with findings on the relative ease of hydrogen transfer to these same categories of structures under donor-solvent coal liquefaction conditions.[13-15] The purpose of this presentation is to address the question of where the hydrogen comes from and how it arrives at the ipso position of these alkylaromatics.

EXPERIMENTAL

Procedures. Pyrolysis experiments were carried out in evacuated fused silica ampoules. The sealed tube and an appropriate quantity of solvent for pressure equalization was placed in an outer jacket of stainless steel tubing capped with compression fittings. The reaction vessel was then immersed in a temperature-controlled molten-salt bath for the desired time, the tube removed and quenched in water. After cooling in liquid nitrogen to condense CO_2 and volatile organics, the ampoule was opened and the sample removed by pipet and repeated washing of the tube with solvent. An internal standard was added and the sample analyzed by capillary gas chromatography with flame ionization and/or mass selective detection. Quantitation was obtained using the FID analyses with molar responses determined separately for those compounds for which we had authentic samples and estimated by comparison with similar species when no sample was available. Generally, at least three split injections of each sample were performed using an autoinjector. For most species the reproducibility was within ± 2% and we estimate the overall analytical accuracy to be within ± 5%. The reaction mixtures were also analyzed by field ionization mass spectrometry (FIMS), using SRI's magnetic sector FIMS instrument, in order to assess the polyaryls and other low volatility products.

Chemicals. n-Hexadecylpyrene (99+% by GC analysis), was obtained from Molecular Probes, Inc. of Eugene, Oregon. Biphenyl was obtained from Aldrich Chemical Co. Toluene used for GC analyses was Malinkrodt reagant grade. These materials were used without further purification. Tetrahydrofuran was used without stabilizer and distilled daily from sodium acetonylacetonate. The added-water pyrolyses employed deionized, low-conductivity water.

RESULTS

Initial pyrolysis experiments with n-hexadecylpyrene were conducted under conditions similar to those used by Savage and coworkers and the products analyzed by GC-MS and FIMS. Subsequently, we performed some experiments with added (supercritical) water. To facilitate comparison, Table 1 gives summary figures relating to the balance of hydrogen, and aromatic and aliphatic carbon for the pyrolysis of 1-dodecylpyrene calculated from the data of Savage and coworkers[11] along with findings from our study.

Perhaps the most striking observation in these and other data of Savage is the very high alkane/alkene ratio in the reported products, particularly at large extents of reaction. It is also clear from these data there is a shortage (in the GC-MS analyzable products) of pyrene rings and of

hydrogen-deficient materials. Evidently, non-volatile, hydrogen-deficient, pyrene-containing products (aka char) have been generated in the course of converting radicals and olefins (produced from ipso-displacement and Rice-Herzfeld alkyl chain scission) into alkanes. The high alkane/alkene ratio, in the absence of an external source of hydrogen, is strikingly reminiscent of the ratios reported by Lewan[1] and others for hydrous pyrolysis of shale kerogen.

Reaction Rates and Hydrogen Balance. The defined first order rate constant (for alkylpyrene disappearance) from the 90-minute quartz ampoule pyrolysis is only about 1/8 of that obtained by Savage[11] in a stainless steel reactor after reaction for the same time. The rate constant derived from the 513-minute run is about three times higher. This increase in first-order rate constant is consistent with the auotcatalysis described in reference 11, although it is difficult at this point to precisely compare the degree of autocatalysis in the two reactor types. The product distributions are quite similar, with there again being a marked excess of alkanes over alkenes and a substantial shortage of pyrene-containing products at higher extents of reaction. The extent of this excess and shortage are shown in Table 1. The mol % yield of alkanes is numerically equivalent to the mol % of "extra" hydrogen required to produce cleaved and reduced (non-olefinic) products. As the conversion of the alkyipyrenes approaches 90%, the yield of extra hydrogen in the reduced products can also approach 90%, meaning that out of every ten original alkylpyrenes that have disappeared, there have been nine chain cleavages that have utilized this extra hydrogen coming from somewhere. Savage and coworkers pointed out this hydrogen imbalance,[11] but were unable to address with GC-MS the nature of the incipient "char" that was presumably providing the hydrogen.

The last two columns in Table 1 show the products obtained when water was included in the reaction mixture along with the organic substrate (at ca. 0.1 and 0.4 g/cc supercritical fluid density). As indicated above, the question of interest here was whether the addition of water would accelerate the formation of those oxidized products whose generation supplies hydrogen (and therefore accelerates cleavage and reduction). The data in Columns 7 and 8 clearly indicate that this was *not* the case. In fact, there was a consistent and progressive *decrease* in the alkane/alkene ratios seen in the aliphatic products, as reflected by 45 and 80% drops in the overall alkane/alkene ratio shown for the two water runs in Table 1. Thus, the effect of water under these conditions has not only *not* been to increase cleavage and reduction, but to make the volatile products more oxidized (olefinic).

Assuming our originally postulated connection between alkylpyrene pyrolysis and hydrous pyrolysis really does exist, the reason why water failed to accelerate cleavage is likely that here there are virtually no ionic species, other than those provided by the autoionization of the water itself. There is neither the mineral matter, nor the organic heteroatom species, nor the stainless steel surfaces generally present in hydrous pyrolysis of oil shale and other kerogens. In fact, the pyrolysis of alkylpyrenes in fused silica ampoules represents the extreme in terms of a "kerogen surrogate" free from any ionic or polar species that may be contributing to the marked effects that water has in hydrous pyrolysis. It does make sense, after all, that if water as a polar medium and ionic reactant is to somehow help connect the ionic reaction manifold to the radical reaction manifold, this will likely require not only fluid densities approaching normal liquid densities[16] (i.e., above ca. 0.3 g/cc) but also the presence of polar species and redox agents. Accordingly, experiments are now underway to see if any of these factors will enable water to accelerate the redistribution of hydrogen and enhance the production of reduced ipso-displaced products during alkylpyrene pyrolysis.

Identity of the Sources of Extra Hydrogen. Savage describes an acetone-insoluble, toluene-soluble non-elutable "char" as the probable source of the hydrogen that produces high alkane/alkene product ratios. The major elutable unidentified product reported by these workers[11] was a material whose presumed molecular ion was reported as m/z 242. Based upon recent field ionization mass spectrometric analyses we have performed on Wilsonville coal liquefaction resids in conjunction with Consolidation Coal Co.[17], and also on earlier HPLC-FIMS analyses of petroleum-resid-derived vacuum gas oils reported by Sullivan et al.,[18] we can identify m/z 242 as the odd-carbon aromatic derived from pyrene by completion of a $-CH_2CH_2CH_2-$ bridge between

the 1- and the 10- positions.. As an analog of phenalene ($C_{13}H_{12}$) it is an odd-carbon molecule that would have to lose three hydrogens to be fully aromatic, it cannot form a closed shell fully aromatic PAH. However, the radical species formed when three hydrogens are lost is among the most stable of all radicals, and earlier esr studies have found it to be common in thermally processed petroleums *even at room temperature*.

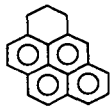

m/z 242

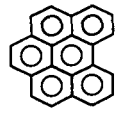

Benzo[ghi]perylene, m/z 276

From our recent analyses of Wilsonville coal-derived resids,[17] it is apparent that m/z 242 is a commonly recurring PAH structure that builds up during catalytic processing. How important it actually is as a step in the ring-growth processes that lead to still larger PAH and eventually char is a critical question, the answer to which has not yet appeared in the literature. However, a partial answer appears here in the form of a second important higher molecular weight product we have detected. At longer reaction times the molar yield of this product approaches 3%, and, from its apparent molecular ion at m/z 276, this product can be identified as benzo[ghi]perylene. Although not previously reported in alkyl pyrene pyrolysis,[10-12] this PAH has been found to be prominent in coal- and petroleum- derived resids and to be correlated with increased problems of coke formation.[18] Benzoperylene could conceivably be formed from the original 1-alkyl pyrene by two successive ring closures, as shown below, proceeding through an intermediate having the m/z 242 ring system.

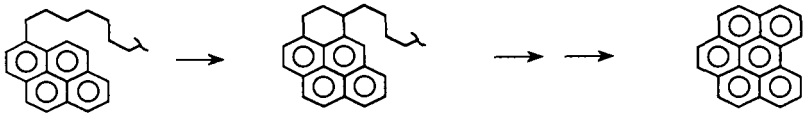

Thus it begins to appear that the phenalene-type structure represented by m/z 242 is in fact important in the ring-growth processes by which higher PAH and eventually char are produced. Benzoperylene (m/z 276) represents five degrees of unsaturation beyond pyrene. Taken together with cleavage of the residual alkyl chain, the net result is the freeing of four units of 2(H) for the production of reduced and cleaved products. For the 513 min run in Table 1, the formation of the single product at m/z 276 accounts for a significant minority of the extra hydrogen made available: the yield of benzo[ghi]perylene represents about 11 percentage points of the 85 mol% of 2(H) generated by "char-forming" reactions.

The operation of ring-growth mechanisms that involve attachment and cylization of alkyl fragments is of course not the only way of generating the larger PAH that eventually become char. The formation of biaryls and their ring-closure (e.g. naphthalene to binaphthyl to perylene) represents passing from pre-existing aromatics to much larger PAH in a minimum number of steps. Furthermore, given that biaryl bonds are the strongest C-C single bonds that can be formed in hydrocarbons, the formation of biaryls can be expected to be very facile *once* aryl radicals have been generated.[19] In contrast, one rather expects that alkylation and cyclization would become much more facile in the presence of acidic catalysts.[20] Hence, we expected in these pure hydrocarbon pyrolyses to find biaryls as the major oxidation products.

We subjected one of the product mixtures from ethylpyrene pyrolysis (supplied to us by Savage) to FIMS analysis to assess the formation of biaryls (which are not analyzable by capillary GC). The spectrum from this analysis is presented in Figure 1. Even though the extent of reaction in this case was only about 35% and the yield of pyrene is only about 5%, the peaks for dimers and

trimers of ethylpyrene are clearly visible. In contrast, the peak at m/z 242 is barely above background and there is no peak visible at m/z 276. Thus it would appear that under these nominally non-ionic conditions, biaryl formation is indeed a more important source of hydrogen than alkylation and ring-closure processes.

FIMS analysis of the 513-minute reaction product (sample from Row 6 in Table 1) does not show such clear presence of biaryls, presumably because rather than having dimer intensity primarily at three masses (2(230) - 2, 2(230) - 2 + 28, and 2(230) - 2 - 28) as in Figure 1, the class of dimers will be distributed over at least 32 different masses.(i.e., m/z = 2(426) - 2 and any mass containing from one to 32 fewer side chain carbons). However, the ring-building species at m/z 240, 242, and 276, and are clearly visible, together with modest amounts of the corresponding 276-alkylation products up to the C_{17} analog. These alkylation products of benzoperylene, in sum, essentially double to about 20 percentage points the extra hydrogen supplied through the formation of all benzo[ghi]perylene species. Thus, both biaryl formation and ring-building processes can each be seen, under different circumstances, to supply substantial percentages of the hydrogen used for ring closure and olefin reduction.

SUMMARY

Pyrolysis of long chain alkylpyrenes at 400°C in fused silica ampoules yields a product distribution and autocatalytic behavior very similar to that detailed by Savage for reaction in stainless steel microreactors, but at about an 8-fold lower rate. The hydrogen needed for the ipso-displacement bond cleavage and for reduction of olefinic products is indeed supplied by the generation of heavy materials. From GC-MS and FIMS analysis, we find both ring-growth and poly-aryl products to be significant sources of this "extra" hydrogen. Some of these ring-growth products, particularly the odd-carbon phenalene analog at m/z 242 and benzo(g,h,i)perylene at m/z 276 have been previously correlated with buildup of coke and refractory resids during catalytic hydrporcessing of heavy petroleums and coal-derived liquids. Somewhat surprisingly, we do *not* find that the addition of supercritical water, at least up to a fluid density of 0.4 g/cc, enhances the formation of biaryls and thereby enhances this supply of extra hydrogen. This observation leads to the tentative conclusion that the interaction of water and the organic matrix that commonly leads to an enrichment in volatile hydrocarbons during hydrous pyrolysis must depend upon the presence of ionic or polar species that are not present during pure hydrocarbon pyrolyses in fused silica. We anticipate that extension of these studies will yield important information on factors controlling coke formation during processing of residual oils as well as on the chemistry responsible for alkane enrichment during hydrous pyrolysis.

ACKNOWLEDGMENTS

The authors wish to acknowledge the Support of the U.S. Department of Energy under Contract No. DE-AC22-91PC91044 and also to thank Drs. Phillip E. Savage and C. Michael Smith for permission to publish the FIMS spectrum in Figure 1.

REFERENCES

1. Lewan, M. D., "Laboratory Simulation of Petroleum Formation: Hydrous Pyrolysis," in *Organic Geochemistry*, eds. M. H. Engel and S. A. Macko, Plenum Publishing Corp., New York, 1989.
2. Hoering, T. C. *Org. Geochem.*, **1984**, *5*, 267.
3. Larter, S. R.; Douglas, A. G. *J. Anal. Appl.Pyrolysis* **1982**, *4*, 1.
4. Khorasheh, F.; Rangwala, H. A.; Gray, M. R.; Dalla Lana, I. G., *Energy and Fuels*, **1989**, *3*, 716.
5. Savage, P. E.; Klein, M. T.; Kukes, S. G., *Energy and Fuels*, **1988**, *2*, 619.

6. Miki, Y.; Yamadaya, S.; Oba, M.; Sugimoto, Y., *J. Catal.*, **1983**, *83*, 371.
7. Billaud, F.; Chaverot, P.; Berthelin, M.; Freund, E. *Ind. Eng. Chem. Res.* **1988**, *27*, 1529.
8. Savage. P. E.; Klein, M. T. *Ind. Eng. Chem. Res.* **1987**, *26*, 488.
9. Mushrush, G. W.; Hazlett, R. N.*Ind. Eng. Chem. Fundam.* **1984**, *23*, 288.
10. Javanmardian, M.; Smith, P. J.; Savage, P. E. *Am. Chem. Soc. Div. Fuel Chem. Preprints* **1988**, *33*(2), 242.
11. Savage, P. E.; Jacobs, G. E.; Javanmardian, M. *Ind. Eng. Chem. Res.* **1989**, *28*, 645.
12. Smith, C. M.; Savage, P. E. *Ind. Eng. Chem. Res.* **1991**, *30*, 331, and other references cited therein.
13. McMillen, D. F.; Malhotra, R.; Chang, S. -J.; Fleming, R. H.; Ogier, W. C.; Nigenda, S. E., *Fuel* **1987**, *66*, 1611.
14. Malhotra, R.; McMillen, D. F. *Energy Fuels* **1990**, *4*, 184.
15. Futamura, S.; Koyanagi, S.; Kamiya, Y. *Fuel*, **1988**, *67*, 1436.
16. Penninger, J. M. L.; Kolmschate, J. M. M. "Chemistry of Methoxynaphthalene in Supercritical Water," in *Supercritical Fluid Science and Technology*, Am. Chem. Soc. Symposium Series, 242.
17. Malhotra, R.; McMillen, D. F.; Huestis, D. L. *Am. Chem. Soc. Div. Fuel Chem. Preprints* **1992**, *37*(2), 908.
18. Sullivan, R. F.; Boduszynski, M. M.; Fetzer, J. C.*Energy &Fuels* **1989** *3*, 603.
19. Fahr, A.; Stein, S. E., *J. Phys. Chem.* **1988**, *92*, 4951.
20. Langlois, G. E.; Sullivan, R. F.; "Chemistry of Hydrocracking," in *Refining Petroleum for Chemicals*, L. J. Spillane, H. P. Leftin, Eds.; Advances in Chemistry, 97; American Chemical Society, Washington, DC, 1970, p. 38.

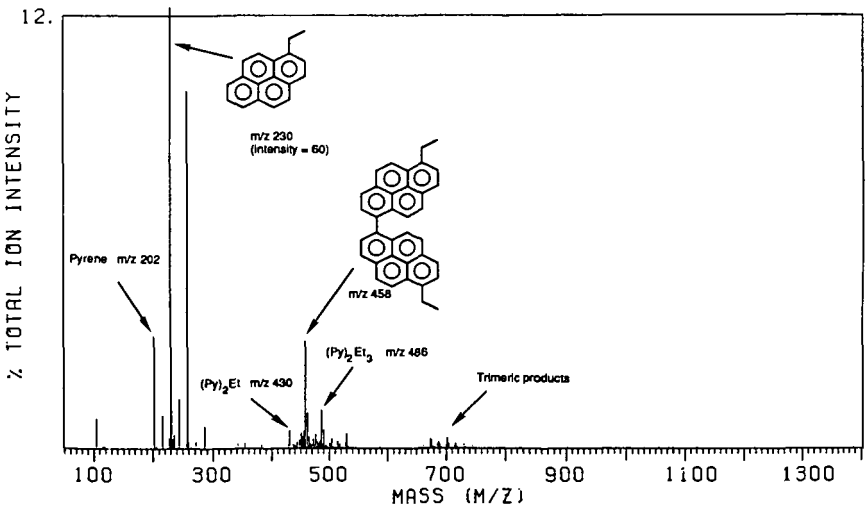

Figure 1. Mass spectrum of a moderate-conversion 1-ethylpyrene pyrolysis product mixture.

Table 1

Comparison of literature and current data on the pyrolysis of long chain alkylpyrenes.

	Literature Data[a]			Current Results[b]			
Time (min)	30	90	180	90	513	90	90
Water density (g/cc)	–	–	–	–	–	0.12	0.40
10^4 Defined k_1 (s^{-1})	1.39	1.84	2.62	0.24	0.60	0.25	0.31
Products (mol%)							
Pyrene	0.74	20.7	43.5	1.91	52.9	1.41	0.28
Me-Pyrene	2.86	6.62	8.38	5.47	9.64	6.04	6.19
Et-Pyrene	1.90	2.08	2.68	1.55	2.35	2.64	1.50
Vinyl-Pyrene	c	c	c	0.033	<0.02	0.14	1.96
Σ(Pyrenes)	82.6	71.9	65.8	Unk	Unk	Unk	Unk
Σ(Identified Pyrene Products)	4.8	34.8	59.9	11.9[d]	80.3[d]	12.4[d]	15.4[e]
Σ(Alkanes)[f,g]	>1.94	>23.5	>54.9	>6.49	>85.14	>5.34	>2.19
Σ(Alkenes)[f]	>2.37	4.60>	>2.61	>4.47	>0.66	>6.74	7.66
Alkanes/Alkenes	0.81	4.60	19.5	1.45	128	0.79	0.29
Excess mols of 2(H)[g]	1.0	24.0	52.3	3.5	77.7	1.9	1.14

a Pyrolysis of 1-dodecylpyrene/biphenyl mixtures at 400°C in stainless steel reactors, Ref. 11.

b Pyrolysis of 1-hexadecylpyrene/biphenyl mixtures at 400°C in quartz ampoules.

c Not reported but stated to be very small due to rapid hydrogenation to ethylpyrene.

d Includes pyrenes with alkyl chain lengths up to C_{12} and selected ring-closure products.

e Includes pyrenes with alkyl chain lengths up to C_{15} and selected ring-closure products.

f Includes aliphatic products from C_8 to C_{16}.

g The mol % yield of alkanes is numerically equivalent to the mol % of excess hydrogen required to produce cleaved non-olefinic products

WATER AS A SOURCE OF HYDROGEN AND OXYGEN IN PETROLEUM FORMATION BY HYDROUS PYROLYSIS

M. D. Lewan
U.S. Geological Survey
Box 25046, MS 977
Denver Federal Center
Denver, CO 80225

The importance of water in laboratory experiments designed to understand natural processes is well documented in the studies of granite melts (Goranson, 1932; Tuttle and Bowen, 1958), metamorphic reactions (Winkler, 1974, p. 15; Rumble et al., 1982; Ferry, 1983), coal formation (Berl and Schmidt, 1932; and Schuhmacher et al., 1960), and clay mineral diagenesis (Whitney, 1990). Prior to 1979, organic geochemists did not fully appreciate the ubiquity of water in sedimentary basins and its role in petroleum formation. A notable exception is the work by Jurg and Eisma (1964). Noting difference in the thermal decomposition of behenic acid in the presence and absence of liquid water, these investigators suggested that water played an important role in petroleum formation. Although a subsequent study in 1969 by Brooks and Smith employed water in laboratory simulations of petroleum generation from coals, laboratory experiments over the next decade did not consider the role of water in petroleum formation (e.g., Tissot et al., 1974; Larter et al., 1977, Harwood, 1977). Lewan and others (1979) reported that heating organic-rich rocks submerged in liquid water resulted in the generation and expulsion of a free-flowing oil that accumulated on the water surface above the submerged rock. Physically, chemically, and isotopically this expelled oil pyrolyzate was similar to natural crude oils. This experimental approach was referred to as hydrous pyrolysis. Although hydrous pyrolysis has since been shown to provide useful information on primary migration, stages and kinetics of petroleum generation, and thermal maturity indices (Lewan, 1983, 1985, 1987; Winters et all., 1983; Lewan et al., 1986), the actual role of water in petroleum formation has not been determined.

In order to better understand the role of water in petroleum formation, a series of pyrolysis experiments were conducted on aliquots of a sample of Woodford Shale under hydrous and anhydrous conditions. The experiments involved isothermally heating 400 g of thermally immature, gravel-sized (0.5-2.0 cm) rock in one-liter stainless steel-316 reactors at 300°, 330° and 350°C for 72 hours. Hydrous experiments included 320 g of deionized water and 241 kPa of helium in the headspace. No water was added to the anhydrous experiments and the head space was evacuated at the start of the experiment. The experiments were conducted at these three temperatures for 72 hours because previous experiments with Woodford Shale showed that the two overall reactions responsible for petroleum formation occur in part over these conditions. The first overall reaction occurs at temperatures below 330°C for 72-hour experiments, and involves the cleavage of

weak noncovalent bonds in the kerogen to form a soluble, high-molecular-weight tarry bitumen (kerogen to bitumen). This bitumen impregnates the ground mass of the rock to form a continuous organic network. The second overall reaction occurs at temperatures from 330°C to 350°C for 72-hour experiments, and involves the cleavage of covalent bonds in the bitumen to form an immiscible oil that is expelled from the organic network in the rock (bitumen to oil).

Pyrolyzate yields from these comparative experiments are given in Table 1 in terms of generated gas, expelled oil, bitumen extract, and total pyrolyzate (i.e., gas + oil + bitumen). The most obvious difference is the total lack of expelled oil in the anhydrous experiments, with no signs of oil droplets or an oily film on the surfaces of the rock chips. At 300°C for 72 hours, only a small amount of expelled oil is generated in the hydrous experiment and the amount of total pyrolyzate generated is essentially the same in the hydrous and anhydrous experiments. Partial decomposition of kerogen to bitumen predominates at this time-temperature condition and the presence of water appears to have no significant effect on this overall reaction. However, distinct differences in the amounts of total pyrolyzate are evident in the 330°C and 350°C experiments (Table 1), which represent conditions for the partial decomposition of bitumen to oil. Amounts of total pyrolysate and bitumen decrease significantly under anhydrous conditions, but the amount of bitumen decreases to a lesser extent and the amount of total pyrolyzate increases under hydrous conditions. These results indicate that bitumen degrades to an insoluble pyrobitumen under anhydrous conditions, while it decomposes to an expellable immiscible oil under hydrous conditions.

Another difference between the hydrous and anhydrous experiments is the significantly higher amounts of CO_2 generated by the former. Table 2 shows the total amount of aqueous and gaseous CO_2 to be one order of magnitude higher under hydrous conditions than under anhydrous conditions at 350°C for 72 hours. Mass balance calculations for the loss of oxygen from kerogen at 350°C for 72 hours indicate that under hydrous conditions the kerogen oxygen accounts for only 64 percent of the oxygen in the generated CO_2. The lack of carbonate minerals in the original rock implicates H_2O as the source of the excess oxygen in the generation of CO_2 under hydrous conditions. Several reactions, including gas-shift reactions, have been considered to explain this excess oxygen, and the most feasible reaction appears to be oxidation of carbonyl groups in the kerogen or bitumen by H_2O. A working hypothesis envisages formation of carboxylic intermediates that are decarboxylated with increasing thermal stress to generate CO_2.

Regardless of the specific mechanism responsible for H_2O to act as a source of the excess oxygen generated as CO_2, the remaining hydrogen from the reacted H_2O would be available for terminating free radical sites. This source of hydrogen is supported by a hydrous pyrolysis experiment that was conducted on the Woodford Shale at 330°C for 72 hours with D_2O instead of water. Deuterium-NMR analyses of the pyrolyzate products from this experiment showed that the expelled immiscible

oil as well as the bitumen and kerogen retained in the rock contained significant quantities of deuterium. Quantification of the deuterium content of the isolated kerogen was not performed, but the NMR spectrum was typical for powdered solids containing deuterium. Quantification of the deuterium content of the oil and bitumen was determined from the NMR analyses with an internal standard of deuterated dichloromethane. Assuming hydrogen contents of 13 wt. % for undeuterated oil and 10 wt. % for undeuterated bitumen, dueterium substitution for hydrogen is approximately 40% for the expelled oil and 33% for the extracted bitumen in the D_2O experiment. This high degree of deuterium substitution is interpreted to be the result of free radical sites being terminated by deuterium atoms derived from the oxidation of carbonyl groups by D_2O.

The ability of hydrous pyrolysis to generate an expelled oil while anhydrous pyrolysis generates a pyrobitumen may be explained by differences in the availability of hydrogen and type of free-radical terminations that occur during bitumen decomposition. Figure 1 diagramatically presents a working hypothesis for hydrous and anhydrous reaction pathways involving a hypothetical bitumen molecule (Figure 1a) subjected to a barrage of extraneous free radicals thermally generated from other bitumen molecules or the kerogen (Figure 1b). Under hydrous conditions, the free radical sites formed on the bitumen molecule by encounters with incoming free-radicals are frequently terminated with water derived hydrogen (Figure 1c) before β-sission in the molecule occurs. Free-radical fragments that do occur by the infrequent β-sissions are also frequently terminated by water-derived hydrogen (Figure 1d). As a result, a liquid oil is generated. H_2O in this reaction pathway occurs as a dissolved species in the bitumen that impregnates the rock. Although the solubility of hydrocarbons in water is low, the solubility of water in hydrocarbons is two orders of magnitude higher. This solubility is sufficient to supply H_2O for the proposed reactions within the bitumen impregnated rock (Lewan, 1992). Dissolved water in the bitumen network of the rock is maintained at a fully saturated level by the water surrounding the rock in the reactor. Lewan (1992) proposes that this H_2O-saturated bitumen is also responsible for the development of an oil that is immiscible in the bitumen network of the rock. Under anhydrous conditions, the lack of water-derived hydrogen for terminating free-radical sites that occur on the bitumen molecule results in frequent β-sissions (Figure 1e). The numerous free-radical fragments that consequently occur are also deprived of terminations by water-derived hydrogen, and resort to termination by recombination with other free radical sites on the bitumen molecule or on neighboring molecular fragments (1f). In a closed pyrolysis system, these carbon-carbon bond terminations result in the formation of pyrobitumen through the development of a highly cross-linked structure that aromatizes through disproportionation.

REFERENCES

Berl, E., and Schmidt, A., 1932, Über die Entstehung der Kohlen, II. Die Inkohlung von Cellulose and Lignin in neutralem Medium, *Ann. der Chemie* 493:97.

Brooks, J. D., and Smith, J. W., 1969, The diagenesis of plant lipids during the formtion of coal, petroleum, and natural gas - II. Coalification and the formation of oil and gas in the Gippsland Basin, *Geochim. Cosmochim. Acta* 33:1183.

Butler, J. N., 1982, *Carbon Dioxide Equilibria and Their Applications*, Addison-Wesley, London, 259p.

Ferry, J. M., 1983, Regional metamorphism of the Vassalboro Formation, south-central Maine, U.S.A.: A case study of the role of fluid in metamorphic petrogenesis. *J. Geol. Soc.* London 140-551.

Goranson, R. W., 1932, Some notes on the melting of granite, *Am. Jour. Sci.*, 23:227.

Harwood, R. J., 1977, Oil and gas generation by laboratory pyrolysis of kerogen. *Am. Assoc. Petrol. Geol. Bull.* 61:2082.

Jurg, J. W., and Eisma, E., 1964, Petroleum Hydrocarbons: Generation from fatty acid. *Science* 144:451.

Larter, S. R., Horsfield, B., and Douglas, A. G., 1977, Pyrolysis as a possible means of determining petroleum generating potential of sedimentary organic matter, *in*: *Analytical Pyrolysis*, (C. E. R. Jones and C. A. Cramers, eds.), Elsevier, Amsterdam, pp. 189-202.

Lewan, M. D., 1983, Effects of thermal maturation on stable organic carbon isotopes as determined by hydrous pyrolysis of Woodford Shale, *Geochim. Cosmochim. Acta* 47:1471.

Lewan, M. D., 1985, Evaluation of petroleum generation by hydrous pyrolysis experimentation, *Phil. Trans. Roy. Soc. Lond.* A315-123.

Lewan, M. D., 1987, Petrographic study of primary petroleum migration in the Woodford Shale and related rock units, *in*: *Migration of Hydrocarbons in Sedimentary Basins* (B. Doligez, ed.), Editions Technip. Páris, pp. 113-130.

Lewan, M. D., 1992, Primary oil migration and expulsion as determined by hydrous pyrolysis, *13th World Petroleum Congress Proceedings*, Topic 3 (in press).

Lewan, M. D., Bjorøy, M., and Dolcater, D. L., 1986, Effects of thermal maturation on steroid hydrocarbons as determined by hydrous pyrolysis of Phosphoria Retort Shale, *Geochim. Cosmochim. Acta* 50:1977.

Lewan, M. D., Winters, J. C., and McDonald, J. H., 1979, Generation of oil-like pyrolyzates from organic-rich shales, *Science* 203:897.

Rumble, D., III, Ferry, J. M., Hoering, T. C., and Boucot, A. J., 1982, Fluid flow during metamorphism at the Beaver Brook fossil locality, New Hampshire, *Am. Jour. Sci.* 292-886.

Schuhmacher, J. P., Huntjens, F. J., and van Krevelen, D. W., 1960, Chemical structure and properties of coal XXVI. Studies on artificial coalificaiton, *Fuel* 39:223.

Tissot, B., Durand, B., Espitalié, J., and Combaz, A., 1974, Influence of nature and diagenesis of organic matter in formation of petroleum, *Am. Assoc. Petrol. Geol.* 58:499.

Tuttle, O. F., and Bowen, N. L., 1958, Origin of granite in the light of experimental studies in the system $NaAlSi_3O_8$-$KAlSi_3O_8$-SiO_2-H_2O, *Geol. Soc. Am. Mem,.* 74.

Whitney, G., 1990, Role of water in the smectite-to-illite reaction, *Clays and Clay Minerals* 38:343.

Winkler,. G. F., 1974, *Petrogenesis of Metamorphic Rocks,* 3rd ed., Springer-Verlag, New York.

Winters, J. C., Williams, J. A., and Lewan, M. D., 1983, A laboratory study of petroleum generation by hydrous pyrolysis, *in: Advances in Organic Geochemistry, 1981* (M. Bjorøy, ed.) John Wiley & Sons, New York, pp. 524-533.

Table 1. Comparison of pyrolyzate yields from hydrous and anhydrous pyrolysis of crushed aliquots (0.5-2.0 cm) of an immature sample of Woodford Shale (WD-26). All of the experiments were conducted with 400g of rock in one-liter stainless steel-316 reactors.

Experimental Conditions (temp./time)	Generated Gas (wt. % of rock)	Expelled Oil (wt. % of rock)	Bitumen Extract (wt. % of rock)	Total Pyrolyzate[1] (wt. % of rock)
300°C/72 hr				
Hydrous[2]	**0.43**	**0.65**	**8.35**	**9.43**
Anhydrous3	0.78	0.00	8.66	9.44
Δ%	-81.4	+100.0	-3.7	-0.1
330°C/72 hr				
Hydrous[2]	**1.05**	**2.79**	**8.19**	**12.03**
Anhydrous3	1.74	0.00	6.62	8.36
Δ%	-65.7	+100.0	+19.2	+30.5
350°C/72 hr				
Hydrous[2]	**1.68**	**4.15**	**5.71**	**11.54**
Anhydrous[3]	2.40	0.00	3.30	5.70
Δ%	-42.9	+100.0	+42.2	+50.6

$$\Delta\% = [(\text{Hydrous-Anhydrous})/\text{Hydrous}] \times 100$$

[1]Total pyrolyzate = generated gas + expelled oil + bitumen extract.

[2]Crushed rock with 320g of deionized (ASTM type I) water under an initial He pressure of 241 kPa.

[3]Crushed rock initially in an evacuated reactor.

Table 2. Millimoles of headspace gas (g) and dissolved aqueous gas (aq) generated from 400 grams of Woodford Shale sample WD-26. Total gas quantities do not include species dissolved in expelled oil or bitumen.

EXPERIMENT	300°C/72 h		330°C/72 h		350°C/72 h	
CONDITIONS	**Hydrous**	Anhydrous	**Hydrous**	Anhydrous	**Hydrous**	Anhydrous
CO2 (g)	**20.07**	14.39	**31.17**	20.88	**44.01**	21.56
CO2 (aq)*	**15.06**	–	**49.12**	–	**196.14**	–
TOTAL CO2	**35.13**	14.39	**80.29**	20.88	**240.15**	21.56

$*CO_2(aq) = H_2CO_3 + HCO_3 + CO_3 = K_H\ PCO2\ \{1+(k_1/H^+)+(k_1k_2/(H^+)^2)\}$
where PCO_2 = partial pressure of CO_2 gas (atm), $K_H = 10^{-1.47}$ mol/l.atm (Butler, 1982), H^+ = hydrogen ion concentration (mol/l), k_1 = first disassociation constant ($10^{-6.352}$), and k_2 = second disassociation constant ($10^{-10.329}$).

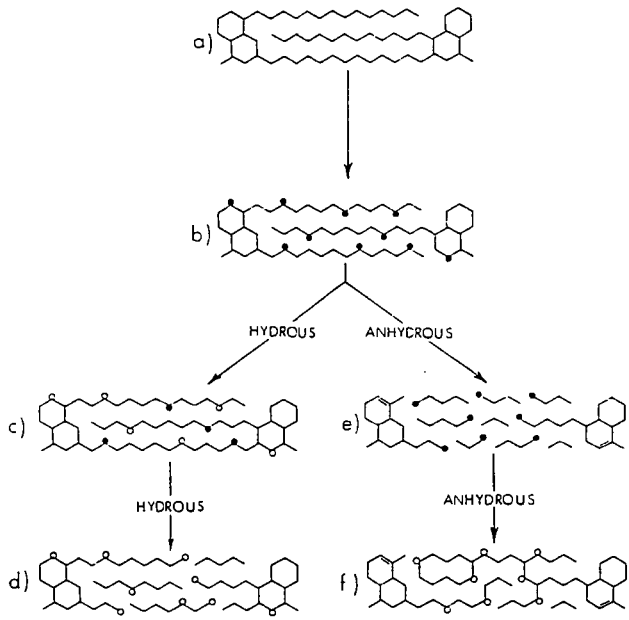

Figure 1. Reaction pathways suggested for thermal maturation of bitumen under hydrous and anhydrous closed-system pyrolysis. Solid circles denote free radicals formed by the loss of hydrogen atoms. Open circles denote terminated free radicals. a) Hypothetical molecule representing aliphatic component of bitumen. b) Molecule with free radical sites, after being subjected to a barrage of extraneous free radicals. c) Termination of free radical sites with water-derived hydrogen atoms before β-sission of chains and disproportionation of cyclics occurs. d) Termination of free-radical fragments with water-derived hydrogen atoms from dissolved water in bitumen. e) Free-radical fragments resulting from frequent β-sissions, which are infrequently terminated by hydrogen atoms due to the lack of dissolved water. f) Termination of free-radical fragments by recombination to form carbon-carbon bond cross linking in the absence of hydrogen atoms from dissolved water.

ALTERNATIVE MECHANISMS FOR RADICAL CATION BOND CLEAVAGE

John H. Penn,* Jin-hai Wang, and You-quan Liu
West Virginia University
Department of Chemistry
Morgantown, WV 26506

Keywords: radical cation, coal liquefaction, mechanism

INTRODUCTION

Recently, a new set of model compounds has been advocated for understanding the reactivity occurring under processing conditions of fossil fuel substrates. These compounds possess multiple functionality and high molecular weight in order to better simulate the reactions which occur in real fuel conversion processes.[1] Chief among these compounds are 4-(naphthylmethyl)bibenzyl, hereafter referred to as Model Compound I, and 4-(2-naphthylethyl)diphenylmethane, II (see structures below). These compounds contain a dicyclic aromatic compound in addition to the monocyclic phenyl groups. Chemical reactivity can then be inferred from the position of the cleavage of the linkages between the aryl groups.

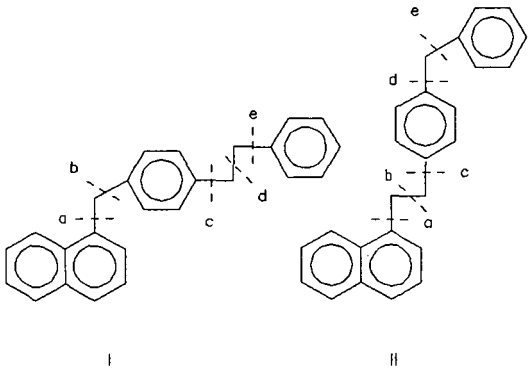

These compounds have been used to test the reactivity of various catalysts. For both compounds, these catalysts cleave bond *a*, *i.e.*, the bond next to the naphthyl ring. Radical cation reactivity has been implicated in these reactions because the naphthyl group is the moiety most likely to lose an electron in these compounds and because the catalytic behavior originates at temperatures in which the surface of the catalyst becomes charged.[2] Theoretical calculations have also been used to support radical cation cleavage of bond a in these compounds.[3]

This reactivity contrasts with the known radical cationic cleavage pathways of monocyclic arenes. For example, the radical cation of 1,1,2,2-tetraphenylethane (**TPE**) is known to cleave at bond *b*, as shown in eq (1).[4] The radical cation of bibenzyl also cleaves at bond *b*, albeit at a much slower rate. The slow cleavage of the radical cation of bibenzyl presumably results from loss of resonance stabilization in the incipient radical and cation formed in this reaction.

In order to distinguish between the contrasting reactivity patterns exhibited by the polycyclic aromatic radical cations and the monocyclic aromatic compounds, we have attempted to independently generate and observe the bond cleavage of the radical cations of naphthyl-containing compounds I, di-(1-naphthyl)methane (**DNM**), and 1,2-di(1-napthyl)ethane (**DNE**). Our strategy for these reactions was to use the photoinitiated electron transfer reactions from 9,10-dicyanoanthracene (**DCA**).[5] In these reactions, **DCA** absorbs a photon of light to produce an excited state of **DCA** (*i.e.*, **DCA***) which does a one-electron oxidation of compounds with oxidation potential $\leq$2.88 V *vs SCE*.[5] These reaction are usually performed in methanol or acetonitrile solutions to facilitate electron transfer and to trap the resulting cations which are expected to be produced in these reactions.

(1)

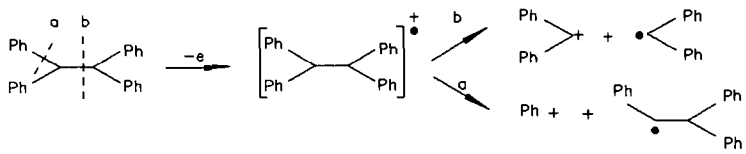

RESULTS AND DISCUSSION

Generation of the Radical Cation of I, DNM, and DNE Under Degassed Conditions: Irradiation of a freshly distilled acetonitrile solution of **I** (2.0 mM) and **DCA** (0.1 mM) using light of 350 nm from a Rayonet reactor for 96 h yielded no product when the reaction solution was degassed with N_2 for 15 min prior to the irradiation and then sealed with a latex septum. The lack of reaction was initially indicated by the lack of low molecular weight products by GC analysis of the reaction solution and was confirmed by the use of internal standards which were added prior to initiation of the reaction. The reactions of **DNM** and **DNE** were similar in that no reactions were detectable after 96 h of irradiation. Again the lack of reactivity was conclusively demonstrated by the use of internal standards.

Since the interpretation of negative results can be often ascribed to poor technique or the inability of a laboratory to reproduce other worker's results, we have generated the radical cation of **TPE** using this methodology. As expected, diphenylmethane and diphenylmethyl methyl ether were produced in quantitative yield in just 24 h of irradiation. These results are consistent with the results obtained in Reference 4 and demonstrate that the radical cations of these substrates are being generated under these conditions.

The significance of these results is that the radical cations of **DNM** and **DNE** do not cleave readily at room temperature. These results are analogous to those reported for bibenzyl (*i.e.*, 1,2-diphenylethane)[6] in which a very low quantum efficiency for cleavage has been reported using the photoinitiated electron transfer methodology for radical cation generation. While the lack of bond cleavage from the radical cation of these 1,2-diarylethanes does not rule out the bond cleavage reactions of radical cations under catalytic conditions where higher temperatures may lead to faster reactions from these intermediates, the lack of bond cleavage suggests that these intermediates have higher energy bond dissociation energies which makes their intermediacy more difficult to postulate without further characterization of their reactivity.

Generation of the Radical Cation of I, DNM, and DNE With O_2 in the Solution: Similar experiments to those above were performed after bubbling of O_2 for 15 min prior to irradiation. In contrast to the lack of reactivity observed under degassed conditions, bond cleavage is observed for **I**, **DNM**, and **DNE** (Note Figure 1). In all cases, bond *a* cleavage is noted in addition to a variety of other products.

Complete interpretation of the reaction results is not possible since the mass balances in these reactions are poor at the present time. We speculate that secondary reactions involving O_2 and the $DCA^{\bullet-}$ (formed by electron transfer from the $DCA^{\bullet}$ and the aromatic moiety) to yield $O_2^{\bullet-}$, followed by a H^+ transfer to yield a pair of radicals which initiate a chain reaction may be responsible for the observed reactivity (Note Figure 2). However, definitive interpretation must await better mass balances and more detailed work to explore the bounds of this

reactivity.

ACKNOWLEDGEMENTS
This work was supported by the Consortium for Fossil Fuel Liquefaction Science under contract to the U.S. Department of Energy.

REFERENCES

1. Farcasiu, M.; Smith, C.M. Ladner, E.P.; Sylwester, A.P. *Prepr. Pap. Am. Chem. Soc. Div. Fuel Chem.*, **1991**, 36.

2. Farcasiu, M.; Smitth, C.M. *Energy Fuels*, **1991**, *5*, 83.

3. Ades, H.F.; Companion, A.L.; Subbaswamy, K.R. *J. Phys. Chem.*, **1991**, *95*, 2226, 6502.

4. Okamoto, A.; Snow, M.S.; Arnold, D.R. *Tetrahedron*, **1986**, *42*, 6175.

5. Mattes, S.L.; Farid, S. *Organic Photochemistry*, **1983**, *6*, 233.

6. Arnold, D.R.; Lamont, L.J. *Can. J. Chem.* **1989**, *67*, 2119.

FIGURES

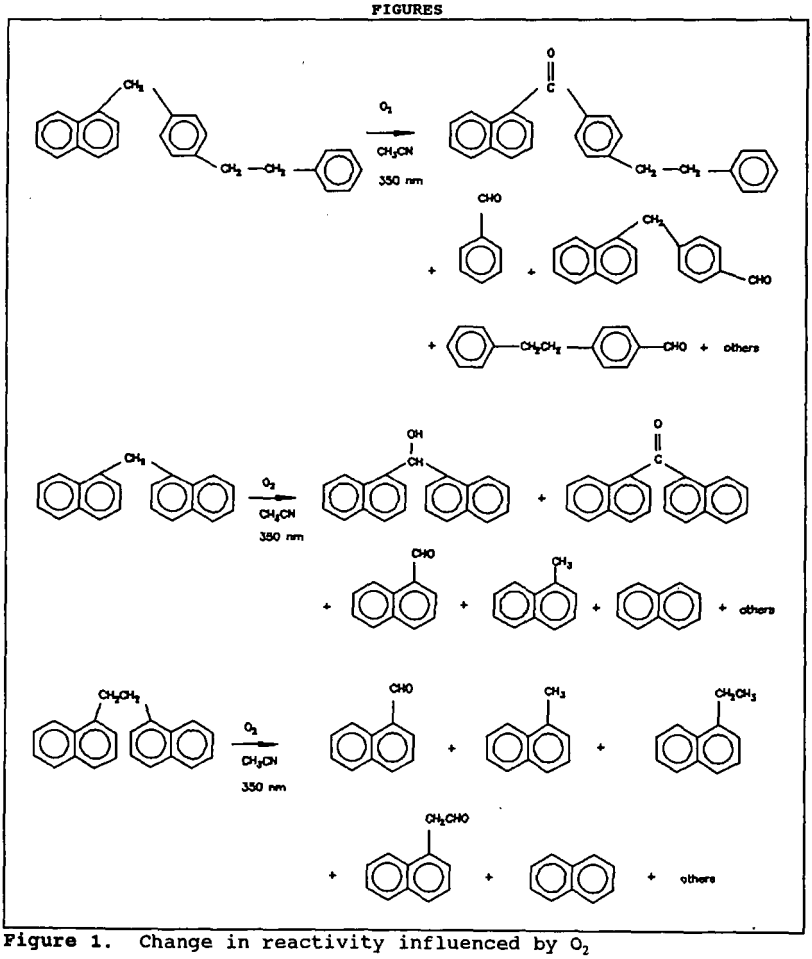

Figure 1. Change in reactivity influenced by O_2

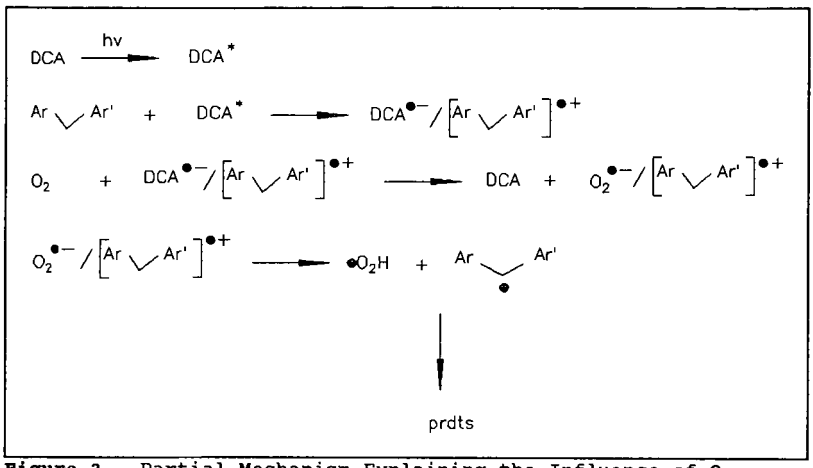

Figure 2. Partial Mechanism Explaining the Influence of O_2.

Hydrogen-Transferring Pyrolysis of Cyclic and Straight-Chain Hydrocarbons. Enhancing High Temperature Thermal Stability of Aviation Jet Fuels by H-Donors

Chunshan SONG*, Wei-Chuan LAI and Harold H. SCHOBERT

Fuel Science Program, Department of Materials Science and Engineering, 209 Academic Projects Building, The Pennsylvania State University, University Park, PA 16802

Keywords: Pyrolysis, Hydrogen-Transferring pyrolysis, Jet fuel, Thermal stability

INTRODUCTION

The present work is a fundamental study of condensed-phase pyrolysis of saturate hydrocarbons including alkylcyclohexanes, trans- and cis-steric isomers of decalin and straight-chain paraffins as well as hydroaromatics such as tetralin. This work is a part of an on-going research program for developing advanced jet fuels thermally stable at high temperatures. One of the critical problems in developing thermally stable jet fuels for high-Mach aircraft is the formation of solid from hydrocarbon fuels in pyrolytic regime (Roquemore et al., 1989; Hazlett, 1991). In studying the pyrolytic degradation of jet fuels, it occurred to us that hydrogen-transfer from H-donors, such as those present in coal-derived JP-8C jet fuel, could play an important role in suppressing thermal decomposition and solid formation (Song et al., 1991a, 1991b, 1992a, 1992b). The hydrogen-transferring pyrolysis described in this paper refers to the thermal decomposition of straight-chain and cyclic hydrocarbons in the presence of H-donors.

This paper reports on 1) pyrolytic degradation of the above-mentioned cyclic and straight-chain hydrocarbons; 2) inhibiting effects of H-donors on the decomposition and solid-forming tendency of n-tetradecane (n-C_{14}), n-butylcyclohexane (n-BCH), cis-decalin (cis-D) and n-butylbenzene (n-BB) as well as a petroleum-derived JP-8P jet fuel; and 3) the mechanisms of the pyrolysis and H-transferring pyrolysis. It should be noted that the experimental conditions used in this work are such that they are close to the high-temperature thermal environment of jet fuel in the future high-Mach aircraft under consideration. These conditions are characterized by condensed or supercritical phases, relatively high pressure, static reactor, and long residence time. Such conditions are distinctly different from those used in most previous paraffin pyrolysis work (vapor phase, low-pressure, flow reactor, short residence time).

EXPERIMENTAL

Reagent-grade n-C_{14}, n-BCH, ethylcyclohexane (ECH), trans-decalin (trans-D) and cis-decalin (cis-D), decalin, tetralin, n-butylbenzene (n-BB) from Aldrich and a petroleum-derived JP-8P jet fuel (Song et al., 1992a) were used. Several compounds including tetralin, decalin, cis-D and trans-D were also examined as H-donors. The pyrolysis was conducted at 450°C for 0-8 h under 0.69 MPa UHP-N_2 (cold) in 25 mL tubing bombs using 5 mL sample. A fluidized sandbath preheated to 450°C was used as heater. The products were identified by capillary GC-MS and quantified by GC. More experimental details may be found in a companion paper (Lai et al., 1992).

RESULTS AND DISCUSSION

I. Pyrolysis of Cyclic and Straight-Chain Hydrocarbons

We first conducted a comparative examination of thermal stability of several cyclic and straight-chain hydrocarbons, which are representative components in coal- and petroleum-derived jet fuels, respectively. Figure 1 shows the time-pressure profiles for the pyrolysis of these compounds. Since static reactor was used, the sample is always confined within the reactor. Therefore, the increase of system pressure after equilibrium boiling is indicative of the extent of thermal decomposition. As shown in Figure 1, when tetralin was heated under 0.69 MPa N_2 (cold) pressure, the system pressure increased to 3.4 MPa within 10 minutes, then the pressure maintained nearly constant. All the other compounds displayed more or less pressure increase. Their t-p profile patterns provide a convenient measure for the extent and rate of their thermal decomposition to form smaller molecules. It should also be noted from Figure 1 that the temperature of 450°C and pressures at 450°C ($\geq$ 3.5 MPa) are higher than the critical temperatures and critical pressures of all the compounds, suggesting the occurrence of supercritical-phase pyrolysis.

Figure 2 shows the conversion of several compounds versus residence time at 450°C for 0-8 h. The typical component of petroleum jet fuels, n-C14, exhibited the highest degree of decomposition, and its pyrolysis led to 50% conversion in just 30 min. For the cycloalkanes, the rate of *n*-BCH decomposition is faster than that of ECH, indicating that increasing the length of side chain on alkylcyclohexane decreases the thermal stability. Decalin appears to

be more stable than the other saturates (Eser et al., 1992, Song et al., 1992b) but it is originally a mixture of trans- and cis-D (see below). Tetralin was the most stable compound when stressed alone. Combination of the data in Figures 1 and 2 indicates that cycloalkanes are much more stable than the long-chain paraffins; the increase in the length of side-chain of alkylcycloalkanes or straight-chain paraffins decreases the stability and increases the decomposition rate.

Alkylcyclohexanes. Figure 3 shows the distribution of products from n-BCH as a function of conversion. At low conversion level of 11.8 mol%, the major products are cyclohexane (3.0, mol%), methylenecyclohexane (2.3), methylcyclohexane (1.9) and cyclohexene (1.1). Scheme I shows the possible reaction mechanisms proposed based on the identified products. The initiation reaction of n-butylcyclohexane is likely the homolytic cleavage of the C-C bond between the ring and the side-chain to form cyclohexyl and 1-butyl radicals. The formation of the four predominant initial products can be rationalized by the radical reaction pathways I, II, III, and IV, respectively. After 1 h at 450°C, the yield of methylenecyclohexane begins to decrease with further increasing residence time, presumably due to hydrogenation to form methylcyclohexane.

In regard to the reaction mechanisms for alkylcyclohexane pyrolysis, there is little information in the literature except for the recent report of Savage and Klein (1988), who found that there are only two major pathways for pyrolysis of n-tridecylcyclohexane. The pathways I and II for n-BCH are also consistent with their observations. However, the present work reveals that other major pathways, III and IV, also exist for the alkylcyclohexanes with shorter side-chains, as shown in Scheme I. Interestingly, when the residence time was extended to 2.5 h and longer, cyclohexane and methylcyclohexane become the two most predominant products, and their yields were several times higher than those of all the other products. These results suggest that pathways I and III dominate in long-duration n-BCH pyrolysis.

Scheme I. Possible Mechanisms for Pyrolysis of n-Butylcyclohexane

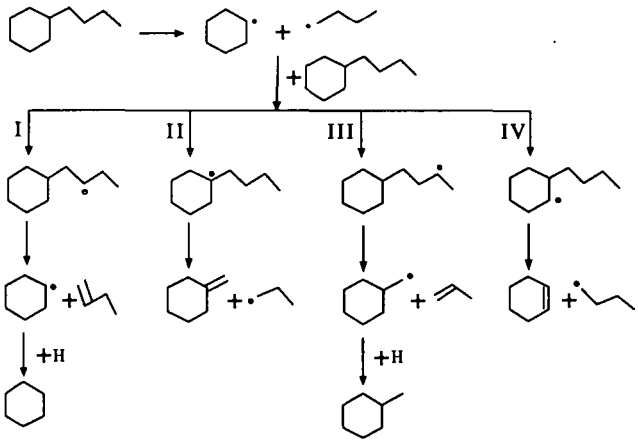

Figure 4 shows the distribution of products from ECH. At low conversion level (7.3 mol%), the major products from ECH are cyclohexene (1.50 mol%), methylcyclohexane (0.83 mol%), methylcyclohexene (0.87 mol%). The preference of cyclohexene formation indicates that the reaction via cyclohexyl radical is a major path, similar to path IV for n-BCH. However, methylenecyclohexane is a minor product in this case (0.17 mol%), indicating that one of the major pathways for n-BCH becomes a minor one for ECH. Another major difference between ECH and n-BCH is the higher yields of isomerization products from ECH pyrolysis, such as methylcyclopentane.

Decalin. Figure 5 shows the product distribution for pyrolysis of decalin, which was originally a mixture of nearly equivalent weights of trans- and cis-D. After decalin pyrolysis at 450°C, the yield of trans-D increased slightly and that of cis-D decreased monotonically with increasing time up to about 4 h. There are two possible reasons for such observations: isomerization of cis- to trans-D or decomposition of cis-D. To gain further insight, we performed the runs of pure trans-D and cis-D, as shown in Figure 6. It was found that cis-D is not stable and tends to isomerize into trans-D as outlined in Scheme II. Amount of trans-D formed from cis-D increased from 6% in 30 min to 41% after 4 h at 450°C. Roberts and Madison (1959) found that di-t-butylperoxide can initiate such an isomerization. Probably

this is initiated via H-abstraction by a radical from 9-position. On the other hand, trans-D is much more stable than cis-D. Its isomerization to cis-D also occurred but the extent was very limited, even after 8 h, as can be seen from Figure 6. In fact, trans-D was found to be one of the most stable components in coal-derived jet fuel JP-8C (Song et al., 1992a).

Scheme II. Isomerization of cis-Decalin to trans-Decalin

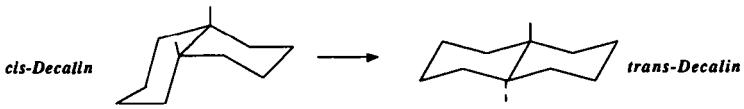

We also observed substantially higher gas yields from cis-D (5.4 wt% in 4 h) than from trans-D (0.8 wt% in 4h), showing higher degree of ring-opening cracking and subsequent dealkylation with cis-isomer. In the case of cis-D, 1-butylcyclohexene was also detected as a major cracking product (0.7 mol%) after 30 min at 450°C. It was formed probably via the 9-decyl radical and subsequent β-scission which caused the ring-openning cracking. The cracking via 9-decyl radical was also suggested for hydropyrolysis of decalin by Shabtai et al. (1979). Therefore, the ring-opening cracking and isomerization of cis-decalin may share the same initiation path, because the latter also involves 9-decyl radical formation as the first step. In summary, the steric conformation of cycloalkanes also affects their thermal stability, and for decalin, trans-isomer is much more stable.

n-Tetradecane Pyrolysis. Pyrolysis of n-tetradecane at 450°C for 0-8 h produced up to about 175 compounds, and the products ranged from lightest molecules such as hydrogen and methane to heavy polyaromatics such as pyrene and solid deposits. After 30 min at 450°C, 49% of n-C_{14} has been decomposed, and the main products are C_1-C_{13} alkanes and C_2-C_{13} 1-alkenes. Scheme III shows the possible reaction pathways for thermal cracking of long-chain n-alkanes such as n-tetradecane under the conditions employed. The first substrate radicals from n-C_{14} include both sec-$C_{14}H_{29}\bullet$ (eq.2) and 1-$C_{14}H_{29}\bullet$ (eq. 3). Formation of the primary radical requires higher activation energy than that of secondary radical, but the difference is not very large in H-abstraction reaction. For example, the activation energies for H-abstraction from n-butane to form 2-$C_4H_9\bullet$ and 1-$C_4H_9\bullet$ at 427°C are 10.4 and 12.3 kcal/mol, respectively (Allara and Shaw, 1980).

There are two extremes of the same fundamental mechanism for radical reactions: the Rice-Kossiakoff mechanism and the Fabuss-Smith-Satterfield mechanism (Fabuss et al., 1966; Poutsuma, 1990), which afford different product spectra. Pyrolysis of long-chain paraffins is still the subject of many investigations. Several recent papers reported the preferential formation of 1-alkenes from vapor-phase pyrolysis of long-chain paraffins (Zhou et al., 1987; Fairburn et al., 1990). In the present work, significant amounts of olefins, mainly 1-alkenes, were also detected, both in liquid and gaseous products. However, unlike the literature results for high temperature and short-residence time pyrolysis, the olefins are not dominant species for most product groups with the same carbon number under the present conditions, except the C_{12} group in which 1-dodecene yield was higher than dodecane for 30 min run.

Scheme III. Possible Mechanisms of Pyrolysis of n-Alkanes C_mH_{2m+2}

$$C_mH_{2m+2} \rightarrow 1\text{-}R\bullet + 1\text{-}R\bullet \qquad 1)$$

$$1\text{-}R\bullet + C_mH_{2m+2} \rightarrow \text{sec-}C_mH_{2m+1}\bullet + RH \qquad 2)$$

$$1\text{-}R\bullet + C_mH_{2m+2} \rightarrow 1\text{-}C_mH_{2m+1}\bullet + RH \qquad 3)$$

$$\text{sec-}C_mH_{2m+1}\bullet \rightarrow 1\text{-}C_{m-n}H_{2(m-n)+1}\bullet + 1\text{-}C_nH_{2n} \qquad 4)$$

$$1\text{-}C_mH_{2m+1}\bullet \rightarrow 1\text{-}C_{m-n-2}H_{2(m-n-2)+1}\bullet + C_2H_4 \qquad 5)$$

$$1\text{-}C_{m-n}H_{2(m-n)+1}\bullet + C_mH_{2m+2} \rightarrow C_{m-n}H_{2(m-n)+2} + \text{sec-}C_mH_{2m+1}\bullet \qquad 6)$$

$$C_mH_{2m+1}\bullet + C_nH_{2n+1}\bullet \rightarrow C_{m+n}H_{2(m+n)+2} \qquad 7)$$

The differences between the present and literature results can be explained as follows. At high temperature (≥ 550°C)-low pressure-short residence time (< 1 min) conditions, as employed in most previous pyrolysis work, radicals tend to undergo β-scission, which leads to products rich in 1-alkene and ethylene. Analytical data show that pyrolysis under our conditions (about 3.4-8.9 MPa system pressures at 450°C for 0-4 h) leads to more alkanes, which can be rationalized based on the Fabuss-Smith-Satterfield mechanism. Under high-pressure conditions, which in general tend to enhance bimolecular reactions, β-scission (eqs. 4,5) will be in competition with hydrogen abstraction (eq.6). Because C_8-C_{12} alkanes and alkenes were still the major components in liquid products after 30 min at 450°C, it is likely that

the first radical formed by β-scission of $C_{14}H_{29}$• radicals (eqs. 4,5) will already prefer to undergo hydrogen-abstraction (eq. 6), which yield one 1-alkene molecule and one alkane molecule. The activation energy required for H-abstraction by a radical from a hydrocarbon or molecular H_2 is smaller than that required for β-scission of the same radical. For example, the energy for β-scission of 1-C_5H_{11}• to form 1-C_3H_7• plus C_2H_4 is 29 kcal/mol, while that for its H-abstraction from another hydrocarbon or H_2 is about 10-12 or 15-17 kcal/mol at 427°C (Allara and Shaw, 1980).

II. H-Transferring Pyrolysis and Inhibition of Solid Formation

The present work on H-transferring pyrolysis seeks to clarify whether and how the hydrogen-donors affect the pyrolytic degradation and solid-forming tendencies of jet fuel components. Figure 7 shows the inhibiting effect of tetralin on solid deposit formation from JP-8P fuel, n-C14, and n-BB, respectively, at 450°C for 4 h. In the absence of H-donor, the amounts of deposits formed were n-BB (5.6 wt%) > JP-8P (3.1 wt%) ≥ n-C14 (3.0 wt%). These figures are extremely large if one considers the deposit formation inside fuel lines in aircraft. It is clear from Figure 3 that adding a small amount of tetralin significantly reduced the deposit formation from all these compounds. As for the efficiency of H-donor, adding 10 vol% tetralin to JP-8, n-C_{14} and n-BB reduced the formation of deposits by 90% (from 3.1 to 0.3 wt%), 77% (from 3.0 to 0.7 wt%) and 54% (from 5.6 to 2.6 wt%), respectively. These results demonstrate that by means of H-transferring pyrolysis, hydrocarbon jet fuels can be used at high operating temperatures in pyrolytic regime with little or no solid deposition.

Multi-ring cyclic alkanes such as decalin can also serve as H-donors at high temperatures, although decalin is not as active as tetralin for inhibiting solid formation (Song et al., 1991c). Table 1 shows that decalin can also suppress the deposit formation from JP-8P jet fuel, n-C_{14} and n-BB. In fact, adding both trans- and cis-D by 50 vol % almost eliminated solid formation from n-C_{14}, JP-8P, and n-BB. Since decalin and n-C_{14} are also representative components of coal- and petroleum-derived jet fuels, respectively, their mixture can also be viewed as a fuel blend. These results also account for the fact observed in previous work that the presence of significant amounts of C_{12}-C_{18} in coal-derived JP-8C did not cause remarkable solid formation (Song et al., 1991b, 1992a).

Based on the foregoing, the reduced solid formation and the enhanced stability of hydrocarbons in H-transferring pyrolysis can be attributed to the stabilization of the reactive radicals via hydrogen-abstraction from tetralin or decalin type compounds, which contributes mainly to inhibiting the secondary radical reactions and suppressing solid formation, as shown in Scheme IV.

Scheme IV. Radical Stabilization via H-Transfer from Tetralin and Decalin

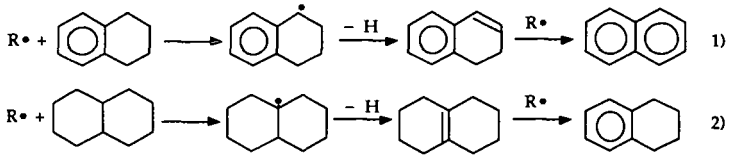

We further examined the effect of adding 10 vol% H-donor tetralin on pyrolysis of n-C_{14}, n-BB, n-BCH, and cis-D at 450°C for 0.5 h (Table 1). Adding tetralin significantly suppressed the n-C_{14} decomposition, and its conversion decreased from 49 to 37 mol%. Surprisingly, it was found that the yields of lower alkanes decreased more than those of corresponding 1-alkenes upon tetralin addition. For example, the ratio of 1-dodecene to n-dodecane increased from 1.6 to 2.6, and that of 1-undecene to undecane increased from 0.5 to 0.6 upon addition of 10 vol% tetralin. In long duration runs, the effect of tetralin in suppressing n-C_{14} decomposition becomes smaller. This is because H-donors inhibit the radical-induced reactions but do not suppress the homolytic C-C bond cleavage. After 4 h, the major effects of H-donor appear to be the inhibition of solid and C_1-C_4 gas formation, as can be seen from Table 1.

For 30 min run of n-BCH, adding tetralin decreased its conversion from about 12 to 6 mol%. In addition to the conversion decrease, the product distribution pattern changed upon tetralin addition. It was found that the decreasing extents in yields of cyclohexane, methyl- and ethylcyclohexane were higher than those for cyclohexene, methyl- and ethylcyclohexene. For cis-D, adding 10 vol% tetralin suppressed the isomerization and decomposition of cis-decalin: the conversion decreased from 12 to 8 mol%, and the cis-D/trans-D ratio increased from 14.2 to 18.9.

III. Reactions of H-donors in H-Transferring Pyrolysis

Tetralin is quite stable when stressed alone at 450°C. The major products from pyrolysis of pure tetralin are 1-

methylindan and naphthalene as well as a small amount of n-butylbenzene. Even after 8 h pyrolysis at 450°C, the total gas products were still within 1 wt%, indicating the ring-opening cracking and dealkylation reactions were very limited with tetralin. On the basis of the findings of Benjamin et al. (1979) and Franz et al. (1980), the isomerization proceeds through the 2-tetralyl radical to form 1-indanylmethyl radical, as shown in Scheme V.

Scheme V. Isomerization of Tetralin to 1-Methylindan

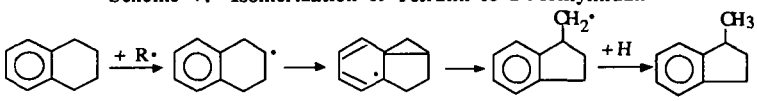

In the H-transferring pyrolysis of n-C_{14} and n-BB, the distribution of products from tetralin shows a significantly different pattern. n-BB is a reactive alkylbenzene (Peng et al., 1992) As shown in Scheme VI, in the presence of n-C_{14} or n-BB, tetralin mainly undergoes dehydrogenation reaction to form naphthalene. For the mixtures of 10 vol% tetralin with reactive compounds such as n-C_{14} or n-BB, the ring-contraction isomerization was enhanced slightly at 450°C for 30 min but further increasing residence time increased mainly dehydrogenation. After 4 h, more than 90% of tetralin has been dehydrogenated in the case of its mixture and its isomerization was reduced significantly as compared to the run of itself. For 30 min runs, the radicals from n-BB were more active in dehydrogenating tetralin, although n-BB conversion was lower than that of n-C_{14} under this condition. For the mixtures of 25 vol% tetralin with n-C14, however, the yield of 1-methylindan from tetralin increased significantly after 4 h run, the value of which is close to that from pure tetralin.

Scheme VI. Products from Tetralin in Pyrolysis & H-Transferring Pyrolysis

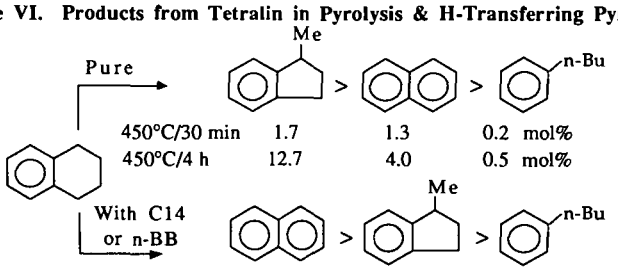

10%Tetralin-C14

450°C/30 min	5.9	4.5	mol%
450°C/4 h	90.9	5.7	mol%

10%Tetralin-BB

450°C/30 min	27.1	3.6	mol%
450°C/4 h	97.0	2.3	mol%

25%Tetralin-C14

450°C/4 h	64.1	12.6	mol%

25%Tetralin-BB

450°C/4 h	92.3	5.6	mol%

Taking into account the difference in reaction mechanisms of dehydrogenation (Scheme IV) and isomerization (Scheme V), our results show that when the H-donor concentration is relatively low, the radicals from n-C_{14} and n-BB mainly abstract benzylic hydrogen to yield 1-tetralyl radical. In such case, the formation of 2-tetralyl radical is very limited and hence the isomerization is not very important. This also confirms that the reactions via 1-tetralyl radical shown in Scheme IV are the major reactions. When tetralin is present at high levels, however, radicals from n-C_{14} abstract hydrogens from both 1- and 2-positions. As a result, n-C_{14} not only promotes tetralin dehydrogenation, but also enhances its isomerization to form 1-methylindan, although the former is still the dominant reaction. It is also interesting to note that the presence of 90 vol% n-BCH caused little increase in reactions of tetralin, neither dehydrogenation nor isomerization, although tetralin suppressed the n-BCH decomposition from 12 to 6 mol% at 450°C

for 0.5 h. On the contrary, adding 10 vol% tetralin to n-BB had little impact on n-BB conversion and gas formation at 450°C for 0.5 h, although tetralin dehydrogenation was more remarkable than in the case of n-BCH.

CONCLUSIONS

High temperature thermal stability of hydrocarbons depends mainly on their chemical structure, carbon number, length of main-chain or alkyl side-chain, and steric conformation (cis, trans). Cycloalkanes are more stable than long-chain paraffins. The stability of straight-chain paraffins decreases with increasing carbon number. Increasing the length of side-chain of alkylcyclohexanes decreases the thermal stability. Steric conformance also affects thermal reactivity, and it was found that trans-decalin is much more stable than cis-decalin.

Pyrolysis of n-tetradecane, a JP-8P jet fuel and n-butylbenzene at 450°C can result in significant amounts of solid deposits. Adding small amounts of H-donors such as tetralin and decalins was found to be effective for inhibiting fuel decomposition and solid formation at 450°C. By taking advantage of hydrogen-transferring pyrolysis reported in this work, hydrocarbon jet fuels can be used at high temperatures in pyrolytic regime with little or no solid deposition.

ACKNOWLEDGMENTS

This project was jointly supported by the U.S. Department of Energy, Pittsburgh Energy Technology Center and the Air Force WRDC/Aero Propulsion Laboratory. Funding was provided by the U.S. DOE at Sandia National Laboratories under contract DE-AC04-76DP00789. We are pleased to thank Drs. W.E. Harrison III and D.M. Storch of WRDC, E. Klavetter of SNL, and S. Rogers of PETC for their support and technical advice. We also wish to thank Dr. P.G. Hatcher of PSU for instrumental support to the maintenance of analytical equipments for the jet fuel project.

REFERENCES

Allara, D.L.; Shaw, R. J. Phys. Chem. Ref. Data, **1980**, 9 (3), 523-559.
Benjamin, B.M.; Hagaman, E.W.; Raaen, V.F.; Collins, C.J. Fuel, **1979**, 58, 386.
Eser, S.; Song, C.; Copenhaver, R., Parzynski, M., ACS Div. Petrol. Chem. Prepr., **1992**, 37 (2), 493-504.
Fabuss, B. M.; Smith, J.O.; Satterfield, C.N., Adv. Petrol. Chem. Refin., **1964**, 9, 158-201.
Fairburn, J.F.; Behie, L.A.; Svrcek, W.V., Fuel, **1990**, 69 (12), 1537-1545.
Franz, J.A.; Camaioni, D.M., J. Org. Chem., **1980**, 45, 5247-5245.
Hazlett, R.N., Thermal Oxidation Stability of Aviation Turbine Fuels, ASTM, 1991, and references cited therein.
Lai, W.-C.; Song, C.; Schobert, H.H.; Arumugam, R., Paper in this issue.
Peng, Y.; Schobert, H.H.; Song, C.; Hatcher, P.G., Paper in this issue.
Poutsma, M.L., Energy & Fuels, **1990**, 4 (2), 113-131.
Roberts, R.M.; Madison, J.J., J. Am. Chem. Soc., **1959**, 81, 5839.
Roquemore, W.M.; Pearce, J.A.; Harrison III, W.E.; Krazinski, J.L.; Vanka, S.P. ACS Div. Petrol. Chem. Prepr., **1989**, 34 (4), 841.
Savage, P.E.; Klein, M.T., Ind. Eng. Chem. Res., **1988**, 27, 1348-1356.
Shabtai, J.; Ramakrishnan, R.; Oblad, A.G., Adv. Chem. Ser., **1979**, 183, 297.
Song et al., Compositional Factors Affecting Thermal Degradation of Jet Fuels, Technical Progress Report for Period October 1990-January 1991, Air Force Aero Propulsion Laboratory, 42-3462-TPR-2, February, **1991a**.
Song et al., Advanced Thermally Stable Jet Fuel Development Program Annual Report, Vol. 2, Final Report for Period July 1990-July 1991, Air Force Aero Propulsion Laboratory, WL-TR-91-2117, Vol. II, August **1991b**.
Song, C.; Nihonmatsu, T.; Nomura, M., Ind. Eng. Chem. Res., **1991c**, 30 (8), 1726-1734.
Song, C.; Eser, S.; Schobert, H.H., Hatcher, P.G., ACS Div. Petrol. Chem. Prepr., **1992a**, 37 (2), 540-547.
Song, C.; Peng, Y.; Jiang, H.; Schobert, H.H., ACS Div. Petrol. Chem. Prepr., Vol. 37, **1992b**, 37 (2), 484-492.
Zhou, P.; Hollis, O.L.; Crynes, B.L., Ind. Eng. Chem. Res., **1987**, 26, 846-852.

Abbreviations

n-BB:	n-Butylbenzene
n-BCH:	n-Butylcyclohexane
n-C10:	n-Decane
n-C_{14}:	n-Tetradecane
cis-D:	cis-Decalin or cis-Decahydronaphthalene
trans-D:	trans-Decalin or trans-Decahydronaphthalene
ECH:	Ethylcyclohexane
JP-8P:	Petroleum-derived JP-8 jet fuel
JP-8C:	Coal-derived JP-8 jet fuel

Table 1. Deposit Formation and Liquid Depletion during H-Transferring Pyrolysis of Hydrocarbons and JP-8P Jet Fuel

Feedstocks		Condition		Products (wt%)			
Sample	+ vol% H-Donor	Temp, °C	Time, h	C1-C4 Gas	≥ C5 Liquid	Solid Deposit[a]	Recovered Deposit[b]
n-Tetradecane		450°C	4.0	38.3	58.8	3.0	1.9
Tetradecane	+ 50% cis-Decalin	"	"	19.5	80.3	0.1	0
Tetradecane	+ 50% trans-Decalin	"	"	18.2	81.7	0.1	0
Tetradecane	+ 10% Tetralin	"	"	27.3	72.0	0.7	0.2
Tetradecane	+ 50% Tetralin	"	"	9.1	90.8	0.1	0
cis-Decalin		"	"	5.4	94.6	0	0
trans-Decalin		"	"	0.8	99.2	0	0
Tetralin		"	"	0.7	99.4	0	0
n-Butylbenzene (n-BB)		"	"	17.2	77.2	5.6	5.0
n-BB	+ 50% cis-Decalin	"	"	14.3	85.9	0	0
n-BB	+ 50% trans-Decalin	"	"	12.1	87.9	0	0
n-BB	+ 10% Tetralin	"	"	15.4	82.0	2.6	2.5
n-BB	+ 50% Tetralin	"	"	9.8	90.2	0	0
JP-8P Jet Fuel		"	"	26.8	70.2	3.1	1.9
JP-8P	+ 50% trans-Decalin	"	"	13.3	86.6	0.1	0
JP-8P	+ 10% Tetralin	"	"	20.0	79.7	0.3	0.1
JP-8P	+ 50% Tetralin	"	"	7.9	92.0	0.1	0
n-Tetradecane		450	0.5	5.9	94.1	0	0
n-Tetradecane	+ 10% Tetralin	"	"	2.3	97.7	0	0
n-Butylbenzene		"	"	5.1	94.9	0	0
n-BB	+ 10% Tetralin	"	"	5.4	94.6	0	0
n-Butylcyclohexane		"	"	1.8	98.2	0	0
n-Butylcyclohexane	+ 10% Tetralin	"	"	0.7	99.3	0	0
cis-Decalin		"	"	0.3	99.7	0	0
cis-Decalin	+ 10% Tetralin	"	"	0.2	99.8	0	0
Tetralin		"	"	0.1	99.9	0	0

a) Solid deposit on the reactor wall determined by measuring weight gain of the microreactor after the stressing, pentane washing and drying; b) Solid deposit recovered from the reactor wall.

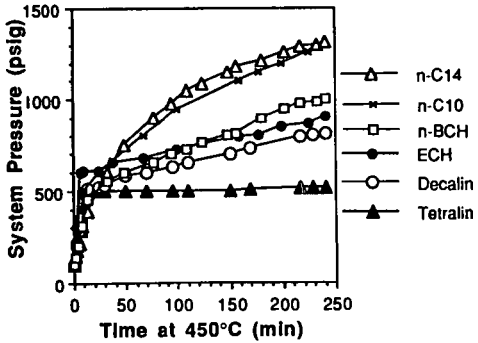

Fig.1. System t-p profiles for pyrolysis of model compounds

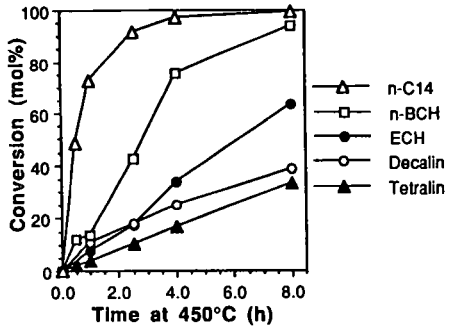

Fig.2. Conversion of model compounds in pyrolysis

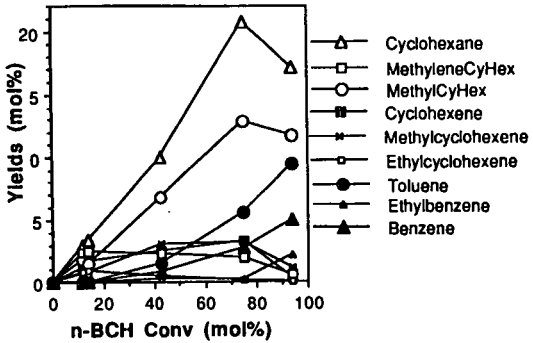

Fig.3. Product distribution for n-BCH pyrolysis

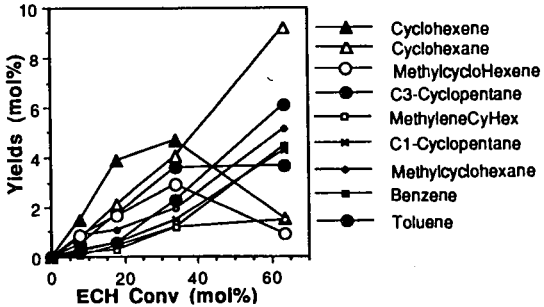

Fig.4. Product distribution for ECH pyrolysis

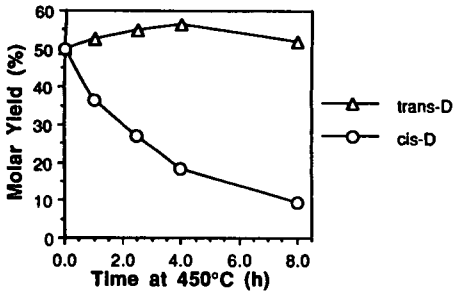

Fig.5. Compositional change during decalin pyrolysis

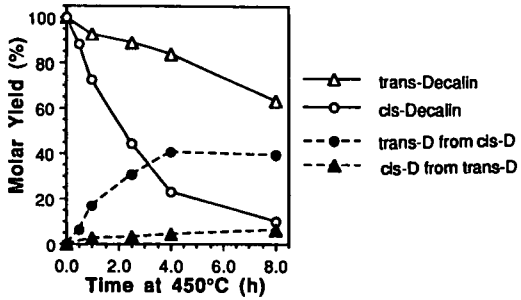

Fig.6. Conversion and isomerization during pyrolysis of pure cis-decalin and pure trans-decalin

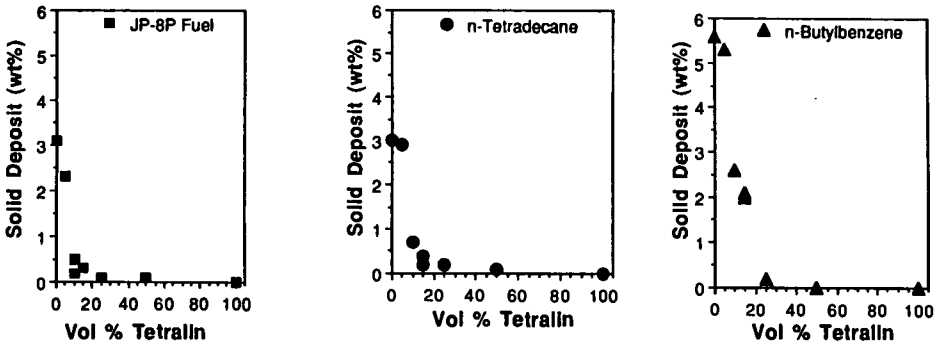

Fig.7. Inhibiting effect of H-donor tetralin on the solid formation from JP-8P, n-tetradecane and n-butylbenzene

POTENTIAL STABILIZERS FOR JET FUELS SUBJECTED TO THERMAL STRESS ABOVE 400°C: 2. NMR STUDIES.

Maria Sobkowiak, Leena Selvaraj, Emily Yoon and Michael M.Coleman*
Department of Materials Science and Engineering
The Pennsylvania State University
University Park, PA 16802

Keywords: Jet Fuels, Thermal Stabilizers, NMR

INTRODUCTION

We recently reported[1,2] the results of Fourier transform infrared (FTIR) and visual studies of Jet A-1 samples that had been subjected to thermal stresses for varying periods of time at a temperature of 425°C. FTIR spectroscopy was shown to be an excellent experimental method that has just about the right degree of sensitivity for our purposes, as it probes at the level of the functional group and is capable of unveiling the major reactions that lead to the formation of carbonaceous solids during thermal stressing at these high temperatures. From these leads we have been successful in identifying a number of additives, specifically benzyl alcohol and 1,4-benzene dimethanol, that appear to function as hydrogen donors and which perform well as thermal stabilizers, significantly retarding the onset of carbonaceous solid formation in jet fuels at temperatures in excess of 400°C.

Evidence obtained from the infrared studies performed to date suggests that the primary route to carbonaceous deposits at temperatures above 400°C may well be the formation of olefins, followed by cyclization and aromatization, similar to the mechanism suggested for the degradation of polyacrylonitrile copolymers used in the formation of carbon fibers[3]. The focus of our research thus turned to studying molecules that might act as hydrogen donors in the anticipation that they might resaturate the double bonds as they are produced and ultimately retard the subsequent reactions that result in the formation of carbonaceous solids. Hydrogenation agents employed in coal liquefaction, such as tetralin or tetrahydroquinoline, do act as thermal stabilizers and significantly retard the formation of carbonaceous solids.

Surprisingly, however, the best thermal stabilizers we found were methalol derivatives, such as benzyl alcohol and 1,4-benzene dimethanol[2]. From infrared studies of the Jet A-1 fuels containing these two alcohols we know that methalol groups *slowly* transform over a period of hours in the jet fuel to aldehydes. A simple mass balance indicates that this is achieved with the loss of two hydrogen atoms and this suggests that benzyl alcohol and benzene 1,4-dimethanol act as *in situ* hydrogenation agents at high temperatures, similar to coal liquefaction reagents, resaturating olefinic double bonds as they are formed and interfering with the process of aromatization and subsequent formation of carbonaceous solids.

While the infrared studies performed to date have been rewarding, parallel NMR studies, which are the main focus of this preprint, were initiated to assist in the interpretation of the changes observed in the infrared spectra as a function of thermal stressing. NMR studies also provide additional information that is useful for the elucidation of the principal reaction pathways that lead to a retardation of carbonaceous solid formation.

EXPERIMENTAL

Samples for these studies were prepared from an essentially additive free Jet A-1 fuel supplied by the Air Force/WRDC Aero Propulsion Laboratory (No. 90-POSF-2747). Benzyl alcohol and benzene 1,4-dimethanol were purchased from Aldrich Chemical Company and used without further purification.

Thermal stressing was performed on 10 ml samples at 425°C in 15 ml type 316 stainless steel micro reactors[2] under 100 psi of air. The micro reactor containing the sample was purged

* To whom correspondence should be addressed.

with UHP-grade N_2 five times at 1000 psi to minimize the presence of dissolved oxygen and finally pressurized with 100 psi of air. It was then placed in a preheated sand bath at 425°C for the required reaction time, followed by quenching into cold water and depressurization to remove head space gases.

Samples for NMR analyses were prepared as 15 wt % solutions in deuterated chloroform. The spectra were recorded on a Brucker WP200 instrument at a field strength of 200 MHz.

RESULTS AND DISCUSSION

1. Thermal Stressing of Neat Jet A-1 Fuel at 425°C.

The physical appearance of the neat Jet A-1 fuel after thermal stressing at 425°C under 100 psi of air, changes from a clear, colorless, transparent liquid to a transparent, light yellow liquid after 1h, a slightly turbid, light brown liquid after 3h and a black liquid after 6h. Between 6 and 24h the black liquid becomes progressively more turbid and there is an obvious increasing presence of black carbonaceous solids (color pictures are shown in ref. 2). Changes observed in the infrared spectra of neat Jet A-1 fuel as a function of thermal stressing time led us to consider hydrogen donors as potential stabilizers. Prominent bands at approximately 1642 /1652 and 890 / 910 cm^{-1} in the spectra were assigned to C=C stretching vibrations resulting from the formation of olefins during thermal stressing. Between 6 and 18h these bands decrease in intensity and are barely detected after 12h in air at 425°C. Other relatively broad bands are observed at approximately 880 and 675 cm^{-1} and these become increasingly prominent in spectra of the samples after reaction times exceed 6h. These bands were attributed to substituted aromatics and their presence correlates well with the observation of the black carbonaceous material in the thermally stressed fuel at long reaction times.

Figure 1 shows ^1H NMR spectra (0-10 ppm) recorded at room temperature of Jet A-1 fuel samples thermally stressed under air after time periods of 0, 1, 3, 6, 12, 18 and 24h at 425°C. The NMR spectrum of the neat unstressed fuel is representative of a typical complex hydrocarbon mixture[4] with prominent lines attributed to paraffinic methyl and γ-methyl protons (0.5-1.05 ppm); paraffinic methylene, γ-methylene, β-methyl and β-methylene protons (1.05-2.0 ppm); α-methyl protons (Ar-CH_3*; 2.0-2.6 ppm); α-methylene protons (Ar-CH_2*-R; 2.6-3.4 ppm); α-methylene protons (Ar-CH_2*-Ar; 3.4-4.5 ppm) and aromatic protons (6.0-9.0 ppm). For completeness, olefinic protons, which are not detected at this scale expansion, resonate between 4.5-6.0 ppm. Upon thermal stressing at 425°C the distribution of aliphatic to aromatic moieties changes in favor of the latter. Systematic increases in the intensity of α-methyl, α-methylene and aromatic protons with corresponding decreases in the intensity of paraffinic methyl and methylene groups are observed. Figure 2 shows ^1H NMR spectra of the same samples (figure 1) scale expanded in the olefinic proton region (4.5-6.0 ppm). In the unstressed Jet A-1 fuel olefinic protons are not detected. However, in the spectra obtained after the sample had been thermally stressed for 1 and 3h there is the obvious presence of NMR resonances that may be attributed to internal and external olefins. In common with the infrared results[2], the concentration of olefins appears to maximize between 3 and 6h. Thus the NMR results obtained on the thermally stressed neat Jet A-1 corroborate the infrared spectroscopic findings.

2. Thermal Stressing of Jet A-1 Fuel Containing 5% Benzyl Alcohol at 425°C.

As we have demonstrated previously[2] the addition of 5% benzyl alcohol to Jet A-1 fuel results in a significant improvement in the thermal stability at 425°C, as confirmed by the retardation of carbonaceous solids formation by some 3h. Infrared spectroscopic analysis was informative. A band at 1720 cm^{-1}, assigned to the carbonyl stretching vibration of benzaldehyde was observed to increase in intensity to a maximum after approximately 3h of thermal stressing, decrease somewhat at 6h and was essentially absent at 12h of thermal stressing. Concomitant with these observations bands assigned to C=C stretching vibrations are detected at 1h, rise to a maximum at about 6h and are barely detected at 12h of thermal stressing. Significantly, after 12h of thermal stressing bands assigned to substituted aromatics are present and this again correlates

well with the observation of the black carbonaceous material in the thermally stressed fuel. The interpretation of these results was as follows. Benzyl alcohol and similar molecules *slowly* transform over a period of hours in the jet fuel to aldehydes with the loss of two hydrogen atoms. We believe that they act as *in situ* hydrogenation agents at high temperatures, similar to coal liquefaction reagents, resaturating olefinic double bonds as they are formed and interfering with the process of aromatization and subsequent formation of carbonaceous solids.

Figure 3 shows ^{1}H NMR spectra (0-10 ppm) recorded at room temperature of Jet A-1 fuel samples containing 5% benzyl alcohol and thermally stressed under air after time periods of 0, 10, 60, 180, 360, and 720 min. at 425°C. A comparison of the spectra of the unstressed Jet A-1 fuel with (figure 3) and without (figure 1) the additive, reveals that benzyl alcohol has a convenient characteristic resonance at 4.74 ppm attributable to the hydroxyl proton of the methalol group. Figure 4 shows ^{1}H NMR spectra of the same samples (figure 3) scale expanded in the olefinic proton region (4.5-6.0 ppm). In the unstressed sample there is no evidence of resonances attributable to olefinic protons and the spectrum is dominated by the intense line associated with the methalol group of benzyl alcohol at 4.74 ppm. It is significant that the intensity of this line at 4.74 ppm decreases as a function of thermal stressing, but is still present in the spectrum recorded after 6h at 425°C. This implies that benzyl alcohol gradually transforms to benzyladehyde (see infrared results[2]) in the Jet A-1 fuel over a period in excess of 6h under air at 425°C. At the same time, the olefinic resonances are clearly observed in the sample thermally stressed for 6h which is consistent with the infrared results and lends support for the *in situ* hydrogenation hypothesis.

ACKNOWLEDGMENTS

This project was jointly supported by the US Department of Energy, Pittsburgh Energy Technology Center and the U. S. Air Force WRDC/Aero Propulsion Laboratory, Wright-Patterson AFB. Funding was provided by the US DOE at Sandia National Laboratories under contract DE-AC04-76DP00789. We also wish to thank Mr. W.E.Harrison III of WRDC, Dr. E. Klavetter of SNL, Professor H. H. Schobert, and Dr. C. Song of PSU for their encouragement and many helpful discussions.

REFERENCES

(1) Selvaraj, L., Sobkowiak, M. and Coleman, M. M., ACS *Division of Petroleum Chemistry Preprints*, 37(2), 451 (1992).
(2) Coleman, M.M., Selvaraj, L., Sobkowiak, M. and Yoon, E., *Energy and Fuels*, submitted.
(3) Sivy, G.T., Gordon, B. and Coleman, M.M., *Carbon*, 21, 573 (1983).
(4) Song, C. et al., Compositional Factors Affecting Thermal Degradation of Jet Fuels Annual Report, Report for period July 1990 to July 1991, The Pennsylvania State University.

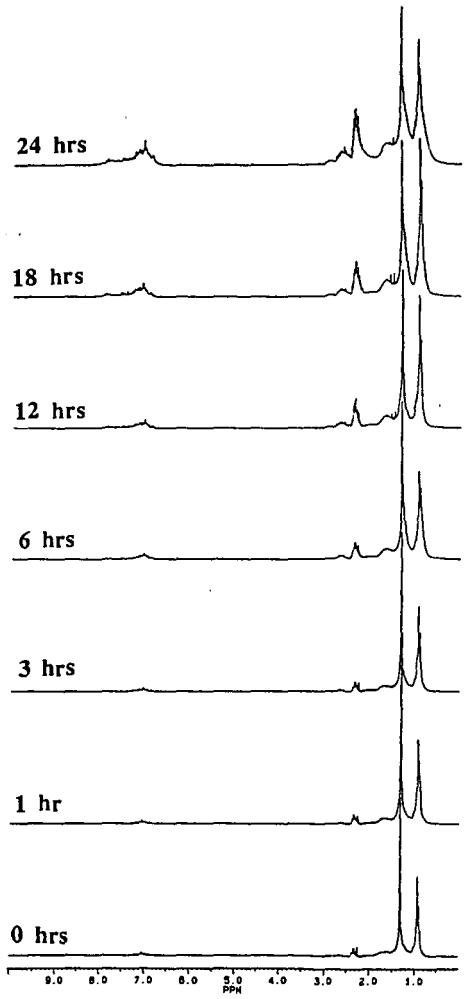

Figure 1. ^{1}H NMR spectra of neat Jet A-1 fuel thermally stressed for the times indicated over air at 425°C.

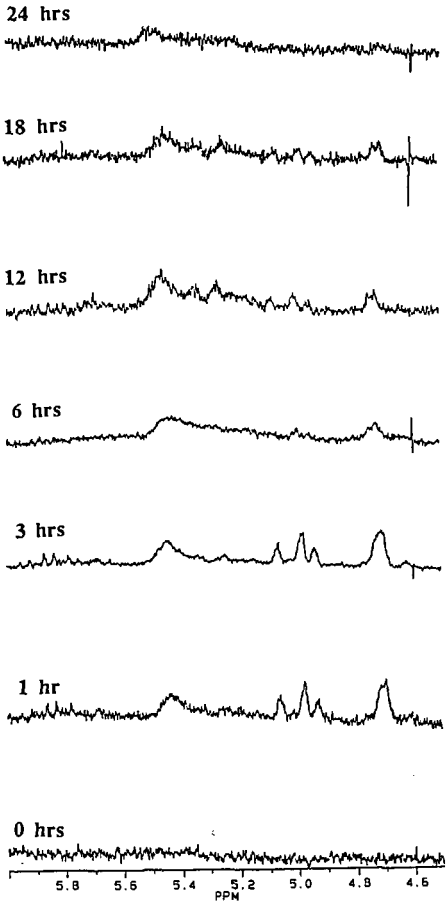

Figure 2. Scale expanded ^{1}H NMR spectra in the olefinic region of neat Jet A-1 fuel thermally stressed for the times indicated over air at 425°C.

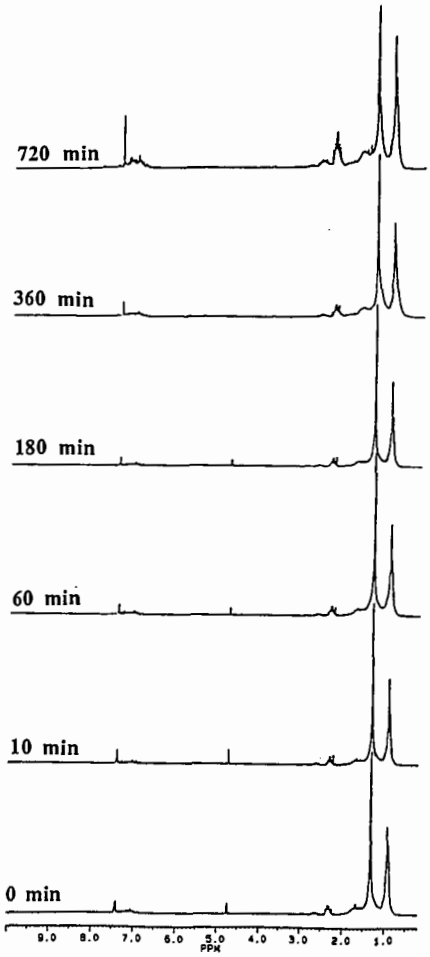

Figure 3. ^{1}H NMR spectra of Jet A-1 fuel containing 5% benzyl alcohol thermally stressed for the times indicated over air at 425°C.

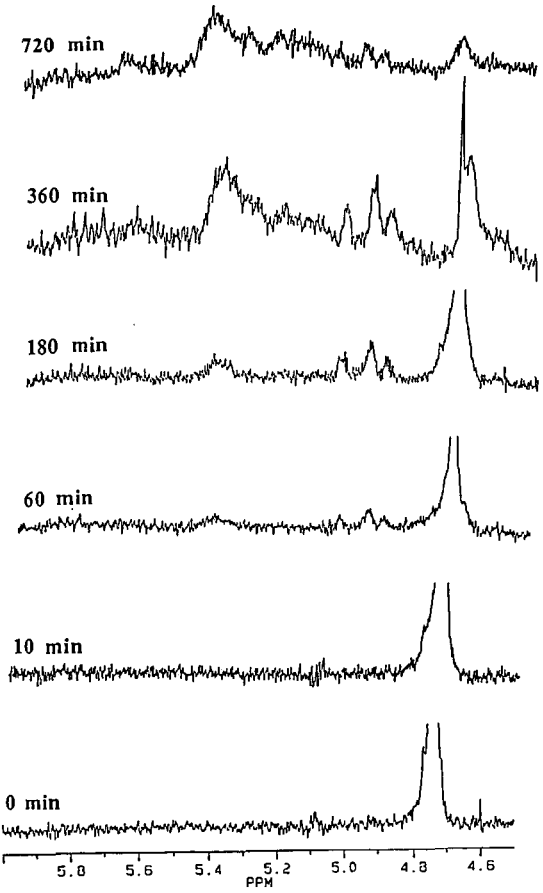

Figure 4. Scale expanded ^{1}H NMR spectra in the olefinic region of Jet A-1 fuel containing 5% benzyl alcohol thermally stressed for the times indicated over air at 425°C.

PYROLYTIC DEGRADATION OF COAL- AND PETROLEUM-DERIVED AVIATION JET FUELS AND MIDDLE DISTILLATES

Wei-Chuan Lai, Chunshan Song, Harold H. Schobert, and Rathnamala Arumugam
Fuel Science Program
Department of Materials Science and Engineering
209 Academic Projects Building
The Pennsylvania State University
University Park, PA 16802

Keywords: pyrolysis, jet fuels, middle distillates, thermal stability

INTRODUCTION

The thermal stability of jet fuels plays an important role in the design and development of future hypersonic aircraft. It was reported that the fuel in these new hypersonic aircraft may reach temperatures higher than 500°C. The temperatures are much higher than the current maximum operating temperature for the conventional aviation jet fuels. When the fuels are exposed to such high temperatures, serious pyrolytic degradation of the fuels will occur and will result in the formation of solid deposits on critical aircraft systems such as fuel pipeline, filter, and engine parts (Roquermore et al., 1989). This means that advanced jet fuels are required for hypersonic aircraft. The development of such fuels warrants detailed study of pyrolytic degradation of hydrocarbon fuels.

The ultimate goal of our research project is to develop advanced jet fuels that are thermally stable at high temperatures. The objectives of this work are to rank the thermal stability of current fuels, to identify thermally stable compounds in fuels, to clarify the chemistry of pyrolytic degradation and mechanisms of solid formation, and to enhance the intrinsic stability of jet fuels by optimizing fuel composition. The future fuels might derive not only from petroleum, but also from hydrocarbon resources such as coal, tar sands, and oil shale. The scope of this paper will concentrate on the thermal stability study of ten fuels including four coal-derived fuels and six petroleum-derived military and commercial jet fuels. The results concerning the effects of hydrogen-donors on the fuel stability are presented in Song et al. (1992b). In this study, the relative thermal stabilities of the fuels have been elucidated by their chemical composition.

EXPERIMENTAL

Apparatus and Procedures

Thermal stressing of the jet fuels and middle distillates were studied in tubing bomb reactors at 450°C for a heating period of 0-8 hours under 0.69 MPa UHP-N_2. The tubing bomb reactors were described in detail elsewhere (Eser et al., 1990). A 5 ml sample was confined in a leak-tested reactor. The sample was deoxygenated through repetitive (6 times) pressurization to 6.9 MPa with UHP-N_2 and purging to remove oxygen/air in the reactor or dissolved in the sample. The reactor was pressurized to the desired starting pressure of 0.69 MPa with UHP-N_2 before being immersed into a fluidized sand bath which has been preheated to 450°C. After the experiment was started, the reaction pressure was closely monitored. The experiment was ended after the desired stressing time by removing the reactor from the fluidized sand bath and immediately quenching in a cool water bath. The headspace gas was collected in a gas sampling bag.

Product Chemical Analysis

The gas samples were analyzed for their compositions and quantities by using a Perkin-Elmer Autosystem gas chromatograph (GC). Two detectors, a thermal conductivity detector (TCD) and a flame ionization detector (FID), were used to analyze the gas composition. The TCD was used to determine CH_4, C_2H_2, C_2H_4, and C_2H_6 as well as non-hydrocarbon gases such as H_2, CO, and CO_2. The FID was used to detect hydrocarbon gases from C_1 to C_6. The GC columns used were a 10 feet long, 1/8 inch diameter stainless steel column packed with 100/120 Carbosieve SII (Supelco) for TCD and a 6 feet long, 1/8 inch diameter stainless steel column packed with 80/100 Chemipack C 18 for FID. There are two liquid samples collected from each experiment: one is the liquid residue directly collected

from the reactor and the other is washed from the reactor wall with pentane. The compounds in the liquid products were identified by a HP 5890 Series II GC coupled with HP 5971A Mass Selective Detector (MSD) and quantified by a Perkin-Elmer GC 8500. The column used was a 30 m, 0.25 mm i.d., DB-17 Fused Silica Capillary Column (50% phenyl, 50% methyl silicone) with a film thickness of 0.25 μm. The solid deposits are operationally defined as the materials which are not soluble in the resulting liquid co-products and pentane (washing solvent). The solid deposits are to be analyzed by Fourier transform infra-red spectroscopy and NMR spectroscopy.

Samples

Ten jet fuels and middle distillates were studied. Four coal-derived fuels include JP-8C from hydrotreating of liquids produced from the Great Plains Gasification plant, and middle distillates derived either from direct coal liquefaction (WI-MD from Wilsonville plant and HRI-MD from HRI) or from indirect coal liquefaction (FT-MD from Fischer-Tropsch synthesis). Six petroleum-derived military and commercial jet fuels include JPTS (thermally stable jet fuel), JP7, JP-8P, JP-8P2, Jet A, and Jet A-1. The basic information of these fuels is presented in Table 1, and the properties of the samples are discussed in the following section.

RESULTS AND DISCUSSION

Properties of Samples

The fuel densities range from 0.76 g/cm^3 (FT-MD) to 0.96 g/cm^3 (WI-MD) with most falling in a smaller range of 0.79 to 0.81 g/cm^3 (JPTS, JP-7, JP-8P, Jet A, Jet A-1, and JP-8P2). The densities of JP-8C and HRI-MD are 0.84 and 0.92 g/cm^3, respectively. All the fuels were analyzed by GC and GC-MS before and after thermal stressing, and they are all complex mixtures of hundreds of compounds. Because of the large number of compounds in the fuels, one way to visualize their compositions is employing the total ion chromatograms (TIC) and specific ion chromatograms (SIC) of GC-MS analysis. Figure 1 presents the TIC and SIC (ions of m/z 57, 83, 91, 105, and 142) of JP-8P2. The fragment ions of m/z 57, 83, and 142 are characteristics of long-chain paraffins, alkylcyclohexanes, and alkylnaphthalenes, respectively. The ions of 91 and 105 imply the presence of alkylbenzenes. From the resemblance between TIC and SIC of m/z 57, we can find that the dominant constituents in JP-8P2 are the long-chain paraffins with carbon-number ranging from C_8 to C_{17} with most falling between C_{10} to C_{15}. The alkylbenzenes (C_2- ~ C_6-, mainly C_3- ~ C_5-) content is about 20 percent. JP-8P2 also includes 5% alkylcyclohexanes (C_3- ~ C_8-) and low concentrations of tetralin, alkylindan, and alkylnaphthalenes.

JP-8P, Jet A, JP-7, FT-MD, JPTS, and Jet A-1 are also paraffinic fuels derived from petroleum with long-chain paraffins as the dominant constituents, but the overall compositions and paraffins distributions are somewhat different. Figure 2 shows the SIC (m/z 57) for six of the seven paraffinic fuels. We can see that JP-8P and Jet A are quite similar to JP-8P2 in terms of the long-chain paraffins distributions. Jet A-1 has a narrower band from C_{10} to C_{14} with most falling between C_{11} and C_{12}. JPTS has a band from C_9 to C_{15}. JP-7 has a band from C_{11} to C_{16} with an average carbon number of 12. FT-MD is also a paraffinic fuel, although derived from coal, having almost exclusively paraffins (C_9 ~ C_{21}) with very low concentration of cycloparaffins. Table 2 summarizes the approximate compositions of the seven paraffinic fuels based on the three major hydrocarbon types found in fuels (paraffins, alkylbenzenes, alkylcyclohexanes) and others (such as alkylnaphthalenes, alkylindans, etc).

JP-8C, WI-MD, and HRI-MD are all coal-derived fuels, but their compositions are quite different from petroleum-derived paraffinic fuels. JP-8C is composed mainly of monocyclic and bicyclic alkanes, and two-ring hydroaromatic compounds. The major components are alkyl-substituted cyclohexanes (about 45%), decalin (6.3%), C_1-decalin (4%), and tetralin (3.9%). There are also about 10% alkylbenzenes. HRI-MD is a heavy fuel, i.e., with many high molecular-weight components compared with the paraffinic fuels and JP-8C. HRI-MD consists of (alkyl) bicyclic alkanes, alkyl two-ring aromatic compounds and some alkylbenzenes. There are about 15% alkyl-substituted (mainly, C_0- ~ C_3-) cyclohexanes and only 8% long-chain paraffins. There are also some (C_0- ~ C_2-) 3-ring or 4-ring aromatics. Regarding WI-MD, it is heavier (with carbon number ≥12) than the other nine fuels with few light molecular weight compounds. It has very high content of aromatics (with ring size not less than 2). The most abundant peaks are pyrene (4%) and multi-hydropyrenes (total about 8%), and less than 10% paraffins (C_{14} ~ C_{25}).

Degradation Product Distributions and Stability Comparison

The relative thermal stabilities of hydrocarbons in fuels as well as the whole fuels themselves were identified based on the overall reaction products (gas, liquid, and solid) distributions and GC/GC-MS analysis of the liquid products. For the hydrocarbons in fuels, it was found that at 450°C long-chain n- and iso-paraffins ($\geq C_{11}$), and n-alkylbenzenes (alkyl$\geq C_3$-) are some of the unstable compounds. Some compounds that are relatively more stable compounds include long-chain paraffins ($\leq C_8$), long-chain paraffins (C_9 and C_{10}, up to 4 hr), C_0- to C_3-cycloalkanes, and C_0- to C_2-benzenes. One example is shown in Figure 3, which presents the total ion chromatograms of the neat sample of, and the liquid products from, FT-MD after thermal stressing at 450°C for 1-8 hours. Recall that FT-MD is a paraffinic fuel which has paraffins ranging from C_9 to C_{21}. We can clearly find that long-chain paraffins of C_{11} through C_{21} decompose quickly; the decomposition rate increases with increasing chain size. Quantitative results from GC and qualitative results from GC-MS indicate that the main reactions occurring in the first 2.5 hours include cracking of the paraffins into lower alkanes and olefins, and cyclization to form alkylcyclic alkanes and olefins. The alkylcyclic compounds were then subjected to dehydrogenation to form alkylbenzenes. This observation is consistent with the mechanisms proposed by Song et al. (1992a). A quantitative presentation of how the paraffins content changes with time is shown in Figure 4 for the same sample. The paraffins were divided into 12 groups based on the carbon numbers; each group consists of straight and branched alkanes with the same carbon number. Figure 4 shows that at 450°C long-chain paraffins with carbon number no less than 11 (i.e., C_n, $n\geq 11$) are unstable. C_{15} through C_{21} decompose completely by 2.5 hours. Notice that the content of C_9 increases from the initial 0.5% to 5.7% at 1 hour and then decreases to 3.1% after 2.5 hours. The initial increase is contributed from cracking yield from longer chain paraffins, and the C_9 later decomposes and results in the C_9 fraction decreasing with increasing time.

The yields of the gas components from JP-8P thermally stressed at 450°C for 1-8 hours are presented in Figure 5. Methane is always the most abundant gaseous product (in mmole) followed by ethane and propane over the stressing range; this is also true for all other nine fuels studied. Another common characteristic for the fuels is that the paraffinic gases (CH_4, C_2H_6, C_3H_8, and C_4H_{10}) increase with increasing time but the olefinic gases (C_2H_4, C_3H_6, C_4H_8) increase initially then decrease with increasing time. Continuous cracking accounts for the progressive increase of paraffinic gases and the initial increase of olefinin gases. Olefins are known to be less stable and highly reactive because of unsaturation; this results in the later decrease of olefinic gases.

The decomposition extents of the ten fuels are significantly affected by their compositions. Figure 6 shows the gas yields from the ten fuels stressed for 1-8 hours. The figure indicates that the three coal-derived non-paraffinic fuels, i.e., JP-8C, HRI-MD, and WI-MD, are more stable than the other seven paraffinic fuels in terms of less gas formation. The difference in stability in terms of the gas formation is attributed to the composition difference. Paraffinic fuels produce more gases because the major reaction for long-chain paraffins is cracking into lighter gases of alkanes and olefins. On the other hand, the compositions of the three coal-derived non-paraffinic fuels are quite different from the paraffinic fuels; they have low fraction of paraffins but are rich in cyclic alkanes and hydroaromatics. Thus the major reaction for them is dehydrogenation to form alkylbenzenes (liquid yields) instead of the formation of low molecular-weight gases. It can be seen that HRI-MD and FT-MD produce the gas the least and the most, respectively. For example, the gas yields for HRI-MD and FT-MD are respectively 3.3% and 17% at 1 hour, 10% and 33% at 4 hours, and 16% and 52% at 8 hours. The six petroleum-derived paraffinic fuels (JP-8P, Jet A, JP-7, FT-MD, JPTS, and Jet A-1) have similar gas yields (ranging from 37% to 40%) for 8-hour stressing. However, for 1- ~ 4-hour stressing, Jet A-1 has the lowest or second to the lowest gas yields; this is consistent with the fact that among the paraffinic fuels, Jet A-1 has the lowest paraffin content and the narrowest paraffin band (from C_{10} to C_{14}, with most falling between C_{11} and C_{12}).

The solid yields from the ten fuels stressed for 1-8 hours are presented in Figure 7. The figure shows that there is no solid formed after 1-hour stressing for all the ten fuels, and the solid starts to form between 1 and 2.5 hours. The induction time, which is the time period needed for the formation of solid precursors (such as polyaromatics) from reactive intermediates, differs for each fuel. It was found that fuels rich in hydrogen-donors (such as cyclic alkanes) have longer induction period and tend to have better stability. The hydrogen abstracted from hydrogen-donors stabilizes the reactive radicals; this in consequence inhibits the secondary radical reactions and suppresses solid formation (Song et al., 1992b). Two of the three coal-derived non-paraffinic fuels, JP-8C and HRI-MD, have much better stability than other fuels in terms of much less solid formation. This is again attributed to the composition

difference and the fact that JP-8C and HRI-MD have high concentration of hydrogen donors. Figure 7 also shows that JP-7 and JPTS have higher stability among the seven paraffinic fuels in terms of less solid formation. This is also attributed to their lower aromatics content and higher hydrogen-donor compounds (alkylcyclohexanes).

WI-MD, on the other hand, does not have good stability in the long run, judging from its high solid formation at 8-hour stressing. Figure 8 presents the total ion chromatograms of the neat sample of, and the liquid products from, WI-MD after thermal stressing at 450°C for 1-8 hours. It can be seen that WI-MD has very high content of aromatics and hydroaromatics. The hydroaromatics decomposed quickly to form saturated aromatics through dehydrogenation, and these aromatic compounds subsequently form more polycyclic aromatic hydrocarbons and solid deposits. WI-MD seems to be stable in terms of low gas formation; however, GC-MS analysis of the liquid products shows that in fact WI-MD is quite unstable and decomposes quickly to form aromatics and precursors to solid. In short, WI-MD tends to form more solid than other fuels due to its high aromatic content nature, and it can not be a good jet fuel.

CONCLUSIONS

The thermal stability of the fuels is significantly affected by their chemical composition. Pyrolysis of ten jet fuels and middle distillates has been studied in a tubing bomb reactor. The compositions of the stressed as well as neat fuels were all qualitatively and quantitatively characterized by GC and GC-MS. This information is useful in explaining and evaluating the thermal stability of fuels. The relative thermal stabilities of hydrocarbons in fuels as well as the whole fuels themselves were identified. The fuels with higher contents of 1-3 ring cycloalkanes and/or hydroaromatics are more stable than those with higher contents of long-chain paraffins in terms of less gas formation. The former includes JP-8C, HRI-MD and WI-MD, and the latter covers the remaining 7 fuels including six petroleum-derived paraffinic fuels and one paraffinic fuel from indirect coal liquefaction. Among the paraffinic fuels, higher stability in terms of less gas formation was observed for those fuels having narrower distribution of paraffins with relatively shorter chain, e.g., Jet A-1; those with lower aromatics content and higher hydrogen-donor compounds exhibits less solid formation . Overall, coal-derived JP-8C and HRI-MD have the best thermal stability among the ten fuels studied either in terms of less gas or solid formation.

ACKNOWLEDGMENTS

This project was jointly supported by the U.S. Department of Energy, Pittsburgh Energy Technology Center and the Air Force WRDC/Aero Propulsion Laboratory, Wright-Patterson AFB. Funding was provided by the U.S. DOE at Sandia National Laboratories under contract DE-AC04-76DP00789. We are pleased to thank Drs. W.E. Harrison III, D.M. Storch and S.D. Anderson of WRDC for providing technical advice, support and jet fuel samples, Drs. E. Klavetter of SNL and S. Rogers of PETC for their support and helpful discussions, and Drs. G. Stigel and R. Hickey of PETC and Dr. P. Zhou of Burns & Roe Service Co. for the WI-MD and FT-MD samples. We also wish to thank Dr. P.G. Hatcher of PSU for instrumental support to the maintenance of analytical equipments for the jet fuel project.

REFERENCES

Eser, S., Song, C., Schobert, H. H., Hatcher, P. G. et al., "Advanced Thermally Stable Jet Fuels Development Program Annual Report", Volume II, Interim Report for period July 1989 to June 1990, WRDC-TR-90-2079, Vol. II, September 1990.

Roquermore, W. M., Pearce, J. A., Harrison III, W. E., Krazinski, J. L., and Vanka, S. P., *Preprints, American Chemical Society, Division of Petroleum Chemistry*, 34(4), *1989*, 841.

Song, C., Peng, Y., Jiang, H., and Schobert, H. H., "On the Mechanisms of PAH and Solid Formation during Thermal Degradation of Jet Fuels", *Preprints, American Chemical Society, Division of Petroleum Chemistry*, 37(2), *1992a*, 484-492.

Song, C., Lai, W.-C., and Schobert, H. H., "Hydrogen-Transferring Pyrolysis of Cyclic and Straight-Chain Hydrocarbons. Enhancing High Temperature Thermal Stability of Aviation Jet Fuels by Hydrogen-Donors", Paper to be presented at the 204th ACS National Meeting, Washington, D.C., August 23-28, *1992b*.

Table 1. Coal- and Petroleum-Derived Jet Fuels and Middle Distillates

Fuel	Description	Received	Supplier/Source	Sample No.
Coal-Derived Fuels				
1) JP-8C	Hydrotreated JP-8	5-30-89	WPAFB	89-POSF-2685 ?
2) WI-MD	Middle distillates from coal liquefaction at Wilsonville	4-20-90	DOE PETC	259E MD
3) FT-MD	Middle distillates from Fischer-Tropsch Synthesis	8-16-91	DOE PETC	PETC F-T
4) HRI-MD	Middle distillates from coal liquefaction at HRI	11-26-91	WPAFB	83-POSF-0849
Petroleum-Derived Jet Fuels				
5) JP-8P	Petroleum-Derived JP-8	5-30-89	WPAFB	
6) JP-8P2	Petroleum-Derived JP-8	5-31-90	WPAFB/Tank S-15	
7) JP-7	Petroleum-Derived JP-7	5-31-90	WPAFB/Tank S-16	
8) Jet A-1	Commercial jet fuel	8-16-91	WPAFB/Tank S-7	90-POSF-2747
9) JPTS	Thermally stable jet fuel	8-16-91	WPAFB	91-POSF-2799
10) Jet A	Commercial jet fuel	8-16-91	WPAFB	90-POSF-2827

Table 2. Approximate Compositions of Paraffinic Fuels

	Weight %			
Fuel	Paraffins	Alkylbenzenes	Alkylcyclohexanes	Others
JP-8P2	~ 70%	~ 20% (C_2- ~ C_6-)	~ 5% (C_3- ~ C_8-)	
JP-8P	~ 75%	~ 12% (C_2- ~ C_4-)	~ 8% (C_3- ~ C_7-)	
Jet A	~ 80%	~ 10% (C_2- ~ C_4-)	~ 6% (C_1- ~ C_6-)	
JP-7	~ 90%	very low	~ 10% (C_5- ~ C_8-)	
FT-MD	~ 100%		low	
JPTS	~ 70%	~ 8% (C_2- ~ C_4-)	~ 13% (C_1- ~ C_7-)	
Jet A-1	~ 65%	~ 26% (C_3- ~ C_5-)	~ 6% (C_4- ~ C_5-)	

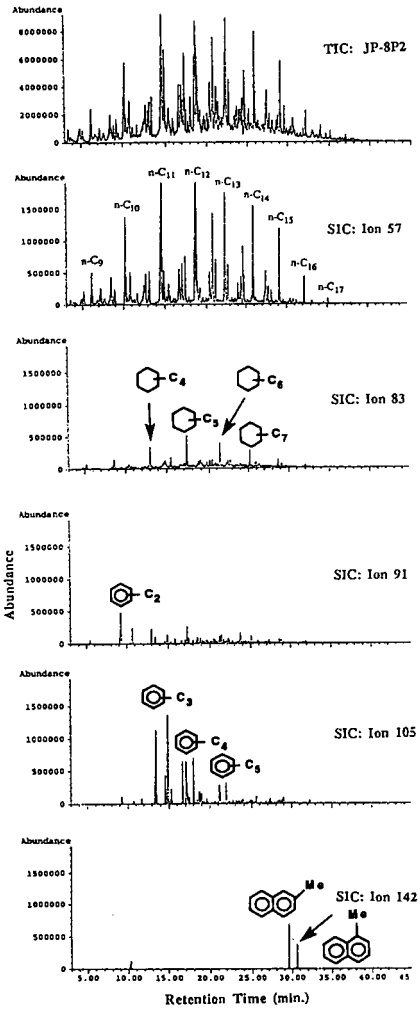

Figure 1. Total and specific ion chromatograms (ions of m/z 57, 83, 91, 105, and 142) of JP-8P2 from GC-MS analysis.

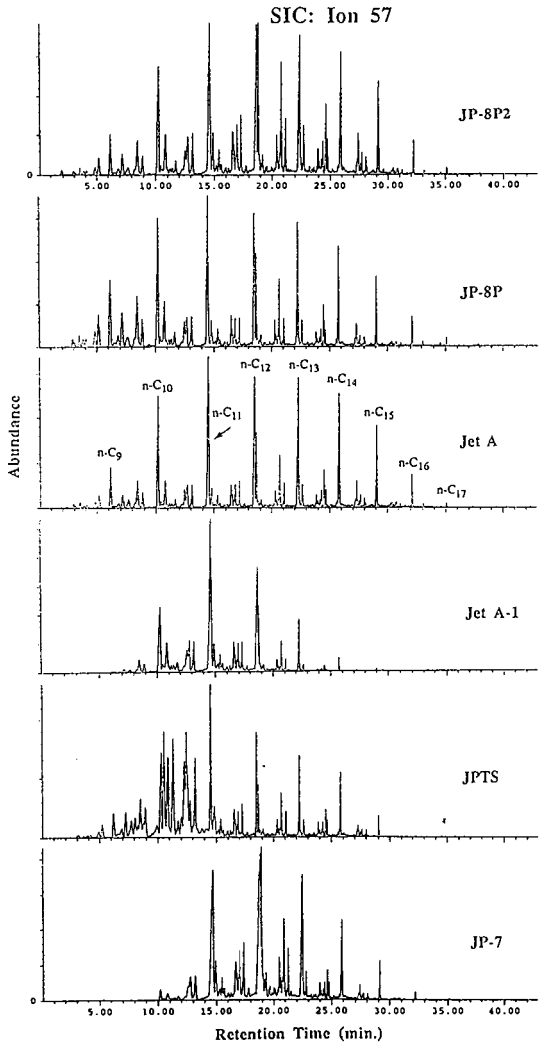

Figure 2. Specific ion chromatograms (ion of m/z 57) of six paraffinic fuels.

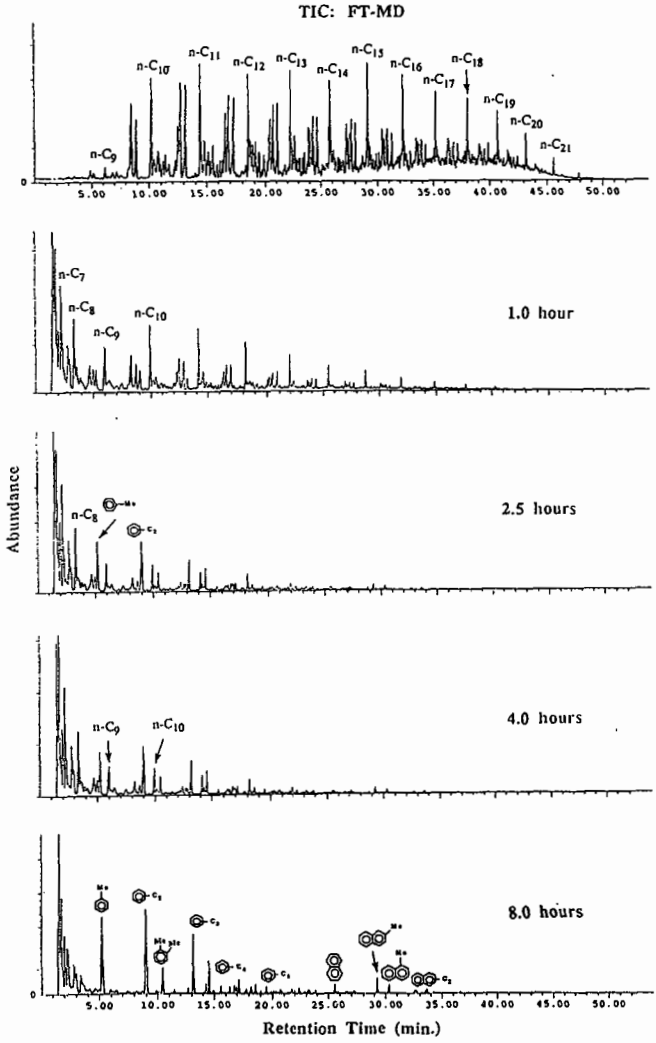

Figure 3. Total ion chromatograms of the neat sample of, and the liquid products from, FT-MD after thermal stressing at 450°C for 1-8 hours.

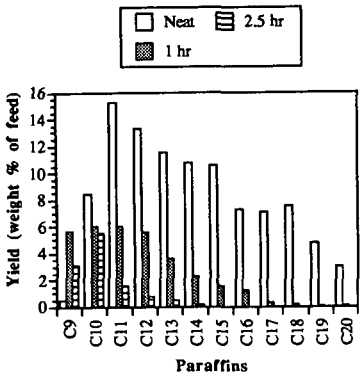

Figure 4. Paraffins distribution of liquids from FT-MD

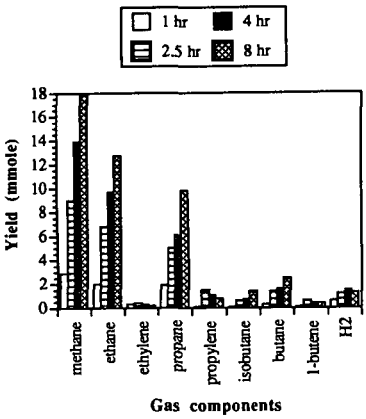

Figure 5. Yields of H_2 and $C_1 \sim C_4$ gases from JP-8P

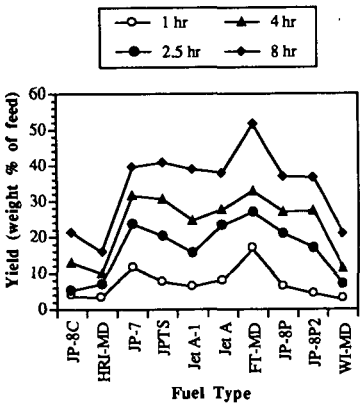

Figure 6. Yields of gases at 450°C

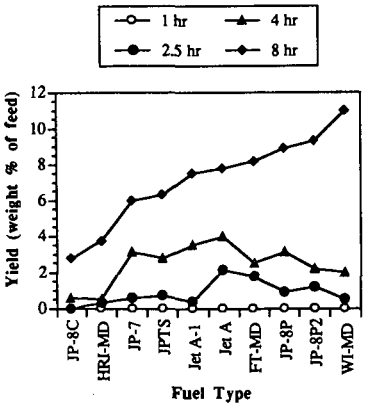

Figure 7. Yields of solid deposits at 450°C

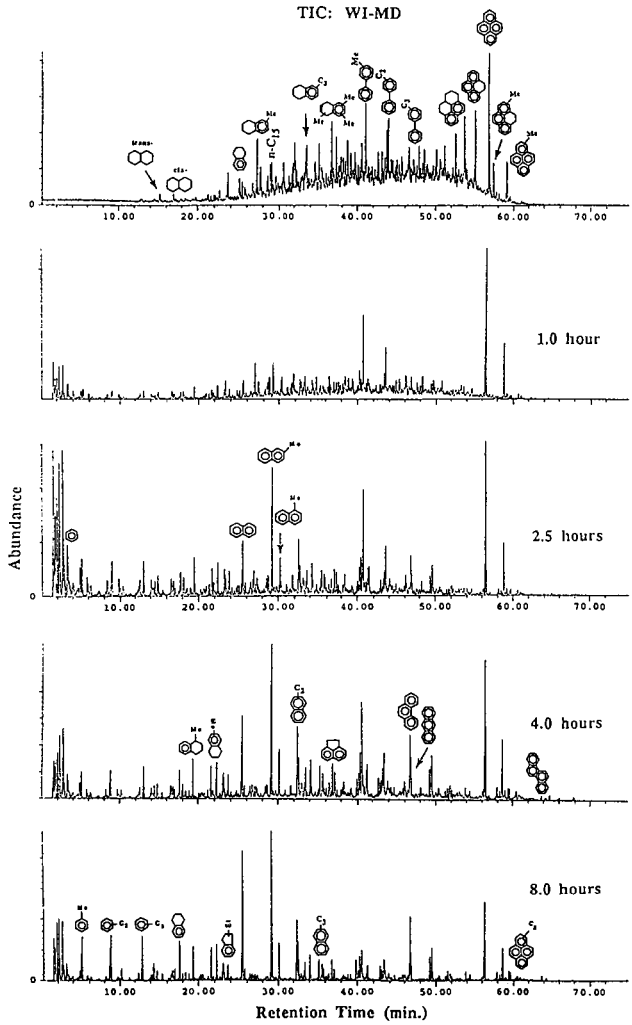

Figure 8. Total ion chromatograms of the neat sample of, and the liquid products from, WI-MD after thermal stressing at 450°C for 1-8 hours.

HYDROUS PYROLYSIS OF FOUR ARGONNE PREMIUM COALS

Michael A. Serio, Erik Kroo, Sylvie Charpenay, and Peter R. Solomon

Advanced Fuel Research, Inc.
87 Church Street
East Hartford, CT 06108

Keywords: Hydrous Pyrolysis, Pretreatment, Argonne Premium Coals

ABSTRACT

Pretreatment experiments were done under hydrous pyrolysis conditions with four Argonne Premium coals (Zap lignite, Wyodak subbituminous, Illinois bituminous, Pittsburgh bituminous) over a range of temperatures (250 -350 °C) and pressures (1000 - 4000 psig). The residues from these experiments were further studied by programmed pyrolysis in a TG-FTIR system. The yields of pyrolysis tar were found to increase sharply at short pretreatment times (< 60 min at 350 °C) and decline slowly at longer times. The yields of pyrolysis methane increase monotonically with pretreatment time, while the yields of pyrolysis CO_2 decline monotonically. All of these trends are in agreement with the contention that hydrous pyrolysis is similar to an accelerated geological aging of the coal. The results for CO evolution were somewhat contrary in that there was usually an initial increase followed by a decline. It is believed that this CO results from decomposition of hydroxy and dihydroxy structures which are created by the hydrous pyrolysis process.

INTRODUCTION

Hydrous pyrolysis (hydrothermal treatment) of coal has been studied previously as a pretreatment step to increase the yields of liquid products from extraction (1-5), pyrolysis (3-7), or liquefaction (8-11) of coal. However, the mechanisms of this process and the applications to coals of a wide range of ranks are still a subject of considerable debate. The similarity between the effects of steam or water pretreatment and accelerated geological aging of coal has recently been noted by several authors (8-11). Landais, Monthioux and coworkers have also discussed the analogy between pyrolysis in confined systems and accelerated geological aging (12-16), otherwise known as "artificial" maturation.

Siskin and Katritzky (17) have recently reviewed the reactivity of organic compounds in hot water, including a consideration of the geochemical implications. Their review indicates that, under conditions where conventional wisdom suggests that water is inert, it may be acting as a catalyst, reactant, and/or solvent. Based on work with model compounds with linkages and functional groups corresponding to those found in coals and shale kerogens, it was concluded that water has important effects on the conversion of plant and animal material into organic fuels under geological conditions of time, heat, and pressure. Much of their work was done in the range of 250 to 350 °C which is the temperature range of interest for hydrothermal treatment of coal. Because of significant changes in the physical and chemical properties of water with increasing temperature, it becomes more likely to react with organic compounds. For example, in the presence of water, ether and ester crosslinks can be readily broken by hydrolysis at relatively low temperatures (17).

The principal conclusions of their work as it relates to hydrothermal treatment of coal are: 1) it

is the ionic chemistry of water that is important under the pretreatment conditions; 2) that reactions in water systems are often "autocatalyzed" by water soluble organic reaction products; 3) aqueous chemistry provides cleavage pathways for major oxygen crosslinks which are too stable to cleave thermally; 4) water can act as a highly effective acidic or basic catalyst or even as an acid-base bicatalyst 5) reactions of water with organics can be catalyzed by clays. Siskin and coworkers (17-19) have demonstrated that there are plausible pathways for water to remove or reduce oxygen functional groups (e.g., conversion of alcohols to methyl groups) under conditions which are relevant to water pretreatment of coal.

EXPERIMENTAL

Sample Selection - The selection of coal samples was made from the Argonne Premium Sample Bank (20). The coals used were the Zap Lignite, the Wyodak subbituminous and the Illinois No. 6 bituminous. Selected experiments were also done with the Pittsburgh Seam bituminous coal from the same sample bank.

Steam/Water Pretreatment Experiments - A new reactor system was designed to carry out high pressure (up to 6000 psig), high temperature (up to ~ 400°C) hydrothermal treatment of coal in a closed bomb (20 ml) reactor. After 1-3 g coal is fed into the bomb and the reactor head is screwed on to get a gas tight seal, the system is purged with N_2 or evacuated, the high temperature, high pressure valve on the reactor base is closed, and the water is injected directly into the coal through the capillary tube with a ~ 0.1-1.0 ml/min rate. Deaerated and deionized water is used throughout the reaction.

Simultaneously with the water injection, the reactor is immersed into the fluidized sand bath held at the required temperature. The pressure is measured in the water feed capillary tubing directly after the pump. The amount of water pumped in and the temperature determines whether steam and/or water pretreatment is done. The results described in the current paper are for pretreatment with subcritical water at 350°C, 4000 psig and pretreatment times from 10 to 1200 minutes. Additional details of the experiments have been provided previously (11).

Product Analyses - The residues from the water pretreatment experiments with the four coals were subjected to analysis by programmed pyrolysis (TG-FTIR), solvent extraction, FT-IR, SEM/x-ray analysis and liquefaction experiments in a donor solvent. The liquefaction and solvent extraction experiments have been discussed previously (11). The current paper focuses primarily on the results from TG-FTIR (21) and FT-IR (22,23) analysis of the residues.

RESULTS AND DISCUSSION

Experimental Results - Figure 1 compares the TG-FTIR results for raw, water pretreated and demineralized Wyodak samples. Figures 1a, 1d, and 1g show the time-temperature profile, the TGA balance (lower curve) and the sum of gases (by FT-IR). Figures 1b, 1e, and 1h show the differential and integrated evolution curves for tar, while Figures 1c, 1f, and 1i show the same curves for CO_2. In addition, Figures 1f and 1i have the differential curves for the raw coal superimposed as dashed lines for comparison. The water pretreatment was done at 350 °C, 4000 psig for 20 minutes.

The results in Fig. 1 show that both hydrothermal treatment and demineralization lend to increases in the pyrolysis tar yield and a reduction in the pyrolysis CO_2 yield. These results are consistent with previous work which has suggested that crosslinking is associated with CO_2 evolution, i.e., the increase in tar is a result of a reduction in crosslinking (24,25). In the case of demineralization, the removal of divalent cations which act as crosslinks in the structure is

believed to be responsible for the observed result (25). In the case of hydrothermal treatment, the divalent cation content is essentially unchanged (10), so a different mechanism must be important.

A variety of explanations for the effects of hydrothermal treatment have been proposed:

- Hydrothermal treatment adds hydrogen (which can stabilize reactive fragments) and removes oxygen groups (which cause retrogressive reactions).

- Hydrothermal treatment partially depolymerizes the coal structure by breaking covalent bonds and disrupting hydrogen bonds.

Evidence for the former comes primarily from spectroscopic and elemental analysis (6-11) while evidence for the latter comes primarily from data on pyridine extractability (1-5,10,11). The relative importance of each mechanism is likely a function of coal type. Both are consistent with work that has been reported in the organic geochemistry literature on the artificial and natural maturation of organic matter (12-17). Landais and coworkers (12-16) conclude that pyrolysis in confined systems, such as occurs in hydrothermal treatment, can mimic the natural maturation process for coal and other organic matter. However, they also conclude that the presence of water may not be as important as close confinement of the sample with the products of primary pyrolysis. Of course, for low rank coals one of the principal primary pyrolysis products is water. The work of Siskin and Katritzky (17) would suggest more prominent role for water as a reactant species and in providing a medium in which ionic reactions can occur (based on an extensive series of studies with model compounds). However, they also agree that the artificial maturation reactions are auto-catalyzed, i.e., the products of the initial reactions become reactants in subsequent reactions.

Figure 2 shows a comparison of evolution curves from TG-FTIR analyses of (a-d) water pretreated Zap lignite residues (350 °C, 4000 psig) and (e-h) four Argonne premium coals of a range of rank. This figure shows four sets of plots of the differential evolution rate curves for tar, CH_4, CO_2, and CO. In the case of tar, the results in Fig. 2a indicate a sharp increase in tar yield at short pretreatment times followed by a gradual decline at long pretreatment times. This trend is consistent with the observed trend in the rank series shown in Fig. 2e. It is also true that the T_{max} values for tar increase with increasing pretreatment time, which is again consistent with the observed rank variation. As discussed above, the initial increase in the tar yield could be due to loss of crosslinking agents (oxygen functional groups) and/or depolymerization of the coal structure. The decline in tar yield at long pretreatment time could be due to an increase in the aromatic cluster size of the average repeating unit which would lend to lower volatility and/or a loss of aliphatic hydrogen which can stabilize reactive fragments (26). There is also evidence from recent solvent swelling measurements done at Advanced Fuel Research that short time water pretreatment loosens up the coal structure, while long time pretreatment makes it more compact.

The results for the CH_4 evolution rate with increasing pretreatment time (Fig. 2b) also shows the same trend that is observed in the rank series (Fig. 2f). A major source of CH_4 gas evolution is believed to be methyl groups. These can be created by rupture and stabilization of CH_2 - CH_2 bridges or CH_2 - O bridges. The latter groups are known to be reactive under hydrothermal treatment conditions. Katritzky et al. (19) have also shown that benzyl alcohols can react under these conditions to form toluene as a major product.

Figure 2c indicates significant reductions in the CO_2 yield with increasing pretreatment time which also parallel the changes with increasing rank (Fig. 2g). The removal of carboxyl groups by

hydrothermal treatment has been demonstrated by FT-IR analysis of pretreated samples (7,11,14). Siskin et al. (18) have shown that hydrothermal treatment at 343 °C of 1-naphthoic acid yielded only naphthalene.

The results for the change in CO evolution with hydrothermal treatment (Fig. 2d) are interesting in that they do not directly follow the trend of decreasing CO with increasing rank (Fig. 2h), i.e., there is an initial increase in CO evolution. The evolution of CO can occur from the decomposition of hydroxy or dihydroxy functionalities. Evidence from FIMS (27) and FT-IR analysis (6,11) of water pretreated coal residues shows an initial increase in the formation of phenols and catechols during water pretreatment which is consistent with the initial increase in pyrolytic CO formation. Siskin et al. (18) have shown from model compound studies that certain diaryl ethers could be readily converted to phenols under hydrothermal treatment conditions. An examination of proposed structures for low rank coals (28) would reveal several ether and hydroxyether structures where this type of chemistry could occur.

The results in Figs. 3-5 show the integral yields of tar, CH_4, CO_2, and CO from water pretreatment of Zap, Wyodak, and Illinois No.6 coals for a range of pretreatment times. The trends for Zap, shown in Fig. 3, are consistent with the more limited set of data shown in Figs. 2a-d. The results for the Wyodak coal shown in Fig. 4, are similar to those of the Zap. The results for the Illinois coal, shown in Fig. 5, appear to depend on the "freshness" of the coal sample. The freshly opened samples (indicated by the darkened circles) appear to follow the same trends as the two lower rank coals, except for the CO_2 yield. The results for samples which were opened and stored in a nitrogen purged glove box are more scattered, but appear to follow similar trends, except for the CH_4 yields. This sensitivity of the Illinois coal to aging at ambient conditions has been reported previously (29,30) and is probably related to catalytic activity of the pyrite.

Quatititative Modeling - Work was begun on using the AFR FG-DVC pyrolysis model (26) to simulate the results of the water pretreatment experiments with Zap lignite. It was decided to use the Zap data from pretreatment at 350°C for short pretreatment times, since it appears that the behavior at long pretreatment times is more complex. The pyrolysis version of the FG-DVC model was successful at predicting the increase in pyrolysis tar yield based on the lower amounts of CO_2 and the higher amounts of extractables and CH_4, which are inputs into the model (26). A comparison of the measured (*-*) and predicted (---) pyrolysis yields is given in Fig. 6 for the raw and water pretreated coals.

In Fig. 7, a plot is shown of a van Krevelen diagram for the Argonne coals. The simulation of the standard FG-DVC model for maturation conditions is shown as a solid line. The simulation of a modified FG-DVC model for maturation in which CO and CO_2 are removed with a higher rate process is shown as a dashed line. This work is discussed in more detail by Solomon et al. (31). The results for the gas yields (discussed above) and FT-IR analysis of the water pretreated residues indicate that hydrothermal pretreatment more closely follows the dashed line than the solid line, since oxygen is removed faster than hydrogen. This is especially true for the two low rank coals (Zap, Wyodak). The total hydrogen and the sum of ether and hydroxyl oxygen amounts determined by FT-IR analysis of the water pretreated residues from four coals are shown in Table 1, below. Previous work has shown that FT-IR analysis provides a good estimate of the total hydrogen content when compared to standard elemental analysis (32). It also provides a measure of the sum of ether and hydroxyl oxygen which correlates with the total oxygen content. This will be confirmed by doing elemental analysis of the residues.

TABLE 1

FT-IR ANALYSIS OF WATER PRETREATED RESIDUES FROM FOUR COALS

COAL	PRETREATMENT TIME (mins. at 350°C, 4000 psig)	H_{TOTAL}	O_{SUM}
ZAP	- - - -	3.9	10.5
	20	4.9	9.7
	180	4.4	8.2
	1080	4.5	6.7
WYODAK	- - - -	5.1	10.2
	20	5.4	8.8
	180	5.0	8.0
	1080	4.0	7.0
ILLINOIS #6	- - - -	5.7	6.0
	20	4.4	5.4
	300	4.3	5.1
	1080	3.4	4.5
PITT	- - - -	5.8	4.4
	20	5.9	6.3
	180	5.3	5.0
	1200	4.7	4.1

CONCLUSIONS

The conclusions can be summarized as follows:

1. The analysis of pyrolysis data from water pretreated Zap lignite and Wyodak subbituminous coal (reduction in CO_2 yield, maximum in tar yield, increase in CH_4 yield) shows a strong similarity of hydrothermal treatment to an accelerated geological aging process. The results for the Illinois and Pittsburgh bituminous coals were generally similar, though less dramatic.

2. The geological aging analogy is also consistent with results that were obtained in the literature on hydrothermal treatment, since it explains why the treatment is effective in increasing pyrolysis yields for low rank coals and is ineffective or reduces pyrolysis yields for high rank coals. However, there are certain trends, such as the fact that the CO yield appears to follow the tar yield (goes through a maximum along with the tar) which do not agree completely with this analogy.

3. The FT-IR data indicate a rapid reduction of oxygen groups during water pretreatment for low rank coals, although there is an initial increase in hydroxy functionalities, and a slower loss of hydrogen after an initial increase.

ACKNOWLEDGEMENTS

The support of this work by the U.S. DOE Pittsburgh Energy Technology Center under Contract No. DE-AC22-89PC89878 is gratefully acknowledged.

REFERENCES

1. Bienkowski, P.R., Narayan, R., Greenkorn, R.A., Choa, K.W., IEC Res., **26**, 202, (1987).
2. Bienkowski, P.R., Narayan, R., Greenkorn, R.A., and Choa, K.C., Ind. Eng. Chem. Res. **26**, 206, (1987).
3. Graff, R.A. and Brandes, S.D., Proceed. of the New Fuel Forms Workshop, U.S. DOE Fossil Energy, p. 35, (1986).
4. Graff, R.A. and Brandes, S.D., Energy & Fuels, **1**, 84, (1987).
5. Zhou, P. and Brandes, S.P., "Steam Conditioning of Coal for Synfuels Production", 7th Annual Gsaification Contractors Review Meeting, (June 16-19, 1987).
6. Brandes, S.D., Graff, R.A., Gorbaty, M.L., and Siskin, M., Energy & Fuels, **3**, 494, (1989).
7. Khan, M.R., Chen, W.-Y., and Suuberg, E.M., Energy & Fuels, **3**, 223, (1989).
8. Ross, D.S. and Hirschon, A., ACS Div. of Fuel Chem. Prepr., **35**(1), 37, (1990).
9. Ross, D.S., Hirschon, A., Tse, D.S., and Loo, B.H., ACS Div. of Fuel Chem. Prepr., **35**(2), 352, (1990).
10. Serio, M.A., Solomon, P.R., Kroo, E., and Charpenay, S., ACS Div. of Fuel Chem. Prepr., **36** (1), 7, (1991).
11. Serio, M.A., Kroo, E., and Solomon, P.R., ACS Div. of Fuel Chem. Prepr., 37 (432), (1992)
12. Landais, P., Michaels, R., and Poty, B., and Appl. Pyrol., **16**, 103, (1989).
13. Landais, P., Monin, J.C., Monthioux, M., Poty, B., and Zaugg, P., C.R. Acad. Sci., Paris, t, **308**, Serie II, p. 1161, (1989).
14. Monthioux, M., and Landais, P., Energy & Fuels, **2**, 794, (1988).
15. Landais, P., and Monthioux, M., Fuel Proc. Tech., 20, 123, (1988).
16. Monthioux, M., Fuel, 67, 843, (1988).
17. Siskin, M., and Katritzky, A.R., Science **254**, 231 (1991).
18. Siskin, M., Brons, G., Vaugh, S.N., Katritzky, A.R., and Balasubramanian, M., Energy & Fuel, **4**, (5), 488, (1990).
19. Katritzky, A.R., Balasubramanian, M., and Siskin, M., Energy & Fuel, **4**, (5), 499, (1990).
20. Vorres, K.S., Energy & Fuels, **4**, (5), 420, (1990).
21. Solomon, P.R., Serio, M.A., Carangelo, R.M., Bassilakis, R., Gravel, D., Baillargeon, M., Baudais, F., and Vail, G., Energy & Fuels, **4**, (3), 319, (1990).
22. Solomon, P.R., and Carangelo, R.M., Fuel, **61**, 663 (1982).
23. Solomon, P.R., and Carangelo, R.M., Fuel, **67**, 949 (1988).
24. Solomon, P.R., Serio, M.A., Deshande, G.V., and Kroo, E. Energy & Fuels **4**, (1), 42, (1990).
25. Serio, M.A., Solomon, P.R., Kroo, E., Bassilakis, R., Malhotra, R., and McMillen, D., ACS Div. of Fuel Chem. Prep., **35**, (1), 61, (1990)
26. Solomon, P.R., Hamblen, D.G., Carangelo, R.M., Serio, M.A., and Deshpande, G.V., Energy & Fuels, **2**, 405, (1988).
27. Ross, D.S., Hirschon, A., Tse, D.S., and Loo, B.H., Fuel, **70**, 289 (1991).
28. Hatcher, P.G., Org. Geochem., 16, 959, (1990).
29. Gethner, J.S., Fuel, **66**, 1091, (1987).
30. Kelemen, S.R., Freund, H., Energy & Fuels, **3**, 498-505, (1989).
31. Solomon, P.R., Serio, M.A., Carangelo, R.M., Bassilakis, R., Yu, Z.Z., Charpenay, S., and Whelan, J., Paper, Anal.. App. Pyrolysis, 19, 1, (1991).
32. Teng, H., Serio, M.A., Bassilakis, R., Knight, K.S., Bates, S.C., and Solomon, P.R., Paper to be Presented at ACS Washington Meeting, (1992).

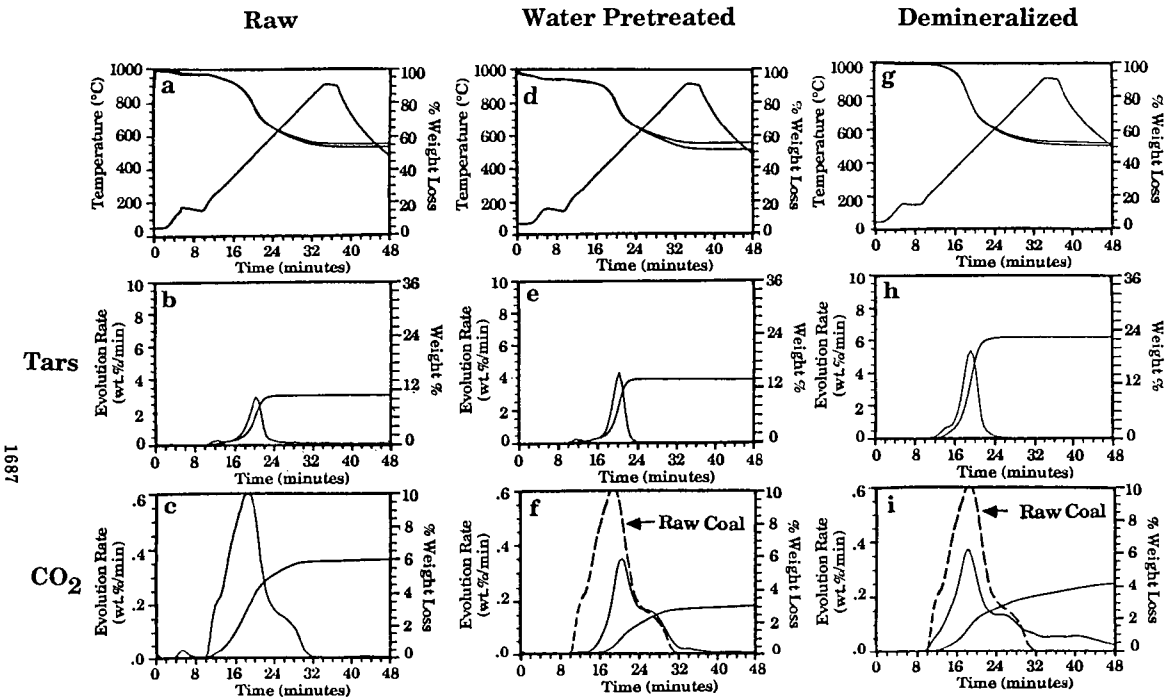

Figure 1. Product Evolution Curves for Raw, Water Pretreated and Demineralized Wyodak Subbituminous Coal. a,d,g) Weight Loss and Temperature Profile; b,e,h) Tar Evolution and Weight Loss; c,f,i) CO_2 Evolution and Weight Loss. Raw Coal Evolution Curve is Indicated in (f) and (i) as a Dashed Line for Comparison. The Water Pretreatment was done at 350°C, 4000 psig for 20 min.

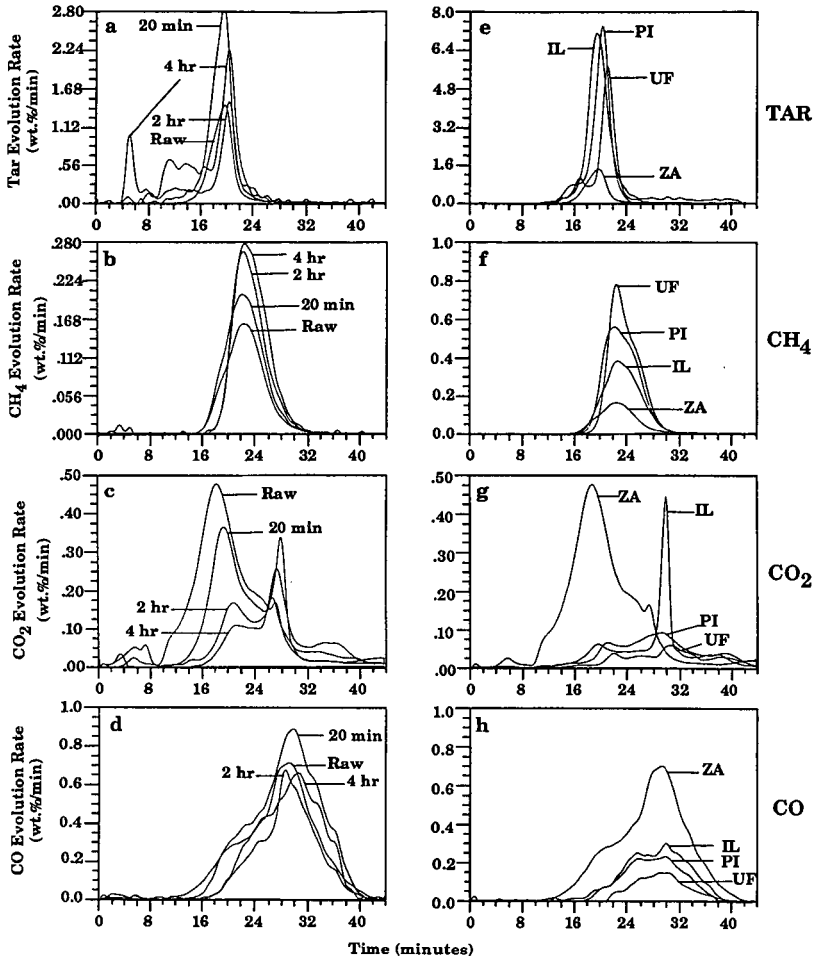

Figure 2. Comparison of Evolution Curves from TG-FTIR Analysis of a-d) Water Pretreated Zap Lignite Residues (350°C, 4000 psig) and e-h) Four Argonne Premium Coal Samples. The Evolution Rates are Given on an As-Received Basis. For the Water Pretreated Samples, the Rates are Normalized to the Moisture Content of the Raw Coal. The Samples are Heated to 150°C for Drying and then at 30°C/min to 900°C (starting at about 10 minutes).

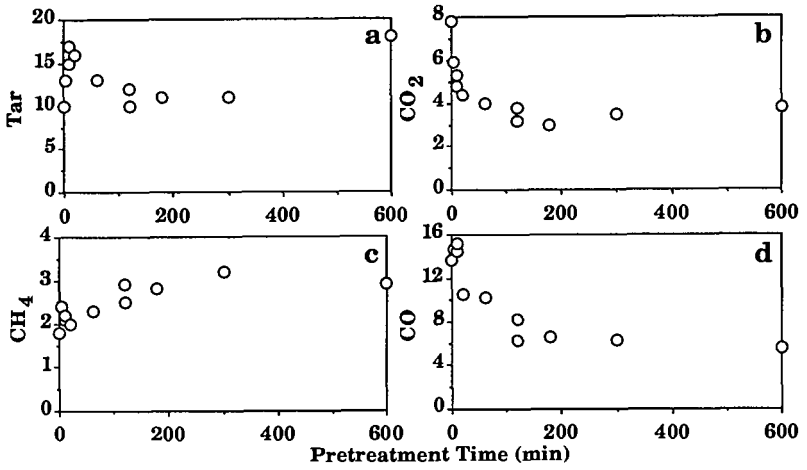

Figure 3. Results from TG-FTIR Analysis of Zap Residues Produced by Water Pretreatment at 350°C, 4000 psig for a Range of Pretreatment Times. All Results are Given on a DAF Basis.

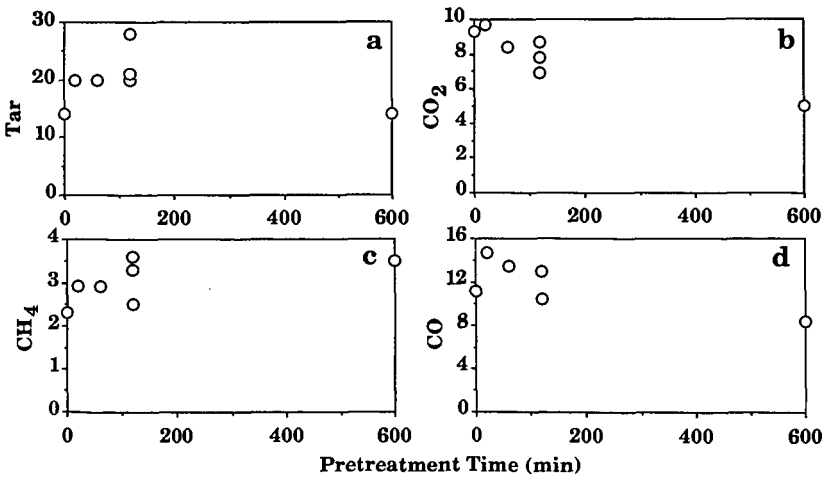

Figure 4. Results from TG-FTIR Analysis of Wyodak Residues Produced by Water Pretreatment at 350°C, 4000 psig for a Range of Pretreatment Times. All Results are Given on a DAF Basis.

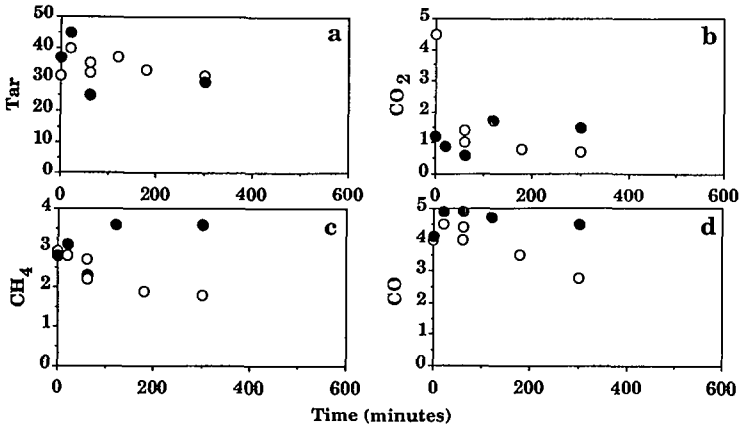

Figure 5. Results from TG-FTIR Analysis of Illinois Residues Produced by Water Pretreatment at 350°C, 4000 psig for a Range of Pretreatment Times. All Results are Given on a DAF Basis. Solid Circles are for Freshly Opened Samples. Open Circles are for Samples which had been Previously Open.

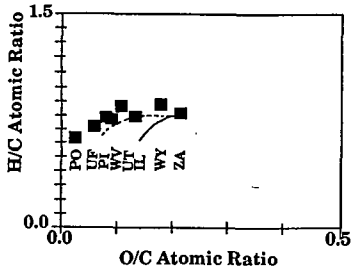

Figure 7. Maturation of Coal. Comparison of Predictions for FG-DVC Pyrolysis Model (solid line), FG-DVC Maturation Model (dashed line) and the Data for the Argonne Coals (symbols).

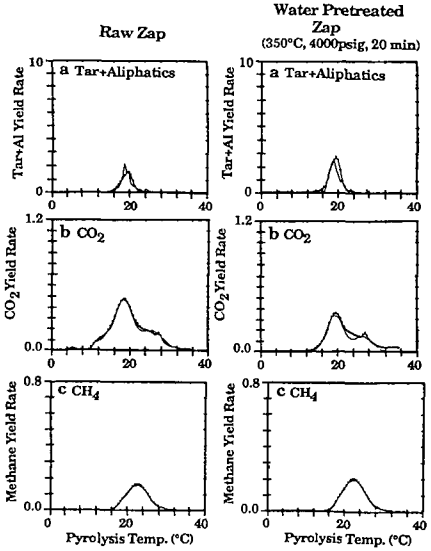

Figure 6. Comparison of Measured and Predicted Yields from Pyrolysis of Raw Zap and Water Pretreated Zap Lignites.

PYROLYSIS AND HYDROPYROLYSIS OF DIPHENYLMETHANE AND SULPHUR-CONTAINING COMPOUNDS IMMOBILISED ON SILICA

Stuart C. Mitchell[1], Christopher J. Lafferty[1], Roberto Garcia[1], Khudzir Ismail[1], Colin E. Snape[1], A.C. Buchanan III[2], Phillip F. Britt[2] and Elmer Klavetter[3]

[1] University of Strathclyde, Dept. of Pure & Applied Chemistry, Glasgow G1 1XL, UK.

[2] Chemistry Division, Oak Ridge National Laboratory, P.O. Box 2008, Oak Ridge, Tennessee 37831, USA

[3] Sandia National Laboratories, Albuquerque, NM 87185,USA

Keywords: Immobilised substrates, pyrolysis, hydropyrolysis, temperature programmed reduction.

ABSTRACT

The use of high pressures and dispersed catalysts, such as sulphided molybdenum (Mo) in fixed-bed hydropyrolysis of coals give rise to increased tar yields. In order to improve our understanding of these phenomena, particularly in relation to cleavage of C-C and C-S bonds, experiments have been conducted on samples of silica-immobilised benzene, diphenylmethane, thioanisole and dibenzothiophene (DBT). These model substrates have the inherent advantage that they do not soften and thus stay in the reactor. Moreover, for the surface-immobilised benzene, the SiO-C bond linking the substrate to the surface is reasonably stable and does not show significant cleavage until 550°C (peak maximum) with a high yield of benzene being achieved at 150 bar hydrogen pressure. For the diphenylmethane substrate, the use of 150 bar hydrogen pressure and the Mo catalyst both reduced the peak evolution temperatures for benzene and toluene clearly demonstrating their separate contributions to promoting C-C bond cleavage. Desulphurisation of the DBT substrate occurred only in hydrogen and the thermal decomposition of the thioanisole substrate was altered markedly by the Mo catalyst.

INTRODUCTION

Diphenylalkanes have been extensively used as model substrates to probe the free radical mechanisms involved in C-C bond cleavage reactions in coal liquefaction (1). However, the fact that the macromolecular structure in coals is undoubtedly subject to highly restricted motion suggests intuitively that free radical pathways are likely to be somewhat different from those encountered in the vapour phase. Indeed, this has been confirmed by the use of silica-immobilised substrates where bimolecular reaction steps are significantly perturbed in the cases of diphenylethane, propane and butane compared to the corresponding vapour phase reactions (2-4). Thus far, immobilised diphenylalkanes have only been studied at temperatures close to 400°C, but the fact that silicas do not melt below *ca* 1000°C means that the immobilised substrates also have considerable potential for probing coal and oil shale pyrolysis mechanisms at temperatures in the range 500-600°C which are generally used to maximise tar yields in both fluidised-beds and well-

swept fixed-beds [5-7]. The maximum temperature at which the substrates can be used will clearly be dictated by the cleavage of the C-O bond between the immobilised species and the silica. However, there are a number phenomena related to coal pyrolysis, particularly under hydrogen pressure (hydropyrolysis), which cannot be adequately modelled using model compounds in the vapour phase [8]. For example, the use of hydrogen pressure increases tar yields but without a concomitant increase in hydrocarbon gas yields at relatively low temperatures (< 600°C) where char hydrogasification would not appear to occur to a significant extent [5]. Secondary reactions of volatiles in coal pyrolysis are often implicated to explain reduced tar yields but, again, these are difficult to model, for example, with respect to non-thiophenic sulphur forms where C-S bonds are inherently weak but readily inter-convert to thiophenes [9].

In this study, pyrolysis and hydropyrolysis experiments have been conducted on silica-immobilised samples of benzene, diphenylmethane, thioanisole and dibenzothiophene (DBT) to begin to quantify the effects of hydrogen pressure and dispersed catalysts on C-C and C-S bond cleavage. The sulphur-containing substrates are also particularly useful in relation to temperature programmed reduction (TPR) where the authors from University of Strathclyde have devised a well-swept high pressure reactor [10] to enable virtually all the organic sulphur in coals to be released as hydrogen sulphide and, to a much lesser extent, as thiophenic compounds in tars. The only model substrates which can be possibly used to determine standard reduction temperatures in this regime for different organic sulphur forms are those which do not soften below the decomposition temperatures of the C-S bonds.

EXPERIMENTAL

The silica-immobilised benzene, diphenylmethane, thioanisole and DBT substrates were prepared as described previously [2-4] from the appropriate phenol. In the case of the sulphur-containing substrates, commercially available thioanisole and 3-hydroxyDBT synthesised from the corresponding bromo derivative were used [11]. The purity and loadings for the substrates as determined by base hydrolysis and subsequent gas chromatographic analysis of the silylated products were as follows. For DBT, GC/MS indicated that the remainder of the substrate appears to be derived from dihydroxyDBTs in the starting material.

	Loading, mmol g^{-1}	purity, %
Benzene	0.36	98.4
Diphenylmethane	0.45	99.5
Thioanisole	0.60	99.9
Dibenzothiophene	0.60	94.7

The sulphided Mo catalyst was prepared from ammonium dioxydithiomolybdate as previously described [12,13] which was loaded onto the substrates in methanol to give nominal Mo loadings of 2 or 5% w/w substrate. This helped to agglomerate the fine silica particles but there is the possibility that hydrolysis may have occurred to a limited extent. However, little difference was observed in the volatile evolution profiles without catalyst for the thioanisole substrate when the sample was contacted with methanol as a control experiment.

The high pressure apparatus used here is the same as that used recently for TPR [10]. The reactor tube was smaller but otherwise identical to that used previously in fixed-bed hydropyrolysis

studies (18" c.f. 42" both with 9/16" o.d., Incoloy) [12,13]. Between 0.2 and 0.5 g of sample (<75 μ) mixed with sand (up to 1:5 mass ratio, 75-250 μ sand to limit pressure drop across the reactor) was loaded into the reactor and held in place with steel wool plugs. The reactor tube was heated resistively up to 600°C at either 2 or 5°C min^{-1}. Hydrogen and nitrogen pressures of 30 and 150 bar were used with superficial gas velocities in the range 0.2-0.5 m s^{-1}. After pressure let-down through either a metering valve or a mass flow controller, the gas stream was sampled through a 1.8 m length of heated capillary tubing at a rate of 25 cm^3 min^{-1} into a quadrupole mass spectrometer (VG Monitorr, 0-100 a.m.u.). The signal from the control thermocouple situated in the coal bed was also fed to the mass spectrometer facilitating the construction of direct plots of evolved gas concentrations against temperature. The evolution profiles for the various species monitored can be fitted using the Redhead equation [14] to derive activation energies assuming first-order kinetics are operative.

RESULTS AND DISCUSSION

Benzene

The evolution profiles for benzene in 150 bar nitrogen and 150 bar hydrogen with and without catalyst and those for benzene, methane and toluene in 150 bar hydrogen are shown in Figures 1 and 2, respectively. In both nitrogen and hydrogen, the peak maxima for benzene are close to 550°C although, in nitrogen, there is also a peak at 500°C. However, much less benzene evolves in nitrogen and it is estimated that the amount is below 20% of that obtained with hydrogen at 150 bar. This is to be expected because the only source of hydrogen is the coupling of two molecules of surface-attached benzene. Indeed, the samples recovered from the nitrogen pyrolysis experiments were black qualitatively confirming that much less benzene had been released than in hydrogen where a small amount of methane and a trace of toluene were also observed at *ca* 570-600°C suggesting that hydrogasification is beginning to occur. No methane and toluene were observed with nitrogen confirming that hydrogasification does not occur under these conditions. Further, no phenol was detected indicating that the Si-O bond is unaffected. Benzene pyrolysis in fluid phases is a complicated process that follows an incompletely understood pathway [1] but it is interesting to note that the pyrolysis of benzene to give diphenyl and hydrogen begins to occur at reasonable rates at *ca* 550°C, the same temperature found here for benzene formation.

Catalyst addition at 150 bar hydrogen pressure vastly reduced the amount of benzene released. Further, the peak evolution temperature for the relatively small amount evolved was close to *ca* 500°C which is significantly lower than without catalyst (Figure 1). However, ions corresponding to methane and a number of alkene species including C_4H_8 and C_5H_8 were also observed suggesting that the benzene released above *ca* 500°C had been hydrocracked to a siginificant degree.

Diphenylmethane

The peak evolution temperatures for benzene and toluene formation are both 550°C with nitrogen (Figure 3) and the recovered sample was coloured indicating that some char must be formed on the substrate. Taking into account the response factors (benzene/toluene = *ca* 1.3 for the ions monitored), it is evident that more toluene is released than benzene (Figure 3, mass ratio being *ca* 2.5). Activation energies for fluid diphenylmethane have been found to be highly dependent on reaction conditions [1]. At low pressures, they are governed by dissociation of the weakest bonds (C-C and C-H are comparable at *ca* 82 kcal mol^{-1}) and hence temperatures in excess of 700°C are

required. However, at higher pressures (18-62 bar in diphenyl diluent), the activation energy is 66 kcal mol^{-1} in the temperature range 550-600°C [1] and this is close to the value of 63 kcal mol^{-1} derived from the evolution profile of benzene with nitrogen. The reaction mechanism in nitrogen is not well-understood but the hydrogen must come from the diphenylmethane itself probably through cyclisation to fluorene. Hence, it is possible that surface-immobilisation and the *para*-silyloxy substituent are lowering the activation energy for toluene release in some unknown fashion.

In hydrogen (without catalyst), roughly equal amounts of benzene and toluene evolve (Figure 4) with the white colour of the residue suggesting qualitatively that the char yield is small. Indeed, comparing the peak areas for benzene and toluene with those in the traces for the nitrogen runs, it is evident that, as anticipated, the amounts evolved are greater (*ca* 60 % more toluene and 4 times as much benzene). However, both evolution profiles would appear to be comprised of two components. The higher temperature one (550-580°C) is consistent with that anticipated for cleavage of the SiO-C bond in surface-immobilised benzene and toluene is similarly formed following the prior hydrogenolysis of the C-C linkages in diphenylmethane according to the reaction scheme below.

$$\text{-SiOPhCH}_2\text{Ph} + 2\text{H}_2 \text{ -------> } \text{SiOPhH} + \text{PhCH}_3 + \text{-SiOPhCH}_3 + \text{PhH}$$

Interestingly, the peak evolution temperature from C-C bond cleavage for toluene (495°C) is lower than that for benzene (530°C). The peak areas in the evolution profiles for the run with catalyst are lower than with hydrogen pressure alone (Figure 5) even allowing for the fact that less sample was used. The peak evolution temperatures for benzene and toluene are in the range 430-450°C and are significantly lower than those without catalyst. Further, with catalyst, no high temperature components in the evolution profiles of benzene and toluene are evident presumably because hydrocracking has occurred in a similar manner to the immobilised benzene (see above). The results clearly demonstrate that the use of hydrogen pressure and then the catalyst vastly reduce the activation energies for the disociation of the C-C linkages in the immobilsed diphenylmethane .

Thioanisole

Without catalyst at 150 bar hydrogen pressure, a H_2S peak with a maximum at *ca* 360°C is observed between 320-480°C (Figure 6) but there is no detectable CH_3SH. The methane profile comprises two components and the lower temperature one would appear to match the H_2S peak. Benzene, and to a lesser extent toluene, evolve from 380°C with the bulk evolving between 480 and 600°C probably from cleavage of the SiO-C bond as found for the benzene substrate (Figure 2). Further, the high temperature component of the CH_4 peak between 520 and 600°C broadly corresponds to the tail off in toluene concentration.

With catalyst, a low temperature CH_3SH peak is observed (Figure 7) with only a small amount of H_2S and a hint of methane being evolved at this stage. Some of the H_2S is undoubtedly from the thermal decomposition of the ammonium dioxydithiomolybdate but the overall H_2S concentration is considerably lower with catalyst which might be partly attributable to chemisorption of H_2S on the sulphided Mo (see below for DBT). The component of the methane peak at 350°C observed without catalyst has almost disappeared. Again, high temperature benzene and toluene peaks are observed from SiO-C bond cleavage but the ratio of benzene to toluene is much higher than without catalyst due to more sulphur being eliminated as CH_3SH. These experiments clearly

demonstrate the catalyst markedly affects the desulphurisation pathways of the immobilised thioanisole favouring cleavage of the phenyl-SCH_3 bond.

Dibenzothiophene

No detectable H_2S is evolved in nitrogen from the DBT substrate but, as anticipated from previous TPR and pyrolytic experiments on coals [10], significant quantities are released with hydrogen pressures of 30 and 150 bar (Figure 8). The peak evolution temperature of *ca* 500°C (slighty lower at the higher pressure) is close to those in the range 450-500°C found in high pressure TPR for a number of coals [10] confirming that the dominant peaks arise from thiophenes; lower temperature peaks between 300 and 400°C, attributed to non-thiophenic forms are also observed for low-rank coals.

Catalyst addition to the DBT substrate vastly reduces the amount of H_2S evolved at 150 bar (Figure 8). This is thought to arise from chemisorption of of H_2S on the sulphided Mo catalyst as the mole ratio of Mo to evolved sulphur is relatively high (*ca* 0.4). The peak maximum of *ca* 430°C is again similar to those observed thus far for coals in TPR [10]. However, because the mole ratio of Mo to evolved H_2S was much lower for the coals, no loss of intensity was observed upon catalyst addition.

CONCLUSIONS

The benzene results have demonstrated that immobilised model compounds are stable enough to be used in the type of pyrolysis and hydropyrolysis regimes used here. It has been shown using the diphenylmethane substrate that dispersed sulphided Mo catalyses the hydrocracking of C-C bonds in the solid-state. The thioanisole and DBT samples have demonstrated the promise of using immobilised sulphur compounds as standards in TPR.

ACKNOWLEDGEMENTS

The research was supported at the (i) University of Strathclyde by the Science & Engineering Research Council (Grant No. GR/G/26600) (ii) Oak Ridge National Laboratory by the Division of Chemical Sciences, Office of Basic Energy Sciences, US DoE under contract DE-AC05-840R21400 with Martin Marietta Energy Systems, Inc. and (iii) Sandia National Laboratories by the US DoE.

REFERENCES

1. M.L. Poutsma, *Energy & Fuels*, **4(2)**, 113 (1990) and references therein.
2. A.C. Buchanan III and C.A. Biggs, *J. Org. Chem.*, **54**, 517 (1989).
3. A.C. Buchanan III, P.F. Britt and M.L. Poutsma, *Prepr. Am. Chem .Soc. Div. Fuel Chem.*, **35(1)**, 217 (1990).
4. P.F. Britt and A.C. Buchanan III, *J. Org. Chem.*, **56**, 6132 (1991).
5. C.E. Snape, *Fuel*, **70**, 285 (1991) and references therein.
6. Z.S. Gonenc, J.R. Gibbins, I.E. Katheklakis and R. Kandiyoti, *Fuel*, **69**, 383 (1990).
7. A.M. Ruben and T.T. Coburn, *Proc. 1981 Eastern US Oil Shale Symp.*, 21.
8. R. Cypres, C. Braekman-Danheux and A. Progneaux, *Fuel*, **65**, 1299 (1986).

9. M.L. Gorbaty, S.R. Kelemen, G.N. George, P.J. Kwiatek and M. Sansome, *Fuel*, **70**, 396 (1991) and references therein.
10. C.J. Lafferty, S.C. Mitchell, R. Garcia and C.E. Snape, *Fuel*, accepted for publication and C.J. Lafferty, C.E. Snape, R. Garcia and S.R. Moinelo, *Prepr. Am. Chem. Soc. Div. Fuel Chem.*, **36(3)**, 877 (1991).
11. M. Gates and W.G. Webb, *J. Am. Chem. Soc.*, **80**, 1186 (1957).
12. C.E. Snape and C.J. Lafferty, *Prepr. Am. Chem. Soc. Div. Fuel Chem.*, **35(1)**, 1 (1990).
13. C.E. Snape, C.J. Lafferty, S. Mitchell, F. Donald, C. A. McArthur, G. Eglinton, N. Robinson and R. Collier, *Final Report, EC Project EN3V-0048-UK(H)* (1991).
14. P.A. Redhead, *Vacuum*, **12**, 203 (1962).

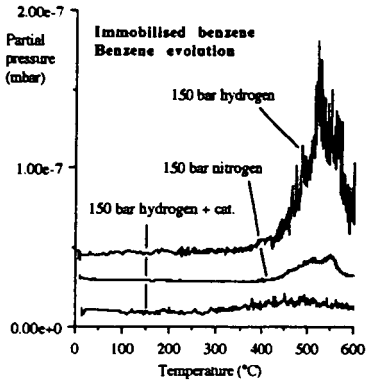

Figure 1. Evolution profiles of benzene from immobilised benzene.

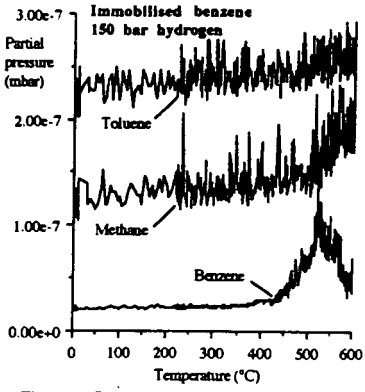

Figure 2. Evolution profiles of benzene, methane and toluene from immobilised benzene in 150 bar hydrogen.

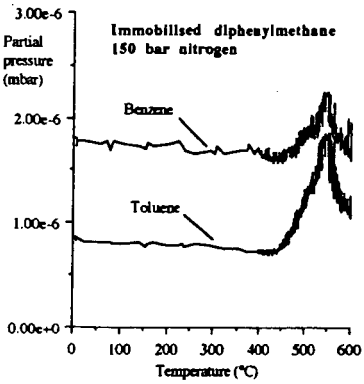

Figure 3. Evolution profiles of benzene and toluene from immobilised diphenylmethane in 150 bar nitrogen.

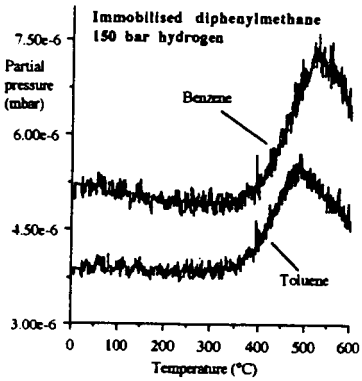

Figure 4. Evolution profiles of benzene and toluene from immobilised diphenylmethane in 150 bar hydrogen.

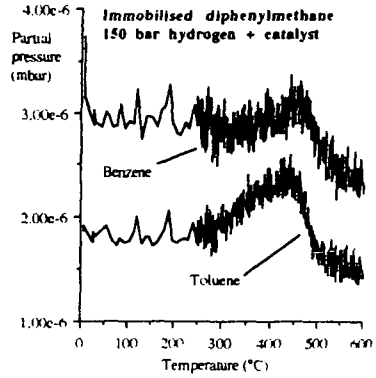

Figure 5. Evolution profiles of benzene and toluene from immobilised diphenylmethane in 150 bar hydrogen with the Mo catalyst.

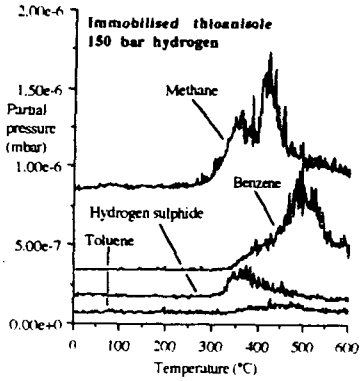

Figure 6. Evolution profiles of hydrogen sulphide, methane, benzene and toluene from immobilised thioanisole in 150 bar hydrogen.

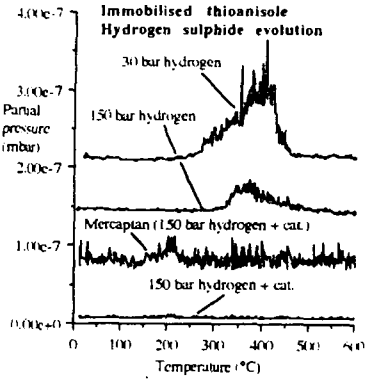

Figure 7. Evolution profiles of hydrogen sulphide and mercaptan from immobilised thioanisole.

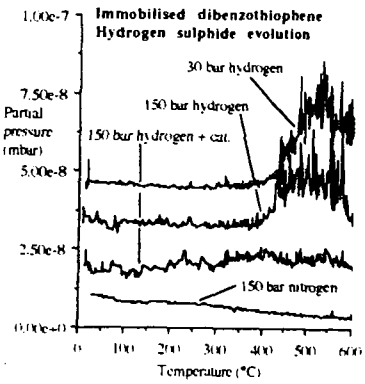

Figure 8. Evolution profiles of hydrogen sulphide from immobilised dibenzothiophene.

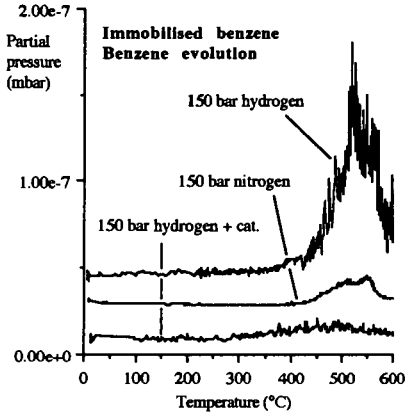

Figure 1. Evolution profiles of benzene from immobilised benzene.

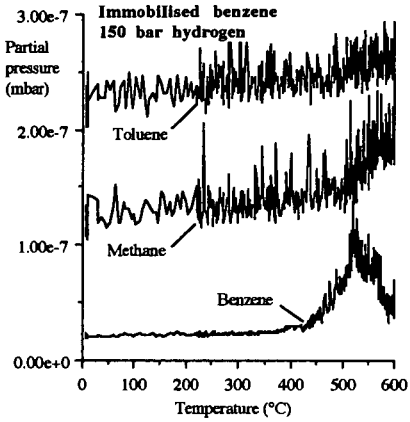

Figure 2. Evolution profiles of benzene, methane and toluene from immobilised benzene in 150 bar hydrogen.

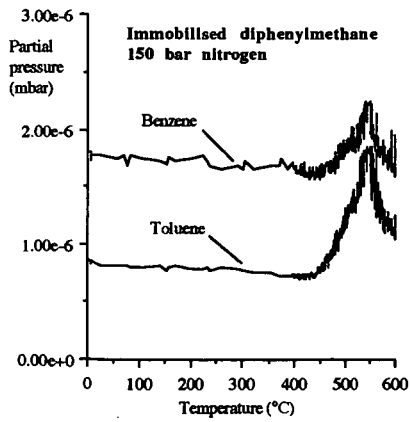

Figure 3. Evolution profiles of benzene and toluene from immobilised diphenylmethane in 150 bar nitrogen.

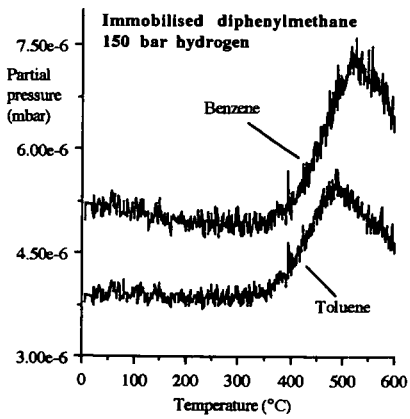

Figure 4. Evolution profiles of benzene and toluene from immobilised diphenylmethane in 150 bar hydrogen.

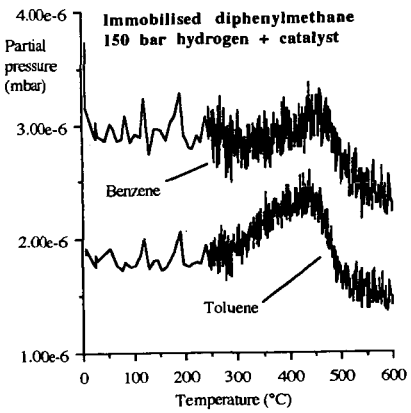

Figure 5. Evolution profiles of benzene and toluene from immobilised diphenylmethane in 150 bar hydrogen with the Mo catalyst.

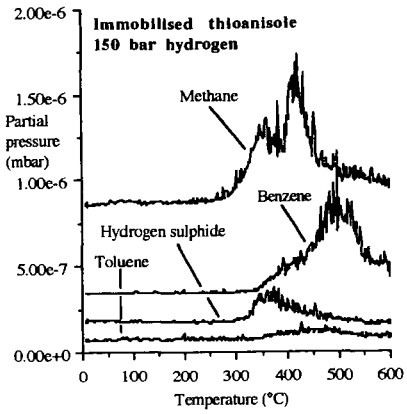

Figure 6. Evolution profiles of hydrogen sulphide, methane, benzene and toluene from immobilised thioanisole in 150 bar hydrogen.

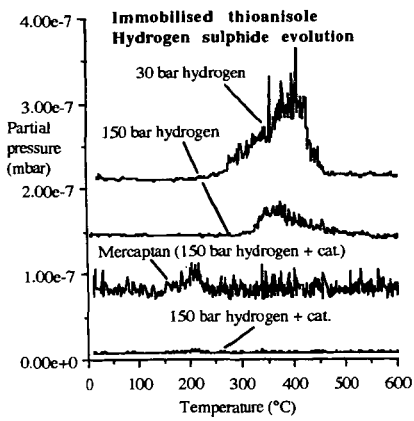

Figure 7. Evolution profiles of hydrogen sulphide and mercaptan from immobilised thioanisole.

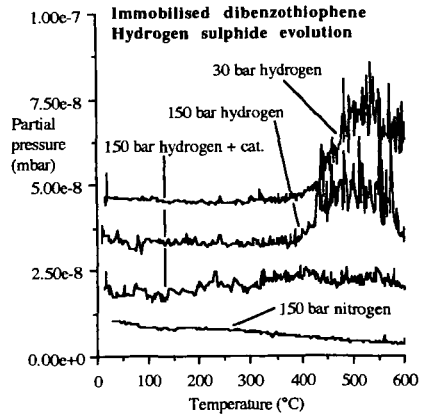

Figure 8. Evolution profiles of hydrogen sulphide from immobilised dibenzothiophene.

A ROLE OF DEVELOPING PORES FOR ORGANIC SULFUR RELEASE IN HYDROPYROLYSIS OF COAL

T. Sugawara and K. Sugawara

Division of Materials Process Engineering, Mining College
Akita University, Akita 010 Japan

Key words: hydrodesulfurization, sulfur form, rapid hydropyrolysis

INTRODUCTION

In our previous papers [1-4] , we examined the dynamic behavior of sulfur forms during hydropyrolysis of coal, changing heating rates from 40 K/min (fixed bed pyrolyzer, 1 atm hydrogen pressure) and 10 K/min (fixed bed pyrolyzer,30 atm hydrogen pressure) to 6000 K/s (free fall pyrolyzer, 1 atm hydrogen pressure). The desulfurization feature was characterized by a kinetic model as shown later, and the simulation of observed results was successful by applying the volume reaction model. We noticed that the extent of sulfur release from solid depended on the operating hydrogen pressure and on the heating rate. As for the organic sulfur in solid, it efficiently decreased when a rapid pyrolysis condition was adopted [4] . We pointed out that the release rate of volatile organic sulfur to tar and gas increased with increasing the release rate of volatile matter and with increasing the internal surface area at an initial stage of heating. The purpose of the present paper is to elucidate a role of developing pores which facilitate the organic sulfur release during rapid hydropyrolysis of coal.

EXPERIMENTAL

Table 1 shows the proximate, ultimate (daf basis), and sulfur form (% of total sulfur) analyses of sample coals: PSOC-830 (Indiana), Rosebud (Montana). A schematic diagram of the free fall pyrolyzer is shown in Fig.1. Coal particles (ca. 0.5 mm) were supplied from the hopper into the reactor at a feed rate of 0.2 g/min. The heating section length was controlled by changing the number of heating blocks from one to five as seen in the figure. Hydrogen gas flowing upwards (2.0 l NTP/min) encountered the coal particles and flowed out with gaseous products and tar. Volatile matter was determined by the difference of the weight of coal supplied and that of char received at the bottom of reactor. Hydrogen sulfide in gaseous products, the sulfur forms in coal and char were analyzed quantitatively [4] . The internal surface areas of the coal and char were measured by applying the Dubinin-Polanyi equation to CO_2 adsorption isotherms at 273 K.

KINETIC MODEL FOR DYNAMIC BEHAVIOR OF SULFUR FORMS

We proposed a kinetic model as illustrated in Fig. 2 where C and D were assumed firstly [2] to be present in void and later [4] in pores. Based on the Dusty Gas Model [5] , we assume here that C represents organic sulfur in tar in macropores and D hydrogen sulfide in gaseous products also in macropores. Micropores would play an important role for the surface reaction of reactants in solid. Decomposition of organic sulfur in coal, A into C and D, occurs at an initial stage of heating with volatile matter release. C and D in macropores could be reattached to solid phase, however, pressure increase in macropores with the evolution of volatile matter would facilitate the release of C and D to outside of a particle. As a consequence, we assume that only D forms refractory organic sulfur B at a later stage of heating where the remarkable evolution of volatile matter almost ends. Rate constants are the 1st order for k_1 - k_3, k_6 - k_8, the 0.5th order for k_4, and the 2nd order for k_5. Further reduction of iron sulfide F is negligible in the atmospheric treatment [4] . The release rates of C and D from macropores to outside of a particle are assumed to be the 1st order to their concentrations in macropores and the rate constants to be equal to the observed 1st order rate constant k for volatile matter release [4] .

EXPERIMENTAL RESULTS AND DISCUSSION

The top section of Fig. 3 shows a calculated curve of particle temperature Tc for PSOC-830 coal along with the distance from the coal hopper X. A set of simultaneous differential equations derived from the momentum, heat, and material balances for a particle were solved iteratively to give the relations of Tc and X and particle residence time t_R. Details of the calculation method are the same as in the reference [4] . A vertical dashed line denotes the point where the temperature begins to rise: particle residence time t_R was set to be 0 at X = 56 cm. Another calculation was also conducted for Rosebud coal which kept a larger apparent density in the pyrolyzer. The particle residence times t_Rs were 0.17, 0.25, 0.33, 0.41, 0.49 s for PSOC-830 coal, and 0.16, 0.24, 0.30, 0.36, 0.42 s for Rosebud coal , respectively, with the heating section lengths of 30 (X=116), 60 (146), 90 (176), 120 (206), 150 (236) cm. The middle section demonstrates change in internal surface area: a drastic change for PSOC-830 coal and a moderate increase for Rosebud coal. It should be noticed that the dynamic feature was quite different within the order of 100 ms even if the final value attained nearly the same. The bottom section of Fig. 3 represents the observed relation between volatile matter released V and the distance from the hopper X. Dashed lines are the calculated values with Eqs. (1) and (2):

$$dV/dt_R = k_0 \cdot \exp(-E/RTc) \cdot (V^* - V) \quad (1)$$

$$V = 0 \text{ at } t_R = 0 \quad (2)$$

where V^* means the ultimate value. A smaller value of the activation energy for PSOC-830 coal, 18 kcal/mol, would relate to the rapid development of micropores, compared with a larger value of 30 kcal/mol for Rosebud coal.

Figures 4 and 5 are observed changes in the sulfur forms distribution with X or t_R for PSOC-830 and Rosebud coals, respectively. Simulation curves are also drawn with one boldfaced and three lightfaced lines in each figure. The part below the boldfaced line in the figure indicates inorganic and organic sulfurs in solid. One can see that the organic sulfur content in solid in PSOC-830 coal decreases more rapidly and efficiently than Rosebud coal. When we concentrate our attention on the sulfur behavior at an initial stage of heating, i.e. t_R<0.2 s, we can evaluate the reaction characteristics of organic sulfur in solid with the rate constants, k_1 - k_3. The simulated values at 1233 K are as follows:

	k_1 [1/s]	k_2 [1/s]	k_3 [1/s]	k [1/s]
PSOC-830	10.1	12.6	25.2	27.7
Rosebud	6.9	4.0	10.1	19.2

Calculated values of the rate constants for volatile matter release with Eq.(1) and (2) are also included. The data suggest that the role of developing micropores is very important for efficient release of organic sulfur from solid.

ACKNOWLEDGEMENTS

This work was supported by Grant in Aid for Scientific Research, Ministry of Education, Science and Culture, Japan, Project no. N16B-01 (03453122). The Pennsylvania State University and Montana College of MineralScience and Technology are appreciated for the supply of coal samples.

REFERENCES

1. Sugawara, T., Sugawara, K., the late Ohashi, H., *Fuel* **67** 1263 (1988).
2. idem, *ibid* **68** 1005 (1989).
3. Sugawara, T., Sugawara, K., Sato, S., Chambers, A. K., Kovacik, G., Ungarian, D., *i bid* **69** 1177 (1990).
4. Sugawara, T., Sugawara, K., Nishiyama, Y., Sholes, M.A., *ibid* **70** 1091 (1991).
5. Bliek, A., van Poelje, W. M., van Swaaij, W. P. M., van Beckum, F. P. H., *AIChE J.* **31** 1666 (1985); Mason, E. A., Malinauskas, A. P., Evans III, R. B., *J. Chem. Phys.* **46** 199 (1967).

Table 1 Ultimate, proximate and sulfur form analyses

Sample	C	H	N	S	Diff.	VM(daf)	FC(daf)	Ash(dry)	FeS_2	SO_4^{2-}	Organic
PSOC 830	71.0	4.4	1.1	1.3	22.2	40.7	59.3	5.6	13	7	80
Rosebud	72.9	4.5	0.9	0.9	20.8	44.3	55.7	10.2	32	3	65

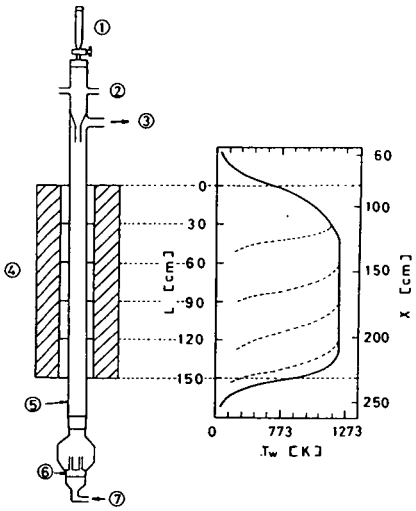

Fig.1 Schematic diagram of free fall pyrolyzer and longitudinal wall temperature profiles of reactor.

1, coal hopper
2, entrained gas inlet
3, gas outlet
4, furnace(5 blocks, 30 cm per block)
5, reactor (fused silica tube, 36 mm i.d.)
6, glass filter
7, gas inlet
L, length of furnace
X, distance from coal hopper

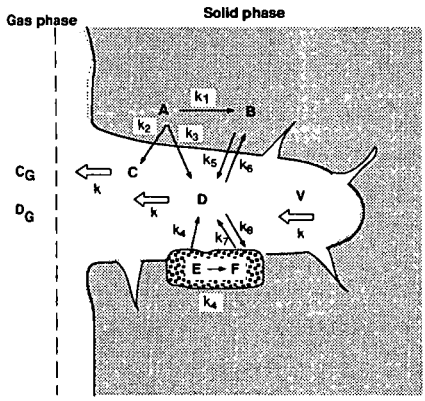

Fig.2 Image of desulfurization of coal.

A : (S_{org})coal
B : (S_{org})char
C : (S_{org})tar
D : S_{H_2S}
E : S_{FeS_2}
F : S_{FeS}
V : Volatile matter

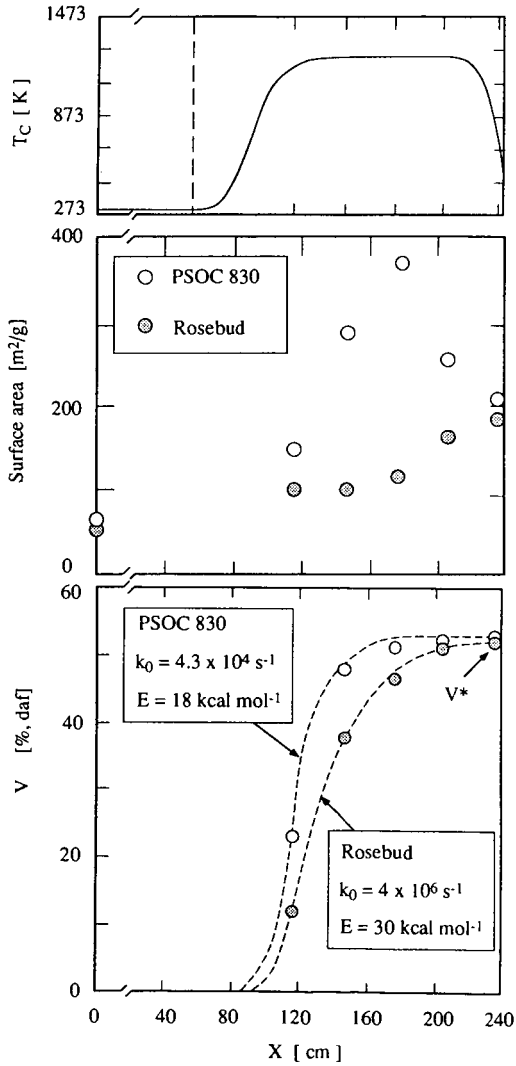

Fig.3 Estimated particle temperature T_c, internal surface area observed and volatile matter released V with simulation curve along with distance from coal hopper X.

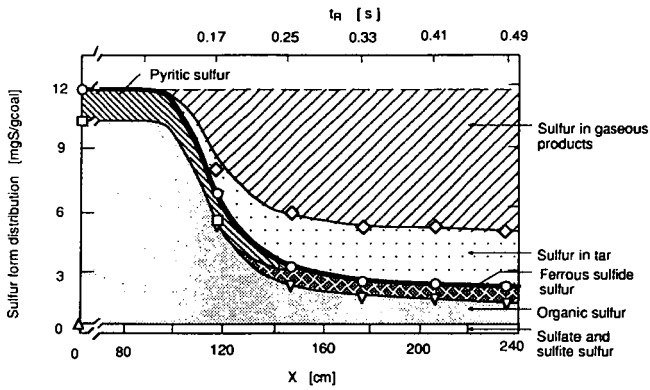

Fig.4 Change in sulfur form distribution with distance X from coal hopper or with particle residence time t_R for PSOC-830 coal.

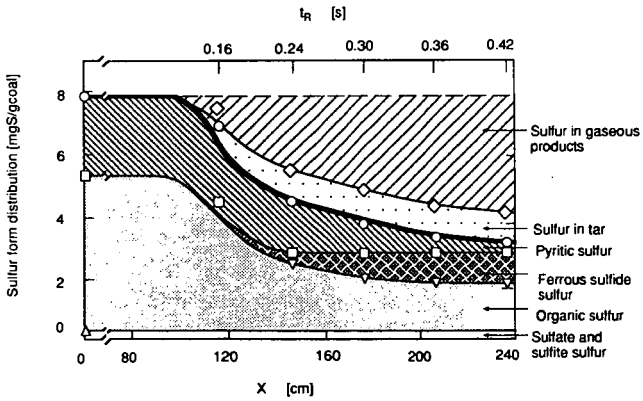

Fig.5 Change in sulfur form distribution with distance X from coal hopper or with particle residence time t_R for Rosebud coal.

CHANGES IN ORGANIC OXYGEN CONTENTS OF ILLINOIS #6 COAL DURING COAL LIQUEFACTION

Bongjin Jung, W. D. Provine, W. H. Calkins*, and M. T. Klein
Center for Catalytic Science and Technology
Department of Chemical Engineering
University of Delaware
Newark, DE 19716

Charles Scouten
Amoco Oil Company
Naperville, IL 60566

INTRODUCTION

The initial stage of direct coal liquefaction is generally presumed to involve the cleavage of the weak bonds in coal. While these weak bonds have not been identified, it appeared possible that they are ether oxygen bonds, and probably benzylic ether bonds because of their low bond strength, and the low activation energies observed in coal liquefaction (1). This view has been strengthened by the observation that coal liquefaction products frequently contain more phenolic components than do the coals from which they were derived (2), suggesting the cleavage of ethers to form phenols. To check this hypothesis, it would be of interest to follow the oxygen content of coal at very low liquefaction conversions, even before much of the coal actually becomes liquid. To do this requires a liquefaction reactor system capable of sampling at very short contact times and low conversions. This system must be such that temperatures and pressures are carefully controlled, and reaction times and reaction time distributions are known. Such a liquefaction reactor has been constructed in our laboratory (3). A preliminary report of the aromaticity of such low conversion products have already been reported (4). In this paper, we present a preliminary report on the total organic oxygen and organic oxygen species in these low conversion solid products.

EXPERIMENTAL

Reactor and Sampling System. The reactor system used is a 1 liter CSTR (continuous stirred tank reactor) described previously (3). A constant flow of tetralin (7 liters/hour) is maintained in a 900 psig nitrogen atmosphere (450 sccm nitrogen) at a temperature of 390°C. 50 gram charges of coal in a tetralin slurry (1:2 coal to solvent) are injected through a rupture disk almost instantaneously by diverting solvent into the charging bomb. Product samples taken in an automated sampling manifold (in this study at 2, 23, 55, 87, 119, and 151 seconds) after injection are quenched to 150°C with a countercurrent water heat exchanger. The system was tested with samples of dibenzylether to check the behavior of a compound with well-known kinetics in the system (5).

Sample Work-Up. The solids were filtered and washed with methylene chloride at room temperature, to remove residual tetralin and coal liquids, and dried in a vacuum oven.

Conversion. Conversion of the coal was determined by measuring the low-temperature ash content of the solid residue and comparing it to that of the unreacted coal (6). A low-temperature asher (LFE Corporation, LTA-302) was operated at 100 watts. The oxygen flow rate was kept at 100 cc/min. Samples were ashed to constant weight.

Organic Oxygen Content. Fast neutron activation analysis (FNAA) was used to determine the oxygen content of the dried reactor sample and the derived low temperature ash. The total

organic oxygen content was determined by correcting the FNAA value of the dried reactor sample for the oxygen content of the mineral matter in the ash (7,8).

Organic Oxygen Speciation. The organic oxygen species (carboxyl, hydroxyl and carbonyl) in the dried reactor samples were determined by the chemical methods of Blom and Schafer (9,10). The organic ether contents of the samples were determined by the difference of the total organic oxygen by FNAA and the oxygen species determined by the chemical methods mentioned above.

Coal Sample. The coal studied was Illinois #6 obtained from AMOCO Corporation. The entire sample was finer than 200 mesh. The analysis of this coal is summarized in Table 1.

RESULTS AND DISCUSSION

The changes in the solid coal at various reaction times are shown in Table 2.

It is apparent from the kinetics of coal conversion (Fig. 1) that a portion of the coal is liquefied more rapidly than the bulk of the coal. That this is not due to the conversion of a particularly reactive maceral is shown by the petrographic analysis summarized in Table 3. Fusinite and semifusinite are generally less reactive than vitrinite (11).

Moreover, these differences are not likely due to particle size effect since the entire sample was extremely fine. In short, a portion of the vitrinite appears to be more reactive than other parts of the vitrinite.

The data gathered thus far suggest that only a relatively small change in the total organic oxygen content occurred (perhaps 10%), even though up to 20% of the coal went into solution. The carboxyl or carbonyl contents of the solid coal are very low to begin with and show little or no change. On the other hand, the hydroxyl content dropped significantly (30–35%) and the ether groups, determined by difference, therefore increased. The explanation for the change in hydroxyl is not clear at this point. However, these results are consistent with the condensation of phenolic groups within the coal to form furane type ring structures (12).

SUMMARY AND CONCLUSIONS

Previous NMR results (4) and the present experiments show clearly that chemical changes occur in solid coal before it becomes a liquid. Further and more extensive measurements will be required before the details of these changes can be resolved. These experiments also show significant conversion of solid to liquid 390°C even at very short contact times. If the formation of these liquid products occurs by cleavage of benzyl ether bonds, they must have occurred in components of the coal having quite different reactivities than the rest of the coal, and to represent only a small proportion of the original ether groups present.

ACKNOWLEDGEMENTS

This research was sponsored in part by Amoco Oil Company and in part by the State of Delaware as authorized by the State Budget Act of Fiscal Year 1988. We also acknowledge the Radioanalytical Services of the University of Kentucky for doing the FNAA and Prof. John Crelling of Southern Illinois University for the petrographic analysis.

REFERENCES

1. Szladow, A. J. and Given, P. H. Ind. Eng. Chem., Process Des Dev. 1981, 20, 27-30.

2. Wachowska, H. and Pawlak, W. Fuel 56, 422 (1977).

3. Provine, W. D.; Poro, N. D.; LaMarca, C.; Foley, H.C.; Bischoff, K. B.; Scouten, C. G.; Cronauer, D. C.; Tait, A. M.; Klein, M. T. "Development of a Pulse Injection CSTR COal Liquefaction Flow Reactor" presented at the AIChE National Meeting, Chicago, IL, Nov. 1991.

4. Provine, W. D.; Jacintha, M. A.; Klein, M. T.; Calkins, W. H.; Dybowski, C. ACS Fuel Div. Preprints 37 (2), 670 (1992).

5. Cronauer, D. C.; Jewell, D. M.; Shah, Y. T.; Modi, R. S. Ind. Eng. Chem. Fund. 1979, 18, 153.

6. Shou, J. K. and Pitts, W. Fuel 1977, 54, 343.

7. James, W. D.; Ehmann, W. D.; Hamrin, C. E.; and Chyi, L. L. J. Radioanal. Chem. 32, 195, (1976).

8. Volborth, A.; Miller, C. E.; Garner, C. K. and Jerabek, P. A. Fuel 56, 204 (1977).

9. Blom, L.; Edelhausen, L. and van Krevelen, D. W. Fuel 36, 135 (1957).

10. Shafer, H. N. S. Fuel 49, 147 (1970).

11. Given, P. H.; Cronauer, D. C.; Spackman, W.; Lovell, H. L.; Davis, A. and Biswas, B. Fuel 54, 40 (1975).

12. Poutsma, M. L. and Dyer C. W. J. Org. Chem. 47, 3317 (1982).

Table 1. Elemental Analysis of Illinois #6 Coal Used.

Carbon	67.18	
Hydrogen	5.00	
Nitrogen	0.98	
Sulfur	3.63	
Chlorine	0.19	
Oxygen (by diff)	12.34	
Ash (ASTM D3174)	10.68	(High Temperature)

Table 2. Total Organic Oxygen Content and Oxygen Functional Groups in the Coal Liquefaction Residues as a Function of Reaction Time at 390°C.

Reaction Time (sec)	0	23	55	87	119	155
% Conversion	0	9.5	16.4	19.5	17.6	20.1
% Organic Oxygen	10.5	10.0	9.6	9.1	10.3	
% Oxygen as Hydroxyl	7.5	5.3		4.7		
% Oxygen as Carboxyl	0.6	0.4		.5	0.65	
% Oxygen as Carbonyl	0.6	0.9		0.6	0.7	
% Oxygen as Ether	2.1	3.3		3.4		

Table 3. Petrographic Analysis of Illinois #6 (AMOCO)

maceral	Volume %	
	Southern Ill. Univ.	Argonne National Laboratory
Vitrinite	86	85
Semifusinite	10.4	10
Fusinite	2.0	
Liptinite	1.6	5

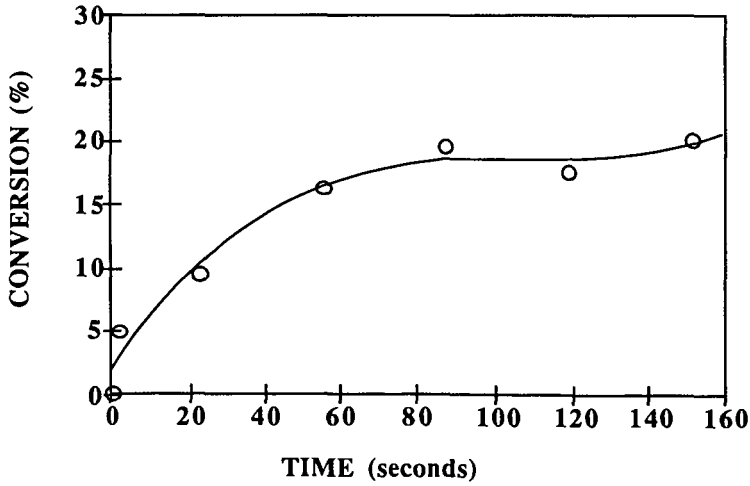

Figure 1. Conversion vs. Time

SULFUR AND NITROGEN EVOLUTION IN THE ARGONNE COALS

R. Bassilakis, M.A. Serio, and P.R. Solomon
Advanced Fuel Research, Inc., 87 Church Street, East Hartford, CT 06108

Keywords: Argonne Premium Coals, Sulfur, Nitrogen

INTRODUCTION

In a previous study (1), the major volatile products evolving from the Argonne Premium coals were investigated using TG-FTIR temperature programmed pyrolysis and combustion. The focus of this study is on the evolutions of two minor volatile products, sulfur and nitrogen, using the same TG-FTIR technique. Although sulfur and nitrogen are small contributors to the mass loss from coal during pyrolysis, their oxides are a major cause of environmental pollutants during coal combustion.

EXPERIMENTAL APPARATUS

Details on the TG-FTIR system appear elsewhere (1,2,3). Its components are as follows: a DuPont 951 TGA, a hardware interface, an Infrared Analysis 16 pass gas cell with transfer optics, and a Michelson 110 FT-IR (resolution, 4 cm^{-1}; detector, MCT). A helium sweep gas (250 cm^3/min) is employed to bring evolved products from the TGA directly into the gas cell. The system is operated at atmospheric pressure.

PROCEDURE

A 50 mg sample loaded in the platinum sample pan of the DuPont 951 is taken on a 30°C/min temperature excursion in helium first to 150°C to dry for 4 minutes and then to 900°C at 30°C/min for pyrolysis. Upon reaching 900°C and holding the temperature for 3 minutes, the sample is immediately cooled to 250°C over a 20 minute period. After cooling, a small flow of O_2 (20 cm^3/min) is added to the helium sweep gas and the temperature is ramped to 900°C in order to combust the remaining char. Infrared spectra are obtained once every 41 seconds.

A post-oxidation method was employed to collectively study sulfur evolution. In this procedure, heat (approximately 900°C) and oxygen (10 cm^3/min) is added to the volatile product stream after the furnace but before the analysis cell. This added step allows detection of H_2S, a very weak infrared absorber; elemental sulfur; and tar sulfur by monitoring SO_2 evolution rate. Details of this post-oxidation method appear elsewhere (1).

RESULTS AND DISCUSSION

Sulfur Evolution - The total sulfur evolution from pyrolysis of the Argonne Premium coals is presented in Figure 1. Sulfur was studied collectively by post-oxidizing the pyrolysis products and monitoring the SO_2 evolution rate. The SO_2 evolution curves exhibit two main evolution peaks. For each peak, the temperature of the maximum evolution rate (T_{max}) increases with increasing rank. Similar rank dependance has been reported by Kelemen et al. (4) and Oh et al.(5). Furthermore, the low temperature SO_2 evolution peak coincides with the coal's tar evolution peak.

To determine the pyritic sulfur contributions to the SO_2 evolutions, Illinois #6 and Pittsburgh #8 coals were subjected to ASTM D-2492 (6) under a nitrogen atmosphere. In this method, sulfate sulfur is extracted from the coal with dilute hydrochloric acid and pyrites (FeS_2) are removed using dilute nitric acid. Results from temperature programmed pyrolysis and combustion of raw and ASTM D-2492 modified Illinois #6 coal are presented in Figures 2 and 3 respectively. Figures 2a and 3a are the balance and thermocouple curves and Figures 2b and 3b are the SO_2 evolution and weight curves. The tar evolution curve for the raw Illinois #6 coal (obtained with out the post-oxidizer in line) is included in Figure 2a to demonstrate how the tar peak overlays the low temperature SO_2 peak. The ASTM D-2492 procedure removed a substantial amount of the low temperature SO_2 peak, the entire high temperature SO_2 peak and the "sharp" portion of the combustion cycle SO_2 peak. These results indicate that pyritic sulfur evolves during the low and the high temperature SO_2 peak, an observation that has been reported by others (5,7). Temperature programmed pyrolysis and combustion of raw and ASTM D-2492 modified Pittsburgh #8 coal showed similar trends as the Illinois #6 coal.

Table 1 compares the TG-FTIR's pyritic and organic sulfur values with those provided by Argonne National Laboratory (8) and also gives the pyrolysis and oxidation contributions to the pyritic and organic sulfur amounts. For Illinois #6 coal, 53 percent of the pyritic sulfur and 62 percent of the organic sulfur along with 47 (ash-free) weight percent of the volatiles evolved during pyrolysis while for Pittsburgh #8 coal, 64 percent of the pyritic sulfur and 48 percent of the organic sulfur along with 43 (ash-free) weight percent of the volatiles evolved during pyrolysis. Consequently, both coals are preferentially evolving sulfur during pyrolysis.

To compare coal pyrite with pure pyrite, a pure pyrite sample from Custer, South Dakota was subjected to temperature programmed pyrolysis and combustion and the evolution curve is presented in Figure 4. The pyrite sample shows no low temperature SO_2 and has a high temperature SO_2 T_{max} (609°C) slightly higher than that of Illinois #6 coal in Figure 2b (578°C).

What causes the low temperature pyrite decomposition in coals during pyrolysis? Since for each Argonne Premium coal the tar evolution and the low temperature SO_2 evolution have similar T_{max}'s, it is feasible that the tars are responsible for the low temperature pyrite decomposition in coal. In support of this possibility, presented in Figures 5a and b are Arrhenius plots comparing the mean reaction rates (r) for tar evolution and low temperature SO_2 evolution for Illinois #6 and Pittsburgh #8 coals respectively. The Arrhenius parameters were generated using the method of evaluating the T_{max} shift with heating rate as described by Braun et al. (9). In this method, a plot of $\ln H_r/T_{max}^2$ versus $1/T_{max}$, where H_r is the experimental heating rate, produces a line with the slope equal to $-(E_a/R)$. The Arrhenius plots show that the mean tar and low temperature SO_2 reaction rates differ by a factor of 4 for the Illinois #6 coal and are virtually identical for the Pittsburgh #8 coal.

As noted from Figure 1, the high temperature SO_2 T_{max} which is a result of pyrite decomposition demonstrates rank dependence. The SO_2 T_{max} increases from 564°C in the case of Zap coal, to 674°C in the case of Upper Freeport coal. It is unclear as to why pyrite in coal is rank dependent. Pyrolysis experiments are presently being done with pyrite/model compound mixtures and with pyrite in the presence of various gases added to the helium sweep gas in an attempt to address this issue.

Nitrogen Evolution - The NH_3 and HCN evolutions from pyrolysis of the Argonne Premium coals are presented in Figures 6 and 7. The NH_3 evolution curves exhibit two main evolution peaks.

For each peak, the T_{max} increases with increasing rank although the majority of the shift in T_{max} for the high temperature NH_3 peak occurs between Wyodak and Illinois #6 coals. The HCN evolution curves exhibit only one main evolution peak and, with the exception of Zap and Wyodak coals, the HCN evolution curves overlay the high temperature NH_3 evolution curve suggesting that a common source is responsible for their formation. In the cases of Zap and Wyodak coals, HCN evolves at a lower temperature than the high temperature NH_3 evolves.

Table 2 compares that TG-FTIR weight percents for NH_3 and HCN to previously obtained values generated during rapid heating rate pyrolysis in an entrained flow reactor (EFR) (10). For each coal, the total amount of nitrogen evolved in of the each pyrolysis systems is similar. The ratio of HCN to NH_3, however, differs significantly. The dominant product during slow heating rate pyrolysis in the TG-FTIR is NH_3 while the only product during rapid pyrolysis in the EFR is HCN. These results can be explained by the following possibilities: 1) A competitive reaction process leads to the formation of NH_3 at the expense of HCN at low pyrolysis heating rates; 2) In the entrained flow reactor, secondary pyrolysis reactions especially tar cracking, lead to the formation of HCN and the destruction of NH_3; 3) NH_3 is removed in the collection system in the entrained flow reactor (e.g., dissolution into water which condenses on the walls of the gas collection bag).

In an attempt to increase the tar cracking in a slow heating rate pyrolysis run, Utah Blind Canyon coal was pyrolyzed in the TG-FTIR and the pyrolysis products were passed through a hot quartz tube heated to approximately 900°C just prior the gas analysis cell. This post-pyrolysis method utilizes the same apparatus as the post-oxidization method; however, helium is added to the sample stream rather than oxygen. The post-pyrolysis results are presented in Figure 8. Figure 8a displays the HCN evolution curves while Figure 8b shows the NH_3 evolution curves. In the post-pyrolysis experiment, the HCN evolution peak at the 20 minute mark indicates a significant increase in tar cracking. This supports item 2 in the latter paragraph although post-pyrolysis does not show significant reductions in NH_3 evolution.

SUMMARY AND CONCLUSIONS

Sulfur Evolution - The total sulfur evolution during pyrolysis measured by post-oxidation of volatile products demonstrated two main evolution peaks which had consistent rank variations. The first SO_2 peak is from organic and pyritic sulfur while the second SO_2 peak is from pyritic sulfur only. Arrhenius plots showed that tar evolution and low temperature SO_2 evolution had similar mean reactions rates. And, sulfur was found to be preferentially released during pyrolysis.

Nitrogen Evolution - NH_3 evolution exhibited two main peaks whose T_{max}'s showed rank dependence although the majority of the shift in the high temperature NH_3 peak occurred between Wyodak and Illinois #6 coals. HCN evolution curves coincided with the high temperature NH_3 evolutions except in the cases of Wyodak and Zap coals where lower HCN T_{max}'s were observed. Finally, the dominant product during slow heating rate pyrolysis was NH_3 while during rapid heating rate pyrolysis HCN was the only product.

ACKNOWLEDGEMENTS

This work was supported by the Morgantown Energy Technology Center of the United States Department of Energy under contract DE-AC21-86MC23075. We wish to acknowledge the useful discussions with Erik Kroo of Advanced Fuel Research and Professor Eric Suuberg of Brown

University. We also thank Jean Whelan of Woods Hole Oceanographic Institute for supplying the pyrite sample.

REFERENCES

1. Solomon,, P.R., Serio, M.A., Carangelo, R.M., Bassilakis, R., Gravel, D., Bailargeon, M., Baudais, F., and Vail, G., Energy & Fuels, (1990).

2. Carangelo, R.M., Solomon, P.R., and Gerson, D.J., Fuel, **66**, 960 (1987).

3. Whelan, J.K., Solomon, P.R., Deshpande, G.V., and Carangelo, R.M., Energy & Fuels, **2**, 65 (1988).

4. Kelemen, S.R., Gorbaty, M.L., Vaughn, S.N., and George, G., "Transformation Kinetics of Organic Sulfur Forms in Argonne Premium Coals During Pyrolysis," Preprint, Am. Chem. Soc., Div. of Fuel Chem., **36** (3) pp.1225-1232 (1991).

5. Oh, M.S., Burnham, A.K., and Crawford, R.W., Preprints, Div. Fuel Chem., Am. Chem. Soc., **33** (1), 274 (1988).

6. Annual Book of ASTIM Standards, Sec. 5 Petroleum Products, Lubricants, and Fossil Fuels, Vol. 05.05 Gaseous Fuels; Coal and Coke, pp. 356-360, (1985)

7. Khan, M.R., Fuel, **68**, 1439 (1989)

8. Vorres, K.S., "Users Handbook for the Argonne Coal Sample Program," (1989).

9. Braun, R.L., and Burnham, A.K., Energy & Fuels **1** (2) pp.153-161 (1987)

10. Solomon, P.R., Hamblen, D.G., Carangelo, R.M., and Krause, J.L., "Coal Thermal Decomposition in an Entrained Flow Reactor: Experiments and Theory," 19th Symposium (International) on Combustion/The Combustion Institute, pp. 1139-1149 (1982)

Table 1. TG-FTIR and Argonne Values for Pyritic and Organic Sulfur in Illinois No. 6 and Pittsburgh No. 8.

	TG-FTIR (AF Wt.%)						Argonne Values (AF Wt.%)	
	Pyritic			Organic			Pyritic	Organic
	Pyrolysis	Oxid.	Total	Pyrolysis	Oxid.	Total	Total	Total
Illinois	1.73	1.53	3.26	1.17	0.73	1.90	3.02	2.16
Pittsburgh	1.12	0.64	1.76	0.42	0.46	0.88	1.48	0.88

Table 2. NH_3 and HCN Weight Percents from Pyrolysis in TG-FTIR and Entrained Flow Reactor.

	TG-FTIR (as-received wt.%)		EFR 1100°C, 24" (ash free wt.%)	
	HCN	NH_3	HCN	NH_3
Pocahontas	0.034	0.27	0.28	0
Upper Freeport	0.028	0.42	0.78	0
Pittsburgh	0.038	0.47	0.84	0
Stockton	0.051	0.45	0.55	0
Utah Blind Canyon	0.101	0.53	1.21	0
Illinois	0.065	0.45	---	---
Wyodak	0.035	0.28	0.60	0
Zap	0.082	0.40	---	---

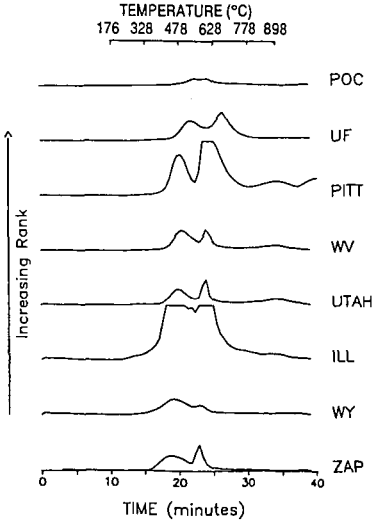

Figure 1. SO_2 Evolution Curves from Pyrolysis of the Argonne Coals with Post-Oxidation of Volatile Products.

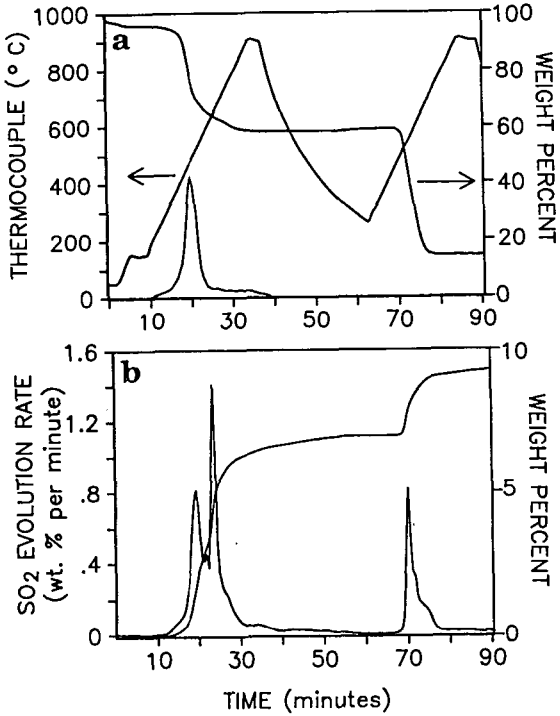

Figure 2. Results from Pyrolysis of Illinois No. 6 Coal with Post-Oxidation of Volatile Products. a) Balance, Thermocouple and Tar Evolution Curves and b) SO_2 Evolution and Weight Curves.

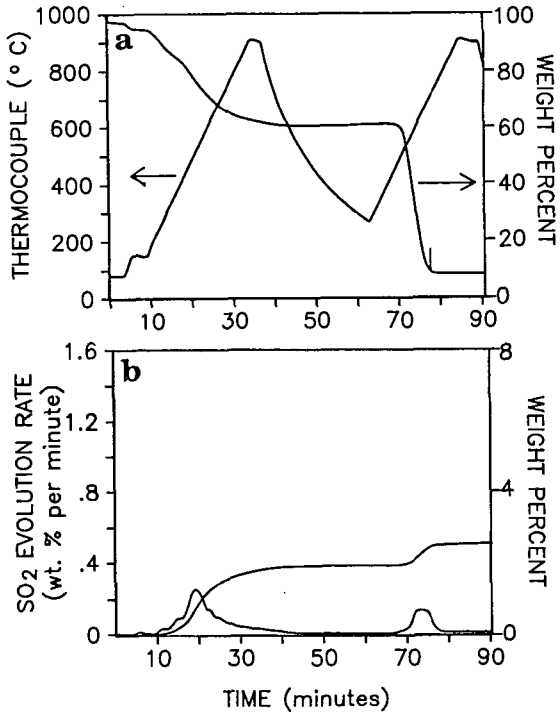

Figure 3. Results from Pyrolysis of ASTM D-2492 Modified Illinois No. 6 with Post-Oxidation of Volatile Products. a) Balance and Thermocouple Curves and b) SO_2 Evolution and Weight Curves.

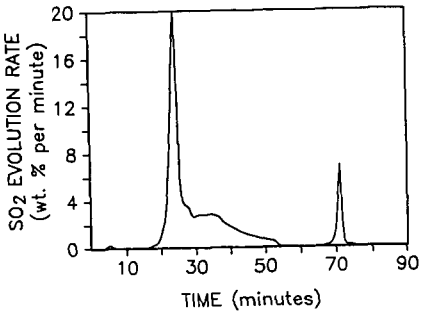

Figure 4. SO_2 Evolution Curve from Pyrolysis of Pyrite with Post-Oxidation of Volatile Products.

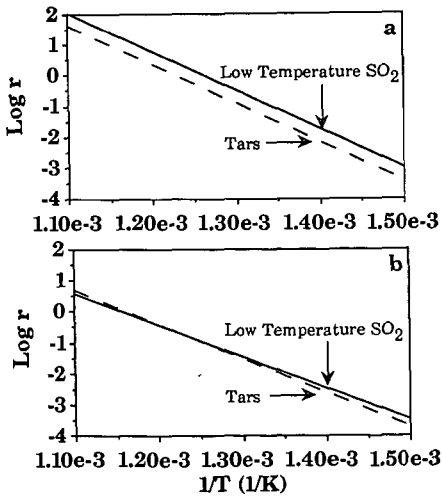

Figure 5. Arrhenius Plots Comparing Mean Reaction Rate (r) of Tar Evolution and Low Temperature SO_2 Evolution for a) Illinois No. 6 and b) Pittsburgh No. 8.

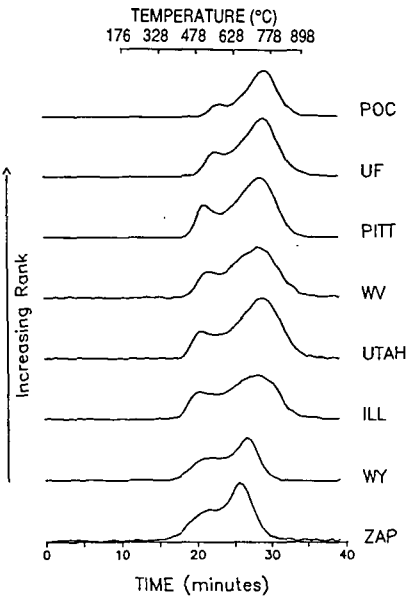

Figure 6. NH_3 Evolution Curves from Pyrolysis of the Argonne Coals.

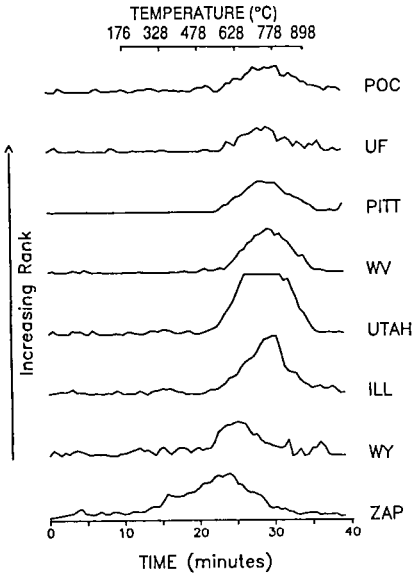

Figure 7. HCN Evolution Curves from Pyrolysis of the Argonne Coals.

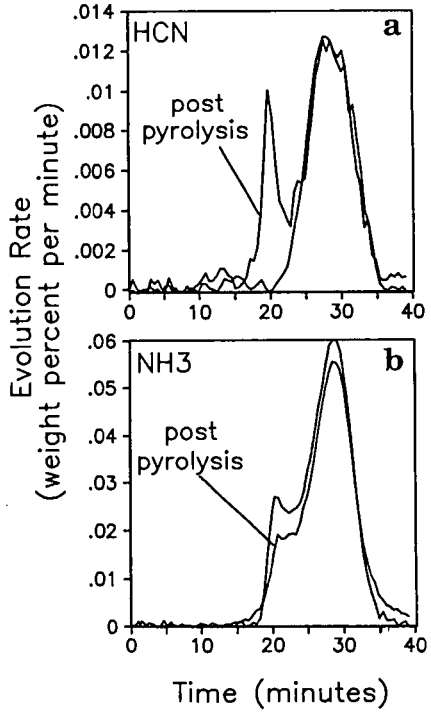

Figure 8. Results from Pyrolysis and Post-Pyrolysis of Utah Blind Canyon. a) HCN Evolution Curves and b) NH_3 Evolution Curves.

DECARBOXYLATION AND COUPLING REACTIONS OF COAL STRUCTURES

Jeffrey A. Manion, Donald F. McMillen, and Ripudaman Malhotra
Molecular Physics Laboratory, SRI International
333 Ravenswood Ave., Menlo Park, Calif. 94025

Keywords: Decarboxylation, cross-linking, retrograde reaction, liquefaction

ABSTRACT

Coupling reactions resulting from decarboxylation have long been associated with the retrograde reactions that hinder the pyrolysis and liquefaction of low-rank coals. The precise chemistry responsible for the coupling has not been proposed, beyond the suggestion that radical recombination or addition must be involved. We have performed a series of decarboxylation/coupling experiments in monomeric benzoic acid systems under liquefaction-relevant, but homogeneous, reaction conditions. The principal findings whose implications will be discussed are: (1) coupling as a result of decarboxylation tends to be very minor (generally < 10%); (2) under strongly oxidizing conditions, namely the absence of scavengers and the presence of one-electron oxidants (which may pertain to the interior of coal particles during the early part of liquefaction), coupling can be as much as 50% of the decarboxylations; (3) amine bases tend to promote decarboxylation but either inhibit or do not affect coupling; (4) H-donors inhibit coupling and, in some circumstances, decarboxylation induced by one-electron oxidants. The limited coupling associated with decarboxylation under most of these liquefaction-related conditions suggests that coupling associated with phenols may be more important.

INTRODUCTION AND OBJECTIVES

It has become increasingly clear in recent years not only that retrograde reactions substantially hinder the liquefaction of low-rank coals, but also that oxygen functional groups in the coal structure are major actors in these retrograde reactions. Carboxyl functions have been implicated in the crosslinking of coals during heating at relatively low temperatures,[1,2] and Serio et al.[3] have been able to model the pyrolytic loss of solvent swelling by including one additional crosslink in the network for every CO_2 evolved. Moreover, pretreatments that have been found to be effective in promoting liquefaction have also shown a corresponding decrease in the early CO_2 evolution.[4] Thus, although crosslinking is correlated with the evolution of CO_2 and H_2O and it therefore seems that carboxyl and/or phenolic groups are involved, we do not know exactly how or why. In order to best mitigate the retrograde reactions it is necessary to better understand their mechanisms—i.e., to know what factors promote and inhibit them.

A recent study by Siskin and coworkers[5] showed that decarboxylation of naphthoic acid under hydrothermal conditions was attended by formation of some binaphthyl, but the coupling aspect was not elaborated in that paper. As a prelude to studies with polymeric compounds, we have carried out and report here on a series of experiments with coal-related monomeric carboxylic acids. We have examined rates of decarboxylation and coupling to see if crosslinking results directly from decarboxylation, as well as how crosslinking is affected by ion exchange, the presence of a hydrothermal environment, and other conditions relevant to pretreatment.

EXPERIMENTAL

Procedures. Experiments on decarboxylation and coupling of monomeric carboxylic acids were carried out in fused silica ampoules. Samples were degassed and sealed under vacuum, with each sample filling approximately one-half of the tube at room temperature. The sealed tube and an appropriate quantity of solvent for pressure equalization was placed in an outer jacket of stainless steel tubing capped with compression fittings. The reaction vessel was then immersed in a temperature-controlled molten-salt bath for the desired time, the tube removed and quenched in water. After cooling in liquid nitrogen to condense CO_2 and volatile organics, the ampoule was opened and the sample removed by pipet and repeated washing of the tube with solvent. An internal standard was

added and the sample analyzed by gas chromatographic analysis using a flame ionization or mass selective detector. Product quantitation was obtained using the FID analyses, with molar responses determined separately for those compounds for which we had authentic samples and estimated by comparison with similar species when no sample was available. Generally, at least three split injections of each sample were performed using an autoinjector. For most species the reproducibility was within ± 2% and we estimate the overall analytical accuracy to be within ± 5%. An exception pertains to the highly polar carboxylic acids, which exhibited excessive peak tailing in the gas chromatograms. These compounds showed much less reproducibility both from injection to injection and in the day-to-day variation in the molar response. For these species we estimate the overall analytical accuracy to be ± 12%.

Chemicals. Benzoic acid (99+% by GC analysis), o-Anisic acid (2-Methoxybenzoic acid, Aldrich, 99%), 3,4-Dimethoxybenzoic acid (Aldrich 99+%), 3-Methoxy-4-hydroxybenzoic acid (Aldrich 97%), m-Hydroxybenzoic acid (Aldrich 99%), Phenylacetic acid (99+% by GC analysis), Cupric acetate monohydrate [$Cu(CH_3CO_2)_2 \cdot H_2O$, Fisher scientific] and Fe_3O_4 powder (supplier unknown, particle size ~ 0.2 μm) were used without further purification.

RESULTS

The Decarboxylation of Activated and Unactivated Benzoic Acids. Table 1 shows the results obtained for a series of benzoic acids under typical "liquefaction" conditions, i.e., 400 °C in tetralin, sometimes with small amounts of other additives such as base.

Data in this table demonstrate that the decarboxylation of benzoic acid itself is slow at 400°C in tetralin (3-5% in 1 hr), unless a fairly strong base or other decarboxylation promoter is present. The substituted but unactivated substrate 3-hydroxybenzoic acid gives a similar degree of decarboxylation. Surprisingly, the decarboxylation of calcium benzoate in tetralin is no faster than that of the free acid. None of these compounds gave significant coupling, either with the starting acid, benzene, tetralin, or naphthalene. In cases where species with hydroxyl groups, e.g. naphthol, were present, there was a small amount (up to several percent) of esterification together with small amounts of the rearranged product of this ester. Since esters will not survive liquefaction conditions when water is present, as it typically is in coal liquefaction, we currently do not consider these "non-permanent" linkages to be of great importance with regard to retrograde reactions.

The near-absence of coupling, together with the slow decarboxylation of benzoic acid itself at 400°C, would make it appear that unactivated aromatic carboxylic acids do not represent the acid species that undergo facile decarboxylation between 250° and 350°C during the heating of low-rank coals. Therefore, we performed additional experiments to examine the behavior of benzoic acid derivatives known[6,7] to be activated toward decarboxylation via electrophilic attack. For all of these, except for meta hydroxy benzoic acid and veratric acid (3,4-dimethoxy benzoic acid, last row in Table 1), decarboxylation in tetralin was almost complete in one hour at 400°C. Again however, there was no substantial level of coupling products. (In some cases there were small chromatographic peaks, as yet unidentified, at higher retention times. We cannot rule out the possibility that these result from some type of coupling associated with decarboxylation, but in any case they amount to less than 5% at most of the decarboxylated acid.)

Perhaps the most interesting result with the activated acids is that obtained with veratric acid. This acid did *not* undergo complete decarboxylation, but was recovered in ca. 25% yield after 1 hour in tetralin at 400°C, in contrast to the analog containing a free -OH in the para position, which underwent complete decarboxylation. Because p-OMe is generally just as activating toward electrophilic attack as p-OH, the above difference indicates that the rate-determining step cannot simply involve attack on the starting material itself. That is, this result suggests that the principal mode of decarboxylation by electrophilic attack either involves reaction of the phenoxy anion or the keto form of the phenolic acid, which is accessible only through the free phenol. One possibility it that the keto form of the acid simply undergoes thermal unimolecular bond cleavage (homolysis) to yield a stabilized radical (phenoxy) and the radical $\bullet CO_2H$, in exact analogy to the thermal cleavage of benzyl and phenoxy

phenols that has been previously elucidated.[8] This possibility, however, is ruled out by the estimated enthalpy requirement for the reaction, which dictates that the decarboxylation would have a half-life of no less than 1000 hours at 400°C.

The Effect of Electron-Transfer Agents and the Acceptor/Scavenger Ratio. Having seen very little coupling resulting from decarboxylation of any of the acids tested thus far, we have broadened the range of reaction conditions under which these acids are being heated, in an attempt to bring about more coupling and perhaps approximate more closely conditions encountered in the thermal processing of low rank coals. Essentially this means reaction in more oxidizing systems, i.e. systems with potential oxidants for carboxylate ions, and with little or no hydro- or alkyl-aromatic. During the early stages of coal liquefaction, such relatively oxidizing conditions might be expected to arise in the interior portions of the coal which are not directly surrounded by the liquefaction solvent. Furthermore, under these conditions, literature data for the reactions of phenyl- and other aryl radicals[11-13] lead us to expect that any phenyl radicals formed will add very readily to essentially any aromatic system, displacing hydrogen to form biaryl linkages. For these experiments we used mixtures of benzoic acid and naphthalene as the basic system and then added various combinations of the reagents that were found from our previous studies to affect decarboxylation, particularly base (pyridine) and the electron transfer agents Fe_3O_4 and $Cu(OAc)_2$.

Table 2 shows the effects of the 1-electon oxidants Fe_3O_4 and $Cu(OAc)_2$ and the solvent H-donating ability on the decarboxylation of benzoic acid. Both electron transfer agents markedly increase decarboxylation (from 3-5% as shown in Table 1 to at least ~50% as seen in Table 2). This increase is qualitatively in accord with the literature data on copper/amine-promoted decarboxylation.[6,7] Decarboxylation is at least ten times faster with $Cu(OAc)_2$ than with Fe_3O_4, but the generation of coupling products is about ten times faster in the presence of Fe_3O_4. In contrast to the experiments reported in Table 1, three main coupling products, phenylnaphthalenes, pyridinylnaphthalenes, and binaphthyls are now observed when either of the electron-transfer agents are present. The similarity of the products suggests that qualitatively similar chemistry is contributing in both systems. However, we still see only relatively low levels of coupling products, particularly in the $Cu(OAc)_2$ system.

The effect of the hydrogen donors on coupling and decarboxylation of benzoic acid can be seen by comparing the latter two experiments in Table 2. In these experiments with cupric acetate, the amount of coupling is decreased by 70% when naphthalene is replaced by a tetralin/1-methylnaphthalene/naphthol mixture. Both the decarboxylation rate and the ratio of coupling to decarboxylation decrease significantly. This result is suggestive that the primary mode of coupling involves aryl radicals, which are readily scavenged by any of the three new components. The most likely mode of aryl radical production is from $C_6H_5CO_2\bullet$, which should rapidly decompose to $C_6H_5\bullet$ and CO_2. Interestingly, decarboxylation itself is also markedly slowed when an H-donor solvent is used, decreasing from ≥ 83% to about 47%. The reason for this is uncertain. Presuming decarboxylation involves $C_6H_5CO_2\bullet$, thermochemical kinetic analysis indicates that the $C_6H_5CO_2\bullet$ radical should decarboxylate much more rapidly than it could abstract hydrogen from e.g. tetralin. It appears, therefore, that the H-donor must be interfering in some other manner with the activity of the electron transfer agent. (For example, a redox reaction within a cupric acetate molecule to produce curpous acetate and $C_6H_5CO_2\bullet$ might possibly be interfered with by tetralin, which, as an added reducing agent might compete with the internal reducing agent, carboxylate anion.)

Coupling Product Distribution. A more detailed breakdown of products from benzoic acid under various conditions is provided in Table 3. The nature and distribution of the coupling products themselves may provide an indication of the factors limiting coupling under the above reaction conditions. GC/MS analysis has allowed us to identify the coupling products 1- and 2-phenylnaphthalene, two isomers of pyridinylnaphthalene, and the 1,1', 1,2', and 2,2'-binaphthyls, as listed in Table 3.

Typically the 1-phenylnaphthalene is two to three times more abundant than the 2-phenylnaphthalene, consistent with a radical mechanism and the relative rates of radical addition and H-transfer to naphthalene that have been reported in the literature.[14,15] In the case of the binaphthyls, the ratio of

1,2'-, 1,1'-, and 2,2'-binaphthyl is typically 3:2:1. This product distribution is consistent with a statistical preference for the 1,2' isomer, a rather small (1-2 kcal/mol) preference for abstraction of the naphthalene 1-hydrogens,[16] and very little kinetic preference for the highly exothermic addition of an aryl radical to the favored[14,15] 1-position of another naphthalene. The least abundant isomer (2,2'-) represents addition of the least favored aryl radical to the least favored position for addition. The isomer distribution reported by Stein,[16] who studied binaphthyl formation starting from the pure hydrocarbons, differs slightly from our product distribution; he reported the 2,2' isomer to be slightly more favored than the 1,1' binaphthyl.

In the case of the pyridinylnaphthalenes, the point of connection of the pyridine to the naphthalene ring is inferred from the phenylnaphthalenes, but the connections to the pyridine ring are unknown. The pyridinyl- and naphthylnaphthalene isomer distributions are generally consistent with those expected from H-abstraction from either pyridine or naphthalene by the initially produced phenyl radical, followed by addition of the new aryl radical to naphthalene. However, the formation of similar amounts of pyridinylnaphthalenes and naphthylnaphthalenes (binaphthyls) is surprising in view of the fact that the reaction mixture contains seven times as much naphthalene as pyridine. In order to check our inference that these products result directly or indirectly from decarboxylation, we performed control experiments with mixtures of benzene, pyridine, and naphthalene in the presence of Fe_3O_4. Although no significant quantity of phenylnaphthalenes were formed, we surprisingly did find pyridinylnaphthalenes and binaphthyls. Their amounts indicate that perhaps 30-40% of the *secondary* coupling products could arise from mechanisms not involving decarboxylation as the original radical source. However, the *primary* coupling products (i.e., those between phenyl and naphthalene) are almost entirely due to decarboxylation.

Rates of Decarboxylation and Coupling. As would be anticipated from the data of Tables 1 and 2, the addition of 10 m% of pyridine to the naphthalene/benzoic acid mixture (Condition 1 to Condition 2) should increase decarboxylation, and it does increase it about a factor of four (to 19%). It does not, however, substantially affect the coupling to decarboxylation ratio, which drops slightly from 0.027 to 0.023. However, if 10 m% of Fe_3O_4 is added instead of pyridine (Condition 1 to Condition 3), decarboxylation is increased by a factor of only two, while the coupling to decarboxylation ratio rises dramatically to 0.49. Apparently, the absence of a reducing agent such as tetralin *and* the presence of a 1-electron oxidant is necessary before coupling reactions become substantial. Finally, if pyridine is added along with the Fe_3O_4, decarboxylation is increased to ≥ 58%, but the ratio of coupling/decarboxylation ratio is reduced by two-thirds when compared to the Fe_3O_4-only case. Thus, although pyridine/Fe_3O_4 synergistically promote decarboxylation, the base leads to an interruption or circumvention of the pathway responsible for coupling.

Mechanistic implications. Although there seem to be relatively few definitive mechanistic investigations of the decarboxylation unactivated acids, decarboxylations have been major synthetic reactions for many years, and the phenomenology is extremely varied, including what appear to be anionic, free radical, and molecular routes.[5-7,9,10] The decarboxylation products we have observed at high temperatures (>300°C) in more oxidizing systems (no donor solvent present, and with an added electron-transfer agent) tend to support one of the traditionally anticipated routes, outlined below, whereby the benzoic acid is converted to benzoate by the base (R1) and the benzoate anion to the radical by the electron transfer agent (R2). The carboxyl radical then decomposes to CO_2 and phenyl radical (R3). Phenylnaphthalenes result from net displacement of a naphthyl hydrogen by phenyl radical (R4). Alternatively, the phenyl radical can abstract hydrogen from pyridine or naphthalene prior to successful addition, resulting in pyridinyl and naphthyl radicals. Attack of these secondary radicals on naphthalene can then explain the formation of pyridinylnaphthalenes and binaphthalenes, as briefly indicated above. The important conclusion is that appearance of these secondary coupling products and the impact of tetralin described above suggest that any radical scavenger should be able to substantially prevent this mode of coupling.

$$C_6H_5CO_2H + C_5H_5N \rightarrow C_6H_5CO_2^- + C_5H_5NH^+ \qquad (R1)$$

$$C_6H_5CO_2^- + Fe_3O_4 \rightarrow C_6H_5CO_2\bullet + Fe_3O_4^- \qquad (R2)$$

$$C_6H_5CO_2\bullet \rightarrow C_6H_5\bullet + CO_2 \qquad (R3)$$

$$C_6H_5\bullet + C_8H_{10} \rightarrow\rightarrow C_6H_5\text{–}C_8H_{10} + H\bullet \quad (R4)$$

It is interesting that a mechanism for the widely used copper/quinoline-promoted decarboxylation of aromatic acids was not published until 1970,[7a] and is still not entirely clear. It is thought to involve the formation of cuprous benzoate as a key intermediate, which then decomposes *without* the formation of a free aryl radical. Since reduction of cupric benzoate to cuprous benzoate can be accomplished by electron transfer from one of the benzoate moieties to the cupric ion, potentially releasing CO_2 and a phenyl radical, both radical and non-radical pathways may be accessible to different degrees and/or under different conditions (copper-quinoline promoted decarboxylations are usually carried out well below 300°C). Thus the scheme in Reactions 1 through 5 is almost certainly simplified and there is very likely more than one mechanism for transition-metal catalyzed decarboxylations operative for different substrates under different conditions.[7,10] In current experiments we are examining the behavior of some activated benzoic acids in the presence of iron oxide, as well as that for a prototypical aliphatic acid.

SUMMARY

The rates of decarboxylation of benzoic acids range from a few percent in 1 hour at 400 °C for unactivated acids to > 98% for species activated in the ortho, para positions. Rates of decarboxylation can be increased by the addition of amine base and/or 1-electron oxidants, but our experiments demonstrate that coupling reactions of activated and unactivated monomeric carboxylic acids are generally *not* important under coal liquefaction conditions in the absence of electron transfer agents. The decarboxylation of the calcium salt of benzoic acid is not significantly faster than that of benzoic acid itself. This is in apparent contrast to the fact the calcium or magnesium forms of low-rank coals produce more CO_2 and show more evidence of crosslinking on heating.[3,17,18] Decarboxylation and coupling reactions of benzoic acid are induced by the electron transfer agents $Cu(OAc)_2$ and Fe_3O_4, and under some highly oxidative conditions one coupling reaction can occur for every two decarboxylations. The rate of coupling in the presence of electron oxidants is greatly reduced by both base and H-donors such as tetralin. The overall conclusion is that, to the extent that monomeric species are representative of coal structures, rather selective conditions are necessary for decarboxylation to result in coupling during coal liquefaction. This suggests either that other mechanisms may be substantially responsible for the retrograde reactions associated with CO_2 evolution, or, if decarboxylation is involved, that it ought to be possible to interrupt these reactions by appropriate control of the conditions.

REFERENCES

1. Suuberg, E. M.; Lee, D.; Larsen, J. W., *Fuel* **1985**, *64*, 1668.
2. Serio, M. A.; Hamblen, D. A.; Markham, J. R.; Solomon, P. R., *Energy Fuels* **1987**, *1*, 138.
3. Solomon, P. R.; Serio, M. A.; Deshpande, G. V.; Kroo, E., *Energy Fuels* **1990**, *4*, 42.
4. Serio, M. A.; Solomon, P. R.; G. V.; Kroo, E.; Bassilakis, R.; Malhotra, R.; McMillen, D.F., *Am. Chem. Soc. Div Fuel Chem. Preprints* **1990**, *35(1)*, 61.
5. Siskin, M., private communication, 1991.
6. March, J., "Advanced Organic Chemistry, 3rd Edition" John Wiley and Sons, New York, 1985, p 507, 562, 653, 842, 928.
7. a. Cohen, T.; Schambach, *J. Am. Chem. Soc.* **1970**, *92*, 3189.
   b. Cairncross, A.; Roland, J. R.; Henderson, R. M.; Sheppard, W. A., *J. Am. Chem. Soc.* **1970**, *92*, 3187
   c. Kaeding, W. W.; Kerlinger, H. O.; Collins, G. R., *J. Org.Chem.* **1965**, *30*, 3754.
   d. Winter, K; Barton, D., *Can. J. Chem.*, **1970**, *48*, 3797.
8. McMillen, D. F.; Ogier, W. C.; Ross, D. S., *J. Org. Chem.* **1981**,*46*, 3322.
9. a. Friedel, C., *Justus Liebigs Ann. Chem.* **1858**, *108*, 122.
   b. Hites, R. A., Biemann, K., *J. Am. Chem. Soc.* **1972**, *94*, 5772.

10. Trahanovsky, W. S.; Cramer, J.; Brixius, D. W., *Am. Chem. Soc.* **1974**, *96*, 1077.
11. Fahr, A.; Stein, S. E., *J. Phys. Chem.* **1988**, *92*, 4951.
12. Fahr, A.; Mallard, W. G.; Stein, S. E., *21st Symposium International On Combusion: The Combustion Institute* **1986**, 825.
13. Chen, R. H.; Kafafi, S. A.; Stein, S. E., *Am. Chem. Soc.* **1989**, *111*, 1418.
14. Herndon, W. C., *J. Org. Chem.* **1981**, *46*, 2119.
15. McMillen, D. F.; Malhotra, R.; Chang, S. -J.; Fleming, R. H.; Ogier, W. C.; Nigenda, S. E., *Fuel* **1987**, *66*, 1611.
16. Stein, S. E.; Griffith, L. L.; Billmers, R.; Chen, R. H., *J. Org. Chem.* **1987**, *52*, 1582.
17. Schafer, H. N. S.*Fuel* **1979**, *58*, 667.
18. Chatterjee, K.; Bal, B.; Stock, L. M.; Zabransky, R. F., *Energy Fuels* **1989**, *3*, 427.

Table 1. Decarboxylation of activated and unactivated benzoic acids.

Acid Structure	Solvent System[d]	Concentration m%	Reaction Time Hrs	% Decarboxylation	% Coupling[a]
$PhCO_2H$ [b,c]	Tet/THQ 75/20	5	1	4	<20
	Tet/THQ/H_2O 55/20/20	5	1	5	<20
	Tet/PipPy 75/20	5	0.5	77	<3
	Tet/THQ/$Zn(OAc)_2$ 75/20	5	1	75	<5
	Tet/1-Naphthol 80/10	10	1	3	<2[e]
$Ca(PhCO_2)_2$	Tet/1-Naphthol 80/10	10	1	3	<2
4-OH-$PhCO_2H$	Tet	20	1	>98	<3
3-OH-$PhCO_2H$	Tet	10	1	2	-
2-OMe-$PhCO_2H$	Tet	10	1	>98	<3
	Tet	20	1	>99	<3
	Tet/Pyrene	10	1	>99	<3
3-OMe-4-OH-$PhCO_2H$	Tet	10	1	>99	<2
3-OMe-4-OMe-$PhCO_2H$	Tet	10	1	~75	<3

a. This figure should be considered an upper limit; it represents the sum of small unidentified high retention time peaks that are potential coupling products, given as a percent of decarboxylation. Thus larger values listed for cases where there is limited decarboxylation do not generally reflect larger absolute amounts of possible coupling products.

b. The first four sets of data for benzoic acid itself are taken from previous work.

c. For economy of space, the symbol "Ph" is used here to represent a single phenyl ring, regardless of whether there are 3, 4 or 5 unsubstituted positions on the ring.

d. "THQ" represents 1,2,3,4-tetrahydroquinoline, "Tet" is tetralin, and "PipPy" is the strong organic base/nucleophile 4-piperidinopyridine.

e. Does not include formation of naphthylbenzoate ester or rearranged product of this ester.

Table 2. Effects of different 1-electron oxidants and solvent H-donating ability on coupling and decarboxylation of benzoic acid[a]

BA (m%)[b]	Solvent System (m%)[b]	Results			
		%Rec. Acid	% Coupling[c]	% Decarbox.[d]	%(Coup/Decarb)
11.3	Naph/Pyridine/Fe_3O_4 68.8/9.8/10.1	19.5	9.34	57.6	16.2
10.4	Naph/Pyridine/Cu Acetate 70.4/8.9/10.3	<0.1	2.96	83.4	3.5
9.8	Tet/MN/Naphthol/Cu Acetate 29.9/29.9/12.2/9.6/9.7	45.9	0.51[e]	46.5	1.1

a. After reaction at 400°C for 1 hr.
b. BA = benzoic acid; Naph. = naphthalene; Tet = tetralin; MN = 1-methylnaphthalene; Naphthol = 1-naphthol; Cu Acet. = cupric acetate monohydrate [$Cu(CH_3CO_2)_2 \cdot H_2O$].
c. As mol% of benzoic acid; refers to all peaks in the "coupling" region of the chromatogram.
d. Based on identified decarboxylation products including benzene and phenyl-containing coupling products.
e. This figure does not include 1% formation of naphthyl benzoate from benzoic acid and naphthol.

Table 3. Effect of Fe_3O_4 and pyridine on decarboxylation and coupling of Benzoic acid during reaction in naphthalene at 400°c for 1 hour

Reactants	Condition 1 mol%	Condition 2 mol%	Condition 3 mol%	Condition 4 mol%
Benzoic Acid	9.57	10.00	10.13	11.26
Naphthalene	90.43	80.23	79.49	68.80
Pyridine	—	9.77	—	9.82
Fe_3O_4	—	—	10.38	10.11
Products				
Benzoic Acid	102.19	92.58	99.74	19.48
Naphthalene	99.80	99.89	98.38	96.08
Pyridine	—	78.88	—	87.54
Benzene	4.26	18.07	6.47	54.11
Naphthalene Impurities	0.77	0.76	0.75	0.76
Biphenyl[a]	< 0.004	< 0.004	< 0.004	0.14
1-Phenylnaphthalene[a]	0.058	0.23	2.36	2.20
2-Phenylnaphthalene[a]	0.055	0.20	1.02	0.99
1-Pyridinylnaphthalene[a]	—	< 0.004	—	2.45
2-Pyridinylnaphthalene[a]	—	< 0.004	—	0.90
1,1'-Binaphthalene[a]	< 0.004	< 0.004	0.91	0.79
1,2'-Binaphthalene[a]	< 0.004	< 0.004	1.44	1.44
2,2'-Binaphthalene[a]	< 0.004	< 0.004	0.44	0.43
% Decarboxylation[b]	4.4	18.5	9.9	57.6
% (Coupling/Decarbox.)[b,c]	2.7	2.3	48.5	16.2

a. Mol percentages are based on the benzoic acid reactant.
b. Based on identified products.
c. For the purposes of this table it is assumed that pyridinylnaphthalenes and binaphthyls are coupling products that stem from decarboxylation after a shift of the radical center from the initial phenyl radical to either pyridine or naphthalene (see text).

CATALYTIC HYDROCRACKING REACTION OF NASCENT COAL VOLATILE MATTER UNDER HIGH PRESSURE IN A TWO-STAGE REACTOR

Hiromi YAMASHITA, Metta CHAREONPANICH, Takayuki TAKEDA, and Akira TOMITA
Institute for Chemical Reaction Science,
Tohoku University, Katahira, Sendai 980, JAPAN.

Keywords: Coal Pyrolysis, Catalytic Hydrocracking, Two-stage reactor

INTRODUCTION

Various products are generated in coal pyrolysis. Usually, the yield of useful chemicals such as benzene, toluene, and xylenes (BTX) is low. If it can be increased to a considerable degree, a combination of flash pyrolysis of coal and gasification/combustion of residual char can become an efficient way to utilize coal. Coal pyrolysis consists of two steps. In the first step, radical species are generated and stabilized. In the second step, the secondary reaction of nascent products occurs in the char pore, in the gas-phase and/or on the char or catalyst surface. In our previous studies [1-4], the modification of the distribution of final products has been tried under the conditions where the primary reaction and the secondary reaction are separated as far as possible. From these studies, it was found that the product yield could be modified by controlling the secondary reaction in which the utilization of catalyst was quite effective.

Previous studies on the utilization of catalyst in coal pyrolysis can be classified into two types: i) hydrocracking of coal volatiles over catalysts added directly on coal [4-6], ii) hydrocracking of volatiles over catalysts placed separately from coal [3, 7, 8]. The results of these studies suggested that the yield of chemicals, such as BTX, can be increased by the following two factors: high H_2 pressure and effective catalyst. However, the coal pyrolysis under high pressure with subsequent catalytic hydrocracking of nascent volatile has not been examined extensively.

In the present study, a two-stage reactor which can be operated under high pressure was made. Using this reactor, coal was pyrolyzed under high pressure of hydrogen in the first stage and the coal volatiles was hydrocracked over sulfided Mo-based catalyst in the second stage. In order to design the distribution of final products, the effects of gas pressure, catalyst, coal type, and reaction temperature on the coal pyrolysis and post-cracking have been clarified.

EXPERIMENTAL

Apparatus and procedure. The schematic diagram of the two-stage reactor used in this study is shown in Fig. 1. The reactor is a SUS-316 tube (i.d. 7.6 mm). H_2 or He at pressure of 0.1-5 MPa was used (200 ml(NTP) min^{-1}). A coal sample (10 mg) was placed in a small quartz boat and was pyrolyzed in the first-stage by heating with an infrared furnace at a rate of 10 K s^{-1} up to a temperature (T_1)

ranging 500-800°C and held there for 2 min. The evolved volatile matter was introduced into the second-stage where the catalyst (800 mg) was packed and the temperature (T_2) was controlled at 400-700°C by another electric furnace. The final products were collected in a cold trap packed with Porapak P. After depressurization, the collected products were allowed to desorb from the trap and subjected to g.c. analysis.

Coal sample and catalyst. Five coals from Australia were used: one bituminous coal; Liddell (C, 83.5 % daf), two subbituminous coals; Wandoan (C, 78.5 %), Millmerran (C, 76.9 %) and two brown coals; Morwell (C, 67.4 %), Loy Yang (C, 66.7 %). Particle size of the coal sample was <100 μm. The sample was dried in N_2 at 107°C for 1 h before use. $Ni/Mo/Al_2O_3$ (NiO: 2.8 wt%, MoO_3: 10.3 wt%) from Harshow and $Co/Mo/Al_2O_3$ (CoO: 3.9 wt%, MoO_3: 10.8 wt%) from American Cyanamid were used as catalysts. Catalyst pellets were crushed to 32-60 mesh. Prior to each series of experiments, the catalyst was calcined in oxygen for 0.5 h, and treatment with hydrogen sulfide (H_2S, 4 %; H_2, balance) was carried out at 500°C for 0.5 h, followed by further treatment with hydrogen for 0.5 h. Ni/Mo/S and Co/Mo/S stand for the sulfided catalysts.

RESULTS AND DISCUSSION

Effect of gas pressure in the first-stage. The effect of gas pressure on the coal pyrolysis in the first-stage was investigated without catalyst in the second-stage (Table 1). The amount of volatile (weight loss) increased with increasing pressure of H_2 and with decreasing pressure of He. Hydrogen stabilizes the radical generated in the primary reaction, increasing the amount of volatile. The BTX yield increased with pressure in both gases. The increase of BTX yield observed in H_2 was larger than that in He. The secondary reaction of volatiles in char pore might be responsible for the pressure effect observed in the inert atmosphere of He.

Effect of catalyst and H_2 pressure in the second-stage. The effects of catalyst and H_2 pressure on the distribution of final products were studied by using several catalysts. The results obtained using Liddell coal at the temperature of T_1=600°C and T_2=500°C are shown in Table 2. Al_2O_3 was not effective to increase BTX yield which was similar to that without catalyst under a high H_2 pressure. On the other hand, Co/Mo/S and Ni/Mo/S catalysts were effective for the secondary reaction even under atmospheric pressure. A high pressure remarkably increased the yields of BTX and hydrocarbons, especially the yield of benzene and methane. Ni/Mo/S catalyst was more effective.

Effect of reaction temperature. Effect of reaction temperature of the first- or the second-stage was investigated with Millmerran coal, Ni/Mo/S, and 5 MPa H_2 (Table 3). With a constant T_2 of 500°C, the BTX yield increased with increasing T_1. On the other hand, at T_1 of 600°C, the maximum yields for BTX and hydrocarbon were obtained at a moderate T_2 (600°C). Using the two-stage reactor, the optimum temperatures for the first- and the second-stage can be selected independently.

Effect of coal types. Effect of coal type on the yield of final products is shown in Table 4. For all the coals, the amount of volatiles increased with H_2 pressure. However, the product distribution pattern was different among coals. Under high H_2 pressure, the highest BTX yield (6.2 %) were observed with Millmerran coal, while the highest C_2-C_7 yield (17.1 %) were obtained with Wandoan coal. The present BTX yields were compared with those obtained using Curie-point pyrolyzer (CPP) under atmospheric pressure of argon without catalyst [1] (Fig. 2). The two-stage reaction with Ni/Mo/S catalyst leads to a large increase in BTX yield. The values obtained under atmospheric pressure were twice and those obtained under high pressure were five times larger than those obtained with CPP. A higher BTX yield was obtained by using coal with higher H/C ratio. This is because the coal with higher H/C ratio generates a larger amount of tar during the primary pyrolysis [1], and BTX is produced by the secondary reaction (hydrocracking) of primary tar over catalyst. It can be concluded that the secondary reaction over Ni/Mo/S catalyst under high H_2 pressure is effective for producing valuable materials.

CONCLUSION

The yield of useful chemicals could be increased to a considerable extent by using catalyst under high H_2 pressure in a two-stage reactor. Coal with higher H/C ratio and operation under higher H_2 pressure are preferable for a high BTX yield. The type of catalyst is also an important factor. The Ni/Mo/S catalyst is the most effective. The higher reaction temperature in the first-stage was preferable and the moderate temperature of the second-stage was suitable for a high BTX yield. In the present study, the highest BTX yield (7.6 %) was observed under the following conditions: Millmerran coal, Ni/Mo/S catalyst, T_1=800°C, T_2=500°C, 5 MPa of H_2

REFERENCES

1. Xu, W. C.; Tomita, A. *Fuel* 1987, **66**, 627.
2. Xu, W. C.; Tomita, A. *Fuel Process. Technol.* 1989, **21**, 25.
3. Xu, W. C.; Yamashita, H.; Tomita, A. *Fuel* 1990, **69**, 1007.
4. Yamashita, H.; Xu, W. C.; Jinoka, T.; Shrotri, V.; Hajima, M.; Tomita, A. *J. Jpn. Inst. Energy* 1992, **71**, 189.
5. Bolton, C.; Riemer, C.; Snape, C. E.; Derbyshire, F. J.; Terrer, M. T. *Fuel* 1988, **67**, 901.
6. Sulimma, A.; Leonhardt, P.; van Heek, K. H.; Juentgen, H. *Fuel* 1986, **65**, 1457.
7. Nelson, P. F.; Tyler, R. J. *Energy Fuels* 1989, **3**, 488.
8. Krabiell, K.; Wanzl, W.; Juentgen, H. *Inter. Conf. Coal Sci.* 1987, pp. 687, Maastricht.

Table 1 Effect of Gas Pressure on Coal Pyrolysis.

Gas	Press. (MPa)	Weight loss (%, daf)	Yield (%, daf)					
			CO_x	CH_4	C_2-C_7	BTX	PCX	Tar
He	0.1	34	5.4	2.4	2.4	0.6	0.9	22.3
	2.0	30	4.6	3.3	3.4	1.0	0.5	17.2
	5.0	28	6.4	3.3	3.2	1.0	0.6	13.5
H_2	0.1	34	4.3	2.7	3.4	0.7	0.8	22.1
	2.0	36	4.7	5.2	3.8	2.1	0.7	19.5
	5.0	39	8.3	7.2	5.6	3.2	0.8	13.9

T_1-T_2: 600-500°C. Coal: Liddell. Catalyst: None.

Table 2 Effect of Catalyst and H_2 Pressure on Product Yields from Secondary Reaction of Volatiles.

Catalyst	H_2 press. (MPa)	Yield (%, daf)				
		CO_x	CH_4	C_2-C_7	BTX	PCX
None	0.1	4.3	2.7	3.3	0.7	0.8
	5.0	8.3	7.2	5.6	3.2	0.8
Al_2O_3	0.1	11.3	1.8	3.7	0.7	0.9
	5.0	10.2	5.0	11.3	2.9	0.9
Co/Mo/S	0.1	7.5	1.7	2.6	2.1	0.8
	5.0	2.0	4.4	7.4	4.7	0.8
Ni/Mo/S	0.1	4.3	4.4	4.3	2.1	0.9
	5.0	0.7	10.8	10.9	5.1	0.8

T_1-T_2: 600-500°C. Coal: Liddell.

Table 3 Effect of T_1 and T_2 on Product Yields from Secondary Reaction of Volatiles.

T_1-T_2 (°C)	Weight loss (%, daf)	Yield (%, daf)			
		CH_4	C_2-C_7	BTX	PCX
500-500	40	5.5	11.6	3.9	0.9
600-500	57	12.4	15.2	6.2	0.9
700-500	60	18.8	18.6	7.0	2.2
800-500	66	18.8	8.3	7.6	1.5
600-400	57	11.0	11.9	5.5	1.5
600-500	57	12.4	15.2	6.2	0.9
600-600	57	16.4	21.6	7.0	0.4
600-700	57	36.4	0.7	4.5	0.1

Catalyst: Ni/Mo/S. Coal: Millmerran.

Table 4 Effect of Coal Types and H_2 Pressure on Product Yields from Secondary Reaction of Volatiles.

Coal	H_2 press. (MPa)	Weight loss (%, daf)	Yield (%, daf)					
			CO_x	CH_4	C_2-C_7	BTX	PCX	Tar
Liddell	0.1	36	4.3	4.4	4.3	2.1	0.9	20.0
	5.0	42	0.7	10.8	10.9	5.1	0.8	13.7
Wandoan	0.1	46	8.8	4.5	6.7	2.5	1.1	22.4
	5.0	56	3.3	13.8	17.1	5.1	1.1	15.6
Millmerran	0.1	53	5.8	4.8	7.4	3.0	1.3	30.7
	5.0	57	1.2	12.4	15.2	6.2	0.9	21.1
Morwell	0.1	50	24.7	3.5	4.8	2.1	1.0	13.9
	5.0	64	2.3	11.4	9.9	5.2	0.8	34.4
Loy Yang	0.1	48	27.1	2.7	3.2	2.0	0.7	12.3
	5.0	56	3.7	14.7	10.8	3.4	0.6	22.8

T_1-T_2: 600-500°C. Catalyst: Ni/Mo/S .

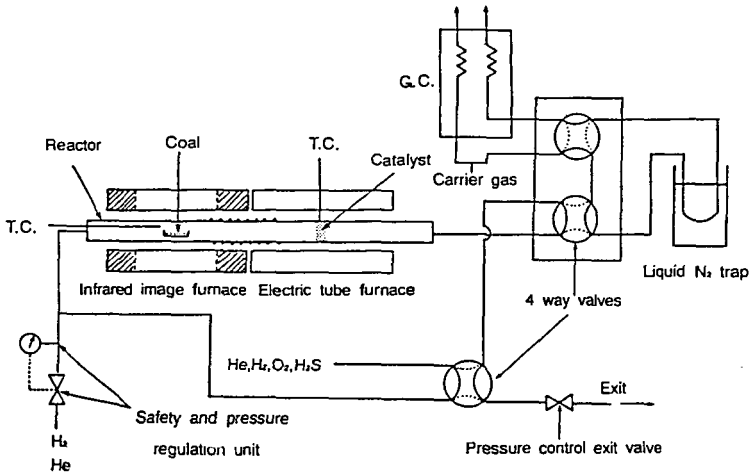

Fig. 1 Schematic diagram of a high pressure two-stage reactor.

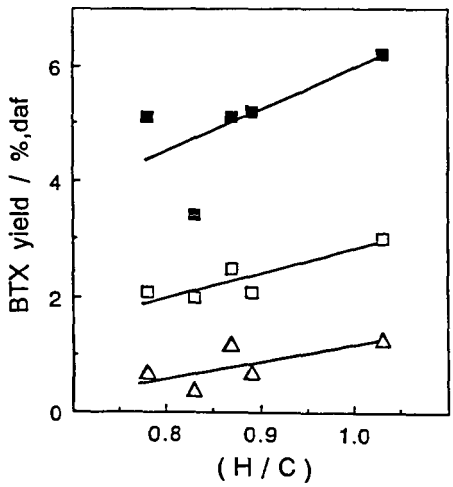

Fig. 2 Effect of H/C ratio of coal on BTX yields obtained in various reaction systems. (■) Two-stage reactor, Ni/Mo/S, 5 MPa H_2; (□) two-stage reactor, Ni/Mo/S, 0.1 MPa H_2; (△) CPP, none catalyst, 0.1 MPa Ar.

Effects of the Structure of the Side Chain on the Pyrolysis of Alkylbenzenes

Ying PENG, Harold H. SCHOBERT, Chunshan SONG
and Patrick G. HATCHER

Fuel Science Program
Department of Materials Science and Engineering
The Pennsylvania State University
University Park, PA 16802

Keywords: Pyrolysis, butylbenzenes

INTRODUCTION

The formation of solids from jet fuels under pyrolytic conditions is a subject of intensive research in the years. The deposit formation is attributed to the thermal breakdown of hydrocarbons at temperatures higher than 350°C (1). Petroleum-derived jet fuels generally consist of about 85% paraffins and less than 10% alkylaromatics (2). When paraffins are subjected to pyrolysis, the formation of unsaturated rings is related to the Diels-Alder type reactions of conjugated alkenes and olefins (3). Upon further heat treatment, these unsaturated rings may undergo dehydrogenation reactions to form alkylbenzenes and solid products. Large amounts of alkylbenzenes are detected in the pyrolysis of long chain paraffins such as decane, dodecane and tetradecane (4). These results suggest that alkylbenzenes are the "precursors" of carbonaceous solid products during the pyrolysis of jet fuels.

The thermal chemistry of alkylbenzenes has been extensively studied, but most of the efforts are directed towards primary products obtained on pyrolysis. The length and types of the alkyl side chains can significantly affect the thermal reactions of alkylbenzenes. As the length of the side chain increases, the reactivity also increases. For instance, the activation energy for the pyrolysis reaction of toluene is higher than that of n-butylbenzene (5). Also t-butylbenzene is found to have a much lower thermal reactivity than its isomer n-butylbenzene (6). Another notable feature is that long-chain alkylbenzenes on pyrolysis exhibit pronounced characteristics of paraffins, i.e., cracking reactions (β-bond scission) become more important (7).

Understanding the secondary reactions that lead to the formation of solid deposit is equally crucial in studying the high-temperature thermal degradation process of jet fuels in an aircraft. This objective is achieved in the following study by using high pressure microautoclave reactors to simulate the situation of the fuel line and fuel nozzles in an aircraft. Preliminary pyrolysis reactions have been performed on four isomeric alkylbenzenes (n-, iso-, sec- and t-butylbenzenes) at 450°C and 0.7 MPa nitrogen over pressure. Solid formation tendencies of these compounds have been compared. Fundamental behavior of these alkylbenzenes that lead to their degradation and the formation of solid deposit have been studied.

EXPERIMENTAL

The experimental apparatus, procedures and product work-up were described in the previous paper (6). All chemicals were obtained commercially and used as received. n-, iso- and sec-butylbenzenes (>99% purity) were purchased from Aldrich Chemical Company. t-Butylbenzene (98% purity) was purchased from TCI America.

RESULTS AND DISCUSSION

1. General Scheme in the High Pressure Microautoclave Reactor

Experiments were carried out in the microautoclave reactors (tubing bombs) at 450°C under 100 psi using ultra-high purity (UHP) N_2. Under this condition, the pyrolysis reactions are extremely complex. In a conventional flow reactor, the dominant reactions are scission of β-bonds, while in microautoclave reactors, this reaction is suppressed and secondary reactions are favored. For jet fuels and related model compounds, generally, three groups of compounds are formed in the quenched tubing bomb reactors. They are: (i) low molecular weight gaseous hydrocarbons with the carbon chain length varying from C_1 to C_4, (ii) liquid products of a wide range of molecular weight, and (iii) carbonaceous solid products. As a result of thermal treatment, the reactions proceed to a thermodynamically stable state. If the treatment is severe, a three-phase thermodynamic equilibrium among gaseous, liquid and solid products can be reached. This appears to be the reason for the changes of the color of the liquid products from white to light yellow to brown to dark brown to light brown. The change of color the from dark brown to light brown after long reaction times seems to be an indication of the achievement of equilibrium state.

2. Substrate Disappearance and Solid Product Formation

Figures 1 and 2 show the rate of disappearance of model compounds and the yield of solid products formed, respectively. Over a time period from 15 min. to 8 h, n-butylbenzene is quickly converted and t-butylbenzene is the most stable isomer, as shown in Figure 1. As the substrate compounds disappear, carbonaceous solids have been observed to form in the reactors. It can be seen from Figure 2 that each compound has a different induction period for the formation of solid products. The induction period reflects the ability of the compound to resist the formation of carbonaceous solid products. The order for the induction time of the four compounds is: n-<sec-<iso-<tert-butylbenzene. The order is the same as that of the rate of their disappearance. The amount of the solids formed increases with the reaction time for sec-, iso- and t-butylbenzene. This behavior is similar to that of jet fuels, which also exhibit a monotonic increase in the amount of solid products (8). Surprisingly, although solid products are quickly formed in the pyrolysis of n-butylbenzene after a short induction period, the amounts leveled off to an asymptotic value at around 5 h. As a result, the least amounts of solids is formed from the reaction of n-butylbenzene after 8 h at 450°C. The unique behavior of n-butylbenzene will be discussed in the following sections.

3. Major Substrate Consumption Pathways

Major substrate consumption pathways are studied in this paper by pyrolyzing the model compounds at very short residence times where little or no solid products are formed, and examining the compositions of the initial gaseous and liquid products.

(1) n-Butylbenzene (n-BB)

The pyrolysis of n-BB for 15 min. at 450°C indicates that ethane is present in the gas phase as a major product and toluene and styrene are major species present in liquid products. These results suggest that the major pathway of consumption n-BB is by breaking C_α-C_β bonds in the side chain (6).

(2) t-Butylbenzene (t-BB)

Although the initiation of t-BB is similar to that of n-BB (C_α-C_β bond cleavage), its initiation process is significantly retarded as shown in Figure 1. This can be explained by the following two reasons. Firstly, the C_α-C_β dissociation energy for t-BB is 73.7±1.5 kcal/mol, which is higher than that for n-BB, 70.0±1 kcal/mol (9). Secondly, the H-abstraction reaction by $C_6H_5C(CH_3)_2$ radicals formed by the homolysis of t-BB is expected to be much slower simply because of the relatively high stability of $C_6H_5C(CH_3)_2$ radicals and the poor stability of $C_6H_5C(CH_3)_2CH_2$ radicals produced. As a result, the

pyrolysis of t-BB is mainly carried out by isomerization reaction to form i-BB and s-BB (6).

(3) s-Butylbenzene (s-BB)

The composition of gaseous products for the reaction of s-BB are shown in Table 1. The major gaseous products after the initial period are methane, ethane and ethylene. As the reaction time increases, the concentration of ethylene decreases. Major liquid products identified include ethylbenzene (0.72 wt%), styrene (0.11 wt%), α-methylstyrene (0.10 wt%), trans-β-methylstyrene (0.70 wt%) and α-ethylstyrene (0.16 wt%). According to these results, removing a CH_3 radical from s-BB appears to be a dominant initiation process:

$$C_6H_5CH(CH_3)CH_2CH_3 \longrightarrow C_6H_5\dot{C}HCH_2CH_3 + CH_3\bullet$$

The presence of C_2 species in relatively high concentration in the gas phase indicates that removing a CH_3CH_2 radical also exists as another initiation process:

$$C_6H_5CH(CH_3)CH_2CH_3 \longrightarrow C_6H_5\dot{C}HCH_3 + C_2H_5\bullet$$

(4) i-Butylbenzene (i-BB)

The composition of gaseous products for i-BB is also shown in Table 1. Methane and propylene are two major gaseous products. Toluene (1.47 wt%) and trans-β-methylstyrene (2.80 wt%) are the major liquid products in the initial period. These data suggest that the following initiation reaction exists in the pyrolysis of i-BB.

$$C_6H_5CH_2CH(CH_3)CH_3 \longrightarrow C_6H_5CH_2\bullet + CH_3\dot{C}CH_3$$

4. Major Liquid Product Selectivities

Liquid products consist mostly of cracking products (4), the molecular weights of which are less than the substrate compounds. Cracking products include mainly benzene, toluene, ethylbenzene, i-propylbenzene and n-propylbenzene. Figures 3, 4 and 5 show the plot of selectivities of benzene, toluene and ethylbenzene from the pyrolysis of butylbenzenes. t-BB has the highest selectivity for benzene as shown in Figure 3. This appears to suggest that the aryl-alkyl bonds in t-BB are weakened by the presence of bulky t-butyl groups. The formation of benzene may also due to the attack of H to the ipso position of t-BB. In Figure 4, the concentration of toluene increases almost linearly with the increase of conversion except that the slope is lower for s-BB. Since β-bond scission to form benzyl radicals is the only initiation process in n-BB and it is easy for the benzyl radicals to abstract H from other species in the reaction system, n-BB has the highest selectivity to form toluene. In contrast, i-BB has two initiation pathways, only one of which forms benzyl radicals that lead to the formation of toluene. This lowers its toluene production. t-BB has been known to pyrolyze mainly by isomerization reactions to form i-BB (and s-BB to a lesser extent). The formation of toluene from t-BB might be attributed to the further dissociation of i-BB. It is obvious that direct decomposition of s-BB does not form toluene. Figure 5 shows the ethylbenzene selectivities. Similar behavior is observed in n-BB, s-BB and i-BB, t-BB. This could be understood from the discussion in the last section. It is possible that ethylbenzene can be formed as an initial reaction product for n-BB and s-BB, while i-BB and t-BB can only be formed between secondary reaction products.

5. Comparison of Solid Formation Tendencies

Compositions of liquid products seem to demonstrate that the reactivity of a model compound is governed by the initial reaction products. Generally there are two competing sets of reactions in the pyrolysis of all four model compounds at the initial stage, i.e.,

isomerizations and the characteristic breakdown for each specific compounds as shown below.

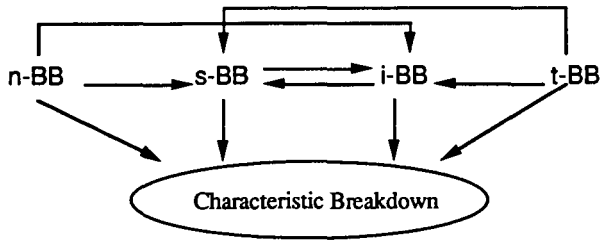

It is obvious from the previous discussion that for the pyrolysis of t-BB, the isomerization reaction to i-BB is more important than its characteristic breakdown. Therefore, the induction time for the solid formation from t-BB mainly depends on the isomerization reaction and the induction period of i-BB. This might account for its low reactivity and long induction period for solid formation (Figures 1 and 2). n-BB is the one that is most easily converted, but not the one that forms the highest amounts of solids. One reason for this is that it appears to be easy for n-BB to form cracking products such as toluene and ethylbenzene as shown in Figures 4 and 5, and stable high molecular weight compounds such as naphthalene as shown in Figure 6. The other reason is that fewer compounds of styrene-series were found in the liquid products of n-BB. In fact, only styrene is identified, and its concentration decreases rapidly as the reactions proceed. In the case of s-BB and i-BB, large amounts of compounds such as styrene, allylbenzene, α-methylstyrene, β-methylstyrene,and ethylstyrenes were present after the initial reaction period. This may constitute the reason for the formation of large amounts of solid products from the pyrolysis of s-BB and i-BB.

CONCLUSIONS

There is a significant effect of the structure of the side chains on the pyrolysis of alkylbenzenes. The rate of the disappearance or reactivity of an alkylbenzene depends on the ease of the dissociation energy of its initiation reactions. The order of reactivity or conversion of substrate was found to be n->sec->iso->tert-butylbenzenes. This indicates that, in general, branching seems to decrease the thermal reactivity of the alkybenzenes. The amount of solids produced is related to the stability of the intermediate products especially at the initial stage. It seems that styrene-series compounds formed at the early stage are responsible for the formation of large amounts of solid products during the pyrolysis of sec- and iso-butylbenzenes.

ACKNOWLEDGEMENTS

This project was jointly supported by the U. S. Department of Energy, Pittsburgh Energy Technology Center and Air Force WRDC/Aero Propulsion Laboratory, Wright-Patterson AFB. Funding was provided by the U. S. DOE at Sandia National Laboratories under contract DE-AC04-76DP00789. We wish to thank Mr. W.E. Harrison III of WRDC, Drs. E. Klavetter of SNL, and S. Lee, M. Baird and S. Rogers of PETC for their support and helpful discussions.

REFERENCES

(1). Frenkenfeld, J.W. and Taylor, W.F., Ind. Eng. Chem. Prod. Res. Dev., 19, 65, 1980

(2). Song, C. and Hatcher, P.G., Preprints, Div. Pet. Chem., ACS, 37(2), 529, 1992

(3). Nohara, D. and Sakai, T., Ind. Eng. Chem. Res., 31, 14, 1992
(4). Song, C., Eser, S., Schobert, H.H. and Hatcher, P.G. et. al., Advanced Thermally Stable Jet Fuels Development Program Annual Report, Volume II, Interim Report for Period July 1990 to July 1991
(5). Leigh, C. H. and Szwarc, M., J. Phys. Chem., 1952, 20, 844
(6). Peng, Y, Schobert. H.H, Song, C. and Hatcher, P.G., Preprints. Div. Pet. Chem., ACS, 37(2), 505, 1992
(7). Savage, P. E. and Korotney, D. J., Ind. Eng. Chem. Res., 1990, 29, 499
(8). Song, C., Peng, Y., Jiang, H. and Schobert, H.H., Preprints. Div. Pet. Chem., ACS, 37(2), 484, 1992
(9). Lide, D.R., CRC Handbook of Chemistry and Physics, CRC Press, 1990-1991

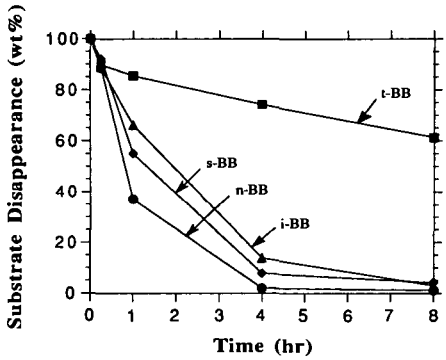

Figure 1. The disappearance of the substrate compounds at 450°C

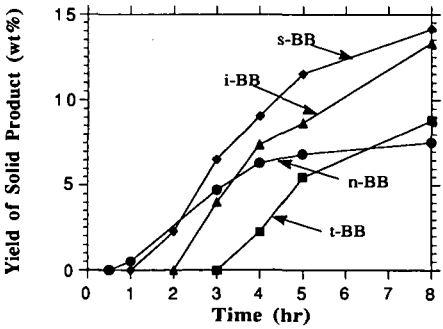

Figure 2. The formation of solid products at 450°C from the pyrolysis of butylbenzenes

Table 1. Composition of Gaseous Products from the Pyrolysis of sec- and iso-Butylbenzenes at 450°C

Time (hr)	CH_4 (mol%)		C_2H_4 (mol%)		C_2H_6 (mol%)		C_3H_8 (mol%)		C_3H_6 (mol%)		Volume (ml)	
	s-BB	i-BB	s-BB	i-BB	s-BB	i-BB	s-BB	i-BB	s-BB	i-BB	s-BB	i-BB
0.25	83.49	71.84	9.52	0.34	6.04	0.87	0.75	3.02	0.08	21.17	44	42
1.00	86.59	62.85	3.13	0.54	8.07	4.11	1.29	7.18	0.80	19.28	293	203
2.00	84.25	68.25	1.50	0.57	10.79	6.35	1.91	9.61	0.59	10.43	497	355
4.00	83.99	63.39	1.08	0.89	12.16	9.58	2.26	14.60	0.32	4.08	687	601
8.00	82.15	62.67	0.54	0.26	13.36	12.16	3.11	15.32	0.23	4.55	727	733

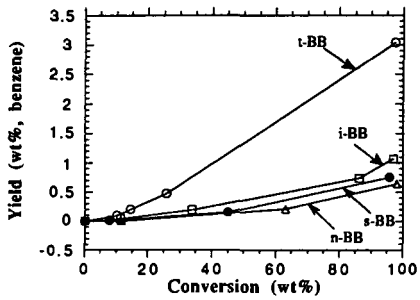

Figure 3. Selectivities of benzene in the pyrolysis of butylbenzenes

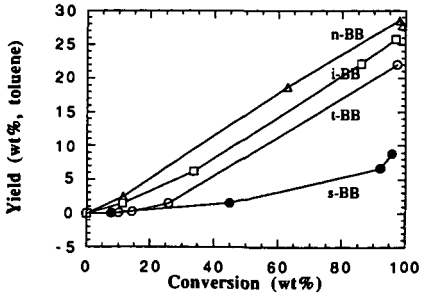

Figure 4. Selectivities of toluene in the pyrolysis of butylbenzenes

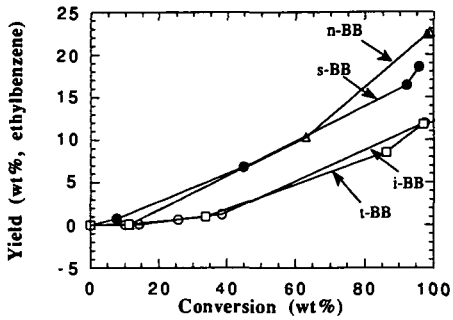

Figure 5. Selectivities of ethylbenzene in the pyrolysis of butylbenzenes

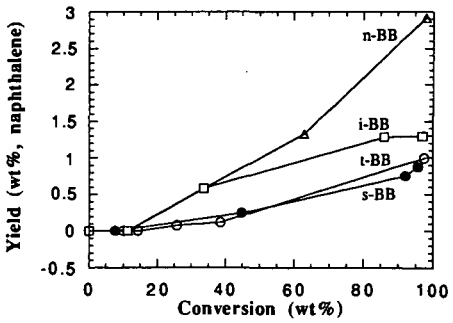

Figure 6. Selectivities of naphthalene in the pyrolysis of butylbenzenes

FORMATION OF POLYCYCLIC AROMATIC HYDROCARBONS AND ELIMINATION OF ALIPHATIC SUBSTITUENTS IN SECONDARY REACTION OF FLASH PYROLYSIS TAR

Jun-ichiro Hayashi, Tsutomu Kawakami, Tomohiro Taniguchi,
Katsuki Kusakabe and Shigeharu Morooka
Department of Chemical Science and Technology,
Kyushu University, Fukuoka 812, Japan

INTRODUCTION

Polycyclic aromatic hydrocarbons (PAHs) derived from coal tar and pitch are very useful for starting materials of various specialty chemicals. To produce PAHs, flash pyrolysis of coal is attractive because its tar yield is much higher than that of other carbonization processes with slow heating rates.[1] However, the quality of flash pyrolysis tar is rather inferior to that of slow pyrolysis tar.[2]

Coal pyrolysis consists of two reactions in series: the primary reaction of the macromolecular network of coal to tar; and the secondary reaction of tar in the gas phase.[3]

Division of reaction zones is indispensable for the quantitative examination of time- and temperature-dependent changes in molecular composition of tar, as indicated by Xu et al.[4] and Serio et al.[5] who separated these reaction zones by using the two-stage reactors comprising of a fixed bed of coal and a tubular reactor connected downstream.

In the present study, the two-stage concept is applied to the flash pyrolysis of a subbituminous coal with a fluidized-bed reactor divided into two zones: a dense bed for the primary reaction and a freeboard above the dense bed for the secondary reaction. Tar is processed in the freeboard at a temperature different from that in the dense bed. PAHs in the tar is characterized by FIMS and ^{1}H-NMR after the separation based on ring structure of molecule. The temperature dependence of the following features are determined: molar yield of homologues having the same ring structure; and number-based distribution of aliphatic carbons per molecule for each homologue.

EXPERIMENTAL

Flash pyrolysis

Wandoan subbituminous coal (C:76.2, H:5.77, N:1.03 in wt.%, daf) was employed for the experiment. The coal sample was pulverized, sized to 0.37-0.74 mm and dried in vacuo at 100°C. The fluidized-bed reactor was divided into dense and freeboard zones, and they were heated separately with external furnaces whose temperatures were independently controlled. The temperature was set in the range of 600-900°C for the freeboard and fixed at 600°C for the dense bed. Coal particles were introduced into the dense bed at a constant rate of 4.2 mg/s. The total gas flow rate was 33.3 ml/s at 20°C. The total residence time of tar vapor was 4.0-4.5 s.

Separation and characterization of tar samples

The tar was separated into benzene-soluble (asphaltene) and insoluble (preasphaltene) portions. The asphaltene was further fractionated into saturates, aromatic hydrocarbons, nitrogen-containing compounds, hydroxylic compounds and the uneluted components by the elution chromatography with neutral alumina.[6] The yield of the uneluted component was added to that of the preasphaltene.

The aromatic hydrocarbons was further separated by HPLC on the basis of ring structure with a semipreparative NH_2 column (Hiber Column, Merck) with n-heptane as the mobile phase.[7] By this method, aromatics were classified by number of double bonds per molecule (d.b.) into 3 (monocyclic), 5 (dicyclic), 6 (dicyclic), 7 (tri-cyclic), 8 (tetracyclic), 9 (tetracyclic), 10 (pentacyclic), 11 and 12 (pentacyclic and greater PAHs). Each double-bond fractions were analyzed by ^{1}H-NMR and FIMS.

RESULTS AND DISCUSSION

Temperature dependence of yield and chemical composition of tar

Figure 1(a) shows the effect of freeboard temperature on the tar yield. When fine coal particles were fed into the dense bed, most particles were entrained by the gas flow. When coal particles were in the size range of 0.21-0.42 mm, however, entrainment hardly occurred. The tar yield by the pyrolysis of the 0.21-0.42 mm particles was virtually identical to that shown in Figure 1. Thus the tar evolution was completed in a short period compared with the residence time of gas in the freeboard.

Figure 1(b) shows yields of components normalized by total tar yield as a function of freeboard temperature. There are three patterns of temperature dependence. The yield of PAHs and nitrogen-containing compounds increases with increasing temperature and then attains ca. 80 wt.% of the total tar yield at 900°C, while that of saturates and preasphaltene decreases monotonously above 600°C. Ethers and hydroxylic compounds show their maximum yield at 700°C. It is clear that the increase in yield of PAHs is compensated by the decrease of the other components, and their roles as precursors of PAHs vary by component.

Yield and structural distribution of PAH component

The FIMS analysis reveals that a PAH molecule has 5 to 12 double bonds. Figure 2 shows the FIMS spectra of the 6, 7 and 8 d.b. fractions separated from tar at 800°C. The spectra shown in Figure 2(a) consist of two series of signals appearing at the mass number 152+14n and 154+14n (n = integer). The former is attributed to the homologue of acenaphthylene (MW = 152) and fluorene (MW = 166), and the latter to that of biphenyl (MW = 154). These homologues have the same double-bond number of 6. Figure 2(b) and (c) show that the 7 and 8 d.b. fractions are composed of the homologues of phenanthrene (or anthracene) and pyrene (or fluoranthene) respectively. Each fraction is a mixture of compounds having the same number of aromatic rings and a different number of methylene units. Peaks with the smallest mass in the FIMS spectrum of each homologue are assigned to the PAHs listed in Table 1.

All the PAH homologues are composed of an unsubstituted PAH and its alkyl-derivatives. Since alkyl substituents are sensitive to the reaction temperature, the total mass of compounds is not a reliable indicator of the yield of homologue. Therefore, the mass of a substituted PAH having aliphatic carbons is converted to that of an

unsubstituted PAH. Figure 3 shows the yield of the 6-12 d.b. homologues. All of them monotonously increase with increasing temperature. This suggests that the formation of PAHs below 900°C is predominant over the soot formation that causes a decrease in the PAH yield. The homologues of 6, 7 and 8 d.b. are most abundant. Each of them comprises more than 1.0 wt% of coal on daf basis at 900°C. The temperature profile of PAH yield varies by homologue. The larger the d.b. number, the higher the temperature at which the slope changes steeply. The yields of the 11 and 12 d.b. homologues increase remarkably above 700°C in accord with the evo-lution of hydrogen gas. In this temperature range, a part of the 11 and 12 d.b. homologues is formed via condensation of smaller aromatic rings, and hydrogen gas is produced as a result.

Aliphatic carbons attached to aromatic ring

The number-based distribution of aliphatic carbons (methylene units) per molecule is shown in Figure 4 for the 8 and 9 d.b. homologues. The FIMS analysis combined with the HPLC separation allows the determination of the yield of molecules composed of a specific aromatic ring and a specific number of aliphatic carbons. The number of aliphatic carbons per molecule is distributed over the range of 0 to 9 at 600°C, where aliphatic carbons are most abundant. Teo and Watkinson[8] pyrolyzed coals in a spouted bed and characterized the molecular composition of tar by HPLC and GC-MS. They found that the number of aliphatic carbons was less than four for aromatic homologues with 1 to 4 rings. Our results, on the other hand, reveal that PAHs bearing more than four or five aliphatic carbons are abundant, particularly in low-temperature tars.

The distribution shown in Figure 4 moves toward the small-number side with increasing secondary reaction temperature. The mole fraction of unsubstituted PAHs is only ca. 5% in the homologues obtained at 600°C, but is ca. 50% at 900°C. The temperature dependence of the yield of substituted molecules varies with the number of aliphatic carbons. In the case of the 7 d.b. homologue, the yield of C_1 and C_2 derivatives shows a maximum at 800°C, while that of C_3 and C_4 derivatives at 700°C. The yield of molecules having more than five aliphatic carbons decreases monotonously over the temperature range tested.

Classification of aliphatic carbons

The NMR data of each d.b. fraction are analyzed by assuming the existence of only methyl-, ethyl- and propyl-chains. This is reasonable because the b-hydrogen content is at most half that of α-hydrogen even at 600°C, where the ratio of β- to α-hydrogen is the highest for all the fractions. The number of chains is given by the following equations.

$$N(\text{propyl}) = N(H_\gamma)/3 \quad (1)$$

$$N(\text{ethyl}) = [\, N(H_\beta) - 2N(\text{propyl}) \,]/3 \quad (2)$$

$$N(\text{methyl}) = [\, N(H_\alpha) - 2N(\text{ethyl}) - 2N(\text{propyl}) \,]/3 \quad (3)$$

$$N(\alpha,\alpha\text{-methylene}) = N(H_{\alpha,\alpha})/2 \quad (4)$$

where $N(H_\alpha)$, $N(H_\beta)$ and $N(H_\gamma)$ are respectively the number-based content of α-, β- and γ-hydrogen normalized by the total hydrogen content. The total number of aliphatic carbons is

$$C_{al} = N(\text{methyl}) + 2N(\text{ethyl}) + 3N(\text{propyl}) + N(\alpha,\alpha\text{-methylene}) \quad (5)$$

The sum of the number of protonated and alkylated aromatic carbons is

$$C_{pa} = N(\text{methyl}) + N(\text{ethyl}) + N(\text{propyl}) + N(H_{ar}) + 2N(\alpha,\alpha\text{-methylene}) \quad (6)$$

where $N(H_{ar})$ is the number-based content of aromatic hydrogens. The total number of aromatic carbons is given as

$$C_{ar} = C_{pa} + C_b \quad (7)$$

where C_b is the number of bridgehead carbons. The ratio of Cpa to Cb is determined from the ring structure. The value of C_{pa}/C_{ar} is calculated from the composition of PAHs by the FIMS analysis in all the fractions of different d.b., and is for instance 10/14 for the 7 d.b. homologue. The averaged number of aliphatic carbons per molecule is

$$N(CH_2) = C_{al}/(C_{ar}/ARC) \quad (8)$$

where ARC is the averaged number of aromatic carbons per molecule. The value of N(CH2) can also be determined by the FIMS data as shown in Figure 4. The values of $N(CH_2)$ calculated from Equation (8) are in agreement with those by the FIMS analysis within an error of 10%.

Figure 5 exhibits the composition of aliphatic carbons in the fractions of 8 and 9 d.b. The number of α-, β- and γ-carbons decreases with increasing temperature. The number of α,α-carbons is independent of temperature in the range of 600-800°C, while it decreases above 800°C.

Figure 6 shows the number of methyl and ethyl chains per molecule for the 8 and 9 d.b. fractions. The number of ethyl chains decreases by 65-85% in the range of 600-700°C, while that of methyl chains hardly changes. This result suggests that the decrease in the number of a-carbons at 600-700°C is due to detachment of ethyl and propyl chains by the selective bond cleavage at aryl-α positions.

REFERENCES

1. Peters, W.; Bertling, H. *Fuel* 1965, **44**, 317.
2. Khan, M.R. *Fuel* 1989, **68**, 1522.
3. Serio, M.A.; Hamblen, D.G.; Markham, J.R.; Solomon, P.R. *Energy and Fuels* 1987, **1**, 138.
4. Xu, W.-C.; Tomita, A. *Fuel Process. Tech.* 1989, **21**, 25.
5. Serio, M.A.; Peters, W.A.; Howard, J.B. *Ind. Eng. Chem. Res.* 1987, **26**, 1831.
6. Schiller, J.E.; Mathiason, D.R. *Anal. Chem.* 1977, **49**, 1225.
7. Boduszynski, M.M.; Hurtubise, R.J.; Allen, T.W.; Silver, H.F. *Anal. Chem.* 1983, **55**, 225.
8. Teo, K.C.; Watkinson, A.P. *Fuel* 1986, **65**, 949.

Table 1. Molecular mass of initial peaks in FIMS spectra of each d.b. homologue.

d.b.	Molecular mass
5	128 (naphthalene)
6	152 (acenaphthylene), 154 (biphenyl)
7	178 (anthracene, phenanthrene)
8	202 (pyrene and fluorenthene)
9	226, 228 (chrysene)
10	252 (benzo(a)pyrene, perylene), 254 (phenylphenenthrene)
11	276, 278 (picene, dibenzanthracene)
12	300 (coronene), 302 (dibenzpyrene), 304 (phenanthrenoanthracene)

[a] Compounds indicated in parenthesis are PAHs to which the peaks are assigned.

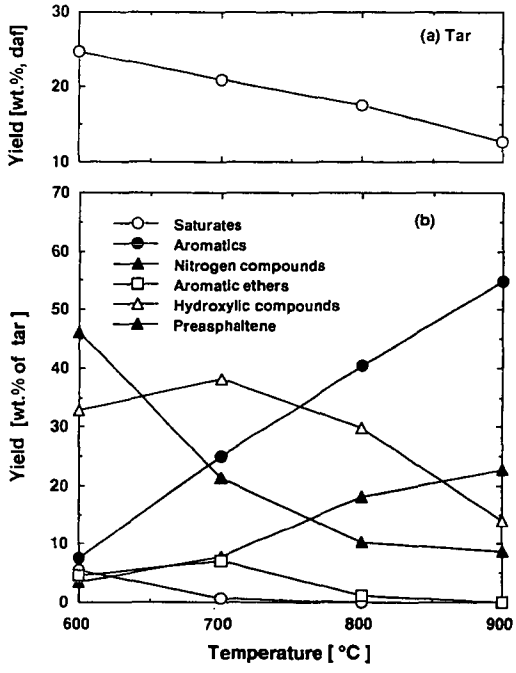

Figure 1. Temperature dependence of yield and composition of tar.

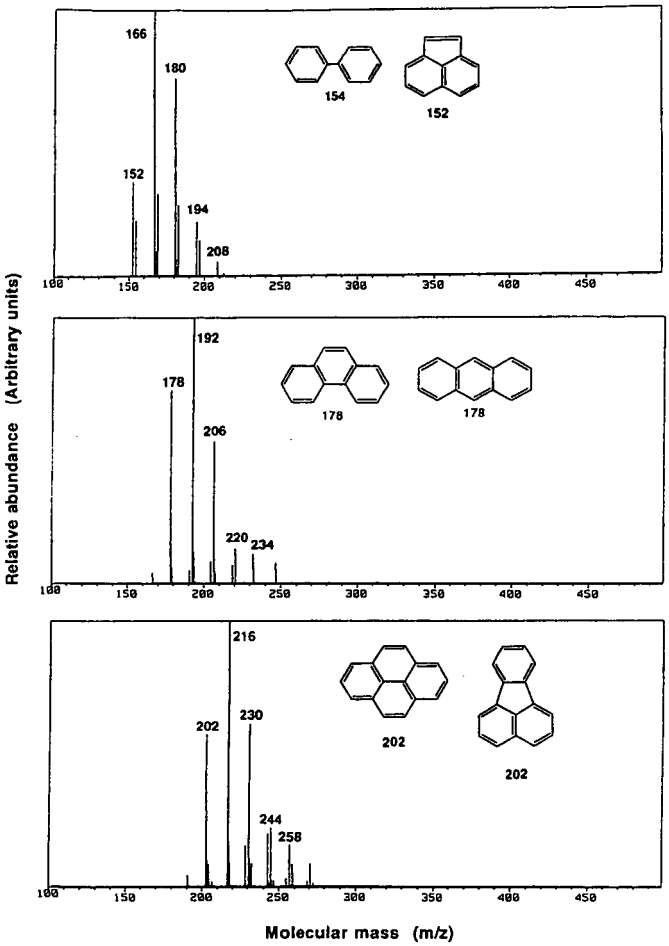

Figure 2. FIMS spectra of 6, 7 and 8 d.b. fractions at 800°C.

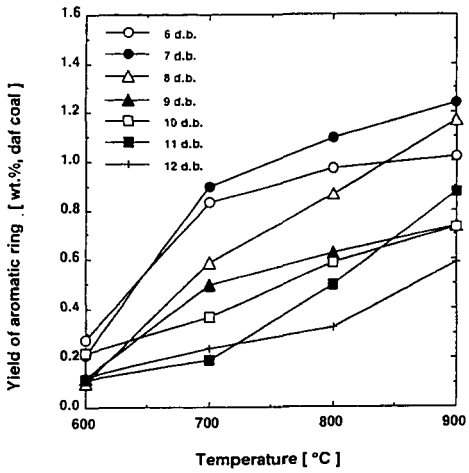

Figure 3. Yield of individual double-bond homologues converted into that of unsubstituted PAH.

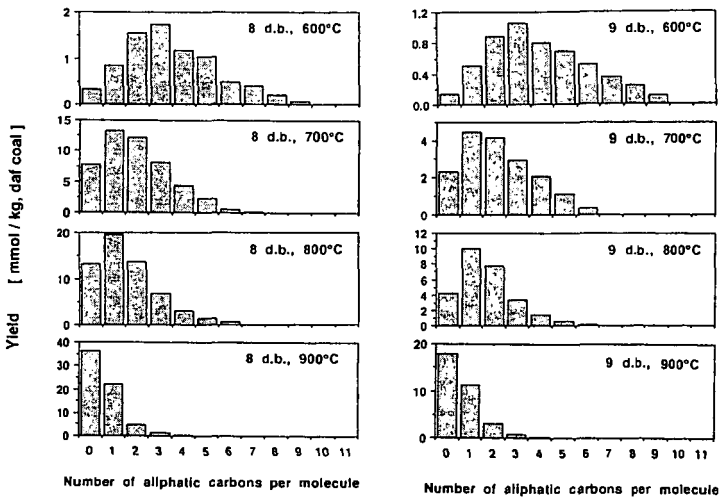

Figure 4. Distribution in number of aliphatic carbons per molecule for 8 and 9 d.b. homologues.

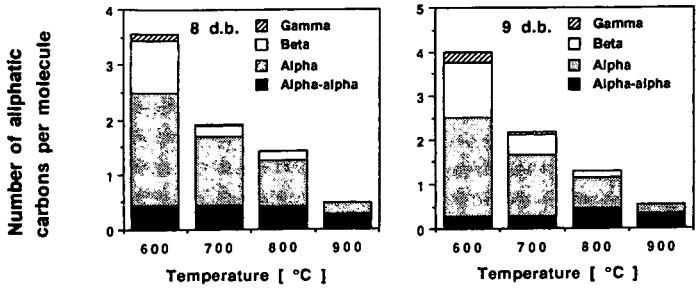

Figure 5. Composition of aliphatic carbons in 8 and 9 d.b. fractions.

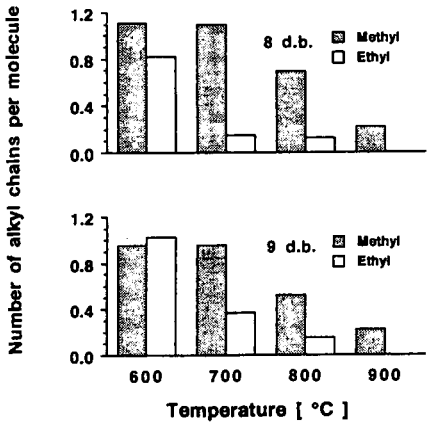

Figure 6. Number of methyl and ethyl chains per molecule for 8 and 9 d.b.fractions.

HYDROUS PYROLYSIS OF n-$C_{32}H_{66}$ IN THE PRESENCE AND ABSENCE OF INORGANIC COMPONENTS

Roald N. Leif[1], Bernd R. T. Simoneit[1] and Keith A. Kvenvolden[2]

[1] Petroleum Research Group, College of Oceanography, Oregon State University, Corvallis, OR 97331

[2] U. S. Geological Survey, 345 Middlefield Road, Menlo Park, CA 94025

Keywords : hydrocarbon cracking, n-alkanes, n-alkenes, n-alkanones

Introduction

There has been much research on catagenetic processes by laboratory simulations. These experiments are performed over short durations but at elevated temperatures to compensate for the lower temperature organic reactions which occur over geologic timescales. Experimental designs for achieving these reactions have been quite diverse. In addition to varying time and temperature, many different combinations of experimental parameters have been used including: vacuum or controlled atmosphere conditions, open or closed systems, different reaction vessel materials, aqueous or anhydrous conditions, varied mineral assemblages, and a wide range of organic source materials (e.g., 1-7). Hydrous pyrolysis is a closed system procedure of heating a sample which is submerged in water and not in contact with water vapor or supercritical water (8). It appears to be the most promising system since it most closely mimics the conditions found in nature, especially those found in hydrothermal systems (9). In this paper, the study of the aqueous high temperature organic chemistry of n-$C_{32}H_{66}$ in the presence or absence of several selected inorganic components is presented. The experiments were performed under nitrogen in a stainless steel reaction vessel, the only variable being the addition of inorganic species. The results of these experiments are relevant for hydrous pyrolysis studies of sedimentary source materials where large amounts of inorganic salts and minerals are present.

Experimental

A 250 mL stainless steel vessel (Parr Instrument T316SS) used for the reactions was equipped with a thermocouple for temperature control (± 2°C) and a gage block assembly for recovery of volatiles. Conditioning of the vessel prior to each experiment was done by heating it with 63.5 mL water at 350°C for 24 h. No effort was made to remove air from the system during the conditioning process. The experiments are summarized in Table 1. For each experiment 0.050 g of n-$C_{32}H_{66}$ and 63.5 mL of deoxygenated water alone or water and an equimolar amount of inorganic species were combined in the reaction vessel. The deoxygenated water was prepared by bubbling N_2 gas into distilled water for twenty minutes before each experiment. Assembly of the reaction vessel was done in a glove bag under a nitrogen atmosphere. The vessel was then placed in a heater and temperature maintained at 350°C for 72 h. In the case of the H_2O - n-$C_{32}H_{66}$ - sulfide system, the interior of the vessel was coated with a sulfide formed by heating the vessel with 0.5 g elemental sulfur and 63.5 mL water for 24 h. After cooling to room temperature, the excess sulfur was rinsed from the vessel leaving a uniform sulfide coating. Then under a N_2 atmosphere, 0.050 g of n-$C_{32}H_{66}$ and 63.5 mL of deoxygenated water were combined and allowed to react.

The vessel was cooled to room temperature before opening and contents transferred to a separatory funnel. The interior of the vessel was rinsed with methanol and methylene chloride, which were added to the separatory funnel, and the organic fraction was separated. The water was extracted with two additional 20 mL portions of methylene chloride. The organic fractions were combined and concentrated.

The products were fractionated by thin layer chromatography (20 x 20 cm, 250 microns Silica Gel G) into four fractions using heptane as developer. Hydrogenation of selected

samples was done by bubbling H_2 gas into the sample for 30 minutes in the presence of platinum (IV) oxide (Adams' catalyst).

Gas chromatography (GC) was performed using a Hewlett-Packard 5890 gas chromatograph equipped with a DB-5 open tubular column (30 m x 0.25 mm ID, 0.25 μm film) programmed from 65° (isothermal 2 min.) to 310°C at 4°C / min. (isothermal 30 min.). Compound identification was aided by comparison with authentic standards.

Results

Although a large amount of cracking occurred, there was no gas pressure in any of the heating experiments. Most of the unreacted starting material along with the cracking products was in the form of a wax disk floating on the water. The walls of the vessel were also coated with the wax which made it difficult to ensure that all of the organic material was completely transferred from the vessel for analysis.

The GC traces of the total extracts are shown in Fig. 1. They are characterized by a broad distribution of cracking products with a large amount of unreacted starting material. The cracking products range in carbon number from C_9 to C_{31}. The cracking products in all experiments maximized at C_{16}, half the carbon number of the starting material. The total extracts consisted primarily of a nonpolar fraction of n-alkanes and n-alkenes and a polar fraction made up of oxygenated compounds. A low amount of branched and aromatic compounds were formed under these conditions.

H_2O - n-$C_{32}H_{66}$. Chromatograms of the nonpolar fraction before and after catalytic hydrogenation confirms the presence of the n-alkene isomers (Fig. 2a and 2b). The n-alkanes were the major products of hydrocarbons with 16 or more carbon atoms. No particular series dominated in hydrocarbons less than C_{16}. The polar fraction consisted of homologous n-alkanal and n-alkan-2-one series in addition to other oxygenated species (Fig. 2c).

H_2O - n-$C_{32}H_{66}$ - NaCl. The nonpolar and polar fractions were similar to the H_2O - n-$C_{32}H_{66}$ system but the n-alkane predominance of the heavier hydrocarbons was not observed.

H_2O - n-$C_{32}H_{66}$ - HCl. The acidic conditions favored the formation of n-alkanes over n-alkenes. No significant differences in the polar fraction was observed.

H_2O - n-$C_{32}H_{66}$ - NaOH. A simple product distribution was generated which was composed primarily of terminal n-alkenes with a minor amount of n-alkanes. A similar distribution of polar compounds was generated in this experiment.

H_2O - n-$C_{32}H_{66}$ - NH_4Cl. The formation of n-alkanes over n-alkenes was slightly favored in this system when compared to the H_2O - n-$C_{32}H_{66}$ system but a similar distribution of polar compounds were formed.

H_2O - n-$C_{32}H_{66}$ - Na_2SO_4. Cracking products below C_{14} were low in this experiment. The nonpolar fraction consisted mainly of n-alkanes and terminal n-alkenes in approximately equal amounts for each carbon number.

H_2O - n-$C_{32}H_{66}$ - Elemental Sulfur. The formation of n-alkanes was favored by the addition of elemental sulfur. The n-alkan-2-ones were present but formed in lower amounts.

H_2O - n-$C_{32}H_{66}$ - Sulfide. This system greatly favored the formation of n-alkanes over any other products, and n-alkan-2-ones were the major series in the polar fraction (Fig. 3).

Discussion

These preliminary experiments were designed to study the effects that some selected inorganic components have on the aqueous pyrolysis of a representative n-alkane. The choice of systems was not comprehensive but does include some major components likely to be found when experimenting with sediments and whole rocks.

Hydrous pyrolysis of n-$C_{32}H_{66}$ results in the formation of alkanes, alkenes, and to a lesser extent oxygenated species. Relative amounts of the products were affected by the inorganic species present in the system. The formation of n-alkene isomers by these pyrolysis experiments confirms the results previously described where terminal n-alkenes and a range of internal n-alkenes, formed by double bond migration, were produced during aqueous pyrolysis of n-hexadecane at 317°C (10). Acid-catalyzed double bond migration was also observed in

the aqueous pyrolysis of 1-decene to form 2-, 3-, 4- and 5-decene (11). The low hydrogen ion concentration under alkaline conditions (H_2O - n-$C_{32}H_{66}$ - NaOH) did not permit much double bond migration. This lack of secondary double bond migration resulted in terminal n-alkenes as the major products, preserving the original cracking products formed by the homolytic bond cleavage of n-$C_{32}H_{66}$. The increase in the hydrogen ion concentration in the NH_4Cl and HCl systems favored a higher alkane to alkene ratio relative to the H_2O - n-$C_{32}H_{66}$ system, indicating an enhancement of hydrogenation occurred under acid conditions. This result may be due to the interaction with the stainless steel vessel to alter the hydrogenation capacity of the reaction system. The corrosion of the stainless steel reaction vessel by the following reaction has been proposed to account for a change in pH observed in some experiments (12) :

$$Fe + 2H^+ \longrightarrow Fe^{2+} + H_2$$

The increased hydrogen ion concentration in the acidic systems could drive this reaction to the right, producing a larger amount of hydrogen gas. This could provide the increased hydrogenation capacity necessary to result in the observed increases in the alkane to alkene ratios. The alkaline conditions of the NaOH system resulted in a greatly diminished hydrogenation capacity to produce a low alkane to alkene ratio. The role of the initial oxidation state of the sulfur species can be seen by comparing the sulfate, elemental sulfur and sulfide systems. The distribution of n-alkanes and terminal n-alkenes as primary products of the H_2O - n-$C_{32}H_{66}$ - Na_2SO_4 system suggests that aqueous sulfate consumes hydrogen ions to decrease both the acid-catalyzed double bond isomerization and the hydrogenation capacity of the system, resulting in a nonpolar fraction similar to the alkaline H_2O - n-$C_{32}H_{66}$ - NaOH system. Both elemental sulfur and sulfide generate acidic systems but the lack of n-alkenes indicates a strongly hydrogenating system. The polar fraction of the sulfide system consisted mainly of n-alkan-2-ones. The n-alkan-2-ones are one of several series of polar compounds commonly found in oils collected from interiors of high temperature hydrothermal vents of the Guaymas Basin hydrothermal system (13). The results of these laboratory experiments suggest that these oxygenated compounds may be formed entirely by thermogenic processes.

Conclusions

The products generated by the heating experiments appear to be the result of primary cracking of n-$C_{32}H_{66}$ to form alkenes followed by secondary reactions of these cracking products. The main findings are listed below :

1. Primary cracking of n-$C_{32}H_{66}$ produced a homologous series of terminal n-alkenes.
2. Specific acid-catalyzed double bond isomerization of the terminal alkenes occurred where a sufficient hydrogen ion concentration existed.
3. The extent of alkene hydrogenation was affected by the hydrogen ion concentration, possibly by corrosion of the stainless steel reaction vessel.
4. The initial oxidation state of sulfur had a major effect on controlling the product distribution, with elemental sulfur and sulfide favoring n-alkane generation.

These experiments provide information on how some inorganic species influence the predominant chemical reactions which n-paraffins undergo under high temperature aqueous conditions. These preliminary results suggest that care should be taken when comparing the results from simple aqueous pyrolysis systems to whole rock and whole sediment pyrolyses where the mineral and salt contents are vastly different.

Acknowledgements

We thank the National Science Foundation, Division of Ocean Sciences (Grant OCE-9002366), the Donors of the Petroleum Research Fund administered by the American Chemical Society and the Gilbert Fellowship Program of the U. S. Geological Survey, for support of this research.

Literature Cited

(1) B. Horsfield and A. G. Douglas, *Geochim. Cosmochim. Acta* **44**, 1119 (1980).
(2) K. E. Peters, B. G. Rohrback and I. R. Kaplan, *Am. Assoc. Pet. Geol. Bull.* **65**, 688 (1981).
(3) M. D. Lewan, *Phil. Trans. R. Soc. Lond.* **A315**, 123 (1985).
(4) P. A. Comet, J. McEvoy, W. Giger and A. G. Douglas, *Org. Geochem.* **9**, 171 (1986).
(5) T. I. Eglinton, S. J. Rowland, C. D. Curtis and A. G. Douglas, in *Advances in Organic Geochemistry 1985*, D. Leythaeuser and J. Rullkötter, Eds., *Org. Geochem.* **10**, 1041 (1986).
(6) E. Tannenbaum, B. J. Huizinga and I. R. Kaplan, *Am. Assoc. Pet. Geol. Bull.* **70**, 1156 (1986).
(7) B. J. Huizinga, E. Tannenbaum and I. R. Kaplan, *Org. Geochem.* **11**, 591 (1987).
(8) M. D. Lewan, J. C. Winters and J. H. McDonald, *Science* **203**, 897 (1979).
(9) B. R. T. Simoneit, in *Productivity, Accumulation and Preservation of Organic Matter in Recent and Ancient Sediments*, J. K. Whelan and J. W. Farrington, Eds. (Columbia University Press, New York, 1992), pp. 368-402.
(10) O. Weres, A. S. Newton and L. Tsao, *Org. Geochem.* **12**, 433 (1988).
(11) M. Siskin, G. Brons, A. Katritzky and M. Balasubramanian, *Energy Fuels* **4**, 475 (1990).
(12) Y. K. Kharaka, W. W. Carothers and R. J. Rosenbauer, *Geochim. Cosmochim. Acta* **47**, 397 (1983).
(13) R. N. Leif and B. R. T. Simoneit, unpublished data.

Table 1. Summary of reaction systems performed in 63.5 mL H_2O at 350°C for 72 h.

Figure	System Description	Reactant Amounts
1a	H_2O - n-$C_{32}H_{66}$	0.050 g n-$C_{32}H_{66}$
1b	H_2O - n-$C_{32}H_{66}$ - NaCl	0.050 g n-$C_{32}H_{66}$ 0.111 mmol NaCl
1c	H_2O - n-$C_{32}H_{66}$ - HCl	0.050 g n-$C_{32}H_{66}$ 0.111 mmol HCl
1d	H_2O - n-$C_{32}H_{66}$ - NaOH	0.050 g n-$C_{32}H_{66}$ 0.111 mmol NaOH
1e	H_2O - n-$C_{32}H_{66}$ - NH_4Cl	0.050 g n-$C_{32}H_{66}$ 0.111 mmol NH_4Cl
1f	H_2O - n-$C_{32}H_{66}$ - Na_2SO_4	0.050 g n-$C_{32}H_{66}$ 0.111 mmol Na_2SO_4
1g	H_2O - n-$C_{32}H_{66}$ - Sulfur	0.050 g n-$C_{32}H_{66}$ 0.111 mmol Sulfur
1h	H_2O - n-$C_{32}H_{66}$ - Sulfide	0.050 g n-$C_{32}H_{66}$ Sulfide coated vessel

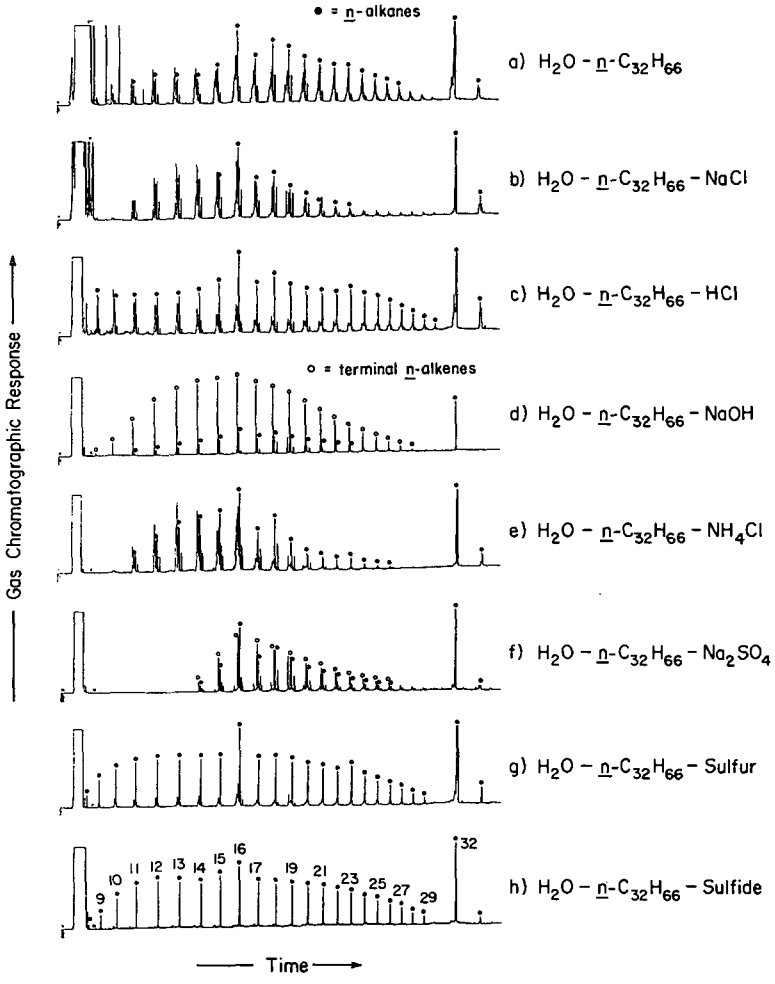

Fig. 1. Gas chromatograms of the total extracts from the hydrous pyrolysis experiments : a) H_2O - n-$C_{32}H_{66}$; b) H_2O - n-$C_{32}H_{66}$ - NaCl; c) H_2O - n-$C_{32}H_{66}$ - HCl; d) H_2O - n-$C_{32}H_{66}$ - NaOH; e) H_2O - n-$C_{32}H_{66}$ - NH_4Cl; f) H_2O - n-$C_{32}H_{66}$ - Na_2SO_4; g) H_2O - n-$C_{32}H_{66}$ - Sulfur; h) H_2O - n-$C_{32}H_{66}$ - Sulfide. [GC conditions : oven was temperature programmed from 65° (isothermal 2 min.) to 310°C at 4°C / min. (isothermal 30 min.)]. Numbers refer to carbon chain lengths of the n-alkanes.

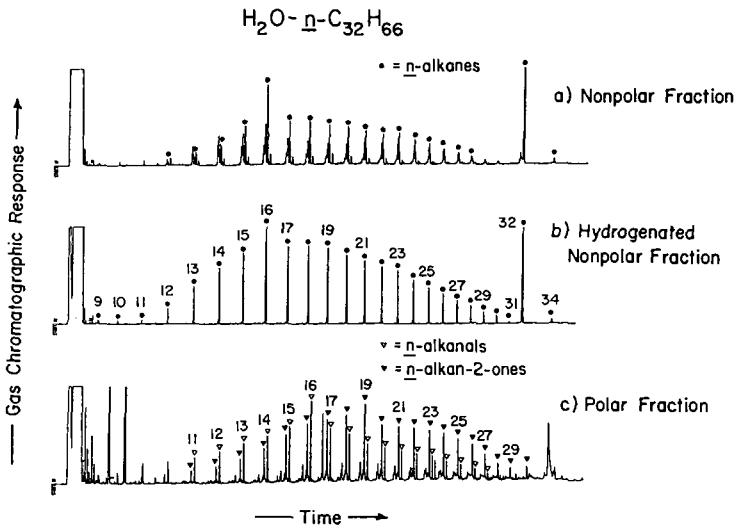

Fig. 2. Gas chromatograms of the H_2O - n-$C_{32}H_{66}$ system : a) nonpolar fraction before catalytic hydrogenation; b) nonpolar fraction after catalytic hydrogenation; c) polar fraction. Numbers refer to carbon chain lengths.

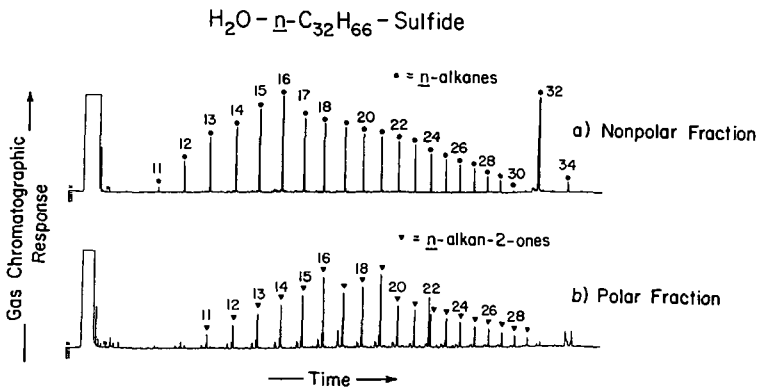

Fig. 3. Gas chromatograms of the H_2O - n-$C_{32}H_{66}$ - Sulfide system : a) nonpolar fraction; b) polar fraction. Numbers refer to carbon chain lengths.

THE EFFECT OF MINERALS ON TRACE ELEMENT DISTRIBUTIONS IN HYDROUS PYROLYSATES OF KEROGENS FROM THE NEW ALBANY SHALE

S. L. Fitzgerald and R. H. Filby
Department of Chemistry
Washington State University
Pullman, WA 99164-4630

Keywords: Minerals, Trace Elements, Pyrolysis

INTRODUCTION

Trace element complexes are present in most crude oils and source rock bitumens (1). Past studies have used trace element distributions in oil-oil (2-10) and to a lesser extent in oil-source rock correlation studies (11,12). Unfortunately, the use of trace element distributions in correlation studies is limited because, other than the nickel and vanadyl porphyrins, very little is known about the nature of these trace element complexes. Even less is known about the parameters controlling their distributions in oils and bitumens (1).

Mineral matter has been shown to play an important role during the catalytic alteration of kerogen to form petroleum (13-18). Kaplan and co-workers (13-15) demonstrated that, during kerogen pyrolysis, the presence of clays decreases the pyrolysate yield due to adsorption of polar constituents and the increase in gaseous products. Work by Rose et. al (19). also showed that while the addition of minerals did not increase the aromatization of the kerogen, they did alter the pyrolysate yields.

Considering the effect that minerals in the source rock have on the hydrocarbon distributions during petroleum formation, it seems reasonable that they also influence the trace element contents in crude oils. In order to study this influence, kerogen from the New Albany shale was subjected to hydrous pyrolysis in the presence and absence of added minerals. A comparison of the trace element abundances in the generated pyrolysates and in the whole shale bitumen indicates the extent to which minerals control the trace element contents in the New Albany bitumen.

EXPERIMENTAL

Kerogens were isolated from the New Albany shale as described previously (20). The bitumen-II was removed from the kerogen by soxhlet extraction (48 hrs.) using chloroform,

the kerogen was then separated into float/sink fractions by suspension in chloroform to remove residual minerals (mostly pyrite). The minerals added in the pyrolysis experiments were calcite, pyrite, Na-montmorillonite, kaolinite, and illite.

In a typical experiment, 30g of kerogen and 30g of mineral were mixed in a Pyrex "sleeve" with 130 mL deionized water. The "sleeve" was then placed in a 1L autoclave. The system was flushed with nitrogen, and heated for 5 hours at 300°C. Temperatures were monitored through a thermo-well placed directly into the sample. For comparative purposes, the bitumen-I extracted shale was pyrolysed under hydrous conditions (150g shale, 200 ml H_2O) for 5 hrs. at 300°C.

The pyrolysates were recovered after each pyrolysis by the same extraction method used to recover the bitumen-II. Pyrolysate yields were determined relative to the amount of kerogen originally pyrolysed and were not corrected for mineral content,mechanical sample loss, or losses due to formation of gaseous products. Trace element concentrations for all samples were determined by instrumental neutron activation analysis (INAA) using the method described previously (21).

RESULTS AND DISCUSSION

Pyrolysate yields. The pyrolysis of kerogen with calcite gave the lowest yield of all the runs (table 1). This is consistent with the observations of Huizinga et. al. (15) who noted (for short heating times) lower pyrolysate yields for kerogens with calcite during both dry (and to a lesser degree) hydrous pyrolysis. They attributed this decrease in yield to inefficient heating due to the large amount of mineral present. It seems more likely that this effect is the result of an interaction between the kerogen and the calcite, however, since similar results were obtained under the conditions of this study (i.e. lower kerogen to mineral ratio, hydrous conditions, and temperature measured from within the sample).

The decrease in pyrolysate products generated in the presence of montmorillonite, and illite also agreed with the findings of Huizinga et. al.(15). They demonstrated that these clays have high adsorptive capacities for the more polar components of the pyrolysate, and thermocatalyticly induce the formation of more gaseous products. These two effects cause a net reduction in pyrolysate yield. In contrast, however, the kerogen heated with kaolinite gave an increase in yield. This seems to indicate that kaolinite provides some thermocatalytic activity with a substantially lower adsorption capacity for pyrolysate products than illite or montmorillonite.

Trace Elements. The concentrations of twenty trace elements in the bitumens, kerogen, and related pyrolysates are

shown in Table 1. For the sake of brevity only the nickel and vanadium values and their ratios will be discussed here. As can be seen from the graph in Figure 1, the vanadium concentrations for the different kerogen pyrolysates are fairly constant. This indicates that the minerals used have very little if any affect on the abundance of vanadyl porphyrins in the pyrolysates. The nickel concentrations (Fig. 2), however, show substantial variation among the pyrolysates. The most noticeable trend is the increase in nickel concentrations from Na-montmorillonite to kaolinite to illite. One explanation for this trend could be the preferential adsorption of nickel porphyrin with montmorillonite being the strongest adsorbent and illite the weakest. However, this is inconsistent with the pyrolysis yield data which indicates that kaolinite is the least adsorbent of the three clays. Another explanation for this trend is that the clays are causing the preferential decomposition of the nickel porphyrins on the surface as a function of surface acidity (Na-montmorillonite being the most acidic).

The value for the nickel concentration from the kerogen-pyrite (KP) pyrolysis shows a dramatic drop which is comparable to the concentration from the montmorillonite run. It has been shown that at temperatures above 240 C, porphyrins in the presence of H_2S are partially decomposed. Also in the presence of H_2S and a Co-Mo catalyst, nickel and vanadyl porphyrins can be demetallated with nickel porphyrins having the higher demetallation rate (22). The generation of large amounts of H_2S during pyrolysis with pyrite could possibly explain the observed drop in the nickel concentration. The pyrolysis with calcite also shows a drop in nickel concentration similar to the value seen in the kaolinite run. It is uncertain at this time why calcite would have this effect on the nickel porphyrins and further investigation is needed to determine the cause of this effect.

A comparison of the Ni/V ratios for the bitumens, kerogen, and related pyrolysates is shown in Figure 3. It can be seen from this comparison that the Ni/V ratios are similar for the kerogen, and for the pyrolysates from the original kerogen, the kerogen float, and the whole shale. This is unsurprising since the kerogen is the source of the Ni and V complexes in these pyrolysates. Variations in the Ni/V ratio in pyrolysates generated in the presence of minerals reflect the variations in the nickel concentrations for the pyrolysates.

A comparison of the bitumen-II Ni/V ratio with that from the Na-montmorillonite pyrolysate shows the two have very similar values. This indicates that the Ni pophyrin in the bitumen-II, which is more intimately associated with the mineral component of the shale, may be decomposing due to interaction with clays.

CONCLUSIONS

The work presented here indicates that the mineral matrix of the shale plays an important role in determining the trace element distributions during petroleum formation. The data show variations in the Ni during pyrolysis of kerogen with clays and pyrite, whereas the V concentration remains essentially constant. Further investigation is needed to determine if this loss is due to the adsorption or the decomposition of the nickel complexes present.

ACKNOWLEDGMENTS

The authors thank Cathy Grimm and the Nuclear Radiation Center staff for their prompt aid during the instrumental neutron activation analysis.

REFERENCES

1. Branthaver, J.F. and Filby, R.H., in "Metal Complexes In Fossil Fuels", eds. Filby, R.H.and Branthaver, J.F., ACS Symposium Series No. 344, American Chemical Society: Washington, DC, 1987.
2. Hodgson, G.W., *Bull. Am. Assoc. petrol. geol.*, 1954, **38**, 2737-54.
3. Hodgson, G.W., Fiores, J., Baker, B.L. *Bull. Am. Assoc. Petrol. Geol.* 1959, **43**, 311-28.
4. Hitchon, B., Filby, R.H. *Alberta Research Council Open File Report* 1983-02, 144 p.
5. Hitchon, B., Filby, R.H. *Bull. Am. Assoc. Petrol. Geol.* 1984, **68**, 838-49.
6. Hyden, H.J., *U.S. Geol. Serv. Bull. 1100-B*, 1961.
7. Saban, M., Vitorovic, O. and Vitorovic, in "Symposium on Characterization of Heavy Crude Oils and Petroleum Residues", Editions Technip: Paris, 1984.
8. Al-Shahristani, H. and Al-Atyia, M.J., *Geochim. Et Cosmochim. Acta*, 1972,**36**, 929-37.
9. Curiale, J.A. In "Exploration for Heavy Oil and Bitumen"; Am. Assoc. Petrol. Geol. Research Conference, Santa Maria, Calif., Oct. 28-Nov. 2, 1984, Vol.1, pp.1-39.
10. Curiale, J.A., in "Metal Complexes in Fossil Fuels", eds. Filby, R.H. and Branthaver, J.F., ACS Symposium Series No. 344, American Chemical Society: Washington, DC, 1987.
11. Hirner, A.V., in "Metal Complexes in Fossil Fuels", eds. Filby, R.H. and Branthaver, J.F., ACS Symposium Series No. 344, American Chemical Society: Washington, DC, 1987.
12. Chakhmachkev, V.A., Lositskaya, I.F., Punanova, S.A.., Semenova, R.A. *Geokhimiya* 1985, 703-09.

13. Lu, S.-T., Kaplan, I.R. *Geochim.et Cosmochim. Acta*, 1985, **49**, 2589-2604.
14. Tannenbaum, E., Huizinga, B.J. and Kaplan, I.R. *Amer. Assoc. Petrol. Geol. Bull.*, 1986, **70**, 1156-1165.
15. Huizinga,B.J., Tannenbaum, E. and Kaplan, I.R. *Org. Geochem.*, 1987, **11**, 591-604.
16. Lu, S.-T., Ruth, E. and Kaplan, I.R. *Org. Geochem.*, 1989, **14**, 491-499.
17. Lu, S.-T. and Kaplan, I.R. *Org. Geochem.*, 1989, **14**, 501-510.
18. Espitalie, J., Makadi, K.S. and Tricket, J. *Org. Geochem.*, 1984, **6**, 365.
19. Rose, H.R., Smith, D.R., Hanna, J.B., Palmisano, A.J. and Wilson, M.A. *Fuel*, 1992, **71**, 355-360.
20. Mercer, G.E., Fitzgerald, S.L., Day, J.W. and Filby, R.H. *ACS Fuel Div. Preprints*, 1991, **36**, 1180-1189.
21. VanBerkel, G.J., Ph.D. Thesis, Department of Chemistry, Washington State University, 1987.
22. Rankel, L.A. *Preprints Div. Petrol. Chem.ACS*, 1981, **26**, 689.

Table 1. Trace element concentrations in kerogen pyrolysates(WK-KL), bitumens (BI, BII), shale pyrolysate (SP), and kerogen (KER).

	WK	K	KP	KC	KM	KK	KL	BI	SP	BII	KER
As (ppm)	18.1	3.07	32.0	1.54	1.76	4.43	3.24	1.78	4.36	120	89
Br (ppm)	14.0	17.6	14.6	12.0	6.73	12.1	10.1	32.1	30.6	102	12.6
Cl (ppm)	5920	12600	6210	6230	2200	9540	2620	617	1680	13500	59100
Co (ppm)	26.2	2.24	2.08	10.6	1.50	1.18	14.8	4.46	64.6	17.7	67.0
Cr (ppm)	22.2	34.5	95.0	0.866	0.396	21.4	2.28	0.794	<0.516	1.29	35.8
Cu (ppm)	232	269	42.2	<27.9	<35.9	96.6	53.3	<68.7	<71.3	308	<1070
Fe (ppm)	237	566	121	892	26.0	566	130	152	492	1600	33800
Ga (ppm)	31.5	20.5	13.2	4.43	4.40	15.8	23.6	0.498	2.82	14.4	27.6
Hg (ppm)	7.64	9.58	15.0	5.14	18.6	9.44	12.0	93.6	20.6	370	33.8
La (ppb)	496	254	193	104	60.3	130	432	38.4	<57.6	214	33000
Mn (ppb)	243	337	620	356	194	330	273	529	1180	602	27700
Mo (ppm)	4.79	7.94	7.26	1.27	1.46	5.47	3.98	4.35	3.72	101	1230
Na (ppm)	29.7	23.2	157	34.8	30.1	13.6	20.8	31.4	25.6	36.0	3280
Ni (ppm)	3290	2600	1560	1940	1600	1920	2700	2180	3460	2405	1830
Sb (ppb)	743	348	330	130	90.5	376	170	<89.4	130	23100	26000
Sc (ppb)	3.11	2.12	19.7	3.38	1.81	2.66	<3.74	1.68	<6.14	<8.26	4190
Se (ppm)	32.2	33.1	62.2	20.9	77.8	39.2	50.8	373	82.2	1510	136
Th (ppb)	24.6	<28.3	<31.8	<32.6	<23.3	<27.5	24.4	<35.6	65.6	<105	3560
V (ppm)	1430	1120	1040	1040	1200	1050	1160	2540	1560	2070	741
Zn (ppm)	36.6	24.0	274	20.3	2.95	14.4	9.10	11.0	56.6	61.8	570
Ni/V	2.30	2.32	1.50	1.87	1.33	1.83	2.33	0.86	2.22	1.16	2.47
Pyrolysate Yield	3.97%	4.84%	3.40%	2.87%	3.04%	5.59%	3.38%	n/a	0.97%	n/a	n/a

WK=untreated kerogen, K=kerogen float, KP=kerogen+pyrite, KC=kerogen+calcite, KM=kerogen+montmorillonite
KK=kerogen+kaolinite, KL=kerogen+illite, BI=bitumen I, SP=extracted shale pyrolysate, BII=bitumen II, KER.=kerogen

*Percentages refer to original kerogen mass (not corrected for mineral content), except for NAP which refers to extracted shale mass.

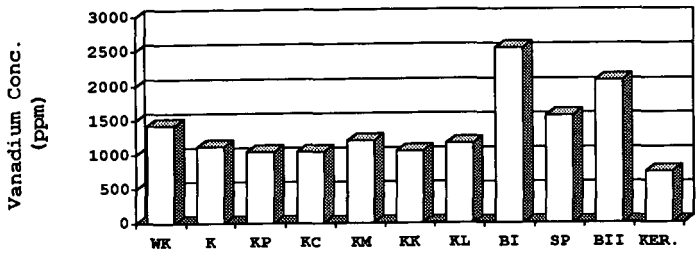

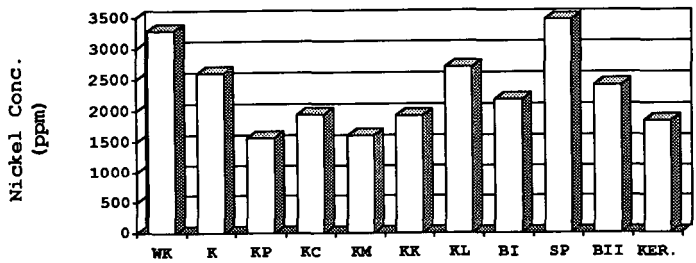

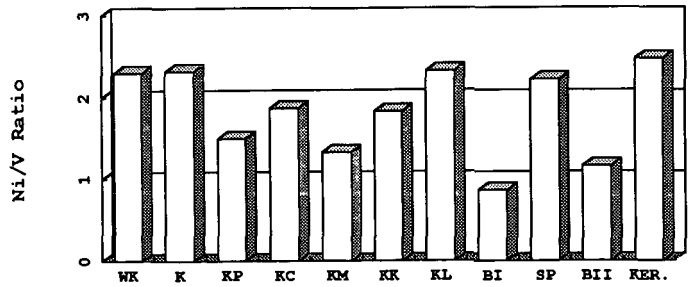

Figure 1 (upper); 2 (middle); 3 (lower) Vanadium, Nickel, and Nickel/Vanadium Ratios in New Albany Kerogen Pyrolysates.

WK=untreated kerogen, K=kerogen float, KP=kerogen+pyrite, KC=kerogen+calcite, KM=kerogen+montmorillonite, KK=kerogen+kaolinite, KL=kerogen+illite, BI=bitumen I, SP=extracted shale pyrolysate, BII=bitumen II, KER.=kerogen

TRACE ELEMENT DISTRIBUTIONS IN KEROGEN, BITUMENS AND PYROLYSATES ISOLATED FROM NEW ALBANY SHALE

Gregory E. Mercer Adam J. Regner, and Royston H. Filby

Department of Chemistry
Washington State University
Pullman, WA 99164-4630

Keywords: pyrolysis, metal complexes; oil-source rock correlation

INTRODUCTION

Although trace element distributions have been used to correlate oils (1-8), there have been few similar studies on oil-source rock correlations (9).

The bitumen, kerogen or a pyrolysate from a source rock may, in principle, be used to correlate a source rock to an oil. However, if trace element abundances are to be used for oil-source rock correlations, the bitumen, kerogen and the pyrolysates of a source rock should show correlation in their trace element distributions. For example, it has been shown (10) that the kerogen of the New Albany shale releases Ni(II) and VO(II) porphyrins during pyrolysis in amounts that are directly proportional to organically combined Ni and V, in the kerogen.

In this study trace element distributions were measured in the bitumen and kerogen from the New Albany shale and in pyrolysates generated from the shale under different conditions (i.e., dry, hydrous, toluene, toluene/methanol). Trace element distributions were also compared in chromatographic fractions of the bitumen and pyrolysates. Implications for oil-source rock correlation are discussed.

EXPERIMENTAL

Detailed geological information on New Albany shale (Clark County, Indiana) are reported elsewhere (11). The procedures for the extraction of the bitumen I and II and the isolation of kerogen by demineralization were similar to those of Mercer et al. (12). Boscan (Venezuela) crude oil was also analyzed for comparison.

Shale samples (150 g) were pyrolysed for 5 hours at 300°C in a 1L autoclave in toluene, toluene/methanol (7:3), or water (200 mL each) and without solvent ("dry" conditions) at initially 1 atm N_2. The pyrolysed shale samples were extracted as for the bitumen-I. The shale which was pyrolysed in toluene was re-pyrolysed four times in toluene and for a fifth time in toluene/methanol (7:3) under the same conditions.

Liquid chromatography (silica gel) was used to separate the bitumen and pyrolysate samples into fractions for analysis. The first fractions were eluted with a) hexanes (saturates), b) CH_2Cl_2 in hexanes (porphyrin aggregate), c) $CHCl_3$ (polar material), and d) 7:3 toluene/methanol followed by 100% methanol (asphaltenes plus other highly polar fractions).

Trace element concentrations were determined by instrumental neutron activation analysis (INAA) using the method published previously (12,13).

RESULTS

The concentrations of 13 elements in New Albany bitumens, kerogen and pyrolysates are listed in Tables 1 and 2.

The kerogen is the source of Ni and V complexes found in the pyrolysates (10) and, through maturation, of the complexes in the bitumen I and II. Hence, it might be expected that the pyrolysates should have similar Ni/V ratios as the kerogen (1.91 after accounting for inorganic Ni contributions, 12). The first toluene pyrolysate, however, has a Ni/V ratio similar to that of the bitumen-I (0.91 and 0.95, respectively) rather than that of the kerogen (1.91). Subsequent toluene pyrolysates, as well as the hydrous, dry, and toluene-methanol pyrolysates, have Ni/V ratios which are similar to that of the kerogen. Thus the first toluene pyrolysate may represent residual bitumen I but the subsequent pyrolysates reflect the Ni/V ratio of the kerogen. Previous electron microprobe work with the New Albany shale (14) indicates that the kerogen is intimately associated with the clay minerals present in the rock. Hence, the extraction of the bitumen-I by sonication in a solvent at 40°C is probably incomplete. Thus, the first heating in the presence of toluene may generate a pyrolysate which is predominantly an improved extraction of the remaining inherent bitumen in the bitumen-I extracted shale, while the subsequent pyrolysates are generated primarily from the breakdown of kerogen. A similar conclusion was reached by Van Berkel, et al (15) to explain the similarity of an initial toluene pyrolysate of the New Albany kerogen and the bitumen-II extracted from the kerogen.

The data in Tables 1 and 2 show that the solvent plays a role in determining the resultant Ni/V ratio of the pyrolysate. Variations of the Ni/V ratio are probably related to the composition of the pyrolysate (i.e., polar versus nonpolar material) which is dependent on the polarity of the solvent and possibly to solvent-mineral interactions. The composition of the bitumen-I and the pyrolysates can be compared using the relative abundances of nonpolar (fractions 1 plus 2) and polar material (fractions 3 plus 4) measured by the chromatographic separation. Table 3 shows the Ni/V values compared to the non-polar/polar ratio. The hydrous and toluene/methanol pyrolysates contain the highest proportion of asphaltic/polar material and have Ni/V ratios very similar to that of the kerogen. A possible explanation is that water and methanol (in the toluene/methanol pyrolysis) deactivate the clay mineral-bitumen-kerogen interface, thus reducing conversion of asphaltic material to nonpolar hydrocarbons. Similarly, Ni and V complexes released by the kerogen are poorly adsorbed by the deactivated mineral matrix and thus the Ni/V ratios are similar to that of the kerogen. The higher Ni/V ratio (relative to the hydrous and toluene/methanol pyrolysates and the kerogen) observed for the dry pyrolysate is probably due to the high yield of the nonpolar fraction resulting from catalytic action of the clays. The large amounts of nonpolar organic matter generated during pyrolysis may

act as a nonpolar solvent and preferentially extract more of the less-polar Ni(II) porphyrins than the polar VO(II) species, thereby producing a pyrolysate with a higher Ni/V ratio than that of the hydrous or toluene/methanol pyrolysates. Similarly, under non-hydrous conditions the active clay surfaces retain the more polar VO(II) species relative to the less polar Ni(II) species. The second and third toluene pyrolysates were also likely to be derived from the breakdown of kerogen in which the catalytic action of the clays is not inhibited, such that conditions are similar to those of the dry pyrolysis.

For elements other than Ni and V the data in Tables 1 and 2 indicate that considerable variations in concentration relative to the bitumen I are observed. None of the pyrolysis conditions produces a pyrolysate that contains trace element distributions identical to that of the bitumen I; the hydrous pyrolysate is closest.

Distribution of Trace Elements in Pyrolysate Fractions. The four chromatographic fractions of each pyrolysate and the bitumen I were analyzed for trace elements. Distributions of trace elements among these fractions (i.e., percentage of element in each fraction relative to original sample) were similar for all pyrolysates and the bitumen I. Data for Ni, V, Se, Cr, Co, Fe and As in the bitumen I and the hydrous pyrolysate are shown in Figure 1. Figure 1 shows that Ni, V, and Se (Fig. 1a,b) are distributed differently from Cr, Cu, Fe, and As (Fig. 1c,d). Data for Ga, Mo, Sb, Zn, and Mn show similar patterns to Cr, Fe, Co and As. Nickel and vanadium are present predominantly as metalloporphyrins in the bitumen and the hydrous pyrolysate (porphyrin aggregate plus the $CHCl_3$ fraction which contains Ni(II) and VO(II) porphyrins). Only minor amounts of Ni and V are present in the asphaltene-polar fraction (<17%) and part of this is probably porphyrinic because weak Soret peaks at 390-410 nm are observed in this fraction. Hence, greater than 80% of the Ni and V in the bitumen and in the hydrous pyrolysates is present as metalloporphyrins. The distribution of Se in the bitumen I and the hydrous pyrolysate is related to that of sulfur. The non-polar (hexanes) fraction contains elemental sulfur and analysis of this fraction of the bitumen-II shows that approximately 86% of the sample was elemental sulfur. The mass spectrum of some of the sulfur crystals (Figure 2) revealed that the sulfur occurs predominantly as S_8 and that Se substitutes for a S in the S_8 ring to give the S_7Se molecule. Therefore, the Se observed in the nonpolar fractions of the pyrolysates is associated with elemental sulfur. The elemental sulfur is probably formed by the breakdown of sulfides, primarily pyrite and marcasite (FeS_2), during pyrolysis. The data also suggests that there is a considerable amount of elemental S/Se in the bitumen-I. This "inherent" elemental sulfur could be derived from weathering, bacterial activity or exposure to any other conditions which are capable of oxidizing sulfide minerals and could have occurred at any point in the history of the rock.

The distributions of Cr, Co, Fe and As (and other elements not shown in Fig. 1) in the hydrous pyrolysate and the bitumen I are similar. These elements are concentrated in the polar fraction (asphaltenes) although mass balance calculations show some retention of the column of these elements, presumably associated with highly polar asphaltenes that did not elute.

The similarity in trace element distributions in the chromatographic fractions of the bitumen I and the hydrous pyrolysate (and other pyrolysates) of the shale indicate that metal species or complexes generated by the kerogen by maturation in the bitumen I and by pyrolysis are also similar. Differences in absolute concentrations among the pyrolysates and the bitumen are probably due to kerogen-mineral or metal species-mineral interactions during interaction of pyrolysis.

CONCLUSION

1. The trace element concentrations in the pyrolysates vary significantly. It is necessary, therefore, to be consistent when choosing pyrolysis conditions for comparative purposes or for correlation work. Hydrous pyrolysis appears to give trace element concentrations closest to those of the bitumen I.

2. The Ni/V ratios observed for the pyrolysates are significantly different from that of the bitumen-I, except for the first toluene pyrolysate which may be residual bitumen-I released during initial pyrolysis. Excluding the first toluene pyrolysate, the Ni/V ratio of the pyrolysates resembled that of the kerogen. The major factor controlling the Ni/V ratio in the pyrolysates appears to be the polarity of the pyrolysis solvent and its deactivating effect on clay catalysis and related adsorption of metal species on clays. Deactivation of clay surfaces by water or methanol (hydrous or toluene/methanol pyrolysis) results in a pyrolysate with a higher proportion of polar material and Ni/V ratios similar to that of the kerogen. Pyrolysis under dry conditions or in toluene (pyrolysates 2 and 3) results in higher proportions of nonpolar material and pyrolysates have higher Ni/V ratios than those generated under hydrous or toluene/methanol conditions.

3. The elemental S and Se in the bitumen II result from decomposition of sulfides (FeS_2) during demineralization and are present primarily as S_8 and S_7Se which elute in the nonpolar fraction. Thus, the S and/or Se content of the nonpolar fraction of pyrolysates may be related to the amount of sulfide mineral breakdown during pyrolysis.

ACKNOWLEDGEMENTS

The help of Cathy Grimm and the Nuclear Radiation Center staff in the INAA analysis is acknowledged.

LITERATURE CITED

1. Hodgson, G.W., Bull. Am. Assoc. Petrol. Geol., 1954, 38, 2737-54.

2. Hyden, H.J., U.S. Geol. Serv. Bull. 1100-B, 1961.

3. Al-Shahristani, H. and Al-Atyia, M.J., Geochim. et Cosmochim. Acta, 1972, 36, 929-37.

4. Saban, M., Vitorovic, O. and Vitorovic, in "Symposium on Characterization of Heavy Crude Oils and Petroleum Residues", Editions Technip: Paris, 1984.

5. Ellrich, J., Hirner, A.V. and Stark, H., Chem. Geol., 1985, 48, 313-23.

6. Abu-Elgheit, M., Khalil, S.O. and Barakat, A.O., Prepr. Div. Petrol. Chem. ACS, 1979, 24, 793-97.

7. Curiale, J.A., in "Metal Complexes in Fossil Fuels", eds. Filby, R.H. and Branthaver, J.F., ACS Symposium Series No. 344, American Chemical Society: Washington, DC, 1987.

8. Hitchon, B. and Filby, R.H., Bull. Am. Assoc. Petrol. Geol., 1984, 68, 838-49.

9. Hirner, A.V., in "Metal Complexes in Fossil Fuels", eds. Filby, R.H. and Branthaver, J.F., ACS Symposium Series No. 344, American Chemical Society: Washington, DC, 1987.

10. Van Berkel, G.J. and Filby, R.H., in "Metal Complexes in Fossil Fuels", eds. Filby, R.H. and Branthaver, J.F., ACS Symposium Series No. 344, American Chemical Society: Washington, DC, 1987.

11. Hasenmueller, N.R. and Woodward, G.S., "Studies of the New Albany Shale (Devonian and Mississippian) and equivalent strata in Indiana", Indiana Geological Survey Contract Report to U.S. Department of Energy, Contract DE-AC-21-76MC05204, 1981, 100.

12. Mercer, G.E., Fitzgerald, S.L., Day, J.W. and Filby, R.H., ACS Fuel Div. Preprints, 1991, 36, 1180-89.

13. Van Berkel, G.J., Ph.D. Thesis, Department of Chemistry, Washington State University, 1987.

14. Fitzgerald, S.L., Day, J.W. and Mercer, G.E., (unpublished data).

15. Van Berkel, G.J., Quirke, J.M.E., and Filby, R.H., Org. Geochem., 1989, 14, 119-128.

Table 1. Concentrations of trace elements in the kerogen, bitumens and pyrolysates of the New Albany shale and in Boscan crude oil.

Element	Elemental Concentration (μg/g)							
	Kerogen[1]	Bitumen I	Bitumen II	Dry Pyr.	H_2O Pyr.	Toluene Pyr.	Tol/MeOH Pyr.	Boscan Crude
As	36.4	75.8	89.1	86.3	64.5	536	406	0.320
Co	115	8.63	113	14.3	10.6	13.4	61.2	0.224
Cr	35.2	1.04	12.3	1.75	0.865	1.65	1.39	0.401
Fe	0 by defn.	353	3140	556	744	992	1180	15.9
Ga	11.0	7.93	32.6	2.30	4.77	6.78	7.12	0.147
Mn	0	0.32	1.24	0.62	0.43	0.53	0.59	0.109
Mo	2400	28.7	460	17.4	6.24	54.6	29.8	4.26
Na	1240	156	816	8.57	171	53.0	53.7	25.0
Ni	2160	2560	3710	896	2760	1710	2300	97.2
Sb	72.6	0.598	56.0	12.2	0.561	1.40	1.38	0.296
Se	175	79.5	3840	18.9	215	43.8	7.86	0.320
V	1130	2700	3400	365	1540	1880	1230	1200
Zn	71.9	65.7	252	10.5	66.5	53.6	67.3	0.608
Ni/V Ratio	1.91 ±0.25	0.95 ±0.02	1.09 ±0.03	2.45 ±0.17	1.80 ±0.06	0.91 ±0.03	1.87 ±0.13	0.081 ±0.006
Yield (%)	25%	1.4%	0.37%	3.6%	1.0%	1.0%	1.5%	--

[1] Corrected for inorganic contributions by the density fraction method described by Mercer *et al.* (22).

Table 2. Concentrations of trace elements in the sequential pyrolysates and residual bitumen (bitumen-III) from the pyrolysed New Albany shale.

Element	Elemental Concentration (μg/g)						
	Pyr.[1] #1	Pyr. #2	Pyr. #3	Pyr. #4	Pyr. #5	Pyr. #6	Bitumen III
As	536	85.1	80.0	290	77.7	8.74	118
Co	13.4	7.04	4.81	3.30	0.360	0.834	7.13
Cr	1.65	2.50	0.786	1.41	0.770	0.50	6.82
Fe	992	594	389	395	151	65.5	1405
Ga	6.78	2.77	2.65	5.87	0.815	0.579	21.6
Mn	0.53	1.18	0.380	0.546	0.42	0.48	0.61
Mo	54.6	17.3	25.9	45.3	17.6	14.1	344
Na	53.0	230	50.0	70.0	45.3	86.0	18.6
Ni	1713	1189	933	777	276	458	516
Sb	1.40	0.267	0.960	0.545	0.17	0.135	15.6
Se	43.8	80.1	51.1	169	131	18.0	956
V	1883	484	393	471	126	242	384
Zn	53.6	12.2	7.03	13.0	7.31	37.0	52.1
Ni/V Ratio	0.91 ±0.03	2.46 ±0.06	2.37 ±0.10	1.65 ±0.10	2.19 ±0.11	1.89 ±0.92	1.34 ±0.07
Yield (%)	1.0	0.54	1.3	0.29	0.16	0.22	0.33

[1] Pyrolysis runs 1-5 in toluene, run 6 in toluene/MeOH
[2] Bitumen-III = extractable organic material of shale after six pyrolyses and demineralization.

Table 3. Ni/V and Non-Polar/Polar Ratios.

Sample	Ni/V	Non-Polar/Polar*
Kerogen	1.91	--
Bitumen I	0.95	1.04
Toluene Pyr. 1	0.91	0.94
Toluene Pyr. 2	2.46	1.54
Toluene Pyr. 3	2.37	1.81
Dry Pyr.	2.45	1.64
Hydrous Pyr.	1.80	0.65
Toluene/MeOH Pyr	1.87	0.68

*Computed from fractional yields of fractions (1+2)/(3+4).

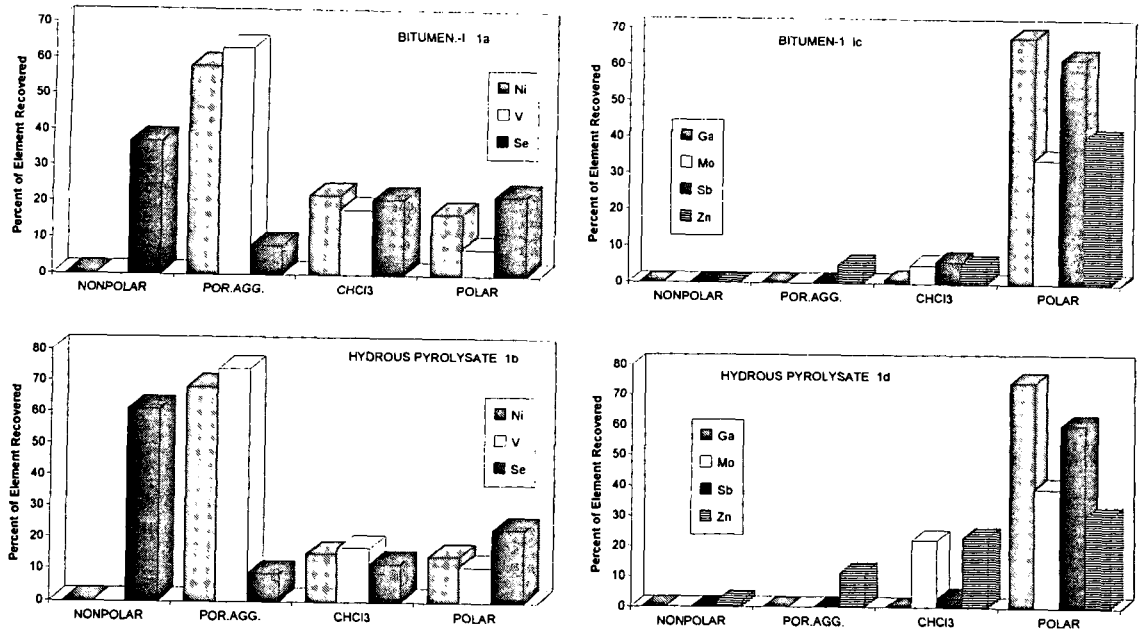

Figure 1: Comparison of elemental distributions in the bitumen I (a,c) and *the hydrous pyrolysate (b,d)*

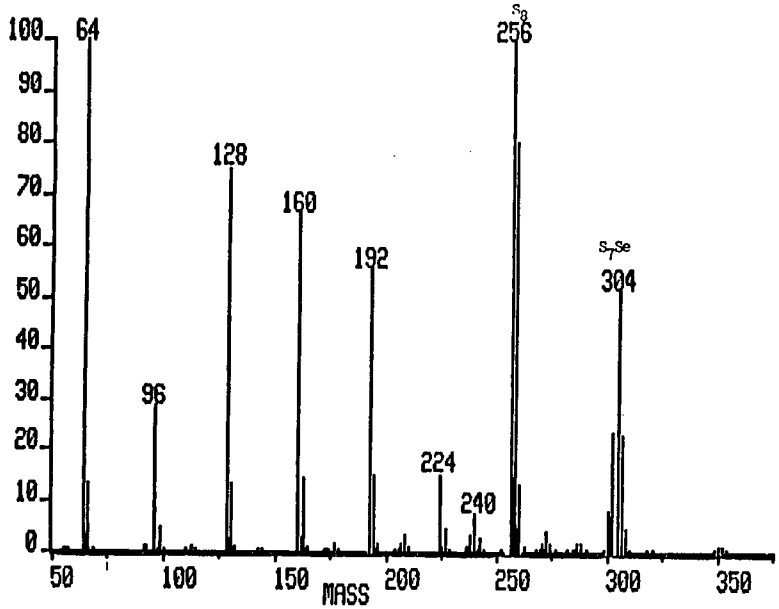

Figure 2: EI/MS spectrum of the non-polar fraction of the bitumen II of the Albany Shale

AN INVESTIGATION OF HYDROGEN TRANSFER IN COPROCESSING USING MODELS AND REDUCED RESIDS

Shu-Li Wang and Christine W. Curtis
Chemical Engineering Department
Auburn University, AL 36849-5127

Abstract

Hydrogen donor reactions in the coprocessing of coal and petroleum resids have been investigated using different hydrogen-rich models and reduced resids as donors and aromatics as acceptors. Three hydrogen-rich donor species were compared: cyclic olefins, hydroaromatics, and cycloalkanes; the aromatic acceptors included pyrene and anthracene; and the resids were reduced by the Birch method. Hydrogen was transferred most readily at 380°C by cyclic olefins, followed by hydroaromatics, and the least was transferred by cycloalkanes. Catalysis by thiophenol promoted the hydrogen transfer by the cycloalkanes at 380°C but had little effect at 440°C. Reduced resids transferred substantially more hydrogen to an aromatic species than did the untreated resids. In a tertiary system of reduced resid, cycloalkane, and aromatic, the reduced resids yielded more hydrogen transfer and promoted hydrogen donation from the cycloalkanes in a nitrogen atmosphere. Reduction of resids by the Birch method appeared to be an effective means of increasing the hydrogen donor ability of resids.

Introduction

Hydrogen donor reactions are important in the transfer of hydrogen from hydrogen-rich compounds to aromatic species in the liquefaction of coal. Different hydrogen-rich compounds have different propensities for donating hydrogen under liquefaction conditions; just as different hydrogen acceptors have different propensities for accepting hydrogen. In this study, the ability of three different hydrogen donors to donate hydrogen and the efficiency of their hydrogen transfer to aromatic species were compared under both hydrogen and nitrogen atmospheres.

The compounds compared were cyclic olefins, which have been shown to release their hydrogen quickly under liquefaction conditions, hydroaromatics, that are typically present in coal liquids and are known hydrogen donors, and cycloalkanes, that are present in resids and do not readily donate their hydrogen. Promotion of hydrogen transfer from the hydrogen-rich cycloalkanes to aromatics is of special interest because these structures are prevalent in resids and offer an indigenous source of hydrogen. Rudnick [1986a,b] has shown that the introduction of an organic sulfur compound promotes this type of hydrogen transfer. In this work, catalytic reactions with organic sulfur were performed to evaluate the effect on the hydrogen transfer from cycloalkanes to aromatics at 380°C and 440°C under both nitrogen and hydrogen atmospheres. These results were compared to thermal reactions at the same conditions.

In the coprocessing of coal with resid, resids have limited ability to solvate coal and to donate hydrogen because of the predominance of indigenous saturated structures. Increasing the hydrogen donability of the chemical species of the resid should enhance the ability of the resid to solvate coal. This enhancement was induced by reducing resids by the Birch reduction method [Birch and Rao, 1972] which is known for producing cyclic olefinic structures from

aromatic species. The ability of these reduced resids to transfer hydrogen to aromatics was determined and compared to the parent resids.

Experimental

Materials and Analysis. Reactions were performed using the following hydrogen-rich compounds: cyclic olefins, isotetralin (ISO) which was synthesized in our laboratory, and hexahydroanthracene (HHA) from Aldrich; hydroaromatics, tetralin (TET) and 9,10-dihydroanthracene (DHA) both from Aldrich; and a cycloalkane, perhydropyrene (PHP) from Aldrich. The compounds used as hydrogen acceptors in these reactions were anthracene (ANT) and pyrene (PYR) both obtained from Aldrich. Thiophenol was used as a catalyst for promoting the transfer of hydrogen from cycloalkanes to aromatics. The catalyst was introduced at a level of 2,000 ppm of sulfur. The reaction products were analyzed by gas chromatography using a Varian 3300 gas chromatograph with FID detection and biphenyl as the internal standard. Qualitative analysis of the products was conducted with a VG70 EHF GC-mass spectrometer.

Thermal and catalytic reactions were performed with the parent resids and treated resids which had been reduced by the Birch method [Birch and Rao, 1972]. The Birch reduction method reduces aromatics in the resid to cyclic olefins and other partially saturated forms by adding Na, alcohol, and ammonia to the resid which is dissolved in tetrahydrofuran (THF) as the solvent. The resids that were used in these reactions were Maya obtained from Amoco Oil Co., a deasphalted resid from a deasphalting resid unit (DAU) from Exxon and south Louisiana resid (S. LA) also from Exxon; the hydrogen acceptor for the reactions was ANT; and the catalyst was 2000 ppm sulfur introduced at thiophenol. The products from these resid reactions were analyzed by gas chromatography to determine the reaction products from both the model donors and acceptors and by solvent fractionation to determine the products from the resid. The solvents used in the extraction of the thermal products were toluene (TOL) and THF, but in the catalytic reactions, hexane (HEX) was also used.

Reaction Procedures. Reactions were performed in 20 cm^3 stainless steel tubular microreactors with single reactants charged at 0.1 g and with binary reactants charged at 0.1 g aromatic and the hydrogen-rich compound introduced at a 1:1 or 5:1 weight ratio to the aromatic. The reaction conditions for the thermal model reactions were 380°C, 30 minutes, nitrogen or hydrogen at 400 psi at ambient, and horizontal agitation at 435 cpm.

Definitions. The following definitions were used: Percent hydrogenation (% HYD) is defined as the moles of hydrogen required to achieve the liquid products as a percentage of the moles of hydrogen required to produce the most hydrogenated product. In the case of ANT, octahydroanthracene (OHA) was considered the most hydrogenated product; in the case of pyrene, the most hydrogenated product was taken to be hexahydropyrene (HHP). Hydrogen efficiency is defined as the moles of hydrogen accepted by the hydrogen acceptor divided by the moles of hydrogen released by the hydrogen donor. The amount of gaseous hydrogen that was accepted by the hydrogen donor is defined as the moles of hydrogen accepted by the hydrogen acceptor under a hydrogen atmosphere minus the moles of hydrogen accepted by the hydrogen accepted under a nitrogen atmosphere.

Results and Discusssion

Thermal Reactions of Hydrogen-Rich Compounds with Aromatics. Reactions of hydrogen-rich compounds, cyclic olefins, hydroaromatics and cycloalkanes, with aromatic species, ANT and PYR, were performed in N_2 and H_2 atmospheres. The purpose of these

experiments was to determine how much hydrogen was released from the hydrogen donor and how much of that hydrogen was accepted by the aromatic species. The reaction of the cyclic olefins with the aromatics resulted in the products of tetralin (TET), 1,2- and 1,4-dihydronaphthalene (DHN), and naphthalene (NAP) from ISO and of OHA, tetrahydroanthracene (THA), DHA and ANT from HHA. The hydroaromatics produced NAP from TET and THA plus ANT from DHA. The cycloalkane PHP only produced PYR as its product. The amount of hydrogen released from the hydrogen-rich compounds was in the order of cyclic olefins > hydroaromatics > cycloalkanes. The amount of hydrogen released from each species was dependent upon the type of atmosphere and acceptor present as well as upon the amount of hydrogen-rich compound present. These results are shown in Table 1.

ANT, as an acceptor, formed DHA and THA as products while PYR formed dihydropyrene (DHP), tetrahydropyrene (THP) and hexahydropyrene (HHP) as products. The % HYD of the aromatic species in individual reactions and in binary reactions with hydrogen-rich species is presented in Table 1. The most hydrogenation of the aromatic species occurred in the presence of the cyclic olefins and in a H_2 atmosphere. ANT was more reactive than PYR when reacted with the same hydrogen donor and at the same conditions.

The hydrogen efficiency of the systems was also compared in Table 1. As the value for hydrogen efficiency approached one, then the amount of hydrogen released was equal to the amount of hydrogen accepted. The hydrogen efficiency of the systems in the N_2 atmosphere showed that the cyclic olefins were the least efficient since they released substantially more hydrogen than the aromatic species was able to accept. In the H_2 atmosphere, hydrogen efficiencies of greater than one were obtained which indicated that gaseous hydrogen was participating in the reactions. The moles of gaseous H_2 incorporated into the reaction products from the hydrogen acceptor varied with the system as shown in Table 1.

Catalytic Reactions of Hydrogen-Rich Compounds with Aromatics. Catalytic reactions were performed with a reaction system of PHP with ANT at a weight ratio of PHP to ANT of 1:1 and 5:1 in both N_2 and H_2 atmospheres at reaction temperatures of 380 and 440°C. The catalyst was 2000 ppm of sulfur introduced as thiophenol. The products produced from PHP were HHP and PYR at both reaction temperatures; the products produced from ANT were DHA at 380°C and DHA, THA, and OHA at 440°C. The amount of hydrogen donated and accepted from these reactions was compared to that in the thermal reactions at the same conditions (Table 2).

The addition of the sulfur catalyst increased the amount of hydrogen donation from PHP. The catalyst also increased the amount of hydrogen acceptance and, hence, hydrogenation of ANT to DHA in both atmospheres. Under thermal conditions, PHP produced only PYR as the product while under catalytic conditions HHP was formed in larger amounts than PYR. The catalysis of hydrogen donation and acceptance by S was observed most in the PHP/ANT system at a 5:1 weight ratio at 380°C in H_2 and N_2 compared to the thermal reaction where a substantial increase in the hydrogenation of the aromatic was obtained compared to the thermal reaction. The promotion of the reaction by S was also observed in N_2 but not in H_2 at 440°C. The higher temperature of 440°C with H_2 as the atmosphere seemed to have more effect on hydrogen donation and acceptance than did the catalyst, because the % HYD's of ANT were equivalent in thermal and catalytic reactions.

The hydrogen efficiency in N_2 shown in Table 2 was always less than one with the hydrogen efficiency of 5:1 PHP to ANT reaction systems frequently having a higher efficiency than the 1:1 ratio. The hydrogen efficiencies for the reactions in the hydrogen atmosphere were always greater than one indicating incorporation of gaseous hydrogen into the reaction

products. The number of moles of gaseous hydrogen incorporated was substantially higher for the higher temperature reactions at 440°C than those at 380°C.

Hydrogen Transfer from Resids. The purpose of this work was to evaluate the efficacy of hydrogen transfer from hydrogen-enriched reduced resids to an aromatic species and to compare that to the hydrogen transfer from the parent resid. The systems used were the reduced and parent resids with the acceptor ANT and the ternary system of a reduced or parent resid with ANT and the hydrogen-rich species, PHP.

The reactions of the reduced and parent resids with ANT in both N_2 and H_2 atmospheres are presented in Table 3. All three of the reduced resids yielded substantially more hydrogenation of ANT to DHA and THA than did the parent resids. The hydrogen atmosphere promoted more hydrogenation of ANT than did nitrogen regardless of whether the resid was reduced or was the parent. The product distributions from each of the resid reactions are given in Table 4. The binary system of resid with ANT produced some THF soluble material and insoluble organic material (IOM) in each reaction regardless of resid or atmosphere. The reduced resids showed a higher propensity for having THF soluble materials in the presence of ANT than did the parent resids.

When PHP was added to the resid/ANT system, the change observed was fairly small in terms of the hydrogenation of ANT. However, more hydrogen uptake appeared to be achieved from hydrogen transferred from hydrogen-rich species than from gaseous hydrogen. The %HYD of ANT in N_2 was higher in the systems with PHP present than in those without PHP. Small increases in %HYD were also observed in the hydrogen atmosphere. The product distributions for the ternary systems (Table 4) showed that all of the resids remained toluene soluble. The amount of hexane solubles produced was greater in the hydrogen atmosphere than in the nitrogen for all but one of the systems.

Summary

Hydrogen donation from three types of hydrogen-rich species resulted in substantial hydrogen donation from cyclic olefins, less from hydroaromatic species, and a very small amount from cycloalkanes by comparison. The hydrogen transfer by cycloalkanes to aromatics was promoted by the presence of sulfur. This promotion, however, appeared to be condition specific with more catalysis apparent at 380°C in N_2 than at any other condition. Reduced resids produced by the Birch method were more effective hydrogen donors than their parent resids. Hydrogen enrichment of these resids produced a solvent more effective for the thermal hydrogenation of aromatic species such as are present in coal.

References

Rudnick, L.R., European Patent 195, 541, 1986a; European Patent 195, 539, 1986b.
Birch, A.J., G.S. Rao, Advances in Organic Chemistry, Methods and Results, Vol. 8, E.C. Taylor, ed., Wiley Interscience, NY, NY, 1972.

Table 1. Thermal Reaction Systems

Reaction Conditions	Mole of Hydrogen Released x 10^4		Percent Hydrogenation (%)		Hydrogen Efficiency		Moles of H_2 From Gaseous H_2 Moles X 10^4
	H_2	N_2	H_2	N_2	H_2	N_2	H_2
ISO	10.73(0.17)	11.39(0.06)					
ISO/ANT (1:1)	11.08(0.03)	17.00(0.06)	19.24(0.27)	18.32(0.14)	0.39(0.01)	0.24(0.00)	0.21(0.09)
ISO/ANT (5:1)	44.69(0.61)	45.42(0.13)	24.88(0.07)	24.39(0.18)	0.12(0.00)	0.12(0.00)	0.12(0.05)
TET	0.05(0.03)	0.03(0.00)					
TET/ANT (1:1)	0.05(0.02)	0.00(0.00)	4.53(0.26)	0.25(0.05)	19.77(2.89)	---*	0.96(0.06)
TET/ANT (5:1)	0.11(0.03)	0.39(0.03)	4.45(0.25)	0.93(0.07)	8.84(1.68)	0.54(0.14)	0.40(0.08)
PHP	0.00(0.00)	0.00(0.00)					
PHP/ANT (1:1)	0.27(0.02)	0.28(0.05)	3.08(0.28)	0.46(0.17)	2.57(0.22)	0.35(0.09)	0.59(0.08)
PHP/ANT (5:1)	0.18(0.01)	0.25(0.02)	3.97(0.42)	0.63(0.02)	4.91(0.84)	0.57(0.07)	0.74(0.09)
ISO/PYR (1:1)	10.99(0.13)	11.80(0.19)	6.02(0.25)	4.11(0.30)	0.08(0.00)	0.05(0.00)	0.28(0.07)
ISO/PYR (5:1)	49.46(0.79)	47.65(0.32)	17.30(0.27)	13.20(0.75)	0.05(0.00)	0.04(0.00)	0.61(0.15)
TET/PYR (1:1)	0.00(0.00)	0.00(0.00)	0.00(0.00)	0.00(0.00)	---	---	0.00(0.00)
TET/PYR (5:1)	0.07(0.00)	0.28(0.19)	0.41(0.09)	0.16(0.01)	0.79(0.18)	0.17(0.12)	0.02(0.01)
HHA	9.95(0.31)	9.95(0.09)					
HHA/PYR (1:1)	9.93(0.01)	9.52(0.31)	13.59(0.23)	8.14(0.84)	0.20(0.00)	0.13(0.02)	0.81(0.15)
HHA/PYR (5:1)	35.84(0.48)	43.67(0.82)	30.35(0.97)	10.40(2.48)	0.13(0.01)	0.04(0.01)	2.95(0.50)
DHA	0.35(0.06)	0.28(0.00)					
DHA/PYR (1:1)	0.43(0.01)	0.52(0.05)	2.46(0.18)	1.63(0.85)	0.87(0.06)	0.44(0.20)	0.15(0.13)
DHA/PYR (5:1)	1.96(0.03)	1.78(0.19)	11.27(0.35)	8.58(2.17)	0.85(0.04)	0.72(0.17)	0.40(0.37)

* --- means no hydrogen was released in that condition.

ISO = isotetralin PYR = pyrene TET = tetralin DHA = dihydroanthracene
PHP = perhydropyrene ANT = anthracene HHA = hexahydroanthracene

Nb49/hyd-tran.pap

Table 2. Catalytic Reaction Systems

Reaction Conditions	Mole of Hydrogen Released x 10^4		Percent Hydrogenation (%)		Hydrogen Efficiency		Moles of H_2 From Gaseous H_2 Moles X 10^4
	H_2	N_2	H_2	N_2	H_2	N_2	H_2
380°C Thermal							
PHP/ANT (1:1)	0.27(0.02)	0.28(0.05)	3.08(0.28)	0.46(0.17)	2.57(0.22)	0.35(0.09)	0.59(0.08)
PHP/ANT (5:1)	0.18(0.01)	0.25(0.02)	3.97(0.42)	0.63(0.02)	4.91(0.84)	0.57(0.07)	0.74(0.09)
380°C Catalytic							
PHP/ANT (1:1)	0.75(0.01)	0.71(0.16)	4.83(0.53)	0.96(0.14)	1.44(0.18)	0.31(0.91)	0.88(0.14)
PHP/ANT (5:1)	1.05(0.14)	1.44(0.22)	11.11(0.60)	4.40(0.09)	2.38(0.28)	0.70(0.12)	1.49(0.13)
440°C Thermal							
PHP/ANT (1:1)	0.24(0.13)	0.55(0.09)	15.44(0.64)	0.30(0.04)	14.13(0.27)	0.13(0.04)	3.40(0.14)
PHP/ANT (5:1)	0.61(0.13)	0.77(0.15)	15.47(0.16)	2.60(0.19)	5.88(1.27)	0.78(0.15)	2.88(0.07)
440°C Catalytic							
PHP/ANT (1:1)	0.61(0.03)	0.55(0.27)	14.93(0.19)	1.48(0.13)	5.48(0.30)	0.77(0.49)	3.01(0.09)
PHP/ANT (5:1)	0.67(0.08)	1.18(0.22)	14.51(0.33)	3.25(0.22)	4.91(0.55)	0.64(0.17)	2.55(0.14)

PHP = perhydropyrene ANT = anthracene

Nb49/hyd-tran.pap

Table 3. Resid Reaction Systems

Reaction Conditions	Moles of Hydrogen Accepted x 10^4		Percent Hydrogenation (%)		Moles of H_2 From Gaseous H_2 Moles X 10^4
	H_2	N_2	H_2	N_2	H_2
Maya/ANT	3.15(0.19)	1.62(0.07)	7.03(0.42)	3.61(0.16)	1.52(0.26)
Maya/ANT (Reduced)	8.02(0.31)	4.26(0.06)	17.90(0.60)	9.50(0.15)	3.76(0.37)
DAU/ANT	4.69(0.15)	1.61(0.11)	10.03(0.51)	3.59(0.23)	3.07(0.26)
DAU/ANT (Reduced)	8.31(0.14)	5.08(0.15)	17.94(0.44)	11.34(0.34)	3.22(0.29)
S.LA/ANT	3.26(0.05)	0.97(0.10)	7.28(0.11)	2.15(0.24)	2.29(0.15)
S.LA/ANT (Reduced)	5.26(0.07)	3.25(0.17)	11.73(0.17)	7.24(0.38)	2.01(0.24)
Maya/PHP/ANT	4.98(0.18)	3.09(0.36)	11.10(0.42)	6.90(0.81)	1.88(0.54)
Maya/PHP/ANT (Reduced)	7.88(0.07)	5.84(0.21)	17.60(0.15)	13.03(0.47)	2.04(0.28)
DAU/PHP/ANT	4.72(0.23)	3.59(0.09)	10.54(0.52)	8.02(0.21)	1.12(0.32)
DAU/PHP/ANT (Reduced)	8.08(0.09)	5.85(0.04)	18.02(0.22)	13.06(0.08)	2.22(0.13)
S.LA/PHP/ANT	3.02(0.17)	1.95(0.14)	6.73(0.38)	4.36(0.31)	1.06(0.31)
S.LA/PHP/ANT (Reduced)	6.15(0.14)	5.06(0.13)	13.73(0.32)	11.29(0.29)	1.09(0.27)

DAU = deasphalted resid
S.LA = South Lousiana resid
PHP = perhydropyrene
ANT = anthracene

Nb49/hyd-tran.pap

COAL/OIL COPROCESSING USING SYNGAS :REACTIVITY OF CYCLOALKANES AS THE SOLVENT.

Yuan C. Fu, Kotaro Tanabe, Makoto Akiyoshi
Department of Applied Chemistry,
Muroran Institute of Technology,
Muroran, Japan 050.

Keywords: Coprocessing, Coal, Model Compounds, Syngas

ABSTRACT

Coprocessing of coal or model compounds with petroleum solvents was conducted in the presence of catalysts using syngas(H_2+CO) with steam in place of hydrogen. NiMo/Al_2O_3 impregnated with potassium carbonate and NiMo/MgO catalysts exhibited good activities for hydrogenation and desulfurization. High coal conversion was obtained at a mild temperature of 400℃ for the coprocessing of coal with petroleum solvents using syngas and steam. With the solvents containing n-paraffin and cycloalkane, it was observed that decalin underwent dehydrogenation and isomerization, and that the extent of hydrodesulfurization increased with the increase of trans/cis ratio of the remaining decalin after the reaction. The presence of aromatic compounds with decalin in the solvent mixtures increased the coal conversion, suggesting that aromatic compounds could be acting as hydrogen shuttlers to transfer hydrogen from decalin to coal.

INTRODUCTION

We have reported previously[1] that coal and model compounds could be hydrogenated and desulfurized in the presence of petroleum solvents and catalyst under coprocessing conditions by using syngas with steam in place of hydrogen. Nickel molybdate on alumina support impregnated with potassium carbonate exhibited good activity with syngas and steam, presumably owing to the simultaneous water-gas shift reaction took place to form active hydrogen. We have continued our quest for catalysts that may also be active in promoting water-gas shift reaction as well as hydrotreating coal in the syngas system. It would be more economical[2] if syngas could be used in place of expensive hydrogen in coal liquefaction or coprocessing even at the initial stage of two-stage processes.

Another aspect of this investigation is to determine the hydrogen donating ability of cycloalkanes as the solvent in coal/oil coprocessing. It appears that decalin is dehydrogenated and that hydrogen transfer to coal or model compounds takes place under coprocessing conditions. The hydrogen donating ability of decalin is enhanced in the presence of aromatic compounds.

EXPERIMENTAL

The coprocessing reactions of coal and model compounds were conducted in a shaking 25-ml microreactor with syngas (H_2:CO=1:1) or H_2 at an initial pressure of 70 kg/cm^2. The reactor was quickly heated up in a fluidizing sand bath and maintained at 400℃ for 45 minutes, and then rapidly quenched in a cold water bath. The catalysts used include a commercial NiMo/Al_2O_3 catalyst (Nippon Mining Co.) containing 12.0% MoO_3 and 2.8% NiO, a MgO supported NiMo catalyst containing 12.0% MoO_3 and 4.0% NiO. For syngas runs, the NiMo /Al_2O_3 catalyst was impregnated with 10% K_2CO_3.

Anthracene and benzothiophene were used as the model compounds, and mixtures of n-paraffin, cycloalkane, and aromatic compound were used as petroleum solvents. The ratio of solvent to model compounds was 5:1. For experiments using syngas, 10 weight % of H_2O based on the total amounts of the model compounds and solvent (roughly equivalent to H_2:CO :H_2O=1:1:0.5 in the gas phase) was added. In all runs the amount of ground catalyst powders charged was also 10 weight %.

Table 4. Product Distribution from the Resid in Binary and Ternary Systems

Reaction System	Product Distribution, wt%							
	H_2				N_2			
	HEX Solubles (%)	TOL Solubles (%)	THF Solubles (%)	IOM (%)	HEX Solubles (%)	TOL Solubles (%)	THF Solubles (%)	IOM (%)
Maya/ANT		98.8(0.2)	1.3(0.2)	0.0(0.0)		97.9(1.2)	1.8(1.2)	0.3(0.1)
Maya/ANT (Reduced)		98.2(0.2)	1.4(0.1)	0.4(0.0)		95.5(0.4)	3.6(1.1)	0.4(0.6)
DAU/ANT		96.9(0.3)	2.9(0.2)	0.2(0.1)		99.1(0.4)	0.9(0.4)	0.1(0.0)
DAU/ANT (Reduced)		96.3(0.6)	3.5(0.6)	0.2(0.1)		96.9(2.0)	2.9(2.0)	0.2(0.1)
S.LA/ANT		98.7(0.3)	1.1(0.1)	0.2(0.1)		98.2(1.1)	1.7(1.0)	0.1(0.1)
S.LA/ANT (Reduced)		98.4(0.7)	1.5(0.6)	0.2(0.1)		98.6(0.5)	1.4(0.5)	0.0(0.0)
Maya/ANT/PHP	76.8(1.2)	23.2(1.2)	0.0(0.0)	0.0(0.0)	73.7(0.9)	26.3(0.9)	0.0(0.0)	0.0(0.0)
Maya/ANT/PHP (Reduced)	78.1(2.1)	21.9(2.1)	0.0(0.0)	0.0(0.0)	81.9(0.0)	18.1(0.0)	0.0(0.0)	0.0(0.0)
DAU/ANT/PHP	81.1(1.4)	18.9(1.4)	0.0(0.0)	0.0(0.0)	76.5(0.6)	23.4(0.6)	0.0(0.0)	0.0(0.0)
DAU/ANT/PHP (Reduced)	88.4(6.1)	11.6(6.1)	0.0(0.0)	0.0(0.0)	83.0(0.3)	17.0(0.3)	0.0(0.0)	0.0(0.0)
S.LA/ANT/PHP	100.0(0.0)	0.0(0.0)	0.0(0.0)	0.0(0.0)	100.0(0.0)	0.0(0.0)	0.0(0.0)	0.0(0.0)
S.LA/ANT/PHP (Reduced)	100.0(0.0)	0.0(0.0)	0.0(0.0)	0.0(0.0)	100.0(0.0)	0.0(0.0)	0.0(0.0)	0.0(0.0)

DAU = deasphalted resid
S.LA = south Lousiana resid
PHP = perhydropyrene
ANT = anthracene

Nb49/hyd-trm.pep

For coal runs, Illinois No.6 bituminous coal with an ultimate analysis of C 78.3, H 5.4, N 1.32, O 11.12, S 3.86 (maf basis), ash 10.9% and Wandan coal with C 67.5, H 5.3, N 0.9, O 15.3, ash 10.9 (mf basis) were used. The ratio of solvent to coal was 2.3:1. The coal conversion was determined from tetrahydrofuran insolubles, and the solubles were analyzed by a gas chromatograph using OV-1701 fused silica capillary column.

RESULTS AND DISCUSSION

Coprocessing Using Syngas. In general, the hydrogenation and hydrodesulfurization activities are somewhat lower with the use of syngas than with hydrogen. It is probably due to the lower partial pressure of H_2 and the existence of other components such as H_2O, CO, and CO_2 in the gas phase. Table 1 shows that the hydrogenation and hydrodesulfurization activities with $NiMo/Al_2O_3$ catalyst are somewhat reduced when the initial H_2 pressure is reduced from 70 kg/cm^2 to 35 kg/cm^2. Using syngas (without adding H_2O), we observe some decrease of hydrodesulfurization activities even at the same H_2 partial pressure of 35 kg/cm^2. With syngas, it is postulated that CO may compete with H_2 for active sites and be adsorbed on the catalyst surface. When H_2O is added, the H_2O vapor adsorbed on the surface may poison the catalyst. Therefore, it is presumably important that, for coprocessing using syngas, a suitable catalyst is used and an adequate amount of H_2O is added to promote the formation of active hydrogen via water-gas shift reaction. As was observed previously[1], the extent of the isomerization of decalin increased with the extent of hydrogenation and hydrodesulfurization. Clarke et al[3] also reported the occurence of isomerization to trans-decalin during extraction of coal using decalin as solvent.

Hydrogen Donation by Decalin. In order to find out the circumstances at which the isomerization of decalin occurs, trans-decalin and cis-decalin alone were solely hydrotreated under H_2 pressure at 400℃ in the presence of $NiMo/Al_2O_3$ catalyst. The results in Table 2 show that 30.4% of cis-decalin and 7.7% of trans-decalin are isomerized, respectively. When the decalin containing both isomers at the trans/cis ratio of 1.6 was hydrotreated under the similar condition, the trans/cis ratio increased to 2.4. It is evident that decalin tends to isomerize from cis-from to trans-form under the hydroteating condition. However, in the presence of reactants (anthracene and benzothiophene), the extent of isomerization of cis-decalin solvent increased to 47.8%. On the other hand, only 7.8% of trans-decalin isomerized, indicating the difficulty for trans-decalin to isomerize to cis-form. It appears that both cis- and trans-decalin undergo dehydrogenation (to form tetralin) and hydrogen tranfer equally, but the tetralin formed probably forms trans-decalin preferentially as it is rehydrogenated. In fact, an experiment hydrotreating tetralin yielded trans-decalin preferentially (Table 2). With decalin containing both isomers as the solvent, in the presence of reactants, the trans /cis ratio after the reaction was also higher, 4.6 compared to 2.4 (see Tables 1 and 2). Coprocessing experiments using syngas with cis- and trans-decalin solvents also showed that the isomerization to trans-form was favored, but the extent of isomerization was lower.

NiMo/MgO Catalyst. In the quest for catalysts that may be active in the H_2-CO-H_2O system, a NiMo/MgO catalyst was prepared and tested. The results in Table 3 show that NiMo/MgO catalyst exhibits comparable activities with $NiMo/Al_2O_3$ catalyst for coprocessing of model compounds. In the syngas system, the alkaline MgO was able to promote CO conversion and no impregnation with K_2CO_3 was necessary. Of various catalysts tested, including synthetic pyrite, $ZnCl_2/SiO_2$-Al_2O_3, Fe_2O_3/SO_4^{2-}, cobalt molybdate, and nickel molybdate, NiMo catalysts with various characteristics of supports may be the most interesting area to explore.

Coprocessing of Coal with Petroleum Solvents. Table 4 shows the experimental results of coprocessing Illinois No.6 coal and Wandoan coal with petroleum solvents. At the mild temperature of 400℃, $NiMo/Al_2O_3$ catalyst impregnated with K_2CO_3 exhibited good activities with syngas, and high coal conversions obtained were comparable to those obtained with hydrogen. At temperatures greater than 425℃, because of lower H_2 partial

pressures with syngas, the fragments from thermally decomposed coal tend to polymerize to form char. The experimental runs using NiMo/MgO catalysts show that coal conversions were somewhat lower with either H_2 or syngas.

It was also observed that hydrogen donating properties of paraffin-cycloalkane solvent mixtures were enhanced by the presence of cyclic compounds containing benzene rings such as tetralin and 1-methylnaphthalene. Even though 1-methylnaphthalene is not a hydrogen donor, its addition to the dodecane-decalin mixture increased the coal conversion, equivalent to that obtained with the addition of tetralin (see Table 4). This suggests that aromatic compounds, in paraffin-cycloalkane solvents, may act as hydrogen shuttlers to transfer hydrogen from cycloalkane to coal.

ACKNOWLEDGEMENTS

We thank the support of Grant-in-Aid of Scientific Research provided by the Ministry of Education, Japan. We also thank Nippon Mining Co. for providing catalyst samples.

References

1. Fu, Y.C., Akiyoshi, M., Tanaka, F., Fujiya, K., Preprints. Div. Fuel chem., Am.chem.soc. Vol 36, No.4, 1887(1991)
2. Batchelder, R.F., Fu, Y.C., Ind.Eng.Chem. Process Des. Dev. Vol.18, No.4, 599(1979)
3. Clarke, J.W., Rantell, T.D., Snape, C.E., Fuel, Vol.63, 1476(1984)

Table 1 Coprocessing of Model Compounds with Petroleum Solvents
(Catalyst:NiMo/Al_2O_3, Reaction temp.:400℃, Time:45min)

Gas	H_2	H_2	Syngas	Syngas+H_2O[a]
Initial pressure kg/cm^2	70	35	70	70
Solvent[b]	DO/DL	DO/DL	DO/DL	DO/DL[c]
Anthracene conv.,%	89.4	65.3	63.1	90.6
Benzothiophene conv.,%	100	80.0	71.6	52.6
Decalin remained,%	76.2	66.5	88.5	75.3
cis	13.7	15.5	62.5	47.0
trans	62.5	51.0	26.0	28.3
trans/cis ratio	4.6	3.3	2.4	0.6
CO conv.,%	-	-	13.1	35.2

DO:Dodecane, DL:Decalin

a) NiMo/Al_2O_3 impregnated with K_2CO_3

b) Equal wt% of each component

c) 100% cis-Decalin

Table 2 Coprocessing Using Decalin Isomers as Solvents
(Initial Pressure:70 kg/cm^2, Temperature:400℃, Time:45min)

Gas	H_2						Syngas+H_2O	
Catalyst	NiMo/Al_2O_3						NiMo-K_2CO_3/Al_2O_3	
Solvent	c-DL	DO/c-DL	t-DL	DO/t-DL	DO/DL	T	DO/c-DL	DO/t-DL
Model compound	-	A,B	-	A,B	-	-	A,B	A,B
A conv.,%	-	98.5	-	98.9	-	-	90.6	83.0
B conv.,%	-	94.9	-	94.3	-	-	52.6	46.5
EB formed,%	-	69.3	-	62.8	-	-	19.1	23.5
Decalin remained,%	96.1[a]	94.7	98.9[a]	82.3	92.4	11.0[b]	75.3	87.0
cis	65.7	46.9	7.7	7.8	27.4	2.8	47.0	6.4
trans	30.4	47.8	91.2	74.5	65.0	8.2	28.3	80.5
trans/cis ratio	0.46	1.0	11.8	9.6	2.4	2.9	0.6	12.5
CO conv.,%	-	-	-	-	-	-	35.2	28.7

c-DL:cis-Decalin, t-DL:trans-Decalin, DO:Dodecane, T:Tetralin

A:Anthracene, B:Benzothiophene, EB:Ethylbenzene

a) The remainder converted to tetralin.

b) Decalin formed, Tetralin remained is 84.2%, and the remainder converted to naphthalene.

Table 3 Coprocessing of Model Compounds on NiMo Catalysts
(Solvent:n-Decane/Decalin/Tetralin, Initial Pressure:70 kg/cm^2, Temp.:400℃, Time:45min)

	H_2		Syngas+H_2O	
Catalyst	NiMo/Al_2O_3	NiMo/MgO	NiMo/Al_2O_3[a]	NiMo/MgO
Anthracene conv.,%	100	100	96.1	99.2
Benzothiophene conv.,%	100	100	93.9	100
Ethylbenzene formed,%	80.5	78.8	83.7	88.3
H_2 consumption,%[b]	7.0	5.1	0.3	-0.5
CO conv.,%	-	-	37.2	40.6
Decalin remaind,%	116.4	85.5	92.5	96.3
cis	27.2	24.5	26.7	27.3
trans	89.2	61.0	65.8	69.0
trans/cis ratio	3.3	2.5	2.5	2.5
Tetralin conv.,%	34.4	24.4	12.2	19.0
Naphthalene formed,%[c]	6.8	3.8	4.1	9.3

a) Impregnated with K_2CO_3
b) Wt.% of coal models
c) Based on the initial amount of tetralin

Table 4 Coprocessing of Coals with Petroleum Solvents at 400℃

Gas	H_2				Syngas (H_2:CO=1:1)			
Catalyst	NiMo/Al_2O_3			NiMo/MgO	NiMo/Al_2O_3[a]			NiMo/MgO
Solvent	DO/DL/T	DO/DL/MN	D/DL/T	D/DL/T	DO/DL/T	DO/DL/MN	D/DL/T	D/DL/T
Coal conversion,%	89.0[b]	86.5[b]	89.9[c]	76.7[c]	87.9[b]	85.5[b]	87.3[c]	74.8[c]
H_2 consumption,wt% of maf coal	3.9	4.5	5.5	2.3	0.9	0.9	-1.3	-0.2
CO conv.,%	-	-	-	-	7.3	12.0	46.0	28.5
Decalin remained,%	98.1	89.9	88.4	96.6	95.8	94.3	85.3	97.9
cis	33.7	29.8	33.7	36.5	33.3	34.5	31.9	36.9
trans	64.4	60.1	54.7	60.1	62.5	59.8	53.4	61.0
trans/cis ratio	1.9	2.0	1.6	1.6	1.9	1.7	1.7	1.7
Tetralin conv.,%	2.3	10.3[d]	3.5	0.3	11.1	7.7[d]	17.1	1.0

D:n-Decane, DO:Dodecane, DL:Decalin, T:Tetralin, MN:1-Methylnaphthalene
a) Impregnated with K_2CO_3 solution
b) Illinois No.6 coal
c) Wandoan coal
d) Conversion of 1-Methylnaphthalene

Nanoscale Fe-based Catalysts from Laser Pyrolysis

P. C. Eklund, Xiang-Xin Bi, and F. J. Derbyshire
Center for Applied Energy Research
University of Kentucky
Lexington, KY 40511-8433

Keywords: Ultrafine particle, catalyst, coal liquefaction, laser pyrolysis

Introduction

Iron-based catalysts have been extensively investigated for their catalytic behavior in direct coal liquefaction[1]. Although they are generally less active than other catalysts containing transition metals such as molybdenum, vanadium, etc, they are favored for economical reasons. The catalytic activity of these iron-based catalysts depends mainly on their chemical composition and effective contact area with the coal-solvent slurry. The contact area relates closely to the particle diameter, surface morphology, and particle agglomeration. Research to produce nanoscale (~10 nm dia.) ultrafine particle (UFP) catalysts with *controllable* chemical composition and particle size is of fundamental importance to study the effect of these factors on the catalytic activity.

In this paper, we report the results of a study to synthesize and characterize nanoscale (5-20nm) UFP Fe-based catalysts for direct coal liquefaction. The UFPs were produced by the laser-driven gas phase reaction of $Fe(CO)_5$ with C_2H_4. By adjusting the reaction conditions we have found it possible to produce reasonably pure phase (~95%) batches of α-Fe, Fe_3C and Fe_7C_3 particles with a size distribution of ~2-4 nm. Typical production rates are ~ 1 g/hr. By adding H_2S to the reactant gas stream we have succeeded recently in producing UFP pyrrhotite ($Fe_{1-x}S$). Results from our studies to determine the catalytic benefit of UFP Fe-carbide catalysts in coal liquefaction have produced some promising results[2]. These experiments were carried out in a microautoclave with dimethyl disulfide (DMDS) added to improve conversion to iron sulfide. Our studies have shown that, under liquefaction conditions, the UFP Fe-carbide catalysts are transformed into pyrrhotite. This transformation complicates the identification of the active catalyst phase and, of course, raises questions about the activity and the role of the carbides in the conversion of coal into liquids and gases. Our recent success in synthesizing UFP pyrrhotite should allow us to study these questions, as well as evaluate the activity of UFP $Fe_{1-x}S$.

We have characterized the physical properties of our UFP catalysts by X-ray diffraction (XRD), optical spectroscopy(reflectivity and Raman scattering),

transmission and scanning electron microscopy (TEM and SEM) and ^{57}Fe Mossbauer spectroscopy.

The CO_2 laser pyrolysis technique, invented by Haggerty et al.[3], has been established as a useful technique for the synthesis of ultrafine particles(UFP) in the size range 5 - 30 nm. In the past, a variety of UFPs have been produced using this technique; they include {Si, SiC, Si_3N_4 }[3], { ZrB_2, TiO_2 }[4], Fe_3C[5], {WC, MoS_2}[6]. These UFPs (e.g., SiC and Si_3N_4) have been found to be free from contamination and exhibit a narrow particle size distribution[3]. The synthesis of UFP Fe_3C using laser pyrolysis was first explored by Fiato et al. at Exxon[5]. They proposed a basic chemical reaction involving the thermal decomposition of $Fe(CO)_5$ and subsequent reaction with C_2H_4 at high temperature sustained by CO_2 laser illumination which couples strongly to the vibrational bands of C_2H_4. They found that UFP Fe_3C forms as a product of this process. Fiato et al.[5] demonstrated that the particle composition, i. e., carbon to iron ratio, could be controlled by varying the preparation conditions. Prior to our work, no studies have been reported which correlate the reaction parameters with particle size, chemical composition or crystalline phase. Furthermore, the Exxon group did not report the formation of Fe_7C_3, which exhibits a hexagonal structure[12].

Experiment

Our laser pyrolysis system[3-5, 7, 8] is shown schematically in Fig. 1. The reactant gases flow vertically out of a stainless steel tube with a nozzle of area A. Studies of the effect of A on particle production have been carried out over the range A ~2 - 5 mm^2. The pyrolysis reaction zone is formed at the intersection of the horizontal infrared beam from a continuous (CW) CO_2 laser, tuned at the P20 line, and the vertical flow of reactant gases from the nozzle. The reactant gases and associated particle growth are confined within the reaction zone by a coaxial flow of Ar gas which passed through a larger tube concentric with the much smaller reactant gas tube (Fig. 1). Argon gas is also introduced into the entrance and exit windows in such a way as to continually sweep any stray particles off the NaCl windows (Fig. 1). Mass flow controllers are used to establish steady gas flows of Ar, and to regulate the flow of C_2H_4 (2–30 sccm) and H_2S(2-20 sccm). The total pressure in the cell was controlled by a needle valve located between a rotary vacuum pump and the stainless steel reaction chamber (6-way cross). Particles are collected downstream in a Pyrex trap indicated in Fig. 1. Since the α-Fe, Fe_3C and Fe_7C_3 particles are ferromagnetic, we have employed a magnetic field to trap the particles using a stack of permanent magnets placed beneath the trap (Fig. 1).

The pyrrhotite $Fe_{1-x}S$ UFPs were synthesized by adding H_2S to the C_2H_4

and $Fe(CO)_5$ reactant gas stream, at a flow rate of 7 sccm. The other reaction parameters are set at the values which would otherwise produce α-Fe particles(Table 1). These sulfide particles are non-magnetic and are not attracted to the magnets beneath the collection trap(Fig. 1). As a result, the particles tend to drift toward the far end of the trap and clog the 0.2 μ pore size membrane filter, which complicates the steady state production of these particles. Other means of trapping pyrrhotite particles are being investigated to solve this problem. It is interesting to speculate that the non-magnetic properties of pyrrhotite UFPs may lead to much less particle agglomeration compared to ferromagnetic carbide UFPs, and thus better dispersion in the coal slurry.

To handle most of our Fe-based UFPs in air, we have found it necessary to passivate the surface in situ in the collection trap. The passivation is carried out by flowing 4-10% O_2–in–He_2 for several hours.

Results and Discussion

Shown in Fig. 2 are the XRD results for UFP α–Fe, Fe_3C and Fe_7C_3 using the reaction parameter values given in Table 1. In this figure, the dots represent experimental data and the lines are calculated using a sum of Lorentzian functions whose peak positions and relative strengths are obtained from published powder diffraction data[9]. The same width parameter is used for all diffraction lines, and an exponential function is introduced to simulate the background. The Debye-Scherrer equation has been used to convert the X-ray line width into an average particle diameter. We find that these X-ray derived values for the particle diameter are in good agreement with Transmission Electron Microscopy (TEM) results, indicating that the UFPs are, for the most part, single crystal particles. The calculated diffraction pattern is seen to agree reasonably well with the data[9], leading to our identification of the three phases as α-Fe, Fe_3C and Fe_7C_3. The signature of Fe_3O_4 in the XRD data of α-Fe is believed to stem from the O_2 passivation.

We have found that higher chamber pressures(> 300 torr) and higher reactant gas flow rates(> 30 sccm) favor the formation of high carbon content crystalline phases such as Fe_7C_3. On the other hand, lower chamber pressures and reactant gas flow rates favor the formation of α-Fe. A detailed study of the correlation between reaction parameter values and the associated solid UFP phases produced will appear elsewhere[8]. Presented in Fig. 3a and 3b are, respectively, the XRD results for several batches of Fe_3C and Fe_7C_3 particles produced with different average particle sizes. The particle size indicated in the figure was estimated using the Debye-Scherrer equation[13] and the data near $2\theta \sim 58°$.

In Fig. 4, we show ^{57}Fe Mossbauer spectra collected at 12K for both Fe_3C and Fe_7C_3. The solid line in Fig. 4 represents the calculated Mossbauer spectrum by fitting the data in the usual way. The results from the fit to room temperature data including internal magnetic field, isomer shift and quadruple splitting parameters are listed in Table 2. The parameter values for the Fe_3C particles at room temperature[8] are compared with the results of Le Caer et al.[11], and are found to be in good agreement. To our knowledge, Mossbauer results for Fe_7C_3 have not been reported. We find in this study that a model with four inequivalent magnetic sites is necessary to fit the data. Fe_7C_3 has three chemically inequivalent sites[10]. Further Mossbauer and neutron scattering studies are underway to determine the magnetic structure of Fe_7C_3 UFPs.

Shown in Fig. 5 by the dotted lines are XRD data for iron sulfide (pyrrhotite) UFPs. For comparison, the solid lines in the figure represent the XRD data of Fe_7C_3 particles after reaction in our microautoclave with dimethyl disulfide(DMDS) at 375 °C. The vertical lines represent the standard powder diffraction intensities for pyrrhotite. As can be seen in the figure, the Fe-sulfide UFPs exhibit a diffraction pattern quite similar to pyrrhotite. However, on the basis of the XRD data, it is not possible to rule out that there may be significant incorporation of carbon into the UFP pyrrhotite lattice. Mossbauer studies are currently underway to address this point. One can also conclude from the XRD data in the figure that liquefaction conditions (and the presence of DMDS) rapidly converts UFP Fe-carbide into UFP pyrrhotite with slightly smaller particle size (and possibly with significant carbon content).

New results from coal liquefaction studies using nanoscale Fe-based catalysts, including UFP-pyrrhotite, will also be presented.

Acknowledgement

We thank Bhaswati Ganguly, Dr. Frank E. Huggins and Dr. Gerald P. Huffman for the Mossbauer studies. This work is supported by DOE Advanced Concepts, DE-AC22-91PC91040.

References

1. Derbyshire, Frank J., *Catalysis in Coal Liquefaction: New Direction for Research*(1988) IEA Coal Research, p. 2
2. Hager, Bi, Derbyshire, Eklund, Stencel, "Ultrafine Iron Carbide as Liquefaction Catalyst Precursor", ACS Preprints- Division of Fuel Chemistry, 36(4) 1900-8(1991)
3. J. S. Haggerty, *Sinterable Powders from Laser-Driven Reactions,* in *Laser-induced Chemical Processes,* J.I. Steinfeld, Editor. 1981, Plenum Press: New York.
4. G. W. Rice, and R. L. Woodin, J. Am. Ceram. Soc., 1988. **71**: p. C181.
5. R. A. Fiato, G. W. Rice, S. Miseo, and S. L. Soled, United States Patent, 1987. **4,637,753**.
6. R. A. Fiato, G. W. Rice, and S. L. Soled, U. S. Patents, 1988. **4659681, 4668647**.
7. G. W. Rice, and et al., United States Patent, 1987. **4,659,681**.
8. G. W. Rice, and R. L. Woodin. *Applications of Lasers to Industrial.* in *SPIE.* 1984.
9. Powder Diffraction File of the Joint Committee on Powder Diffraction Standard(International Center for Diffraction Data, Swarthmore, PA, 1991).
10. Xiang-Xin Bi, P. C. Eklund, et al., in preparation.
11. R. L. Cohen, *Applications of Mossbauer Spectroscopy.* ed. R.L. Cohen, 1980, New York: Academic Press.
12. H. L. Yakel, International Metals Reviews, 1985. **30**: p. 17.
13. B. D. Cullity, *Elements of X-Ray Diffraction.* 1967, Addison-Wesley Publishing Company, Inc.

Table 1 Typical laser pyrolysis reaction parameters.

	α-Fe	Fe_3C	Fe_7C_3
Laser Intensity(W)	30	50	54
Beam Width(mm)	1	1	0.2
Nozzle Diameter(mm)	1.7	0.8	0.8
Chamber Pressure(Torr)	100	300	500
C_2H_4 Flow Rate(sccm)	9	9	25

Table 2 Room-temperature ^{57}Fe Mossbauer parameters including hyperfine magnetic splitting(H_0), isomer shift(I. S.) and quadropole splitting(Q. S.) for UFP Fe_3C and Fe_7C_3.

	H_0 (KG)	I. S. (mm/s)	Q. S. (mm/s)
Fe_7C_3*	228	0.32	-0.17
	210	0.23	0.03
	185	0.20	-0.04
	163	0.21	0.07
Fe_3C*	210	0.19	0.02
	198	0.19	0.01
Fe_3C[11]	208	0.18	0.02
	206	0.18	0.02

* present work.

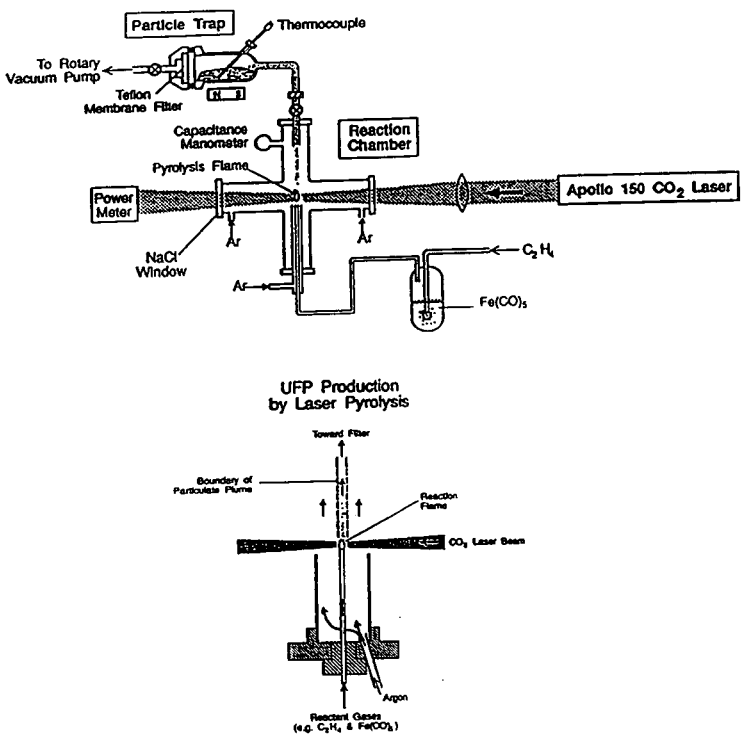

Fig. 1 Laser pyrolysis system for the synthesis of ultrafine iron carbide and sulfide particles.

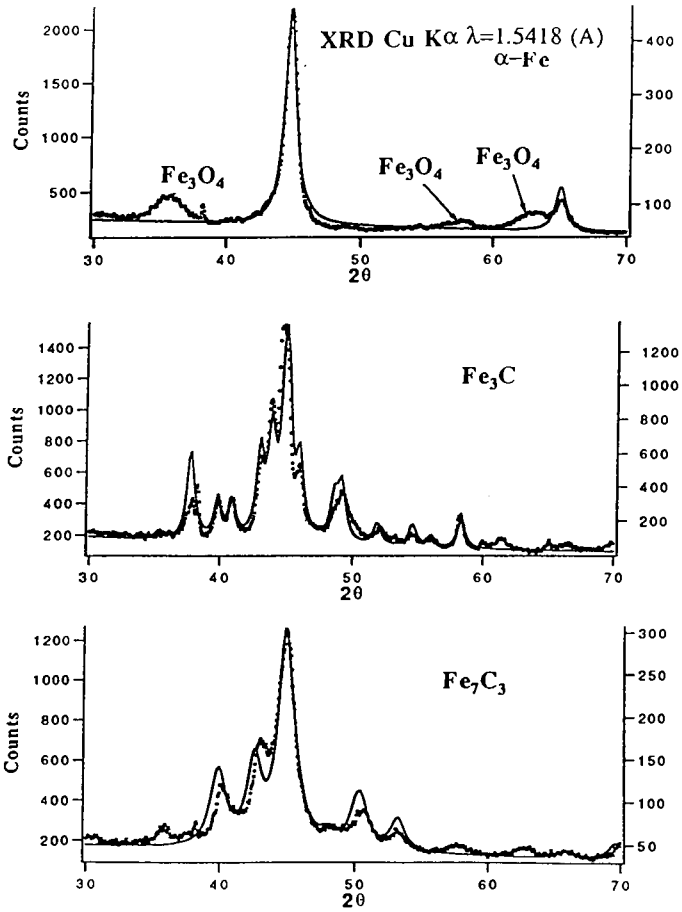

Fig. 2 XRD data(dots) for α-Fe, Fe_3C and Fe_7C_3 UFPs and calculated results (solid curves) using standard diffraction data[9] with an exponential background.

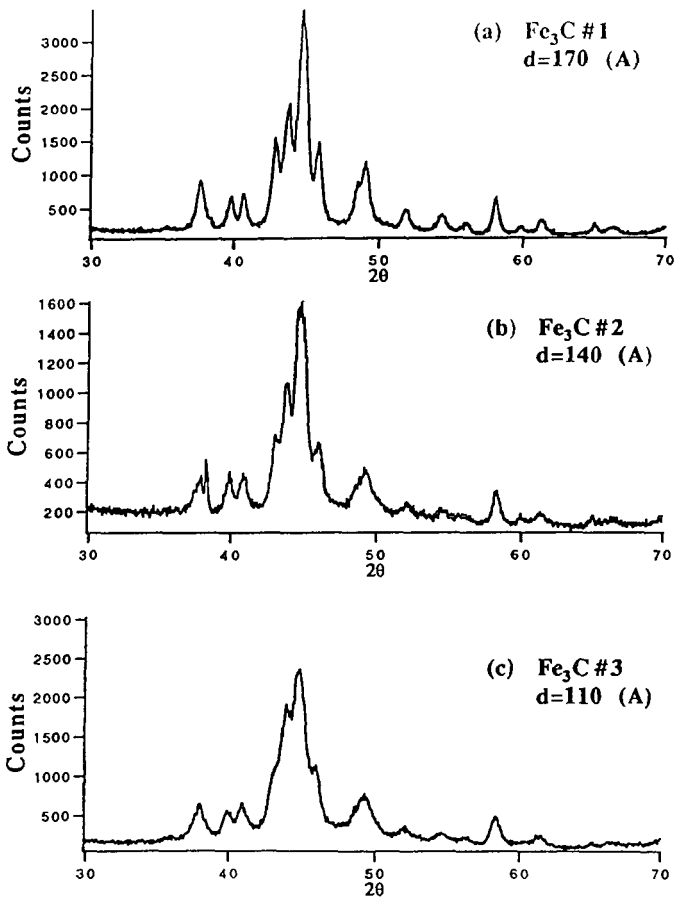

Fig. 3(a) XRD data for Fe_3C UFPs of different particle size.

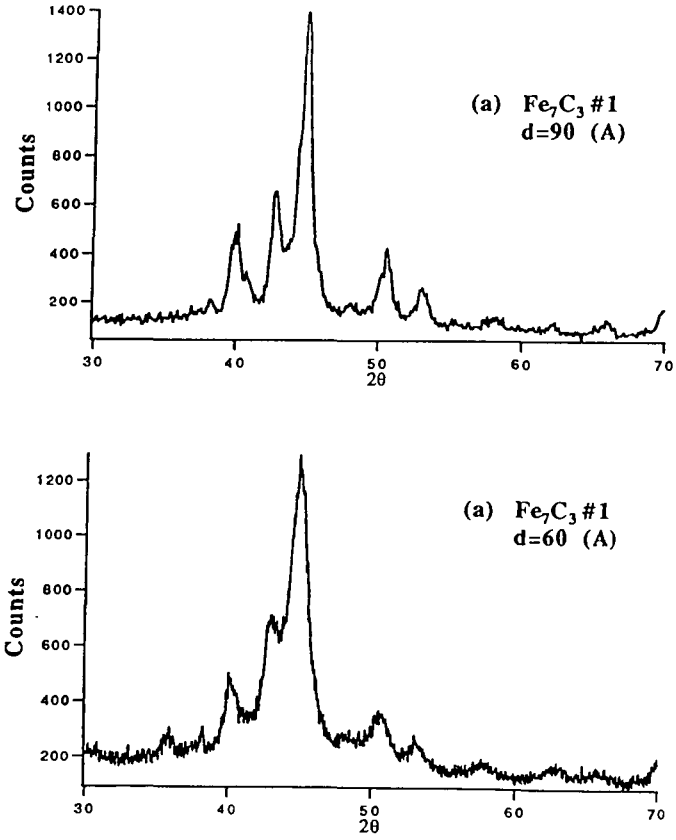

Fig. 3(b) XRD data for Fe_7C_3 UFPs of different particle size.

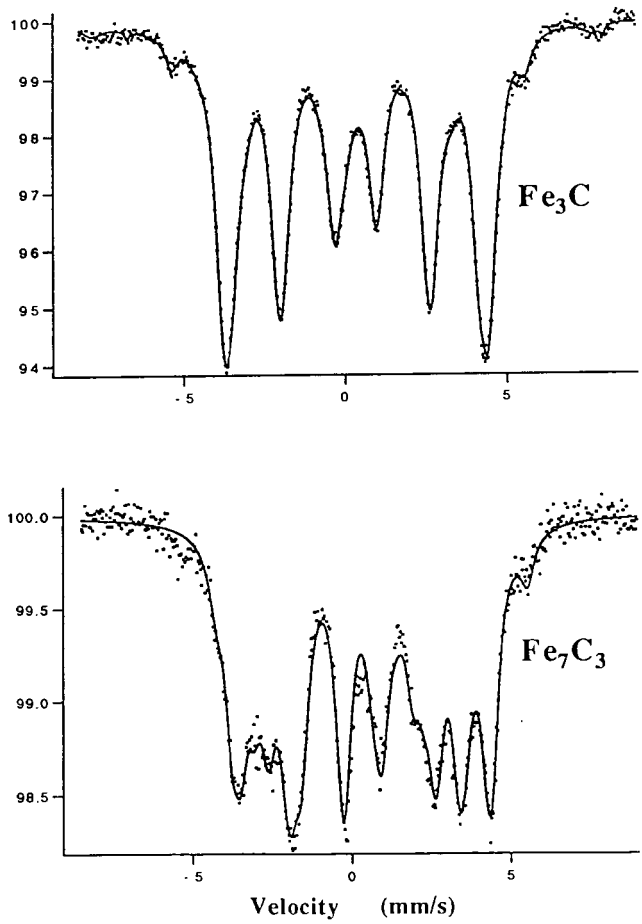

Fig. 4 ^{57}Fe Mossbauer spectra(dots) at T=12 K for Fe_3C and Fe_7C_3. Solid lines are calculated using a set of parameters that fit the data.

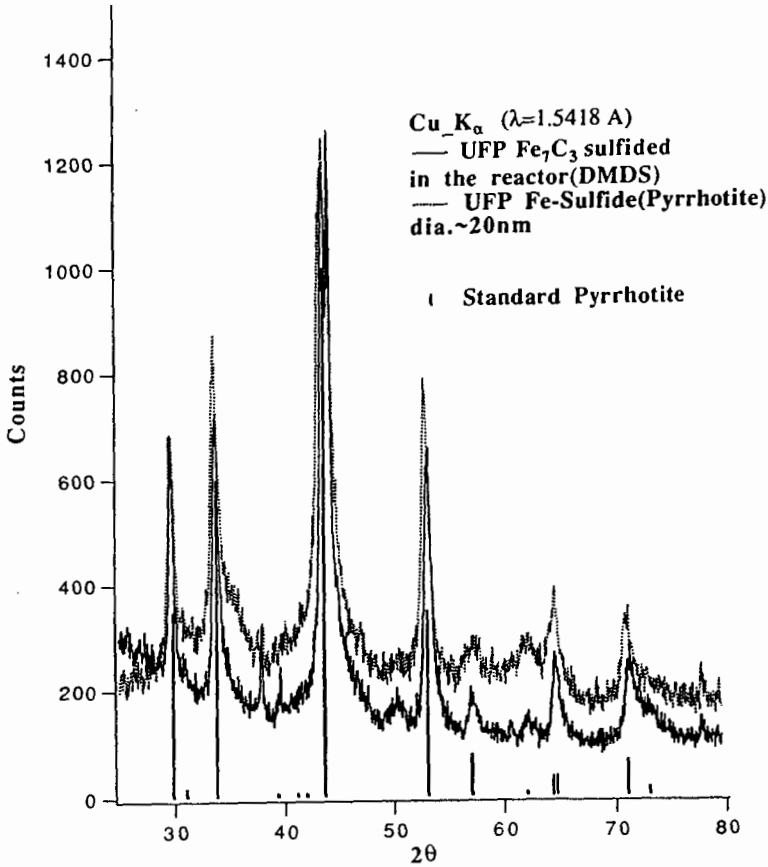

Fig. 5 Dotted lines are XRD results for the pryyhotite $Fe_{1-x}S$ UFPs obtained by using laser pyrolysis, and solid lines by sulfiding iron carbide Fe_7C_3 UFPs with DMDS at 375 °C(solid lines). The vertical lines represent standard powder diffraction data[9] for $Fe_{1-x}S$ phase.

CONVERSION OF RESID COMPONENTS IN CC-ITSL PROCESSING AT WILSONVILLE

G. A. Robbins, R. A. Winschel, F. P. Burke
CONSOL Inc.
Research & Development
4000 Brownsville Road
Library, PA 15129

Key words: Liquefaction, Resid, Kinetics

INTRODUCTION

Integrated Two-Stage Liquefaction technology has evolved to its current configuration, in which high recycle rates of solids and non-distillable materials contribute to high conversions and distillate yields. At the Wilsonville, Alabama, 6 ton/day pilot plant, the feed stream contains 29-33 wt % coal, 27-34 wt % resid (850°F$^+$), and 8-16 wt % cresol insolubles (CI). Only 25-28% of the feed is distillable. In a recent assessment of analytical needs,[1] it was concluded that the chemistry of residual materials is an important area for study, including improved analytical methods for resid characterization and more extensive kinetic modeling. CONSOL has characterized process oils from each of the last nineteen Wilsonville runs; Close-Coupled Integrated Two-Stage Liquefaction (CC-ITSL) operation of the plant spanned fifteen runs since 1985. This paper represents an initial attempt to review and refine some areas of our investigations of resid conversion chemistry in Wilsonville runs.

EXPERIMENTAL

The experimental methods used in the analysis of whole process oils were reported elsewhere in detail.[2-4] A brief description is provided here. Each whole process oil is distilled to 850°F to produce a distillate and a resid. Tetrahydrofuran (THF) solubles are obtained by repeated washing of distillation bottoms with distilled THF and recovery by rotary evaporation. Phenolic -OH concentration in the THF-soluble resid is determined by Fourier Transform infrared spectroscopy in THF solution. The THF-soluble resid is fractionated successively into oils (hexane-solubles), asphaltenes (benzene-solubles), and preasphaltenes (pyridine-solubles) with analytical quantitation by flame ionization detection (using different response factors for each feed coal represented). Each insoluble resid fraction is ashed at 800°C to constant weight and insoluble organic matter (IOM, also referred to as unconverted coal, or UC) is determined by difference between weights of ash and THF-insolubles.

The process oils analyses are used to calculate conversions (forced ash balance method) of the 850°F$^+$ material and its various components in each reactor stage. The 850°F$^+$ conversions are used to calculate conversion rate constants, conversion activities, and a catalyst deactivation rate constant.[5] Equations used are:

$$C = \text{Conversion} = \left(\frac{850°F^+ \text{ In/Ash In} - 850°F^+ \text{ Out/Ash Out}}{850°F^+ \text{ In/Ash In}} \right) \times 100\%$$

$$K = \text{Rate Constant} = \text{WHSV} \left(\frac{C}{100 - C} \right)$$

$$A = \text{Conversion Activity} = Ke^{E_{act}/RT}$$

where E_{act} is assumed to be 23,500 cal/mol. In addition to conversion of the total 850°F$^+$ resid, it is possible to calculate conversion of any component, including IOM, THF-solubles, oils, asphaltenes, preasphaltenes, and phenolic -OH.

RESULTS AND DISCUSSION

Background. Table 1 summarizes the major operating conditions for CC-ITSL Runs 257 through 262. Generally several significant differences exist among runs. Detailed discussions of each run have been reported by Wilsonville[6] and CONSOL[7]. A block diagram of the Wilsonville plant appears in Figure 1.

Comparison of CONSOL and Wilsonville Distillation Procedures and Resid Conversions. CONSOL uses an 850°F atmospheric equivalent distillation endpoint; the Wilsonville laboratory uses a 1050°F endpoint.[8] Therefore, the 850 x 1050°F boiling fraction is considered resid in CONSOL's analyses, but distillate in Wilsonville's analyses. Table 2 illustrates this. On average, CONSOL typically measured about 14 wt % more resid than did Wilsonville. The amount of the difference may be related to reactor volume either directly or indirectly (see Table 2). Because of the difference, conversions calculated from CONSOL data are of 850°F$^+$ material; Wilsonville's conversions are of 1050°F$^+$ material. Some implications of this difference have been discussed elsewhere.[5]

One way to compare the (850°F$^+$) conversions obtained by CONSOL with those obtained by Wilsonville (for 1050°F$^+$) is to calculate the CONSOL/Wilsonville conversion ratio (R(C/W)) (Figure 2). Several observations were made from these data. First, R(C/W) averaged 0.8-1.0 in most runs, indicating CONSOL conversions were generally somewhat lower than Wilsonville conversions. Second, the R(C/W) ratio did not correlate with CONSOL and Wilsonville values for V-131B resid content (Table 2). Third, Run 262 was unprecedented in the low R(C/W), in each stage (not shown) and total system. It is not obvious why the 850 x 1050°F conversion was so low relative to the conversion of 1050°F$^+$ material, but perhaps paraffinic components present in the 850 x 1050°F fraction were not readily converted to distillate in Run 262. Several points can be made regarding this: 1) Wilsonville found significant quantities of waxes in the Run 262 distillate products, and experienced unprecedented handling problems with them. 2) CONSOL found the heavy distillate paraffinicity to be very high in Run 262. 3) The Run 262 resid alkyl beta protons were high, but not unprecedented; they were consistently this high only in one other CC-ITSL run (Run 257). How these results may be related to the use of Molyvan L (dispersed catalyst precursor first used in Run 262) is unknown. Perhaps dispersed Mo is not a good paraffin cracking catalyst, or the high coal space velocity during Run 262 was a contributor to poor cracking.

Corresponding first- and second-stage results are not shown, but are summarized here. R(C/W) for the first stage (typically slightly lower than one) in any given period is usually greater than that of the second stage (typically 0.8). These observations seem consistent with the first stage conversion which is dominated by IOM, and is not highly subject to variation in distillation conditions. The conversion of material in the second stage is more sensitive to distillation conditions and shows a greater difference in CONSOL and Wilsonville results. There was more scatter in the second-stage ratios.

Catalyst Deactivation in Run 258. Kinetic rate constants and activities (pre-exponential factors) for 850°F$^+$ conversion were calculated for Run 258 material balance periods to evaluate catalyst activity and deactivation. In many recent runs, a look at catalyst deactivation was impossible because most operating periods were obtained at similar (equilibrium) catalyst ages. However, tests at several catalyst ages (some were from batch aging) in Run 258 allowed a catalyst activity evaluation. In order that the calculation would not be skewed by many data points near the equilibrated age of ca. 2500 lb (resid + CI)/lb cat, all of those data (periods B through F, H, and I) were averaged to a single value (transitional periods were omitted). The deactivation rate constant is evaluated by considering the conversion activity, A, to have an exponential dependence on catalyst age, t, as $A = A'e^{\alpha t}$, where A' is the initial conversion activity. As written, catalyst deactivation will result in negative values of α, the deactivation rate constant. The value of α was determined by regression of ln A on t. The results (Table 3 and Figure 3) indicate no significant effect of second-stage catalyst age on first-stage activity, as is expected for the thermal first stage (in the absence of any solvent donor effect). However, a deactivation rate constant is obtained for the second-stage catalyst with a high correlation, although for only four data points. The α and A' values for the second-stage catalyst are similar to those CONSOL found for Wilsonville Runs 250 through 257.[5] However, the correlation of catalyst activity with age in Run 258 was much stronger than in those prior runs.

Conversion of Resid Components. Conversions of components of the 850°F$^+$ resid (850°F$^+$ resid, THF-solubles, oils, asphaltenes, preasphaltenes, and phenolic -OH) were calculated for Runs 257 through 262 (Figure 5). In Run 262 (Black Thunder coal, see Figure 5a), the resid + IOM conversion was positive in the first stage and low in the second stage, resulting in equivalent first-stage and total conversions. The conversion of THF-soluble resid and its components showed negative first-stage and total conversions, with higher second-stage conversions. The negative conversions represent gains in those components, from conversion of coal to solubles. Second-stage conversions of THF solubles, oils, and asphaltenes were approximately zero, making the corresponding first-stage and total conversions equivalent. Conversions of

preasphaltenes and phenolic -OH differ from those of the other components: they are greater in magnitude, showing greater first-stage and total gains (negative conversions); and the second-stage conversions are large and positive, resulting in increases in the total system conversions. The large negative conversion (net gain) of preasphaltenes in the first stage implies that preasphaltenes are primary coal solubilization products and that they are an intermediate form in the transition from coal to distillate. In the second stage, little additional coal is converted, and the conversion of preasphaltenes to other products is positive. The phenolic -OH conversion shows a similar trend with reactor stage, presumably because preasphaltenes are high in phenolic -OH (but the other fractions contain phenolics, as well). These results suggest that preasphaltenes and/or phenolic -OH could be important to include as a group in lumped kinetic modeling. This could be important in overall evaluations of performance, since heteroatom removal is a significant role of the catalyst, and since refining of the liquids to final products has a major impact on process economics.

Figure 5b shows the average results from Run 261, a catalytic/catalytic, low/high temperature run, with Illinois 6 feed coal. The preasphaltene and phenolic -OH conversions show the same trends as in Run 262. Trends in conversions of resid + IOM and other components somewhat resemble those in Run 262, but a number of differences are evident. In Run 261, the second-stage conversion of resid + IOM was relatively high and contributed a great deal to the total conversion. Conversions of THF-solubles and asphaltenes were positive in the second stage in Run 261, contributing to the respective total conversions. Total conversions of THF-solubles, oils and asphaltenes, and conversion of oils in each stage, were all close to zero. The results for Run 257 (another catalytic/catalytic Illinois 6 coal run) were very similar to those for Run 261, in spite of the fact that Run 257 used a high/low temperature configuration.

Resid component conversion results from two segments of Run 260 (Black Thunder coal) are shown in Figures 5c and 5d. One is thermal/catalytic, high/low operation (periods A-C), and the other is catalytic/thermal, low/high operation (periods D-F). The trends in resid component conversion during thermal/catalytic operation are quite similar to those seen in Run 261 (Figure 5b). Run 260 resembles the other subbituminous thermal/catalytic runs (262 and 258), however, in the relatively low second-stage resid + IOM conversion. That situation changed during catalytic/thermal operation in Run 260 (Figure 5d), when the two reactors more equally shared the contribution to conversion of resid + IOM. Also during catalytic/thermal operation, the first-stage, second-stage, and total conversions of most resid components were approximately zero. The preasphaltene conversions were still the most sensitive, but their magnitude was greatly reduced relative to the other runs discussed. The phenolic -OH conversions were quite small in magnitude, and were close to zero. Overall, it appears as if catalytic/thermal operation in Run 260 nearly balanced the work performed by each reactor and put the reactors into a near-equilibrium situation with respect to resid conversion. Thus, for most components, there was little net conversion or gain. A net conversion of coal to preasphaltenes occurred in the first stage and total system. In the second stage, coal conversion to resid was balanced by resid conversion to distillate.

CONCLUSIONS

In the latest Wilsonville CC-ITSL runs, the first stage primarily converts coal to solubles; conversion of soluble components takes place principally in the second stage. Preasphaltenes (which are high in phenolics) seem to be the primary coal solubilization product, and their conversion is effected primarily in the second stage. Including preasphaltenes and/or phenolic -OH components in lumped kinetic models may be useful, because defunctionalization and upgrading are important roles of catalytic reactor systems. Second-stage conversions of the oil and asphaltene components were typically low (relative to preasphaltenes conversions), and in many cases were close to zero. These results are consistent with the conventional wisdom regarding thermal/catalytic processing, in which solubilization and upgrading take place primarily in different stages, but appear to apply as well to catalytic/catalytic operation. Trends in resid component conversions in two catalytic/catalytic runs with the same feed coal (Runs 257 and 261) were very similar, in spite of a difference in temperature configuration (high/low vs. low/high). Catalytic/thermal operation in the last part of Run 260 seemed to balance the load in each reactor and result in a near-equilibrium situation with respect to resid conversion (little net conversion or gain of most resid components in either reactor). This situation was not typical of the other runs investigated (Runs 257-262).

Second-stage resid + IOM conversion activities in Run 258 material balance periods decreased significantly with catalyst age, indicating catalyst deactivation. The thermal first stage conversion activity showed no dependence on second-stage catalyst age.

The concentration of 850 x 1050°F material in the recycle oil seems to be influenced primarily by reactor volume in use, perhaps by changing the reactor dynamics (such as the relative thermal and catalytic reaction volumes). During Run 262, the 850°F$^+$ conversion relative to 1050°F$^+$ conversion was quite low in each stage, possibly due to the presence of paraffinic components not easily converted to final products.

RECOMMENDED FUTURE WORK

The resid conversion chemistry of Wilsonville runs prior to Run 257 should be explored in more detail and more-detailed analysis of runs after 257 may also be warranted. Calculation of kinetic rate constants and conversion activities for individual components (instead of only the resid + IOM) might also be of interest. Addition of one more analysis would make it possible to obtain conversions of various hydrogen (proton) types, perhaps providing additional information on the nature of the converted resid.

What more is needed in the future? Innovative kinetic modeling is needed, even for empirical yield and conversion data. For example, experience indicates that bituminous coal converts readily to soluble resid, but less readily to distillate. Conversion of subbituminous coal to solubles is more difficult, but the solubles are readily converted to distillate. An adequate model of liquefaction phenomena would have to account for differences in the coal and resid conversion kinetics in various coals. A comprehensive kinetic model (of proper reaction order) should include the following (preferably mathematically separable) terms: coal (separate terms for IOM and resid reactivity), catalyst (activity and deactivation susceptibility by various routes), and processing conditions (temperature, space velocity, resid concentration, coal and ash recycle concentration, etc.). Current models do not adequately separate processing condition effects from those of the coal and catalyst.

ACKNOWLEDGEMENT

This work was supported by the U. S. Dept. of Energy under contract DE-AC22-89PC89883.

REFERENCES

1. Brandes, S. D.; Robbins, G. A.; Winschel, R. A.; Burke, F. P. "Coal Liquefaction Process Streams Characterization and Evaluation, Analytical Needs Assessment Topical Report", DOE/PC 89883-18, March 1991.
2. Burke, F. P.; Winschel, R. A.; Robbins, G. A. "Recycle Slurry Oil Characterization Final Report - October 1980 through March 1985", DOE/PC 30027-61, March 1985.
3. Winschel, R. A., Robbins, G. A.; Burke, F. P. "Coal Liquefaction Process Solvent Characterization and Evaluation, Technical Progress Report, July 1 through September 30, 1985", DOE/PC 70018-13, December 1985.
4. Winschel, R. A.; Robbins, G. A.; Burke, F. P. *Fuel* 1986, *65*, 526-532.
5. Burke, F. P.; Winschel, R. A.; Robbins, G. A. "Coal Liquefaction Process Solvent Characterization and Evaluation - Final Report", DOE/PC 70018-70, September 1989.
6. Detailed Wilsonville Technical Review Meeting handouts and run reports under U. S. DOE Contract DE-AC22-90PC90033 and others preceding it; also see, for example, papers from recent DOE Liquefaction Contractors' Review Meetings and from recent EPRI Clean Fuels Conferences.
7. Various reports under U. S. DOE Contracts DE-AC22-80PC30027, DE-AC22-84PC70018, and DE-AC22-89PC89883.

Table 1. Conditions Used in Recent Wilsonville Runs

Condition	Wilsonville Run					
	257	258	259	260	261	262
Coal* (MF Ash Content, wt %)	BS 2 (11.3)	SC (5.6), BT (7.3)	Ire. (4.5), Ire. (14.9)	BT (6.2)	BS 2 (11.8)	BT (6.4)
Coal Feed Rate, MF lb/hr	166-531	193-293	230-356	251-352	357-548	242-346
Coal Concentration, MF wt %	30-34	30	30-33	30	29-33	30
Resid in Recycle Solvent, wt %	40-50	40-41	40-51	39-40	33-49	32-41
Solids in Recycle Solvent, wt %	12	20-25	6-13	20-21	11-12	19-20
Reactor Vol., % Stg 1/Stg 2	100/100, 50/50	50/50	50/50	100/75, 75/100	100/100	50/50
Catalyst Configuration	Cat/Cat	Th/Cat	Cat/Cat	Th/Cat, Cat/Th	Cat/Cat	Th/Cat, Th/Th
Temperature Configuration	High/Low	High/Low	High/Low	High/Low, Low/High	Low/High	High/Low
Interstage Separation	No	Yes	Yes	Varied	Yes	Yes
Temp. in Stage 1, °F	760-810	825-865	810-825	775-840	790-810	825
Temp. in Stage 2, °F	760-805	740-790	760-790	775-805	800-825	760-810
Stage 1 Catalyst**	Am 1C	None	Am 1C, Sh 324	None,Sh 324	EXP, Cr 324	None
Replace. Rate, lb/T MF Coal	0-3	-	0-4	-, 3	0-3	-
Stage 2 Catalyst**	Am 1C	Sh 324	Am 1C, Sh 324	Sh 324,None	EXP, Cr 324	Cr 324, -
Replace. Rate, lb/T MF Coal	0-3	0-3	0-4	3, -	0-3	3, -
Thermal Stage Space Vel., lb MF Coal/hr/ft^3, (C=Constant)	-	51C-78C	-	31C-43C	-	64C-92C
Catalytic Space Vel., Stg 1/Stg 2, lb feed/hr/lb cat.	3.7-6.7/ 3.7-7.0	-/3.6-5.7	1.8-6.8/ 1.7-6.5	-/3.1-3.9, 2.8-4.0/-	2.9-6.4/ 2.6-6.0	-/4.7-6.6, -/-
Stage 1 Catalyst Age, lb (Resid+Solids)/lb cat.	926-2308	-	895-1918	1415-1497	1324-2812	-
Stage 2 Catalyst Age, lb (Resid+Solids)/lb cat.	727-2314	415-3452	718-2710	1330-1368	1090-2238	1315-1545
Slurry Catalyst and Feed Rate:						
Fe_2O_3, wt % MF Coal	0	2	0	2	0	2
Molyvan L, Mo ppm of MF Coal	0	0	0	0	0	100-1000

Coals are: Black Thunder and Spring Creek (subbituminous), and Burning Star 2 and Ireland (bituminous).
**Catalysts are: Amocat 1C, Shell 324, Criterion 324, and EXP-AO-60.

Table 2. Comparison of CONSOL and Wilsonville Resid Concentrations in Wilsonville Pasting Solvent (V-131B)

Wilsonville Run	Reactor Volume Used, % (1st/2nd Stage)	Resid in V-131B Pasting Solvent, wt %		Fraction of 1050°F$^+$ in 850°F$^+$ (Wilsonville wt %/CONSOL wt %)
		Wilsonville	Difference (CONSOL-Wilsonville)	
Run 262	50/50	37.2 ±2.9	12.5 ±2.0	0.75 ±0.03
Run 261	100/100	43.3 ±6.7	18.5 ±3.5	0.70 ±0.07
Run 260	100/75 (A-C), 75/100 (D-F)	39.4 ±0.8	15.2 ±3.4	0.72 ±0.05
Run 259	50/50	47.4 ±4.1	13.4 ±1.7	0.78 ±0.02
Run 258	50/50	40.8 ±0.4	7.1 ±1.5	0.85 ±0.03
Run 257	100/100, 50/50	46.0 ±4.8	19.1 ±4.9	0.71 ±0.07
257A-257H	100/100	45.7 ±4.9	21.9 ±1.2	0.67 ±0.03
257I-257K	50/50	46.8 ±5.4	11.7 ±0.4	0.80 ±0.02

Table 3. Catalyst Deactivation Rate Calculation For Wilsonville Run 258

Period	Cat. Age, lb (Resid+Cl)/ lb Cat.	First Stage A, 10^7	Second Stage A, 10^7
K	559	1.84	3.75
L	1130	1.36	2.22
M	1314	1.57	2.16
Equilibrated (Avg. B, C, D, E, F, H, I)	2523 ±84	1.81 ±0.43	1.05 ±0.61

First Stage: $\alpha = 0.30 \times 10^{-4}$, $\sigma(\alpha) = 1.17 \times 10^{-4}$, $A' = 1.56 \times 10^7$, $\sigma(A') = 1.18$, $R^2 = 0.03$
Second Stage: $\alpha = -6.2 \times 10^{-4}$, $\sigma(\alpha) = 0.06 \times 10^{-4}$, $A' = 4.96 \times 10^7$, $\sigma(A') = 1.09$, $R^2 = 0.98$
Note: Units of A' are lb total feed/hr/lb cat, units of α are lb Cat./lb (Resid + Cl).

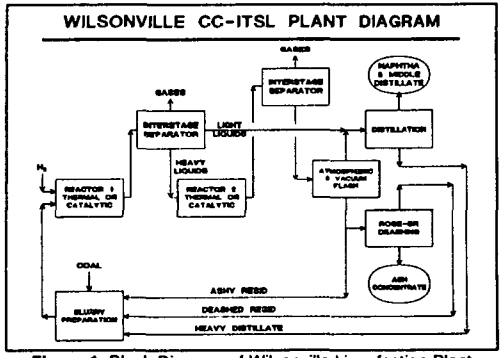

Figure 1. Block Diagram of Wilsonville Liquefaction Plant

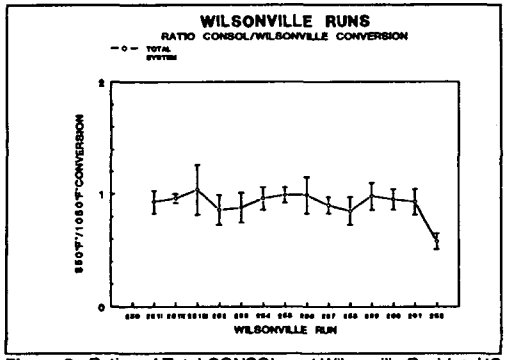

Figure 2. Ratios of Total CONSOL and Wilsonville Resid + UC Conversions for CC-ITSL Runs

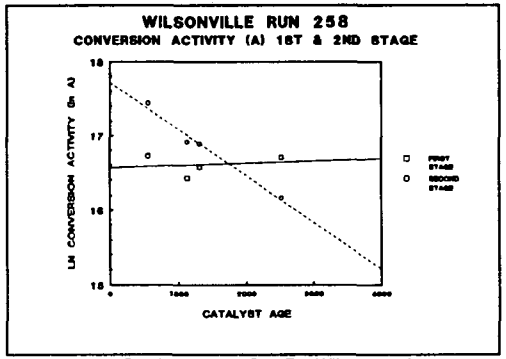

Figure 3. Catalyst Activity Plot For Wilsonville Run 258

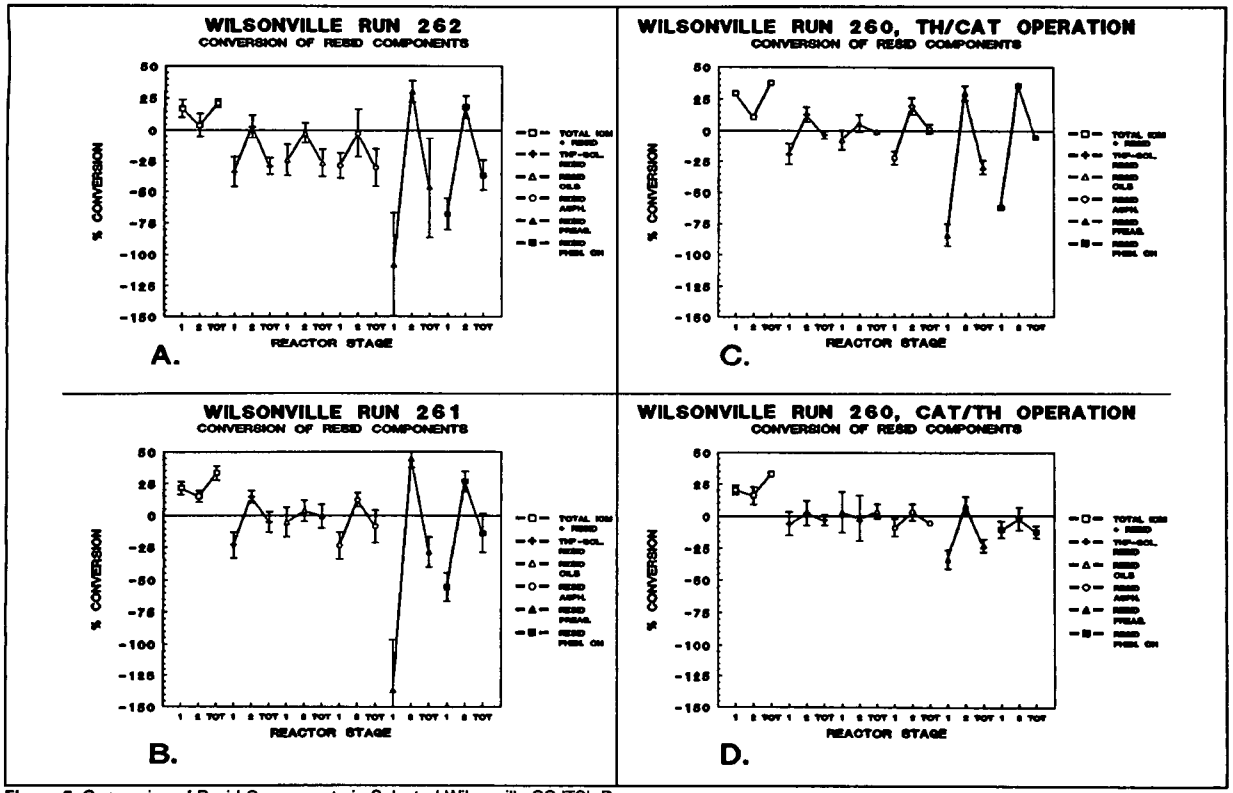

Figure 5. Conversion of Resid Components in Selected Wilsonville CC-ITSL Runs.

SEPARATION AND CHARACTERIZATION OF COAL LIQUIDS FROM WILSONVILLE

S. M. Fatemi, D. C. Cronauer, and R. T. Lagman

Amoco Corporation and Amoco Oil Company
Amoco Research Center, P.O.Box 3011, Naperville, Illinois 60566

Keywords: coal liquefaction, LC separation, ion-exchange, coal characterization

ABSTRACT

Ion-exchange and silica gel adsorption techniques were used to isolate and characterize six distillate cuts from three coal liquids generated at the Advanced Coal Liquefaction Facility in Wilsonville, Alabama. Distillates from Black Thunder subbituminous coal liquids contain much higher levels of acidic components than the distillates of Illinois No. 6 or Pittsburgh No. 8 bituminous coal liquids. Saturate fractions of 450-650 °F distillates of all coal liquids were mainly straight chain aliphatics with some indication of branching. The major components identified in the acid fractions from the Black Thunder coal liquid were methyl, ethyl, propyl, and vinyl substituted phenols, benzaldehydes, and methoxy-benzenes. The major components identified in the base fractions from these liquids were methyl and ethyl substituted quinolines, benzene substituted quinolines and carbazoles, methyl-acridines, methyl substituted phenanthrolines and anthracenecarbonitriles. The major aromatic components of the aromatic fractions from Black Thunder coal liquid were methyl, ethyl, and vinyl substituted benzenes and naphthalenes, methyl-anthracene, methyl and ethyl substituted phenanthrene, fluoranthene, pyrene and chrysene.

INTRODUCTION

A typical coal liquid mixture contains a wide range of compound types including acidic, basic, neutral, and various hydrocarbons. The objective of this investigation was to fractionate distillates from coal liquids of varying rank, characterize the fractions and identify the major components of the fractions. Six distillate cuts of three coal liquids from the Advanced Coal Liquefaction Facility in Wilsonville, Alabama, were selected. The samples were 450-650 °F and 650+ °F distillates of coal liquids from Black Thunder subbituminous and Illinois and Pittsburgh seam bituminous coals. The yields of these fractions as a percentage of MAF feed coal are given in Table I.

EXPERIMENTAL

Samples were separated into acid, base, and neutral (ABN) fractions using a non-aqueous ion-exchange separation technique in which a sample dissolved in cyclohexane is passed through two consecutive ion-exchange LC columns. The first was packed with anion resin and the second with cation resin. The material which is not retained by either column was the neutral fraction. Acids were extracted using formic acid in toluene and bases using propylamine in toluene. The fractions were then filtered and stripped of solvent. The neutral fractions were separated into saturate and aromatic (Sat/Ar) fractions using an activated silica gel column. The saturates were eluted from the column with cyclohexane. The retained aromatics were eluted using a mixture of methanol, diethylether, and toluene.

Proton (^1H) NMR spectrometry was used to study the molecular structure of saturate and aromatic fractions. FT-IR spectroscopy was used to study the functional groups in the acid, base, saturate and aromatic fractions from distillates of Black Thunder coal liquid. Thermogravimetric analysis (TGA) in combination with FT-IR was used to determine the decomposition of neutral fractions from 450-650 °F cuts. A gas chromatograph/mass spectrometer (GC/MS) unit was used for detailed characterization and component type identification of acid, base, neutral, saturate and aromatic fractions from distillates of Black Thunder coal liquid.

RESULTS AND DISCUSSION

Separation Data - Recoveries from acid, base, and neutral (ABN) separation cuts are shown in Table II. The ABN recoveries of the 650+ °F cuts of the Illinois and Pittsburgh coal liquids were reasonable and were within the expected ranges. However, that of the neutral fraction from the lower boiling distillate (450-650 °F) was low, possibly due to the loss of light components of the neutral fraction.

Recoveries from the separation of the neutral fractions into saturate and aromatic fractions are shown in Table II. While the saturates and aromatics of the lower boiling distillates (450-650 °F) were clear and thin brownish liquids, respectively, the saturate and aromatic fractions from the higher boiling distillates (650+ °F) were opaque solids and thick brownish liquids. The total recoveries for higher boiling distillates were reasonable, but the total recoveries for the lower boiling distillates were low. Significant amounts of light components were lost from the aromatic fractions of 450-650 °F cuts.

Elemental Analyses Data - Elemental analyses and calculated H/C ratio are given in Table III. The atomic H/C ratio is highest for the saturate fractions, intermediate for the acid, base, and neutral fractions and lowest for the aromatic fractions. The acid fractions have the highest oxygen and the base fractions have the highest nitrogen content. Neither fraction is free of other heteroatoms. In general, the lower boiling cuts had higher oxygen contents than the higher boiling cuts.

NMR Spectrometry Data - The proton NMR data of the saturate and aromatic fractions of both cuts from Black Thunder coal liquid are shown in Table IV. The saturate fractions of 450-650 °F cuts were mainly straight chain aliphatics with some branching. The aromatic, olefinic, and alpha proton values shown for the saturate fractions of light distillates are negligible. While the aromatic fraction of the 450-650 °F distillate exhibits aromatic compounds with highly branched aliphatics attached to the ring(s), the aromatic fraction of the 650+ °F distillate exhibits aromatics with mostly linear aliphatics. Some methyl substituted aromatics were also present in this fraction.

FTIR Spectroscopy Data - FTIR spectra were obtained for the acid, base, saturate and aromatic fractions of both distillates from Black Thunder coal liquid. Spectra of the acid and base fractions of the 650+ °F cut are shown in Figure 1. The main difference between the FTIR spectra of the acids and bases is the presence of a broad band in the 3600-3100 cm^{-1} region of the spectra of the acids. The broad band in this region is assigned to the absorption of O-H and/or N-H groups associated with the intermolecular hydrogen bonding in phenolic, hydroxyl and pyrolytic type compounds. The aromatic C-H stretches are evident from the peaks in the 3050-3000 cm^{-1} and 900-680 cm^{-1} regions of the acid fractions. The peak assigned to the aromatic C=C stretch at 1600 cm^{-1} is also present in the spectra of the acid fraction. Alkanes, both $-CH_2-$ and $-CH_3$ groups, are also evident in the 2960-2850 cm^{-1} region of the spectra of the acids. Carbonyl bands (1710-1700 cm^{-1}) can be assigned to the carboxilic acid functional group (COOH). Comparison of spectra of the acid fractions of the 450-650 °F and 650+ °F cuts suggests that; 1. the intensities for the bands assigned to the aromatic ring substitutions (900-680 cm^{-1}) are much lower for the acid fraction from 450-650 °F cut, 2. the aromatic to alkane ratio is higher for the acid fraction of high boiling cut, and 3. the methyl functionalities are slightly higher in the acid fraction from 650+ °F distillate.

The aromatics were still evident in the FTIR spectra of the base fractions, but at a much lower concentration. The presence of the carbonyl peak at 1727 cm^{-1} and the pattern of the bands in the aromatic ring substitution region (900-680 cm^{-1}) suggest the presence of 1,2-disubstituted ester compounds. Alkanes ($-CH_2-$ and $-CH_3$) were also evident. The spectra patterns for the two base fractions were nearly identical. The only differences between the spectra of the two bases from the two cuts were the higher ester to alkane and aromatic ratios for the 650+ °F cut.

TGA-FTIR Analyses Data - Stack plots of selected bands from TGA-FTIR analyses of 450-650 °F Black Thunder neutrals are shown in Figure 2. At a TGA temperature up to 300 °F, the neutrals from the Illinois and Pittsburgh coals show very little loss of functional groups. However, the neutral from the Black Thunder coal liquid indicates significant losses of $-CH_2-$ and $-CH_3$ functional groups at about 150 °F. There are significant losses of aliphatic, aromatic, phenolic and C-H stretch functional groups from all three neutrals at temperatures above 300 °F.

GC/MS Analyses Data - GC/MS chromatograms were obtained for the acid, base, neutral, saturate and aromatic fractions of both distillates from Black Thunder coal liquid. Only selected major components were identified. While there are some similar components in both acid fractions from the high and low boiling cuts (i.e. methyl, ethyl, and propyl-phenols), substituted pyrene and fluoranthene are only present in the acid fraction from the 650+ °F cuts. The major components identified in both acid fractions were methyl, ethyl, propyl, and vinyl substituted phenols, benzaldehydes, and methoxy-benzenes. Methyl substituted carbazoles were also seen in both acid fractions.

The major components identified in the base fraction of 450-650 °F cut were methyl and ethyl substituted quinolines. 2,4-Dimethyl-benzaldehyde, which was identified in both acid fractions, was also identified in the two base fractions. 3-propyl-phenol and anthracene were seen in both the acid and base fractions of 450-650 °F distillates, and components such as pyrene and fluoranthene were seen in the acid and base fractions of 650+ °F distillate. The base fraction of the 450-650 °F cut contained benzene substituted quinolines and methyl substituted acridines, and the base fraction of the 650+ °F cut were methyl substituted phenanthrolines, anthracenecarbonitriles, and benzene substituted carbazoles.

The saturates of both distillate cuts were mostly straight chain alkane with limited branching. Some components with functional groups such as hydroxylamine and alcohols were also identified. The major components of the aromatic fraction of the 450-650 °F cut were methyl, ethyl, and vinyl substituted benzenes and naphthalenes. Those in the aromatic fractions of the 650+ °F cut were methyl and ethyl substituted phenanthrene, fluoranthene, pyrene and chrysene.

CONCLUSIONS

The first step in the analysis of coal-derived liquids is the separation of coal liquid into fractions. Distillates from Black Thunder subbituminous coal contain much higher levels of acidic components than those derived from the bituminous coals. The saturate fractions of all coal liquids were mainly straight chain aliphatics with some branching. The aromatic fraction of the low boiling cut derived from Black Thunder coal liquid contained highly branched aliphatics attached to the rings. However, that of the high boiling cut contained both branched and linear aliphatics attached to the rings. The acid fractions of the distillates derived from Black Thunder coal liquid were methyl, ethyl, propyl, and vinyl substituted phenols, benzaldehydes, methoxy-benzenes, methyl substituted carbazoles, and substituted anthracenes, pyrenes and fluoranthenes. The base fractions of the distillates derived from Black Thunder coal liquid were methyl and ethyl substituted quinolines, benzene substituted quinolines, methyl substituted acridines, methyl substituted phenanthrolines, anthracenecarbonitriles, and benzene substituted carbazoles. The aromatic fractions of these distillates contained methyl, ethyl, and vinyl substituted benzenes, naphthalenes, and anthracene, phenanthrene, fluoranthene, pyrene and chrysene.

ACKNOWLEDGMENTS

We acknowledge K. R. Smith of Mattson Instrument and R. E. Lumpkin of the Amoco Alternative Feedstock Development (AFD) Program for their support.

Table I

Yield of Distillate Cuts (Wt.%, MAF Feed Coal)) from Coal-Derived Liquids of Illinois No. 6, Pittsburgh No. 8 and Black Thunder

Feed Coal	Fraction	Yield
Black Thunder	450-650 °F	60
	650+°F	2
Illinois No. 6	450-650 °F	40
	650+°F	31
Pittsburgh No. 8	450-650 °F	44
	650+°F	20

Table II

Recoveries (Wt.%) from Acid, Base, Neutral, Saturate and Aromatic Separations of Distillate Cuts from Illinois No. 6, Pittsburgh No. 8 and Black Thunder

Coal Liquid Cut	Acid	Base	Neutral	Total Recovery
B.T. (450-650 °F)	13.30	3.27	70.10	87.30
Ill. No. 6 (450-650 °F)	3.24	4.18	73.60	81.10
Pitt. No. 8 (450-650 °F)	4.66	3.06	90.60	98.30
B.T. (650+ °F)	17.80	5.42	75.40	98.60
Ill. No. 6 (650+ °F)	3.51	2.95	86.20	92.60
Pitt. No. 8 (650+ °F)	7.32	3.74	90.40	101.50

	Saturate	Aromatic	Total Recovery
B.T. (450-650 °F)	25.2	63.3	88.5
Ill. No. 6 (450-650 °F)	23.8	38.6	62.4
Pitt. No. 8 (450-650 °F)	26.8	45.3	72.1
B.T. (650+ °F)	19.8	81.7	101.5
Ill. No. 6 (650+ °F)	23.4	75.1	98.5
Pitt. No. 8 (650+ °F)	26.2	73.4	99.6

Table III

Elemental Analyses (Wt.%) of Acid, Base, Neutral, Saturate and Aromatic Fractions of Distillates from Illinois No. 6, Pittsburgh No. 8 and Black Thunder

Fractions	C	H	N	O	S	H/C
BT (450-650 °F)						
Acid	77.84	8.34	1.71	8.08	0.13	1.28
Base	81.66	8.99	4.43	2.73	0.18	1.31
Neutral	86.55	10.08	< 0.30	-------	0.12	1.39
Saturate	84.39	13.13	< 0.30	-------	870 (ppm)	1.85
Aromatic	88.31	9.25	< 0.30	-------	639 (ppm)	1.25
Ill.#6 (450-650 °F)						
Acid	78.41	8.60	1.57	9.47	0.47	1.31
Base	80.16	9.30	3.80	3.64	0.18	1.38
Neutral	87.99	11.55	< 0.30	------	427 (ppm)	1.56
Saturate	86.12	12.93	< 0.30	------	------	1.79
Aromatic	89.09	9.73	< 0.30	------	568 (ppm)	1.30
Pitt.#8 (450-650 °F)						
Acid	77.78	8.61	0.72	10.15	0.32	1.32
Base	78.50	9.60	2.04	8.89	0.38	1.46
Neutral	88.45	11.63	< 0.3	-------	371 (ppm)	1.57
Saturate	85.47	11.13	< 0.3	-------	------	1.55
Aromatic	88.69	9.85	< 0.3	-------	385 (ppm)	1.32
BT (650+ °F)						
Acid	81.47	7.67	1.25	7.74	772 (ppm)	1.12
Base	84.62	8.20	4.10	1.79	0.36	1.15
Neutral	89.52	9.52	< 0.3	------	399 (ppm)	1.27
Saturate	83.97	14.01	< 0.3	------	239 (ppm)	1.99
Aromatic	89.60	8.04	< 0.3	------	291 (ppm)	1.07
Ill.#6 (650+ °F)						
Acid	82.06	8.44	2.11	5.82	0.29	1.23
Base	83.83	8.89	3.55	2.09	------	1.26
Neutral	89.12	9.97	< 0.30	------	315 (ppm)	1.33
Saturate	86.12	11.83	< 0.30	------	------	1.64
Aromatic	90.27	8.88	< 0.30	------	393 (ppm)	1.17
Pitt.#8 (650+ °F)						
Acid	80.46	8.06	1.00	8.63	0.24	1.19
Base	81.80	8.87	1.70	7.13	0.58	1.29
Neutral	89.50	10.27	< 0.3	------	219 (ppm)	1.37
Saturate	86.25	11.70	< 0.3	------	------	1.62
Aromatic	90.28	9.14	< 0.3	------	289 (ppm)	1.21

Table IV

Proton NMR Data (atom%) from Saturate and Aromatic Fractions of Distillates from Illinois No. 6, Pittsburgh No. 8 and Black Thunder

Sample	Aromatic	Olefinic	Alpha	Methylene	Methyl
BT (450-650 °F)					
Saturate	0.7	0.8	1.4	69.8	27.4
Aromatic	20.5	0.9	32.9	36.8	8.9
Ill.#6 (450-650 °F)					
Saturate	0.4	0.2	0.6	68.5	30.4
Aromatic	17.2	1.0	33.2	39.3	9.3
Pitt.#8 (450-650 °F)					
Saturate	0.2	0.3	0.9	67.8	30.7
Aromatic	15.6	0.8	32.1	41.4	10.1
BT (650+ °F)					
Saturate	0.3	0.4	0.8	78.0	20.5
Aromatic	29.3	1.2	30.2	32.5	6.9
Ill.#6 (650+ °F)					
Saturate	0.8	0.6	1.7	71.2	25.8
Aromatic	21.5	0.8	30.3	37.9	9.5
Pitt.#8 (650+ °F)					
Saturate	0.3	0.4	1.3	71.7	26.3
Aromatic	20.1	0.8	29.8	39.0	10.3

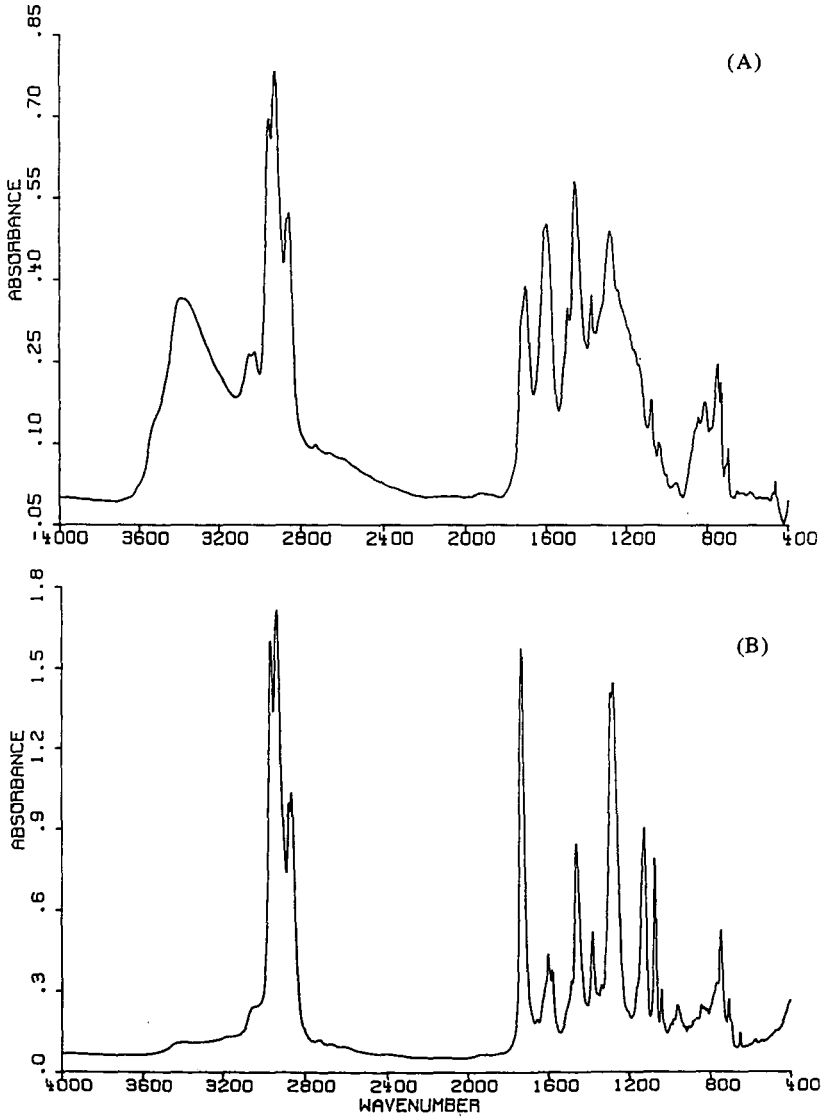

Figure 1. FTIR Spectra of Acid (A) and Base (B) Fractions from 650+ °F Distillate cut of Black Thunder Coal Liquid.

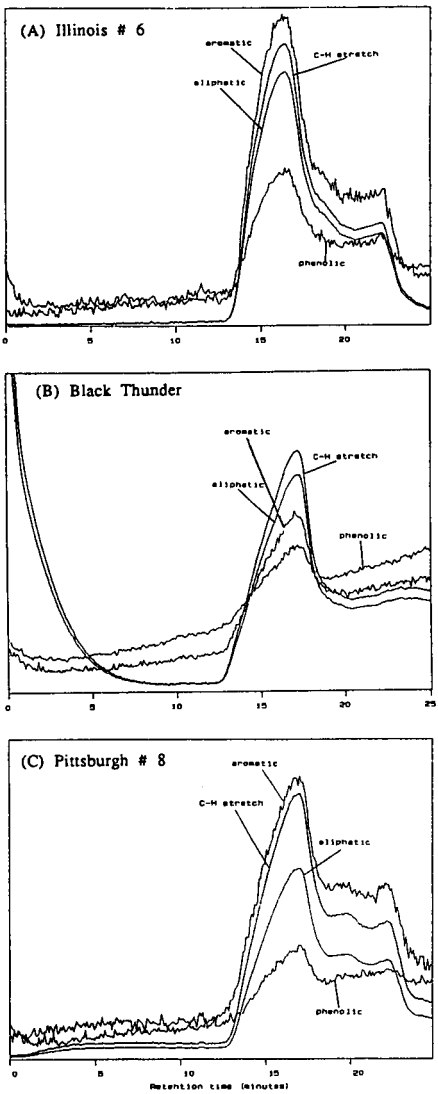

Figure 2. Stack Plots of Selected Bands from TGA-FTIR Spectra of Neutrals from 450-650 °F Distillates of Coal Liquids.

COMPOSITIONAL DIFFERENCES IN NAPHTHA DERIVED FROM NON-CONVENTIONAL FOSSIL FUELS

Robert A. Keogh, Buchang Shi, Shuh-Jeng Liaw, Arthur Fort and Burtron H. Davis

Center for Applied Energy Research
University of Kentucky
3572 Iron Works Pike
Lexington, KY 40511-8433

Keywords: naphtha, heteroatoms, hydrocarbons

INTRODUCTION

Naphtha derived from non-conventional fossil fuel feedstocks- that is, coal, bitumen, and shale - have the potential to augment the supply of naphtha obtained from petroleum feedstocks. To obtain transportation fuels which meet the current and future environmental regulations, these naphtha will have to be further upgraded. A number of studies suggest that more severe conditions (1-5) are required to obtain suitable heteroatom removal to meet current catalyst requirements both in reforming and hydrotreating.

A number of the studies report on the bulk properties of the naphtha feedstocks and products (elemental analysis, boiling point distributions, etc.). A detailed compositional analysis of the heteroatom and hydrocarbon distribution of the naphtha may offer potential explanations for the severe conditions required and be an important initial step in planning future catalyst formulations for upgrading strategies. These later analyses are not usually reported, at least in significant detail.

EXPERIMENTAL

Samples of naphtha were obtained from the catalytic processing of a western Kentucky tar sand bitumen and for the coprocessing of the bitumen with a Western Kentucky #9 coal in the CAER 1/8 tpd pilot plant. Details of the run and syncrude distillation to obtain the naphtha (IBP-400°F) samples are given elsewhere (6).

Naphtha samples (IBP-380°F) derived from processing an Illinois #6 (bituminous coal) and Black Thunder (subbituminous coal) were obtained from the Wilsonville, Alabama Advanced Integrated Two Stage Liquefaction facility. A light shale oil derived from processing a Cleveland shale (eastern shale) in the CAER Kentort II pilot plant was also included for comparison. Details of the process are given elsewhere (7).

The as-received samples were analyzed by gas chromatography using an HP 5890 series II instrument with a DB-5 column (60m x .32mm; .25μm film thickness). Sulfur compounds were analyzed using a Sievers Model 350B chemiluminescence sulfur detector coupled with an HP 5890 Series II gas chromatograph containing a SPB-1 column (30m x .32mm; 4.0μm film thickness).

Identification of the hydrocarbons was done by GC/MS and injection of standard compounds. Identification of the nitrogen and sulfur compounds was accomplished by injection of standard compounds. However, the lack of commercially available alkyl

substituted thiophenes and benzothiophenes prevented a number of peaks in the sulfur chromatogram to be identified using this method. From the retention times obtained from the injection of the available standards and current literature (8), it was possible to separate the sulfur chromatogram into classes of sulfur compounds such as thiophenes and benzothiophenes for comparison.

The elemental analyses of the samples are given in Table 1. Carbon, hydrogen, nitrogen and sulfur were obtained using standard methods. Oxygen was determined for the bitumen, coprocessing and coal-derived naphtha by FNAA. The oxygen content of the shale oil was determined by difference.

RESULTS AND DISCUSSION

A. Hydrocarbon Distribution. The major hydrocarbon classes in the two naphtha samples from Wilsonville are shown in Figure 1. Compounds which are present in greater than .5 wt.% of the total FID chromatogram were identified by GC/MS. The only heteroatom compounds which had a sufficient response in the FID chromatogram are the phenols and these are included in Figure 1 for comparison. Using these guidelines, 65.5 wt.% (Illinois #6 naphtha) and 53.5 wt.% (Black Thunder naphtha) of total areas were identified in the chromatograms.

The major class of hydrocarbons in both coal-derived naphtha samples are cyclohexanes. This class of hydrocarbons includes cyclohexane and one carbon to four carbon substituted cyclohexanes. Methylcyclohexane is the major component in this class for the Illinois #6 derived naphtha. The 2-carbon substituted cyclohexanes are the major components in the Black Thunder derived naphtha. The Illinois #6 naphtha contains higher concentrations of all the cyclohexanes when compared to the Black Thunder naphtha, and this accounts for the overall higher concentration of the cyclohexanes in the Illinois #6 naphtha.

The Illinois #6 naphtha also contains a higher concentration of cyclopentanes than the Black Thunder naphtha. This hydrocarbon class includes cyclopentane and one to three carbon cyclopentanes. The Illinois #6 naphtha contains higher concentrations of all cyclopentanes identified; however, the differences in concentrations of the cyclopentanes in the two naphtha samples are smaller than is observed for the cyclohexanes.

An additional difference in the hydrocarbon distribution is the amount of alkanes, both normal and branched, in these naphtha samples. The Illinois #6 naphtha has significantly more branched and normal alkanes than the Black Thunder naphtha. The normal alkane distributions in both naphtha samples are in the C_4 to C_{12} range.

The hydrocarbon distribution of the naphtha samples derived from catalytically processing a western Kentucky tar sand bitumen and from the catalytic coprocessing the bitumen with a Western Kentucky #9 coal is shown in Figure 2. The major differences in the compositions between the two naphtha samples are in the yields of normal alkanes and aromatics. Coprocessing the bitumen with the coal produced a naphtha with slightly lower amounts of normal alkanes and aromatics when compared to the naphtha produced from processing the bitumen alone using the same process conditions, catalyst, etc. (6). The carbon number distribution of the normal alkanes ranges from C_6 to C_{12} in both naphtha samples. The carbon number distributions in the branched alkanes are the same for both

naphtha samples and range from C_7 to C_{13}. The major class of branched alkanes are also the same for both naphtha samples, and are the C_{10} branched alkanes.

A comparison of the naphtha samples from the coal liquefaction process (Figure 1) and the naphtha samples shown in Figure 2 indicate major differences in the hydrocarbon distributions. The bitumen and coprocessing naphtha samples have a significantly higher amount of alkanes, both normal and branched, and aromatics when compared to the coal liquefaction naphtha samples. Another major difference is in the cycloalkane distributions. The naphtha samples derived during the processing of the bitumen and bitumen plus coal have more alkyl substitutions than the naphtha samples derived from the coal liquefaction process. Five carbon substituted cyclopentanes and cyclohexanes were identified in these two naphtha samples. The coal liquefaction derived naphtha samples have a maximum carbon number of 4 as alkyl substituents.

The hydrocarbon distribution of a distillate sample derived from retorting an eastern shale (Cleveland member) in the Kentort II process (7) is shown in Figure 3. In addition to the hydrocarbons, oxygen and sulfur compounds are in sufficient concentrations to have a response in the FID detector and are included for comparison. The hydrocarbon distribution for processing the shale is distinctly different from the distillates described previously. The major class of hydrocarbons were aromatics (24.4 wt.%), normal alkanes (12.4 wt.5) and olefins (0.3 wt.%). Olefins are only detected in the shale-derived distillate and included a small amount of cyclo-olefins. In addition to the presence of olefins, the major composition difference between the shale derived distillate and the previously described naphtha samples is the low yield of cycloalkanes.

B. Nitrogen Compounds. The nitrogen compound class distributions of this sample set are shown in Figure 4. Identification of the nitrogen compound is made using available standard compounds and the thermionic detector (TSD) as described in the experimental section. The concentrations of the nitrogen compound classes are given in area percent of the total area in the TSD chromatogram.

The major nitrogen class in the Illinois #6 and Black Thunder naphtha samples and the bitumen and coprocessing naphtha samples are the anilines. The anilines include aniline and 1 to 4 carbon alkyl substituted anilines. The 1 carbon substituted anilines are the most abundant compounds in this nitrogen class in the Illinois #6 naphtha. The 2 carbon substituted anilines are the most abundant compounds in this class for the other samples in this study.

The pyridines and quinolines are the next most abundant nitrogen classes of compounds identified in the Illinois #6, Black Thunder, bitumen and coprocessing derived samples. The 1 carbon pyridines are the most abundant compounds in this class in the Illinois #6 and Black Thunder naphtha samples. The 2 carbon substituted pyridines are the compounds with the highest concentration in this class for the bitumen derived naphtha and pyridine is the abundant compound found in this class in the coprocessing derived naphtha.

Quinoline and tetrahydroquinoline have the highest concentrations in this compound class in the Illinois #6, Black Thunder, bitumen and coprocessing samples. One and 2 carbon quinolines were identified in the Black Thunder and Illinois #6 naphtha samples. Substituted quinolines were not detected in the bitumen and coprocessing derived samples.

The distribution of nitrogen compounds in the shale derived distillate are significantly different. The number of compounds represented in the TSD chromatogram are larger than those of the other samples and only 26% of the compounds are identified at this time. The data indicate that the amounts of the pyridine, anilines and quinolines in this distillate are similar. The number of alkyl substitutions are similar to those discussed above.

C. Sulfur Compounds. The sulfur classes of the naphtha samples are shown in Figure 5. The major components identified using the Sievers CSD detector are thiophenes and benzothiophenes. Small concentrations of thiols and sulfides were also identified. The thiophene and benzothiophene classes are characterized by 1 to 3 carbon substitutions and their concentrations depend on their source.

SUMMARY

The hydrocarbon and heteroatom compositions of naphtha samples from non-conventional fossil fuels are reported. This on-going project should provide a well characterized set of samples for future research in hydrotreating and reforming of non-conventional fossil fuels.

ACKNOWLEDGMENT

This work was supported by the DOE contract #De-AC22-90PC90049 and the Commonwealth of Kentucky. The authors also acknowledge the personnel at the Wilsonville liquefaction facility for providing the naphtha samples and for their helpful advice.

REFERENCES

1. L. Xu, R. A. Keogh, C. Huang, R. L. Spicer, D. E. Sparks, S. Lambert, G. A. Thomas, and B. H. Davis, *Prep. - Am. Chem. Soc., Div. Fuel Chem.*, **36 (4)**, 1909 (1991).
2. R. J. Parker, P. Mohammed, and J. Wilson, *Prep. - Am. Chem. Soc., Div. Fuel Chem.*, **33 (1)**, 135 (1988).
3. U. R. Gaeser, R. Holighaus, K. D. Dohms, and J. Langhoff, *Prep. - Am. Chem. Soc., Div. Fuel Chem.*, **33 (1)**, 339 (1988).
4. V. E. Smith, C. Y. Cha, N. W. Merriam, J. Faky, and F. Guffy, Proceedings of the Third Annual Oil Shale, Tar Sand and Mild Gasification Contractors Review Meeting, 166, 1988.
5. H. Frumkin, R. F. Sullivan, and B. E. Strangeland, in "Upgrading Coal Liquids", (R. F. Sullivan, ed.), ACS Symp. Series 156, American Chemical Society, Washington, DC, 1981, pg. 75.
6. R. J. Medina, R. A. Keogh, W. P. Barnett, D. E. Sparks, R. L. Spicer, and B. H. Davis, *Fuel Proc. Tech.*, **27 (2)**, 161 (1991).
7. D. N. Taulbee and S. D. Carter, *Fuel*, **70**, 1245 (1991).
8. B. Chawla and F. J. Di Sanzo, *J. Chromatogr.*, **589 (1-2)**, 271 (1992).

Table 1

Elemental Analysis of Samples

	Wilsonville Samples		CAER PIPU Samples		Kentort II Eastern Shale Liquid
	Bituminous	Subbituminous	Bitumen	Coprocessing	
C (Wt.%)	86.19	85.34	85.20	84.81	84.58
H (Wt.%)	13.34	12.25	13.66	13.54	11.84
N (Wt.%)	.07	.35	.48	.41	.40
S (Wt.%)	.05	.05	.37	.29	1.79
O (Wt.%)[1]	.35	2.01	.29	.95	1.39

[1] Oxygen determined by FNAA for all samples except the shale liquid. This oxygen content was determined by difference.

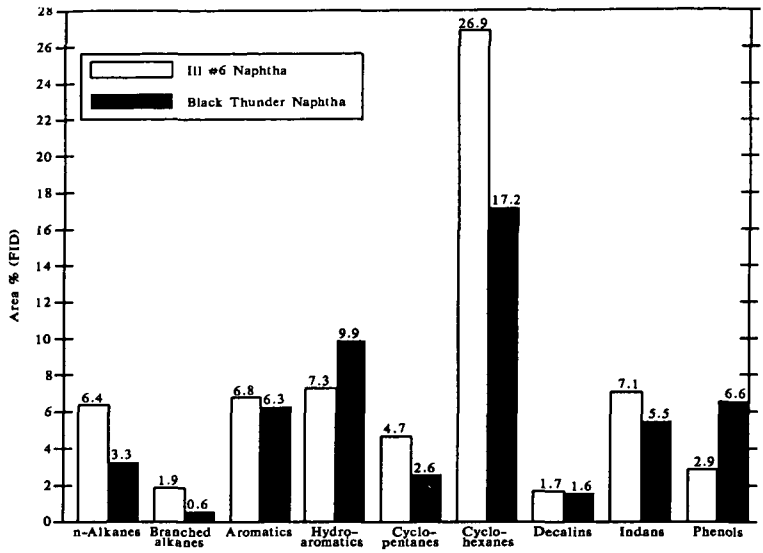

Figure 1. Analysis of Wilsonville naphtha derived from a bituminous and subbituminous coal.

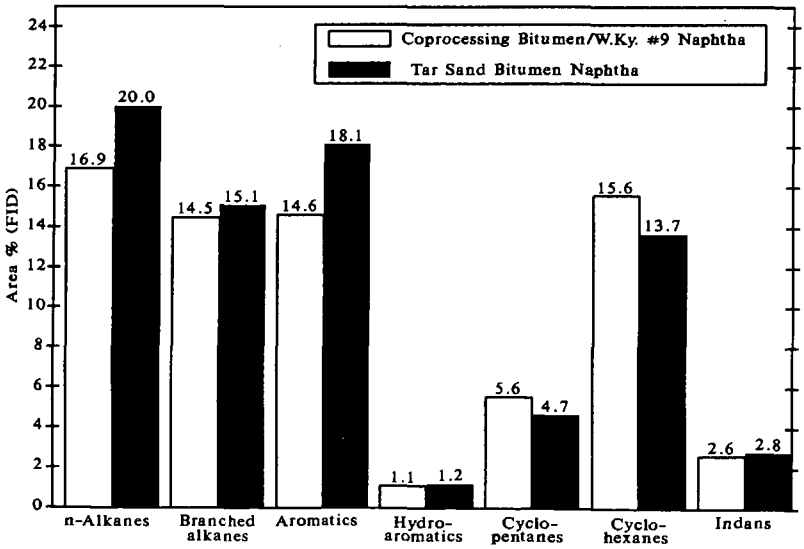

Figure 2. Analysis of naphtha derived from catalytic processing of tar sand bitumen and coprocessing bitumen and a W.Ky. #9 coal.

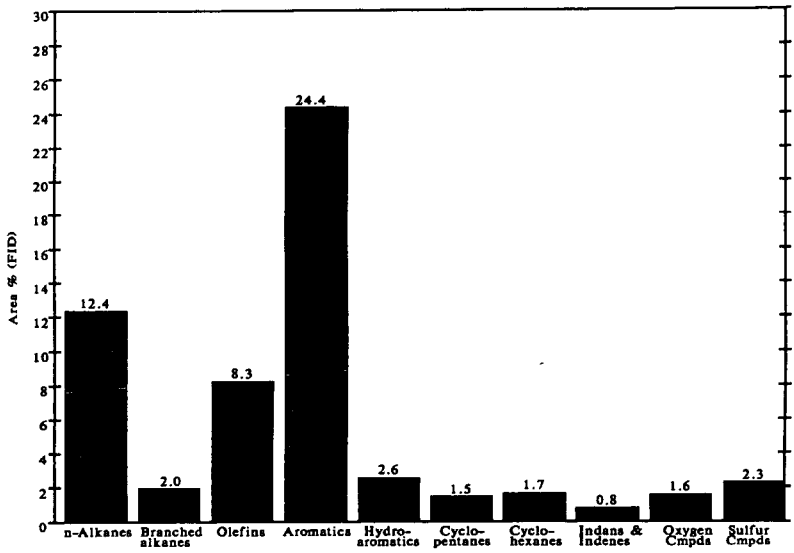

Figure 3. Analysis of a shale derived distillate sample from the Kentort II process.

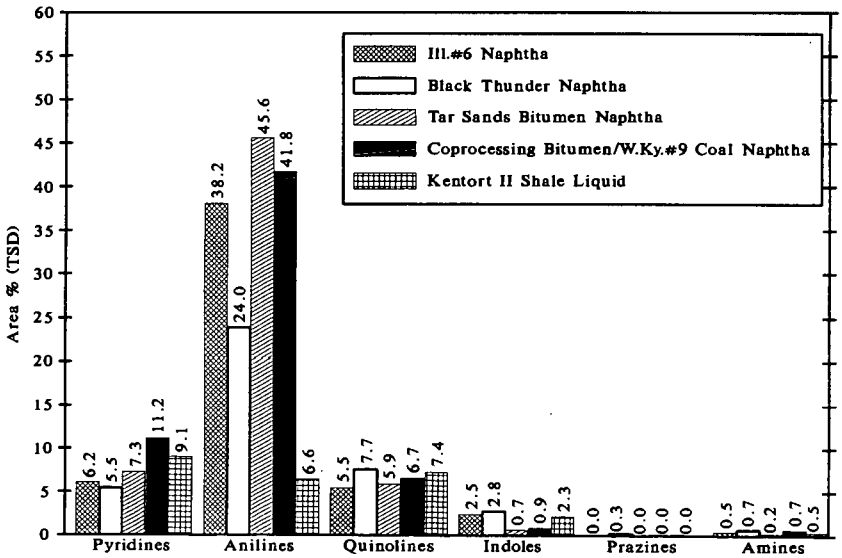

Figure 4. Nitrogen compound class distribution in the sample set.

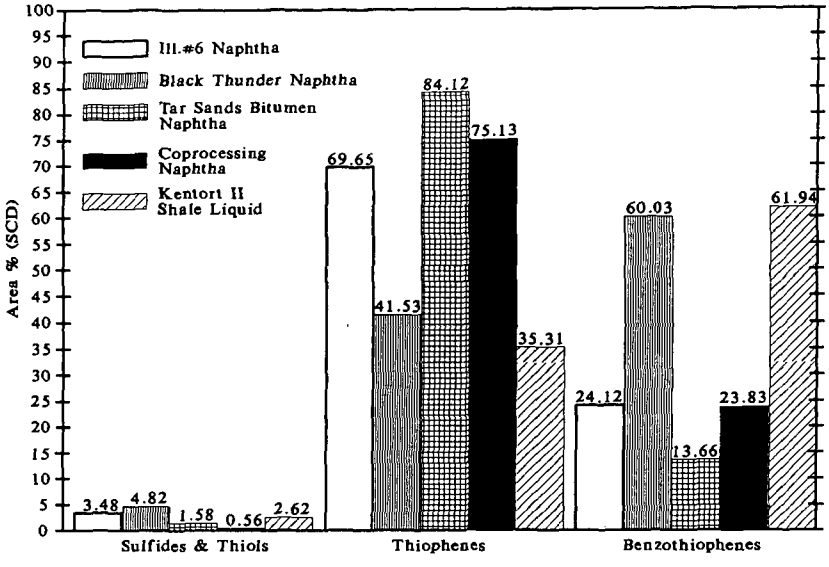

Figure 5. Sulfur compound class distribution in sample set.

ISOBUTENE FROM ISOBUTANOL/METHANOL MIXTURES OVER INORGANIC ACID CATALYSTS

Owen C. Feeley, Marie A. Johansson, Richard G. Herman, and Kamil Klier

Zettlemoyer Center for Surface Studies and
Department of Chemistry, S.G. Mudd #6
Lehigh University, Bethlehem, PA 18015

Keywords: Isobutene, isobutanol, methanol, oxygenates, acid catalysts

INTRODUCTION

The increasing demand for octane boosting oxygenate compounds, particularly methyl tertiarybutyl ether (MTBE), has led to research efforts investigating alternative sources of these valuable compounds. Currently, MTBE is manufactured from methanol and isobutene *via* a liquid phase synthesis over acid resin catalysts, where isobutene is obtained as a side product from petroleum refinery FCC units (1-3). Although older FCC units can produce 8 wt% C_4 products in their output (4), the typical FCC refinery product slate now contains 1.4 wt% C_4 compounds (5), and improved processes utilizing catalytic additives such as improved ZSM-5 tend to decrease the yield of C_3 and C_4 olefins in the light ends further still (6). Thermal cracking of the isobutane in the light ends can also be carried out to obtain isobutene (5). In any case, the supply of refinery supplied isobutene is limited.

Since MTBE is now the seventh largest produced synthetic organic chemical today (7) and has also been the fastest growing catalytic process during the last decade, a ready supply of both methanol and isobutene is needed. Indeed, it has been predicted that due to continuing and increasing clean air restrictions, the demand for oxygenates (ethers and alcohols) in fuels could increase more than 10-fold by the year 2001 (8). Various alternatives have been sought for increasing the availability of isobutene, and one source of C_4 is butane from natural gas. Although, the butane content in natural gas is low, this source of C_4 is increasingly gaining importance. Among the processes that have been developed for the synthesis of pure isobutene is the endothermic dehydration of tertiary butanol (9).

Another possible source of isobutene for ether synthesis is isobutanol that is produced from synthesis gas. Methanol and isobutanol are the predominant products formed from H_2/CO synthesis gas over alkali promoted Cu/ZnO-based catalysts (10-14). Since the two alcohols are produced together, direct coupling of these two alcohols to produce high octane ethers is also of interest. It has been shown (15,16) that over acid catalysts, the dominant reaction is direct coupling that results in the formation of methyl isobutyl ether (MIBE), a lower octane (17) isomer of MTBE. In addition to ethers, butenes were also observed, and these tended to become more abundant products over inorganic catalysts that were employed at higher temperatures than were the resin catalysts (16).

If a selective catalyst were found for converting isobutanol to isobutene with subsequent reaction with methanol, a desirable route to high octane MTBE from natural gas or coal-derived synthesis gas would be provided, as represented by Equations 1 and 2.

$$(CH_3)_2CHCH_2OH \rightarrow (CH_3)_2C{=}CH_2 + H_2O \quad [1]$$

$$(CH_3)_2C{=}CH_2 + CH_3OH \rightarrow (CH_3)_3C\text{-}O\text{-}CH_3 \quad [2]$$

Such a process would alleviate isobutene dependence on petroleum feedstocks. Over the inorganic catalysts previously studied, it was shown that an equimolar mixture of methanol and isobutanol could be directly converted to a methanol/isobutene mixture in high yields with high selectivity using a sulfate-modified zirconia catalyst (16). This catalyst was found to be superior to other solid acid catalysts such as zeolites, silica-alumina and ion exchange resins. The strongly acidic zeolite H-Mordenite, on the contrary, was found to be highly selective for dehydrating the methanol in the mixture to dimethyl ether (DME) (16). No mixed ether was formed and very little dehydration of isobutanol to isobutene was seen. In the present work, the coupling and dehydration reactions were studied over H-ZSM-5 zeolite and γ-alumina. In addition, the pressure dependence of isobutene formation from an isobutanol/methanol mixture was examined over the ZrO_2/SO_4^{2-} catalyst.

EXPERIMENTAL

The preparation of the sulfate-modified zirconia (ZrO_2/SO_4^{2-}) was carried out according to the work of Hino and Arata (17). $ZrOCl_2{\cdot}8H_2O$ was added to aqueous ammonia to precipitate high surface area $Zr(OH)_4$ that was washed and dried at 100°C overnight. The dried $Zr(OH)_4$ weighing 10 g was placed on a folded filter paper, and 150 ml of 1 N H_2SO_4 was poured through it. The wet powder was dried at 110°C overnight and then calcined at 620 °C for 3 hr. The BET surface area of this catalyst, determined from N_2 adsorption/desorption data, was found to be 60 m^2/g and the sulfur content was 0.84% by weight.

The H-ZSM-5 zeolite (Mobil MZ-289) was calcined in air at 400°C for 2 hr prior to loading in the reactor. The Catapal-B was calcined in air at 500°C for 3 hr in order to activate and convert the pseudoboehmite precursor into the γ-alumina phase.

Operating Conditions. The following standard test conditions were used to study the activity and selectivity of H-ZSM-5 zeolite and γ-alumina:

Temperature	90, 125, 150, 175°C (also 200, 225, 250°C for γ-alumina)
Pressure	1 atm (100 kPa)
Methanol feed	1.72 mol/kg catalyst/hr
Isobutanol feed	1.72 mol/kg catalyst/hr
He (+ N_2 trace) flow	16.0 mol/kg catalyst/hr
Catalyst weight	5.0 g

For determining the pressure dependence of the alcohol dehydration reactions and the ether synthesis reactions over the ZrO_2/SO_4^{2-} catalyst, the gas composition was maintained while the total reaction pressure was sequentially increased. The following reaction conditions were used:

Temperature	157°C
Pressure (total)	1-62 atm (0.1-63 MPa)
Methanol feed	42.2 mol/kg catalyst/hr
Isobutanol feed	21.1 mol/kg catalyst/hr
He (+ N_2 trace) flow	756 mol/kg catalyst/hr
Catalyst weight	2.0 g

RESULTS AND DISCUSSION

Reactions of Methanol/Isobutanol Over H-ZSM-5 Zeolite. The space time yields of the major products obtained over H-ZSM-5 zeolite and γ-alumina from methanol/isobutanol = 1/1 reactants at 1 atm with He(N_2) carrier gas are given in Table 1 for a range of temperatures beginning at 90°C, along with those of two of the other inorganic catalysts, H-mordenite and ZrO_2/SO_4^{2-}, originally reported in previous work (16). The H-ZSM-5 sample was found to be active for isobutanol (i-BuOH) conversion to methylisobutylether (MIBE) and butenes as well as methanol (MeOH) conversion to dimethylether (DME). Of special note is that as the temperature was increased from 125°C to 175°C, the yield of MIBE decreased while the yield of butenes significantly increased. The activation and conversion of i-BuOH over this zeolite catalyst contrasts sharply with that of the H-mordenite studied previously. The H-mordenite sample had been found to be inactive for mixed ether formation from the methanol and isobutanol mixture over the temperature range studied, as shown in Table 1. DME was formed highly selectively and in high yield with only slight conversion of isobutanol, and this was explained in terms of "shape selectivity". Although H-ZSM-5 has smaller pores than H-mordenite, 5.3 x 5.6 Å interconnecting 5.1 x 5.5 Å *vs* 6.5 x 7.0 Å, respectively (19), it is very active for mixed ether formation and butene formation. This shows that the high selectivity toward DME formation observed over H-mordenite is not a general feature of acidic zeolites. This rules out sieving as an explanation for the selectivity pattern seen in H-mordenite. The relative accessibility of the reactants to the zeolitic protons at the low temperatures employed (90-175°C) may be a factor. The intersecting channels of the H-ZSM-5 structure may allow transition state geometries or better access of isobutanol to active sites than the straight non-interconnecting channel system of H-mordenite.

Reactions of Methanol/Isobutanol Over γ-Alumina. The γ-alumina was rather inactive for the conversion of the methanol/isobutanol = 1/1 reactant mixture at the lower reaction temperatures where the other inorganic catalysts were active, and, therefore, higher temperatures (200, 225, and 250°C) were utilized. As seen in Table 1, the selectivity of γ-alumina was unique among the catalysts. The ethers MIBE and DME were selectively formed between 125 and 175°C, while at higher temperatures isobutene formation became more significant. Although not indicated in Table 1, small quantities of iso-octene were also

produced. It is notable that the only butene formed over this γ-alumina was isobutene, whereas for all of the other catalysts under reaction conditions that produce isobutene, significant amounts of the linear butenes, mostly cis- and trans-2-butene, were also produced. The molar fraction of linear butenes to all butenes formed over the inorganic catalysts, excluding γ-alumina, was generally about one third at 150 to 175°C. The quantities of linear butenes observed were below those calculated for thermodynamic equilibrium. Figure 1 shows the equilibrium constant ratios, i.e. ratio of each linear butene to isobutene, as a function of temperature. The selectivity of isobutanol dehydration over γ-alumina has been studied by several workers (20,21), and it was found that isobutene was formed with over 95% selectivity. The pronounced selectivity of the γ-alumina may be explained by the absence of strong Brønsted acid sites on the surface of alumina (22). The γ-alumina surface has been shown to contain Lewis acid sites associated with basic sites (22). It has been proposed that the acidic and basic sites act concertedly to remove, respectively, the OH^- from the alcoholic carbon and an H^+ from the neighboring tertiary carbon of isobutanol. The presence of strong Brønsted acid sites in the other catalysts, both organic and inorganic, has been associated with carbenium ion chemistry, which leads to rearranged products in isobutanol dehydration (23). Thus, the absence of strong Bronsted acidity in γ-alumina may explain the absence of linear butenes in the product.

Pressure Dependence of Ether and Olefin Synthesis Over Sulfated Zirconia. The effect of reactant pressure on the activity and selectivity of the dehydration of a methanol and isobutanol mixture to butenes and ethers was studied. Nunan et al. (15) had previously studied this reaction over the very strongly acidic ion-exchange resin Nafion-H. It was shown that the rate of butene production decreased and the rate of ether production, mostly MIBE and DME, increased with increasing alcohol pressure. Their kinetic studies indicated that over Nafion-H, dehydration of isobutanol to isobutene required two acid sites. As a consequence, at higher pressures isobutanol inhibited its own dehydration. In studying the pressure dependence of these reactions over ZrO_2/SO_4^{2-}, the reaction conditions chosen in the present study are similar to those of Nunan et al. (15), and conversions were kept well below 10%.

The space time yields of the products of the reaction of methanol and isobutanol over ZrO_2/SO_4^{2-} are presented in Figure 2 as a function of alcohol pressure. Isobutene production decreased strongly with increasing pressure and ether production increased somewhat with increasing pressure. These results are similar to those observed with the Nafion-H resin catalyst (15), and this suggests that the same catalytic functions and properties are occurring on ZrO_2/SO_4^{2-} as were found for Nafion-H. The effect of pressure was reversible, i.e. when alcohol pressure was decreased to its original value, isobutene production increased and ether production decreased to their original rates. Even with the ratio of methanol to isobutanol of 2/1, it is clear that at low pressures isobutanol is selectively dehydrated to isobutene with little conversion of methanol to DME or MIBE.

It is apparent from Figure 2 that the reaction pressure hardly affected the yields of the ethers but that low pressures were needed to maximize the selective dehydration of isobutanol to isobutene. It is also evident from Figure 1 that low temperatures are needed when pathways exist (*via* carbenium ion chemistry with Brønsted acids) for the formation

of linear butenes in order to minimize the linear butenes and maximize the proportion of isobutene in the product stream.

CONCLUSIONS

A route to the precursors of MTBE, *viz.* methanol and isobutene, from the products of higher alcohol synthesis from synthesis gas over alkali-promoted Cu/ZnO catalysts, i.e. methanol and isobutanol, can be made in one step *via* selectively dehydrating isobutanol in the alcohol mixture to isobutene over a sulfate modified zirconia, ZrO_2/SO_4^{2-}, catalyst at moderate temperatures and pressures (e.g. selectivity was ≈88% at 157°C with methanol/isobutanol = 2/1 under the reaction conditions in Figure 2 and 89% at 175°C with methanol/isobutanol = 1/1 under the conditions in Table 1). On the other hand, the H-ZSM-5 zeolite displayed a selectivity toward isobutene plus linear butenes of 77% at 175°C under the reaction conditions given in Table 1, and the selectivity of γ-alumina toward isobutene, with no detectable linear butenes, was 53% at 250°C. In contrast, H-mordenite selectively produced DME from the methanol/isobutanol mixture.

ACKNOWLEDGEMENT

This research was supported by the U.S. Department of Energy (PETC) contract DE-AC22-90PC90044.

REFERENCES

1. Chase, J. D. and Galvez, B. B., Hydrocarbon Process., **60(3)**, 89 (1981).

2. Chase, J. D., in "*Catalytic Conversions of Synthesis Gas and Alcohols to Chemicals*," ed. by R. G. Herman, Plenum Press, New York, 307 (1984).

3. Hydrocarbon Process., **68(11)**, 96 (1989); and Satterfield, C. N., "*Heterogeneous Catalysis in Industrial Practice*," 2nd Ed., McGraw-Hill, Inc., New York, 260 (1991).

4. Haggin, J., Chem. Eng. News, **67(23)**, 31 (1989).

5. Monfils, J. L., Barendregt, S., Kapur, S. K., and Woerde, H. M., Hydrocarbon Process., 71(2), 47 (1992).

6. Krishna, A. S., Hsieh, C. R., English, A. R., Pecoraro, T. A., and Kuehler, C. W., Hydrocarbon Process., 70(11), 59 (1991).

7. Chem. Eng. News, **70(15)**, 17 (1992).

8. Chem. Eng. News, **70(19)**, 26 (1992).

9. Abraham, O. C. and Prescott, G. F., Hydrocarbon Process., 71(2), 51 (1992).

10. Klier, K., Herman, R. G., and Young, C.-W., Preprint, Div. Fuel Chem., ACS, 29(5), 273 (1984).

11. Klier, K., Herman, R. G., Nunan, J. G., Smith, K. J., Bogdan, C. E., Young, C.-W., and Santiesteban, J. G., in "*Methane Conversion*," ed. by D. M. Bibby, C. D. Chang, R. F. Howe, and S. Yurchak, Elsevier, Amsterdam, 109 (1988).

12. Nunan, J. G., Bogdan, C. E., Klier, K., Smith, K. J., Young, C.-W., and Herman, R. G., J. Catal., 116, 195 (1989).

13. Nunan, J. G., Herman, R. G., and Klier, K., J. Catal., 116, 222 (1989).

14. Herman, R. G., in "*New Trends in CO Activation*," ed. by L. Guczi, Elsevier, Amsterdan, 265 (1991).

15. Nunan, J. G., Klier, K., and Herman, R. G., J. Chem. Soc., Chem. Commun., 676 (1985).

16. Klier, K., Herman, R. G., Johansson, M. A., and Feeley, O. C., Preprint, Div. Fuel Chem., ACS, 37(1), 236 (1992).

17. Spindelbalker, C. and Schmidt, A., Erdoel, Erdgas, Kohle, 102, 469 (1986).

18. Hino, M. and Arata, K., J. Chem. Soc., Chem. Commun., 851 (1980).

19. Meier, W. M. and Olson, D. H., "*Atlas of Zeolite Structure Types*," Butterworths & Co. Ltd., Cambridge, 102 (1988).

20. Knozinger, H. and Scheglila, A., J. Catal., 17, 252 (1969).

21. Herling, J. and Pines, H., Chem. & Ind., 984 (1963).

22. Peri, J. B., J. Phys. Chem., 69, 231 (1965).

23. Kotsarenko, S. and Malysheva, L. V., Kinet. Katal., 24, 877 (1983).

TABLE 1. Yields over Inorganic Catalysts (mol/kg cat/hr)

Pressure	1 atm
Methanol feed	1.72 mol/kg catalyst/hr
Isobutanol feed	1.72 mol/kg catalyst/hr
He + N_2 flow	16.0 mol/kg catalyst/hr
Catalyst weight	5.0 g

	$T_{Reaction}$	DME	Butenes	MIBE	MTBE	C_8 ether
H-Mordenite *	90°C	0.060	-----	-----	-----	-----
	125°C	0.660	-----	-----	-----	-----
	150°C	0.830	0.068	-----	-----	0.004
ZrO_2/SO_4^{2-} *	90°C	-----	-----	0.003	-----	-----
	125°C	0.006	0.067	0.020	0.003	0.008
	150°C	0.027	0.696	0.068	0.009	0.017
	175°C	0.103	1.29	0.049	0.007	-----
H-ZSM-5	90°C	0.005	0.001	0.012	-----	-----
	125°C	0.071	0.169	0.350	0.004	0.003
	150°C	0.261	0.339	0.134	0.003	0.003
	175°C	0.185	1.086	0.131	0.005	0.002
γ-Alumina	90°C	-----	-----	-----	-----	-----
	125°C	0.006	-----	0.007	-----	-----
	150°C	0.035	-----	0.038	-----	-----
	175°C	0.118	0.002	0.160	-----	-----
	200°C	0.253	0.023	0.450	-----	-----
	225°C	0.342	0.242	0.831	-----	-----
	250°C	0.470	1.073	0.493	-----	-----

* Reference 16.

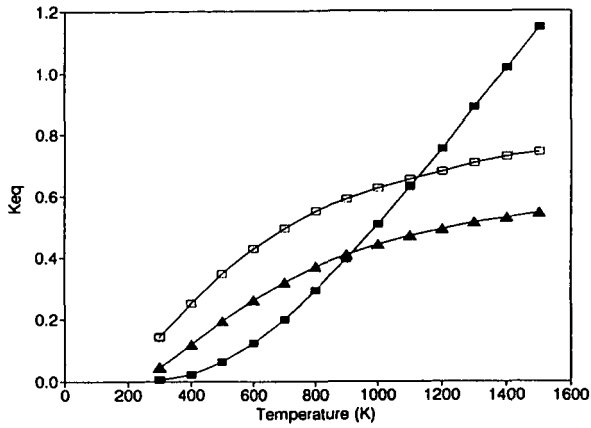

FIGURE 1. The dependence of the calculated equilibrium constants, i.e. mole ratio of linear butenes to isobutene, on the reaction temperature for the conversion of isobutene into 1-butene (■), cis-2-butene (▲), and trans-2-butene (□), beginning at STP conditions.

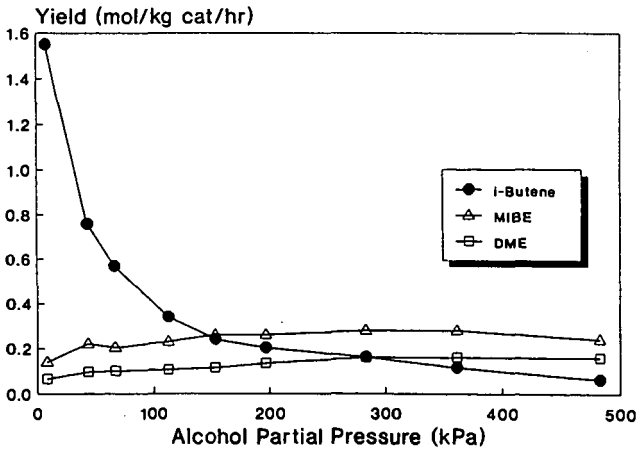

FIGURE 2. Variations of the product yields with the total alcohol partial pressure (methanol/isobutanol = 2/1) over the ZrO_2/SO_4^{2-} catalyst at 157°C. The reaction conditions are described in the Experimental Section.

ACCEPTABILITY OF ALCOHOLS AS GASOLINE SUBSTITUTES

R G Temple and S J Sidhu
Department of Chemical Engineering & Applied Chemistry
Aston University, Birmingham B4 7ET, U.K.

Keywords: Alternative Fuels, Alcohols, Corrosion.

Automobile engines and their fuel systems were developed to use gasoline and their design has been progressively improved for that specific mixture of hydrocarbon fuels. Minor variations in design may render one engine more suitable for "regular" grade (92 RON) fuel while another may be able to use 98 octane fuel to a higher efficiency, but most vehicle owners wish to take advantage of their own preference at the filling station so that one versatile design of engine is required.

The introduction of alcohols (or other oxygenates) presents a range of new properties which may affect engine performance in various ways. Significant differences in volatility, calorific value and latent heat of vapourisation indicate the need for some major adjustments in engine and fuel system dimensions and design for engines which are to use 100% alcohol fuels.

However, there is much to gain by the use of gasohol mixtures since redesign of the internal combustion engine can then proceed by incremental changes rather than a "step change" of unacceptable magnitude. In a large population it is not easy to introduce new fuels unless and in so far as they can be used with minor adjustments only. e.g. to carburettor needle valves or idling controls, etc.

The research described in this paper studied the extent to which alcohols may be substituted without major alterations and especially their acceptability with regard to possible corrosive or deleterious effects on engine and fuel system materials.

Oxidation and corrosion test procedures

Test procedures were designed to simulate actual conditions during engine operation. Small samples of metal or carburettor parts etc., were totally immersed in the test fuel for periods of upto many weeks. While many tests were carried out at ambient temperatures, some higher temperature tests (50°C, 65°C, 90°C) were studied. In all cases periodic aeration of the test fuel reservoir (15 minutes each four hour period) was instigated in order to simulate actual conditions which would obtain in engine operation. Prior to the tests, specimens were ultrasonically cleaned in acetone and similarly cleaned before subsequent weighing and examination.

Corrosion and Oxidation

Corrosion of metals will usually proceed through the formation of an oxide layer on the accessible surface. If this layer is discontinuous as for example in the rusting of iron then corrosion proceeds steadily "eating" into the original material depth. However, if a continuous oxide film results as with some non-ferrous metals then,as oxidation progresses, flakes of oxide layers will detach themselves from the metal surface leaving new accessible surface. In general oxidation follows three courses. Most equations which explain the transient growth at lower temperatures involve logarithmic or exponential terms. They are grouped together as the log laws. At higher temperatures the oxide thickening obeys a parabolic law. This pattern involves a greater risk of flaking or cracking (Fig.1).

Depending on the temperature and time a metal-oxygen system may follow any one of the above curves. A material which thickens by the parabolic law is accepted as reasonably resistant. However, there is a higher risk of cracking and flaking. If, in contrast the oxidation process follows the log laws then oxidation will almost reach a stand still at a small oxidation thickness. Component designers must therefore seek a material which thickens according to a favourable growth law. Alloying materials can often be found which though not altering the growth law will vary the rate of growth. In some cases the alloying constituent may introduce a new phase at the base of the oxide layer and then the effect of the alloy may give rise to a log law. To some extent the oxidation pattern may then be more predictable. At lower temperatures, as in this work, mechanical separation of the oxide layer may be greatly delayed, at least for a considerable time until a critical thickness is reached. The growth pattern may be altered so that a parabolic thickening at one temperature range may be replaced by rectilinear growth at higher temperatures. Material selection is thus founded on a range of complex ambient influences.

In the case of carburettor components, temperature variation is naturally restricted to liquid phase fuel temperatures and thus growth law prediction is simplified.

Corrosion in engine fuel systems

Corrosion and oxidation rates will be governed by several variables which in engine fuel systems will be dependent on ambient conditions, driving modes, and several design features. Oxidant concentration (in blends) will usually increase corrosion rate. Increased temperatures will also normally increase corrosion rates except where the increased temperature reduces oxygen content of the blend. Acidity (pH value) of the liquid corrodant is a crucial factor determining the likelihood and/or extent of corrosion. Since the oxidation products of alcohols and other oxygenates are carboxylic or other acids, the "strength" of the acid resulting from oxidation is of prime importance. Aeration, resulting in greater access to oxygen, will normally accelerate corrosion/oxidation effects unless the metal or material surface is passive. Flow velocity effects may be significant if corrosion reactions are "diffusion-controlled". Increased velocity will ensure a plentiful supply of fresh ions and will remove corrosion/oxidation products which otherwise would be potentially inhibiting.

In the case of vehicle engines, corrosion/oxidation rates may be of less direct significance than flaking or spalling and consequent weight loss effects. Thus, in this work we placed greater emphasis on any weight loss or gain resulting from corrosion. Samples were treated in significantly lengthy experiments being periodically removed from the test fuel reservoir for weighing. In this way a progressive weight gain and loss profile gave a more or less quantitative indication of corrosion and spalling effects. Figures 2 and 3 are typical of such measurements.

As a further indicator of potential corrosive attack, electrical conductivity of the substitute fuels and of gasohol blends was measured. Methanol (and its blends with gasoline) was shown to be more electrically conductive than ethanol. Some correlation with greater corrosion by methanol was found but other factors contributed significantly, masking this effect.

Vulnerability of metals to alcohols

A longer term study of a greater range of metals and alloys would be needed to identify the most resistant material for use with alcohols in fuel systems. However this work provided some clear indication of which metals might be the most vulnerable in the longer term.

The brasses for example showed greater surface damage in methanol than ethanol but their general resistance to spalling or weight loss indicated that brass components would be satisfactory at elevated temperatures and with aeration. Higher temperature accelerates acid formation in the alcohols giving rise to more severe attack on some metal surfaces. Copper surfaces for instance are highly vulnerable to pitting when in contact with formic acid in methanol. Aluminium is also severely attacked by methanol although the presence of formic acid shows little added effect.

Stainless steel components in methanol (with or without acid) are largely unaffected but this material would be too costly for many components and does not lend itself to simple fabrication techniques as do the "softer" non-ferrous metals copper, zinc, aluminium and their alloys.

Zinc carburettor components showed greater surface damage in methanol than ethanol as judged by the dulling in appearance. This can be related back to the fact that methanol is more electrically conductive than ethanol. However, zinc or zinc-plated components would be much better than aluminium for use with the oxygenates. Copper can be used in the carburettor but care must be taken since this metal can yield large amounts of oxide in the presence of methanol with consequent danger to needle valves and generally inefficient fuel metering.

Conclusions

Our results point the may to material selection for the next generation of carburettors. However, existing materials were not shown to be in imminent danger of corrosive collapse after use of oxygenates. These corrosion studies were carried out in parallel with wide ranging studies of oxygenate fuel performance in a Fiat 127 903cc engine. Visual inspection of the carburettor on this engine after 3-4 years of use with oxygenates and with oxygenate/gasoline blends showing that some pitting of the carburettor had occurred. It is difficult to predict the useful life of carburettor components under these circumstances but this could reasonably be estimated to be several years. It must also be noted that carburettors have until now been largely designed for use with hydrocarbon fuels. As oxygenates begin to feature more prominently as potential alternatives, carburettor design will almost certainly change to use more resistant materials.

Furthermore many of the existing carburettor materials might be retained if some form of inexpensive protective coating were used. These may include polymeric or metallic coating on entire surfaces such as the carburettor body or inlet ducts etc., or on specific vulnerable areas such as the point of a needle valve.

In many countries of the world a finite percentage of alcohol is already used as an extender and to enhance resources of motor fuels. Research studies of this type provide clear indications of where engine designers must seek alternative construction materials for some components.

References

1. Sidhu, J. S., "The Acceptability of Alcohol Fuels for Automobile Engines", Ph.D. Thesis, Aston University, U.K. (1988).

2. Evans, U. R.,"The Corrosion and Oxidation of Metals: Scientific principles and practical applications", Edward Arnold Publishers Ltd., London (1976).

Figure 1. Main Types of Growth Laws (2.)

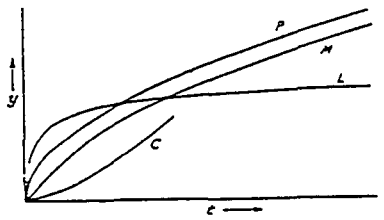

P - simple parabolic
M - mixed paraboilc
L - log laws
C - concave upwards

FIG: 2 THE OXIDATION AND CORROSION OF ZINC IN METHANOL/GASOLINE BLENDS AT 50 C

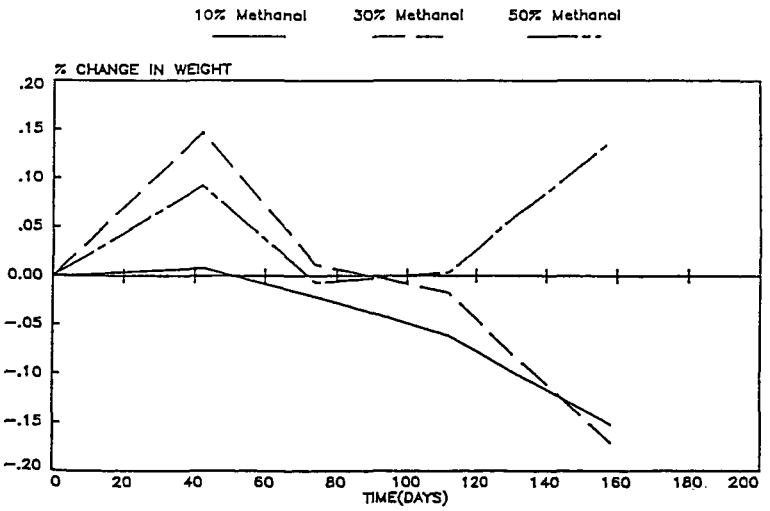

FIG: 3. EFFECT OF TEMPERATURE AND FORMIC ACID ON OXIDATION AND CORROSION OF ALUMINIUM IN METHANOL

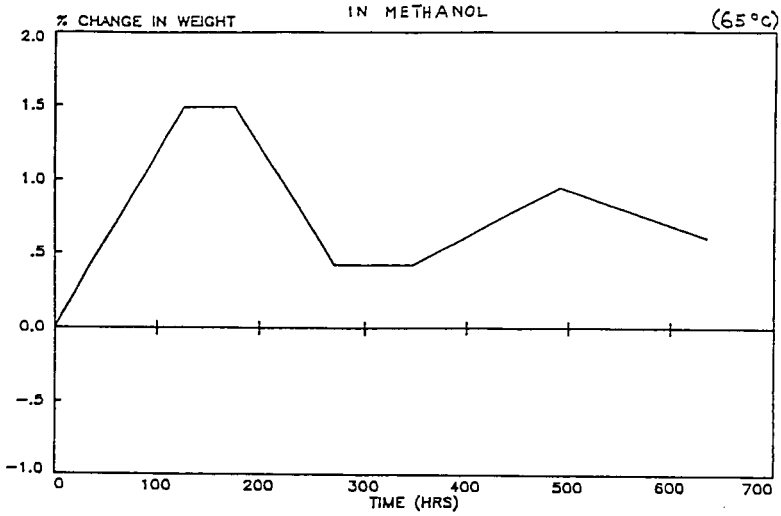

ALCOHOLS AND OTHER OXYGENATES AS MOTOR FUELS

R G Temple and N R Gribble
Aston University, Birmingham, UK

Keywords: Alcohols, oxygenates, alternative motor fuels

Alcohols and other low molecular weight oxygenates are known to be potentially valuable gasoline substitutes. While these are generally of interest in relation to the long-term need to secure future motor fuel supplies, there is a more urgent need for substitutes which will improve the octane rating of unleaded fuels. For environmental reasons, oxygenates including alcohols may be preferred to other fuel ingredients which are currently proposed or introduced to replace lead compounds. In addition to octane improvement qualities, oxygenates were assessed with regard to power output and exhaust emissions thus confirming that no great deficiencies in these parameters would be introduced.

TEST PROCEDURES

Oxygenates were studied in a Fiat 127 903 cc engine connected to a Heenan Froude dynamometer to apply a steady variable load. A standard fuel-measuring device and Alcock viscous air flowmeter enabled fuel-air ratios to be closely monitored. Oil, cooling water, and air temperatures etc were continuously monitored to ensure that these remained within the normal range of operational variability. Compression ratios between the four cylinders ranged from 8.92 to 9.13 and this variation was deemed to be acceptable since our concern was to establish the comparative behaviour of these fuels in commercially available engines rather than in single-cylinder studies. The incidence of engine knock was readily detectable at low engine speeds. For routine detection at high engine speeds, a Bruel and Kjaer piezoelectric accelerometer and a CEL piezoelectric pressure washer were installed. The Bruel & Kjaer accelerometer required amplification through a Kistle charge amplifier to give a satisfactory oscilloscope signal, while the "knock" washer gave a satisfactory pressure trace without amplification.

A standard low-leaded base gasoline of the F-7 series was used for comparison and as a base for alcohol and oxygenate blends.

Oxygenates used:

The following alcohols, ethers, esters, and ketones were used in blends containing between 5 and 20% oxygenate in gasoline .

Alcohols	Methanol
	Ethanol
	Tert Butanol
Ethers	Methyl tert butyl ether
	Diiso propyl ether
	Anisole
Esters	Dimethyl carbonate
	Methyl acetate
Ketones	3 methyl butan-2-one
	4 methyl pentan-2-one
	Acetone
	Methyl ethyl ketone

The alcohols and MTBE are well known gasoline substitutes, some having been considered and used over the last sixty years. Other oxygenates in this list were chosen because of their branched structure, small molecular size and, in some cases, prior knowledge of their RON and MON. Current production cost was also important although bulk production and new methods of synthesis could make many other similar oxygenates viable.

The concentrations used in experiments were varied so as to limit total blend oxygen content to a maximum of around 4% by weight. This is within the limits of good drivability ie giving no observed problems caused by the leaning effect due to the extra oxygen in the combustion process.

The experiments aimed to test the various oxygenates with regard to improved octane rating and to test various mixtures of oxygenates combining two or more chemical types and changing individual components to assess whether a synergistic effect is exhibited.

The results obtained for single oxygenates showed several chemicals to have similar effects in similar concentrations provided that their oxygen content was comparable. Dual combinations of oxygenates were all tested as 10% vol/vol blends producing 2-4% wt/wt oxygen in the blends. Treble combinations were blended at 15% vol/vol.

Methanol/MTBE/3 methyl butan-2-one and methanol/MTBE/4 methyl pentan-2-one were seen to be superior while methanol/MTBE/TBA also exhibited good knock "protection". (Figs. 1 and 2)

Comparison of multicomponent blends with the effect of individual components is not always readily seen, since the individual effect of a smaller oxygenate percentage is not always very obvious. Comparing results on the basis of percentage weight of oxygen in the blend showed little significant correlation. Blending octane numbers cited in the literature vary dramatically with notable gaps for some of the ketones.

EXPERIMENTAL RESULTS

Octane Improvement To determine apparent increase in quality due to oxygenate addition several engine runs were performed using the base fuel. Then oxygenate blends showed a clear comparison. Combinations of oxygenates were regarded as most important in order to study synergistic effects especially of mixtures of chemical type and components so as to establish where chemical type was of the greater importance.

The results initially suggested methanol plus MTBE with a ketone was better than average and methanol plus MTBE with TBA was promising. Later results showed dual blends may be equally valuable. For example MTBE and methanol was one of the best combinations while TBA and ketones in the triple blends were valuable in replacing the ether but did not improve the anti knock quality.

CFR tests were carried out and showed that the oxygenates led to a greater RON than MON increase. This is due to the higher sensitivity of the oxygenates compared with the base gasoline. However the replacement of MTBE by 4 methyl pentan-2-one reduced the sensitivity of the blend due to its own very low sensitivity. Small amounts of 4 MP2 imparted no change in RON but a decrease in MON.

Power output A number of blends showed increased power output when oxygenates were present with the greatest increase exhibited at low speeds. This may result in better acceleration performance with maximum power output largely unaffected. Increases of up to 5% were exhibited and in our work a 6:3:2 blend of methanol/MTBE/and 4 MP2 gave some of the best results.

Viability of ketones as blending components

Acetone, MEK and 4 MP2 are among the hundred largest volume production organic chemicals, and some may be close in price to more usually accepted blending components. Their very high octane numbers make them worth further consideration. Tonnage production of such compounds may, however, be dependent on other industrial useage. For example, 4 MP2 is used widely as a solvent and degreasant. Tonnage used as an automobile paint solvent is being reduced in an attempt to reduce evaporative emissions to the atmosphere. Replacement by water-based solvents should release large tonnages of this ketone for fuel blends in the medium term as production plants are left with reduced total demand. Although this reduction may not augur well for future price stability, the medium term availability may provide a period in which the merits of 4 MP2 as an engine fuel ingredient could be well established.

CONCLUSIONS

This work showed that combinations of oxygenates including alcohols, ethers and ketones can be highly advantageous in raising octane ratings by 3 or 4 without modification to engine and fuel system. Lower exhaust emissions are to be expected with more oxygen in the fuel and these and improved power output are additional benefits.

Alcohols and MTBE are used individually by many countries and some, notably Switzerland, include them together in some gasoline blends. Increasing interest is being shown in other ethers (such as dimethyl ether in the USA and elsewhere) and production plants for such fuel components are coming to be seen as potentially viable. The higher cost of ketones such as 4 MP2 has limited the interest in these as gasoline substitutes but current demand changes may release lower cost supplies and a world wide interest, increasing production for automobile fuel use, could well bring massive economies of scale.

The inexorable moves to unleaded fuels will bring these oxygenates a higher profile as potentially viable gasoline substitutes with major advantages in terms of octane requirement, power output and atmospheric quality.

Clean air legislation in the USA and elsewhere is giving a boost to several of the oxygenates which we have studied. For example, the 1990 US Clean Air Act placed tough restrictions on gasoline blending

while tightening constraints on exhaust emissions. A 25% reduction in high octane aromatic compounds is called for by 1995. New blending ingredients are needed which meet the Act's requirements and replace the lost octane rating. MTBE has been widely recommended for this role[2] but Dimethyl ether (DME) may be equally promising.

A new one-step synthesis yields methanol **and** DME from CO-rich synthesis gas and is expected to show cost advantages over traditional catalytic dehydration of methanol. The DME/methanol product could be used as a transport fuel since the DME gives the methanol an improved cold-start facility. Thus, as a separate synthetic fuel or as an octane improver, DME could compete with MTBE without competing for a C_4 feedstock.

Another oxygenate which has attracted interest as an octane booster is di methyl carbonate (DMC). This compound was synthesised in the 1980's as a replacement for phosgene in carbonylation reactions[3]. Found to be "environmentally-friendly", DMC is finding other demands in pharmaceuticals and plastics but its greatest potential may be as an octane booster. Again it does not compete with MTBE being synthesised from methanol:

$$CO + 2CH_3OH + \tfrac{1}{2}O_2 \longrightarrow (CH_3O)_2CO + H_2O$$

A 12,000 t/y plant is operating in Italy and the feasibility of production in the USA is under consideration with methanol and methane more readily available. As a fuel blending component DMC reduces the amount of ozone emitted by the engines of older vehicles and shows the other cleaner exhaust properties typical of oxygenates.

As the world-wide trend towards unleaded fuels gathers pace, all the oxygenates will gain a higher profile as gasoline substitutes and octane boosters. Relying mainly on synthetic production routes the choice of "best oxygenate" will depend primarily on ease of synthesis to keep costs within reasonable limits.

Synthetic oxygenate mixtures such as the methanol/DME product referred to above could well prove the most viable. As with petroleum fractionation the usefulness of a mixture of compounds (c/f the "gasoline fraction") may well be decisive in settling which formulation will win the "best oxygenate" label.

Apart from compliance with the general constraints on emissions of CO, hydrocarbons, and NOX, there will be increasing concern to combat the "greenhouse effect". Apart from enhancing engine performance efficiency, alcohols, especially ethanol, may hold their place as the most "environmentally-advantageous" automobile fuels. This is especially true if the alcohol can be produced from a short-rotation biomass source such as cane-sugar. Agricultural production of the sugar cane absorbs CO_2. If one then produces ethanol by the well-known fermentation route, the subsequent combustion of the alcohol as motor fuel is merely **recycling** that CO_2 to the earth's atmosphere.

While the choice of feedstock for automobile fuel will remain largely dependent on price, such environmental issues will maintain the interest in the alcohols. In the next decade one may well see a range of fuels based on alcohols making further inroads into the world-wide gasoline demand.

REFERENCES

1. Gribble, N.R. "Alcohols and other Oxygenates as Motor Fuels" Ph.D. Thesis, Aston University, U.K. 1987.

2. Ottewell, S. "One-Step DME clears the Air". The Chemical Engineer, 25 July 1991.

3. Bolton, L. Enichem synthesis unpacks DMC potential". The Chemical Engineer, 9 April 1992.

ACKNOWLEDGMENT: The authors wish to thank Esso Research, U.K. for a cooperative (CASE) award in support of this research.

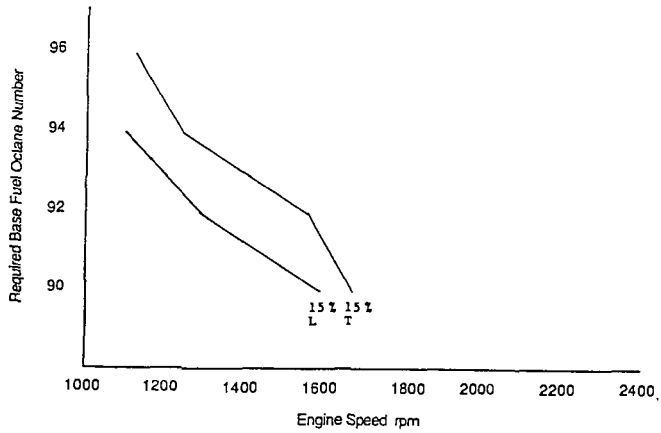

Figure 1 1 : 1 : 1 Methanol : MTBE : TBA

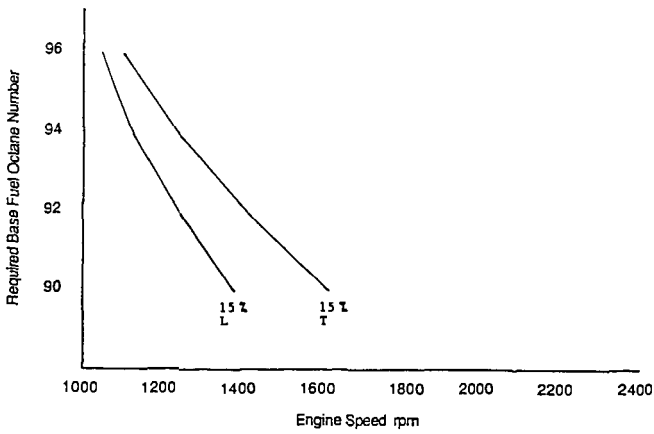

Figure 2 1 : 1 : 1 Methanol : MTBE : 3MB2

LIQEFACTION OF HYDROCARBON-RICH MICROALGA

Yutaka Dote, Shigeki Sawayama, and Shinya Yokoyama
National Institute for Resources and Environment
16-3 Onogawa, Tsukuba, Ibaraki 305, Japan

Keywords: liquefaction, Botryococcus braunii, liquid fuel

INTRODUCTION

A colonial green microalga, Botryococcus braunii, accumulates hydrocarbons(terpenoids) 30-70 % of its dry weight by fixing carbon dioxide in the atmosphere (1). Thus, the use of B. braunii could contribute to the reduction of the greenhouse effect if the hydrocarbons could be used as alternative liquid fuel. In laboratory, hydrocarbons of algal cells have been separated by extraction with organic solvent after freeze-drying and sonicating the algal cells. However, these procedures are not suitable for separation on a large scale because these are costly. Therefore, an effective method is expected for separating hydrocarbons as liquid fuel from harvested algal cells with high moisture content. We have proposed a new method for separating liquid fuel from algal cells of B. braunii by direct thermochemical liquefaction. The direct thermochemical liquefaction can convert wet biomass such as wood and sewage sludge to liquid fuel at around 300°C and 10 MPa using catalyst such as sodium carbonate (2,3). At the same time, the liquid oil can be easily separated (4). Therefore, it is expected that an amount of oil more than that of hydrocarbons in algal cells could be obtained because of the liquefaction of organic materials such as fiber, cellulose, and protein other than hydrocarbons in algal cells. In this paper, we discussed the applicability of the liquefaction of algal cells of B. braunii and the yield and properties of the liquid oil obtained by the liquefaction.

EXPERIMENTAL

Botryococcus braunii Kutzing Berkeley strain was used for liquefaction. Culture conditions were as follows: continuous light at 3000 lx and 25°C in a modified Chu 13 medium (5). Algal cells were washed three times by filtration with a nylon sheet of 20 μm mesh. The properties of the algal cells are listed in Table 1. The algal cells contained 92 % of water. Hydrocarbons in algal cells were separated as follows: freeze-dried algal cells were sonicated with 50 ml of hexane for 30 min by a Sonicator 201M(Kubota, Japan). The suspension was filtered through No.2 filter paper(Toyo Roshi, Japan) and the hexane solution was evaporated at 30°C under vacuum conditions.

Liquefaction was performed in a 300ml autoclave made of stainless steel. The wet algal cells(about 30g) were charged in the autoclave. After purging the residual air with nitrogen, nitrogen was added to 2 MPa and then the autoclave was sealed. The reaction was started by heating the autoclave by an electric furnace. After heating the autoclave up to the required temperature(200 and 300°C), the temperature was maintained for 1 h, and then the autoclave was cooled.

The procedure for the separation of products is shown in Fig. 1. The oil obtained by liquefaction was defined as dichloromethane soluble(in this paper referred to as primary oil). Hydrocarbons in primary oil was extracted with hexane(10 ml-hexane/g-dichloromethane soluble x 5).

The analysis of elemental composition(carbon, hydrogen, and nitrogen) was made by a Perkin Elmer Elemental Analyzer(Model 240) and the content of

oxygen was calculated by difference. Heating value(MJ/kg) was calculated according to Dulong's formula, Q=0.3383C+1.442(H-O/8), where C, H, and O are the weight percentage of carbon, hydrogen, and oxygen, respectively. Viscosity was measured by a viscometer(HAAKE, RV12) at 50°C.

RESULTS AND DISCUSSION

Properties of hexane soluble of the raw algal cells. The properties of the hexane soluble of the raw algal cells are shown in Table 2. The hexane soluble was obtained in the high yield of 58 % of its dry weigh, and had the good fluidity(56 cP) and the high heating value(49 MJ/kg).

Primary oil. The properties of primary oil are shown in Table 3. The yield of the primary oil obtained at 300°C were 52.9 % and that at 200°C was 56.5 %; these values were a little lower than the yield of the hexane soluble of the raw algal cells. This suggests that hydrocarbons of the raw algal cells were partly converted to dichloromethane insoluble materials such as char.

The heating value of the primary oil obtained at 300°C was 47.5 MJ/kg and that at 200°C was 42.0 MJ/kg; these values were equivalent to petroleum oil. Especially, the heating value of the primary oil obtained at 300°C was much higher than that of the oil obtained by liquefaction of other biomass. The viscosity of the primary oil obtained at 300°C was as low(94 cP) as that of the hexane soluble of the raw algal cells. However, the viscosity of the primary oil obtained at 200°C was too high to measure it; the primary oil was like a rubber. Therefore, the primary oil obtained at 300°C could be used as fuel oil.

The oxygen content of the primary oil obtained at 300°C was a little higher than that of the hexane soluble of the raw algal cells. However, it was much lower than that of the oil obtained by liquefaction of other biomass.

Hexane soluble. The properties of the hexane soluble of primary oil are shown in Table 4. The yield of the hexane soluble of the primary oil obtained at 300°C was 44 % and that at 200°C was 39 % on a dry algal cells basis. This meant that the primary oil obtained at 300°C contained 83% of hexane soluble and that at 200°C contained 69 % of hexane soluble. The elemental composition of the three hexane solubles was almost equal. The hexane solubles of the primary oil obtained at 300 and 200°C had good fluidity as well as the hexane soluble of the raw algal cells. In spite of thermal treatment at high temperature, the same properties of the hexane soluble of primary oil as that of the hexane soluble of the raw algal cells.

In summary, The direct thermochemical liquefaction could provide an effective method for separating liquid fuel from the hydrocarbon-rich microalga, *B. braunii*. Although the yield of primary oil was a little lower than that of the hexane soluble of the raw algal cells, the yield of primary oil might be possibly improved by use of suitable catalyst such as sodium carbonate. The bench-scale plant to continuously liquefy sewage sludge run successfully (6); thus, it might be possible to liquefy the algal cells on a large scale.

ACKNOWLEDGMENT

The authors thank Professor Katsumi Yamaguchi of The University of Tokyo for graciously providing *Botryococcus braunii* Kutzing Berkeley strain.

References

1) K. Yamaguchi, H. Nakano, M. Murakami, S. Konosu, O. Nakayma, M. Kanda, A. Nakamura, and H. Iwamoto, Agric. Biol. Chem. 51, 493-498, 1987

2) T. Ogi, S. Yokoyama, T. Minowa, and Y. Dote, Sekiyu Gakkaishi 33, 383-389, 1990
3) S. Yokoyama, A. Suzuki, M. Murakami, T. Ogi, K. Koguchi, and E. Nakamura, Fuel 66, 1150-1155, 1987
4) A. Suzuki, T. Nakamura, S. Itoh, and S. Yokoyama, Kagaku Kogaku Ronbunshu 15, 326-334, 1991
5) C. Largeau, E. Casadevall, C. Berkaloff, and P. Dhamelincourt, Phytochemistry 19, 1043-1051, 1980
6) A. Suzuki, T. Nakamura, S. Itoh, and S. Yokoyama, Research Journal of Japan Sewage Works Association 27, 104-112, 1990

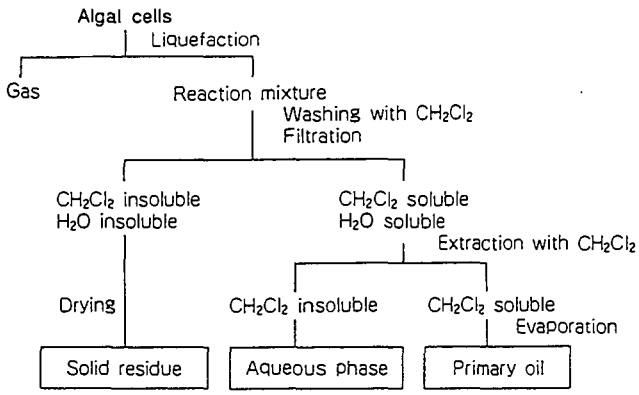

Fig.1 Procedure for the separation of primary oil

Table 1 Properties of microalga used for liquefaction

Moisture content (%)	Dry solid (%)	Ash (%)[1]	Organics (%)[1]
92.0	8.0	2	98

Elemental analysis (%)[1]			
C	H	N	O
68.7	10.9	1.3	19.1

1) On a dry algal cells basis

Table 2 Properties of the hexane soluble of raw algal cells

Yield (%)[1]	Heating Value (MJ/kg)	Viscosity (cP, @50°C)	Elemental analysis(%)			
			C	H	N	O
58	49.4	56	84.6	14.5	0.1	0.9

1) On a dry algal cells basis

Table 3 Properties of primary oil

Temp. (°C)	Yield (%)[1]	Heating Value (MJ/kg)	Viscosity (cP, @50°C)	Elemental analysis(%)			
				C	H	N	O
300	52.9	47.5	94	83.3	13.7	0.4	2.6
200	56.5	42.0	-	78.6	11.9	0.0	9.5

1) On a dry algal cells basis

Table 4 Properties of the hexane soluble of primary oil

Temp. (°C)	Yield (%)[1]	Heating Value (MJ/kg)	Viscosity (cP, @50°C)	Elemental analysis(%)			
				C	H	N	O
300	44	49.2	77	84.5	14.3	0.1	1.1
200	39	50.3	170	83.5	15.3	0.1	1.1

1)On a dry algal cells basis

CATALYTIC ACTIVITY OF OXIDIZED (COMBUSTED) OIL SHALE FOR REMOVAL OF NITROGEN OXIDES WITH AMMONIA AS A REDUCTANT IN COMBUSTION GAS STREAMS

John G. Reynolds, Robert W. Taylor, and Clarence J. Morris

University of California
Lawrence Livermore National Laboratory
Livermore, CA 94551

Keywords: Oil Shale, NO_x Removal, Combustion Flue Gas

ABSTRACT

Oxidized oil shale from the combustor in the LLNL hot recycle solids oil shale retorting process has been studied as a catalyst for removing nitrogen oxides from laboratory gas streams using NH_3 as a reductant. Combusted Green River oil shale heated at 10°C/min in an $Ar/O_2/NO/NH_3$ mixture (~ 93%/6%/2000 ppm/4000 ppm) with a gas residence time of ~ 0.6 sec exhibited NO removal between 250 and 500°C, with maximum removal of 70% at ~ 400°C.

Under isothermal conditions with the same gas mixture, the maximum NO removal was found to be ~ 64%. When CO_2 was added to the gas mixture at ~ 8%, the NO removal dropped to ~ 50%. However, increasing the gas residence time to ~ 1.2 sec, increased NO removal to 63%.

These results are not based on optimized process conditions, but indicate oxidized (combusted) oil shale is an effective catalyst for NO removal from combustion gas streams using NH_3 as the reductant.

INTRODUCTION

Green River oil shale contains 10+ wt % organic material. Pyrolyzed for a few minutes at 500°C, this shale releases ~ 80% of the organic matter as oil vapors and non-condensable gases. The balance of this organic material is left in the retorted shale as a solid (char). Efficient oil shale processes, such as the LLNL hot recycle solids (HRS) retort process, burn this char to heat the raw feed shale (1).

The ratio of nitrogen to organic carbon in Colorado Oil shale and retorted shale is higher than in most other fossil fuels. As a result, the concentration of NO_x and NH_3 in the combustion flue gas of the HRS process are high. Under normal HRS pilot plant operations, the combustion flue gas contains ~ 5% O_2, ~ 50 ppm NH_3, and ~ 500 ppm NO. This NO emission level is high by a factor of ~ two for current coal combustion standards in the U. S. (2). Under oxygen starved (fuel rich) combustion, the concentration of NO falls to ~ 250 ppm.

At present, a practical way of lowering NO_x emissions in industrial boilers employs selective catalytic reduction (SCR) using NH_3 at ~ 300°C (3). Non catalytic reduction of NO_x by NH_3 at about 950°C (thermal denox) is also practiced (4).

We are investigating factors which influence emissions of NH_3 and NO during oxidation of retorted shale. We have reported on the oxidation and thermal decomposition of NH_3, as well as utilizing retorted oil shale for NO reduction (5). Here we report the use of NH_3 as a reducing agent for NO over oxidized (combusted) oil shale.

EXPERIMENTAL

Experiments were performed at constant heating rates or isothermally at ambient-pressure in a 2.5-cm diameter, 50-cm long silica glass tube mounted vertically in an electric furnace. The thermal center of the tube was filled over a length of ~ 8 cm with the material being examined. Bed materials were either oxidized (combusted) Green River oil shale (22 gal/ton) or porous white firebrick. The shale bed used in the constant heating rate experiments was prepared by burning shale at temperatures as high as 850°C in air which assured that a significant fraction of the calcite ($CaCO_3$) in the shale was decomposed to lime (CaO), and no organic carbon remained. The shale used in the isothermal experiments was taken from the HRS pilot plant where combustion was at temperatures below 750°C, resulting in little $CaCO_3$ decomposition. This shale sample contained ~ 0.3 wt % unburnt char, typical of processed shale. Both shale samples weighed 27 g and had a particle size range from 1.4 to 2.8 mm. The bed porosity was ~ 40%, and the porosity of the individual shale grains was ~ 25%.

Temperature of the bed was measured with a thermocouple located at the center of the bed. The gas mixtures were passed down flow at a rate of either ~ 1 or ~ 0.5 L/min. At the 1 L/min rate, the transit or contact time between the flowing gas and shale at 300°C was about 0.6 sec. The gas compositions were constructed to simulate an idealized HRS combustor output, with and without CO_2. Ar was selected as the carrier gas to facilitate detection of product N_2.

Analysis of NH_3, NO, NO_2, N_2, H_2, O_2, H_2O, and Ar was by an EXTREL Questor model mass spectrometer. Calibration for all gases except H_2O was accomplished by means of commercial gas standards and air. The mass spectrometer was connected to the reactor by a 304 SS line heated at 150°C. Data was taken every 10 to 15 sec. Because both N_2O and CO_2 have m/z 44, they can not be differentiated in the mass spectrometer. In the cases where CO_2 was absent in the inlet gas, m/z 44 was considered due mainly to N_2O. In the initial experiments at constant heating rates, the N_2O was also measured by a BIO-RAD FTS 40 FTIR. In the cases of CO_2 in the inlet gas, m/z 44 was assumed to be all CO_2, and no N_2O measurements were made. In all cases, m/z 28 was corrected for CO fragmentation from CO_2. No NO_2 was observe.

Whenever NH_3 and O_2 were passed into the mass spectrometer, H_2O and N_2 were observed as products. The ratio of H_2O to N_2 corresponded to NH_3 combustion. Approximately 20% of the NH_3 was burnt in the hot MS source. This side reaction was accounted for by measuring a baseline concentrations of these species before each run.

RESULTS AND DISCUSSION

Nitrogen oxide removal utilizing SCR with NH_3 as the reductant is chemistry which could go through several reactive oxide intermediates, such as N_2O, NO_2, N_2O_4, N_2O_3 (6). In this initial study, we make no attempt to study the mechanism(s) of the reactions. We only use the stoichiometry of suspected reactions to substantiate (but not necessarily prove) the overall global reactions. The general global reactions which need to be considered are:

$$NO + NH_3 + 1/4O_2 \rightarrow N_2 + 3/2H_2O \quad (1)$$
$$NH_3 + 3/4O_2 \rightarrow 1/2N_2 + 3/2H_2O \quad (2)$$
$$NO \rightarrow 1/2N_2 + 1/2O_2 \quad (3),$$

where reaction (1) is a combination of reactions (2) and (3). Potential competing reactions which may be observed under the conditions of these experiments are:

$$NH_3 + 3/2NO \rightarrow 5/4N_2 + 3/2H_2O \quad (4)$$
$$NH_3 + 5/4O_2 \rightarrow NO + 3/2H_2O \quad (5).$$

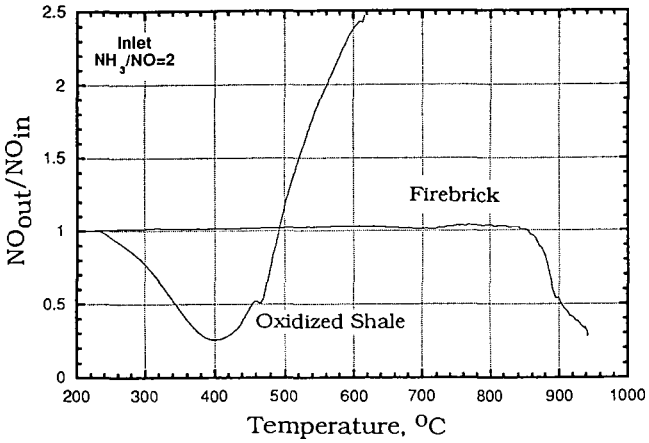

Figure 1. Loss and formation of NO from a mixture of ammonia and NO passed over heated oxidized shale and firebrick (5% O_2, $NH_3/NO = 2$, rate of heating 10°C/min).

NO Reduction at the Heating Rate of 10°C/min

Oxidized Oil Shale. Oxidized (combusted) Green River oil shale was heated at 10°C/min in a gas mixture of Ar with ~ 5% O_2, 2000 ppm NO, and 4000 ppm NH_3 at a gas residence time of ~ 0.6 sec from 200 to 700°C. Figure 1 shows the results. At 250°C, the NO concentration of the reactor effluent begins to decrease with respect to the NO concentration in the reactor inlet ($NO_{out}/NO_{in} < 1.0$). This decrease continues to 400°C where a maximum NO removal of 70% is reached. For temperatures above this maximum, NO removal activity steadily decreases. At temperatures above ~ 500°C, there is a net production of NO, which continues to increase the concentration of NO in the reactor effluent with increasing temperature.

The decrease in NO in the reactor effluent at temperatures from 250 to ~ 500°C is probably due to NO reduction by NH_3, mostly by reaction (1). Rough nitrogen balances for N_2 production and NO and NH_3 consumption support this. This behavior is in the temperature range observed for SCR of NO by commercially available V-Ti NO reduction catalysts (3). At temperatures above ~ 500°C, net NO is produced ($NO_{out}/NO_{in} > 1$). Rough mass balance indicates this

is probably due to due to ammonia oxidation, reaction (5), and nitrate decomposition (see below). Note at ~ 600°C, a large fraction of NH_3 appears to be converted to NO.

Even without NH_3 as a reducing agent, this lime-bearing sample of burnt shale (see experimental) removed NO from the gas stream at temperatures of ~ 380°C. No N_2 was released, and the amount of oxygen consumed is consistent with the following reaction for the formation of calcium or some other nitrate:

$$2NO + 3/2O_2 + CaO \rightarrow Ca(NO_3)_2 \qquad (6).$$

After this shale has been reacted with NO and O_2, heating above 400°C results in the release of NO and O_2, consistent with published data on the thermal stability of some nitrate compounds (7). However, x-ray diffraction did not reveal any nitrates (possibly due to low concentrations).

Firebrick. Figure 1 also shows the behavior of the same gas mixture flowing over firebrick under the same conditions. Obvious is total the lack of NO removal activity until temperatures above 850°C. This is in the temperature range assigned to thermal denox (4). Although not shown, NH_3 over firebrick (with no NO) begins to oxidize at temperatures above 500°C, not yielding any significant amount of NO, but yielding $H_2O/N_2 = 3$, suggesting reaction (2) is occurring. Full oxidation of NH_3 is seen only at 950°C, where thermal denox is taking place at the same time.

We presume that if the mixture of NO and NH_3 had been heated to 900°C over oxidized (combusted) shale, NO would have decreased to the values observed over firebrick. This prediction is based on the assumption that at high temperatures thermodynamic equilibrium is likely to prevail, and at 900°C, NO remains unstable with respect to N_2 and O_2.

***Table 1.* Removal of NO over Combusted Oil Shale (Isothermal)**

Experiment, #	T, °C	NH_3/NO	CO_2	NO Removal, %	~ Residence Time (sec)
1	365	2.8	No	64	0.6
2	365	0[a]	No	19	0.6
3	375	2.8	Yes	49	0.6
4	383	2.8	Yes	50	0.6
5	374	0[a]	Yes	8	0.6
6	385	1.3	Yes	62	1.2
7	402	1.0	Yes	63	1.2
8	385	1.0	Yes	61	1.2

a. No NH_3 in gas stream

NO Reduction at Isothermal Conditions

Figure 1 shows the temperature for maximum NO reduction over oxidized (combusted) shale is 400°C at the 10°C/min heating rate. In efforts to optimize removal conditions and obtain better mass balances, NO removal was performed isothermally over the oxidized (combusted) oil shale. Table 1 lists these results using the shale from the HRS pilot plant (contains 0.3 wt % char).

Oxidized (combusted) shale (Experiment 1). The first experiment listed in the table was carried out with the same gas composition as in the constant heating rate experiments shown in Figure 1. The NO removal is slightly lower than the maximum removal found for the constant heating rate experiment. We do not know the source of this difference, and more experiments are being performed to assess the reason. However, this may be due to the shale bed in the isothermal experiments contained little or no lime preventing NO removal by nitrate formation as a supplement to SCR.

***Table 2.* Normalized Nitrogen Balances for Removal of NO over Combusted Oil Shale (Isothermal)**

	Consumed		Produced	Net
Experiment #	N from NO	N from NH_3	N as N_2*	$\Sigma_{pro} - \Sigma_{con}$
1	1.00	1.46	2.58	0.12
2	1.00	0.15	2.09	0.94
3	1.00	1.44	2.44	0.00
4	1.00	1.20	2.34	0.14
5	1.00	0.10	0.11	-0.99
6	1.00	0.85	1.95	0.10
7	1.00	0.94	2.12	0.18
8	1.00	0.81	1.87	0.06

* m/z 28

Overall normalized nitrogen balance of the experiments in Table 1 are shown in Table 2. If all of the NO is consumed by reaction (1) ($NO/NH_3/N_2$ stoichiometry, 1/1/1; that is one N is released for each NO lost and one N is released for each NH_3 lost), an additional 0.46 moles of N from NH_3 remains to be accounted for by some other reaction. This could be almost all accounted for by the oxidation of NH_3 by reaction (2) which would produce 0.46 moles of N as N_2.

This reaction could be verified by H_2O and O_2 balances. However, O_2 and H_2O balances are complicated by the combustion of char ($CH_{0.4}$). For example, in experiment 1, the predicted net O_2 loss through the bed (normalized to NO as in the case of Table 2) would be 0.52 from NH_3 combustion and NO decomposition (reactions (1) and (2)) whereas the measured loss in O_2 was 2.5. The predicted H_2O production would be 2.0 but the measured production of H_2O was 2.9. The observed production of CO_2 was ~ 2, accounting for the observed extra O_2 loss. The CO_2 concentration decreased with time, due to the consumption of char. Furthermore, low temperature combustion of char can release CO (m/z 28) which may explain why more N_2 (m/z 28) was seen than can be accounted for by NH_3 and NO loss.

Oxidized (combusted) shale without NH_3 (Experiment 2). The second experiment in Table 1 shows the reaction of NO over the oxidized (combusted) shale in the absence of NH_3 as the reductant. (Very low levels of NH_3 were detected in both the inlet and product streams, probably because of desorption from prior runs, or background correction errors.) Some decrease in the NO concentration in the product effluent compared to the inlet stream does occur without the presence of NH_3. This could be through reaction (3), or by reduction by char. A 2000 ppm concentration of CO_2 is observed indicating char oxidation. A CO content of 200 ppm in the gas stream from the char oxidation chemistry would explain the observed N balance.

Oxidized (combusted) shale with CO_2 (Experiments 3 and 4). To simulate the real combustion stream for the HRS process, ~ 8% CO_2 was added to the reaction gas mixture. The third experiment in Table 1 shows the NO removal with NH_3 present in excess. Although the removal is almost 50%, which demonstrates the oxidized (combusted) oil shale has catalytic properties even with CO_2 in the gas stream, the removal is reduced to 75% of the removal found without CO_2 in the gas stream. (This is even with the reactor temperature 10°C higher.) Raising the reactor temperature from 375°C to 383°C showed only a 1% increase in removal of NO.

Table 2 shows the normalized nitrogen balance for Experiment 3. If reaction (1) is considered as the sole consumer for the NO, 0.44 moles of NH_3 reacted and 0.44 moles of N as N_2 formed remain unaccounted for. However, these remaining quantities can be accounted for by the oxidation of NH_3 by reaction (2). Although exhibiting poorer closure, the normalized nitrogen balance for Experiment 4 shows a similar result. Probably the improved N balance compared to earlier experiments is due to most of the char has been already consumed in previous experiments, so there is less contribution to m/z 28 from CO producing reactions. This is suggested because of 75% of the H_2O produced can be accounted for by NH_3 oxidation in this experiment. Also, the concentration of CO_2 in the exit gas was only 400 ppm compared to nearly 2000 ppm in the earlier experiments 1 and 2.

Oxidized (combusted) shale with CO_2 and without NH_3 (Experiment 5). The CO_2 in the gas stream also appears to have an effect on the ability of the catalyst to remove NO with or without the presence of the NH_3 reductant. Comparing the second and fifth experiments in Table 1 shows the NO removal with CO_2 but no NH_3 in the gas stream is ~ 50% lower than in the case without CO_2 in the stream. This may be due to the absence of char as a reducing agent or due to absorption (see above) instead of catalysis, suggesting the CO_2 is competing with NO for absorption sites on the shale. This will be addressed in detail in another paper.

Effect of Flow Rate and NH_3 to NO ratio on NO Removal (Experiment 6-8). Experiments 6-8 in Table 1 also show NO removal increases significantly when the gas stream residence time (containing CO_2) is doubled to ~ 1.2 sec. These conversions are comparable to the baseline case where no CO_2 is in the gas stream. Because the NH_3 to NO ratio was decreased for this set of experiments, a direct comparison to NO removal at the higher flow rate is not possible. However, these results indicate changing the flow rate (or residence time) is an important variable in maximizing the NO reaction chemistry, particularly when temperature change has an upper limit of ~ 400°C where NO formation (through reaction (5)) begins to compete.

The two experiments (6 and 8) at 385°C reactor temperature and the 1.2 sec residence time show little dependence of NO removal on the NH_3 to NO ratio. This dependence has been studied for a broader range of NH_3 to NO ratios (0 to 2.8) for thermal denox over firebrick. Those results showed a greater difference than seen for NO removal by oxidized oil shale. At 933°C, the firebrick showed for NO_{out}/NO_{in} ~ 0.48, NH_3/NO = 1.0; for NO_{out}/NO_{in} ~ 0.25, NH_3/NO = 1.30.

Table 2 shows for NH_3/NO = 1 (Experiment 8), the amount of NO reacted that can be accounted for by reduction with NH_3 (reaction (1)) is 80%. The source of the consumption of the balance of NO is uncertain. Experiment 5 at the higher gas-flow rate indicates ~ 10% decrease in NO concentration in the gas stream even when NH_3 is not present, probably by reduction by char. However, all the char was probably consumed by the time this experiment was done. Also, lime formation can not take place in the presence of CO_2 at this temperature, so NO consumption by nitrate formation probably does not occur. Reaction (3), though, when applied to

the balance of NO gives excellent N closure. Further experiments are being conducted to clarify this.

CONCLUSIONS

Oxidized (combusted) oil shale from the HRS process exhibits catalytic activity for the removal of NO from laboratory gas streams using NH_3 as the reductant. The activity and conditions have not been optimized, but typical NO removal is 60+% at a 1.2 sec gas residence time, a reactor temperature range of 380 to 400°C, and for a gas containing ~ 2000 ppm NO, 2000 ppm NH_3, and 8% CO_2. Temperature limitations potentially due to competing NH_3 oxidation suggest residence time is the important variable to study for improving removal of NO from flue gas. Optimizing this process variable, as well as application to actual retort combustor gas streams will be addressed in a later paper.

ACKNOWLEDGMENTS

We thank Russ Sanborn for assistance with the N_2O measurements, Henrik Wallman and Mary Singleton for useful discussions. This work was performed under the auspices of the U. S. Department of Energy by the Lawrence Livermore National Laboratory under contract no. W-7405-ENG-48.

REFERENCES

1) R. J. Cena and R, G, Mallon. 19th Oil Shale Symposium Proceedings, Colorado School of Mines, 102-125 (1986).
2) Clean Coal/Synfuels Letter. 4-8 Oct. 22 (1990).
3) H. Bosch, H. and F. Janssen. Catal. Today, 2, 369 (1988).
4) R. K. Lyon, Int. J. Chem. Kinetics, 8, 315 (1976).
5) R. W. Taylor, and C. J. Morris, Lawrence Livermore National Laboratory, UCRL-89806 October (1983).
6) J. B. Joshi, V. V. Mahajani, and V. A. Juvekar. Chem. Eng. Commun., 33, 1-92 (1985).
7) R. A. Robie, B. S. Hemingway, and J. R. Fisher. *Thermodynamic Properties of Minerals and Related Substances at 298.15 K and 1 Bar (105 Pascals) Pressure and at Higher Temperatures*, U. S. Geological Survey Bulletin 1452 (1979).

STRATEGIC CONSIDERATIONS OF COAL LIQUID REFINING

P.-Z. Zhou, J.J. Marano (Burns and Roe Services Corp.)
R.A. Winschel (CONSOL, Inc.)

The development of the two-stage coal liquefaction process over the past decade has resulted in remarkable improvements in process efficiency, including increased liquid yield, better product quality, improved hydrogen efficiency, and dramatic reduction in production costs. At this stage in liquefaction development, serious consideration should be given to the refining of coal liquids into marketable transportation fuels.

PROPERTIES OF COAL-DERIVED LIQUIDS

Properties of coal liquids representative of various single-stage and two-stage liquefaction (TSL) processes were compiled in a comprehensive review [Zhou and Rao, 1992]. The major differences between current two-stage liquefaction coal liquids and those from earlier processes are the higher hydrogen and lower heteroatom contents of the former. TSL liquids are usually richer in middle distillates than are single-stage liquids, probably due to the lower hydrogenation severity of the two-stage processes which leads to the lower hydrogen consumption and higher liquid yields.

Coal liquids produced from coals of the same rank under similar conditions are quite similar in properties. For coal liquids obtained from bituminous coals, the hydrogen content is high, in the range of 11.3-12.2 wt%; and heteroatom contents are low: 0.1- 0.3 wt% nitrogen, less than 0.1 wt% sulfur, and 1-2% oxygen [Lee et al. 1991]. Liquid products from lower-rank coals are characterized by more oxygen and higher paraffinicity than bituminous coal liquids. The subbituminous Black Thunder coal liquids have a greater concentration of normal paraffins, olefins, and phenols than Pittsburgh seam coal liquids [Robbins et al. 1992].

As complex mixtures of hydrocarbons and hetero-compounds, coal liquids and petroleum exhibit many fundamental similarities; therefore, coal liquids can be refined into liquid transportation fuels by current petroleum refining technologies. Extensive research on coal-liquid refining done by Chevron, UOP, and Exxon demonstrated that environmentally clean, quality liquid fuels, can be produced from coal liquids. Modern TSL liquids, however, have a lower boiling range than petroleum, with an end point around 427°C, and are free of residual materials and metals. The H/C ratio of TSL liquids falls within the H/C range of crude oils, although at the lower end, reflecting the cyclic nature of coal liquids. Coal liquids have very low sulfur contents, moderate nitrogen contents, and relatively high oxygen contents. These unique features of coal liquids require somewhat different refining strategies than those conventionally used for the refining of petroleum.

Oxygen compounds in coal liquids are concentrated in the 175-315°C boiling range, with a peak at 230°C [Pauls et al. 1990]. For Black Thunder coal liquid, 3.6 wt% of the naphtha (IBP - 193°C) and 10 wt% of the 193-266°F fraction are phenolic compounds and can be extracted easily by caustic washing [Burke et al. 1991]. This naphtha phenolic extract contains phenol, cresols, xylenols, ethyl phenol, methylethyl-phenol and propyl-phenol [Robbins et al. 1992].

Some coal liquids produced recently at Wilsonville are characterized in Table 1. Tables 2 through 4 compare the properties of respective fractions of these coal liquids with corresponding specifications for gasoline, jet fuel, and diesel fuel.

HYDROPROCESSING -- THE MAJOR TOOL FOR COAL-LIQUID REFINING

Based on the characteristics of coal liquids, hydroprocessing is obviously the most important refining technology for coal-liquid upgrading. Coal liquefaction is a hydrogenation process, and coal-liquid refining can be envisioned as an extension of the coal-to-liquid fuel conversion process. The hydrogenation conditions in the liquefaction step determine the yield and properties of the coal liquids produced, which in turn dictate the extent of upgrading required for coal-liquid fuel production.

Current liquefaction practice is to recycle resids to extinction to produce a total distillate product with an end point in the range of 370-427°C. With improved liquefaction operation, it is possible to lower the end point further to around 350°C, as suggested by some authors [Zhou and Rao, 1992]. This is particularly advantageous to the downstream refining facility which may have limited cracking (either catalytic or hydrocracking) capacity, and provides the added benefit of confining the toxicologically active polycyclic aromatic hydrocarbons within the boundary of the liquefaction plant. In fact, Exxon's new liquefaction process is generating 350°C- coal liquids, which make a naphtha plus distillate product slate [Stuntz 1991].

Hydroprocessing, e.g. hydrotreating and hydrocracking, of coal liquids is highly versatile in that the extent of hydrogenation can be adjusted to produce different product slates (maximum gasoline or maximum distillate) as well as product quality (primarily aromatics content).

UTILIZATION OF EXISTING PETROLEUM REFINERY INFRASTRUCTURE

It appears to be more realistic to consider the co-refining of coal liquids with petroleum in an existing petroleum refinery rather than in a grass-roots, dedicated coal-liquid refinery.

Coal liquids can be introduced into a refinery either as a single feed or as previously fractionated individual cuts. The unique properties of coal liquids warrant a different refining strategy than that for petroleum. Mixing the total coal liquid with petroleum would eliminate many possible refining schemes suitable for each of these two feedstocks. More flexibility in processing can be achieved if coal liquids are distilled in the liquefaction plant and individual fractions are introduced into the refinery at points where their properties are most compatible with petroleum counterparts.

Much work has been done on the hydrotreatment of total coal liquids; however, evidence shows that hydrotreating the individual naphtha, kerosene, and diesel fractions is advantageous from a product-quality standpoint. For example, jet fuels with higher smoke points may be obtained by hydrotreating the respective fractions rather than the total coal liquid [Sullivan 1987b, Zhou and Rao 1992]. Depending on the coal liquid properties, the product slate, and the refinery infrastructure, coal liquid fractions may be hydroprocessed together with or separately from their petroleum counterparts.

REFINERY LINEAR PROGRAMMING

Linear programming (LP) techniques are used routinely within the refining industry to evaluate the economics of petroleum processing. Linear programming can also be applied to coal liquids to determine their value as refinery feedstocks. LP is potentially a very powerful tool since the products from most liquefaction processes are intermediates which must be further upgraded or blended with petroleum-derived intermediates to meet product specifications. Thus, LP allows the effects of variations in yields and quality between different liquefaction operations to be quantified, and can provide a benchmark for comparing and ranking different coal liquid products.

The effect of feeding coal-liquid fractions to a refinery is being studied with the linear programming technique and preliminary results are reported here. The LP model used in this study was developed by Bechtel, Inc. as part of the DOE-funded Direct Liquefaction Baseline Design project [Bechtel, work in progress]. It is a model of the typical midwestern U.S. refinery, producing the average U.S. midwest product slate. Incremental quantities of different coal-liquid cuts are introduced into the refinery model, which calculates the effect of each cut on refinery net profit. In general, liquids produced by direct liquefaction are found to be more valuable than crude petroleum. The results reported here are expressed as a coal liquid premium defined as the percentage difference between the value of the coal liquid and the price of crude oil.

GASOLINE PRODUCTION FROM COAL NAPHTHA

Coal-liquid naphthas are similar to the naphtha fraction from a naphthenic crude oil. Data in Table 2 show that the oxidation stability, caused by heteroatoms (mainly oxygen), and lack of light ends are the two major problems in the manufacture of gasoline from coal liquids. Coal naphtha, however, has a high octane number and low aromatics content and is an ideal source for gasoline production. The clear motor octane of coal naphthas is in the range of 76-83 [Zhou and Rao, 1992]. The aromatics content of coal naphthas from recent TSL runs, contrary to conventional views, are fairly low (7-13 vol%), and the naphthene content is very high (60-70 vol%), as shown in Table 2. It is an excellent reformer feedstock to make gasoline components with a research octane number above 105 [Sullivan 1987b], which is attractive at the present time. However, conversion of naphthenes to aromatics by catalytic reforming may no longer be advisable due to provisions in the U. S. Clean Air Act Admendments. A cost-effective means of gasoline production from coal naphthas is to maintain the current level of naphthenes, which have fairly high octane numbers, and improve the oxidation stability of the coal naphtha via mild hydrotreating to remove the heteroatoms. Isomerization of light coal naphtha is also a promising option. Volatility requirements can be easily remedied by blending.

LP studies show that for a refinery not deficient in high- octane gasoline blendstocks, this scheme results in a premium for coal naphtha of 12% over the price of crude oil. Under the assumptions used in the calculation, straight blending of the hydrotreated coal naphtha is preferable to catalytic reforming which has a premium of 6.5%. This difference is due primarily to the loss of volume which occurs during reforming. In this study, the refinery product slate was assumed to be unchanged. Further studies are planned to explore various scenarios in which the refinery infrastructure and product slate are modified to take best advantage of coal liquid potentials. Higher premiums are anticipated.

PHENOLICS EXTRACTION

Since oxygen is the major heteroatom found in coal liquids, hydrogen used for oxygen removal during hydrotreating accounts for the major part of hydrogen consumption. The oxygen compounds in the 232°C- fraction are mostly single-ring phenolics, which can be easily extracted by caustic washing.

A promising approach is, therefore, to extract these phenolics before hydrotreating as chemicals by-product. Preliminary work indicated that this has good potential for raising the coal-liquid premium for the naphtha fraction.

JET FUEL PRODUCTION

As illustrated in Table 4, the coal-derived kerosene fractions have lower hydrogen contents than do naphthas from the same source. This follows the general trend that hydrogen content decreases with increasing boiling point. The hydrogen level of the coal-derived kerosene fraction is low compared with that of petroleum-derived jet fuels (H 13.5-14.0 wt%), and is a reflection of its high aromatics content, typically around 50%. As a result, the API gravity and smoke point, two major properties for jet fuels, are much lower than specifications.

The jet fuel fraction obtained from an EDS distillate by hydrotreating do not meet gravity and smoke point specifications [Erwin and Sefer 1989]. It was reported, however, that through appropriate hydrotreatment smoke points of at least 20 mm can be obtained for jet fuels from Illinois No. 6 coal liquids (aromatics content 10 vol% or lower) and for jet fuels from Wyodak coal liquids (aromatics content about 15 vol%) [Sullivan 1987a]. Hydrocracking appears to be a more efficient way of making specification jet fuels from coal liquids [Sullivan and O'Rear 1981]. In essence, this is a matter of the depth of hydrogenation. Jet fuels with no aromatics and no sulfur can be produced and meet all of the current ASTM specifications for jet fuel [Stuntz 1991].

Due to the compositional uniqueness, traditional density specification is more difficult to meet than smoke point for coal-derived jet fuel fractions, which comprise largely two-ring cycloparaffins. However, the high naphthene content of coal liquids makes them a remarkable feedstock for manufacturing high-density, high-energy jet fuels, a range-extender for high-mach aircrafts. More work is required in this area.

DIESEL FUEL PRODUCTION

With an even lower hydrogen content than the kerosene fraction, the coal-derived middle distillates have low cetane numbers, usually in the twenties. Upgrading of the middle distillates is necessary to increase the hydrogen content and remove hetero-compounds. However, saturation of a large part of the aromatics in the diesel fuel fractions may not be justified economically, and the use of multi-purpose additives may be advisable [Sefer and Erwin 1989]. The coal-derived diesel fuel does show good susceptibility to ignition improvers [Sullivan et al. 1981].

With all the aromatic hydrocarbons in coal diesel fractions saturated, a zero-aromatics, zero-sulfur diesel fuel is made by Exxon, which has a cetane value in the 42-53 range and considerably reduced particulate emissions relative to a typical petroleum diesel fuel [Stuntz 1991].

Initial LP work indicates that low-severity hydrotreating results in a diesel blendstock with a premium of about 4% over crude oil. A better premium may be possible by adjusting the cut points of this fraction.

CRACKING

Coal-derived middle and heavy distillates can be cracked, either by catalytic cracking or hydrocracking, to boost yields of gasoline or light distillate fuels. In order to be a good cat-cracker feedstock comparable to petroleum feedstocks, coal distillates must be hydrogenated to a 11.5-12.0 wt% hydrogen content [Riedl and deRosset 1980].

A decision on whether the hydrotreated middle distillate should be used as a diesel fuel blending stock or subjected to catalytic cracking should be based largely on economic considerations. Product slate constraints, however, will probably dictate that a certain part of the middle distillate should be blended to diesel fuel and the rest cracked to generate gasoline blending components. Heavy distillate or vacuum gas oil, if produced by the liquefaction plant, should be cracked. Hydrocracking of coal-derived heavy distillates can produce quality gasoline, jet, and diesel fuels. The choice between catalytic cracking and hydrocracking depends on the refinery infrastructure. The mode of operation for the hydrocracker, all-gasoline mode or maximum-jet-fuel mode, depends on refinery economics. Further LP work is under way to study this and other related options.

CONCLUSION

Coal liquids can be refined by modern refining technologies, primarily hydroprocessing, into specification transportation fuels. Mild hydrotreatment of coal naphtha to produce a gasoline blendstock is preferred over catalytic reforming in the long run. The middle distillate can be hydro-upgraded into high-density jet fuel or diesel fuel with the use of an appropriate additive package. Heavy distillates may be cracked to boost gasoline yield. By adjusting the depth of hydrogenation, zero-aromatics liquid fuels can be obtained with high quality. A high degree of product slate flexibility is possible with coal-liquid refining. Suitable refining strategies will result in a considerable premium for coal liquids over the price of crude oils. More research is recommended on coal-liquid characterization, including detailed analysis and development of correlations for property prediction; and on coal-liquid processing, including experimental and LP studies.

ACKNOWLEDGEMENT

This work was sponsored by the U.S. Department of energy (DOE), Pittsburgh Energy Technology Center (PETC), in part under Contract No. DE-AC22-89PC89883 (CONSOL) and in part under Contract No. DE-AC22-89PC88400 (8RSC). Special thanks go to Mr. S.R. Lee (DOE/PETC) for his support and comments on this paper.

REFERENCES

Bechtel, Inc. work in progress. "Direct Coal Liquefaction Baseline Design and System Analysis," DOE Contract DE-AC22-90PCB9857.

Burke, F.P.; Winschel, R.A.; Robbins, G.A.; and Brandes, S.D. 1991. CONSOL Project Status Report under DOE Contract DE-AC22-89PC-89883, November 6, 1991.

Erwin, J., and Sefer, N.R. 1989. "Synthetic Fuels from Coal-Derived Distillate as Jet Fuels for High Mach AiRcraft," presented at ACS Meeting, Div. Petrol. Chem. September 10-15, 1989. Miami Beach, FL.

Kramer, R.L. 1991. Conoco Research Report No. 6210-0003-T000-1-91, August 1991.

Lee, J.M.; Cantrell, C.E.; Gollakota, S.V.; Davies, O.L.; Corser, M.M.; and Vimalchand, P. 1991. Prep. ACS National Meeting, Div. Fuel Chemistry, August 25-30, 1991. New York, N.Y. 36 (4), 1985.

Pauls, R.E.; Bambacht, M.E.; Bradley, C.; Scheppele, S.E.; and Cronauer, D.C. 1990. Energy & Fuels, 4, 236.

Riedl, F.J., and DeRosset, A.J. 1980. "Hydrotreating and Fluid Catalytic Cracking of SRC-II Process Derived Gas Oils," UOP Interim Report, DOE Contract No. EF -77-C-01-2566, July 1980.

Robbins, G.A.; Brandes, S.D.; Winschel, R.A.; and Burke, F.P. 1992. CONSOL, Quarterly Technical Progress Report, Oct. 1 - Dec. 31, 1991. DOE Contract No. DE-AC22-89PC89883.

Southern Electric International, Inc. 1991. "Advanced Coal Liquefaction Research Facility, Wilsonville, Alabama. Technical Progress Report, Run 258 with Subbituminous Coal," DOE Contract No. DE-AC22-82PC50041. May 1991.

Stuntz, G.F. 1991. "Premium Products from Direct Coal Liquefaction," presented at Alternate Energy '91, April 16-19, 1991. Scottsdale, AR.

Sullivan, R.F. 1987a. "High-Density Jet Fuels from Coal Syncrudes," presented at the Symposium on Structure of Future Jet Fuels, Div. Petroleum chemistry, ACS Meeting, April 5-10, 1987. Denver, CO.

Sullivan, R.F. 1987b. "Refining and Upgrading of Synfuels from Coal and Oil Shales by Advanced Catalytic Processes," Final Report, prepared for USDOE, Contract No. DE-AC22-76ET10532, May 1987.

Sullivan, R.F.; O'Rear, D.J.; and Frumkin, H.A. 1981. "Converting Syncrudes to Transportation Fuels," presented at 1981 Fuels and Lubricants Meeting, NPRA, November 5-6, 1981. Houston, TX.

Vimalchand, P.; Lee, J.M.; Gollakota, S.V.; Davies, O.L.; Cantrell, C.E.; and Corser, M.M. 1991. "Recent Developments in Coal Liquefaction at Wilsonville Facility," presented at 16th Annual EPRI Conference, June IB - 20, 1991. Palo Alto, CA.

Winschel, R.A., and Zhou, P. 1991. "Inspection of Integrated Two-Stage Liquefaction Products by Petroleum Assay," presented at 16th Annual EPRI Conference on Fuel Science, June 16-21, 1991. Palo Alto, CA.

Zhou, P.-Z., and Rao, S.N. 1992. "Assessment of Coal Liquids as Refinery Feedstocks," prepared for U.S. DOE/Pittsburgh Energy Technology Center, DOE Contract No. DE-AC22-89PC88400.

TABLE 1
PROPERTIES OF WILSONVILLE TWO-STAGE LIQUIDS

Coal	Spring Creek	Pittsburgh Seam	Black Thunder	Illinois No. 6
Gravity, °API @15°C	16.2-18.3	27.7	23.9	24.5
Elemental				
Carbon, wt%	86.2-86.9	86.9	87.4	87.2
Hydrogen, wt%	10.9-11.3	11.55	11.2	11.8
Sulfur, wt%	0.05-0.10	0.05	0.05	0.02
Nitrogen, wt%	0.40-0.52	0.1	0.3	0.22
Oxygen, wt% (diff)	1.36-2.21	1.4	1.10	0.76
H/C Atom Ratio	1.51-1.58	1.59	1.54	1.62
V, Ni, Fe, Cu, ppm	-	<4.5	<25.0	-
Characterization Factor	-	10.9	10.9	-
Ash, wt%	-	0.002	0.01	-
Conradson Carbon, wt%	-	0	0	-
Pour Point, °C	-	-59	-26	-
Bromine Number, g/100g	-	8	14	-
Aniline Point, °C	-	23.8	-	-
Kin. Viscosity, cSt, @38°C	-	2.1	3.1	-
Phenolic-OH Conc., meq/g	-	0.18	-	-
Acidity, meq/g	-	-	0.38	-
GC Simulated Dist., °C				
IBP	36-57	-	-	-
10%	118-180	85	80.5	-
50%	277-331	253	270	-
95%	363-417	362	379	-

Data Source for Tables 1 through 4:
Burke et al. 1991.
Kramer 1991.
Vimalchand et al. 1991.
Winschel, Burke, and Zhou 1991.
Kowalski and Basu 1984.
SEI 1991.
Winschel and Zhou 1991.
Zhou and Rao 1992.

TABLE 2
PROPERTIES OF WILSONVILLE COAL-DERIVED NAPHTHAS

Coal	Illinois No. 6[1]	Pittsburgh Seam	Black Thunder	gasoline Specs
Cut, °C	IBP-182	IBP-193	IBP-193	
Gravity, °API @15°C	43.1	48.9	50.9	
D86 Distillation, °C				
10%	74[2]	91	80[2]	70 max
50%	121	126	116	77-121
90%	173	172	171	190 max
EP	197	187	204	225 max
RVP, kPa	-	19.3	21.4	62 max[3]
Elemental, wt%				
C	85.2	85.3	84.3	
H	12.9	13.3	13.6	
N	0.008	<0.1	0.1	
S	0.36	0.05	0.08	0.10 max
O (diff)	1.56	1.25	1.92	
Group Analysis, vol%				
Paraffins	15.9	19.3	} 88.0	
Naphthenes	60.7	67.5		
Aromatics	23.4	13.2	7.0	
Olefins	5.5	-	5.0	
Acidity, mg KOH/g	-	-	0.38	
Phenolic-OH, meq/g	-	0.18	0.40	
Motor Octane	73.4	86.5[4]	87.1[4]	
Existent Gum, mg/g	-	7.6	40.2	5 max
Copper Corrosion	-	1A	1A	1 max
Oxidation Stability, min	-	Pass	Fail	240 min
Yield, wt%				
on Total Coal Liquid	18.4	26.7	23.7	
on maf Coal	-	19.7	-	

[1] Wilsonville Run 244.
[2] GC Simulated.
[3] Class A.
[4] by GC method.

TABLE 3
PROPERTIES OF WILSONVILLE KEROSENE FRACTIONS

Coal	Illinois No. 6	Pittsburgh Seam	Black Thunder	Jet A-1 Specs
Cut, °C	182-232	193-266	193-266	
Gravity, °API @15°C	22.9	25.9	21.3	37-51
D86 Distillation, °C				
10%	178[1]	220	2121	205 max
50%	200	227	242	
90%	222	244	259	
EP	379	262	346	300 max
RVP, kPa	-	9.6	-	20.7 max
Flash Point, oC	-	76.1	86.7	38 min
Freezing Point, oC	-	-53.5	dark	-47 max
Elemental, wt%				
C	84.4	87.0	85.8	
H	10.9	11.5	10.6	
N	0.22	<0.1	0.3	
S	0.23	0.04	0.04	0.30 max
Mercaptan S	-	0.003	0.009	0.003 max
O (diff)	4.26	1.36	3.26	
Group Analysis, vol%				
Paraffins	-	-		
Naphthenes	-	-		
Aromatics	-	44.0	50.0	25 max
Olefins	-	3.0	3.0	5 max[2]
Naphthalene	-	-	4.94	
Smoke Point, mm	-	10.8	9.8	25 min
Acidity, mg KOH/g	-	0.05	0.50	0.1 max
Phenolic-OH, meq/g	-	0.25	0.92	
Kin. Viscosity, cSt @ -20°C	-	1.75	18.94	8 max
Existent Gum, mg/g	-	69.0	90.8	7 max
Copper Corrosion	-	1A	1A	1 max
JFTOT	-	Fail	-	25/3 Min.
Net Heat Value, MJ/kg	-	42.1	42.0	42.8 min
Yield, wt%				
on Total Liquid	11.0	31.4	19.0	
on maf Coal	-	23.1	-	

[1] GC Simulated. [2] applicable to Jet B.

TABLE 4
PROPERTIES OF WILSONVILLE COAL-DERIVED MIDDLE DISTILLATES

Coal	Illinois No. 6	Pittsburgh Seam	Black Thunder	No. 1 Diesel
Cut, °C	182-343	266+	266-343	
Gravity, °API	18.6	16.3	17.7	
GC Simulated Dist.,°C				
10%	193	-	256	
50%	250	-	289	
90%	317	365	321	288 max
EP	379	-	346	
Flash Point, °C	-	-	124	38 min
Elemental, wt%				
C	86.3	88.4	87.0	
H	10.7	10.5	10.7	
N	0.23	0.1	0.3	
S	0.22	0.04	0.03	0.50 max
O (diff)	2.48	0.96	1.75	
H/C Atom Ratio	1.49	1.43	1.48	
Aromatic Carbon, %	34.0	-	-	
Bromine No. g/100g	-	7.4	17	
Viscosity, cSt, @40°C	-	8.97	6.2	1.3-2.4
Ramsbottom Carbon, %	0.15	-	-	0.15 max
Hot C. Insolubles, %	0.48	-	-	
Ash, wt%	-	0.02	0.00	0.01 max
Copper corrosion	-	1A	1A	3 max
Cetane Index	21	26.5	27.7	40 min[1]
Yield, wt% on Total Liquid	45.7	41.9	22.9	

[1] Cetane number.

CATALYST SELECTION FOR HYDROTREATING DIESEL FUEL FROM RESIDUE HYDROCRACKING

Patricio S. Herrera, Michael C. Oballa, Arpad F. Somogyvari and Jacques Monnier*
NOVA HUSKY Research Corporation
2928 16th - Street N.E., Calgary, Alberta, Canada, T2E 7K7
* Energy Research Laboratories, CANMET, Energy, Mines and Resources Canada
555 Booth Street, Ottawa, Ontario, Canada, K1A 0G1

Keywords: Hydrotreating, aromatics reduction, sulfur reduction

ABSTRACT

Six commercial catalysts ($NiMo/Al_2O_3$ and NiW/Al_2O_3) were evaluated for the simultaneous reduction of the aromatics and sulfur contents in the diesel fraction (177°C - 343°C) of a hydrocracked atmospheric residue.

The reactions were carried out in a fixed bed reactor operating in an upflow mode. Optimal operating variables were established to maximize aromatics conversion and sulfur removal. In order to rank catalysts according to their performance, short term screening runs were performed. The two best catalysts were selected for which long term runs were carried out. Though the hydrotreated products for all catalysts met required specifications, the optimal operating conditions used in this study were more severe than processing conditions used in existing hydrotreating units.

INTRODUCTION

Diesel fuel properties are said to have an effect on the quantity and type of air polluting emissions from diesel engines. Specifically, the sulfur and aromatics contents of diesel fuels are singled out as the main sources of particulate emissions[1]. In Canada, the contribution of diesel particulates to the total discharges from transportation and industrial diesel engines was estimated at 29 and 23 thousand tons respectively per year[2]. In California, new and stringent emission standards are already set and other states are expected to follow California's example.

To comply with these new regulations, the oil refining industry has been evaluating a number of options to limit the sulfur and aromatics contents of diesel fuels. One way of achieving this goal involves a two-stage process: initial desulfurization with a deep desulfurization-type catalyst (Co-Mo/alumina) followed by aromatics saturation. The second stage may use a Ni-Mo/alumina or noble metal catalyst. Desulfurization would protect the noble metal catalyst against sulfur poisoning[3].

On the other hand, there are new sulfur tolerant catalysts that would achieve both aromatics saturation and sulfur removal in one step[3-5].

The work reported in this paper is part of a project to evaluate available commercial catalysts for simultaneously reducing sulfur and aromatics in diesel oil fractions to be produced at the Bi-Provincial Upgrader (BPU) in Lloydminster, Sask., Canada[6]. This

grassroots facility will upgrade a feedstock containing a 50/50 volumetric blend of Lloydminster/Cold Lake heavy oils to synthetic crude.

The project focused on attaining the proposed specifications for sulfur and aromatics contents in diesel fuel fractions. The selected approach was to study a one-step hydrotreating process using our particular feedstock and several new generation catalysts claiming to achieve the specified reductions.

EXPERIMENTAL

Equipment: Hydrotreating experiments were carried out in a stainless steel tubular fixed bed reactor operated under the following experimental conditions: upflow mode, diluted catalyst bed (reaction zone = 225 mL), isothermal and plug flow, and once through. The experimental system, including the reaction unit, was described and illustrated elsewhere[7].

Catalysts: All commercial catalysts except one (catalyst B) were of the Ni-Mo type on alumina carrier. Catalyst B was a layered arrangement of Ni-Mo and Ni-W catalysts supplied by the same source. Catalyst companies provided a catalyst they considered the most suitable to treat our feedstock. There were no apparent dissimilarities in catalyst properties based on vendor information.

Feedstock: The feedstock was the fraction boiling between 177°C - 343°C obtained from a hydrocracked 50/50 volumetric blend of Cold Lake/Lloydminster residue. The hydrocracked material was distilled on a TBP unit according to procedures described in ASTM D-2892. The properties of the average feed are given in Table 1.

Analytical Methods: Specific gravities were measured at 15.5°C using a Paar DMA instrument. Dynamic viscosities were determined at 25°C on a Brookfield DV II apparatus. Carbon and hydrogen were determined commercially on a Perkin Elmer 240B analyzer. Trace nitrogen was obtained by chemiluminescence using an Antek Model 771 analyzer, while trace sulfur was measured by microcoulometry using a Dohrmann instrument, model MCTS 130. The total per cent aromatics was determined by the fluorescent indicator adsorption (FIA) method (ASTM D-1319). Simulated distillations were performed according to ASTM D-2887. Low resolution mass spectrometry (MS) analyses for aromatic types were determined commercially by ASTM D-3239. Cetane number was determined by ASTM D613 and Aniline Point by ASTM D611.

RESULTS AND DISCUSSIONS

The initial part of the study included catalyst activity runs to select the process conditions which produced a liquid product meeting the specifications established for the BPU middle distillate fraction (177°C - 343°C)[6]. These values correspond to, among others, sulfur content in product at 1000 wppm max. and cetane number at 40 min.

The base conditions chosen after the initial runs were: T = 380°C, P = 12.4 MPa and LHSV = 0.75 h^{-1}. A single catalyst (A) was used for all the initial runs.

The catalyst screening program involved experiments to rank six commercial catalysts according to their efficiencies in sulfur and aromatics conversions. Each catalyst was tested at base conditions and at various temperatures, pressures and liquid hourly space velocities (LHSV) to determine the influence of these parameters on catalyst performance. All experiments were performed using the same hydrogen-to-feed ratio (1000 Std.m^3/m^3).

The properties determined on the total liquid product obtained from each run included measurements of density, viscosity, sulfur and nitrogen content, simulated distillation, total aromatics by FIA and elemental analysis. The properties of the average feedstock and of the products obtained at base conditions are shown in Table 1.

AROMATICS CONVERSION

The aromatics content of the total liquid product was used (instead of the cetane number) to compare catalyst activities. The FIA method was used to measure concentrations of aromatics in feed and products. To confirm the FIA results and to expand the information on aromatics distribution, additional analyses using Robinson and Cook's mass spectrophotometric technique[8] were performed only on products obtained at base conditions. Table 2 shows the aromatics content of hydrotreated products determined by both procedures. The level of aromatics concentration recorded by the MS method was lower than that observed using FIA. The difference may be attributed to some of the problems observed with the FIA method: the analysis includes as aromatics other compounds such as diolefins and sulfur, nitrogen and oxygen containing materials[9]. Nevertheless, the trend observed with FIA for aromatics reduction with different catalysts was confirmed by MS results and, in addition, it was observed that conversion of diaromatics and polyaromatics to monoaromatics was almost complete.

The reduction in total aromatics with increase in reaction pressure is a well known aspect of the hydrotreating process[9,10]. In our work, the effect of pressure on aromatics conversion was studied over a wide pressure range at base values of temperature and LHSV (Figure I). Our results indicate that in order to get aromatic conversions above 50% (or concentrations below 20 vol%), one has to operate at a pressure above 10 MPa. At higher pressures all catalysts exhibited higher aromatic conversions, confirming that the hydrogenation reaction is very much favored by pressure. Catalysts B and C clearly outperformed the others with respect to aromatics reduction. On the other hand, catalysts B and C also presented better hydrocracking activities by producing lighter fractions in the total liquid product (Table 1).

The influence of reaction temperature on aromatics conversion in middle distillate fractions has been studied before[11-13]. An optimum temperature of 380°C was determined[12] to achieve a maximum aromatics conversion. The base temperature found by us agrees with the optimum temperature previously measured. Our study covered the 350 - 380°C temperature range, at base values of pressure and LHSV.

Again catalysts B and C exhibited the best activity for aromatics saturation (Figure II). Aromatics conversion increased linearly with reaction temperature for all catalysts tested in the program. Even at the lowest end of the temperature range (350°C) catalyst B achieved aromatics conversion above 65% (or concentrations of 15 vol%). At 365°C, all catalysts attained conversions exceeding 50% which correspond to concentrations below 20 vol%.

The effect of LHSV on aromatics conversion, at base values of temperature and pressure, is shown in Figure III. At low LHSV, all catalysts achieved conversions above 80%. At the highest LHSV tested, 1.0 h^{-1}, the conversion level surpassed 60% (or aromatics concentration below 18 vol%). Based on equal amount of conversion, the LHSV influence on aromatics reduction is not as marked as that produced by pressure or temperature.

According to the results presented, clearly aromatics saturation was more dependent on pressure than on any other parameter. Also, some of the combinations of the operating conditions reduced the aromatics concentration below the levels established in impending specifications for diesel fuels. The severe process conditions at which these requirements were met are, however, out of line with the operating parameters of existing diesel hydrotreating units.

SULFUR AND NITROGEN CONVERSIONS

Under all experimental conditions tested, sulfur conversions exceeded 90%. At base conditions removal of sulfur surpassed 94% (Table 1). Therefore, the target sulfur concentration was easily achieved by all catalysts at the operating conditions used. On the other hand, nitrogen conversions above 99% (corresponding to less than 5 wppm in product) were achieved in all of the runs performed. No significant differences were observed in the catalysts' performance from the point of view of sulfur and nitrogen removal.

INFLUENCE OF CATALYST PROPERTIES

The catalysts' properties were determined in an attempt to find the origin of the differences observed in catalysts' performance. We wished to compare the various conversions for each catalyst on an equal basis. The basis chosen was the unit surface area conversion. The catalyst components believed to affect in greater extent the conversions were nickel, molybdenum, phosphorus and tungsten. In Figure IV, the [Ni + Mo(W) + P] weight per unit surface area was plotted against the conversion for the same area. The results demonstrated that catalysts exhibiting higher coverage per unit area (B and C) were the ones performing better as far as aromatics, sulfur and nitrogen conversions are concerned. There was little correlation for independent components suggesting the existence of a synergism effect among all these elements.

CATALYST DEACTIVATION EXPERIMENTS

Long term runs of approximately 1000 hours were carried out using the two best catalysts from the screening experiments (B and C). The purpose of this task was to

study the rate of deactivation of the selected catalysts at base conditions. No marked difference in catalysts' performance was found except for hydrogen consumption (Table 3). It was the original intent of this part of the study to project catalyst life based on a deactivation curve. However, this was not possible because within the length of the runs, little deactivation occurred. The layered bed of NiMo and NiW on alumina (catalyst B) showed lower hydrogen consumption for similar aromatics conversions. The cetane number of liquid products showed similar results.

CONCLUSIONS

All six commercial catalysts studied satisfied upcoming specifications on the sulfur content for diesel fuels. Also, at base conditions, all catalysts reduced the aromatics content of the feed to less than 20 vol%. The operating conditions at which these requirements were met are, however, out of line with the operating conditions of existing diesel hydrotreating units. This implies that a single stage process for hydrotreating middle distillates can only meet the impending specifications with a new reactor designed and built specifically for these operating conditions.

Two out of six catalysts (B and C) outperformed the others in aromatics conversion. It was found that the activity of these catalysts showed marked dependence on the total coverage of definite fresh catalyst components. After the catalyst deactivation experiments, the choice between catalysts B and C was based on economics because they exhibited similar technical performance.

ACKNOWLEDGMENTS

The authors thank Mr. Leon Neumann who performed the hydrotreating experiments and was responsible for part of the analytical work. Our thanks also go the Analytical Services Group at NHRC. Part of this work was supported by a 50/50 cost-shared program between Husky Oil Ltd. and CANMET, EMR, Ottawa, under contract number 23440-0-9018/01-SQ.

REFERENCES

1. Weaver,C.S.; Miller,C.; Johnson,W.A.; Higgins,T.S., SAE Technical Paper 860622 (1986).
2. *A Plan to Identify and Assess Emission Reduction Opportunities from Transportation*, Industrial Engines and Motor Fuels, Transportation Systems Division, Environment Canada, TP 9773E (May,1989).
3. Cooper,B.H.; Stanislaus,A.; Hannerup,P.N., Prepr. Am. Chem. Soc. Div. Fuel Chem. 1992, **37**, 41.
4. Nash,R.M., Oil and Gas Journal 1989, **87** (22), 47-56.
5. Parkinson,G.; Johnson,E., Chem. Eng. 1989, **96** (9), 31-46.
6. Chase,S., Paper presented at the Sixth Annual Heavy Oil and Oil Sands Technical Symposium, Calgary, AB, March 1989.
7. Herrera,P.S.; Oballa,M.C.; Somogyvari,A.F., Paper presented at the 41st Annual Canadian Chemical Engineering Conference, Vancouver, B.C., Oct. 1991.
8. Robinson,C.J.; Cook, G.L., Anal. Chem. 1969, **41**, 1548.

9. Assim,M.Y.; Keyworth,D.A.; Zoller,J.R.; Plantenga,F.L.; Lee,S.L., Paper presented at the AKZO Catalysts Seminar, Calgary,AB, July 1990.
10. Nash,R.M., Paper presented at the NPRA Annual Meeting, San Francisco, CA, March 1989, paper AM-89-29.
11. Wilson,M.F.; Kriz,J.F., Fuel 1984, **63** (2),190-196.
12. Wilson,M.F.; Fisher,I.P.; Kriz, J.F., J.Catalysis 1985, **95** (8), 155- 166.
13. Wilson,M.F.; Mainwaring,P.R.; Brown,J.R.; Kriz.J.F., Preprints 10th Canadian Symposium on Catalysis, Kingston, Ontario, June 1986.

TABLE 1

AVERAGE FEEDSTOCK AND PRODUCT PROPERTIES AT BASE CONDITIONS

	FEED STOCK	PROD. A	PROD. B	PROD. C	PROD. D	PROD. E	PROD. F
Density (g/cm^3)	0.8554	0.8308	0.8282	0.8251	0.8333	0.8266	0.8503
Viscosity (cP)	3.2	2.0	2.6	2.3	2.7	2.7	3.6
Carbon (wt%)	86.96	86.01	85.38	85.67	86.13	85.99	86.14
Hydrogen (wt%)	12.23	13.27	13.77	14.22	13.80	13.92	13.30
Sulfur (wppm)	3858	112	181	195	138	82	64
Nitrogen (wppm)	752	5	<1	<1	2	1	<1
Sim. Distribut. (wt%):							
IBP - 177°C	0.9	4.7	6.8	5.8	4.7	5.6	3.5
177 - 249°C	39.6	44.3	47.7	48.2	37.3	47.4	27.5
249 - 343°C	58.6	50.1	43.7	44.7	57.0	45.6	64.1
343 - 524°C	0.9	0.9	1.8	1.3	1.0	1.4	4.9

Notes: (i) A, B, C, D, E, F are commercial catalysts;
(ii) Base Conditions: T = 380°C; P = 12.4 MPa; LHSV = 0.75 h^{-1}

TABLE 2
TOTAL AROMATICS AT BASE CONDITIONS

	FEED-STOCK	PROD. A	PROD. B	PROD. C	PROD. D	PROD. E	PROD. F
F.I.A. (vol.%)	43.6	12.5	6.0	7.1	11.2	9.8	17.0
Mass Spec. (wt%):							
Monoaromatics	30.60	7.31	2.18	5.08	7.74	9.29	11.12
Diaromatics	5.59	0.18	0.07	0.09	0.17	0.18	0.43
Polyaromatics	0.05	0.01	0.00	0.08	0.13	0.03	0.61
Aromatic Sulfur	0.74	0.03	0.04	0.00	0.02	0.00	0.12
Total Aromatics	36.98	7.53	2.29	5.25	8.06	9.50	12.28

TABLE 3
LONG TERM RUNS, AVERAGE QUALITY OF TOTAL LIQUID PRODUCTS

CATALYST	B	C
Cetane Number (ASTM D613)	50.3	50.7
Aniline Point, °C (ASTM D611) Modified	70.70	71.25
Sulfur (wppm)	259	174
Nitrogen (wppm)	3	<1
FIA Aromatics (vol%)	5.1	4.6
Aromatics Conversion (%)	84.40	87.50
Sulfur Conversion (%)	91.07	94.00
Nitrogen Conversion (%)	99.39	99.93
Density (g/cm^3)	0.8240	0.8225
API Gravity	40.2	40.5
Viscosity (cP)	2.4	2.4
Carbon (wt%)	85.98	86.25
Hydrogen (wt%)	13.56	13.74
H_2 Consumption:		
L H_2/L feedstock	56.2	74.6
(SCF H_2/BBL feedstock)	(315)	(419)

Note: Operating Conditions: T = 380°C; P = 12.4 MPa; LHSV = 0.75 h^{-1}

FIGURE I: EFFECT OF REACTION PRESSURE ON AROMATICS CONVERSION

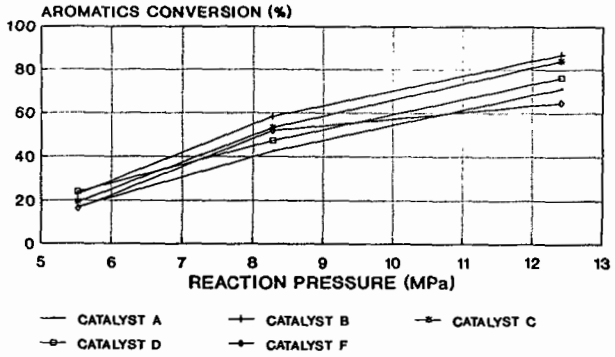

Temperature = 380 deg C
LHSV = 0.75 hr⁻¹

FIGURE II:EFFECT OF REACTION TEMPERATURE ON AROMATICS CONVERSION

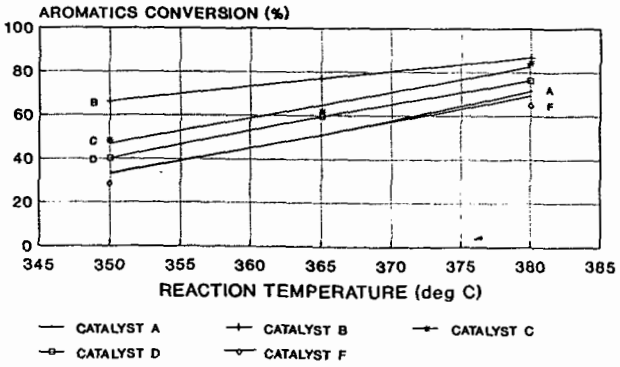

Pressure = 12.4 MPa
LHSV = 0.75 hr⁻¹

FIGURE III: EFFECT OF LHSV ON AROMATICS CONVERSION

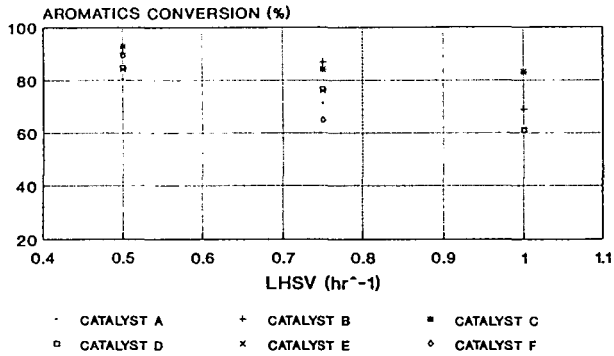

Temperature = 360 deg C
Pressure = 12.4 MPa

FIGURE IV: CONVERSION AS A FUNCTION OF CATALYST COMPONENTS COVERAGE

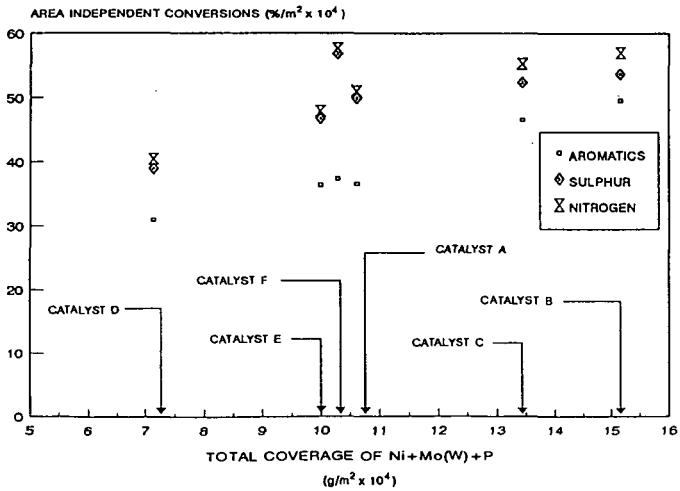

PROMOTED HYDROTREATING CATALYSTS

A. S. Hirschon, L. L. Ackerman, and R. B. Wilson
SRI International

Y. Horita and T. Komoto
Nippon Steel Chemical Corporation

Keywords: Hydrotreating, HDN, catalysts

INTRODUCTION

With dwindling supplies of high quality petroleum feedstocks, efforts are being taken to utilize alternative feedstocks such as heavy crudes and coal liquids as sources for chemicals and alternative fuels. However, these feedstocks are often heavily aromatic and contain large amounts of heteroatoms such as nitrogen, sulfur, and oxygen. Nitrogen and oxygen are so difficult to remove that extremely strenuous conditions are required. However, under these severe conditions the valuable aromatics are also excessively hydrogenated, wasting valuable hydrogen. Attempts to improve the current hydrotreating catalysts such as NiMo, CoMo, and NiW that have been developed for petroleum feedstocks have met with little success. What is needed are catalysts that are more selective toward hydrogenolysis activity rather than hydrogenation reactions. Therefore efforts are being conducted to find catalysts that can selectively remove heteroatoms, in particular, nitrogen. Workers have shown in systematic studies that for each row of the periodic table a correlation occurs between the position and the reactivity of the bulk metal towards hydrogenolysis reactions, with the lower rows being the most active.[1-4] Using this methodology, certain noble metals such as ruthenium have been identified as highly active hydrogenolysis catalysts.

Since the ratio of the hydrogenolysis to hydrogenation activity varies with the nature of the catalyst, various metals and metal combinations have been investigated in efforts to find catalysts with improved selectivity and high ratios of hydrogenolysis to hydrogenation activities.[5-10] Recently it has been shown that when ruthenium was used in conjunction with molybdenum, a very active and selective hydrodenitrogenation catalyst was formed. In this work we investigated several methods of preparation of this catalyst and their respective activities towards both model systems and coal tars.

EXPERIMENTAL

Catalyst Preparation

Alumina extrudates were used for coal tar testing whereas powdered alumina was used for the model system testing. Molybdenum and nickel salts were impregnated into the alumina by standard incipient wetness techniques. Ruthenium was added as the carbonyl for the majority of the catalysts; the methodology for incorporation of ruthenium and activation of the catalyst is described in the text.

Catalyst Testing

The catalysts were evaluated for HDN and HDO using quinoline and diphenylether, respectively. Under nitrogen, 0.100 g of catalyst, 10 mL of a 0.197 M quinoline, and 0.086 M n-tetradecane (internal standard) and/or 0.150 M diphenyl ether were placed in a quartz liner in a 45-mL Parr bomb. The Parr bomb was pressurized with 500 psig of H_2 and heated for the desired times and

temperatures. The quinoline and the diphenyl ether were used to compare the catalysts for HDN and HDO activities, respectively. The HDN reactions were run at 350°C, and the HDO reactions were run at 250° to 300°C. The competitive HDN/HDO reactions were run at 350°C.

The HDN activities of the catalysts were compared by calculating the turnover frequencies (TF) for the disappearance of tetrahydroquinoline (THQ) and formation of propylbenzene (PB) and propylcylohexane (PCH). Selectivities were determined from the relative distribution of PCH, PB, and propylcyclohexene (PCHE) when 5% of quinoline had been converted to these hydrocarbon products. HDO activities were compared by calculating the TF for the disappearance of diphenyl ether (DPE) and appearance of cyclohexane and benzene. HDO selectivities were determined from the relative proportions of benzene, cyclohexane, and phenol at a given level of conversion.

The activities of the catalysts were evaluated for the hydrotreatment of coal tars using a continuous flow reactor with 20 mL of catalyst at 360°C, 180Kg/cm^2 pressure hydrogen and LHSV of 0.5h^{-1}. The reaction was monitored by elemental analysis of the product stream with samples taken after 100 h on-stream.

RESULTS AND DISCUSSION

Hydrogenolysis of Model Compounds

Since both nitrogen and oxygen containing molecules cause the most problems in upgrading coal derived liquids, both HDN and HDO reactivities on model systems were investigated. A summary of the effect of ruthenium promotion of supported NiMo and CoMo alumina catalysts on the HDN reaction of quinoline (Table 1) shows that the promoted CoMo gives exceptional performance; even greater than that of promoted NiMo under these conditions. Furthermore, the promotion shows a large increase in selectivity for the CoMo system from a PCH/PB ratio of 15:1 to 3:1, compared to an increase of 4.9:1 to 2.6:1 for the NiMo system. However, when the RuCoMo catalyst was examined for the HDO of diphenylether, the CoMo catalysts was actually found to be more reactive; but when examined in a competition study with both quinoline and diphenylether present, the reverse order was found and the promoted RuCoMo catalyst was both the most active and selective catalyst. Apparently the amine reduced the HDO activity of the CoMo catalyst to a greater extent than the RuCoMo catalyst. Thus we would expect that the ruthenium promoted catalysts would be most useful in hydrotreating coal liquids and other alternative fuels.

Method of Activation and Preparation

The procedure we used for the formulation of the ruthenium promoted catalyst involved presulfiding the molybdenum based catalyst and then adding ruthenium carbonyl. The objective of this synthesis was to add the ruthenium to the sulfidryl groups of the sulfided metal (molybdenum for instance). This procedure was based on the methods of Yermakov, and was designed to produce a highly dispersed mixed metal cluster.[11] However, in common practice catalysts are not sulfided as an intermediate step, and therefore we varied the order of sulfiding and calcining as follows, to determine if there would be any effects on the activities and selectivities of these ruthenium promoted catalysts. Promoted molybdenum catalysts were prepared by three different methods. Method 1 consisted of impregnating the molybdenum catalyst with the ruthenium carbonyl in THF, evaporating the THF, and then first calcining and then sulfiding the product at 400°C. The method is similar to a conventional catalyst preparation, where each metal is sequentially added and calcined. The calcination step assures that the metals interact with the

support for high dispersion and to prevent loss of metal during use. Method 2 consisted of sulfiding the RuMo product without the second calcining step. In Method 3, we prepared the catalyst our normal way, first sulfiding the molybdenum catalyst and adding the ruthenium to the sulfided molybdenum catalyst, and then sulfiding again.

The activities and selectivities of the catalysts prepared by these methods are listed in Tables 3 and 4 for HDN reactions using quinoline as a model system. As seen in these tables, the selectivity of the catalyst produced by method 1 is high, giving a PCH/PB ratio of 3.0, but the overall activity is much lower than that for the other two methods, having a rate almost 200 times less active than for method 3. As seen for Methods 2 and 3, the activities are greatly improved, with method 3 being the most active for HDN activity. We believe that the difference between the activities is due to the sulfiding of the molybdenum prior to the promotion with Ru. Thus method 1 should give strong Al-O-Ru interactions, whereas method 3 should give Mo-S-Ru interactions, which we postulate will allow a synergy between the Mo and Ru.

Testing of Catalysts on Coal Tars

In order to verify these results on model systems, samples of RuCoMo, RuNiMo, and RuMo were evaluated for hydrotreating of coal tars. Table 5 lists some of these results. As seen from this table, there were both similarities and differences from the results on the model systems. For instance, the promotion of the CoMo catalyst (2A) to form RuCoMo (2B) gave little difference in the HDN of the coal tar (HDN rates of 0.47 and 0.44, respectively). However, promotion of the CoMo catalyst gave a very dramatic increase in reactivity and selectivity for quinoline HDN. In contrast, the promotion of NiMo (1A) with ruthenium to form RuNiMo (1B) did indeed increase the reactivity towards coal tars, and increasing both the rate of nitrogen removal (from 0.43 to 0.55) as well as increasing the selectivity of HDN to hydrogenation reactions. Catalyst 3A and 3B were RuMo catalysts designed to compare the method of preparation as previously described in the model systems. Catalyst 3A was prepared by first sulfiding the molybdenum and then adding ruthenium (Method 3), and 3B was prepared by adding the ruthenium to the calcined molybdenum, calcining again, and then sulfiding (Method 1). Again, as with the model systems, the presulfiding increased the activity of the catalyst.

CONCLUSIONS

Ruthenium promotion enhances HDN activity under low-severity hydrotreating of coal tars, confirming our previous studies with model systems. Promotion of CoMo is not as effective on coal tars as with model systems, and may depend upon the type of feedstock. However, promotion of NiMo gave enhanced HDN activity and selectivity for both systems. The key to the high activity and selectivity appears to be adding the ruthenium to a previously sulfided molybdenum catalyst. The reason for this high activity, we believe, is the formation of a Ru-S-Mo interaction, which may allow a better synergistic relationship. However, alternative explanations may be possible, and a more detailed study of these catalysts may lead to a better description of the active site.

REFERENCES

1. H. Sinfelt, Prog. Sol. St. Chem. (1975), 10, 55-69.

2. T. A. Pecoraro and R. R. Chianelli, J. Catal. (1981), 67, 430

3. S. Harris and R. R. Chianelli, J. Catal. (1984), 86, 400-412.

4. A. S. Hirschon and R. M. Laine, Energy and Fuels, (1988), 2, 292-295.

5. A. S. Hirschon, R. B. Wilson, Jr. and R. M. Laine, Amer. Chem. Soc. Div. Pet. Prepr. (1987), 32(2), 268-270.

6. A. S. Hirschon, R. B. Wilson Jr., and R. M. Laine, Appl. Catal. (1987), 34, 311-316.

7. J. Shabtai, N. K. Nag, K. Balusami, B. Gajjar and F. E. Massoth, Amer. Chem. Soc. Div. Pet. Prepr., 31 (1986) 231.

8. J. Shabtai, N. K. Nag and F. E. Massoth, J. Catal., 104 (1987) 413.

9. T. G. Harvey and T. W. Matheson, J. of Catal., 101, (1986) 253-261.

10. S.-M. Koo, M. L. Hoppe, and R. M. Laine, Amer. Chem. Soc. Div. Pet. Prepr. (1992), 37(1), 290-297.

11. I. Yermakov, Catal. Rev.-Sci. Eng., (1976)., 13, 77-120.

Table 1

TURNOVER FREQUENCIES FOR QUINOLINE FOR QUINOLINE HDN[a] USING PROMOTED CATALYSTS

		TF[b]		
No.	Catalyst	THQ	PCH	PB
1	CoMo	54	8.9	0.5
2	RuCoMo	141	27	8.0
3	NiMo	86	15	1.7
4	RuNiMo	128	14	5.5

[a]Reaction of 10 mL of 0.197 M quinoline in n-hexadecane and 0.100 g of sulfided catalyst at 350°C and 500 psi H_2.
[b]TF = moles reactant or product/mol Metal/h.

Table 2

SELECTIVITY AT 5 mol % CONVERSION[a]

No.	Catalyst	% PCH	% PB	% PCHE	PCH/PB
1	CoMo	82.2	4.6	13.2	17.8
2	RuCoMo	76.6	23.4	0	3.3
3	NiMo	73.3	14.9	11.8	4.9
4	RuNiMo	71.5	27.5	1.0	2.6

[a]Reaction of 10 mL of 0.197 M quinoline in n-hexadecane and 0.100 g of sulfided catalyst at 350°C and 500 psi H_2.

Table 3

EFFECT OF METHOD OF PREPARATION OF RuMo CATALYST FOR QUINOLINE HDN[a]

No.	Method	TF[b] THQ	TF[b] PCH	TF[b] PB
1	$Ru/O_2/H_2S$[c]	50	0.3	0.1
2	$O_2/Ru/H_2S$[d]	67	14	2.3
3	$O_2/H_2S/Ru/H_2S$[e]	180	48	11

[a]Reaction of 10 mL of 0.197 M quinoline in n-hexadecane and 0.100 g of sulfided catalyst at 350°C and 500 psi H_2.
[b]TF = moles reactant or product/mol Metal/h.
[c]Ru added to calcined Mo, calcining Ru, and then sulfiding.
[d]Ru added to calcined Mo, and then sulfiding.
[e]Ru added to sulfided Mo, and sulfided again.

Table 4

SELECTIVITY AT 5 mol % CONVERSION[a]

No.	Method	% PCH	% PB	% PCHE	PCH/PB
1	$Ru/O_2/H_2S$[b]	63	21	16	3.0
2	$O_2/Ru/H_2S$[c]	80	14	6	5.7
3	$O_2/H_2S/Ru/H_2S$[d]	75	21	4	3.6

[a]Reaction of 10 mL of 0.197 M quinoline in n-hexadecane and 0.100 g of sulfided catalyst at 350 C and 500 psi H_2.
[b]Ru added to calcined Mo, calcining Ru, and then sulfiding.
[c]Ru added to calcined Mo, and then sulfiding.
[d]Ru added to sulfided Mo, and sulfided again.

Table 5

EFFECT OF CATALYST ON HYDROTREATMENT OF COAL TARS

Run No.	Catalyst Type	HDN			Hydrogenation			Selectivity
		N(wt%)[a]	DNR (%)[b]	Kn[c]	C(wt%)[a]	H/C[d]	ΔH/C[e]	Kn/ΔH/C
1A	NiMo	0.43	57.8	0.43	91.37	1.00	0.31	1.39
1B	RuNiMo	0.33	67.6	0.55	90.62	1.07	0.38	1.45
2A	CoMo	0.38	62.7	0.47	91.24	1.06	0.37	1.27
2B	RuCoMo	0.42	58.8	0.44	91.16	1.06	0.37	1.19
3A	RuMo-3[f]	0.40	60.8	0.46	90.61	1.08	0.39	1.17
3B	RuMo-1[g]	0.54	47.1	0.32	91.82	0.93	0.24	1.33

[a]Wt % in product.
[b]Degree of nitrogen removal.
[c]Rate of nitrogen removal hr^{-1}.
[d]Mole ratio.
[e]H/C(product)-H/C(feed).
[f]Mo(sulfided) + Ru.
[g]Mo + Ru, then sulfided.

HYDROCRACKING OF HEAVY OILS: DEVELOPMENT OF STRUCTURE/REACTIVITY CORRELATIONS FOR KINETICS

Ralph N. Landau, Styliani C. Korré, Matthew Neurock and Michael T. Klein

Center for Catalytic Science and Technology, Department of Chemical Engineering
University of Delaware, Newark, DE 19716

and Richard J. Quann

Mobil Research and Development Corporation
P.O. Box 480, Paulsboro, NJ 08066-0480

KEYWORDS

Hydrocracking, Phenanthrene, 1-methyl naphthalene, Linear Free Energy Relationships

ABSTRACT

The catalytic hydrocracking reaction pathways, kinetics and mechanisms of 1-methyl naphthalene and phenanthrene were investigated in experiments at 350 °C and 68.1 atm H_2 partial pressure (190.6 atm total pressure), using a presulfided Ni/W on USY zeolite catalyst. 1-methyl naphthalene hydrocracking led to 2-methyl naphthalene, methyl tetralins, methyl decalins, pentyl benzene and tetralin. Phenanthrene hydrocracking led to dihydro, tetrahydro and octahydro phenanthrene, butyl naphthalene, tetralin to butyl tetralin and dibutyl benzene. The rate constants for the dealkylation of butyl tetralins produced in the phenanthrene hydrocracking network conform to a linear free energy relationship (LFER), with the heat of formation of the leaving alkyl carbenium ion as the reactivity index.

INTRODUCTION

Catalytic hydrocracking is a versatile process for increasing the hydrogen to carbon ratio and decreasing the molecular weight of heavy oils. This versatility may prove extremely valuable in the search for optimal processing conditions and catalysts for production of "reformulated" gasolines. Associated reaction models will likely increase in detail as increasingly molecular output is desired. However, the complexity of hydrocracking feedstock structure and reactivity has kept traditional models somewhat global and, thus, often feedstock dependent. Therefore, the new, feedstock-sensitive, "molecular" models of hydrocracking reaction chemistry require the development of a critical mass of consistent molecular reaction pathways and kinetics as an essential data base. To this end, we report here on hydrocracking reaction pathways of 1-methyl naphthalene and phenanthrene, components among a broader set aimed at sampling the structural attributes of hydrocracking feedstocks. Special attention is devoted to the efficient organization of the resolved kinetic information into quantitative structure/reactivity correlations that will serve as a component of a broader kinetic data base.

The present work builds on the significant current understanding of the hydrocracking of paraffins (Froment, 1987) and extends to examine aromatic hydrocarbons. The aromatics' hydrocracking literature is less comprehensive. Several investigations on hydrocracking model bare ring polynuclear aromatic hydrocarbons involved Al_2O_3 or Si/Al_2O_3 catalysts (Qader, 1973; Shabtai et al., 1978; Lemberton and Guisnet, 1984). The effect of zeolite catalysts is examined in more recent publications (Haynes et al., 1983; Lapinas et al., 1987).

We report here on the reactions of 1-methyl naphthalene and phenanthrene. The experiments were focused on the target of discerning reaction families and characterizing them in terms of Quantitative Structure/Reactivity Correlations. We describe the work by first considering the experimental methods. The kinetics of 1-methyl naphthalene and phenanthrene hydrocracking are considered next. Finally, discernible linear free energy relationships are examined.

EXPERIMENTAL

Cyclohexane (HPLC grade, 99.99%, Aldrich) served as the solvent for the study of the reactions of the remaining compounds. Phenanthrene (98%+, Aldrich), served as the prototype three-ring aromatic moiety. Its staggered structure, makes it thermodynamically more stable than anthracene, and thus more abundant in heavy oils. 1-methyl naphthalene (98%, Aldrich) could in principle be obtained from the phenanthrene network, but its high rank in the network made parameters estimated statistically insignificant. All reactants were used as received.

The catalyst was a Mobil conditioned Zeolyst 753 Ni/W on USY zeolite, received in standard 3.0 mm pellets. Prior to all experiments, it was sulfided for two hours at 400° C by a 10% H_2S in H_2 gas stream (99%, Matheson Gas Products) at a flow rate of 30 cm^3/min. The catalyst was equilibrated by reaction with phenanthrene at 350 °C and 68.1 atm H_2 for ≈10 hours to achieve a steady-state activity that lasted about 50 more hours on stream.

A one-liter spinning basket batch autoclave (modified from original as received from Autoclave Engineers) was the core of the reaction system. A detailed description of the system is available elsewhere (Landau, 1991). The catalyst basket was mounted on the autoclave's agitator which was equipped with baffles to ensure turbulence. Varying the stirring speed revealed the absence of diffusion limitations for a stirring rate of 10 s^{-1} or greater. Also, phenanthrene hydrocracking with powdered catalyst (50-200 mesh) in a slurry exhibited the same kinetic behavior as with the 3.175mm pellets, which suggested that internal transport limitations were not important.

Experiments were routinely performed at 350°C and 68.1 atm H_2 (190.6 atm total pressure, the balance from cyclohexane vapor pressure), with 10g of catalyst in the spinning basket arrangement. The stirring rate was 15 s^{-1}, increased by 50% for 10 min. immediately following the injection. Total pressure was regulated with continuous hydrogen makeup. Sampling was scheduled to remove no more than 5% of the total liquid volume.

Products were identified using a Hewlett Packard 5970 Mass Selective Detector and a Hewlett Packard 5880A Gas Chromatograph, employing a fused silica capillary column and flame ionization detector. Dibenzyl ether (Aldrich, > 99.9%)was used as an external standard. Finally, the

RESULTS

Hydrocracking of 1-methyl naphthalene

Reaction of 25% wt 1-methyl naphthalene took place in cyclohexane as a solvent at 68.1 bar H_2 at 350 °C, and led to 6 identified isomeric lumps, representing 99%+ material balance closure. Kinetics are summarized in Fig. 1. There are two primary products of 1-methyl naphthalene hydrocracking, both with high selectivity : methyl tetralins (lump including 1, 2, 5, and 6-methyl tetralins) and 2-methyl naphthalene (isomerization product). The balance consists of methyl decalins, pentyl benzenes and tetralins.

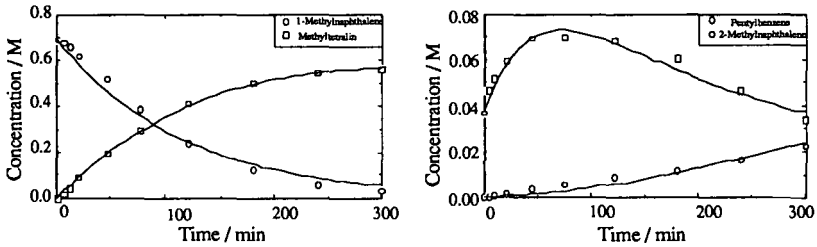

Fig. 1 : Temporal yields of some 1-methyl naphthalene hydrocracking products. Solid lines represent parameter estimation results

Delplot analysis classifies pentyl benzenes as secondary products (direct cracking of methyl tetralins), as well as methyl decalins. Tetralin appeared to be weakly primary product, which implies that their formation is the result of disproportionation reactions of methyl tetralins with the solvent, since no bare-ring naphthalene has been observed.

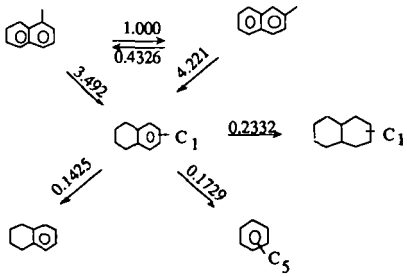

Fig. 2: Proposed network for 1-methyl naphthalene hydrocracking (normalized with 1.49 10^{-3} $l/g_{cat}/min$.)

Parameter estimation for the above network provided more insight into the pathways. Isomerization of 1-methyl naphthalene occurred at a slower rate than its hydrogenation, while 2-

methyl naphthalene hydrogenated at a slightly higher rate than 1-methyl naphthalene. Further reactions of methyl tetralins (hydrogenation to decalins, cracking to pentyl benzenes) occurred with rate parameters one order of magnitude lower.

Hydrocracking of Phenanthrene

Reaction of 3.4 wt% phenanthrene in cyclohexane solvent and at 68.1 atm H_2 at 350 °C led to 11 identified isomeric product lumps, representing 95%+ material balance closure. Each lump represents grouping of molecular weight isomers. For example the tetrahydro phenanthrenes lump includes molecules with cyclohexyl and methyl cyclopentyl saturated rings. *Sym-* and *asym-* octahydro phenanthrenes are in the same lump, and "butyl tetralin" refers to any tetralinic unit sheet with a side chain of four carbon atoms, regardless of its position on the unit sheet.

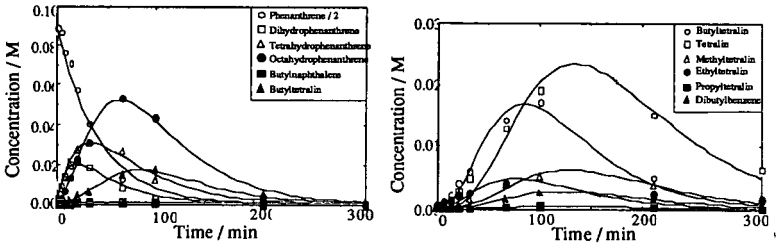

Fig. 3: Temporal yields of some phenanthrene hydrocracking products. Solid lines represent model correlations.

Reaction kinetics are summarized in Fig. 3, which shows, by the initial positive slopes, that dihydrophenanthrene (DHP) and tetrahydro phenanthrenes (THP) were the primary products, DHP forming with higher initial selectivity. Octahydro phenanthrenes (OHP) had very low initial selectivity and were interpreted as secondary products, evolving from THP. Butyl tetralins, ethyl tetralins, tetralins and dibutyl benzenes were higher rank products, evolving mainly from OHP. Butyl naphthalenes, propyl- and methyl tetralins were all clearly of tertiary or higher rank.

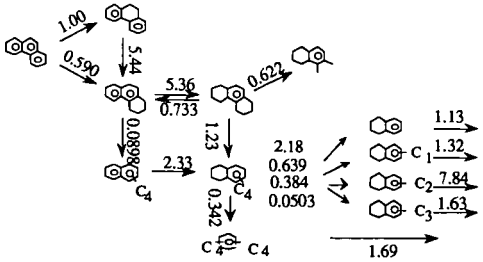

Fig. 4: Proposed network for phenanthrene hydrocracking (normalized with 1.49 10^{-3} $l/g_{cat}/min$.)

DHP did not appear to dehydrogenate back to phenanthrene, as reported over non-acidic catalyst supports (Girgis and Gates, 1991), but rather hydrogenated further to THP. This difference was probably due to the higher H_2 partial pressure employed in this work. THP in turn underwent further hydrogenation to OHP; this was more selective than ring opening to n-butyl naphthalene. The terminal naphthenic ring in OHP was cracked to butyl tetralin, and cleavage of the butyl side chain occurred at various positions.

The optimized kinetic parameter fitting on all the network components of Fig. 4 is presented in Fig. 3, as modeled species' concentration vs. time. Clearly the fit is good. The chemical significance of the rate constants regressed is thus the remaining issue. This is considered more fully below.

LFER DEVELOPMENT

The organization and chemical significance of these kinetics data can be enhanced by the existence of linear free energy relationships (LFER). A LFER will exist for a reaction family with similar transition state sterics (essentially constant A-factor) and reactivities that differ because of differences in activation energies. This will assume the form of a linear correlation between the reactivity of a molecule, as it is expressed through its rate parameter, and its structure, as expressed by a reactivity index pertinent to each reaction. The existence of a LFER not only helps to establish the reaction mechanism, but can also concisely summarize an enormous amount of information in a handful of slopes and intercepts. The data bases constructed in this way will be general and flexible enough to draw useful correlations for process modeling.

The applicability of LFERs in heterogeneous catalysis has been hindered in part because of the uncertainty of controlling elementary steps (Dunn, 1968). Observable kinetics are generally the expression of many elementary steps acting in concert. However, Mochida and Yoneda (1967) uncovered a linear relationship between the logarithm of the observed rate constant for dealkylation of a particular alkyl benzene and the enthalpy change for hydride abstraction from the related paraffin, $\Delta H_c^+(R)$ (Olah et al., 1964). The mechanistic information in this correlation is the suggestion of a rate limiting step for the dealkylation reactions that correlates with the formation of the alkyl carbenium ion. It is also possible that several steps correlate in concert with the same reaction family index. In any case, the modeling value of this correlation is that it allows for the *a priori* prediction of other dealkylation reactions. We follow this perspective in the search for useful correlations to summarize hydrocracking kinetics data.

The butyl tetralin dealkylation reactions observed during hydrocracking of phenanthrene seemed a reasonable point to search for a relationship like that found by Mochida and Yoneda (1967). Careful scrutiny of the kinetic parameters regressed reveals a trend for the dealkylation of butyl tetralins. The dealkylation rate constants increase as the stability of the leaving alkyl carbenium ion increases. This is consistent with the energetics of the formation of the alkyl carbenium ions. This suggests that the formation of the alkyl carbenium ion could contribute to the controlling energetics of the process.

This information was tested more quantitatively using a linear free energy relationship for the butyl tetralin dealkylation reactions with the stability of the dealkylating carbenium ion as the reactivity index. Two options for the value of the reactivity index were available, reflecting the nature of the alkyl carbenium ion: the energetics of either the primary (n-alkyl) or the most stable alkyl carbenium ion could be used. The experimental data were not sufficiently precise to adjudicate.

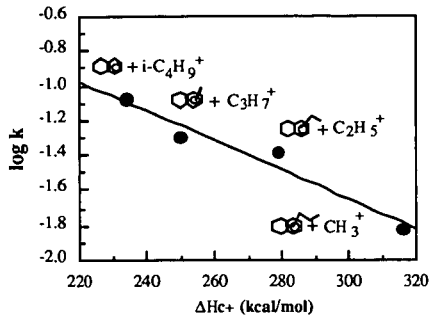

Fig. 5: LFER for the butyl tetralin dealkylation reactions. (k in min.$^{-1}$)

CONCLUSIONS

1-methyl naphthalene hydrocracking resulted in isomerization to 2-methyl naphthalene, as well as hydrogenation to methyl tetralins. Hydrogenation of the single ring in methyl tetralin was one order of magnitude slower than hydrogenation of methyl naphthalenes, and comparable to the naphthenic ring opening reactions. Phenanthrene hydrocracking proceeded mainly through sequential hydrogenation to dihydro, tetrahydro and octahydro phenanthrene, followed by opening of the terminal naphthenic rings and dealkylation of the butyl side chains.

Reasonable structure/reactivity correlations were obtained for the rate parameters of the dealkylation of butyl tetralins produced from phenanthrene hydrocracking. The heat of formation of the leaving alkyl carbenium ion (CH_3^+-$C_5H_{11}^+$) as used from Mochida and Yoneda (1967) was established as a suitable reactivity index.

ACKNOWLEDGEMENT

The authors acknowledge the financial support of Mobil Research and Development Corporation (Paulsboro Research Laboratory), and the State of Delaware, as authorized by the State Budget Act of Fiscal Year 1989.

REFERENCES

Bhore, N. A., Klein, M.T., and Bischoff, K.B. (1990). The Delplot Technique: A New Method for Reaction Pathway Analysis. *Ind. Eng. Chem.*, 29(2), 313-316.

Dunn, I.J. (1968). Linear Free Energy Relationships in Modeling Heterogeneous Catalytic Reactions. *J. Catal.*, 12, 335-340.

Froment, G.F. (1987). Kinetics of the Hydroisomerization and Hydrocracking of Paraffins on a Platinum Containing Bifunctional Y-Zeolite. *Catal. Today*, 1, 455-473.

Girgis, M.J., and Gates, B.C. (1991). Reactivities, Reaction Networks, and Kinetics in High-Pressure Catalytic Hydroprocessing. *Ind. Eng. Chem. Res.*, 30(9), 2021-2058.

Haynes, H.W.J., Parcher, J.F., and Helmer, N.E. (1983). Hydrocracking Polycyclic Hydrocarbons over a Dual-Functional Zeolite (Faujacite)-Based Catalyst. *Ind. Eng. Chem. Process Des. Dev.*, 22, 401-409.

Landau, R.N. (1991) Chemical Modeling of the Hydroprocessing of Heavy Oil Feedstocks. PhD Thesis, University of Delaware.

Lapinas, A.T., Klein, M.T., Gates, B.C., Macris, A., and Lyons, J.E. (1987). Catalytic Hydrogenation and Hydrocracking of Fluoranthene: Reaction Pathways and Kinetics. *Ind. Eng. Chem. Res.*, 26, 1026-1033.

Lemberton, J.-L., and Guisnet, M. (1984). Phenanthrene Hydroconversion as a Potential Test Reaction for the Hydrogenating and Cracking Properties of Coal Hydroliquefaction Catalysts. *Appl. Catal.*, 13, 181-192.

Mochida, I., and Yoneda, Y. (1967). Linear Free Energy Relationships in Heterogeneous Catalysis I. Dealkylation of Alkylbenzenes on Cracking Catalysts. *J. Catal.*, 9, 386-392.

Olah, G.A., Baker, E.B., Evans, J.C., Tolgyesi, W.S., McIntyre, J.S., and Bastien, I.J. (1964). Stable Carbonium Ions. V. Alkylcarbonium Hexafluoroantimonates. *J. Am. Chem. Soc.*, 86(1360-1372).

Pines, H. (1981). The Chemistry of Catalytic Hydrocarbon Conversions. New York, N. Y.: Academic Press.

Qader, S. A. (1973). Hydrocracking of Polynuclear Aromatic Hydrocarbons over Silica-Alumina Based Dual Functional Catalysts. *J. Inst. Pet.*, 59, 178-187.

Shabtai, J., Veluswami, L., and Oblad, A.G. (1978). Steric Effects in Phenanthrene and Pyrene Hydrogenation Catalyzed by Sulfided NiW/Al_2O_3. *Am. Chem. Soc., Div. Fuel Chem. Prepr.*, 23(1), 107-112.

ASPHALTENE AND RESID PYROLYSIS 2: THE EFFECT OF REACTION ENVIRONMENT ON PATHWAYS AND SELECTIVITIES.

Muzaffer Yasar, Daniel M. Trauth and M.T. Klein

Center for Catalytic Science and Technology
Department of Chemical Engineering
University of Delaware
Newark, Delaware 19716.

Keywords

Asphaltene, Kinetic, Pyrolysis.

Abstract

Resids and isolated asphaltenes from four feedstocks were pyrolyzed at temperatures of 400, 425 and 450 °C for holding times ranging from 20 to 180 minutes in micro-batch reactors. Reaction products were recovered as gas, maltene, asphaltene and coke lumps. The maltene, asphaltene and coke product fractions were collected by a solvent extraction sequence where heptane-soluble material was defined as maltene, toluene-soluble material as asphaltene, and toluene-insoluble material as coke. Gas chromatography revealed the presence of C_1-C_5 paraffins, C_2-C_5 olefins, isoparaffins, H_2S and CO_2.

Results were summarized by a lumped reaction network which allowed for quantitative kinetics. Comparison of relative kinetics and apparent activation energies yielded insight into thermal reaction pathways, feedstock effects, and asphaltene environment effects. At 400°C and 425°C, isolated asphaltene reacted selectively to maltenes. At 450°C asphaltene reacted predominately to coke. Isolated maltene pyrolysis indicated that asphaltene and coke formed in series, i.e., M--->A--->C.

Introduction

The increased usage of heavy petroleum feedstocks has focused attention on problems associated with the refining of heavy feedstocks, such as solids formation and catalyst deactivation. On a feedstock structural level, these problems are associated with high aromaticity, high molecular weight, and high heteroatom content[1].

Asphaltene is the aromatic-soluble and paraffinic-insoluble fraction of crude oil. Understanding the effects of environment on asphaltene reaction pathways can provide insight into the processing problems of heavy crudes. Previous asphaltene and resid thermal pyrolysis studies[2] have yielded information on environmental and feedstock effects. The current work is an extension of that study. Arabian Heavy Resid (AHR) and Arabian Light Resid (ALR) were subject to pyrolysis in an isothermal sand bath at 400, 425, and 450°C for holding times between 20 and 180 minutes. The isolated maltene from ALR was also pyrolyzed at 425°C. Gaseous product were collected and analyzed by GC. A soxhlet sequence was used to separate maltene, asphaltene and coke. The time dependence of the product distributions was used to calculate lumped kinetic rate constants. Arrhenius parameters were calculated for each network step.

Experimental Methods

1) Samples

Asphaltenes were precipitated from the resids at a weight ratio of 40/1, n-heptane to resid. The mixture was stirred for 1 hr at 60 °C, and then allowed to cool under continuous stirring for 4 hr. The solution was then allowed to settle overnight prior to filtering. Maltenes were collected by evaporating the n-heptane from the filtrate. The asphaltene was subject to soxhlet extraction to verify the absence of maltenes.

The samples were characterized by elemental analysis , simulated distillation, proton NMR, SARA (saturate, aromatic, resin, asphaltene) and molecular weight by VPO. Molecular weight experiments were carried out at 130°C in nitrobenzene. Molecular weights were extrapolated from measurements at three concentrations. The results are given in Table (I). VPO measurements showed that Maya isolated asphaltene and Arabian Heavy resid had the highest molecular weight in their respective classes. Elemental analysis indicated that heteroatoms were concentrated in the asphaltene fraction. Simulated distillation analysis revealed some variability in cut point for the resids.

2) Pyrolysis Reactions

Reactions were carried out in micro-batch reactors. Briefly, a glass tube containing the sample was loaded into the reactor. It was purged several times with high pressure nitrogen to minimize potential oxidation reactions then reacted in an isothermal sandbath. Reaction products were separated into gas, maltene, asphaltene and coke fractions. Gas products were collected and then analyzed by gas chromatography equipped with a thermal conductivity detector and a 6 ft propak Q column. Maltene, asphaltene and coke fractions were collected by a soxhlet extraction sequence. The yield of each fraction was calculated gravimetricaly.

Results and Discussions

1)Isolated asphaltenes

Figures (1a-c) show the kinetics of pyrolysis of isolated asphaltenes. The curves drawn through experimental data represent a first-order model fit. Asphaltene reactivities were as follows: AH~AL~H>M at 400 and 425°C. At 450°C asphaltene conversion was extremely rapid.

2) Asphaltene in resid

Figures (2a-c) depicts the time dependence of the ratio of the weight of asphaltene to initial weight of asphaltene in the resid. Clearly the reaction paths of asphaltene are influenced by the resid environment. The amount of AL asphaltene approximately doubled at 400°C. At 425 and 450°C the amount of AL asphaltene rapidly rose to 2-3 times its initial value. Further reaction returned the AL asphaltene amount to a value below this initial level. Asphaltene levels in the other three resids did not increase above the ordinate at any reaction temperatures. Reactivities were as follow: H>AH~M>AL

3) Maltene from isolated asphaltene

Figures (3a-c) summarize the temporal variation of the maltene weight fraction. At 400°C the yield of maltene was nearly the same for all feedstocks. H maltene yield

increased at all temperatures. H had highest maltene yield at 450 °C. M produced the most maltene at 425°C. AH and AL produced the greatest amounts at 400 and 425°C.

The maxima exhibited by all isolated asphaltenes at reaction temperatures of 425 and 450°C are indicative of secondary cracking and possible condensation reactions. The complex behavior is indicative of a chemically complex mixture.

4) Maltene from resids

The temporal variations of the maltene weight fractions for AH, AL, H and M resids are shown in Figures (4a-c). As temperature increased the maltene disappearance rate increased for all resids. After 20 minutes, the disappearance rate of maltenes was similar for all feedstocks.

5) Isolated maltenes and reaction pathways

Experimental results from isolated AL maltenes pyrolysis, as shown in figure (5), suggest that isolated maltenes produced asphaltene and then coke in series. These experiments revealed that the previously proposed pathways[2] could be simplified since coke was not formed directly from maltene. The network is shown in Figure (6).

Reaction Kinetics

Optimized rate constants for the network of Figure (6) were obtained as described elsewhere.[3] Briefly, a simplex minimization program[4] coupled to the DGEAR[5] routine minimized the error in the solution of a first-order differential equations developed from figure (6).

The predicted rate constants are shown in Table II. For both isolated asphaltenes and resid, k4, the rate constant for the reaction of maltene to gas was negligible. The rate constant for the reactions of asphaltene to maltene and maltene to asphaltene, k1 and k5, were highest for resids. The selectivities, k1/k5, were between 4.5 and 8.6 for four resids at all temperatures.

The activation energies calculated from network parameters for each reaction step are summarized in the table III both for resids and asphaltenes.

Conclusions

1) AL, AH and H isolated asphaltenes reacted at the similar rates at 400 and 425°C; The M isolated asphaltene reacted more slowly. All of the isolated asphaltenes reacted at about the same rate at 450°C.

2) At 400 and 425°C, the isolated asphaltenes reacted selectively to maltene. At 450°C H isolated asphaltene formed more maltene than M, AL and AH.

3) H asphaltene reacted faster than M, AL and AH in the resid at all temperatures. AL asphaltene in the resid reacted most slowly.

4) Resids and isolated AL maltene pyrolysis showed that important amounts of asphaltene and coke could be formed by maltenes.

References

1) Speight, J.G. 1990. Fuel Science and Technology Handbook. Marcel Dekkar, New york.

2) Trauth, D.M., M. Yasar, M. Nuerock, A. Nigam, M.T. Klein and S.G. Kukes. Asphaltne and Resid Pyrolysis: Effect of Reaction Environment.Accepted for publication in Fuel Science and Technology International 1991.

3) Nuerock, M., A. Nigam, D. Trauth, and M.T.Klein.1990. Asphaltene Pyroysis Pathways and Kinetics: Feedstock Dependence. Preprints AIChE Meeting, San Diego, CA, August 1990 (submitted to AIChE symposium series).

4) Press, W.H., Flanner, S. A. Teukolsky, and W.T. Velterling. 1986. Numerical Recipes. Cambridge University Press.

5) IMSL Inc. 1989. IMSL User's Manual, Volume 1, v1.1.

TABLE I

Chemical analysis of Hondo , Maya, Arabian Light, and Arabian resids and their isolated asphaltenes by Elemental, VPO, Proton NMR, Simulated Distillation, ORA, a Soxhlet Extraction techniques (R=resid, A=asphaltene, - =not measured).

Analysis	Hondo (R)	Maya (R)	A. Light (R)	A. Heavy (R)	Hondo (A)	Maya (A)	A. Light (A)	A. Heavy (A)
% Carbon	81.15	85.66	84.41	83.80	80.35	83.08	82.13	82.00
% Hydrogen	9.95	10.41	10.02	9.31	7.96	7.27	7.59	6.69
% Nitrogen	1.01	0.465	0.15	0.44	1.87	1.09	0.75	0.93
% Sulfur	6.90	3.17	4.04	5.31	7.89	7.11	6.17	7.43
% Oxygen	1.02	0.50	0.008	0.020	0.110	0.170	0.036	0.074
% Vanadium	0.017	0.005	0.002	0.007	0.040	0.032	0.010	0.022
% Nickel	0.010	0.005	-	-	-	-	-	-
% Iron	1.47	1.46	1.40	1.33	1.19	1.05	1.11	0.98
H/C	0.011	0.005	0.002	0.005	0.020	0.011	0.008	0.010
N/C	0.032	0.014	0.018	0.024	0.037	0.032	0.028	0.034
S/C	0.009	0.004	0.009	0.013	0.016	0.008	0.013	0.015
O/C	862	944	1022	1535	2871	5292	1950	2119
MW by VPO								
1H NMR	-	-	-	-	20.6	28.1	28.8	29.8
% H (ME)	-	-	-	-	57.6	60.9	44.9	46.7
% H (N + MY)	-	-	-	-	10.6	5.8	12.2	14.8
% H (alpha)	-	-	-	-	11.2	5.2	14.2	9.7
% H (aromatic)								
Simulated Distillation								
%800-1000°F	12.5	19.0	10.1	9.8	-	-	-	-
%1000°F+	87.5	81.0	89.9	90.2	-	-	-	-
ORA								
%Oils	31.7	12.3	-	-	-	-	-	-
%Resins	55.2	71.6	-	-	-	-	-	-
%Asphaltenes	12.5	15.1	-	-	-	-	-	-
Soxhlet Extracted								
%Maltenes	77	88	94	85	-	-	-	-
%Asphaltenes	23	12	6	15	-	-	-	-
SARA								
%Saturates	13	26	30	30	-	-	-	-
%Aromatics	43	51	45	44	-	-	-	-
%Resins	21	11	19	16	-	-	-	-
%Asphaltenes	23	12	6	2	-	-	-	-

Table II

Network Kinetics of the Pyrolysis of Hondo and Maya Resids and their Isolated Asphaltene (First order units are 1/(hr*wt%))

Rate Parameters.	Hondo Resid	Maya Resid	Arabian Light Resid	Arabian Heavy Resid	Hondo Asphaltene	Maya Asphaltene	Arabian Light Asphaltene	Arabian Heavy Asphaltene
400 °C								
k1	123.62	54.018	2.5800	13.351	0.9369	0.6465	0.7330	48.943
k2	0.3433	0.2689	0.1680	0.3369	3.2014	1.5201	3.0133	2.9273
k3	0.2559	0.1699	0.1390	0.1313	0.4196	0.1503	0.3022	0.3012
k4	0.0025	0.0003	0.0001	0.0003	0.0048	0.0038	0.0000	0.0003
k5	20.044	8.1600	0.3860	2.8021	0.5875	0.6825	0.2540	81.565
425°C								
k1	293.14	115.08	12.757	33.350	2.5700	1.5813	0.9720	114.81
k2	1.4586	0.8568	1.1251	0.8183	3.3700	2.6710	4.3890	6.4369
k3	0.0006	0.3545	0.3565	0.3300	0.5290	0.0010	0.5077	0.7720
k4	0.0765	0.0003	0.0003	0.0005	0.0200	0.4889	0.0000	0.0007
k5	33.910	14.400	2.2291	7.3300	1.1400	0.6977	0.5592	163.81
450°C								
k1	572.53	348.60	34.121	79.350	3.0725	59.438	4.3110	368.58
k2	1.7511	1.4741	1.9663	1.9153	4.2704	203.45	7.3411	13.687
k3	1.1886	0.7349	1.3054	0.9250	1.1481	0.0039	1.5570	2.2512
k4	0.0007	0.0008	0.0007	0.0009	0.0018	0.9305	0.0910	0.0021
k5	97.398	59.571	4.8265	16.380	0.3793	0.4078	9.1011	280.02

Table III

Arhenius parameters for resids and asphaltenes, (Ea (kcal/mol) , * = not calculated).

Parameters	k1	k 2	k3	k4	k5	k1	k2	k3	k4	k5
		Hondo Resid					Hondo Asphaltene			
Ea	29.69	31.81	*	*	30.45	23.16	5.53	19.33	*	*
log A	11.74	9.94	*	*	11.48	7.54	2.28	5.86	*	*
		Maya Resid					Maya Asphaltene			
Ea	35.98	33.04	28.32	18.80	38.24	86.79	93.82	*	106	*
logA	13.38	10.19	8.42	2.53	13.26	27.79	30.36	*	32.53	*
		Arabian Light Resid					Arabian Light Asphaltene			
Ea	50.07	47.88	43.22	42.05	49.07	33.98	17.19	31.58	*	68.74
LogA	16.71	14.87	13.15	9.58	15.58	10.81	6.05	9.68	*	2.16
		Arabian Heavy Resid					Arabian Heavy Asphaltene			
Ea	34.47	33.61	37.72	21.22	34.18	38.97	34.57	38.87	38.23	23.89
LogA	12.32	10.4 4	11.36	3.36	11.55	14.31	11.60	12.08	8.86	9.68

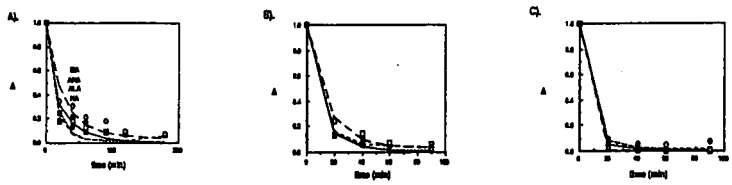

Figure 1. Temporal varition of isolated asphaltene: A) 400°C, B)425°C, C) 450°C

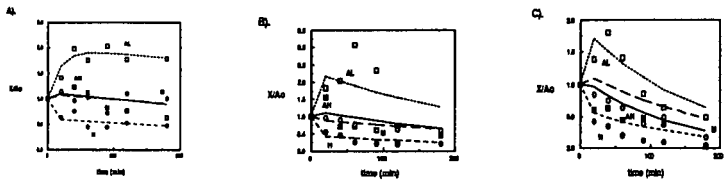

Figure 2. Temporal variation of asphalthene yield in a ratio of asphaltene weight to initial asphaltene weight for resids: A) 400°C, B) 425°C, C) 450°C

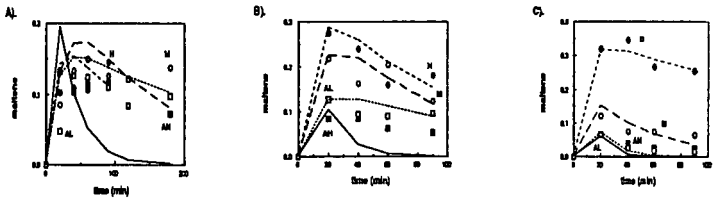

Figure 3. Temporal variation of maltene weight fraction for asphaltenes. A) 400°C, B) 425°C, C) 450°C.

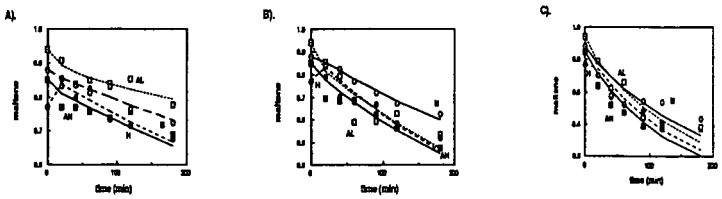

Figure 4. Temporal variation of maltene weight fraction for resids. A) 400°C, B) 425°C, C) 450°C.

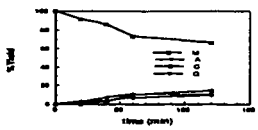

Figure 5. Isolated maltene pyrolysis at 425°C.

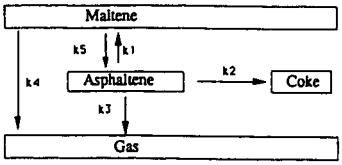

Figure 6. Lumped resid/ asphaltene model

PERFORMANCE OF HYBRID CATALYST SYSTEM IN TWO-STAGE COAL LIQUEFACTION

J. M. Lee, P. Vimalchand, O. L. Davies, and C. E. Cantrell
Southern Electric International, Inc.
P. O. Box 1069, Wilsonville, Alabama 35186

Keywords: two-stage liquefaction, catalyst, distillate

INTRODUCTION

The Clean Coal Research Center at Wilsonville has developed alternate technologies for producing low cost fuels from coal. Process developments of close-coupled integrated (CC-ITSL) configurations using the thermal/catalytic or catalytic/catalytic mode of operation were discussed in earlier articles[1,2].

This paper is primarily focused on the low-rank Black Thunder subbituminous coal performance at steady-state operation with catalyst replacement in the thermal/catalytic mode. Process development results from four runs are discussed: Runs 258, 260, 262 and 263. Three different operation modes with supported, dispersed slurry and hybrid catalyst systems were tested. Runs 258 and 260 studied the supported catalyst system using Shell (or Criterion) 324 catalyst in the second stage without addition of a dispersed catalyst. Runs 262 and 263 (second part) tested the hybrid system using a dispersed molybdenum (Molyvan L or 822 precursor) and Criterion 324 supported catalyst in the second stage. Run 263 (first part) tested the dispersed slurry catalyst system using Molyvan L and 822 as precursors. Half-volume reactors were used for Runs 258, 262 and 263; a combination of full- and 3/4-volume reactors was used for Run 260. Iron-oxide (+ dimethyl disulfide) addition was 1-2 wt % MF coal.

The primary objective of this study was to maximize the distillate production with good quality in order to improve the process economics. High distillate yield and coal throughput increase the distillate production. The distillate production can be enhanced by improving coal reactivity, catalyst conversion activity, and distillate selectivity. The performance of a dispersed molybdenum catalyst was evaluated processing a low-rank coal. Solids buildup in reactor transfer lines and interstage separator was investigated for possible reduction or elimination by using a dispersed molybdenum catalyst. The dispersed molybdenum catalyst may give acceptable conversions at moderate reaction temperatures and reduce the coking reactions, that cause solids to deposit in the transfer lines, by hydrogenating thermally produced free radicals and possibly through the prevention of retrogressive reactions[3]. Dispersed molybdenum catalysts using Molyvan L and Mo octoate as precursors were tested in bench-scale two-stage liquefaction with Illinois No. 6 coal using Amocat 1C bimodal supported catalyst by Amoco Oil Company[4], and UOP[5] and Dow Chemical Company[6] studied dispersed catalysts in bench-scale single stage. Several investigators have studied with dispersed molybdenum and iron catalysts to improve liquefaction conversion and their results can be found in the literature[7-13]. Typical analyses of Black Thunder coal processed for this study are summarized in Table 1. Properties of Shell (or Criterion) Ni-Mo catalyst and dispersed molybdenum precursors tested are shown in Table 2.

PROCESS DESCRIPTION

The current catalytic close-coupled integrated two-stage liquefaction (CC-ITSL) process consists of two H-OIL® ebullated-bed reactors and a Residuum Oil Supercritical Extraction-Solids Rejection (ROSE-SR℠) unit[14]. Both the reactor designs utilize "H-OIL®" technology supplied by Hydrocarbon Research, Inc. The ebullated-bed design helps to maintain a uniform temperature distribution in the reactor. The reactor is used as a thermal reactor in the thermal mode of operation without a supported catalyst. The ROSE-SR℠ is a proprietary extraction process at conditions close to the critical point of the deashing solvent. It was developed and licensed by the Kerr-McGee Corporation.

RUN EXPERIMENTS

Key process variables studied in Runs 258, 260, 262 and 263 are listed below to maximize the distillate production by increasing distillate yield and coal throughput processing Black Thunder subbituminous coal.

(1) Catalyst activity
- Shell (or Criterion) 324 unimodal supported
- dispersed molybdenum (Molyvan L/822 precursors)
- iron-oxide + DMDS (dimethyl disulfide)

(2) Steady-state operation with catalyst replacement
- 1.5 to 3 lb/ton MF coal in catalytic stage

(3) Molybdenum addition concentration (100-1000ppm MF coal)

(4) Iron-oxide addition concentration (1-2 wt % MF coal)

(5) Recycle resid concentration
- 35-45 wt % in the process solvent

(6) High/low thermal severity mode

(7) Heavy vacuum gas oil recycle

(8) Coal space velocity
- 45-110 lb MF coal/hr/ft^3-catalyst in catalytic
- 30-90 (x1/C) lb MF coal/hr/ft^3-reactor in thermal (C: constant equating thermal to catalytic reaction volume in the thermal/catalytic mode)

(9) Reaction temperature
- 760-860/760-810°F in the first/second stage

(10) Inlet hydrogen partial pressure
- 2450-2850 psia in the first stage
- 2400-2550 psia in the second stage

(11) Slurry composition (25-30 wt % coal, 20 wt % CI)

(12) Interstage separation

(13) Reactor operation parameters
- temperature profiles, exotherms
- ebullation rate, gas flow, slurry flow
- slurry viscosity, etc.

Several steady-state operation periods in Runs 258, 262 and 263 with half-volume reactors in operation were selected for comparison of distillate production in three different operation modes with the supported, dispersed slurry and hybrid catalyst systems. Experimental results with Black Thunder subbituminous coal are summarized in the following along with the theoretical distillate production projected for the "all-distillate" product slate with resid extinction using a CSTR first order kinetic model[15]. Illinois No. 6 bituminous coal result from Run 257J using Amocat 1C in the catalytic/catalytic mode is also included for comparison.

run	catalyst	temper. (°F) 1st/2nd	cat. rep. (lb/t MF) 1st/2nd	recycle resid (wt %)	dist.prod. (lb/hr) exp.	the.[a]
(1)	w/ supported catalyst in the second stage					
258H	Shell 324	840/790	-/1.5	40	127	126
258I	Shell 324	850/790	-/1.5	40	132	126
(2)	w/ dispersed molybdenum slurry catalyst					
262F[b]	Molyvan L	825/810	200[c]	40	152	137
263E	Molyvan L	840/810	100[c]	40	147	150
263H	Molyvan 822	840/810	100[c]	45	150	158
(3)	w/ hybrid catalyst with dispersed and supported catalysts					
262E	[d]	825/810	-/3[e]	40	185	181
263I	[d]	840/810	-/3[e]	45	195	207
263J	[d]	840/810	-/3[e]	40	188	197
(4)	w/ Illinois coal in catalytic/catalytic mode					
257J	Amocat 1C	810/760	3/1.5	50	137	133

[a] Using CSTR 1st order kinetic model for resid extinction[15].
[b] Some Criterion catalyst was left in the second reactor.
[c] Unit: ppm based on MF coal.
[d] With a combination of Molyvan L and Criterion 324.
[e] Molyvan L addition at 100 ppm based on MF coal.

RESULTS AND DISCUSSION

DISTILLATE PRODUCTION COMPARISON

Supported, Dispersed Slurry and Hybrid Catalyst Systems

The hybrid system (Runs 262E and 263IJ) with a combination of dispersed molybdenum and Criterion supported catalysts showed the highest distillate production, 185-195 lb/hr, among three catalyst systems tested. Corresponding coal space velocities for these runs were 59-62 MF lb/hr-ft^3-catalyst in 2nd stage or 24-26 (x1/C) MF lb/hr-ft^3-reactors in CCR unit. The distillate production of the hybrid system was 30% higher than that of the dispersed molybdenum slurry catalyst system (147-152 lb/hr in Runs 262F and 263EH at 20 (x1/C) coal space velocity); 50-60% higher than that of the Criterion supported catalyst system (127-132 lb/hr in Run 258H1 at 17 (x1/C) coal space velocity).

The hybrid system with Black Thunder subbituminous coal in the thermal/catalytic mode of operation produced 40-55% higher distillate than the Amocat 1C supported catalyst system with Illinois No. 6 bituminous coal in the catalytic/catalytic mode of operation (Run 257J at 18 (x1/C) coal space velocity). This result suggests that Black Thunder subbituminous coal can produce more distillate than Illinois No. 6 bituminous coal, if process operating conditions are optimized for better coal and resid conversions, even though subbituminous coal has lower distillate yield and selectivity. It seems that due to the addition of the dispersed molybdenum to the supported catalyst system, the hybrid system enhances the distillate production by improving coal and resid conversions, employing higher thermal severity compared to Run 257J with Illinois coal and Amocat 1C catalyst. However, as reported in the previous Run 261 with Illinois bituminous coal using a new bimodal supported catalyst (EXP-AO-60)[15] in the catalytic/catalytic mode with full-volume reactors in operation, the

low/high severity operation significantly improved the distillate production by approximately 40-50%, employing higher thermal severity, increased recycle resid concentration and higher catalyst replacement. Further studies are required for better comparison with bituminous coals using half-volume reactors in operation.

Distillate Product Yield and Selectivity

The addition of a dispersed molybdenum allowed operation at lower thermal severity in the first stage, while the second stage operated at higher thermal severity compared to the supported catalyst system, resulting in higher C4+ distillate product yield and selectivity to resid + UC conversion as summarized below. The potential C4+ distillate yield is estimated by adjusting the resid yield for the "all-distillate" product slate with resid extinction by using an achievable common organic rejection (OR) and distillate selectivity measured in each run.

run	catalyst system	distillate yield, wt % MAF coal experimental	theoretical (OR)	distillate selectivity, %
258HI	supported	55-58	60 (14)	64-68
263EH	slurry	61	62-63 (14)	72-73
263IJ	hybrid	58-61	61-62 (13-14)	71-72

EFFECT OF MOLYBDENUM CONCENTRATION

Varying the molybdenum concentration from 100 to 1000 ppm (based on MF coal) seemed not to affect the resid + UC conversion, but increasing the molybdenum concentration slightly improved coal conversion. Good performance was observed at a low 100 ppm concentration in both slurry and hybrid catalyst systems. Distillate properties were generally the same within the range of molybdenum concentration studied.

The addition of Molyvan L or 822 as a dispersed molybdenum seemed to improve the overall two-stage resid and coal conversions allowing lower temperature and higher space velocity operation. In the hybrid system, with a combination of dispersed and supported catalysts, the resid + UC conversion was 5-10 wt % MAF coal higher and the coal conversion was 3-5 wt % higher than using the catalysts separately, when compared at the same thermal reaction severity operation. The use of just dispersed slurry catalyst (Molyvan L or 822) or Criterion supported catalyst gave similar overall two-stage coal and resid + UC conversions, and conversions improved by the combination of Criterion and Molyvan L or 822 catalysts.

COAL CONVERSION AND ORGANIC REJECTION

Figure 1 illustrates the effect of coal conversion on organic rejection. A good linear correlation was observed with low-rank coals and are summarized as follows.

$$Y = 173.3 - 1.69\ X;\ r^2 = 0.84$$

where Y is the organic rejection (wt % MAF coal), X is the coal conversion (wt % MAF coal), and r^2 is the determination coefficient. The X-intercept in Figure 1 indicates that a deeply cleaned coal could achieve a low organic rejection (4 wt % MAF coal), if extrapolated to 100 wt % coal conversion. A similar observation with bituminous coals was reported in the previous work[2,15].

CATALYST AND THERMAL ACTIVITIES IN RESID + UC CONVERSION

Supported catalyst and thermal activities were calculated assuming that the resid + UC conversion reaction follows first-order kinetics for a continuous stirred tank reactor[2]. Cracking activity (resid conversion) is not the only function of the catalyst. Hydrogenation activity of the catalyst was not considered in these catalyst activity analyses. Catalyst activity analysis is based on the overall activity of combined catalytic and thermal conversions in the catalytic stage.

The Arrhenius plot for temperature dependence (Figure 2) compares first stage thermal conversion activities in Runs 258, 260, 262 and 263 processing Black Thunder subbituminous coal operating in three different modes with supported, dispersed slurry and hybrid catalyst systems. The hybrid system with a combination of Molyvan L or 822 and Criterion 324 catalysts showed the highest thermal conversion activity, compared to the dispersed slurry and supported catalyst systems. The presence of Criterion supported catalyst in the second stage improved the resid + UC conversion in the first stage, due to improved hydrogenation by the supported catalyst in the second stage, producing better recycle process solvent and resulting in better thermal conversion in the first stage. It appears that the dispersed molybdenum catalyzes thermal hydrogenation of coal- and resid-derived free radicals[3] through stabilization by hydrogen transfer from the process solvent, resulting in higher thermal conversion in the hybrid system. The dispersed catalyst system had a higher thermal conversion activity than the supported catalyst system. Apparent activation energies (30000-31000 Btu/lb-mole) for the hybrid and dispersed slurry systems were lower than that (53000-64000 Btu/lb-mole) for the supported catalyst system, although their conversion activity levels were higher than the supported system.

Figure 3 compares second stage conversion activities for Runs 262 and 263. The catalytic resid + UC conversion activity of the hybrid system with a combination of Molyvan L or 822 and Criterion 324 was much higher than the thermal conversion activity of the dispersed slurry catalyst system using Molyvan L or 822 alone. The calculated average rate constant values were 45-115% higher than those obtained without Criterion catalyst. The hybrid system catalytic activity was obtained with 3 lb/ton MF coal catalyst replacement. It seems that the dispersed molybdenum may not be greatly involved in hydrogenation and hydrocracking of the process solvent compared to the supported catalyst, since operations with the dispersed slurry catalyst gave significantly lower hydrogen and higher heteroatoms contents of distillate and process streams. It is possible that nickel or support material of the supported catalyst, which are missing components of the dispersed molybdenum, may play a significant role in hydrogenation and hydrocracking. Apparent activation energy for the hybrid catalyst system was 48000 Btu/lb-mole, higher than that with the supported catalyst (30000-40000 Btu/lb-mole). This high value might have been affected by molybdenum concentration variation in the range of 100-1000 ppm MF coal.

SOLIDS BUILDUP IN PROCESS LINES AND INTERSTAGE SEPARATOR

Problems associated with the formation of deposits in both the process lines and interstage separator between two reactors were discussed in the previous work processing subbituminous coals[16], and two different solids deposition mechanisms suggested by Davis et al. were coking and mineral

deposition[17]. In recent Runs 262 and 263, the addition of Molyvan L or 822 as a dispersed slurry catalyst prevented reactor line plugging. However, solids did deposit in the interstage separator. A different interstage separator design could resolve the deposit problem.

DISTILLATE PRODUCT QUALITY

Table 3 summarizes distillate product qualities from Runs 258HI, 262E, 263EHJ, 257I and 261BD. During Run 259 with Pittsburgh coal and Shell 324, which was the first run tested with a better distillation separation system, the boiling end point of the distillate product was reduced to 715-760°F[2]. In Run 261BD with Illinois coal and EXP-AO-60 bimodal catalyst, the end point was 772-780°F. Runs 257I and 258HI end point data were estimated by assuming steady recycle of heavy distillate as in Runs 259 and 261.

The major observation from Runs 262 and 263 in Table 3 was that operations in the hybrid system with a combination of Molyvan L or 822 and Criterion catalysts produced better quality distillate than just using dispersed slurry catalyst (periods 262E and 263J vs. 263EH). Hydrogen content increased to 11.0-11.4 wt %, while heteroatoms decreased to 0.6 wt % nitrogen and 1.7-2.1 wt % oxygen, respectively. The end point of the distillate product was similar for both catalyst systems (717-755°F). Note that the supported catalyst only system (258HI) had similar distillate product quality as the hybrid system. The presence of Criterion supported catalyst in the second stage seems to improve the product quality in both the hybrid and supported catalyst systems by increasing hydrogenation and heteroatoms removal.

CONCLUSIONS

- Processing Black Thunder subbituminous coal, the hybrid system with a combination of dispersed molybdenum slurry and supported catalysts improved the distillate production by 30-60% compared to using the dispersed slurry and supported catalysts separately.
- The addition of Molyvan L or 822 at a low 100 ppm MF coal as a dispersed molybdenum catalyst precursor significantly improved coal and resid conversions, allowing operation at lower thermal severity in the first stage and higher severity in the second stage compared to the supported catalyst system, resulting in higher C4+ distillate product yield and selectivity to resid + UC conversion.
- Operations in the hybrid system with a combination of Molyvan L or 822 and Criterion catalysts produced better quality distillate than just using dispersed slurry catalyst only. The boiling end point of the distillate product was similar for both catalyst systems (717-755°F).
- The supported catalyst only system had similar distillate product quality as the hybrid catalyst system. It seemed that the presence of Criterion supported catalyst in the second stage improved the product quality in both the hybrid and supported catalyst systems by increasing hydrogenation and heteroatoms removal.
- The dispersed molybdenum seemed to catalyze thermal hydrogenation of coal- or resid-derived free radicals through stabilization by hydrogen transfer from the process solvent, resulting in higher thermal conversion in the hybrid catalyst system, while seemed to have a less role in hydrogenation and hydrocracking of the process solvent compared to the supported catalyst.

- The addition of Molyvan L or 822 as a dispersed molybdenum catalyst precursor improved process operability by preventing reactor line plugging.
- Black Thunder subbituminous coal produced more distillate than Illinois No. 6 bituminous coal, when process operating conditions were optimized for better coal and resid conversions, even though the subbituminous coal had lower distillate yield and selectivity.

ACKNOWLEDGMENTS

This work was supported by the U. S. Department of Energy under Contract DE-AC22-82PC50041, and the Electric Power Research Institute under Contract RP1234-1-2, and was managed by the Southern Company Services, Inc. Dr. Ed Klunder is DOE project manager and Mr. Bill Weber is EPRI project manager. The authors appreciate the contributions made by the technical department staff (M. Sherbert, F. Morton, M. Corser and S. Gollakota). The authors also acknowledge J. Howard, T. Pinkston, G. Styles, N. Stewart, D. Cronauer, A. Basu, R. Lumpkin, G. Robbins, H. Schindler and E. Moroni for their supports.

REFERENCES

1. R. V. Nalitham, J. M. Lee, C. W. Lamb, and T. W. Johnson. Fuel Processing Technology, Vol. 17, 1987, pp. 13-27.
2. J. M. Lee and C. E. Cantrell. Fuel Processing Technology, Vol. 29, 1991, pp. 171-197.
3. B. Bockrath, E. Illig, and M. Keller. ACS Div. Fuel Chem., Prep., 37(1), 133 (1992).
4. A. Swanson. ACS Div. Fuel Chem., Prep., 37(1), 149 (1992).
5. J. Gatsis, R. Roemisch, M. Miller, C. Piasecki, and H. Fullerton. ACS Div. Fuel Chem., Prep., 37(1), 160 (1992).
6. N. Moll and G. Quarderer. Chemical Engineering Progress, 75(11), 1979.
7. A. Cugini, D. Krastman, and R. Hickey. Proceedings of the Eighth Annual International Pittsburgh Coal Conf., Pitts., PA, Oct., 1991.
8. A. Cugini, B. Utz, D. Krastman, R. Hickey, and V. Balsone. ACS Div. Fuel Chem., Prep., 36(1), 91 (1991).
9. A. Hirschon and R. Wilson. ACS Div. Fuel Chem., Prep., 36(1), 103 (1991).
10. F. Derbyshire and T. Hager. ACS Div. Fuel Chem., Prep., 37(1), 312 (1992).
11. D. Sommerfeld, J. Jaturapitpornsakul, L. Anderson, and E. Eyring. ACS Div. Fuel Chem., Prep., 37(2), 749 (1992).
12. C. Burgess, L. Artok, and H. Schobert. ACS Div. Fuel Chem., Prep., 37(1), 200 (1992).
13. C. Curtis and H. Kim. ACS Div. Fuel Chem., Prep., 35(4), 1064 (1990).
14. Catalytic, Inc., Topical Report. DOE Cont. No. DE-AC22-82PC50041, EPRI Cont. No. RP1234-1-2, Doc. No. DOE/PC/50041-82.
15. J. Lee, C. Cantrell, S. Gollakota, O. Davies, M. Corser, and P. Vimalchand. Proceedings of the Sixteenth Annual EPRI Conference on Fuel Science, June 1991.
16. J. M. Lee, S.V. Gollakota, and O.L. Davies. Proceedings of the Fifteenth Annual EPRI Conference on Fuel Science, June 1990.
17. A. Davis, H. Schobert, G. Mitchell, and L. Artok. DOE Technical Progress Reports, No. DOE-PC-89877-3 and -7 (1990 and 1991).

TABLE 1. FEED COAL ANALYSIS
(BLACK THUNDER MINE - WYODAK ANDERSON SEAM)

FC: 49% mf, HV: 11800 Btu/lb mf, Reactives: 92 mmf vol%
Ultimate: 69.5% C, 5.1% H, 1.0% N, 0.6% S, 7.3% Ash, 16.5% O

TABLE 2. CATALYST PROPERTIES

Shell (or Criterion) 324 unimodal supported catalyst
1/16" size, 2.7% Ni, 13.2% Mo
SA: 165 m^2/g, PV: 0.48 cc/g, CBD: 54 lb/ft^3
Dispersed molybdenum slurry catalyst
Molyvan L: 8.1% Mo, 12.3% S, 6.4% P, no N
Molyvan 822: 4.9% 6.0% no yes

TABLE 3. TOTAL DISTILLATE PRODUCT QUALITY COMPARISON

Run	258H	258I	262E	263E	263H	263J	257I	261B	261D
Coal	--------Black Thunder--------						---Illinois---		
Wt % C	86.1	86.0	86.3	85.8	85.1	86.3	87.4	87.3	87.5
H	11.2	11.3	11.4	10.1	10.4	11.0	12.1	11.4	11.3
N	0.5	0.5	0.6	0.9	0.9	0.6	0.1	0.2	0.3
S	0.06	0.06	0.05	0.02	0.05	0.04	0.01	0.04	0.03
O	2.2	2.2	1.7	3.9	3.6	2.1	0.4	1.1	0.9
(dir.)								(0.7)	(0.9)
°API	18	18	24	15	18	22	21	23	22
Wt % Naphtha	21	21	20	10	12	16	18	19	14
Mid.D1	15	15	10	14	17	14	11	11	16
Mid.D2	59	62	44	38	40	40	64	40	40
Gas Oil	5	2	26	38	31	30	7	30	30
End point °F (D1160)	667	665	748	755	719	717	665	772	780
	(estimated)						(est.)		

FIGURE 1

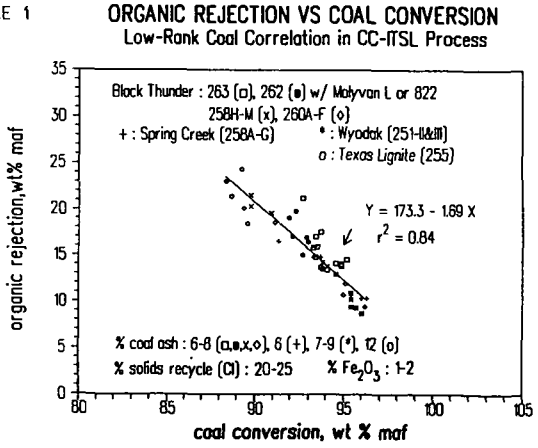

FIGURE 2

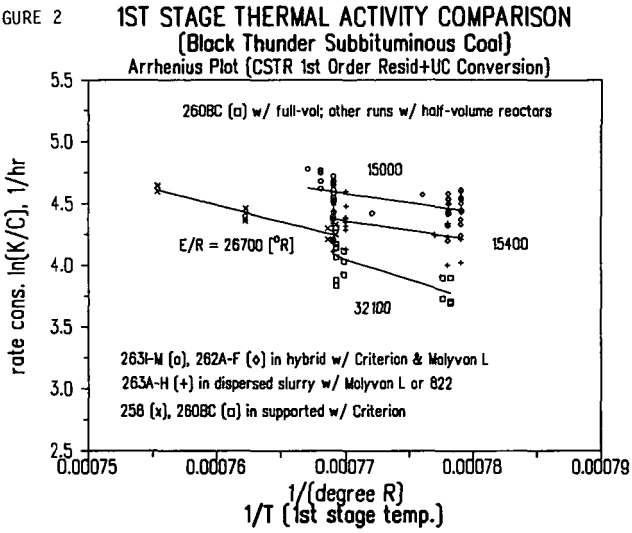

FIGURE 3

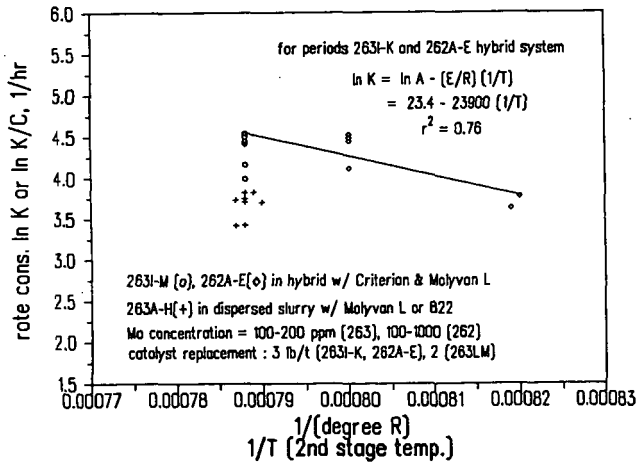

CHLORIDATION AND ACTIVITY OF Pt/Al_2O_3 CATALYSTS

Robert A. Keogh, Dennis E. Sparks, Gerald A. Thomas, and Burtron H. Davis
Center for Applied Energy Research
University of Kentucky
3572 Iron Works Pike
Lexington, KY 40511

Keywords: chloridation, Pt/Al_2O_3, isomerization

INTRODUCTION

Current advanced coal liquefaction processes produce a naphtha that contains a high fraction of naphthenes. This will likely remain true for any improved process at lower temperatures. Conversion of this naphtha to gasoline by today's reforming processes will lead to a gasoline with a very high percentage of aromatics. Environmental considerations require that the aromatic and olefinic content of gasolines be drastically reduced. Petroleum refiners are making an intense effort to produce a gasoline containing more alkanes; for the short term alkylate will be utilized to accomplish this.

The high naphthene content of naphtha from coal liquefaction means that it would not be a suitable transportation fuel for the future. Tomorrow's clean gasoline will be low in heteroatoms and will contain mainly isoparaffins instead of aromatic and naphthenic hydrocarbons. Thus, if coal liquefaction is to advance from an emerging technology to a viable commercial process, a means must be found to reform the naphtha to a clean gasoline that will find acceptance in the market place.

Currently naphtha reforming is conducted at high temperatures and produces a high concentration of aromatics. The objective of this study is to reverse this trend in reforming by operating at low temperatures where thermodynamics favors a high concentration of isoparaffins.

An approach taken was to effect isomerization using an active catalyst (e.g., 1-3). Although a wide range of catalysts were investigated, much effort was centered on a heavily chlorided Pt-alumina catalyst. For example, Pt on a special silica-alumina could only operate at 350°C, and heavily chlorided Pt-alumina catalysts have been used for isomerization of alkanes at higher temperatures (350°C or greater). However, for naphtha reforming to produce alkanes it is desirable to operate at lower temperatures to be able to obtain a high octane product. It is likely that the chlorided Pt-alumina catalyst will have sufficient activity to produce a high fraction of the isoparaffins; however, the question concerning the ability of the catalyst to operate effectively in the presence of a high concentration of naphthenes (such as found in a coal-derived naphtha) requires further study. An objective of this paper was to develop a method to obtain a heavily chlorided Pt-alumina catalyst and to determine the activity and selectivity of these catalysts in reforming coal-derived naphtha and model compounds.

EXPERIMENTAL

Two aluminas, one a commercially available pellet (S.A. = 196 m^2/g) and one which was made in-house (S.A. = 149 m^2/g), were used in this project. The alumina powder was

made by precipitating $AlCl_3 \bullet 6H_2O$ (.5M in Al) with NH_4OH to a pH of 7.6. The gel was copiously washed with distilled H_2O and dried. The dried alumina was calcined at 500°C in air for 16 hours. Platinum was impregnated on the aluminas with chloroplatinic acid. An acetone solution containing the desired concentration of Pt was added to the alumina carrier and stirred overnight. The acetone was removed by rotoevaporation. The catalyst was dried overnight and stirred in a dessictator. Surface areas were determined by the BET method.

A plug flow reactor system was used for reduction, chloridation and activity testing of the catalysts.

Chloride analysis were done using standard ion chromatography techniques.

Methylcyclohexane and n-pentane were obtained commercially and dried using molecular sieves (3A) prior to use. All gases (N_2 and H_2) were ultra high purity (99.999%) and passed over molecular sieves prior to introduction into the reactor system. The naphtha sample was obtained from the Wilsonville advance liquefaction pilot plant. The naphtha was hydrotreated in the CAER PIPU pilot plant prior to use with the chlorided Pt/Al_2O_3 catalyst.

RESULTS AND DISCUSSION

A. Chloride Pretreatment. In the initial set of chloriding experiments, the Pt impregnated alumina powder (S.A. = 149 m^2/g) catalysts were used. The catalyst was reduced prior to the pretreatment using a temperature of 450°C and 260 psig H_2 (100 sccm/min.) overnight. Chloriding was done at 300°C using nitrogen at 250 psig pressure (100 sccm/min.) and CCl_4 as the chloriding agent. The CCl_4 partial pressure in the gas phase was controlled by the temperature of the vessel containing liquid CCl_4 that was used to saturate the nitrogen stream. Gas samples were taken to monitor the CO_2 content of the product gas by gas chromatography. In addition, gas samples were analyzed in the region of maximum CO_2 production and in the initial stage of chloridation by GC/MS. No $COCl_2$ or CO were found in the product gas stream in any of the samples using nitrogen as the carrier. The only compounds detected were N_2, CO_2, and at the end of the final time period of chloridation, CCl_4. Thus, CCl_4 reacts with alumina to produce CO_2 as the only carbon containing product; however, it is not known whether the chloride containing species is AlOCl, $AlCl_3$, or some more complex alumina compound is formed. However, it appears that chloriding occurs in steps with the first product being an alumina oxy chloride followed by subsequent formation of $AlCl_3$. Thus, for discussion purposes the reaction is written in two steps:

$$2\ Al_2O_3 + CCl_4 \rightarrow 4\ AlOCl + CO_2 \qquad [1]$$

$$2\ AlOCl + CCl_4 \rightarrow 2\ AlCl_3 + CO_2 \qquad [2]$$

$$AlCl_3)_{ads} \leftrightarrow AlCl_3)_{gas} \qquad [3]$$

The four Pt/Al_2O_3 catalysts were chlorided using this method. A typical CO_2 generation curve obtained using the .4 wt.% Pt/Al_2O_3 catalyst is shown in Figure 1. Because of the dead volume between the CCl_4 saturator and the catalyst bed, the time taken as zero does not coincide with the time that CCl_4 first contacts the catalyst bed. As can be seen in this figure, the CO_2 generated goes through a maximum at .31 mole % in 90 minutes. The low amount of CO_2 generated, which was typical for this set of catalysts suggested that the amount of chloride added would be lower than the 8-13 wt.% required for an active isomerization catalyst (4). Analysis of the catalyst indicated that the chloride content was 3.66 $\pm$ .30 wt.%. The chloride content of these Pt/Al_2O_3 catalysts did not exceed 4 wt.% and appeared to correlate with the maximum CO_2 content generated during the chloriding pretreatment.

The next set of experiments performed in an attempt to increase the chloride content of the catalyst used the commercially available Al_2O_3 pellets. The method for the chloriding pretreatment was also changed. Nitrogen was used for the CCl_4 entrainment at atmospheric pressure and 100 sccm/min. The reactor temperature remained the same (300°C). The CO_2 concentrations generated during the chloridation of the alumina pellets are shown in Figure 2. As can be seen, the amount of CO_2 produced was significantly greater than the amount shown in Figure 1. The maximum CO_2 generated (23.2 mole %) was also obtained at a shorter reaction time (10 min.). The chloride content of the catalyst was determined to be 13.70 wt.%. These data suggested that the observed increase in chloride added to the alumina pellets may be due to the form of the catalyst (pellets vs. powder).

In the next chloriding experiment, the alumina pellets were ground to -100 mesh (S.A. = 200 m^2/g) to determine if the form of the catalyst affects the amount of chloride addition. The powdered alumina was chlorided using the same procedure as that used for the alumina pellets. The CO_2 generated during the chloridation of this sample is shown in Figure 2. As can be seen, the maximum CO_2 content is lower and required a longer reaction time to obtain. This correlates with the lower chloride content (5.79 wt.%) of the powdered catalyst. One possible explanation for the data shown in Figure 2 is that for the alumina pellets, the CCl_4 penetrates the pellet and reacts rapidly (reactions [1] and [2]) with the alumina to produce a chlorided alumina compound and produce CO_2. The penetration of CCl_4 into the pellet and the escape of the CO_2 out of the pellet was not believed to be diffusion limited. It is believed that the diffusion of $AlCl_3$ from the interior of the catalyst or particle is slow because of diffusion, or a process that resembles diffusional limitations. Thus, it is viewed that $AlCl_3$ forms uniformly throughout the catalyst particle or pellet but that it is lost from the catalyst bed by desorption from the surface boundary of the catalyst particle or pellet. The geometric surface boundary of the pellet is much smaller than that of the same amount of catalyst when it is present in powder form. Hence, it is believed that the rate of chloridation is similar in both the powder and the pellet. However, desorption to the gas in the void volume and transport from the catalyst bed is much slower for the pellet than for the powder.

With the development of a method of chloride addition which produced an alumina with a sufficiently high chloride content, the next set of experiments used the alumina pellets impregnated with 2 wt.% Pt. This catalyst was reduced as described above and chlorided using the same procedure as in the alumina pellet experiments. In addition this catalyst was also chlorided without prior reduction. The chloride content of the resulting catalysts are shown in Figure 3. The data shown in Figure 3 indicate that the addition of Pt to the alumina pellets decreases the chloride content of the catalysts when compared to that of

the alumina pellets. The reduced catalyst produced a slightly higher chloride content than the catalyst which was not reduced prior to chloridation. Without further data, it is not possible to unambiguously determine the cause for the lower chloride content; however, the data does suggest that the impregnation of the alumina with the Pt has removed a number of sites that react with the CCl_4.

The data presented above indicate that a 2% Pt/Al_2O_3 (pellet) can be chlorided to produce a catalyst containing a high chloride content (7.22 wt.%) and that the extent of chloride addition can be monitored by the amount of CO_2 produced during this pretreatment. The reproducibility of this method is illustrated in Figure 4 which shows the CO_2 generation curves for a number or chloride pretreatments. Note that in Test #11, the chloriding pretreatment was terminated just after the CO_2 production reached a maximum. The resulting catalyst had a 5.93 wt.% chloride content. This run suggests that using this method of monitoring the extent of chloridation can accurately produce a series of catalysts with varying chloride contents.

B. Isomerization Activity. The isomerization activity of the 2% Pt/Al_2O_3 catalysts which have different chloride contents is shown in Figure 5. For all of the reaction temperatures studied, the Pt/Al_2O_3 (pellet) catalyst containing 7.22 wt.% Cl affected significantly higher conversions of n-pentane. The product distribution obtained for both of these catalysts were similar. The major product of the runs was isopentane (> 99%). In addition, minor amounts (ca. 0.1 - 0.2 wt.%) of isohexanes were also produced. Very little hydrogenolysis was observed for both of the catalysts. The data obtained from these isomerization runs with n-pentane suggest that the higher conversions are obtained with catalysts with high chloride concentrations.

The chlorided 2 wt.% Pt/Al_2O_3 (pellet) was also tested with methylcyclohexane (MCH) using a number of reactor temperatures. The results indicated that although conversion of MCH were relatively high, the major products were 2-carbon cyclopentanes ($\sim 95^+$ wt.%) which indicated that little ring-opening of the MCH was accomplished. In an attempt to change the selectivity of the catalysts for the conversion of MCH, the total hydrogen pressure of the reactor was increased while holding the temperature constant. The effect of pressure on the conversion of MCH is shown in Figure 6. Increasing the reactor pressure from 100 to 730 psig slightly increases the conversion from 60 to 80 wt.%. However, the increase in pressure significantly changes the product distribution (Figure 7). The 2-carbon cyclopentanes, which are the major products of the conversion of MCH at lower pressures, significantly decrease in concentration with increasing pressure. It appears from these data that in order to obtain ring opening at lower temperatures, higher reactor pressures are required.

A hydrotreated naphtha derived from processing an Illinois #6 coal at Wilsonville was obtained as a reforming feedstock using the chlorided 2% Pt/Al_2O_3 (pellet) catalyst. The catalyst exhibited an initial high activity in producing branched alkanes; however, this activity decreased rapidly with time on stream. It appears that the low concentration of heteroatoms remaining in the hydrotreated naphtha poisons the catalyst rapidly.

SUMMARY

The extent of chloridation of a Pt/Al_2O_3 catalyst can be monitored by determining the CO_2 concentration in the product gas stream. The pellet form of the catalyst can be pretreated to produce a catalyst with a higher chloride content when compared to the powdered form

of the catalyst. The Pt/Al_2O_3 catalyst containing the higher chloride content has a significantly higher isomerization activity using n-pentane as the feedstock. In order to open the cycloalkane ring to produce branched alkanes, higher reactor pressures are required at low reaction temperatures.

ACKNOWLEDGMENT

This work was supported by the DOE contract #De-AC22-90PC90049 and the Commonwealth of Kentucky. The authors also acknowledge the personnel at the Wilsonville liquefaction facility for providing the naphtha samples and for their helpful advice.

REFERENCES

1. E. F. Schvarzenback, *Proc. Am. Petrol. Inst.*, **37**, Section III, 354 (1957).
2. D. H. Belden and V. Haensel, *Proc. Am. Petrol. Ind.*, **37**, Section III, 354 (1957).
3. T. Y. Yan, T. J. Huang, W. O. Haag, U.S. Patent 4,049,539, September, 1977.
4. A. G. Goble, P. A. Lawrance, *Proc. 3rd Int. Cong. Catalysis*, Amsterdam, Vol. 1, 320, 1964.

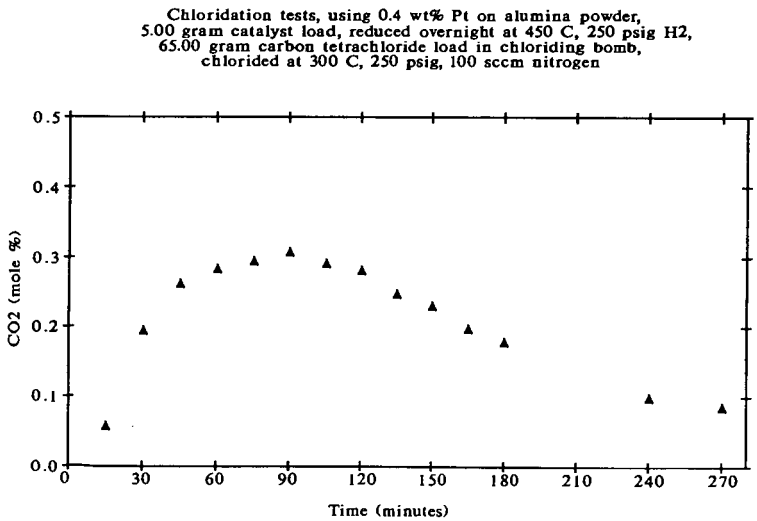

Figure 1. Carbon dioxide content of product gas during chloradation.

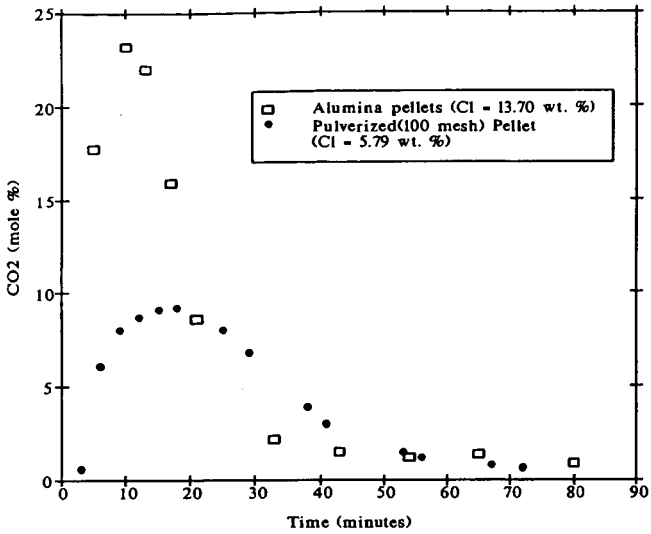

Figure 2. CO2 production during chloridation of alumina catalysts (5.00 gram load,65.00 g CCl4 load in chloriding bomb, chlorided at 300 C, 1 at, N2 @ 50 sccm).

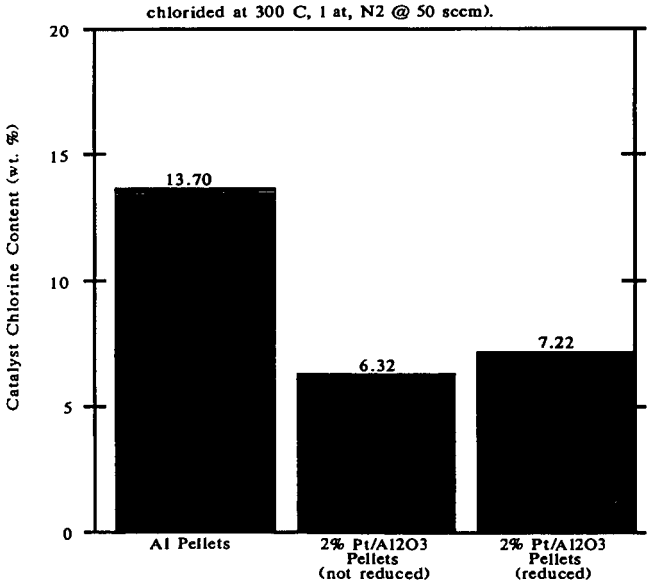

Figure 3. The effect of Pt impregnation and reduction on chloride addition. (same conditions as Figure 2.)

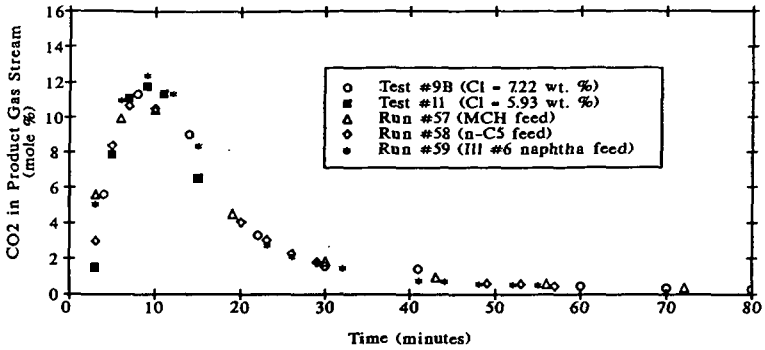

Figure 4. Reproducibility in the chloriding of a 2 % Pt/Al2O3 catalyst (pellet) (same conditions as in Figure 2).

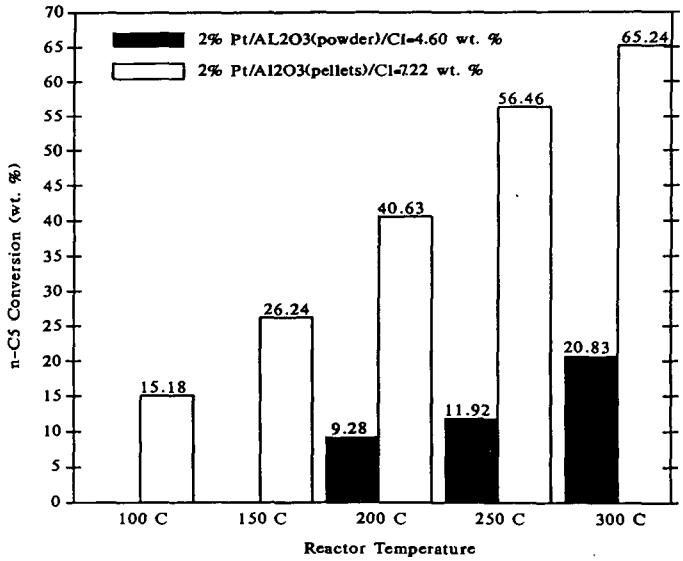

Figure 5. Comparison of n-C5 conversions using catalysts with different Cl contents (WHSV=1.0, pressure=100psig).

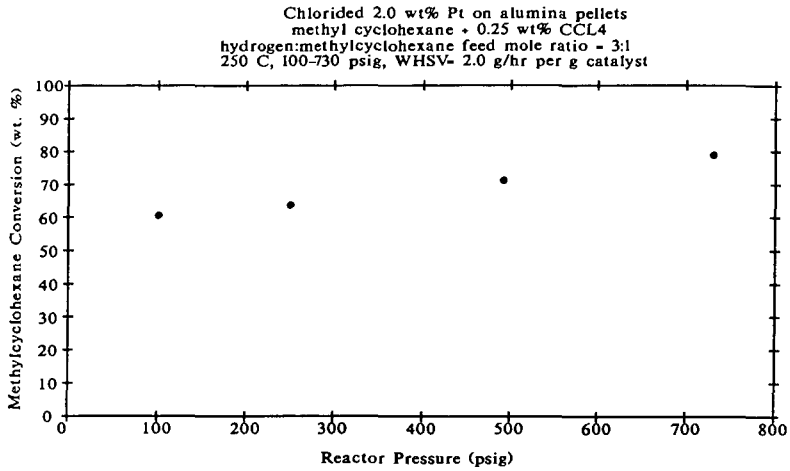

Figure 6. Efect of hydrogen pressure on MCH conversion.

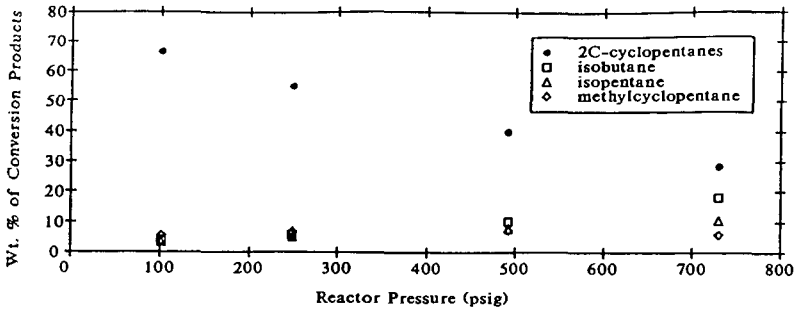

Figure 7 Effect of H2 pressure on product selectivity (same conditions as Figure 6).

THE APPLICATION OF FT-IR METHODS TO THE CHARACTERIZATION OF COAL LIQUEFACTION PROCESS STREAMS

Hsisheng Teng, Michael A. Serio, Rosemary Bassilakis,
Kim S. Knight, Stephen C. Bates and Peter R. Solomon

Advanced Fuel Research, Inc.
87 Church Street
East Hartford, CT06108

Keywords: Coal Liquefaction, FT-IR, Fiber Optics

INTRODUCTION

Fourier transform infrared spectroscopy (FT-IR) is one of the most versatile analytical techniques available for the study of fossil fuel structure and reaction chemistry [1-5]. Among its advantages are: 1) its ability to study feedstocks and reaction products as solids, liquids and gases, since almost all have characteristic absorptions in the infrared; 2) its high sensitivity, allowing the study of strongly absorbing materials such as coal and char, and the use of techniques such as attenuated total reflectance (ATR) or photoacoustic spectroscopy; 3) its speed, allowing the possibility of following chemical reactions on-line. Because of these advantages, FT-IR spectroscopy has achieved increasing use in fuel science.

The objective of this work was to evaluate the use of two FT-IR methods for characterization of distillation resids from coal liquefaction process streams. The first method is quantitative FT-IR analysis of samples pressed into KBr pellets to determine functional group concentrations. The second method is Thermogravimetric Analysis with FT-IR analysis of evolved products (TG-FTIR). In addition, the application of on-line FT-IR Fiber Optic (F-O) ATR analysis to coal liquefaction processes is addressed.

EXPERIMENTAL

Characterization of Coal Liquefaction Products

The samples used in this study were supplied by Consolidation Coal Company (CONSOL), PA, along with chemical and structural information obtained with various techniques. These samples included: 1) Three feed coals (Wyodak, Illinois, and Pittsburgh); 2) Nine whole resid samples produced by distillation of process oils generated from the three different feed coals and obtained from three different sampling points (interstage, recycle, second stage) during liquefaction runs at the Wilsonville (AL) facility; 3) Nine THF soluble portions of the above whole resids; 4) Four additional solids free resids obtained during a catalyst aging study at the HRI (NJ) facility; 5) A single whole process oil for Pittsburgh coal obtained from the Wilsonville facility. These samples were analyzed by both FT-IR and TG-FTIR.

FT-IR Analysis - The samples are analyzed as KBr pellets in a Nicolet 7199 FT-IR. For quantitative analysis of such spectra, a curve analysis program is employed to synthesize the IR spectra [1-3]. The program uses a basic set of adsorption peaks identified with various functional groups. The synthesis routine can produce a spectrum which matches the actual spectrum well. The correction of a whole resid spectrum for scattering and minerals is demonstrated in Figure 1.

TG-FTIR Analysis - The apparatus consists of a sample suspended from a balance in a gas stream within a furnace. As the sample is heated in helium, the evolving volatile products are carried out of the furnace directly into a gas cell for analysis by FT-IR [5]. The results of a typical resid pyrolysis experiment are shown in Figure 2. The system continuously monitors the time-dependent evolution of the gases and tars, and weight of the non-volatile material. At the end of the pyrolysis experiment, oxygen is introduced to burn the residue to obtain the ash content of the sample.

In-Situ FT-IR/F-O/ATR Measurements

A coal liquefaction test cell which incorporates a FT-IR/F-O system is shown in Figure 3. The reactor is made of 3/8" stainless tubing and Swagelok tube fittings. This reactor can withstand a pressure as high as 3800 psig at 400 °C. A sapphire fiber, which is 15" (38 cm) in length and 0.25 mm in diameter, is used as an ATR sensor in the reactor. A zirconium fluoride fiber cable is used as a transmitting fiber to link between the sensor fiber and the FT-IR spectrometer and detector.

Liquefaction of demineralized Zap lignite was performed in the test cell, with 1 g of coal sample mixed with 6 ml of tetralin. The experiment was performed by heating the reactor from room temperature to 400 °C at 20 °C/min, and sustaining the final temperature for 40 minutes. The F-O/ATR spectra of the tetralin/coal liquid mixtures in the reactor were taken at regular intervals. Tetralin spectra at the relevant temperatures were taken and compared with those from coal liquefaction experiments.

RESULTS AND DISCUSSION

Characterization of Coal Liquefaction Products

Characterization of the samples using the FT-IR and TG-FTIR methods provides a good understanding of the average chemical structure of products from the various stages of a coal liquefaction process. In order to demonstrate the reliability of these two FT-IR techniques, correlation and comparison of the results in this study with those supplied by CONSOL using different methods are described below.

FT-IR Analysis

Aromatic and Aliphatic Hydrogen (Proton) Distribution - The comparison of the aromatic to total hydrogen ratio (H_{ar}/H_{total}) using FT-IR analysis with the aromatic proton fraction from the ^{1}H-NMR method for the THF soluble samples is shown in Figure 4a. Figure 4b shows the comparison of the aliphatic hydrogens for the same set of samples. The results show that the FT-IR H_{ar}/H_{total} agrees reasonably well with the fraction of aromatic protons derived from the ^{1}H-NMR method. The same is true of the aliphatic hydrogen. These figures contain two lines. The solid line is the mean value of the ratios between the two sets of measurements. The dashed line is a parity line. Figures 4a and 4b provide a relation between the results obtained by these two methods:

H_{ar}/H_{total} (%, THF sol.), FT-IR = 0.77 [Aromatic Proton Fraction (% THF sol.), ^{1}H-NMR]
H_{al}/H_{total} (%, THF sol.), FT-IR = 1.1 [Aliphatic Proton Fraction (% THF sol.), ^{1}H-NMR]

Hydroxyl Groups - Both this study and CONSOL used an FT-IR method to determine the

concentration of hydroxyl groups in the samples. CONSOL used the -OH stretch band found between 3200 and 3400 cm^{-1} to determine the phenolic -OH concentration from measurements on THF-soluble portions of the samples. In this study, the concentration of hydroxyl groups was determined using the 3200 cm^{-1} O-H stretch to avoid the interference from the KBr-H_2O band which peaks at 3400 cm^{-1} [1]. The hydroxyl results obtained in this study and by CONSOL are in good agreement, considering the differences in sample preparation and the quantitative analysis routines. The relation between them is:

-OH (wt%, THF sol.), FT-IR = 0.90 [Phenolic-OH (wt%, THF sol.), FT-IR | CONSOL]

Oxygen Analysis - In general, most of the oxygen atoms in coal and coal products are contained in hydroxyl, ether, and carbonyl functional groups. In this study, oxygen contents of the samples were determined through quantitative analysis of hydroxyl and ether by the FT-IR method, assuming that the amount of oxygen in carbonyl functions is negligible. The oxygen contents of the samples provided by CONSOL were determined by difference in elemental analyses. The oxygen data in this study and from CONSOL for the whole resids and whole process oil show reasonable agreement, although the data are somewhat scattered. The relation between these two different methods is:

O-Content (wt%, MAF), FT-IR = 1.1 [O-Content (wt%, MAF), Elemental Difference]

Hydrogen Analysis - The total hydrogen content for each of the samples was determined by summing up the aliphatic, aromatic, and hydroxyl hydrogen determined by FT-IR. The hydrogen analysis provided by CONSOL was determined with a Leco CHN-600 elemental analysis instrument. The results of these two methods are in good agreement. The relation between them is:

H-Content (wt%, MAF), FT-IR = 1.1 [H-Content (wt%, MAF), Elemental Analysis]

Carbon Analysis - The carbon content of each sample was determined by mass balance difference with oxygen and hydrogen contents obtained with the FT-IR method, assuming that the fraction of others, such as nitrogen and sulfur, is negligible. The values supplied by CONSOL were obtained from carbon analysis with the Leco CHN-600 instrument. A comparison shows that these two sets of data from different methods are in good agreement, and the relation between them is:

C-Content (wt%, MAF), FT-IR = 1.0 [C-Content (wt%, MAF), Elemental Analysis]

Ash - FT-IR analysis can determine the contents of major minerals, i.e. mixed clays, Kaolinite, Quartz, and Calcite. The total ash content determined by FT-IR is the sum of these four minerals. Since the FT-IR measurement of minerals includes the associated water and is done at ambient temperature, it is expected to be higher than the high temperature ash determinations supplied by CONSOL. However, it is also true that the FT-IR method does not determine pyrite, so it may underestimate the ash content for coals which contain large amounts of this mineral. The comparison of the ash contents determined with FT-IR and by CONSOL is shown in Figure 4c. The results show that the trends in the FT-IR values of the total ash content agreed well with the values supplied by CONSOL, although the latter numbers were lower as expected. The relation between the two measurements is:

Ash (wt%, dry),FT-IR = 1.3 [Ash (wt%, dry), Combustion]

TG-FTIR Analysis

Proximate Analysis of Feed Coals - Pyrolysis up to 900 °C followed by combustion of the residue, when carried out in the TG-FTIR apparatus, gives a good proximate analysis for feed coals. The proximate analysis with TG-FTIR reveals the contents of ash, volatile matter, fixed carbon, and moisture in coal.

Pyrolysis of coal at temperatures as high as 900 °C will produce a char with a high carbon content (>95%, MAF). Therefore, the char yield (MAF) in pyrolysis represents the fixed carbon content in the coal. The comparison of the fixed carbon content obtained by TG-FTIR and that supplied by CONSOL is shown in Figure 4d. It shows that the two sets of values are in good agreement and the relation between them is:

Fixed Carbon (wt%, dry), TG-FTIR = 1.0 [Fixed Carbon (wt%, dry), Proximate Analysis]

The ash content is determined by burning the char in the presence of oxygen. A comparison of ash analyses is shown in Figure 4e, and the results show a good agreement. The relation between the two sets of data is:

Ash (wt%, dry), TG-FTIR = 1.1 [Ash (wt%, dry), Proximate Analysis]

The volatile matter of coal includes all the species evolved during pyrolysis. These species are gases and tars, which are measured by TG-FTIR during the process of pyrolysis. The comparison of the volatile matter contents determined by TG-FTIR with those provided by CONSOL from proximate analysis is shown in Figure 4f. The results show that they are in good agreement with each other and the relation is:

Volatile (wt%, dry), TG-FTIR = 1.0 [Volatile (wt%, dry), Proximate Analysis]

The moisture content of coal is determined by TG-FTIR prior to pyrolysis. The results obtained by TG-FTIR are not in good agreement with those supplied by CONSOL, although the trend is correct. The relation between them is:

Moisture (wt%, as rec.), TG-FTIR = 0.45 [Moisture (wt%, as det.), Proximate Analysis]

This difference is not surprising since the moisture content depends on how the sample is stored and handled.

Ash Analysis for Resids - The ash content of the distillation resids was determined using TG-FTIR by burning the char residue from the resids in the presence of oxygen. The comparison of the resid ash content obtained with TG-FTIR and that supplied by CONSOL is shown in Figure 5a. The results show that the ash contents determined by TG-FTIR are in very good agreement with those provided by CONSOL. The relation between the two sets of data is:

Ash (wt% dry), TG-FTIR = 1.0 [Ash (wt%, dry), Combustion]

Char Analysis for Resids - Coal chars produced at temperatures above 900 °C consist mainly of large condensed aromatic rings. It is expected that the char yield from resid pyrolysis would have a proportional relation with the content of condensed aromatics. The comparison of the char yield for pyrolysis performed in the TG-FTIR and the condensed aromatic proton fraction from NMR is shown in Figure 5b for the THF soluble fractions. The results show that the char

yield in resid pyrolysis increases with increasing condensed aromatic proton fraction. The relation between the two sets of values is:

Char (wt%,THF sol.), TG-FTIR = 0.65 [Cond. Aromatic Proton (%, THF sol.) ^{1}H-NMR]

Data Interpretation in the Context of the Liquefaction Process

The samples from the Wilsonville facility were taken from three locations to represent different degrees of coal processing. The Interstage Product samples were distillation resids obtained from a high pressure flash separation system located between the first stage and second stage reactors. The 2nd Stage Product samples were resids collected from the bottom product hold tank of a separation system following the second stage reactor. The Recycle samples were resids obtained from the solvent surge tank. The Recycle samples are the partially deashed products of the 2nd Stage Product. The structural differences of the samples, revealed in the analytical data, are due to differences in the feed coals and to different degrees of coal processing in liquefaction, as discussed below.

A comparison of -OH contents from THF soluble fractions of the resid samples from different degrees of processing is shown in Figure 6. The results show that the Interstage Product has a higher -OH content than the 2nd Stage Product due to upgrading by the second reactor. The TG-FTIR results show a corresponding reduction of CO evolution in pyrolysis for the 2nd Stage Product, as discussed below. Figure 6 shows a slight -OH reduction due to the deash process. In general, the -OH content of the resids decreases in the order Interstage > 2nd Stage > Recycle. The trends for char yield from TG-FTIR analysis follow the same general order, which is consistent with the role of oxygen functions in retrogressive reactions under pyrolysis [6] and liquefaction conditions [7].

Since the oxygen content of the feedstock would be reduced in the liquefaction process, the amount of CO evolution in pyrolysis is expected to decrease in the order coal > Interstage > 2nd Stage > Recycle, and the results shown in Figure 7 for the whole resids indicate that this is the case. If the results in Figures 6 and 7 are compared, it can be seen that the -OH content and the CO evolution from pyrolysis are related.

Similar to the result of CO evolution in pyrolysis, more CH_4 is evolved in coal pyrolysis than in resid pyrolysis. Because most of the CH_4 forming components in coal are consumed in the liquefaction process in which gaseous product CH_4 is separated from the process stream to become fuel gas, it is reasonable to see less CH_4 evolution in resid pyrolysis. A comparison of CH_4 yields from pyrolysis of the feed coals and various whole resid samples is shown in Figure 8. Since CH_4 forming components would be further reduced by the Second stage reactor, it is also not surprising to see less CH_4 evolution in the pyrolysis of the 2nd Stage Product than the Interstage Product. The amounts of CH_4 evolution from the 2nd Stage Product and from the Recycle are similar, which reveals that the deash process has little effect on the CH_4 forming structures in resids. In general, the amount of CH_4 evolution in the pyrolysis of liquefaction products follows the order coal > Interstage > 2nd Stage ~ Recycle.

The hydrogen content analyses indicate a slight increase in hydrogen concentration in the whole resids from the second stage reactor by comparing the 2nd Stage Product with the Interstage Product (except for Pittsburgh resid). These results are shown in Figure 9. This figure also shows the expected increase in hydrogen concentration for the resid products when compared to the feed coal. Also, as the material is upgraded, the absolute amount of aromatic hydrogen decreases, as shown in Figure 10.

The HRI samples represent production of material from a Continuous Two-Stage Liquefaction facility for different periods of time in a single run. Interpretation of the data reveals a consistent variation of the properties of the samples with the length of run period. The interpretation of these variations is discussed below and is based on information supplied by CONSOL on variations in run conditions as function of time.

The variation of the hydrogen content of the sample with the length of the run period is shown in Figure 11. The results show that the total hydrogen and aliphatic hydrogen content decrease with increasing run time, whereas the aromatic hydrogen shows an opposite trend. The decrease of the hydrogen content of the liquefaction product with run time may be attributable to catalyst aging as well as to a reduction in the solvent/coal ratio and an increase in solvent cut point. It is reasonable to observe a reduction in the aliphatic hydrogen content since the hydrogenation rate slows down with time due to catalyst aging. The increase in H_a, with run time may also result from the increasing reaction temperature which would tend to increase the amount of aromatic hydrogen.

The variation of the hydroxyl and ether contents of the samples with the length of the run period is shown in Figure 12. The results show an increase of the hydroxyl content with run time. The change in -OH concentration is due to catalyst aging as well as to the reduction in the solvent/coal ratio and to the increase in solvent cut point. The FT-IR results also show an increase in the ether content with time. The increase of the ether content in the liquefaction products can be attributed mostly to the catalyst aging which would result in a lower rate of bond cleavage on ether linkages. A second possibility is an increase in the amount of ethers formed from retrogressive reactions involving hydroxy and dihydroxy functionalities structures.

In-Situ FT-IR/F-O/ATR Measurements

In order to accommodate the temperature (~400 °C) and pressure (~3000 psig) requirements of a coal liquefaction process, a sapphire fiber optic element was used in the ATR mode for in-situ measurements. This cuts out the information below about 2500 cm^{-1}, but still allows significant amounts of chemical structural information to be obtained.

Since tetralin is the solvent used in coal liquefaction experiments, it is of interest to know how tetralin behaved under temperature conditions similar to those of coal liquefaction. Non-isothermal experiments which simulate the conditions of coal liquefaction are carried out in the test cell, and the infrared spectra from the F-O/ATR spectroscopy at different temperatures were obtained. Figure 13 shows the tetralin absorbance spectra in the C-H stretching region at different temperatures. Since tetralin does not contain oxygen functional groups, the focus of the analysis was on the C-H stretching region.

It can be seen from the spectra that the infrared absorbance decreases with temperature. This result is expected, since the depth of penetration of the infrared evanescent wave into the sample decreases with temperature. The temperature effect on F-O/ATR spectroscopy requires further study in order to obtain quantitative results.

Since it was known [8] that tetralin would undergo hydrogen transfer reactions to form a mixture of aliphatic and alkyl aromatic compounds by heat treatment, the aliphatic to aromatic ratio in the system would therefore vary with temperature. Based on Figure 13, one should be able to determine the aliphatic to aromatic hydrogen ratios at different temperatures from the absorbance ratios of 2930 cm^{-1} to 3020 cm^{-1}, if the extinction coefficients for each species were

known. This issue, for pure tetralin as well as coal liquefaction measurements, will be discussed in a future publication.

It has been reported [9] that the alkyl CH_3 gives rise to a symmetric stretching mode at 2870 cm^{-1}, and the $-CH_2-$ at 2850 cm^{-1}. Since tetralin does not contain methyl structures, the 2860 and 2840 cm^{-1} peaks shown in Figure 13 are actually from the spliting of the methylene symmetric stretching at 2850 cm^{-1}. By thermal treatment, tetralin will undergo decomposition to form its derivatives, which contain methyl groups. The methyl symmetric stretching at 2870 cm^{-1} would interfere with the 2860 cm^{-1} peak from the methylene, and, therefore, the former peak would not be distinct if its concentration is low. Because of this interference, we cannot see a 2870 cm^{-1} peak emerging at higher temperatures in Figure 13. However, if a series of absorbance spectra from coal liquefaction experiments are examined, as shown in Figure 14 for demineralized Zap, the emergence of the methyl 2870 cm^{-1} absorbance underneath the methylene 2860 cm^{-1} absorbance can be clearly seen. A curve resolving technique has recently been developed in our group to resolve overlapped absorption bands. This technique will be applied to the F-O/ATR spectra to improve quantitative analysis.

The O-H stretching region for the liquefaction run is shown in Figure 15. The absorbance spectrum of O-H stretching is usually a broad band, ranging between 3100 and 3600 cm^{-1} and centered near 3400 cm^{-1} [10]. Figure 15 shows that the absorbance by hydroxyls increases with the degree of liquefaction, indicating increasing amount of OH-containing coal fragments dissolved in the liquid phase.

CONCLUSIONS

Both FT-IR and TG-FTIR have been clearly shown to provide a wide variety of useful information for process stream characterization. Both techniques can be applied to whole process oils, resids, or distillates, including ash components, and require relatively small samples (<50 mg). Significant differences are observed between process stages, coal types, and with catalyst aging. A summary of the composition parameters that can be obtained by FT-IR and TG-FTIR is shown in Table 1. In many respects, FT-IR is probably the single most useful technique for this purpose, since it can provide measurements on both organic and mineral components. It has also demonstrated that on-line FT-IR measurements could be made in-situ using a sapphire fiber optic element in the Attenuated Total Reflectance mode.

ACKNOWLEDGEMENTS

This work was supported by a subcontract from the Consolidation Coal Company under DOE Contract No. DE-AC22-89PC89883, and by the DOE SBIR program under Grant No. DE-FG05-91ER81151. The authors also wish to acknowledge Dr. Susan Brandes and Mr. Richard Winschel of CONSOL Research and Development for many helpful discussions, and Mr. William Stevenson, Dr. Mark Druy, and Mr. Paul Glatkowski of Foster-Miller, Inc. of Waltham, Mass. for assisting with the FT-IR/F-O/ATR measurements. Marie DiTaranto of Advanced Fuel Research did the FT-IR analyses. Robert Carangelo and Erik Kroo consulted on the interpretation of the FT-IR, TG-FTIR and FT-IR/F-O/ATR results.

REFERENCES

1. Solomon, P.R., and Carangelo, R.M., Fuel, **61**, 663 (1982).
2. Solomon, P.R., and Carangelo, R.M., Fuel, **67**, 949 (1988).
3. Solomon, P.R., Hamblen, D.G., and Carangelo, R.M., Am. Chem. Soc. Symp. Ser., **205**, 77 (1982).
4. Painter, P.C., Snyder, R.W., Starsinic, M., Coleman, M.M., Kuehn, D.W., and Davis, A., Am. Chem. Soc. Symp. Ser., **205**, 47 (1982).
5. Carangelo, R.M., Solomon, P.R., and Gerson, D.J., Fuel, **66**, 960(1987).
6. Solomon, P.R., Serio, M.A., Desphande, G.V., and Kroo, E., Energy & Fuels, **4**, (1), 42 (1990).
7. Serio, M.A., Solomon, P.R., Kroo, E., Bassilakis, R., Malhotra, R., McMillen, D., Prepr. Pap. - Am. Chem. Soc., Div. Fuel Chem., **35**, (1), 61 (1990).
8. Vlieger, J.J., Kieboom, A.P.G., and Bekkum, H., Fuel, 63, 334, (1984).
9. Willard, H.H., Merritt, L.L., Jr., Dean, J.A., and Settle, F.A., Jr., Instrumental Methods of Analysis, 6th Edition, D. van Nostrand Co., New York (1981), Chapter 7.
10. Painter, P.C., Sobkowiak, M., and Youtcheff, J., Fuel, **66**, 973 (1987).

TABLE 1. SUMMARY OF FT-IR AND TG-FTIR MEASUREMENTS

FT-IR MEASUREMENT	ALTERNATIVE TECHNIQUE
Hydroxyl Hydrogen	Chemical Titration
Aliphatic Hydrogen	^{1}H-NMR
Aliphatic Carbon*	^{13}C-NMR
Aromatic Hydrogen	^{1}H-NMR
Hydrogen Content	Elemental Analysis
Carbon Content*	Elemental Analysis
Hydroxyl Oxygen	Chemical Titration
Ether Oxygen	- - -
Carbonyl Oxygen**	- - -
Total Ash	TGA
Mineral Components	ICP
TG-FTIR MEASUREMENT	**ALTERNATIVE TECHNIQUE**
Direct	
Volatile Content	Proximate Analysis
Fixed Carbon	Proximate Analysis
Total Ash	Proximate Analysis
Moisture	Proximate Analysis
C,H,N,S	Elemental Analysis
Indirect	
Char Yield →Condensed Aromatics	^{1}H-NMR
CO Yield → Phenolic Content	FT-IR
CH_4 Yield → Methyl Group Content	^{13}C-NMR
Tar Evolution Profile → Boiling Range	Distillation

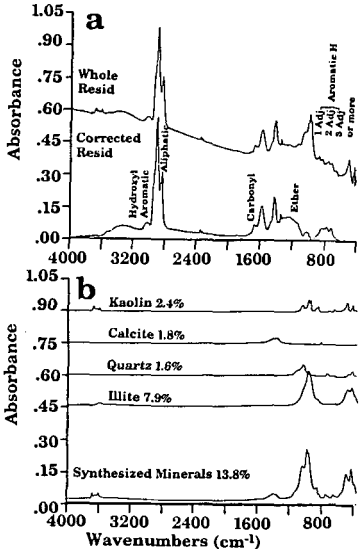

Figure 1. Quantitative FT-IR Analysis of the Coal Liquefaction Product. Correction of Resid Spectrum for Scattering and Minerals. a) Correction of Resid Spectrum; b) Determination of Mineral Spectrum by Addition of Reference Spectra. Data for Whole Resid Sample (interstage) from Illinois No. 6 Coal.

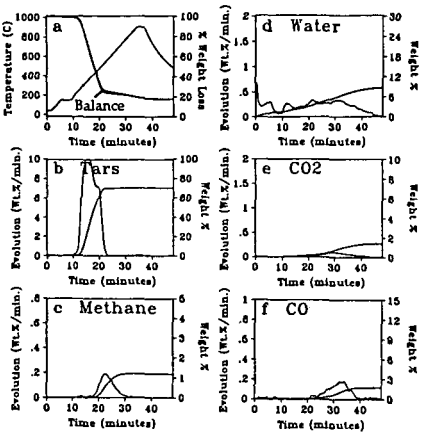

Figure 2. TG-FTIR Results for Interstage Oil Resid from Illinois No. 6 Coal.

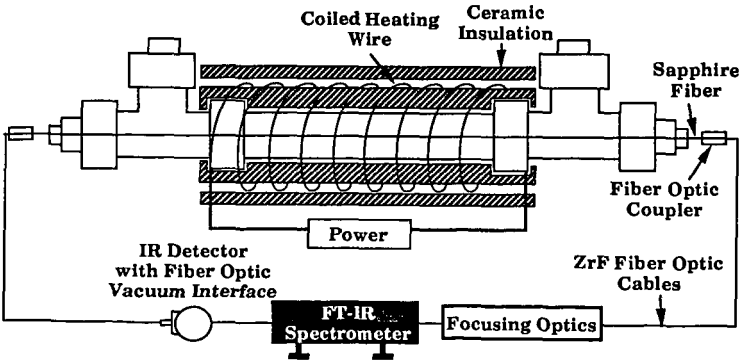

Figure 3. Schematic of FT-IR Fiber-Optic ATR System for Coal Liquefaction.

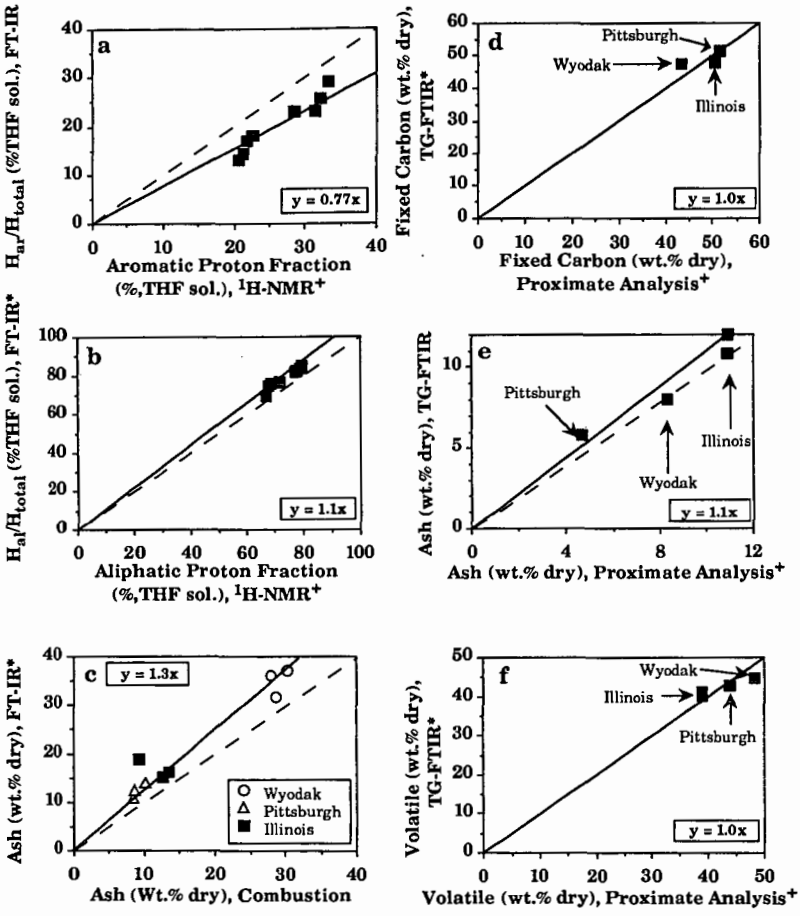

Figure 4. Correlation and Comparison of the Results from FT-IR Techniques and Other Methods. a) Resid Aromatic Hydrogen Distribution; b) Resid Aliphatic Hydrogen Distribution Resid; c) Resid Ash Content; d) Coal Fixed Carbon; e) Coal Ash Content; f) Coal Volatile.
* Present Study; + Data Supplied by CONSOL.

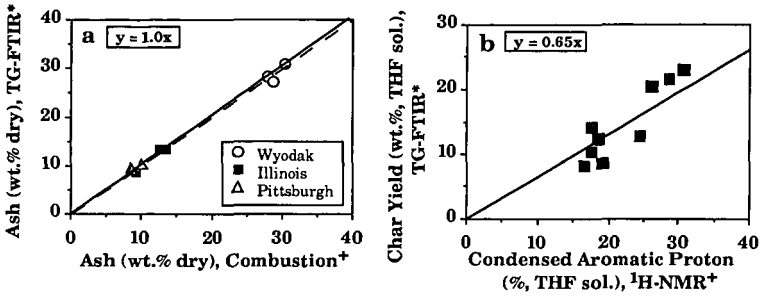

Figure 5. Correlation and Comparison of the Results from FT-IR Techniques and Other Methods. a) Resid Ash Content; b) Char Yield with Condensed Aromatic Proton Fraction. * Present Study; + Data Supplied by CONSOL.

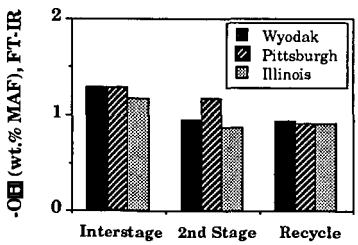

Figure 6. -OH Content at Different Stages for Wilsonville Resids.

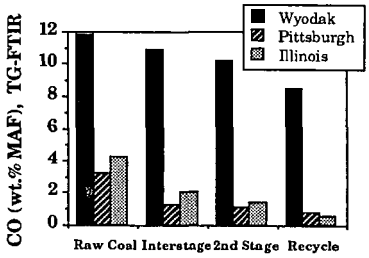

Figure 7. CO Evolution from Pyrolysis of Wilsonville Resids.

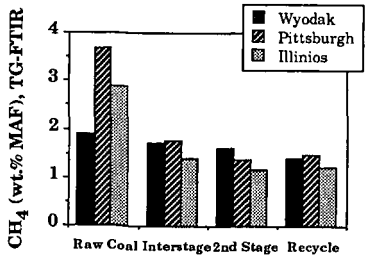

Figure 8. CH_4 Evolution from Pyrolysis of Wilsonville Resids.

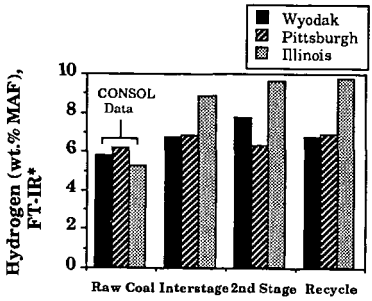

Figure 9. Hydrogen Content at Different Stages for Wilsonville Resids.

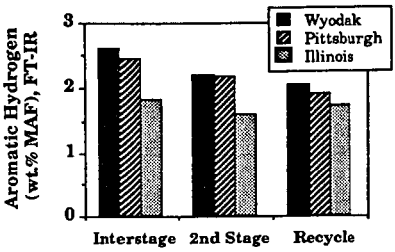

Figure 10. Aromatic Hydrogen Content at Different Stages for Wilsonville Resids.

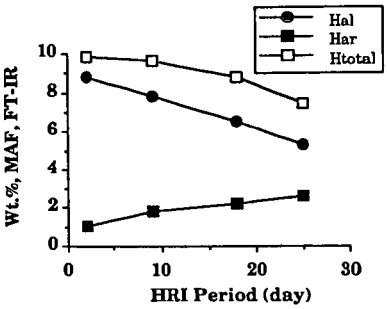

Figure 11. Hydrogen Analysis for HRI Liquids.

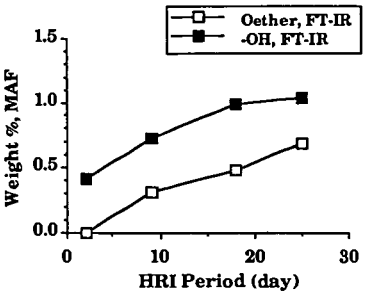

Figure 12. Oxygen Functional Group Analysis for HRI Liquids.

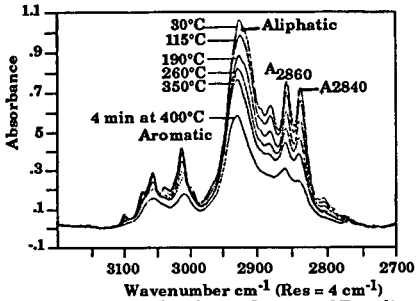

Figure 13. The Absorbance Spectra of Tetralin from F-O/ATR Spectroscopy in a Non-Isothermal Experiment.

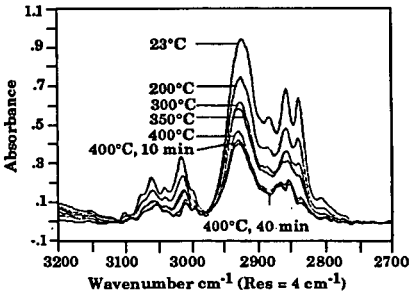

Figure 14. The C-H Stretching Region of the Absorbance Spectra from F-O/ATR Measurements under Coal Liquefaction Conditions for Demineralized Zap.

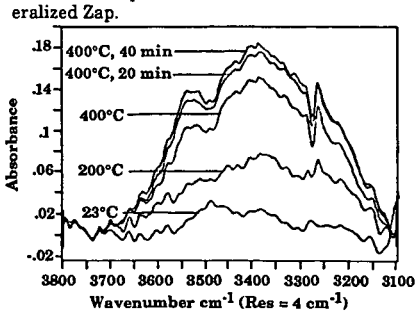

Figure 15. The O-H Stretching Region of the Absorbance Spectra from F-O/ATR Measurements under Coal Liquefaction Conditions for Demineralized Zap.

SYMPOSIUM ON PROCESSING AND PRODUCT SELECTIVITY
OF SYNTHETIC FUELS

Presented before the Division of Fuel Chemistry
American Chemical Society
Washington, D.C., August 23-28, 1992

ASSAY OF DIESEL FUEL COMPONENTS PROPERTIES AND PERFORMANCE

by Jimell Erwin
Southwest Research Institute
P.O. Drawer 28510
San Antonio, TX 78228
(512) 522-2389

Introduction

The increasingly stringent restrictions on exhaust emissions from diesel fuel powered vehicles pose a challenge for both existing petroleum fuels and proposed fuels from alternative sources. The EPA regulation limit governing particulates reduced to 0.25 g/bhp-hr in 1991 for trucks and to 0.1 g/bhp-hr for city buses in 1993. In 1994, the limit will drop to 0.1 g/bhp-hr for all vehicles. It is expected that Canada will adopt the same limits at a later date and Mexico will have similar standards for urban vehicles. EPA has not prescribed the method for meeting the emissions requirements for diesel engines. Engine manufacturers have performed significant development on cleaner engines without meeting the proposed standard in all cases. EPA issued regulations that limit sulfur content of diesel fuel to 0.05 weight percent and imposed a minimum 40 cetane index to "cap" aromatics content at present levels.[1] The California Air Resources Board has also announced regulations effective in 1993 that control diesel fuel sulfur content to less than 0.05 weight percent plus aromatics to less than 10 volume percent.

The objectives in the current work included producing a consistent set of performance, emission, and composition measurements on a set of diesel fuel components distinguished by source and processing history emphasizing aromatics. The components were reduced in sulfur and aromatic content by pilot plant hydrogenation before distillation into selected ranges of boiling points. The resulting fractions of feedstocks and products were analyzed for chemical composition and physical properties that would be most revealing for ignition quality and particulate generation.

This report presents the results to date of this work in progress. With the broad objective of relating diesel exhaust emissions and performance to chemical composition and physical properties, the more specific concerns of the effect of alkane branching and aromatic substituients will be addressed later. The choice of starting materials will give insight about source and upgrading method as they affect ignition quality and emissions from different samples meeting the same limits on sulfur and aromatics but with different processing histories.

Background

Contemporary diesel fuel is a blend of several refinery streams chosen to meet specifications. The need to increase yield of transportation fuel from crude oil has resulted in converting increased proportions of residual oil to lighter products. This is accomplished by thermal, catalytic, and hydrocracking of high molecular weight materials rich in aromatic compounds. The current efforts to reformulate California diesel fuel for reduced emissions from existing engines is an example of the other driving force affecting refining practice. Although derived from petroleum crude oil, reformulated diesel fuel is an alternative to current specification-grade diesel

fuel, and this alternative presents opportunities and questions to be resolved by fuel and engine research.

It has been observed that sulfur and aromatics concentrations increase with boiling point. For example, lower concentrations of aromatics and sulfur typically occur in D-1 fuel whose boiling range of 300-550°F is lower than D-2 fuel with 350-650°F. What has not been shown is which of the highest boiling components are most responsible for particulate emissions or which components of refinery streams would benefit the most from processing to reduce emissions precursors. The approach used for determining the effects of fuel composition on engine behavior has been to blend or measure full boiling range fuels for engine tests. For instance, the work at the University of Wisconsin [2] and the University of Pennsylvania [3] found little effect on performance and emissions attributable to fuel composition. Other studies had different results. Weidmann found that fuel properties have a small, measurable effect on emissions using a VW 1.67 liter, 4-cylinder engine.[4] Hydrocarbon emissions were found to be a function of fuel cetane number with volatility exerting a stronger influence for low cetane number fuels. Particulate formation was a strong function of fuel density and distillation range.

Fortnagel et al., found HC, NOx, CO, and a particulate emissions to be subject to aromatic content in a Mercedes Benz, prechamber-type engine.[5] A study by Gairing found large effects on exhaust emissions and fuel consumption attributable to fuel properties.[6] The diversity of these results is typical of the literature and emphasizes the strong influence that the engine type has on emissions from a given fuel. These studies were also performed with full-boiling fuels that made no attempt to segregate fuel properties by boiling range. Cookson attempted to determine the effect of hydrocarbon type composition on the diesel index (Method IP21) and the cetane index (ASTM D976) in 54 fuels, again using full-boiling materials.[7]

The approach to be used in the current work will attempt to improve on the resolution of previous studies done with full-boiling test fuels by examining the four starting materials in narrow fractions of the diesel fuel boiling range. We will then correlate the resulting measurements with emissions and performance indicators.

Experimental

Materials ➛ Of the refinery streams blended into diesel fuel, the higher boiling and more aromatic ones are implicated in particulate and hydrocarbon emissions. Accordingly, feedstocks for this study were chosen to include products from resid conversion and gas oil cracking. The test components chosen were:

- full-boiling straightrun diesel (SRD)
- light cycle oil from catalytic cracking (LCO)
- light coker gas oil (LCGO)
- coal-derived Fischer-Tropsch distillate (FT)

The parentheses enclose the abbreviated designations used in this paper. The opportunity to include the highly paraffinic FT liquid extended the objectives to see the effect of a material which might provide future solutions to diesel emission problems. These four materials were characterized by a set of laboratory analyses as shown in Table 1.

Processing ➛ The four feedstocks were processed to reduce sulfur and aromatics then distilled into analytical samples. The processing and distillation sequence is shown in Figure 1. The LCO and LCGO were hydrogenated at two severities to reduce sulfur to 0.05 M% and aromatic concentration (by ASTM D1319) to 10 V%. The SRD was naturally low in sulfur and was hydrotreated at one severity to reduce aromatics to 10 V%. The FT required no hydrogenation. The process variables for the hydrogenations are summarized in Table 2.

TABLE 1. FEEDSTOCK PROPERTIES					
Test	ASTM Method	Straight Run Diesel	Lt. Cycle Oil	Lt. Coker Gas Oil	Fischer-Tropsch
Density Specific Gravity °API g/ml	D 1298	0.8458 35.8 0.8453	0.9490 17.6 0.9485	0.8676 31.6 0.8671	0.7770 50.6 0.7767
Distillation, °F	D 86				
IBP/5%		353/428	367/457	385/420	368/396
10/30%		466/523	476/509	435/462	407/449
50/70%		551/581	536/573	492/528	502/550
90/95%		635/657	634/656	574/590	592/606
EP		672	689	608	620
Carbon, Wt%	D 3178	86.82	88.84	85.18	84.92
Hydrogen, Wt%		13.31	9.84	12.58	15.12
Sulfur, Wt%	D 2622	0.052	0.69	1.41	0.003
Hydrocarbon Type, Vol % Aromatics Olefins Saturates	D 1319	 23.6 1.0 74.7	 75.45 3.64 20.91	 52.4 5.9 41.7	 0.9 0.9 98.2
Viscosity @ 40°C @ 100°C	D 445	3.52 1.34	3.16 1.20	2.56 1.10	2.42 1.05
Refractive Index @ 20°C	D 1218	1.4718	1.5537	1.4797	1.4342
Cetane Index	D 976	52.6	26.1	39.3	75.4
	D 4737	54.6	23.89	38.9	81.4
UV Aromatics Analysis Wt% Aromatic Carbon	TOTAL MONO DI TRI	11.4 4.3 5.8 1.3	43.7 6.3 28.3 9.1	15.7 8.4 5.9 1.4	0.2 0.0 0.0
Cloud point, °C/°F	D2500	1/34	-10/14	Too dark	-20/-4
Pour point, °C/°F	D 97	-1/30	-12/10	-30/-22	-20/-4
Aniline point, °C/°F	D 611	73.0/163	9.8/50	47.6/118	92.8/199
Smoke point, mm	D 1322	17.2	6.2	13.3	+35

Each of the four feedstocks and their five products were distilled under vacuum into congruent (corresponding cut point) boiling range fractions. The following boiling point ranges were selected for the cuts:

Fraction 1	Fraction 2	Fraction 3	Fraction 4	Fraction 5	Fraction 6	Fraction 7
IBP - 440°F	440° - 480°F	480° - 520°F	520° - 560°F	560° - 600°F	600° - 640°F	640° - EP

Approximately 40 liters of each material were charged to a stainless steel kettle and column, which was operated along the lines of a ASTM D1160 distillation. The resulting 63 samples were further subsampled for separation by ASTM D2549 into saturates and aromatics fractions.

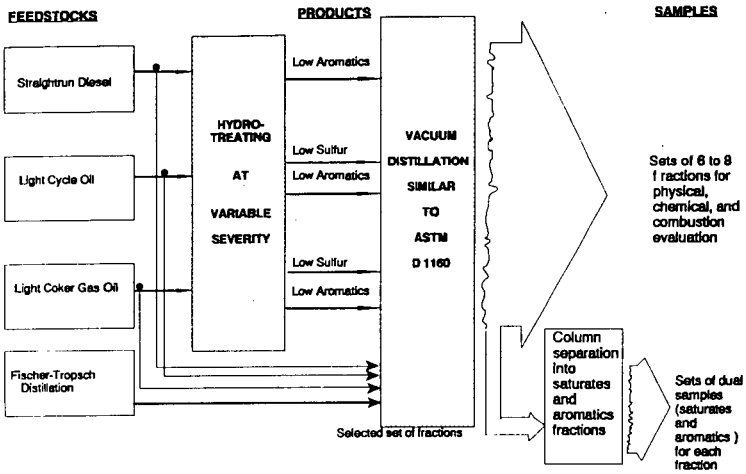

Figure 1. Sequence of Processing for the Diesel Fuel Assay

TABLE 2. PROCESSING PARAMETERS					
	T_{av}, °F	P_{tot}, psig	Feed, gal-hr^{-1}	H_{2tot}, SCFH	LHSV, hr^{-1}
STRAIGHT RUN DIESEL					
High severity - low aromatics	630	1500	1.6	60	1.03
LIGHT CYCLE OIL					
Low severity - low sulfur	710	650	1.9	110	1.05
High severity - low aromatics	686	2300	0.74	130	0.41
LIGHT COKER GAS OIL					
Low severity - low sulfur	650	600	2.2	140	1.22
High severity - low aromatics	676	2200	0.98	117	0.56

Combination of adjacent cuts were made in the middle of the boiling range to limit the number of samples submitted for instrumental analysis. These combinations are indicated by the pairs and triples of sample numbers in brackets in Table 3.

Analyses ➛ The set of laboratory measurements listed in Table 1 are being applied to each of the 63 fractions made by vacuum distillation. The list includes two measures of aromatic content, D1319 and the UV method.[8] The fluorescent indicator analysis (ASTM D1319) is widespread in its use and included in emissions regulations. It is regularly applied to diesel fuel samples, although the method is designed for depentanzed gasoline, and relies on measurements of column length taken up by saturates, olefins, and aromatics made visible by fluorescent dye. The volume percent aromatics determined this way can be affected by cycloparaffins or polar materials.

The UV method compares sample absorbance at selected wavelengths with reference spectra of solutions of aromatics composed of representative compounds in the diesel boiling range. Since the absorbance is proportional to the aromatic rings, weight percent aromatic carbon is reported without regard to substituents. Both methods are indirect; so instrumental analysis by GC/MS and NMR are planned.

The samples will be rated for ignition quality in a constant volume combustion apparatus (CVCA).[9] A single shot of sample is injected into a shaped combustion temperature at controlled temperature and pressure. The temperature, pressure, and stoichiometry of the fuel/air mixture causes the gas mixture to autoignite. When the sample ignites and burns, it results in a pressure rise, which is automatically measured. The ignition delay time from injection to measured pressure rise for various temperatures and reference materials has been correlated with measured cetane numbers for estimating the cetane number of samples. All 72 samples (4 feedstocks, 5 products, & 63 fractions) will be tested in the CVCA.

Engine experiments will be performed with a single cylinder, direct injected, variable compression ratio engine (VCR).[10] The cylinder head can be moved during operation to adjust compression ratio thus allowing knock measurements to be made, which are necessary for measuring cetane number. The piston and intake port are being modified to match contemporary configurations designed to comply with 1991 diesel engine emission standards. Measurements will include cetane number, fuel efficiency, pressures traces, heat release rate, and exhaust emissions of CO, CO_2, O_2, NO, NO_2, C, and unburned hydrocarbons. Selected samples will be tested in the VCR engine.

Results

The processing, distillation, and laboratory analyses are complete, while the instrumental analyses and CVCA measurements continue. The VCR engine is being modified to reflect contemporary design before the engine experiments take place. Table 3 presents some of the measurements on the 63 fractions to date. Density (specific gravity), abbreviated boiling range, and aromatic composition are given in the table, however, each fraction has received the full analysis listed in Table 1. The number of fractions distilled from each feedstock and product vary in number depending on the boiling range of the starting material.

The results for aromatic composition of the LCO are presented in the series of graphs of Figure 2. This series of graphs is representative of the changes made by hydrogenation. The total aromatic carbon was reduced moderately in concentration as the sulfur was reduced by low severity treatment. The distribution of aromatics decreased most in the highest boiling point fractions, which display the most tricyclic compounds. A similar decrease is noted for dicyclic aromatics, but monocyclics increase across the boiling range. The explanation for this increase will await the ASTM D2425 results to confirm the trend, but in addition to creating corresponding cycloparaffins from the two- and three-ring aromatics, the hydrogenation opened rings in the multicycles to form alkylbenzenes distributed throughout the lower boiling ranges.

The trend for high severity hydrogenation to limit total aromatics showed the greatest decrease in polycyclics. The overall reduction in monocyclic aromatics was slightly greater for higher boiling ranges. These changes are expected to reduce emissions and are projected to improve ignition delay as shown in Figure 3.

The plot of cetane index *versus* 50% recovered temperatures (T50) by D86 in Figure 3 was made by two estimating methods; ASTM D976 and D4737. Both correlations use density and T50, but in different ways. D976 uses API gravity and T50 in two terms, while D4737 uses specific gravity and T50 in four terms. Furthermore, the new, four-term correlation used a larger fuel matrix including cracked components and shale oil to develop its correlation. D4737 made lower estimates of cetane number in the front end of the boiling

TABLE 3. PARTIAL RESULTS FOR DISTILLATION FRACTIONS

Property		Feed	#1	#2	#3	#4	#5	#6	#7	#8
STRAIGHT RUN DIESEL										
Sp. Gravity		0.8458	0.8146	0.8445	0.8483	0.848	0.845	0.847	0.859	0.863
Dist. T10/T50		466/551	338/404	465/480	486/498	514/523	544/550	578/584	617/622	666/673
T90/EP		635/672	452/475	501/515	516/529	542/556	564/576	597/610	634/643	687/698
Arom	Tot/Mono	11.4/4.3	12.4/7.9	13.6/4.6	13.3/4.4	12.5/4.3	10.9/4.0	8.7/3.2	9.3/3.1	17.1/5.7
C Wt%	Di/Tri	5.8/1.3	4.4/0.1	8.6/0.4	8.5/0.4	7.4/0.8	5.7/1.2	3.7/1.8	3.5/2.7	6.2/5.2
LOW A SRD										
Sp. Gravity		0.8280	0.7892	0.8251	0.8373	0.8368	0.8304	0.8203	0.8314	0.8373
Dist. T10/T50		442/539	241/278	386/404	440/452	482/494	530/538	567/577	615/620	673/683
T90/EP		622/664	323/351	438/455	474/488	510/526	552/562	587/597	631/641	699/715
Arom	Tot/Mono	3.3/3.0	7.8/7.7	5.8/5.6	5.0/4.6	3.6/3.2	2.6/2.2	1.5/1.3	1.1/0.9	0.8/0.6
C Wt%	Di/Tri	0.3/0.0	0.1/0.0	0.3/0.0	0.4/0.0	0.4/0.0	0.3/0.0	0.2/0.0	0.2/0.0	0.2/0.0
LIGHT CYCLE OIL										
Sp. Gravity		0.9490	0.8849	0.9147	0.9321	0.9440	0.9541	0.9685	0.9979	
Dist. T10/T50		476/536	384/410	447/459	483/490	515/522	548/552	583/588	643/651	
T90/EP		634/689	443/492	473/492	499/518	531/544	562/575	596/614	677/734	
Arom	Tot/Mono	43.7/6.3	42.5/26.7	55.3/14.5	57.2/6.8	60.6/5.1	46.1/4.1	41.2/3.3	46.7/0.1	
C Wt%	Di/Tri	28.3/9.1	15.0/0.8	39.8/1.0	49.6/0.8	53.9/1.6	39.3/2.7	28.6/9.3	10.4/36.2	
LOW S LCO										
Sp. Gravity		0.9200	0.8849	0.9082	0.9153	0.9230	0.9352	0.9484	0.9497	
Dist. T10/T50		462/518	370/424	444/467	472/488	503/519	543/557	595/603	650/663	
T90/EP		614/682	469/510	502/544	521/548	549/572	579/595	617/630	702/738	
Arom	Tot/Mono	35.8/16.6	29.1/23.3	35.4/22.9	35.8/20.4	36.9/16.7	34.1/11.8	32.9/6.8	32.0/2.4	
C Wt%	Di/Tri	15.0/4.2	5.8/0.0	12.5/0.0	15.1/0.3	19.0/1.2	19.6/2.7	17.5/8.6	9.5/20.1	
LOW A LCO										
Sp. Gravity		0.8628	0.8479	0.8623	0.8676	0.8708	0.8745	0.8703	0.8448	
Dist. T10/T50		419/488	362/384	412/422	446/454	477/486	514/520	547/552	606/620	
T90/EP		581/657	406/419	432/453	470/488	499/514	530/544	561/574	669/715	
Arom	Tot/Mono	3.5/3.1	5.6/5.4	3.6/3.4	4.1/3.7	3.9/3.4	2.9/2.5	2.5/2.0	1.4/1.0	
C Wt%	Di/Tri	0.4/0.0	0.2/0.0	0.2/0.0	0.4/0.0	0.5/0.0	0.4/0.0	0.5/0.0	0.4/0.0	
LIGHT COKER GAS OIL										
Sp. Gravity		0.8676	0.8403	0.8565	0.8740	0.8871	0.8927	0.9094		
Dist. T10/T50		435/492	395/410	446/456	486/495	530/537	565/571	603/609		
T90/EP		574/608	429/461	473/491	508/526	547/565	580/595	624/645		
Arom	Tot/Mono	15.7/8.4	10.9/8.5	12.6/7.4	13.7/6.3	14.5/6.0	13.8/5.3	14.4/4.7		
C Wt%	Di/Tri	5.9/1.4	1.7/0.7	4.4/0.8	6.4/1.0	7.2/1.3	6.8/1.7	6.1/3.6		

TABLE 3. PARTIAL RESULTS FOR DISTILLATION FRACTIONS (Continued)

Property		Feed	#1	#2	#3	#4	#5	#6	#7	#8
LOW S LCGO										
Sp. Gravity		0.8463	0.8184	0.8299	0.8403	0.8524	0.8628	0.8697		
Dist. T10/T50		427/476	360/389	399/415	432/447	473/484	512/523	567/577		
T90/EP		552/599	427/457	442/467	473/492	504/526	539/550	598/624		
Arom	Tot/Mono	10.5/8.2	10.0/9.4	10.9/9.8	10.2/8.4	11.0/8.2	11.2/7.7	11.4/7.2		
C Wt%	Di/Tri	2.3/0.0	0.6/0.0	1.1/0.0	1.8/0.0	2.8/0.0	3.4/0.1	3.5/0.7		
LOW A LCGO										
Sp. Gravity		0.8393	0.8203	0.8265	0.8324	0.8418	0.8490	0.8498	0.8524	
Dist. T10/T50		436/491	374/390	404/417	437/448	474/483	508/516	548/556	595/602	
T90/EP		576/612	414/430	440/466	468/485	503/520	530/546	566/574	622/644	
Arom	Tot/Mono	3.3/3.0	4.5/4.3	3.9/3.7	3.6/3.3	3.5/3.1	3.3/2.9	2.7/2.3	2.2/1.8	
C Wt%	Di/Tri	0.3/0.0	0.2/0.0	0.2/0.0	0.3/0.0	0.4/0.0	0.4/0.0	0.4/0.0	0.4/0.0	
FISCHER-TROPSCH										
Sp. Gravity		0.7770	0.7538	0.7633	0.7710	0.7783	0.7853	0.7913	0.7989	
Dist. T10/T50		407/502	355/373	397/416	438/453	478/490	522/531	558/566	607/615	
T90/EP		592/620	420/456	452/474	475/488	507/521	545/557	579/589	628/638	
Arom	Tot/Mono	0.2/0.2	0.4/0.4	0.3/0.3	0.2/0.2	0.2/0.2	0.1/0.1	0.1/0.1	0.1/0.1	
C Wt%	Di/Tri	0.0/0.0	0.0/0.0	0.0/0.0	0.0/0.0	0.0/0.0	0.0/0.0	0.0/0.0	0.0/0.0	

range and higher estimates in the back end. These calculations will be compared with the CVCA and VCR results for verification, but the fractions at highest boiling ranges increased the most in cetane index. This is consistent with the results of Weidmann et al, for full-boiling test fuels.

Conclusions

It has been observed that a consistent set of narrow-boiling samples was unavailable and this work will fill the need, however, this study is in the initial stages permitting few conclusions. The early results obtained to date suggest that the dominant effects for both emissions (by virtue of polycyclic aromatic distribution) and performance (considering the relative increase in cetane index) will be in the higher boiling point fraction. Further instrumental analyses of hydrocarbon type composition and the combustion studies will add to our understanding. The current results offer guidance on where in the boiling range the strongest effects can be found.

The improvement in the high end of the boiling curves is significant for the emissions and performance benefits that were obtained and for resource utilization. It has been suggested generally and implemented in California to reduce the limit for T90 for the D-2 specification. Careful control of upgrading may reduce the necessity to curtail T90 thereby leaving more of each blendstock in the diesel fuel boiling range.

Acknowledgements

This work has been supported by the U.S. Department of Energy Office of Conservation and Renewable Energy Alternative Fuels Utilization Program (AFUP), John A. Russell, manager, first through its operations at the Oak Ridge National Laboratory, Dr. R.L. Graves, project representative then at the National Renewable Energy Laboratory, Kenneth R. Stamper, program manager representative.

The concept of the study was suggested by Norman R. Sefer the first project manager of the AFUP Alternative Fuel Center at Southwest Research Institute. The able technical staff for the processing included: C.C. Cover, D.L. Hetrick, P.M. Rainwater, and G.R. Segura. The engine combustion studies will be conducted by Dr. T.W. Ryan III. The numerous tables and typescript were prepared by Evangelina S. Martin.

REFERENCES

1. "Fuel Quality Regulations for Highway Diesel Fuel Sold in 1993 and Later Calendar Years", Federal Register, Vol. 54, No. 163, August 24, 1989.

2. Foster, D.E., Dimplefeld, P.M. Boggs, D.L., Bair, R.E., and Borman, G.L., "The Effects of Fuel Composition on Ignition Delay in Homogeneous Charge and Direct Injection Compression Ignition Engines", Final Report, Contract DE-AC05-84OR21400, U.S. Department of Energy, Alternative Fuels Utilization Program, Report No. ORNL/Sub/84-89677/1, November 1987.

3. Buzza, T.G., and Litzinger, T.A., "A Comparison of Three Coal-Derived, Middle Distillate, Synthetic Fuels in a Single Cylinder DI Diesel Engine", SAE International Fuels & Lubricants Meeting, Toronto, Canada, November 2-5, 1987.

4. Weidmann, K., Menrad, H., Reder, K., and Hutchenson, R.C., "Diesel Fuel Quality Effects on Exhaust Emissions", SAE International Fuels & Lubricants Meeting and Exposition, Portland, Oregon, SAE Paper No. 881649, October 10-13, 1988.

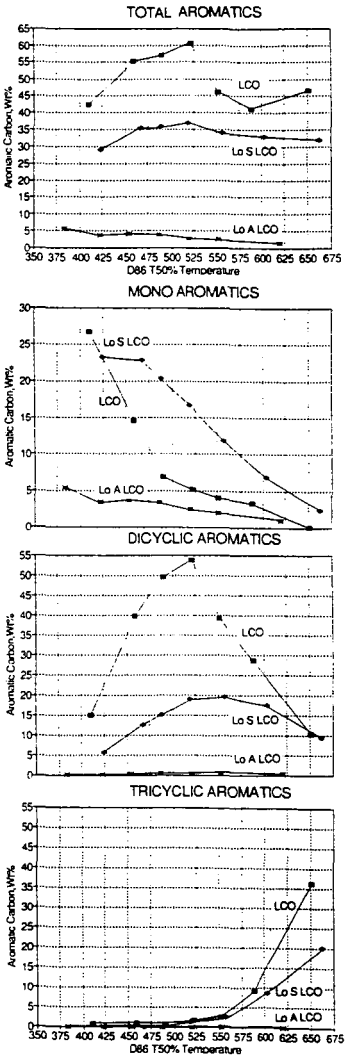

Figure 2. LCO Aromatics Distribution

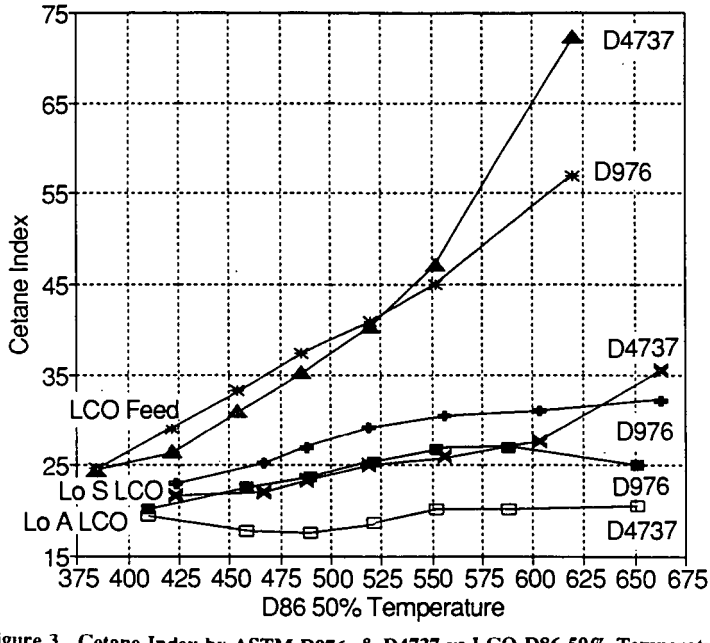

Figure 3. Cetane Index by ASTM D976 & D4737 vs LCO D86 50% Temperature

5. Fortnagel, M., Gairing, M., Wagner, W., "Verbesserung des Diesel-Motors-Verschlechterung des Diesel-Kraftsoffs - ein Eiderspruch", VDI Berichte No. 466, 1983.

6. Gairing, M., "Anforderungen and Diesel-Kraftsoffqualitat-heute und in Zukunft", VDI Berichte No. 559, Emissionsminderung Automobilabgase - Dieselmotoren - VDI Verlag 1985.

7. Cookson, D.J., Lloyd, C.P., and Smith, B.E., "Investigation of the Chemical Basis of Diesel Fuel Properties", Energy and Fuels 2, 854-860, 1988.

8. Kohl, K.B., Bailey, B.K., Newman, F.M., and Mason, R.L., "Chemical Analysis of Aromatics in Diesel Fuels", report for California Air Resources Board A932-125, 20 June 1991.

9. Ryan, T.W. III, "The Development of New Procedures for Rating the Ignition Quality of Fuels for Diesel Engines", U.S. Army Belvoir RD&E Center, Interim Report 223, BFLRF, Southwest Research Institute, December 1986.

10. Ryan. T.W. III, "Ignition Delay as Determined in a Variable Compression Ratio, Direct Injection Diesel Engine", SAE Paper 872036, November 1987.

MASS TRANSPORT IN BIOREACTORS FOR COAL SYNTHESIS GAS FERMENTATION

K. T. Klasson, M. D. Ackerson, E. C. Clausen, and J. L. Gaddy
Department of Chemical Engineering
University of Arkansas
Fayetteville, AR 72701

Keywords: Synthesis gas, bioreactors, hydrogen

INTRODUCTION

Synthesis gas, a mixture of primarily CO, H_2 and CO_2, is a major building block in the production of fuels and chemicals. The gas is derived from non-gaseous raw materials such as coal, shale oil, tar sands, heavy residue and biomass. The composition of synthesis gas is dependent upon the raw materials used and the gasification process. Coal-derived gas is rich in CO and H_2, with lower concentrations of CO_2 and CH_4 and traces of H_2S and COS (1).

A wide variety of both liquid and gaseous fuels may be produced from synthesis gas using Fischer-Tropsch synthesis including light hydrocarbons (methane, ethane), fuel range hydrocarbon distillates and heavy waxes. The stoichiometry for product formation may be characterized by the empirical relation (2):

$$CO + 2.12\ H_2 \rightarrow (HC, Alcohols, Acids) + 0.95\ H_2O \qquad (1)$$

As is noted, about 2 moles of H_2 are required for every mole of CO.

Since typical synthesis gas is deficient i H_2, a catalytic water gas shift conversion is used to adjust the H_2/CO ratio:

$$CO + H_2O \rightarrow CO_2 + H_2 \qquad (2)$$

This same reaction may be carried out biologically at ambient conditions with high yield using bacteria such as *Rhodospirillum rubrum* (3) or *Rhodopseudomonas gelatinosa* (4).

Purpose

The purpose of this paper is to present laboratory data from continuous culture experiments for the conversion of H_2O and CO in synthesis gas to CO_2 and H_2 using a biological process. The photosynthetic bacterium *R. rubrum* is employed. Performance results from continuous stirred tank and trickle-bed reactors are presented and discussed.

BIOREACTOR DESIGN

The choice of a suitable bioreactor for synthesis gas fermentations is a matter of matching reaction kinetics with the capabilities of the various reactors. It has been found that for these slightly soluble gases, the rate

of mass transfer usually controls the reactor size (5,6). Mass transfer capabilities of the reactor must be balanced with the cell density achieved. The proper reactors for these systems will likely be ones that achieve high mass transfer rates and high cell densities. These concepts will be expanded in this and the following section.

Gas-Liquid Mass Transfer Concepts

The transfer of gas phase substrates in fermentation systems involves three heterogeneous phases: the bulk gas phase, the culture medium (liquid) and microbial cells (solid) suspended in the medium. The reactants, present in the gas phase, must be transported across the gas-liquid interface and diffuse through the culture medium to the cell surface to be consumed by the microbes. In general, a combination of the following resistances can be expected (7):

1. Diffusion through the bulk gas to the gas-liquid interface.
2. Movement across the gas-liquid interface.
3. Diffusion of the solute through the relatively unmixed liquid region (film) adjacent to the bubble and into the well-mixed bulk liquid.
4. Transport of the solute through the bulk liquid to the stagnant film surrounding the microbial species.
5. Transport through the second unmixed liquid film associated with the microbes.
6. Diffusive transport across the liquid/solid boundary and into the microbial floc, mycelia, or particle, if appropriate. When the microbes take the form of individual cells, this resistance disappears.
7. Transport across the cell envelope to the intracellular reaction site.

As with the conventional chemical engineering analysis of absorption processes, mass transfer through the bulk gas phase is assumed to be instantaneous. Also, when individual cells are suspended in a medium, the liquid film resistance around the cells is usually neglected with respect to other resistances, because of the minute size and the enormous total surface of the cells (8). Thus, for the transfer of sparingly soluble gases, such as CO, the primary resistance to transport may be assumed to be in the liquid film at the gas-liquid interface.

It can be shown that the substrate transfer rate per unit of reactor volume, $\frac{dN_S^G}{V_L dt}$, is given in terms of the gas phase partial pressures as:

$$\frac{d\,N_S^G}{V_L dt} = \frac{K_L a}{H} \left(P_S^G - P_S^L\right) \qquad (3)$$

where N_S^G = moles substrate transferred from the gas phase, V_L is the volume of the liquid phase, t is time, K_L is the overall mass transfer coefficient,

a is the gas-liquid interfacial area per unit volume, H is Henry's law constant, P_S^G is the partial pressure of the substrate in the bulk gas phase, and P_S^L is the partial paressure (dissolved tension) of the substrate in the liquid phase ($P_S^G = HC_L$). The rate of transport from the gas phase must be equal to the rate of consumption in the liquid phase, given by a Monod relationship:

$$\frac{d\,N_S^G}{V_L dt} = \frac{X\,q_m\,P_S^L}{K_p' + P_S^L + (P_S^L)^2/W'} = \frac{K_L a}{H}\left(P_S^G - P_S^L\right) \qquad (4)$$

where X is the cell concentration and q_m, K_p', and W' are Monod constants.

Equation (4) shows that a bioreactor for these gaseous systems must operate in either of two regimes. In one case, sufficient cells are present to react more solute, but the mass-transfer rate cannot keep pace. Therefore, the liquid phase concentration goes to zero and the reactor is mass transport limited. The cell concentration and rate of consumption are limited by the ability of that particular reactor to transfer substrate. In the other case, sufficient substrate can be supplied, but the cell concentration does not allow consumption at an equal rate. Then the liquid phase concentration is not zero (with possible inhibitory effects) and the rate is limited by the cell concentrations in that particular bioreactor. Obviously, the best bioreactor is one that will achieve high cell concentrations and high mass transfer rates.

Stirred Tank Reactor Studies

The traditional reactor used in continuous fermentation processes is the stirred tank reactor, or CSTR. As it relates to gas phase substrates, the CSTR has continuous gas flow into a constant volume liquid phase reactor. A small liquid feed stream is utilized to supply nutrients to the microorganisms in the reactor system and to remove products. The agitation rate in the system is relatively high in order to promote transfer of the sparingly soluble gas into the liquid culture medium.

Experiments have been carried out in a CSTR at different gas flow rates under mass transfer-limited conditions. In these experiments, the progress of the reaction is followed by the use of an inert component, whose partial pressure does not change throughout the system. Assuming perfect mixing in both the gas and the liquid phases, the CO uptake rate from the gas phase may be described by Equation (5) under mass transfer limiting conditions:

$$\dot{n}_I\,(Y_{CO}^i - Y_{CO}^o) = \frac{K_L a}{H} \cdot V_L \cdot P_{CO}^o \qquad (5)$$

Equation (5) may be easily rearranged to yield:

$$\left(\frac{P_{CO}^i}{P_{CO}^o} - \frac{P_I^i}{P_I^o}\right) = \frac{K_L a}{H} \cdot \frac{V_L \cdot RT}{G^i} \qquad (6)$$

A plot of CO conversion as a function of pseudo retention time in the CSTR (defined as the liquid volume in the reactor divided by the gas flow rate) is shown in Figure 1. As noted, a conversion of about 55 percent was attained at a retention time of 1 h. The maximum conversion was about 85 percent, attained at retention times of 3 h or above. Conversion in the CSTR is limited by the mixed flow pattern inside the reactor.

The mass transfer coefficient, K_La, may be obtained for the CSTR experiments by employing Equation (6). If the left hand side of Equation (6) is plotted as a function of V_L RT/HG a straight line should be obtained with a slope of K_La if the experiments are carried out under mass transfer limiting conditions. Such a plot is shown in Figure 2, where K_La is shown to have a value of 70.0 h^{-1}. It should be noted that these experiments were carried out at a constant agitation rate of 400 rpm. Agitation rate, impeller design and other physical characteristics of the reactor significantly affect the value of the mass transfer coefficient.

Trickle Bed Reactor Studies

Trickle-bed reactors are used conventially to obtain a low pressure drop or low liquid holdup when there is practically no heat to remove or supply, or the liquid is corrosive. They are usually operated countercurrently since a higher driving force can be achieved than with cocurrent operation. However, when an irreversible reaction occurs between the dissolved gases and the absorbent (as in biological systems), the mean concentration driving force is the same for both modes of operation. In this case, the capacity of cocurrent columns is not limited by flooding and at any given flow rates of gas and liquid, the pressure drop in a cocurrent column is less (9).

Experiments were conducted in a cocurrent column packed with ceramic Intalox saddles. In this experimental setup, the liquid and the gas were disengaged in a liquid/gas separator with the culture being recirculated back to the top of the column. In this manner, a high concentration of cells can be maintained inside the reactor while at the same time using high L/G operating conditions inside the column. For this ystem, assuming perfect plug flow in the gas phase ascending through the column and constant partial pressure of the inert gas in the system (as closely substantiated from experimental data), the outlet ratio of CO to the inert can be related to other operating conditions according to the equation (10):

$$\ln \frac{Y^i_{CO}}{Y^o_{CO}} = K_La' \frac{ShRT}{H\bar{G}} \qquad (7)$$

A plot of CO conversion as a function of pseudo retention time in the trickle bed reactor is shown in Figure 3. In contrast to the CSTR results, nearly complete conversion was seen in the trickle bed at a retention time of 0.6 h. Complete conversion was obtained because the trickle bed operates very closely to ideal plug flow behavior.

Figure 4 shows the calculation of the mass transfer coefficient for the trickle bed as a rearrangement of Equation (7). The value of K_La of 23.5 h^{-1} is in good agreement with the value of 27.0 h^{-1} calculated from the results of Charpentier (9).

CONCLUSIONS

The performance of *R. rubrum* in producing H_2 was demonstrated in a continuous stirred tank reactor and a trickle-bed reactor. A conversion of 0.85 was obtained in the CSTR at a pseudo retention time of 3 h. The plug flow trickle-bed reactor gave a conversion of 100 percent at a retention time of only 0.6 h. Mass transfer coefficients were obtained for the two continuous reactors, with K_La equaling 70.0 h^{-1} in the CSTR and 23.5 h^{-1} in the trickle-bed reactor.

REFERENCES CITED

1. McCullough, G. R., Roberts, S. C. and Van der Burgt, M. J., "Shell Coal Gasification Process," *Energy Prog.*, **2**, 69 (1982).

2. Schreiner, M. "Research Guidance Studies to Assess Gasoline from Coal by Methanol-to-Gasoline and Sasol-Type Fischer-Tropsch Technologies," Report No. FE-2447-13, U. S. Department of Energy, Washington, D.C. (1978).

3. Dashekvicz, M. P. and Uffen, R. L., "Identification of a Carbon Monoxide Metabolizing Bacterium as a Strain of *Rhodopseudomonas gelatinosa* (Molisch) van Niel," *Int. J. System. Bacteriol.*, **29**, 145-148 (1978).

4. Uffen, R. L., "Anaerobic Growth of a *Rhodopseudomonas* Species in the Dark with Carbon Monoxide as the Sole Carbon and Energy Substrate," *Proc. Natl. Acad. Sci.*, 73, 3298-3302 (1976).

5. Vega, J. L., Clausen, E. C., and Gaddy, J. L., "Study of Gaseous Substrate Fermentations: Carbon Monoxide to Acetate, 1. Batch Cultures," *Biotechnol. Bioeng.*, **34**, 774 (1989).

6. Vega, J. L., G. M. Antorrena, E. C. Clausen, and J. L. Gaddy, "Study of Gaseous Substrate Fermentations: Carbon Monoxide to Acetate. 2. Continuous Culture," *Biotechnol. Bioeng.* 34, 785 (1989).

7. Bailey, J. E. and D. F. Ollis, *Biochemical Engineering Fundamentals*, McGraw-Hill, New York (1986).

8. Finn, R. K., "Agitation-Aeration in the Laboratory and in Industry," *Bacteriol. Rev.*, **18**, 154-274 (1954).

9. Charpentier, J. C., "Mass-Transfer Rate in Gas-Liquid Absorbers and Reactors," *Adv. Chem. Eng.*, 11, 1 (1981).

10. Antorrena, G. A., Internal Report, Department of Chemical Engineering, University of Arkansas, Summer 1987.

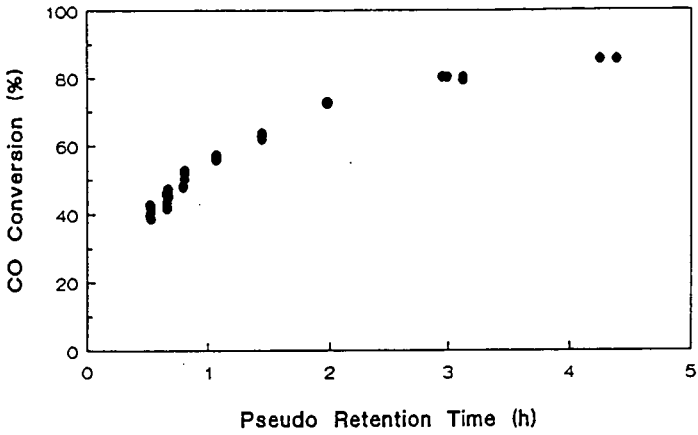

Figure 1. CO conversion profile in the CSTR at various pseudo retention times

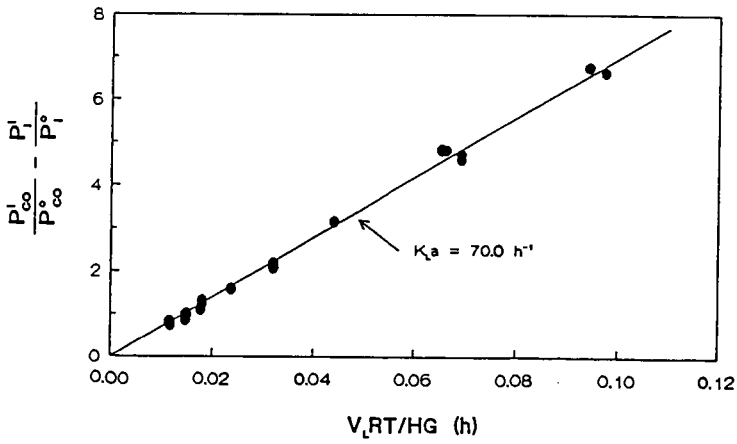

Figure 2. Determination of the mass transfer coefficient in the CSTR

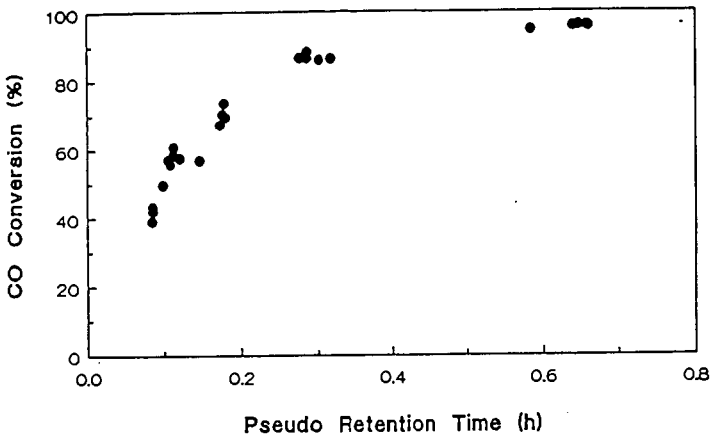

Figure 3. CO conversion profile in the trickle-bed reactor at various pseudo retention times.

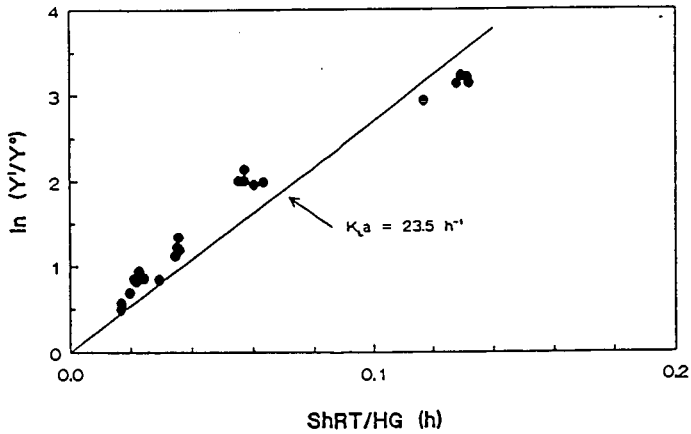

Figure 4. Determination of the mass transfer coefficient in the trickle-bed reactor

EFFECT OF COAL PARTICLE SIZE ON VOLATILE YIELDS DURING RAPID HEATING

J. R. Gibbins, J. Jacobs+, C. K. Man and K. J. Pendlebury.

Dept. of Mechanical Engineering, Imperial College of Science, Technology and Medicine, Exhibition Road, London, SW7 2BX.
+ Rheinisch-westfaelisch-technische Hochschule, Aachen, Germany.

INTRODUCTION

Typically a wide range of particle sizes, with mean diameters between about 10 and 300 um, are present in feed coal streams to entrained flow combustion and gasification processes. The magnitude of any variation in volatile yield with particle size over this range is therefore relevant for computer modelling of such processes, and possibly specification of an optimum feed particle size distribution. The result will also affect the validity of coal characterisation measurements, made on a sample with a limited size range, for predicting the behaviour of a real coal feed.

Mass transport effects should result in a monotonic increase in volatile yields during rapid heating with decreasing particle size, due to the progressive reduction in retrograde char-forming reactions as the residence time of the nascent volatiles within the particles is reduced. In practice, however, the magnitude of such mass transfer effects may be difficult to measure in isolation. One possible source of interference is the differences in heating rate which will also occur between different-sized particles in tests in entrained flow reactors, another is the difficulty in obtaining different size cuts of a coal with identical mineral and maceral composition. The basic tendency will be for finer fractions to become enriched with the more friable constituents of the coal. Less uniform effects may result, however, from the behaviour of intrinsically-homogenous sub-components of a coal (e.g. fossil spores[1]). These may be released virtually intact from the coal matrix by grinding, but are then resistant to further comminution.

Since a captive-sample wire-mesh reactor was used in the present study, differences in heating rate between different size cuts were not considered to be a problem. Under the test conditions used (1000 K/s heating to 950°C) all of the samples softened in the early stages of heating, ensuring good heat transfer between the mesh and the sample. The temperature of the mesh in the area where the sample was distributed was computer-controlled to give typically better than +/- 20 K compliance with the desired value.

To allow for the effect of compositional differences between size cuts a number of approaches were used in the present study.

(a) The ash content of size fractions was measured and data reported on a daf basis to avoid interference from mineral enrichment.

(b) Maceral analyses were performed to identify whether or not maceral enrichment had occurred during grinding.

(c) A second grinding step, using the top size fraction tested as the starting material instead of the raw coal, was used to give more homogenous samples (see below for more details).

(d) A vitrain sample with essentially homogenous (>90% vitrinite) starting composition, and thus largely immune to maceral enrichment effects, was also tested.

EXPERIMENTAL

Coal preparation

Samples of two U.K. bituminous coals (Daw Mill, type 802, and Kellingley, type 602) and one hand-picked Shirebrook Blackshale vitrain sample (>90% vitrinite) were obtained in lump form from British Coal's Technical Services and Research Executive (TSRE) at Bretby. The Pittsburgh No. 8 sample from the Argonne Premium Coal Sample programme[2] was also used.

The lump coal samples were ground to all <150um using a Fritsch Pulverisette II motorised grinder with frequent sieving to remove undersize material. The Pittsburgh No. 8 was ground by hand. The ground coal was screened to produce the following size fractions : <38 um, 38-53 um, 53-75 um, 75-106 um and 106-150 um. The mass distributions from this first grinding process are shown in Table 1.

For the coals (which showed significant maceral enrichment effects) a second grinding stage was also used. The 150-106um size fraction was divided into four equal sub-samples, using a Microscal spinning riffler. Three of these sub-samples were subsequently reground to all pass through 53, 75 and 106 um respectively, and then screened to give 38-53um, 53-75 um and 75-106 um size cuts.

All samples were dried overnight in a nitrogen-purged oven at 105 °C and then stored under nitrogen until required.

Sample analysis

Small samples of each of the coal fractions (approx. 0.5g) were mounted in a fast-setting 'Buehler Epo-thin' low viscosity resin. After polishing, maceral compositions were observed by examination under a light microscope. To obtain quantitative maceral data, 500 point counts were made on each sample.

Because of the limited amounts of sample available, a thermogravimetric analyser (TGA - Stanton Redcroft Model TG-780) was used to measure ash contents. Approx. 10 mg samples were heated at 30 °C min^{-1} to 900 °C in N_2/air.

Wire-mesh apparatus

A version of the wire-mesh reactor previously developed at Imperial College[3,4] was used for devolatilization experiments. This incorporates a computer-based temperature control system, with a two-colour pyrometer for temperature measurements. All experiments were undertaken with a flowing helium sweep gas at atmospheric pressure and using a heating rate of 1000 K/s to 950°C, with 10 s hold at peak temperature. Previous work[5] has shown that volatile yields are insensitive to experimental variations in heating rate, temperature or hold time under these conditions.

The sample holder was made from folded AISI 304 stainless steel mesh (25 um wires x 32 um aperture). A 5-10 mg coal sample was spread within a 15 mm diameter circle at the centre of the sample holder, and total volatile yields were measured by direct weighing before and after experiments.

RESULTS AND DISCUSSION

Total volatile yields and ash, vitrinite, liptinite and inertinite contents for the sized fractions of the coals from the first and second grinding stages and the vitrain are shown in Figs 1-4. Data points are included for the daf volatiles values to indicate the experimental scatter in the data, with lines drawn through the average values. Points are also shown for other quantities if only limited information is available.

Considering first the volatile yields on a dry basis for the 'first grind' size fractions of the coals, it is interesting to note that there appears to be relatively little effect of particle size. Thus, although differences in the grinding methods used make definitive general conclusions impossible, the results in Figs 1-3 do suggest that overall volatile release per unit mass from the different size fractions may be roughly constant under actual plant conditions (before any heating rate effects are taken into account).

Inspection of the ash contents for the coal size fractions shows, however, that this apparent invariance in dry volatile yields is the result of two opposing trends rather than of an underlying uniformity in coal behaviour! In line with previous findings[6] the ash contents of the size fractions generally increase with decreasing size. This then tends to counteract the general trend for an increase in volatile release from the organic constituents of the coal with decreasing size, as shown in the daf yields for the first grind size fractions.

Volatile yields on a daf basis from the first grind size fractions were not observed to increase monotonically, however, suggesting that a simple reduction in mass transfer resistance was not the only factor involved. This supposition is confirmed by the variation in maceral analysis between size fractions, although some allowance must be made for scatter in the maceral data (particularly at the smaller particle sizes when edge effects become more common with the point counting techniques used). No clear general trends for maceral enrichment emerge from the (somewhat limited) data presented, however, beyond a probable decrease in liptinite content for the smaller size fractions.

The significance of changes in maceral composition can be inferred from the results of previous work on maceral concentrates[7]. For similar UK coals and under similar experimental conditions, it was estimated that volatile yields from 'pure' vitrinite, liptinite and inertinite were of the order of 40%, 80% and 30% daf respectively. It was also found that in maceral mixtures (including whole coals and different maceral concentrates obtained by density separation), the contribution of individual maceral components to overall yields were simply additive.

In an attempt to allow the effect of mass transfer to be examined with less interference from maceral enrichment effects, a similar set of size fractions was prepared using the 106-150 um fraction from the first grind, instead of the raw coal, as the starting material. This method was at least partly successful. For the UK coals. ash levels in the samples are relatively constant and, particularly for the Kellingley samples, the overall trend in maceral levels is roughly level. Significant differences still exist in maceral contents for the Daw Mill coal, although the changes are now monotonic. The latter trends perhaps reflect more homogeneity within the individual maceral groups than occurred in the original coal, coupled with grindability differences. The limited data for the Pittsburgh No. 8 sample showed little effect of maceral enrichment in the second grind, but a much more pronounced, monotonic increase in ash content with decreasing particle size. Overall the second grinding strategy can probably be regarded as at least partly successful, in that monotonic changes in daf volatile yields with changing particle size were observed for these samples.

The effect of mass transfer is still not easy to resolve, however, from the second grind daf volatile data. For the Kellingley and Pittsburgh samples volatile yields increased with decreasing particle size, in line with expectations. For the Daw Mill samples no increase was observed, despite maceral changes that suggest that an increase in volatile yield should result even in the absence of any mass transfer effects.

Data from the vitrain samples, shown in Fig. 4, supports the existence of a small mass transfer effect. Two sets of samples were used, obtained by sieving after grinding to all pass 150 um and 300 um respectively. Because of the high vitrinite concentration in the original vitrain it was expected that maceral enrichment would not occur during grinding, although there is some evidence for slight enrichment in the limited data obtained. Interestingly, even with the small ash content of the original sample, high levels of ash enrichment occurred in the smaller size fractions from the -300 um grind. Nonetheless, daf volatile yields from the two sets of samples agreed closely in the overlapping region, despite the significantly different preparation procedures used, suggesting that maceral enrichment was not a major problem.

CONCLUSIONS

When interference from mineral and maceral enrichment effects was minimised, small increases in daf volatile yields for rapid heating have been observed with decreasing particle size. This is likely to result from reduced resistance to volatiles mass transfer within the smaller particles. Volatile yield increases varied from nearly zero to 8 percentage points between the 100-150 um and 38-53 um size fractions.

In practice, selective mineral and maceral enrichment of different size fractions is very difficult to prevent. Without special preparation procedures these enrichment effects can swamp any effect of changing mass transfer resistance.

In ground samples prepared from whole coals selective enrichment effects probably tend to offset mass transfer effects. Because of this, the simplifying assumption of invariant volatile yields with particle size, often made in combustion and gasification models, appears to be reasonably valid.

The unavoidability of maceral enrichment effects imposes a limit on the accuracy with which a characteristic rapid-heating volatile yield for a whole coal can be measured if, as is often the case, the test method used (e.g. wire-mesh, entrained flow reactor) requires a sample with a restricted size range. The present study indicates a potential uncertainty of about +/- 3 percentage points in indicated daf values. More representative measurements are likely to be obtained if the test sample is prepared by grinding all of the original coal to pass the top size required, instead of screening the test sample out of a grind with some wider size distribution.

Acknowledgements

The authors would like to thank the UK Science and Engineering Research Council for their financial support under Grant No. GR/F 89817. The coal maceral analyses were measured by British Coal's Technical Services and Research Executive (TSRE) at Bretby. The TGA experiments were carried out at the British Gas plc London Research Station (LRS).

References

1. Crelling, J.C., Southern Illinois University, Carbondale, personal communication.
2. Vorres, K.S., Energy & Fuels 4(5), 1990, 420-426.
3. Gibbins, J.R., King, R.A.V., Wood, R.J. and Kandiyoti, R., Rev. Sci. Instrum. 60, 1989, 1129-1139.
4. Man, C.K, Pendlebury, K.J. & Gibbins, J.R., ACS DFC Prepr. 37(1), 1992, 103-109.
5. Gibbins, J.R. & Kandiyoti, R., Energy & Fuels, 2, 1988, 505-511.
6. Littlejohn, R.F., J. Inst. Fuel, 39, 1966, 59.
7. Li, C.-Z., Gaines, A.F., Guell, A.J. & Kandiyoti, R., Proc. 1991 Int. Conf. on Coal Science, Newcastle, 1991, 723-726.

Table 1 Mass distributions from first grinding process

Coal	Size fraction , um (wt.%)				
	150-106	106-75	75-53	53-38	<38
Daw Mill	18.8	19.2	18.2	11.8	32.0
Kellingley	15.8	60.2	19.2	4.8	n/a
Pittsburgh #8	12.6	17.0	16.1	10.3	44.0
SB vitrain	26.2	22.0	17.1	22.5	12.2

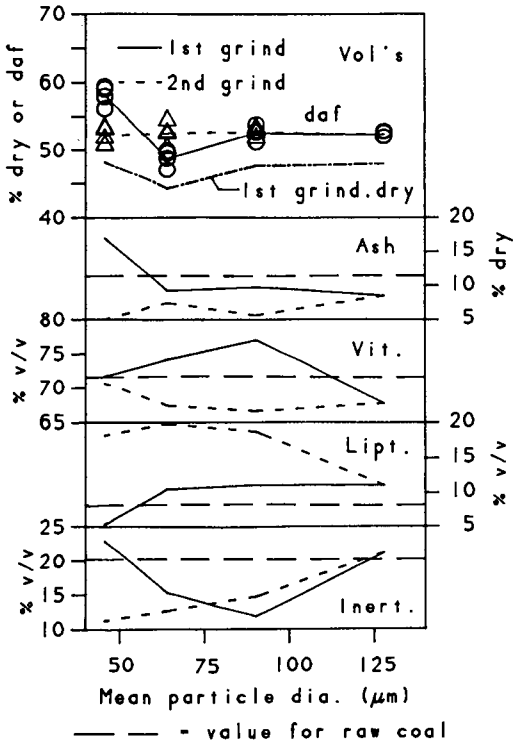

Fig. 1 Daw Mill coal - variation in volatile yields and mineral and maceral enrichment with size fraction.

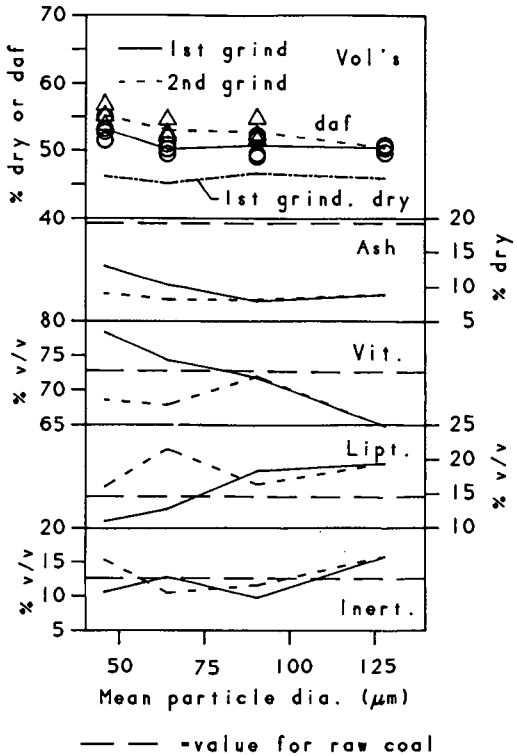

Fig. 2 Kellingley coal - variation in volatile yields and mineral and maceral enrichment with size fraction.

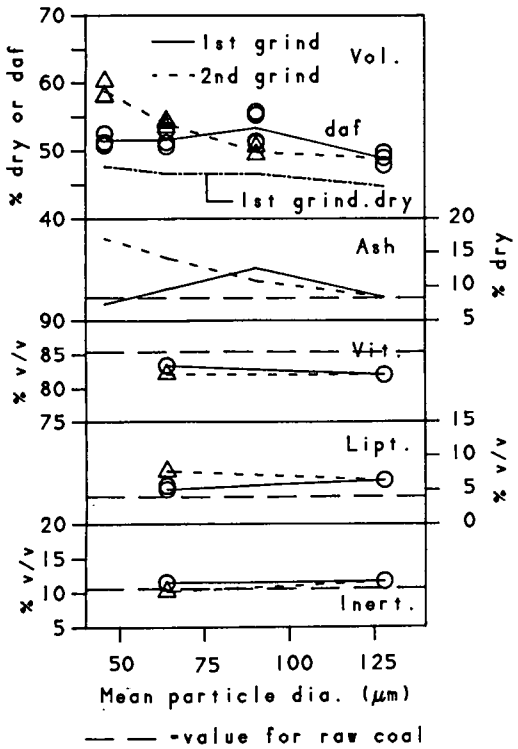

Fig. 3 Pittsburgh No. 8 coal - variation in volatile yields and mineral and maceral enrichment with size fraction.

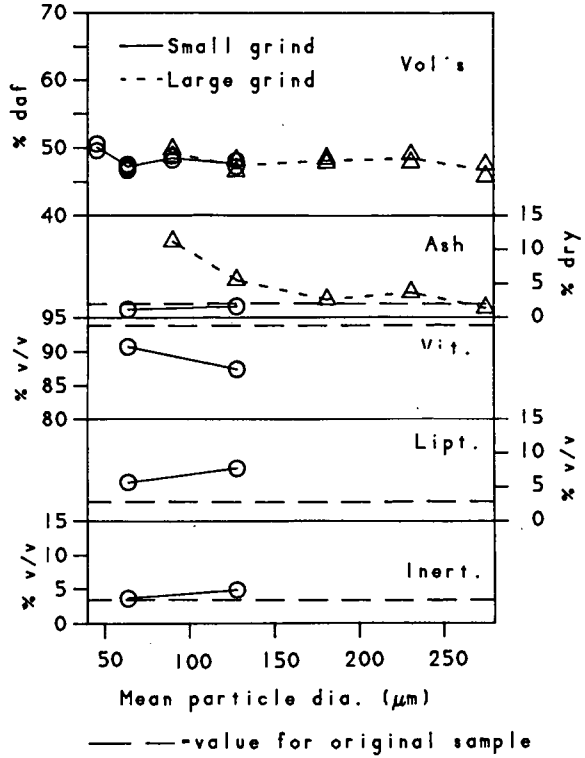

Fig. 4 Shirebrook Blackstone vitrain - variation in volatile yields and mineral and maceral enrichment with size fraction.

THE INFLUENCE OF CHAR STRUCTURE ON LOW TEMPERATURE COMBUSTION REACTIVITY

S. Charpenay, M.A. Serio, H. Teng, and P.R. Solomon
Advanced Fuel Research, Inc., 87 Church Street, East Hartford, CT 06108

Keywords : char structure, combustion reactivity, pore diffusion

INTRODUCTION

Coal char is a porous material with a structure which is intimately related to its combustion properties. In particular, the internal structure influences the degree of intraparticle diffusion limitations present at various temperatures. For fluid coals, the char structure is expected to depend on the extent of "reorganization" during the fluid stage, and should vary with the pyrolysis heating rate, the pyrolysis temperature and the holding time. On the other hand, coals which do not become fluid should produce chars with a structure similar to that of the original coal. It has been shown in a previous study[1] that the pyrolysis heating rate has an impact on the reactivity of fluid chars. Since reactivity was measured in the kinetic regime, this effect should not be related to the char physical structure, except for differences in internal surface area. However, the extent of rearrangement during the period when the char is fluid may well affect both the physical pore structure and the molecular order. The latter quantity will determine the active site concentration. In that previous study[1], the reactivity of low rank coals was found to be relatively independent of the time-temperature history, as long as the same degree of pyrolysis is reached. This is consistent with the fact that no important structure reorganization is expected to occur with these non-fluid coals.

The current study investigated the influence of the starting coal type (softening or non-softening) and of the char formation conditions on the onset of the pore diffusion regime. The reactivity of chars produced from fluid coals at different heating rates, and from non-fluid coals at low heating rate was measured isothermally with a TGA. Cumulative pore volumes and nitrogen surface areas were measured in order to be correlated with the behavior of the chars towards pore diffusion limitations.

The transition from zone I (kinetic regime) to zone II (combination of pore diffusion and kinetic regime) has been observed in a TGA apparatus by several researchers[2,3,4,5]. The chars studied were, in all cases, produced at low heating rate, i.e., a few degrees per minute. Tseng and Edgar[2,3] observed variations in the activation energy for lignite chars (from approximately 28 kcal/mol in the kinetic regime to 14 kcal/mol in the pore diffusion regime) and anthracite and bituminous coal chars (from about 33 kcal/mol to 22 kcal/mol). For an identical particle size of 650 μm, their results show that the lignite chars reach the pore diffusion regime at a much higher reaction rate (roughly an order of magnitude) than the bituminous or anthracite chars. This implies that the structure of the lignite char is probably more "open", thus retarding diffusion limitations. The values of the N_2-BET surface areas at 0% burnoff were measured and were found to be of the order of 100 m^2/g for the lignite char, 15 m^2/g for the bituminous char and 1-2 m^2/g for the anthracite char. These values are consistent with the assumption of a more porous structure for the lignite chars. Su and Perlmutter[4] studied chars produced at different heating rates (in the range 1 to 10 K/min), for different pyrolysis temperatures (873 to 1223 K) and for

different starting coals (anthracite and bituminous coals). They concluded that chars with different pore structures can be generated from the same coals by varying pyrolysis conditions: a higher final pyrolysis temperature or a slower heating rate generate chars of more compact structure. Floess et al.[5] compared the behavior of a microporous sucrose char with a macroporous spherocarb char and observed that the reactivity of the former varied with particle size, while the latter did not display such an effect. They attributed the difference in behavior to the different structure of the chars (purely microporous versus microporous and macroporous), and in particular to the presence of large microporous domains in the sucrose char. As Hurt et al.[6] pointed out, the degree of meso and macroporosity defines the size of the microporous regions, and consequently influences the degree of diffusion limitations in the micropores. In other words, for highly meso/macroporous chars, where the microporous regions are small, the micropores may not be diffusion limited before the meso/macropores themselves. This situation is similar to the one described in Thiele[7] where, even if most of the reaction occurs in small micropores, the meso/macropores configuration is assumed to control intraparticle diffusion. Walker[8] and Simons[9] arrived at the same general conclusion, although using different approaches. Consequently, it is important to estimate the degree of micro and meso/macroporosity of a char in order to predict the degree of pore diffusion limitations.

In order to assess differences in pore structures, multiple techniques such as gas adsorption (for surface areas and pore size distribution measurements), helium pycnometry (densities) and mercury intrusion (macropores distribution) can be used. White et al[10] performed a comprehensive study on representative US coal chars (from lignite to bituminous) in order to determine surface area, pore size and volume distribution, and density. The chars were prepared at high heating rate in a flat flame burner (in the presence of oxygen), which is representative of char formation in pulverized coal combustion processes. They observed large variations in properties between the original coals and the corresponding chars : increase by two to three-fold for CO_2-DP surface area, by 20-200-fold for N_2-BET surface area, by 5-10-fold for pore volume, by three to four-fold for porosity. However, the differences between the chars produced from different coals were not very important, and varied by less than a factor of 2 for surface area, less than a factor of 2 for pore volume, and less than 15% for porosity. All of the chars were fairly porous (porosity of about 0.6-0.7) with most of the pore volume in macropores, and had N_2 surface areas of about 100-200 m^2/g and CO_2 surface areas of about 200-500 m^2/g.

More significant variations between the chars studied in the present work were expected, due to the widely different char formation conditions used.

EXPERIMENTAL

Coal Samples - The coals used are from the Argonne Premium Coal Sample Program. The original coal particle size fraction is -100 mesh.

Char Preparation - The chars prepared in the TGA were produced by heating at 30°C/min in helium up to the pyrolysis temperature. In the case of non-fluid, non-agglomerating chars, the isothermal combustion cycle was done immediately after the pyrolysis cycle (without removing the sample from the TGA). In that case, the coal sample size was approximately 10 mg, which corresponds to a char sample sample of 4 to 7 mg. For fluid coals, since the particles have agglomerated during low heating rate pyrolysis, the char was prepared in larger quantity (150 mg) and was separated into different size fractions. The char average particle size was measured with an ISI Scanning Electron Microscope. The same procedure was applied to the char

prepared in an entrained flow reactor (EFR).

Isothermal Reactivity Measurements - The reaction rates at low temperatures were measured isothermally using a Dupont 951 TGA. The reaction rate is constantly monitored during the entire burnoff process. All experiments were performed using an oxygen partial pressure of 17.2 kPa, a total flow rate of 240 cc/min, and a char sample size of 4 to 10 mg. For the chars prepared in advance in the TGA or the EFR, the char sample was heated under a helium atmosphere at 30°C/min up to the combustion temperature, and the oxygen was introduced after 15 minutes to allow equilibrium.

Nitrogen Adsorption Measurements - Adsorption isotherms in nitrogen were obtained using the dynamic, continuous flow method. The measurements were made using a Quantasorb instrument (Quantachrome Corp.). From the adsorption isotherm, the cumulative pore volume was calculated. The nitrogen surface areas were obtained using the BET equation (single point).

RESULTS AND DISCUSSION

Reactivity Measurements - Chars from the fluid coal Pittsburgh No. 8 were produced at low heating rate in a TGA (Pitts8 TGA) and at high heating rate in an entrained flow reactor (Pitts8 EFR). In order to evaluate the influence of coal rank on pore structure, a char from a Zap lignite was also produced at low heating rate in the TGA (Zap TGA). A char from a demineralized Zap was produced under the same conditions for comparison (Zapd TGA). Table I gives a summary of the properties of the chars studied.

Isothermal measurements of reactivity were obtained for each char over a wide range of temperature, which covered usually 3 orders of magnitude in reactivity. The reported rate was taken at 35% burnoff in all cases, in order to avoid any uncertainty in the calculation of the reaction rate because of the relatively high weight increase due to oxygen adsorption at lower burnoff levels. As shown in Fig. 1, a leveling off of the rate is observed for all chars at a rate of approximately 1 g/g.min. This behavior is due to external mass transfer resistances in the TGA, and would not occur under typical pulverized coal combustion conditions. The Zap TGA char was also found to ignite, which is indicated by the presence of a discontinuity in the reactivity.

As shown in Fig. 1, at low temperature all the chars studied indicated a similar activation energy, which fell in the range of 28 to 34 kcal/mol. The Arrhenius plots for the low heating rate, fluid char Pitts8 TGA showed a gradual change in activation energy, from approximately 28 kcal/mol at low temperature, to 22 kcal/mol at higher temperature. This behavior is observed for the two different particle sizes studied, 150 μm and 800 μm. Following the Thiele[7] model, the observed change in activation energy is believed to represent the transition from regime I (kinetic) to regime II (pore diffusion). However, features relative to the effect of particle size in each regime need to be clarified. In particular, the fact that, at low temperature (i.e. in the kinetic regime), the 150 μm particle size presents a reactivity higher than the one from the 800 μm particle size requires some explanation. This phenomenon has been observed by other researchers[5,11]. van Heek and Mühlen[11] proposed that the enrichment of product gases inside the larger particles caused by too small diffusion coefficients or too large flow resistances is responsible for the inhibition of the reaction rate. On the other hand, at higher temperatures (in the pore diffusion regime), the variation in rate between the two size fractions is smaller than expected : since the two particle sizes differ by about a factor of 5, the same factor should be obtained between the reaction rates. However, only a factor of 2 is found. A possible explanation of this effect may

result from finding out where the diffusion limitations take place in the particle. If we consider the char to be formed by microporous grains (or regions) surrounded by meso or macropores, diffusion limitations can occur either in the grains (if these are large) or in the meso/macropores (in the case of small microporous grains). In other words, for a char with large microporous regions, the diffusion parameter D_{micro}/L^2_{micro} (where D_{micro} is the effective diffusivity and L_{micro} is the diffusion distance in the microporous grains) is lower than the corresponding parameter $D_{meso/macro}/L^2_{meso/macro}$ for the meso/macropores, where $L_{meso/macro}$ represents a distance of the order of the particle size. In such a case, particle size effects may not be present, or would be weak, until the particle size is small enough (i.e. of the size of the microporous regions), in which case the diffusion distance is effectively reduced. The fact that a very low N_2 surface area of 0.5 m^2/g at 0% burnoff is found for that char would also be consistent with this assumption, since it implies that few meso and macropores are present. In such a case, the microporous regions could be fairly large.

In contrast with the low heating rate char, Pitts8 TGA, the char produced at high heating rate Pitts8 EFR, did not show much change in activation energy (i.e. did not reach the pore diffusion regime) before entering the external diffusion limitation regime. Its N_2 surface area (at 0% burnoff) was also found to be higher (4 m^2/g versus 0.5 m^2/g) than the one from Pitts8 TGA. This behavior is consistant with the findings of Su and Perlmutter[4] that low heating rate chars have a more compact structure. The lignite and demineralized lignite chars Zap TGA and Zapd TGA behaved similarly to the Pitts8 EFR. Their surface areas (84 m^2/g and 100 m^2/g respectively) were also much higher than the ones from either of the Pittsburgh No. 8 chars.

Pore structure characterization - In an attempt to characterize the pore structure of the chars studied, nitrogen adsorption measurements were performed. Nitrogen adsorption is done at the temperature of liquid nitrogen (77 K). Adsorption is assumed to occur in the mesopores but not in the micropores (at least in the case of 0% burnoff chars) because of activated diffusion. However, since the micropores open up at higher burnoffs, those also adsorb nitrogen in the case of partially combusted chars.

The N_2 adsorption data at 0% burnoff provide useful information on the number and accessibility of the mesopores of the char. Since mesopores probably constitute the main pathway for oxygen to penetrate into the particle, their characterization is an important step in order to predict diffusion limitations. Fig. 2 shows the adsorption isotherms for the Pitts8 EFR and the Pitts8 TGA at 0% burnoff. Pitts8 EFR char produces an isotherm of type IV (characteristic of the presence of pores in the transitional range) while Pitts8 TGA produces an isotherm of the types II or III (non porous). Also, the adsorbed volume is larger in the case of the Pitts8 EFR than for the Pitts8 TGA. The adsorption isotherm for Zap TGA char is shown in Fig. 3, and is characteristic of a porous material with numerous mesopores. Fig. 4 gives the cumulative pore volume for the three chars. These results confirm, in the case of the high heating rate Pitts8 EFR, the presence of more mesopores than in the low heating rate Pitts8 TGA char and are consistent with the assumption that the latter possesses larger microporous regions than the former. Also, as expected, the structure of the Zap TGA char is much more porous than the chars from the fluid coals. This is consistent with the results from Tseng and Edgar[2,3] who found that for the same particle size, a bituminous char entered the diffusion limited regime before a lignite char. A more quantitative correlation of the pore volume with the degree of diffusion limitations will require additional data in the pore diffusion limited regime for the highly porous chars.

It is well known that the N_2 adsorption pattern changes significantly after a few percent of burnoff.

In order to evaluate those variations, Pitts8 TGA and the Pitts8 EFR chars were produced at 10% and 35% burnoff respectively. Although the degree of burnoff of the two chars is different, it can be reasonably assumed that the internal structure does not vary significantly between 10 and 35% burnoff. The combustion temperature was chosen to be sufficiently low as to be in the kinetic regime. Under these conditions, the pore structure is expected to vary uniformly through the whole particle. It should be noted that this may not be how the structure changes when burnoff is performed at higher temperature, i.e., in the pore diffusion regime (in that case burnoff occurs mostly at the exterior of the particle, with the interior not being modified). Fig. 5 presents the adsorption isotherm for the Pitts8 TGA at 10% burnoff and the Pitts8 EFR at 35% burnoff. The two chars produce an adsorption isotherm characteristic of a microporous structure[12], with most of the pores being smaller than about 20 Å. In that case, the Kelvin equation cannot be utilized to calculate the pore size distribution. The value of the N_2 surface area also increased dramatically, from 0.5 to 98 m^2/g for the Pitts8 TGA char and from 4 to 310 m^2/g for the Pitts8 EFR. These results indicate that the structure of both coal chars is mostly microporous. However, the degree of meso and macroporosity (which is important to estimate for transport processes) cannot be evaluated easily from these measurements. Also, since the burnoff was performed in the kinetic regime, it does not give a representation of the structure obtained when the combustion is done under more severe conditions. Additional data from chars combusted at high temperatures (i.e. in the pore diffusion regime) is needed. This point will be addressed in more detail in a future publication.

CONCLUSIONS

From this study it can be concluded that low heating rate, fluid chars are less macroporous than high heating rate, fluid chars or lignite chars. This conclusion is consistent with the observation that the low heating rate, fluid chars enter the pore diffusion regime earlier than the other chars. It was also shown that char structural parameters such as surface area and cumulative pore volume can be correlated with the behavior of the char towards pore diffusion limitations. However, additional data obtained in the pore diffusion regime is necessary in order to establish a quantitative correlation between structural properties and the onset of diffusion limitations for a wide range of chars.

ACKNOWLEDGEMENT

The authors are grateful for the support of the Morgantown Energy Technology Center of the United States Department of Energy under contract DE-AC21-86MC23075, for support of the study of char reactivity. The authors wish to acknowledge the contributions of Marie DiTaranto of Advanced Fuel Research to the experimental work, and helpful discussions with Prof. Suuberg of Brown University.

REFERENCES

1. Serio, M.A., Solomon, P.R., and Bassilakis, R., ACS Div. Fuel Chem. Preprints, 34 (1), (1989)
2. Tseng, H.P., Edgar, T.F., Fuel, 63, 385, (1984)
3. Tseng, H.P., Edgar, T.F., Fuel, 64, 373, (1985)
4. Su, J.L., Perlmutter, D.D., AIChE J., 31, 973, (1985)
5. Floess, J.K., Longwell, J.P., Sarofim, A.F., Energy and Fuels, 2, 18-26, (1988)
6. Hurt, R.H., Sarofim, A.F., Longwell, J.P., Energy and Fuels, 5, 290-299, (1991)
7. Thiele, E.W., Ind. Eng. Chem., 31, 916, (1939)

8. Walker, P.L., Fuel, 59, 809, (1980)
9. Simons, G.A., Combustion Science and Technology, 20, 107-116, (1979)
10. White, W.E., Bartholomew, C.H., Hecker, W.C., Smith, D.M., Adsorption Science and Technology, vol.7, No.4, 180, (1990)
11. van Heek, K.H., Mühlen, H.J., in "Fundamental Issues in control of carbon gasification Reactivity", J. Lahaye and P. Ehrburger (Eds), Kluwer Academic Publishers, 1-34, (1991)
12. Gregg, S.J., Sing, K.S.W., Adsorption, Surface Area and Porosity, 2nd Edn, Academic Press, New York, (1982)

TABLE I Char Properties

Char	Coal	Reactor	Heating Rate (°C/s)	Final Temp.(°C)	Char Particle Size (μm)	N_2 Surface Area (m^2/g)
Pitts8 TGA	Pitts 8	TGA	0.5	900	800 ± 200* 150 ± 50	0% BO:0.5 10% BO:98
Pitts8 EFR	Pitts 8	EFR	5000	1100	130 ± 30	0% BO:4 35% BO:310
Zap TGA	Zap	TGA	0.5	900	80 ± 40	0% BO:84
Zapd TGA	Zap	TGA	0.5	900	60 ± 20	0% BO:100

* In that case, the combustion cycle was performed immediately after the pyrolysis. The particle size is approximate, since the chars showed a cenospheric agglomerated structure.

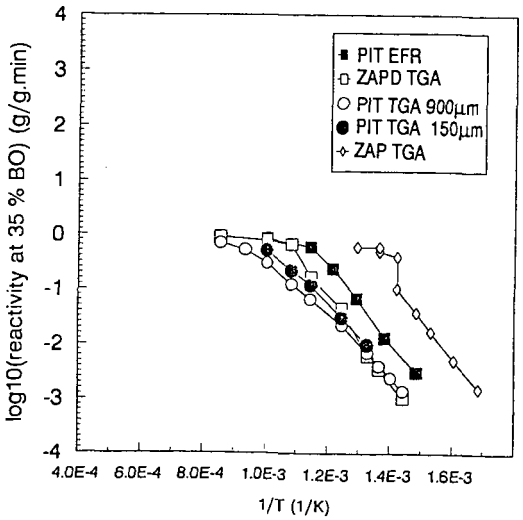

Figure 1. Measured Reactivity at 35% Burn-off of PITTS8 TGA, PITTS8 EFR, ZAP TGA, ZAPD TGA Chars as a Function of 1/T.

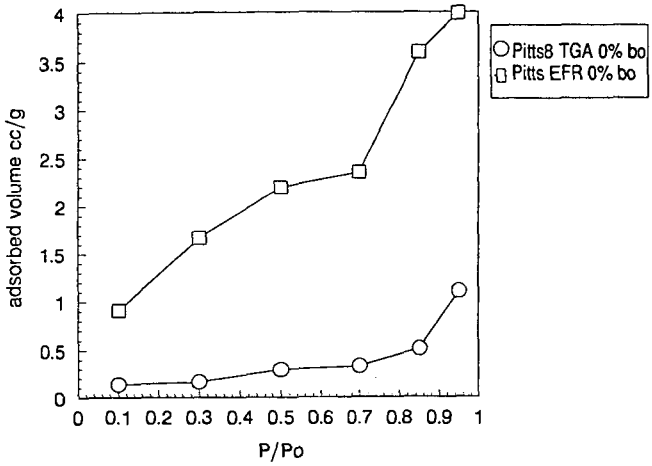

Figure 2. Nitrogen Adsorption Isotherms for PITTS8 EFR and PITTS8 TGA Chars.

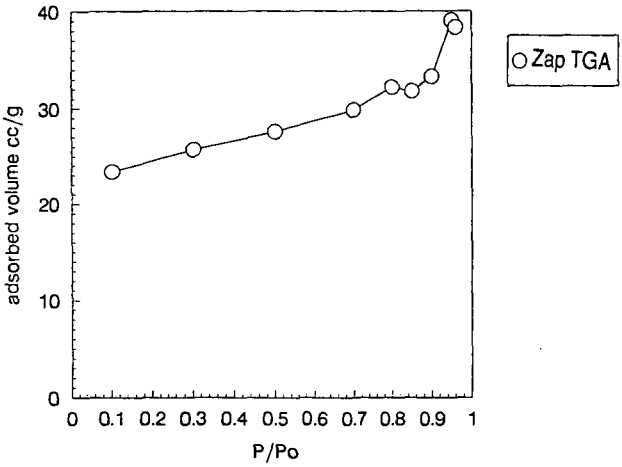

Figure 3. Nitrogen Adsorption Isotherm for ZAP TGA Char.

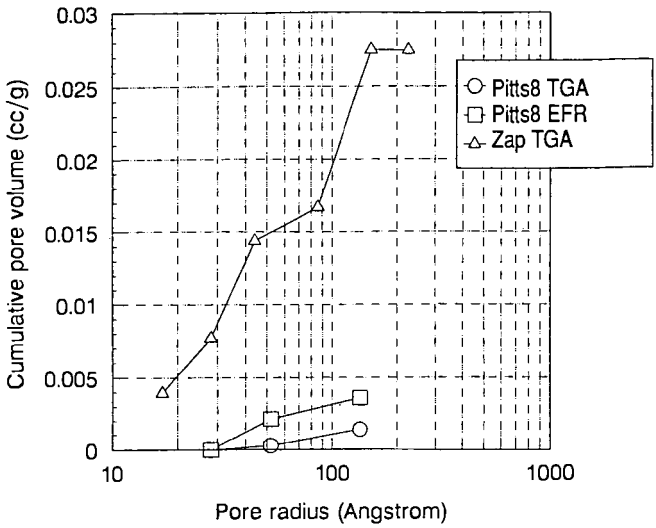

Figure 4. Cumulative Pore Volume for PITTS8 EFR, PITTS8 TGA and ZAP TGA Chars.

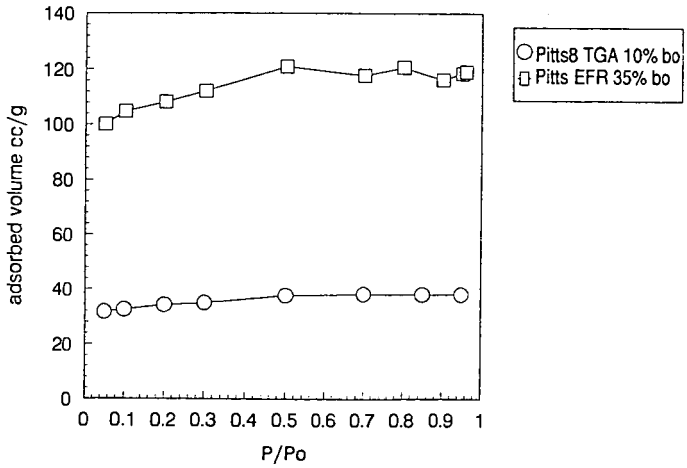

Figure 5. Nitrogen Adsorption Isotherms for PITTS8 EFR at 35% Burn-off and PITTS8 TGA at 10% Burn-off.

GAS EVOLUTION FROM COAL IN SEALED GLASS AMPOULES*

K. S. Vorres
Chemistry Division, Building 211, Argonne National Laboratory
Argonne, IL 60439, USA

INTRODUCTION:

Earlier publications reported studies on the gas content of Argonne Premium Coal Samples (1,2). These samples are available in ampoules of 5 grams of -100 mesh and 10 grams of -20 mesh. They were periodically opened in vacuum and analyzed with a mass spectrometer as part of a quality monitoring program. The samples were originally sealed under nitrogen in a glove box maintained at less than 40 ppm of oxygen. Moisture present in the coal was kept in the samples as much as possible. Determinations of the gases were made and provide an opportunity to observe the changes due to transformations, release of dissolved gases or other processes in the samples. Changes in the gas content were observed and may be useful in interpreting a variety of phenomena.

The eight Argonne Premium Coal Samples are described below:

#	Name	Rank	State	Dmmf C	Dmmf H	Abbrev.
1	Upper Freeport	MVB	PA	88.08	4.84	UF
2	Wyodak-Anderson	SUB	WY	75.01	5.42	WY
3	Illinois #6	HVB	IL	77.67	5.20	IL
4	Pittsburgh	HVB	PA	83.20	5.43	PITT
5	Pocahontas #3	LVB	VA	91.05	4.48	POC
6	Blind Canyon	HVB	UT	80.69	5.81	UT
7	Lewiston-Stockton	HVB	WV	82.58	5.44	WV
8	Beulah-Zap	LIG	ND	74.05	4.90	ND

LVB = Low volatile bituminous, MVB = Medium volatile bituminous, HVB = High volatile bituminous, SUB = subbituminous, LIG = Lignite, State = U. S. A. State of origin, Dmmf = dry mineral matter-free, Abbrev = Abbreviation used later

EXPERIMENTAL:

The Argonne premium coal samples have been sealed in borosilicate glass ampoules in a nitrogen atmosphere (3). A hydrogen-oxygen torch was used for the sealing. The hydrogen and oxygen gas flows were controlled with a gas mass flow controller to maintain stoichiometric conditions during the sealing. The oxygen content of the glovebox system was constantly monitored during the operation and no significant deviations from the expected values were observed.

*This work was supported by the Office of Basic Energy Sciences, Division of Chemical Sciences, U. S. Department of Energy, under contract number W-31-109-ENG-38.

A supply of coal ampoules for each of the eight samples in each of the two mesh sizes was selected to provide samples for analysis over several years at initial sample consumption rates of about two per year. The ampoules were sent to the Analytical Chemistry Laboratory of the Argonne National Laboratory for gas analysis. The ampoules were placed in an evacuable chamber and the surrounding air was pumped out. A magnetic hammer was used to break the ampoule and release the atmosphere above the ampoules.

For the measurements until 1991, the gas was passed into a Consolidated Engineering Corporation (CEC) model 21-620 mass spectrometer and analyzed for nitrogen, methane, carbon dioxide, hydrogen, argon, water vapor, and higher hydrocarbons. Carbon monoxide could not initially be distinguished from nitrogen and was not reported. A VG Gas Analysis mass spectrometer, model 30-01 equipped with electron multiplier detector, was obtained in 1990 to replace the CEC unit and provide better data. Carbon monoxide can now be detected in the nitrogen, and lower limits of detection exist for the oxygen measurements.

The data obtained are condensed in Table I below.

Table I. Methane and Carbon Dioxide Concentrations in Argonne Premium Coal Sample Ampoules.

Coal		-100 mesh						-20 mesh					
		CH_4			CO_2			CH_4			CO_2		
	major gas	trend	max. conc	time	trend	max. conc		trend	max conc	time	trend	max conc	
UF	CH_4	+	.40	79	+	.13		P	.70	79	+	.15	
WY	CO_2	P-	.02	63	P-	.93		P	.02	63	+	1.4	
IL	CO_2	P-	.23	65	P-	.23		P-	.46	65	0	.66	
PITT	CH_4	P-	.8	64	P-	.58		P-	14.5	64	0	3.7	
POC	CH_4	P	1.2	62	+	.78		P-	7.6	62	P	5.1	
UT	CO_2	P-	.03	61	+	.10		0	.02	61	P	.37	
WV	CO_2	P-	.03	59	+	.13		P-	.23	59	0	.53	
ND	CO_2	P-	.02	58	+	2.68		0	.03	58	P	3.3	

major gas = gas at higher concentration in ampoule (other than N_2), trend = trend of changes in concentration (+ = increasing, 0 = constant, - = decreasing, P = plateau before or after trend), P- = decrease after plateau, max conc = maximum concentration of gas in ampoule in %, time = maximum time since sealing in months for data.

The data were plotted as concentration of gas versus time since sealing of the ampoules. Representative plots are shown in Figures 1-4. Figure 1 gives the concentration of CH_4 versus time since sealing for -100 mesh material. Figure 2 gives a similar

plot for the -20 mesh material. Figure 3 gives the concentration of CO_2 versus time since sealing for -100 mesh material, while Figure 4 provides similar information for the -20 mesh material.

RESULTS AND DISCUSSION:

Differences in the gas contents were observed as time passed. Considerable amounts of methane were released during the initial size reduction in the sample processing facility. The gas contents in Table I represent subsequent gas releases. Lower rank (Beulah-Zap and Wyodak-Anderson) and some intermediate rank (Illinois #6, Blind Canyon, Lewiston-Stockton) ampoules contained more carbon dioxide, while several higher rank (Pocahontas #3, Upper Freeport, Pittsburgh seam) ampoules contained more methane. In most cases, if carbon dioxide contents increased then methane contents did not increase, and vice-versa. Oxygen contents remained at or below the limits of detection, indicating the integrity of the ampoules.

The data in Figure 1 indicate the variation in methane for the six most concentrated -100 mesh samples. In general, the concentration increases as the time since sealing increases. The highest rank coal, Pocahontas, shows the largest methane concentration. The next highest rank, Upper Freeport, has a lower methane concentration than the Pittsburgh seam (lower rank in this group). A comparison in a similar plot for -20 mesh particles for these three coals indicates the highest concentration for the Pittsburgh seam followed by the Pocahontas and Upper Freeport in that order. The data are more limited but show an increase with concentration with time. The maximum concentration for the Pittsburgh seam coal was about 14% of the gas volume, or more than an order of magnitude greater than for the -100 mesh material. For early measurements

The data in Figure 3 indicate the carbon dioxide content of the gas space in the ampoules above the -100 mesh lower rank samples. The Beulah-Zap sample (legend ND) clearly released the most carbon dioxide at 2.6%. The Wyodak-Anderson sample released the next largest amount with the concentration increasing almost linearly over time. A similar plot of releases from -20 mesh material indicated that the evolution was only about 50% larger for the Beulah-Zap material. The values for the other coals were two to three times as high. The concentrations for the remaining samples were Pittsburgh > Illinois #6 > Lewiston-Stockton (legend WV) > Blind Canyon (legend UT). The latter three were relatively constant for the period in which the samples were analyzed.

The data in Figure 4 for -20 mesh samples indicate that the carbon dioxide concentrations are higher than those for the -100 mesh samples. This behavior is consistent with that observed for the methane measurements from the different particle sizes. The more striking difference is that the concentrations in the Pocahontas and Pittsburgh samples have increased to exceed that from the Beulah-Zap sample.

It is believed that the gas is dissolved in the coal matter and is released very slowly. Bacterial activity is not considered responsible since either carbon dioxide or methane but generally

not both are released from the samples, as might be expected from many bacterial actions. The most recent data indicate that significant quantities of carbon monoxide are not released in that the concentrations are at or below the limits of detection (.02%).

CONCLUSIONS:

1. Higher rank coals evolve methane, and lower rank coals evolve carbon dioxide with some evolution of both gases for the intermediate ranks.

2. The evolution proceeds over times of years for pulverized coals in sealed ampoules.

3. Gas concentrations are higher above -20 mesh samples than above -100 mesh material.

4. Carbon monoxide is not evolved.

5. The Wyodak sample evolves carbon dioxide approximately linearly with time.

6. The gas evolution seems to be associated with evolution of dissolved species.

ACKNOWLEDGMENTS:

The author expresses his grateful appreciation to A. Engelkemier for her analyses of the coal ampoule atmospheres. Gratitude is also expressed to the U. S. Department of Energy, Office of Basic Energy Sciences, Chemical Sciences Division for support.

REFERENCES:

(1) Vorres, K. S., Proc. 1989 Intl. Conf. on Coal Science, Vol. II, 1083 (1989).

(2) Vorres, K. S., Proc. 1991 Intl. Conf. on Coal Science, Vol. I, 147 (1991).

(3) Vorres, K. S., The Argonne Premium Coal Sample Program, Energy & Fuels, 1990, 4, 420-426.

Fig. 1, Six Highest −100 Mesh Methane

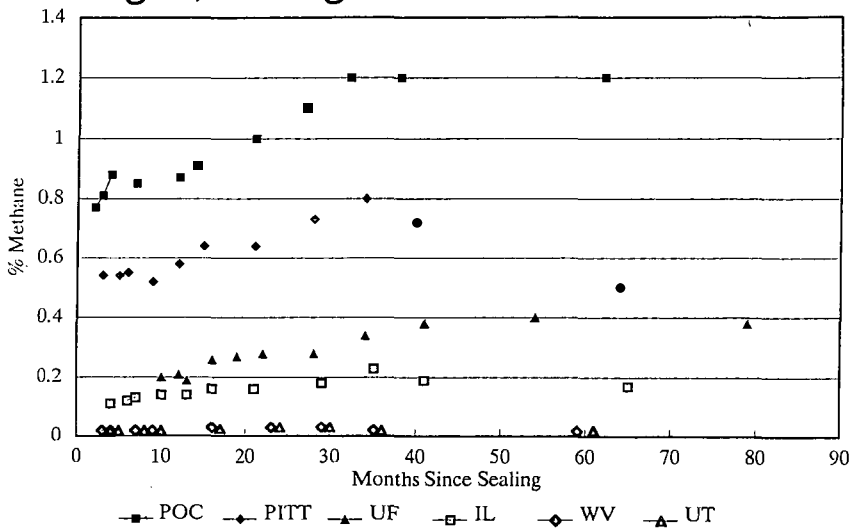

Fig. 2, Six Highest −20 Mesh Methane

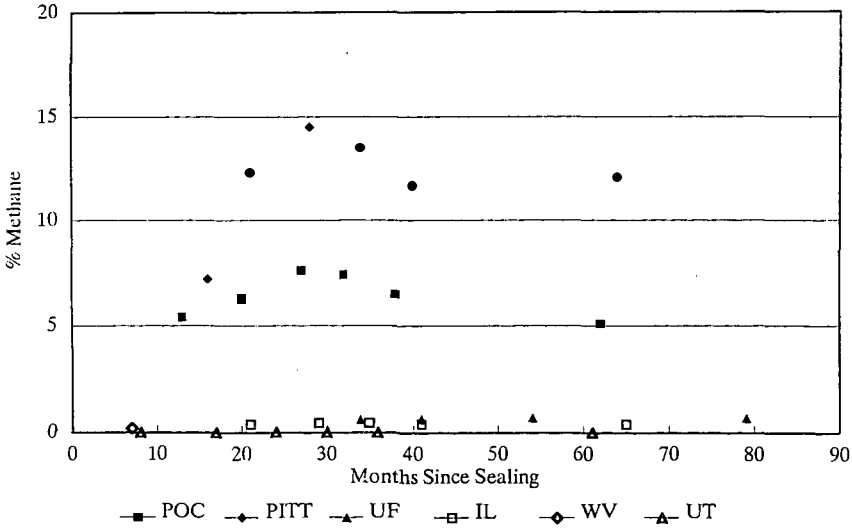

Fig. 3, Six Highest −100 Mesh CO2

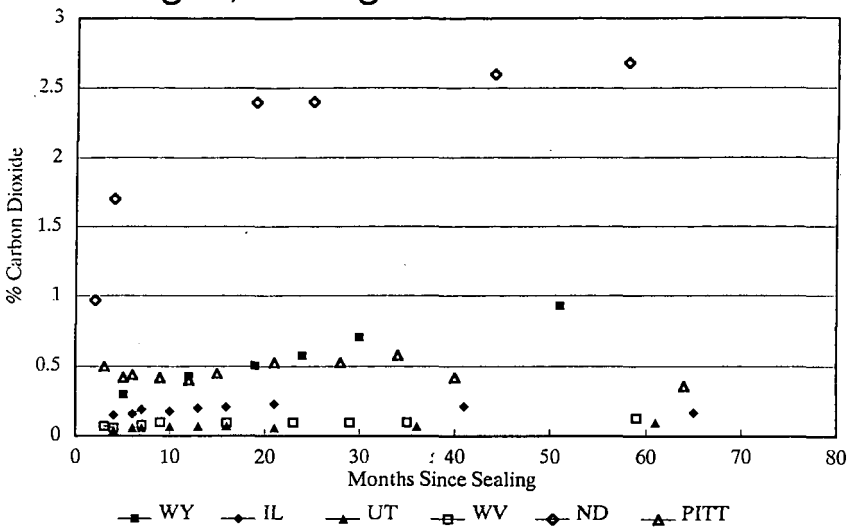

Fig. 4, Six Highest −20 Mesh CO2

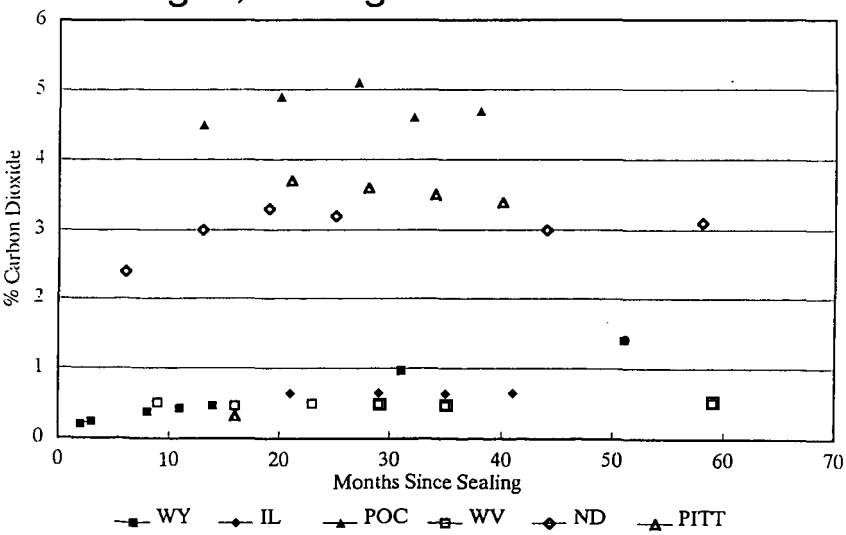

HYDROGASIFICATION OF BROWN COAL WITH ACTIVE IRON CATALYSTS FROM FERRIC CHLORIDE

Kenji Asami and Yasuo Ohtsuka
Research Center for Carbonaceous Resources
Institute for Chemical Reaction Science
Tohoku University, Sendai 980, JAPAN

Keywords: Coal, Hydrogasification, Iron Catalyst

INTRODUCTION

It would be necessary nowadays that coal is converted into the environmentally acceptable fuels. Gasification of coal with hydrogen is an important process for producing clean SNG. Since the reaction rate is very slow, high temperature and high pressure are required in the absence of catalyst [1], and thus an active and inexpensive catalyst should be developed. Iron is one of the most promising catalysts for the hydrogasification of coal. We have been trying to utilize acid wastes from metal pickling and titanium oxide production plants as Fe catalyst sources, because the wastes are cheap and abundant. When Fe chlorides or sulfates of the major components are added onto coal by the conventional impregnation method, they are inactive for the gasification in H_2 at low temperatures [2], and Cl- or S-containing gases evolved during gasification may result in serious problems such as corrosion. However, we have recently found that Cl-free Fe catalysts finely-dispersed on low-rank coals can be successfully prepared from an aqueous solution of $FeCl_3$ using several additives, and exhibit high activities for the low temperature gasification with steam [3,4].

In the present work, these Fe catalysts are applied to the gasification of brown coal in atmospheric H_2 at low temperatures below 1200 K. The relationship between the catalytic activity and the preparation method and the catalytic state is examined.

EXPERIMENTAL

Coal and Catalyst. Australian Loy Yang brown coal with a particle size of 0.15 - 0.25 mm was employed in this study. The proximate analysis was ash, 0.5; volatile matter, 52.4; fixed carbon, 47.1 wt% (dry), and the ultimate analysis was C, 66.7; H, 4.6; N, 0.5; S, 0.3; O, 27.9 wt% (daf).

Three kinds of Fe catalysts were precipitated onto brown coal from an aqueous solution of $FeCl_3$ with different additives, that is, urea ($(NH_2)_2CO$), $Ca(OH)_2$, and NH_3/NH_4Cl buffer solution. These catalysts are abbreviated as Fe(U), Fe(C), and Fe(A), respectively. In the preparation of Fe(U), urea was added to the mixture of coal and $FeCl_3$ solution so that fine particles of FeOOH could be precipitated onto coal [5], and the resulting mixture was stirred at 370 K. For Fe(C) and Fe(A) $Ca(OH)_2$ powder and NH_3/NH_4Cl solution were added instead of urea, respectively, and the aqueous mixture was stirred at room temperature. After each precipitation, the solution was filtered off, and the Fe-bearing coal was washed with deionized water repeatedly to remove the Cl^- or Ca^{2+} ions. The preparation methods have been described in detail elsewhere [3,4].

Hydrogasification. Gasification runs were isothermally conducted in a thermobalance under atmospheric H_2 at 873-1173 K. Since all the samples were quickly heated up to a predetermined temperature, the coal devolatilization first took place, and after the completion within a few minutes char gasification started. The activity of Fe catalyst in the latter stage will be discussed throughout the paper. The reactivity of char after devolatilization is expressed by using both char conversion on a dry ash free and catalyst free basis and the specific rate of char, that is, the gasification rate per unit

weight of remaining char.

X-ray diffraction. X-ray diffraction (XRD) measurements of Fe-bearing coals and chars were made with Mn-filtered Fe-$K\alpha$ radiation to clarify the chemical form and dispersion state of Fe catalyst. The average crystallite size of Fe species was determined by the Debye-Shörrer method.

RESULTS AND DISCUSSION

Catalyst Components. The actual Fe loading of each sample was 3.4, 4.7, and 4.6 wt% for Fe(U), Fe(C), and Fe(A), respectively. The chlorine content determined by a standard Eschka method was nearly equal to that in the original coal (0.08 wt%) in every catalyst, indicating the complete removal of Cl ions from $FeCl_3$ with water washing. A small amount of Ca^{2+} (0.5 wt%) from $Ca(OH)_2$ was retained with Fe(C).

Catalytic Activity for Hydrogasification. Table 1 shows char conversion after 30 min in the hydrogasification at 873 K. The enhancement of the gasification rate by Fe catalyst was observed only in the early period of reaction, though not so high, and all the catalysts seemed to lose the activity in the latter stage. Char conversion showed that the order of the catalytic effectiveness was Fe(A) < Fe(C) < Fe(U).

Figure 1 illustrates the change in char conversion with reaction time at 1073 K. Every catalyst promoted the gasification, and the effectiveness was strongly dependent on the preparation method. The order of the activity was Fe(A) < Fe(U) < Fe(C), which is the same order as observed in the steam gasification [4]. With the most active Fe(C) char was completely gasified within about 100 min. The conversion at 120 min with Fe(U) and Fe(A) increased from 18 % without iron to 52% and 37%, respectively. Figure 2 shows the specific gasification rate as a function of char conversion at 1073 K. The rates for Fe(A) and the original coal were low and almost constant. The initial rates for Fe(U) and Fe(C) were almost the same, and they were about 20 times that without iron. The specific rate for Fe(U) decreased steeply with increasing conversion. On the contrary, the rate for Fe(C) increased gradually as the gasification proceeded. This rate increase was also observed at 1173 K. The change in specific rate with conversion may be determined by the balance between catalyst agglomeration and enrichment due to the consumption of char. When the catalyst enrichment is predominant as in the K-catalyzed gasification [6], the specific rate would increase with increasing conversion. The rate increase observed in the latter part of gasification with Fe(C) may be this case.

Thus, it is found that these precipitated Fe catalysts, especially Fe(C), exhibit high activities for the gasification of brown coal in atmospheric H_2 even at a temperature as low as 1073 K.

Catalyst State. Since no XRD lines of Fe species were detectable for each catalyst, the chemical form of Fe catalyst on coal could not be identified. However, other analytical techniques such as elemental analysis, ESCA, and FT-IR suggested that the catalyst exists as finely dispersed FeOOH [3,4].

The catalyst state immediately after devolatilization in H_2 at 873 K is summarized in Table 1. Major XRD species were α-Fe irrespective of the catalyst type. Small peaks due to cementite (Fe_3C) were also observed for Fe(C). The degree of catalyst dispersion evaluated from the average crystallite size of α-Fe increased in the order of Fe(A) < Fe(C) < Fe(U). This order corresponded to that of the gasification activity, which suggests that the dispersion may be a key factor determining the catalytic effectiveness in this temperature region.

Figure 3 shows the XRD patterns for Fe-bearing chars devolatilized at 1073 K. When the devolatilization temperature was raised from 873 K to 1073 K, the main species for Fe(C) changed from α-Fe to Fe_3C and strong XRD lines of unidentified iron carbides

appeared with small signals of α-Fe for Fe(U), whereas the major species for Fe(A), α-Fe, remained unchanged, though weak peaks of unidentified carbides were observed. As is seen in Figure 1, Fe(C) was the most active catalyst at 1073 K, and it achieved the complete gasification of char. Although Fe_3C is not always the actual active species because of the bulk chemical form identified by XRD, these observations suggest that the formation of iron carbide, perhaps Fe_3C, may be essential for such the high activity in the temperature region of around 1100 K. In other words, the hydrogasification may proceed through the carbon dissolution mechanism [7,8]. On the other hand, the hydrogen spill-over mechanism [1,9] might be predominant in the Fe-catalyzed hydrogasification in the temperature region of around 850 K.

CONCLUSIONS

Hydrogasification of brown coal with Cl-free Fe catalysts precipitated from $FeCl_3$ solution using different additives is carried out at ambient pressure. The activity depends strongly on the preparation method and the gasification temperature. The use of urea as an additive seems to give the most effective catalyst at 873 K. The iron prepared with $Ca(OH)_2$ shows the largest rate enhancement at 1073 K, and realizes complete gasification within a short time. The formation of Fe_3C may be related to the catalytic activity in this case.

ACKNOWLEDGMENTS

Ms. Naoko Yoshida and Ms. Naomi Katahira are gratefully acknowledged for their assistance in carrying out experiments. This work was partly supported by a Grant-in-Aid for Scientific Research from the Ministry of Education, Science and Culture, Japan (Nos. 0245082 and 03203204).

REFERENCES

[1] D.W. McKee, *Chem. Phys. Carbon*, **16**, 1 (1981).
[2] Y. Ohtsuka, Y. Tamai, and A. Tomita, *Energy & Fuels*, **1**, 32 (1987).
[3] Y. Ohtsuka and K. Asami, *Ind. Eng. Chem. Res.*, **30**, 1921 (1991).
[4] K. Asami and Y. Ohtsuka, submitted to *Ind. Eng. Chem. Res.*
[5] K. Kaneko, S. Ozeki, and K. Inouye, *J. Chem. Soc. Jpn.*, **1985**, 1351.
[6] M.J. Verra and A.T. Bell, *Fuel*, **57**, 194 (1979).
[7] C.W. Keep, S. Terry, and M. Wells, *J. Catal.*, **66**, 451 (1980).
[8] W.L. Holstein and M. Boudart, *J. Catal.*, **72**, 328 (1981).
[9] E. Keren and A. Soffer, *J. Catal.*, **50**, 43 (1977).

Table 1 Activity and state of Fe catalysts at 873 K.

Sample	Additive	Conv.[a] (wt%)	Chem. form[b]	Size[b),c)] (nm)
Fe(U)	$(NH_2)_2CO$	20	α-Fe	10
Fe(C)	$Ca(OH)_2$	13	α-Fe, (Fe_3C)	28
Fe(A)	NH_3/NH_4Cl	8	α-Fe	45
Original	—	5	—	—

[a]Char conversion after 30 min.

[b]Immediately after devolatilization in H_2.

[c]Average crystallite size of α-Fe.

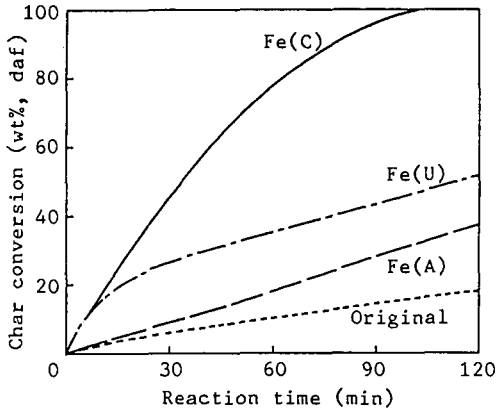

Figure 1 Hydrogasification of Loy Yang coal with iron catalysts at 1073 K.

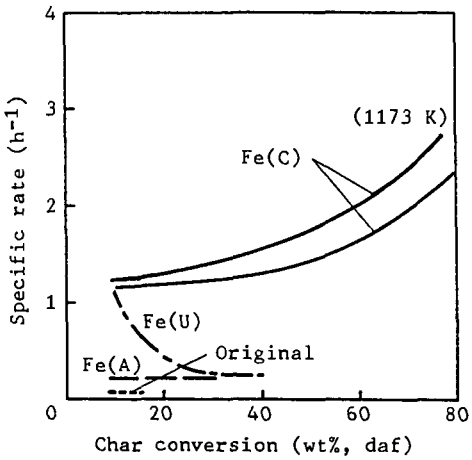

Figure 2 Profiles of specific gasification rates at 1073 K.

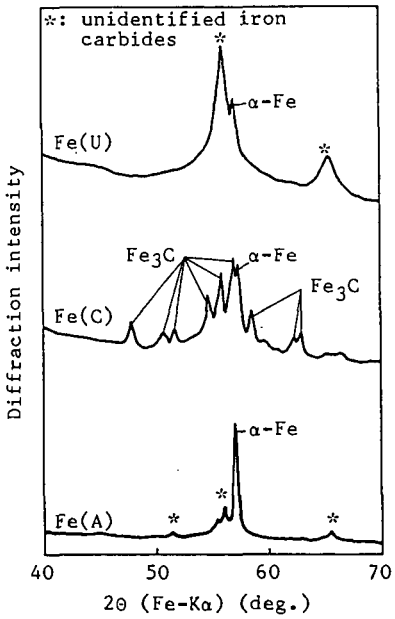

Figure 3 XRD patterns of iron catalysts on the chars devolatilized at 1073 K.

THE CATALYTIC ACTIVITY OF FE/ZSM-5 FOR HYDROCARBON SYNTHESIS AND EXAFS STUDY OF ITS STRUCTURE

Qiwu Wang, Shiqiang Wei and Minming Huang

Department of Modern Chemistry, University of Science and Technology of China, Hefei, Anhui, P. R. China

Keywords: Fe/ZSM-5, Hydrogenation, EXAFS

INTRODUCTION

Hydrogenation of carbon dioxide has been paid more and more attention recently because of its green house effect and for synthesis of hydrocarbons and alcohols[1,2]. Unfortunately, it was observed that carbon dioxide can be converted into only carbon monoxide and methane over the many effective Fisher-Tropsch catalysts. The selectivities forming more than C_2 hydrocarbons and alcohols on them are, if any, very low[3]. In the recent years, Fe, Rh and other catalysts supported on suitable carriers and having some promoters were found to have high selectivities for C_2-C_4 hydrocarbons under high pressures[4,5]. Some studies of adsorption of CO_2 by IR and the catalytical reaction kinetics under different temperatures and pressures were also reported[6,7]. All these researches have given great contribution to develop the catalytic conversion process of carbon dioxide to match the requirement of human environment protection and new energy source.

In this paper it is reported that the Fe/ZSM-5 has good selectivity to C_2-C_4 in the hydrogenation of CO_2 and EXAFS study shows the change of the local environment of Fe on the catalyst during the deactivation process.

EXPERIMENTAL

Preparation of catalysts: The weighed amount of metal nitrate, such as 2.93 g ferric nitrate, was dissolved in water to make a diluted solution in which 5.0 g support, HZSM-5 zeolite, was added. It stands in room temperature for two hrs by frequently stirring and dried at 393K for 10 hrs. The impregnated procursor was calcined at 723K, 2 hrs in flow of 40 ml/min of air, and cooled to room temperature to get the oxidized state of

the catalyst, 7.5% Fe/ZSM-5. It was reduced in a stainless steel reactor in hydrogen at 773K, for 4 hrs before hydrogenation of CO_2.

Hydrogenation: The activity of the catalysts was determined in a flow system at space rate, 6000 ml/g.h with $CO_2:H_2=1:4$ at different temperatures between 500 to 650K and under 1-20 atmospheric pressures. The products were analyzed by a gas chromatographic system with HFD and TCD as detectors for hydrocarbons and the gases.

X-ray absorption: The X-ray absorption experiments were performed on Rigaku, 6KVA anode-rorating X-ray machine. The photon intensity was recorded with a solid detector and TP-801 monitor. All data analysis was carried out with EXAFS program on IBM-PC computer. The fitting was done using experimentally determined Fe-O and Fe-Fe phase shifts and backscattering amplitudes.

RESULTS AND DISCUSSION

1. The effects of supports on activity and selectivities

The same amounts of Fe, such as 15%, were supported on SiO_2, Al_2O_3, HZSM-5, Cr_2O_3, Nb_2O_5 and La_2O_3 individually by impregnation, calcination and then reduction at 773K, in H_2, for 4 hrs. The hydrogenation activity and selectivities were measured in the flow system at 600K, 6000 ml/g.h of the reactant mixture of $CO_2:H_2=1:4$. The activity expressed as the percentage of conversion of CO_2 and the selectivities as percents of the converted CO_2 are listed in Table 1. From the data it can be seen that the properties of supports affect conversion of CO_2 very seriously, HZSM-5 made the Fe catalyst active 50 time more than that on La_2O_3 and the selectivity forming C_2+C_3 can reaches to 33.2% on Fe/ZSM-5, only about 1% on Fe/SiO_2, Fe/Al_2O_3 and Fe/Cr_2O_3 and even nothing on Fe/La_2O_3. The better effect of Nb_2O_5 on the C_2+C_3 selectivities is in agreement with that reported in the literature[8].

2.Loading of Fe on HZSM-5 and its effects on catalytic properties

The results listed in Table 2 indicate that the activity and C_2 and C_3 selectivities gradually increase by loading more and more Fe until 30% on the support. XRD experiments demonstrate that the increasing loading of

Fe resulted in the growing up of Fe particles on the reduced catalysts from 170 to 310Å (average particle diameter) from 5 to 30% Fe on HZSM-5. It can also be seen from Table 2 that the changes of C_2 and C_3 selectivities parallel with each other for loading more Fe and rising reaction temperatures. These results show that the metal Fe surface plays the main role in the hydrogenation of carbon dioxide and for growing of the C-C chains. In this particle size range, the larger, the particle of metal Fe, the better, the catalytical reactivity.

3. The effects of some promoters

Addition of 2.5% Cu, Ni, Ru, Rh, Co, the easily reduced metals to 15%Fe/ZSM-5 increase the activity and C_2, C_3 selectivities at high reaction temperatures. At 650K the conversion of CO_2 reached 30.1% over Fe-Ru/ZSM-5 and CO, CH_4, C_2, C_3 and C_4 selectivities are 30.5, 27.7, 20.8, 14.0 and 7.0 respectively, that is, hydrocarbons become the main products, $C_2+C_3+C_4$, 41.8% besides 27.7% CH_4 and CO only 30.5%. Promoter, Ni lets methane to be the main hydrogenation product, 51.5% in 4.1% converted CO2 at 550K. However at 650K, C_2+C_3 hydrocarbons reach to 21.7% , methane 22.9% and CO, 45.4% in 31.5 % converted CO_2. As shown in the author's TPR experiments[9], Ni and Ru could move the reduction peak temperatures of Fe_2O_3 to the lower positions, that is, they could promote the reduction of Fe to metal state which is necessary to catalytical hydrogenation of CO_2 over Fe catalysts.

Na_2O and MgO and other alkaline and alkaline earth metal oxides can increase a little bit of the hydrogenation activity, however, decrease the C_2 selectivity. They can inhibit the growing of C-C chain making methane as the main products[10].

The transition metal oxides, such as V_2O_5, MoO_3 and Cr_2O_3 decrease both the hydrogenation activity and C_2, C_3 selectivities a lot at low reaction temperatures. In comparison with Fe/ZSM-5, these promoted catalysts have great temperature dependence. At 650K they have a comparable activity to that over Fe/ZSM-5 except the lower selectivities. These phenomena could be related to the inhibition effect to reduction of FeO and this effect would decline at the temperatures as higher as 650K.

4. Stability of the catalysts

In Fig.1 the hydrogenation activity and C_1, C_2 and C_3 selectivities on Fe/ZSM-5, Fe-Cu/ZSM-5, Fe-Ru/ZSM-5, Fe-Cr/ZSM-5 and Fe-Cu-Ru/ZSM-5 were plotted against the reaction time. Although the initial activities on Fe/ZSM-5 and Fe-Cu/ZSM-5 are very high and reach the maxima after 1 hour, they drop very quickly later. After 5 hrs, the selectivities forming C_1, C_2 and C_3 gradually decrease to the lowest values. On the contrary, the effect of Ru is very interesting. Over Fe-Cu-Ru/ZSM-5 the selectivities of C_2 and C_3 keep increasing with reaction time at expense of that of methane when the conversion of CO_2 gradually increases to a stable level, around 10%. After 10 hrs, selectivities of C_1, C_2 and C_3 reach to 38.o, 19.0 and 16.5% respectively. It seems that the active centers which favor to growing of C-C chains were formed with reaction time instead of that for methane. The co-promoters, Cu-Ru, make Fe-Cu-Ru/ZSM-5 the best hydrocarbon synthesis catalyst from CO_2 and H_2 under our experimental conditions.

5. EXAFS study of the structure of the catalysts

EXAFS as a powerful tool has been widely used for study of the structure of catalysts.[12] The data obtained by fitting the filtrated $k^2.x(k)$ with models of Fe-C and Fe-Fe for the Fe local environments of different catalysts at the different reaction times are listed in Table 3. The Radial Structure Functions (RSF) of Fe in Fe/ZSM-5 catalyst measured after 0.5, 2.0 and 24h are shown in Fig.2. It can be seen from Table 3 that the new Fe-C coordination was formed in the deactivated Fe- and Fe-Cu catalysts, the coordination numbers of nearest Fe around Fe centers decrease with time from 7.5 and 8.5 (0h) to 2.5 and 3.0 (24h) and a farther Fe-Fe formed.

From Fig.2 we can see that the peak height of Fe-Fe obviously decrease with time if we know the different Y-scales in the three figures from 40 (0h) to 20 (24h) being used and the large noise level in the third figure. The Fe-Fe interaction was interrupted by the carbon atoms which enter between iron atoms and some kind of Fe-C species are formed owing to the deposit of the carbon atoms on the surface during the reaction process. All these caused the deactivation of the catalysts. On Fe-Cu-Ru/ZSM-5, Fe-Fe coordination number almost does not change comparing 7.0 after 24h to 7.5 for 0h Fe/ZSM-5 and at the same time only 0.4 carbon atoms approach to Fe atoms on Fe-Cu-Ru/ZSM-5 comparing 2.5 on Fe/ZSM-5. It is known that Cu can inhibit the deposit of inactive carbon on Fe surface[13]. The better activity and stability of the Fe-Cu-Ru/ZSM-5 than

that of the others can be explained from the viewpoint of the local structure of Fe on the catalysts by EXAFS study.

Reference

1. Solymosi, F., Erdohelyi, A. & Bansagi, T.; J. Cattal., 68, 371 (1981)
2. Nozaki, F., Sodesawa, T. Satoh, S. & Kimura, K., J. Catal.,104, 339 (1987)
3. Rehmat, A. & Randhava, S. S., Ind. Eng. Chem. Prod. Res. Develop., 9, 512 (1970)
4. Lee, M. D., Lee, J. E. & Chang, C. S., Bull. Chem. Soc. Japan, 62, 2756 (1989)
5. Trovarelli, A., Mustazza, C. & Dolcetti, G., Appl. Catal., 65, 129 (1990)
6. Solymosi, F. & Knozinger, H., J. Catal., 122, 166 (1990)
7. Peebles, D. E., Goodman, D. W. & White, J. M., J. Phys. Chem., 87, 4378 (1983).
8. Weatherbee, G. D. & Bartholomew, C. H., J. Catal., 68, 67 (1981)
9. Wei, S., Huang, M., Chen, S., Rong, J., Wang, Q. & Yang T., Chinese J. Chem. Phys. 4, 303 (1991)
10. Comphell, T. K. & Falconer, J. L., Appl. Catal., 50, 189 (1989)
11. Stockwell, D.M., Bianchi, D. & Bennett, C. D., J. Catal., 113(1988)
12. Wang, Q. & Wei S., J. Petrochemistry (Chinese)20, 500 (1991)
13. Anderson, R.B., "Catalysis IV", Chapter 2, ed. Emmett, P. H.,Reinhold Pub.Corp. (1956)

Table1 Effects of Supports on the Activity and Selectivities

Support	Conv. %	Selectivity, % CO	CH_4	C_2	C_3	C_2+C_3
SiO_2	2.3	89.9	8.9	1.2	0.0	1.2
Al_2O_3	6.4	98.0	1.4	0.4	0.1	0.5
HZSM-5	15.1	43.6	23.2	14.8	18.4	33.2
Cr_2O_3	5.2	92.2	6.5	1.0	0.3	1.3
Nb_2O_5	5.4	74.6	17.9	4.3	3.2	7.5
La_2O_3	0.3	95.2	4.7	0.0	0.0	0.0

Table 2 The Effects of Loading of Fe

Content %	Temp. K	Conv. %	Selectivity % CO	CH_4	C_2	C_3	C_4
1.0	600	1.5	97.0	3.0	0.0	0.0	0.0
	650	5.1	98.8	1.0	0.2	0.0	0.0
5.0	550	1.8	82.0	16.4	1.6	0.0	0.0
	600	6.4	83.7	12.4	3.1	0.8	0.0
	650	11.5	88.8	8.5	2.4	0.3	0.0
7.5	550	2.5	76.8	17.9	2.3	1.2	0.5
	600	6.8	73.1	16.8	5.3	2.6	0.7
	650	5.5	71.5	14.9	6.7	3.2	0.2
15.0	500	1.2	85.0	12.0	2.0	1.0	0.0
	550	3.9	60.0	21.6	6.8	7.6	6.4
	600	5.1	43.6	23.2	14.8	12.0	6.4
	650	30.5	65.1	16.0	9.6	6.8	1.9
30.0	500	1.5	79.6	9.6	3.4	5.4	2.0
	550	5.3	67.3	13.5	5.7	5.6	7.9
	600	25.7	42.6	17.4	13.0	12.8	14.2
	650	39.4	53.8	16.7	12.0	11.4	6.1
60.0	500	3.0	82.9	12.3	1.7	1.7	1.4
	550	11.9	58.5	15.7	8.4	10.5	8.9
	600	27.7	36.9	16.9	11.9	16.7	17.6
	650	35.7	63.2	14.5	9.4	8.3	4.6

Table 3 EXAFS Results of the Catalysts

Catalyst	Bond		Reaction Time (h) 0.0	0.5	2.0	24
15%Fe	Fe-C	R		2.00	2.00	1.90
		CN		0.5	1.5	2.5
	Fe-Fe	R	2.49	2.51	2.55	2.48
		CN	7.5	6.0	5.0	2.5
	Fe-Fe	R			2.60	2.65
		CN			2.5	3.8
15%Fe,10%Cu	Fe-C	R		2.00	2.00	1.87
		CN		0.7	1.5	2.0
	Fe-Fe	R	2.50	2.52	2.50	2.48
		CN	8.5	7.5	4.0	3.0
	Fe-Fe	R			2.60	2.65
		CN			2.5	5.0
15%Fe,10%Cu 2.5%Ru	Fe-C	R			2.00	2.00
		CN			0.3	0.4
	Fe-Fe	R			2.5	2.5
		CN			8.0	7.0

Notes: All catalysts were supported on HZSM-5. The unit of R is Å. CN-coordination number.

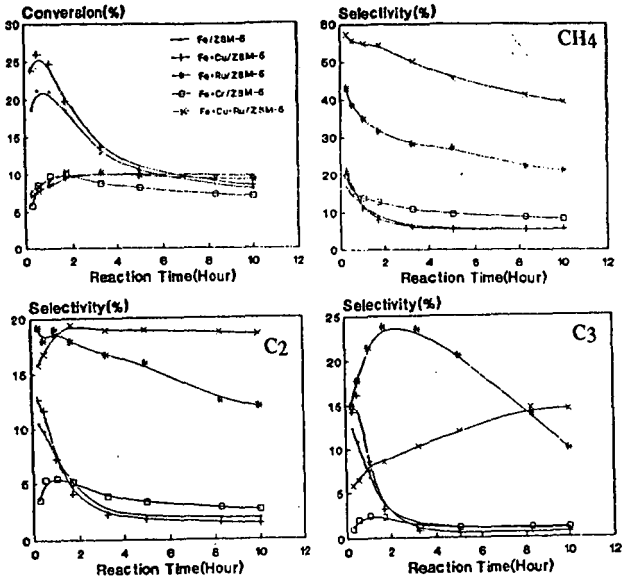

Fig.1 The relationship between the hydrogenation activity, selectivities and reaction time over several catalysts.

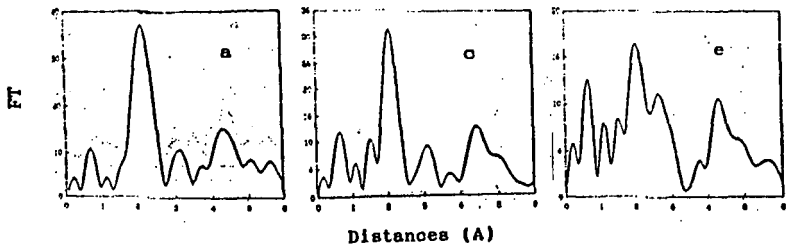

Fig.2 The RSFs of Fe measured at different reaction time. a-0.5h, c-2h and e-24h. The main peak at around 2.5Å is from the Fe-Fe coordination in Fe/ZSM-5.

USE OF ACTIVATED COAL CHAR FOR REMOVAL OF VOLATILE ORGANIC COMPOUNDS FROM WATER

P .J. Beaulieu, S .M. Fatemi, and J .B. Tumidalsky, Analytical Research and Services Division, Amoco Research Center, Box 3011, Naperville, Illinois 60566,
and
C. W. Kruse, M. Chou, and C. Feizoulof, Illinois State Geological Survey, 615 East Peabody Drive,Champaign, Illinois 61820.

Keywords: char, environmental, adsorption, mild gasification, coal

INTRODUCTION

Mild gasification is an alternative to traditional coal burning for coal utilization. Mild gasification produces gas, liquid, and substantial quantities of coke. Coal liquid and gas are being studied as alternatives to petroleum and natural gas, as sources of chemical feedstocks and fuels. This project concentrates on an alternate use for the solid coke, upgrading it to a higher value product, an activated char, and use for sorption of pollutants.

Activated charcoal is conventionally produced from a source such as coconut husk. We reported earlier on the conversion of coke to activated char by a process of controlled oxidation (1). There is a large market for activated charcoal as a sorbent for removal of organic compounds from water supplies and industrial outfalls. Presently, activated charcoal for this purpose is priced at more than $1,000/ton. If coal char can successfully compete in this arena, the value of the coke would be upgraded dramatically, and the economics of coal utilization changed substantially. In this paper, we report on successful testing of activated coal char under laboratory conditions as a sorbent for removal of volatile organic compounds from deionized water.

Organohalogens are common environmental pollutants. We reported earlier that activated coal char catalytically promoted dehydrohalogenation and other elimination reactions, producing olefins (2-5). If an overall process of sorption of organic compounds from water and their catalytic decomposition and conversion to more useful or less noxious compounds can be demonstrated, it would represent an advantage for coal derived char over other charcoal types. Last minute results of experiments testing for decomposition of previously sorbed compounds will also be reported, if ready in time for the meeting.

EXPERIMENTAL

Experimentation consisted of preparation of activated char from coal, equilibration with deionized water containing 37 organic compounds, and GC-MS analysis to measure the amounts of these compounds remaining in the water at the end of the sorption period. Details follow below.

Preparation of Coal Char Activated coal char was prepared from a blend of Illinois #5 (Springfield) and Illinois #6 (Herrin) coals using the following method. The starting material was char from a United Coal Company pilot scale, fixed bed, mild gasification reactor. This material was further devolatilized using a fluidized bed reactor at ISGS, heating in an atmosphere of pure nitrogen at a rate of 20°C/min, and holding a final temperature of 500°C for 15 minutes. After characterization, steam treatment followed. The material was heated at a rate of 20°C/min to 870°C in pure nitrogen. The atmosphere was changed to 50% steam in nitrogen, and conditions held constant for 3 hours to increase porosity. After characterization, mild oxidation followed. The material was heated at 20°C/min to 450°C in pure nitrogen. The atmosphere was changed to 10% oxygen in nitrogen, and conditions held constant for 15 minutes to activate the surface. This product, which had a surface area of 557 meter^2/gram, was used for the sorption studies described below.

Sorbates. A methanolic stock solution of 37 analytes, each at 1000 ppm, was purchased from a vendor of environmental analytical standards (Accustandard). Components are listed in Table I. This solution contains most of the volatile organic compounds (VOC) for which federal and state discharge permits usually require screening. These are also known as VOA, for volatile organic analytes. Portions of this stock solution were injected (spiked) into water as described in the experiments detailed below.

Equilibration Experiments. Samples of char were covered with deionized water, and were either spiked immediately with the stock solution (Experiment 1), or spiked after a four hour conditioning period during which the char equilibrated with the unspiked water (Experiment 2). After spiking, the char was equilibrated with the spiked water for 20 hours (Experiments 1 & 2). Sampling of the water layer for GC-MS analysis followed. To do Experiment 3, several refilled samples from Experiment 2 were used. A second 20 hour equilibration and second GC-MS analysis followed. Experimental details follow.

Experimental Details. A sample of char (either 0.100 gram or 1.00 gram) was placed in a precleaned glass 40 milliliter environmental water sample vial (VOA vial). A second vial was designated immediately as control. Each was filled with deionized water and sealed immediately with its teflon faced septum screw cap. After the unspiked conditioning times described above, each vial was opened momentarily in turn, and a syringe (or glass micropipette) used to add a spike volume (0.002 to 1.00 milliliter) of the sorbate solution to each, injecting it well below the water surface. Taking care to exclude bubbles, the vial was resealed immediately and was mixed by inverting several times.

After the 20 hours spiked equilibration, the vials were sampled for GC-MS analysis. The deionized water needed for a dilution was placed in a VOA vial. Each vial was opened momentarily, and the volume for analysis removed. Except for the vials spiked with the smaller volumes, the aliquot taken was that required to prepare a diluted solution approximating 125 ppb in concentration. The volume was removed either by syringe (or glass micropipette) or by decanting and weighing (when the desired volume exceeded 5.00 milliliters). When a syringe (or glass micropipette) was used, this aliquot was injected below the surface of the deionized water in the analysis vial. When decanted, it was poured without vortex into the water in the analysis vial. For Experiment 3, the water volume removed for the GC-MS analysis in Experiment 2 was immediately replaced with fresh deionized water. The vials were immediately resealed, and equilibrated for 20 hours more. No makeup spike was added. This brought the cumulative equilibration time for Experiment 3 to 40 hours before the second sampling. Immediately after adding the sampled aliquot to the analysis vial, 0.080 milliliter of the internal standard and surrogate solution described below was added by micropipette, the vial topped up with deionized water, resealed and mixed. The resulting solution was analyzed by GC-MS as described below.

Internal Standard Solution. A combination solution of three internal standards (20 ppm each) and three surrogate analytes (25 ppm each) was prepared by diluting methanolic stock solutions (Accustandard, Supelco, or other vendor). High purity methanol was used as solvent. Internal standards are used as GC-MS references, for locating the chromatography peaks of the analytes, and for calculation of concentrations of analytes present. Surrogate analytes are used to ascertain that the GC-MS analysis and calculation methods are in control. Compounds used as internal standards and surrogates are listed in Table II.

Method of Analysis. Concentrations of the volatile analytes remaining in solution were measured by Purge and Trap GC/MS, using an automated version of EPA Method 8240, as was specified by EPA for analysis of waste water regulated under the Resource Conservation and Recovery Act (3). This method is largely the same as the earlier EPA Method 624 for sites regulated under the Clean Water Act (4). The analysis vials prepared as described above were placed in an autosampler, where they were held until a 5 milliliter volume was transferred automatically to the purge and trap device (OI Analytical 4460A). Helium was used to purge the volatile organics from the room temperature water sample, transferring the organic vapors to a multilayer (OV-1, Tenax, Silica Gel, Activated Charcoal) trap where they were held for analysis by GC-MS. On signal from the GC, the organic vapors were thermally desorbed and transferred to the GC, which was equipped with a 2 meter glass column (1% SP-1000 on 60-80 mesh Carbopack B). The temperature programmed GC sequentially eluted the components to the mass spectrometer over a period of about 40 minutes. The mass spectrometer was a Finnigan 4500 quadrupole instrument operating in the EI, positive ion, full scan mode. Scan time was 2 seconds, mass range 34 to 340 M/Z, and tuning was to EPA specifications for the spectrum for bromofluorobenzene.

Standard Finnigan peak search software was used to locate the chromatogra-

phy peaks, integrate the EPA recommended quantitation ion for each compound, and calculate results. To calculate results, the peak area for the analyte and that for the internal standard eluting nearest the analyte peak were obtained for a series of 5 calibration standards in the range 10-200 ppb. Relative response factors ("RRFs", relating analyte area, analyte concentration, internal standard area and internal standard concentration) were calculated. EPA statistical quality control requirements were followed in evaluating the analytical range, establishing initial average RRFs, and then for checking and updating the response factors to be used for calculation on a daily basis. Concentrations were then calculated in the analysis solutions using the library of daily RRFs.

GRAPHICAL PRESENTATION OF RESULTS

Most peaks for the 37 analytes were resolved, either by effective GC separation, or by identification of a unique quantitative mass. However, in the case of two peaks, each of which contained two isomers, resolution was not possible. This resulted in 35 calculated data points to be reported for each solution, including the sum peaks for the isomeric pairs. In addition to the 35 analytes, the three surrogate compounds were determined in the same manner. The amount of methanol was not determined. A value for the amount of each analyte (the ith analyte) sorbed on the char was calculated as a percent, relative to the matching control solution, using the equation:

$$\textbf{Percent Sorbed}_i = 100 \times \frac{[\textbf{Concentration}_i \textbf{ in Control} - \textbf{Concentration}_i \textbf{ in Sample}]}{\textbf{Concentration}_i \textbf{ in Control}}$$

A typical component is illustrated in Figure I, where the data for benzene are shown. A total of 35 similar graphs resulted from the data processing. Several more graphs will be presented at the meeting, as germane to a discussion of the slight differences between sorption properties of the individual components and classes of components.

However, it proved easier to contrast and compare the data after further manipulation. The Average Percent Sorption was calculated for each sample from the percent sorption for the individual analytes in each sample/control pair. Average sorptions are shown in Figure II.

$$\textbf{Average Percent Sorption} = \frac{\sum_{i=1}^{35} \textbf{Percent Sorbed}_i}{35}$$

Figure III shows the relative strength of sorption listed by component. The sorption for benzene can be seen to closely resemble the average sorption. This was seen earlier by comparison of Figure I and Figure II, but the comparison is easier when Figure III is considered. This data for construction of Figure III was obtained by further calculation. Using the sample average sorption described for Figure II, the relative strength of sorption for each (that is, the ith) component in each sample was calculated using the equation:

$$\textbf{Relative Sorption Strength}_i = [\textbf{Percent Sorbed}_i - \textbf{Average Percent Sorption}]$$

The average relative sorption strength for this (the ith) component in for all (j = 17) samples was then calculated and plotted in Figure III.

$$\textbf{Average Relative Sorption}_i = \frac{\sum_{j=1}^{17} \textbf{Relative Sorption Strength}_i}{17}$$

In Figure III, the analytes are listed alongside a bar graph representing the average sorptions of the analytes for all experiments. The analytes which sorb best are to the left of the vertical line. The center of the bar represents the average sorption over all experiments, the length of the bar is a measure of the precision (each bar is 2 standard deviations in length).

DISCUSSION AND CONCLUSIONS

Fresh, dry Activated coal Char can be seen to have sorbed the analytes, with efficiencies improving at lower concentrations. Some individual analytes proved to be more strongly sorbed than others, and the strong sorbency persisted to higher concentrations.

The average results for Experiment 1, as presented in Figure I, will be considered first. In experiments at or below at 100 micrograms of each analyte per gram of char, removal was essentially complete for most analytes (96% sorption at the lowest concentration level studied, 50 ppb, leaving a concentration of only 2 ppb in solution). Above 100 micrograms of each analyte per gram of char, performance degraded. In the experiment at 5000 micrograms of each analyte per gram of char, removal of the sorbates from solution was largely incomplete (approximately 60% of all 35 analytes, at an aqueous concentration of 25 ppm, leaving 10 ppm in solution).

Results for the second (pre-soaked) experiment proved somewhat more variable and the char somewhat less effective. Most of the samples showed lower sorptions (for the same spike amount) than in the case of samples which were not pre-soaked. Two exceptions were noted to lie closer to the line representing the first experiment. These two are believed to represent samples which still contained entrained air. Note was not taken of samples which did not sink, and thus might still contain air, since this was not known to represent an important variable at the time. For the several samples refilled with deionized water, and allowed to reequilibrate with the spiked solutions, the amounts of each analyte sorbed increased.

Since presoaking with water was observed to degrade performance of the char somewhat, it is proposed that water binds active sites which would otherwise be available to the analytes. A hidden component, methanol, is probably also sorbing on the char, occupying active sites. If methanol is also sorbing, the total capacity of the char for organics is then probably much higher than the sum of the 37 analytes, but further work will be needed to measure the total capacity.

Kinetics have not been characterized at this point. In the presence of presoaked char, at a spike level of 50 micrograms of each analyte per gram of char, sorption appears to be approximately 60% complete in 20 hours and increases to the about 75% in 40 hours. Since the 40 hour equilibration never produced sorptions higher than those produced by the 20 hour equilibration with dry char, it is possible that the sorption is essentially complete by 20 hours in the presence of dry char, but further experimentation will be required to be certain.

In summary, activated coal char appears to be an effective sorbent for VOCs, but the equilibrium is displaced somewhat and/or the sorption rate slowed by presoaking the char in water.

References:

1. C. W. Kruse, L. M. Lytle, M. Rostam Abadi, M. Chou, and Feizoulof (ISGS); S. M. Fatemi, J. A. Mahoney, P. L. Beaulieu, and J. O. Schreiner (Amoco) Annual Technical Report to the Center for Research on Sulfur in Coal, 1991. **Upgrading Mild Gasification Char: Evaluation of Oxidized Char as a Catalyst**
2. C. W. Kruse, G. C. Ray, U.S. Patent 3,240,834 Mar. 15, 1966.
3. J. E. Mahan, R. E. Reusser, C.W. Kruse, U.S. Patent 3,352,935 Nov.14 ,1967.
4. C.W. Kruse, U.S. Patent 3,437,695 Apr. 8, 1969.
5. C. W. Kruse, M. I. M. Chou, C. Feizoulof (ISGS); S. M. Fatemi, P. L. Beaulieu, J. O. Schreiner (Amoco); Vol 37#2, 556-563, 1992. 203rd ACS National Meeting, San Francisco, CA. **Evaluation of Oxidized Char as a Catalyst - I. Characterization**
6. United States Environmental Protection Agency; Office of Solid Waste & Emergency Response, Washington, D.C. 20460, November, 1986. **SW-846 Test Methods for Evaluating Solid Waste; Laboratory Manual; Physical/Chemical Methods; Volume IB; Third Edition.**
7. 40 CFR Part 136, United States Environmental Protection Agency **Guidelines Establishing Test Procedures for the Analysis of Pollutants.**

TABLE I. COMPONENTS OF SPIKE SOLUTION
(each at 1000 Micrograms/Milliter, Except Methanol = Balance)

	HALOGENATES	
C-1	C-2 (Unsatd.)	C-3 (Unsat'd.)
Chloromethane	1,1-Dichloroethene	Vinyl Chloride
Bromomethane	Cis-1,2-Dichloroethene	Cis-1,3-Dichloropropene
Methylene Chloride	Trans-1,2-Dichloroethene	Trans-1,3-Dichloropropene
Bromodichloromethane	Trichloroethene	
Dibromochloromethane	Tetrachloroethene	
Chloroform		
Bromoform	C-2 (Satd.)	C-3 (Sat'd.)
Carbon Tetrachloride	Chloroethane	1,2-Dichloropropane
	1,1-Dichloroethane	
	1,2-Dichloroethane	
	1,1,1-Trichloroethane	
	1,1,2-Trichloroethane	
	1,1,2,2-Tetrachloroethane	
	OXYGENATES	
Methanol (Solvent)	Acetone	
Vinyl Acetate	Methyl Ethyl Ketone (2-Butanone)	
	4-Methyl-2-Pentanone (MIBK)	
	2-Hexanone (MBK)	
	AROMATICS	
Benzene	Ortho-Xylene	Styrene
Toluene	Meta-Xylene	Chlorobenzene
Ethylbenzene	Para-Xylene	
	MISCELLANEOUS	
Carbon Disulfide		

TABLE II. COMPONENTS OF INTERNAL STANDARD & SURROGATE SOLUTION

	SURROGATES	
1,2-Dichloroethane-D4	Toluene-D8	4-Bromofluorobenzene
	INTERNAL STANDARDS	
Bromochloromethane	2-Bromo-1-Chloropropane	1,4-Dichlorobutane

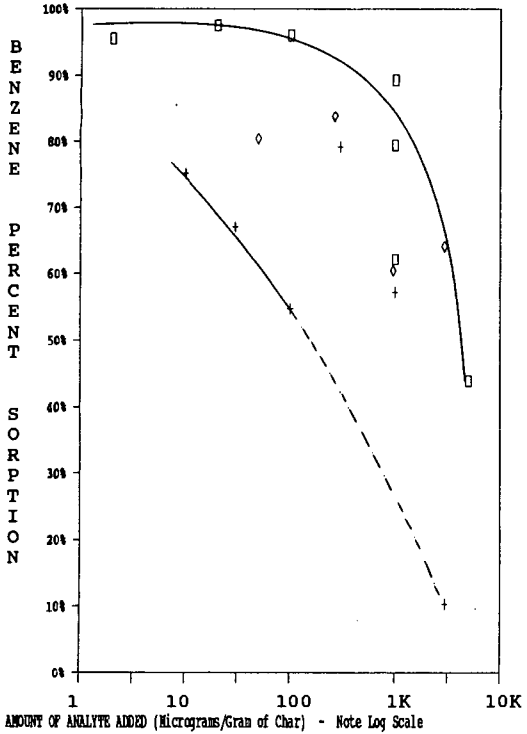

FIGURE I. EFFECTIVENESS OF ACTIVATED COAL CHAR FOR REMOVAL OF BENZENE FROM WATER
[] Experiment 1. + Experiment 2. ◇ Experiment 3.

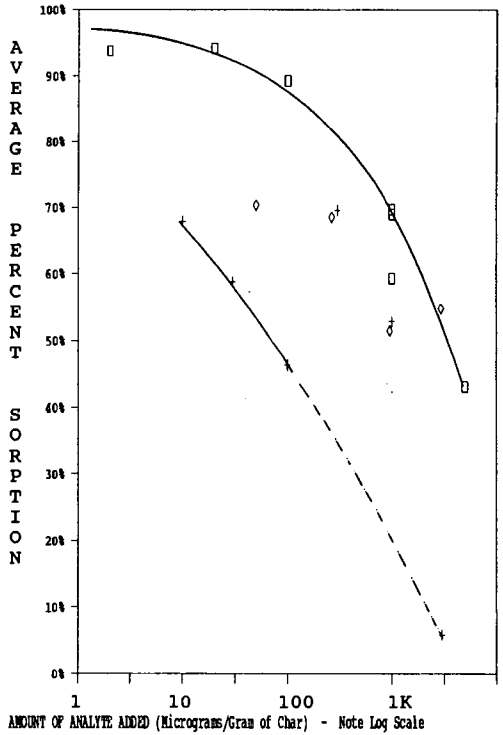

FIGURE II. EFFECTIVENESS OF ACTIVATED COAL CHAR FOR REMOVAL OF VOC FROM WATER
[] Experiment 1. + Experiment 2. ◇ Experiment 3.

FIGURE III. AVERAGE RELATIVE STRENGTH of SORPTION LISTED by COMPONENT

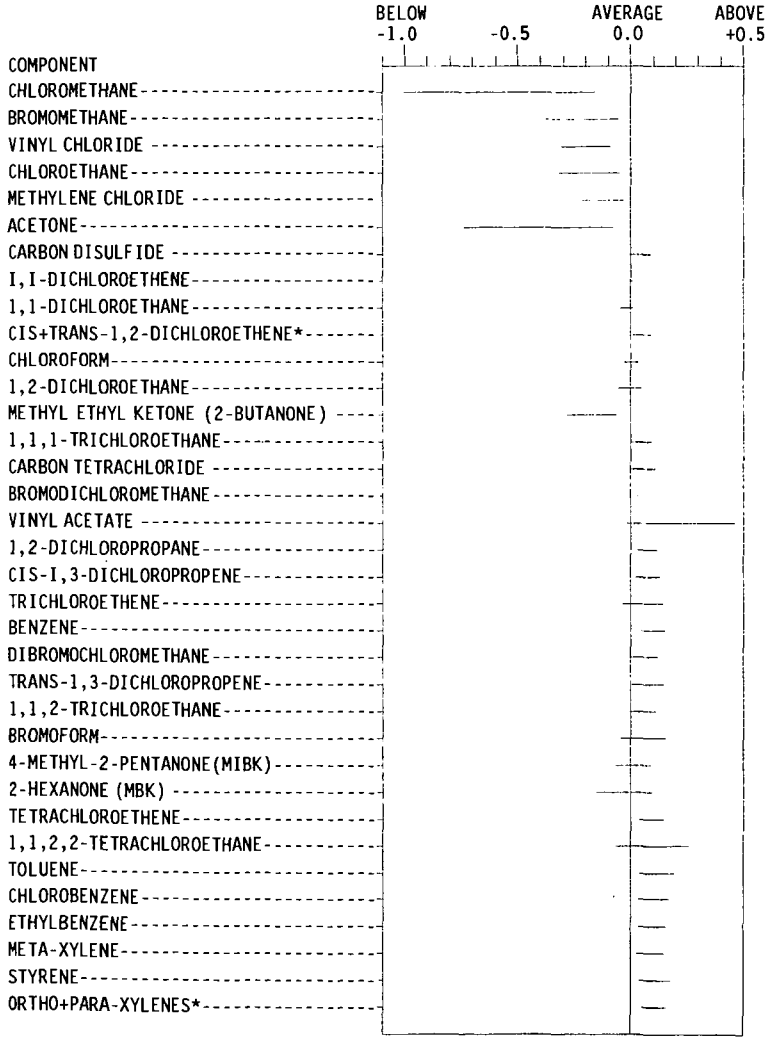

* Coeluting Pair, quantified as single component

CATALYTIC COAL GASIFICATION IN A DRAFT-TUBE SPOUTED BED BY USING CERAMIC PARTICLES AS A THERMAL MEDIUM

Yoshimitsu Uemura, Masahiko Miyauchi, Shigeho Tanaka, Kazuya Ijichi, Yasuhiko Tanaka, Desmond F. King* and Yasuo Hatate
Department of Applied Chemistry and Chemical Engineering, Kagoshima University, Kohrimoto, Kagoshima 890, Japan
* Chevron Research & Engineering Company, 100 Chevron Way, Richmond, 94802 California, USA

Keywords: Coal, Gasification, Spouted bed, Draft tube, Ceramic

INTRODUCTION

Steam gasification of coal is thought to be an important future process for production of hydrogen, which is a nonpolluting energy. We have proposed a draft-tube spouted bed type reactor as a catalytic coal gasifier to produce hydrogen.(1) Some minor modifications have been applied to concept of the gasifier. The schematic diagram of the gasifier is illustrated in Fig. 1. In this apparatus, coal is fed to the devolatilization zone in the annulus section. After devolatilization, the char falls into next zone and is gasified by steam supplied from bottom conical section. The heat of gasification is supplied mainly from circulating ceramic particles, which obtains thermal energy from burning gas within the draft tube and returns to the annulus top.

In previous studies (2,3), cold model experiments were carried out by using an acrylic cylindrical apparatus and by using an acrylic semi-cylindrical one. From the results, flow regimes in a spouted bed with a draft tube were clarified, and several correlations concerning the annulus gas velocity and particles circulation rate were proposed for each flow regime. In next step (4), a cold model apparatus, which has the same dimensions as those of the hot model apparatus used in this study, was constructed and was employed to obtain basic data for the hot model operation.

In this paper, we present the results obtained by operating a hot model apparatus of a spouted bed with a draft tube at 1073 K. The hot model unit was heated by electric furnace in the present study, while the unit was designed in consideration of mass and heat balance.

EXPERIMENTAL

Catalytic steam gasification was carried out in a spouted bed with a draft tube shown in Fig. 2. Figure 3 is the photograph of the unit. The bed was heated by four pieces of electric furnace, which surrounded the bed as shown in Fig. 4. The unit includes a stainless steel spouted bed (150 mm I.D.) with a stainless steel coaxial draft tube (10.9 mm I.D.). The draft tube spacing above the gas inlet nozzle (10.9 mm I.D.) was 3 mm. Air was introduced from the nozzle to spout and recirculate solid particles. The bottom of the column was a conical section with a cone angle of $\pi/3$ rad. Steam was introduced through 40 holes (2.0 mm in diameter) located in the conical section. Figure 5 shows the top view of the bottom conical section before assembly. Steam inlet holes (20x2) are found to be arranged concentrically on the conical section. Draft tube was assembled as shown in Fig. 6.

Table 1 shows the physical properties of ceramic particles and coal particles before devolatilization. The ceramic particles (thermal medium) were Nikkato YTZ ball (95% ZrO_2 and 5% Y_2O_3). The char particles were obtained by the following treatment of a bituminous coal of Alaska (Table 2). A sieved fraction of 14 to 20 mesh (average diameter = 1015 μm, Table 1) coal was impregnated with potassium carbonate (gasification catalyst) aqueous solution at room temperature for 3 h. The slurry of the coal was dried up by a rotary evaporator at 323 K. The coal was devolatilized by a fluidized bed (15.5 cm I.D.) at 1123 K for 7 min. The charged amounts of coal were 1.15 kg and 2.08 kg, respectively. Nitrogen (superficial gas velocity at 1123 K = 1.0 cm/s) was used as the fluidizing gas. The catalyst content was 3.4 meq-K/g-char. The minimum fluidizing velocity of the char was 0.79 cm/s at 1073 K.

Table 1 Characteristics of solid particles

solid particles	average diameter [μm]	particle density [kg/m^3]	bulk density [kg/m^3]	terminal velocity [m/s]	minimum fluidizing velocity [m/s]
ceramic	500	6.0×10^3	3.7×10^3	7.1	0.48
coal	1015	1.2×10^3	7.2×10^2	4.9	0.41

Terminal velocity was calculated. Others were measured.
Terminal velocity and minimum fluidizing velocity are the values at 298 K.

Table 2 Composition of bituminous coal

ash [%]	VM [%]	FC [%]	fuel ratio	elementary analysis [%] S	C	H	O	N
8.7	42.2	35.0	0.83	0.02	62.9	4.5	21.3	0.9

mineral [%] Al_2O_3	SiO_2	Fe_2O_3	CaO	MgO	Na_2O	K_2O	TiO_2	SO_3	P_2O_5	MnO	V_2O_5
14.9	42.3	5.98	23.3	3.42	0.58	1.16	0.85	4.95	0.14	0.24	0.01

The ceramic particles (4.5 kg) were packed into the annulus section. The air was sent through an air filter, an air-oil separator, and an orifice meter before entering the bottom of the bed. The air feed rate was varied to maintain the linear gas velocity within the draft tube as constant (ca. 30 m/s) as possible. Steam was supplied from a vaporizer. The feed rate was controlled by an electric power supply. The particles flowed down through the draft tube spacing above conical section, and were conveyed vertically in the draft tube. At the top, the particles were separated from the carrier gas by a cyclone and returns to the annulus. The temperature of the bed was elevated to 1073 K under spouting by air. As the temperature reached 1073 K, continuous char-feed (0.16 g/s) was started by a rotary feeder. The gasification operation was carried out for 30 min under the conditions summa-

rized in Table 3.

Table 3 Experimental conditions

Gasification temperature	980-1100 K
Packed amounts of ceramic particles	4.5 kg
Circulating rate of ceramic particles	$5x10^{-3}$ kg/s
Feed rate of char	$1.6x10^{-4}$ kg/s
Feed rate of air	2.8 N-m^3/h
Feed rate of steam	0.99 N-m^3/h
Tube-cone clearance	$3x10^{-3}$ m

RESULTS AND DISCUSSION

Figure 7 shows the results of temperature and gas composition. The annulus bed temperature decreased with time, while the external temperature (between upper and lower jacket heater) was maintained at almost constant temperature (990 K). This means poor thermal conduction within the moving bed of the annulus. The gaseous products were hydrogen, carbon monoxide, carbon dioxide and methane as shown in Fig. 7. Hydrogen and carbon monoxide were major products. Since the ratio is unity approximately, the following reaction is thought to be major.

$$C(char) + H_2O \rightarrow CO + H_2$$

The molar rate of ($CO+CO_2+CH_4$) produced was about $7x10^{-3}$ mol/s during the gasification operation. About half of the product gas was exhausted from the outlet of the annulus. Another half was exhausted from the cyclone. Carbon feed rate was $8.5x10^{-3}$ mol/s, which was calculated from the char feed rate, 0.16 g/s, and carbon content of the char, 64wt%. From these values, we obtained the carbon conversion, ca. 80 %.

The experimental data shows that the draft-tube spouted bed type gasifier is superior to product hydrogen, while poor thermal conduction is a significant problem. Another problem is the bypassing of the product gas to the cyclone.

REFERENCES

1. Hatate, Y.; Uemura, Y.; Churei, S.; Imamura, S.; Ijichi, K.; Tanaka, Y. and King, D.F., Proceedings of Second Asian Conference on Fluidized-Bed and Three-Phase Reactors, 1990, 45.
2. Uemura, Y.; Churei, S.; Miyauchi, M.; Imamura, S.; Ijichi, K.; Tanaka, Y.; King, D.F. and Hatate, Y.,"Circulating Fluidized Bed Technology III", Pergamon Press, 1991, 645.
3. Hatate, Y.; Uemura, Y.; Churei, S.; Miyauchi, M.; Ijichi, K.; Tanaka, Y. and King, D.F., Conference Papers Fourth China-Japan Fluidization Symposium, 1991, 236.
4. Uemura, Y.; Miyauchi, M.; Tanaka, S.; Usukubo, M.; Ijichi, K.; Tanaka, Y.; King, D.F. and Hatate, Y., Proceedings of Third Asian Conference on Fluidized-Bed and Three-Phase Reactors 1992, 45.

Figure 1. Schematic diagram of gasifier.

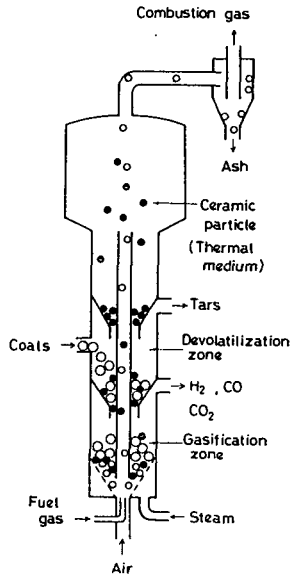

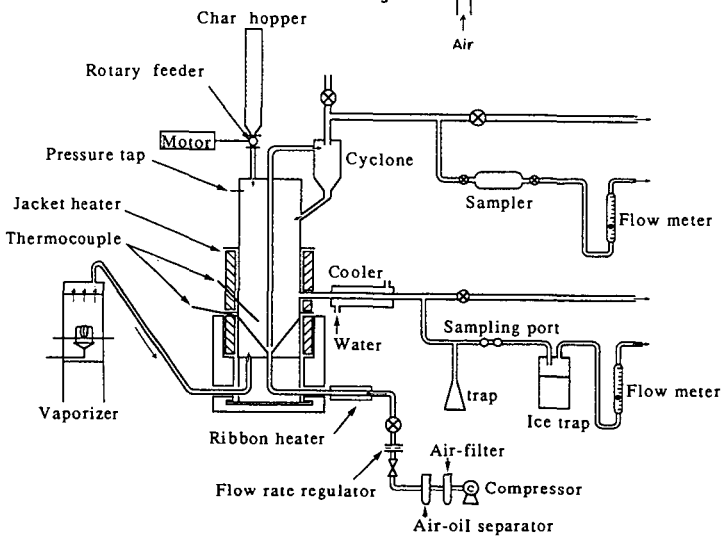

Figure 2. Schematic diagram of hot model unit.

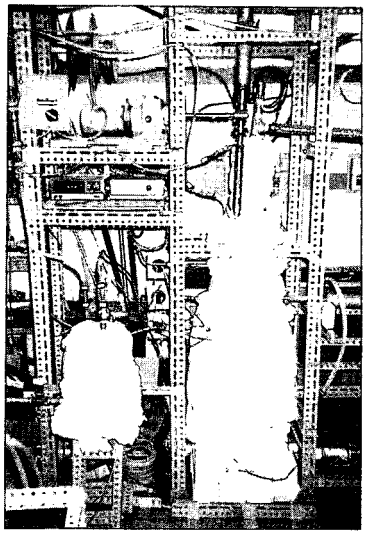

Figure 3. Photograph of hot model unit.

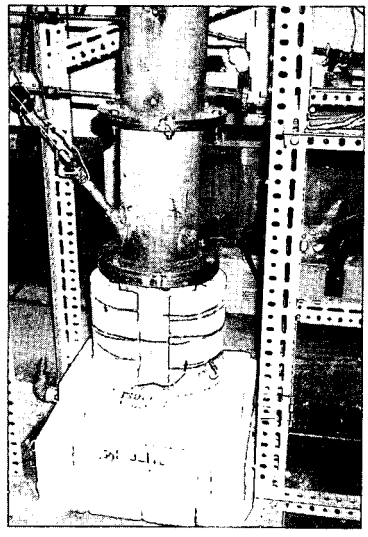

Figure 4. Photograph of hot model unit (under construction).

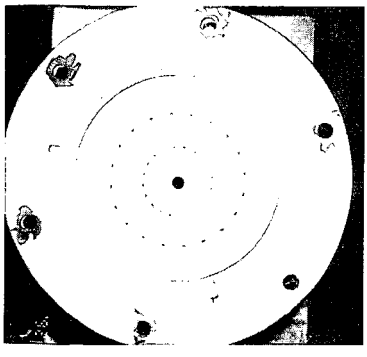

Figure 5. Photograph of bottom conical section.

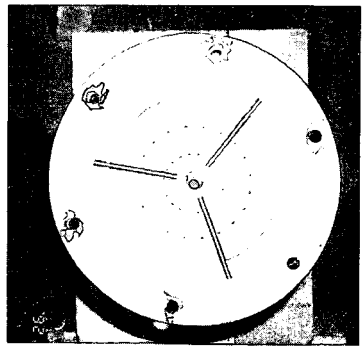

Figure 6. Photograph of bottom conical section with draft tube.

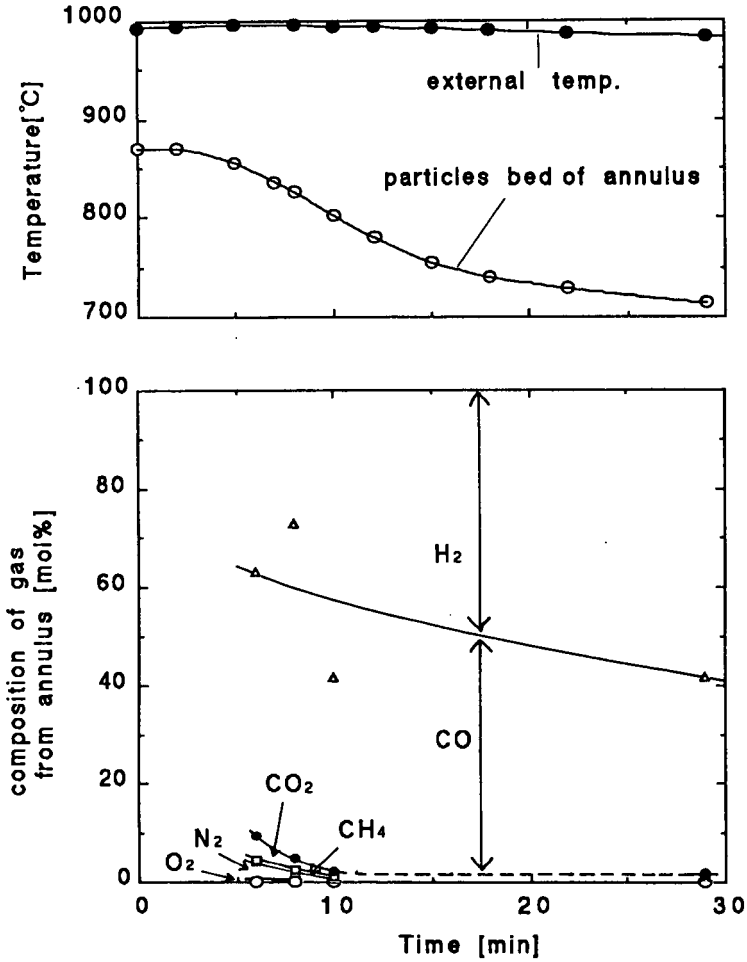

Figure 7. Temperature and gas composition.

BIOLIQUEFACTION OF COAL SYNTHESIS GAS

K. T. Klasson, M. D. Ackerson, E. C. Clausen, J. L. Gaddy
Department of Chemical Engineering
University of Arkansas
Fayetteville, AR 72701

Keywords: synthesis gas, ethanol, coal bioliquefaction

INTRODUCTION

Synthesis gas, a mixture of primarily CO, H_2 and CO_2, is a major building block in the production of fuels and chemicals. The gas may be produced from several sources, including coal, oil shale, tar sands, heavy residues, biomass or natural gas. Most synthesis gas is produced today by catalytic reforming of natural gas, although the partial oxidation of heavy liquids is also practiced (1). Only a small percentage of the synthesis gas currently produced is by gasification of solid fuels. However, because of the large reserves of coal in the United States (300 year supply at the current consumption rate (2)), synthesis gas production from coal will become an important technology in the future.

CO, CO_2 and H_2 in synthesis gas may be used as substrates for the biological production of fuels and chemicals. The bacterium *Rhodospirillum rubrum* uses CO and water in producing H_2 and CO_2 (3,4). Bacteria such as *Peptostreptococcus productus* (5) and *Eubacterium limosum* (6) convert CO, CO_2 and H_2 to acetate. Butanol may be produced from CO using the bacterium *Butyribacterium methylotrophicum* (7) and ethanol may be produced from CO, CO_2 and H_2 by *Clostridium ljungdahlii* (8,9).

The anaerobic bacterium *C. ljungdahlii* produces ethanol and acetate from CO, CO_2 and H_2 by the equations (9):

$$6\ CO + 3\ H_2O \rightarrow C_2H_5OH + 4\ CO_2 \quad (1)$$
$$2\ CO_2 + 6\ H_2 \rightarrow C_2H_5OH + 3\ H_2O \quad (2)$$
$$4\ CO + 2\ H_2O \rightarrow CH_3COOH + 2\ CO_2 \quad (3)$$
$$2\ CO_2 + 4\ H_2 \rightarrow CH_3COOH + 2\ H_2O \quad (4)$$

The bacterium was isolated from animal waste, with the "wild" strain producing predominantly acetate in favor of ethanol. In fact, early studies showed an ethanol to acetate product ratio of 0.05 mol/mol and an ethanol concentration of less than 0.1 g/L (9). A major research effort was undertaken to improve the product ratio and increase the ethanol concentration. Studies at decreased pH (to 4.0) and with yeast extract removed from the liquid medium resulted in product ratios of 0.8 and an ethanol concentration of 1.8 g/L in the CSTR (10).

The purpose of this paper is to present results of continuous laboratory studies with *C. ljungdahlii* in converting CO, CO_2 and H_2 in synthesis gas to ethanol. In addition, the effects of the sulfur gas H_2S on growth and substrate uptake are presented and discussed.

MATERIALS AND METHODS

Clostridium ljungdahlii, Strain PETC, ATCC 49587, was originally ioslated from chicken waste in the University of Arkansas laboratories, and later identified and characterized by Dr. R. S. Tanner, University of Oklahoma, Department of Botany and Microbiology. The recommended medium for growth and ethanol production, as well as the techniques for handling the culture in batch and continuous reactors, have been presented previously (11,12).

RESULTS AND DISCUSSION

CSTR Performance

Growth and product formation in the CSTR are shown as a function of the inlet gas flow rate in Figures 1 and 2. The working liquid volume of the CSTR was approximately 350 mL, so that the minimum pseudo retention time on the figures was 30 min. The corresponding liquid retention time was 2.92 days. As is noted in Figure 1, the cell concentration remained nearly constant at about 1500 m/L for a gas flow rate range of 0.15 - 0.47 mmol/min. The ethanol concentration ranged from 15 to 22 g/L, increasing slightly with gas flow rate (see Figure 2). The corresponding acetate concentration ranged from 2 to 5 g/L. Thus, a maximum product ratio of 14.3 mole ethanol per mole acetate was obtained. This represents a dramatic shift from earlier studies where acetate was the predominant product and low product concentrations were obtained. The specific production rate, calculated as the moles of products (both ethanol and acetate) produced per g cell per hour, was essentially constant at 0.004 regardless of gas flow rate.

Studies were also carried out with *C. ljungdahlii* in a CSTR with cell recycle. In this study, the liquid volume was 1000 mL, the temperature was 36°C and the pH was held constant at 4.5. The agitation rate was increased from 300 to 450 rpm and the gas flow rate was increased from 10 to 30 mL/min during the study to accomodate cell growth in the reactor. The liquid flow rate to the cell recycle reactor was 3.5 to 12 mL/h, decreasing with time of operation.

Figure 3 presents cell concentration measurements for the CSTR with cell recycle. As is noted, the cell concentration increased (with agitation rate and gas flow rate increases) from approximately 800 mg/L to over 4000 mg/L. The maximum in the previous CSTR study without cell recycle (see Figure 1) was 1500 g/L. The CO conversion, shown in Figure 4, hovered around the 90 percent level after 150 h of operation. The corresponding H_2 conversion, on the other hand, averaged 70 percent up to a time of 500 h. At this time, the H_2 conversion fell, probably due to an accumulation of CO in the liquid phase. It is likely that a growth limitation by a liquid constituent prompted a drop in CO conversion, resulting in CO build-up in the liquid phase and CO inhibition.

Product concentration measurements during the study are shown in Figure 5. The ethanol concentration ranged from 6 g/L at the beginning of the study to 48 g/L after 560 h of operation. The corresponding acetate concentrations at these times were 5 g/L and 3 g/L, respectively. The ratio of ethanol to acetate ranged from 1.6 mol/mol to 21 mol/mol. Thus, very high ethanol concentrations are possible with favorable product ratios.

Sulfur Gas Tolerance of *C. ljungdahlii*

Many bacterial cultures capable of converting CO to products have been found to be quite tolerant of the sulfur gases H_2S and COS (13,14). *Peptostreptococcus productus*, for example, which converts CO to acetate, is able to successfully convert CO to acetate in the presence of 19.7 percent H_2S or COS after culture acclimation. The methanogen *Methanobacterium formicicum*, on the other hand, is able to tolerate only 6.6 percent H_2S or COS. However, even this latter result is encouraging, since typical coal-derived synthesis gas contains only 1-2 percent sulfur gases, mainly as H_2S.

C. ljungdahlii, grown in the presence of Na_2S in place of cysteine-HCl as the reducing agent for several weeks, was evaluated for its tolerance to H_2S in batch bottle experiments. The 155 mL bottles containing 50 mL of liquid medium devoid of yeast extract and adjusted to pH 4.3, were first gassed with synthesis gas to a pressure of 10.7 psig. The desired amount of H_2S or COS (2.5 mL-20 mL) at 1 atm was then added. This batch system was allowed to equilibrate overnight. As a final step, 10 mL of *C. ljungdahlii* were added prior to incubation at 34°C.

The effects of H_2S on growth and substrate uptake by *C. ljungdahlii* are shown in Figures 6 and 7, respectively. As is noted in Figure 6, growth was not significantly slowed at H_2S concentrations below 5.2 percent. Upon the addition of 9.9 percent H_2S, however, growth essentially stopped. Similar results are noted with substrate uptake in the presence of H_2S (see Figure 7). The presence of H_2S slowed the rates of substrate uptake only slightly up to an H_2S concentration at 5.2 mole percent. Similar results were obtained with concentrations of COS up to 5.2 percent.

These concentrations are far in excess of maximum sulfur gas concentrations possible in coal synthesis gas. It should also be realized that dramatic effects can be obtained with prolonged sulfur gas acclimation. *P. productus*, for example, was only marginally tolerant of H_2S and COS in initial studies. Concentrations up to 20 percent were tolerated after a period of acclimation to the sulfur gases.

CONCLUSIONS

Clostridium ljungdahlii was shown to grow on synthesis gas with the production of high concentrations of ethanol and acetic acid. The relative amounts of ethanol and acetate can be controlled by nutritional factors, substrate gas supply, and pH. Low pH (4.0 to 4.5), high mass transfer of an adequate supply of substrate gas, and minimal medium all favor ethanol production. A CSTR cell recycle system has been shown to be effective in permitting the cell concentrations necessary for high concentrations of ethanol. An ethanol concentration of 47 g/L with a corresponding acetate of 2 g/L has been attained. Finally, *C. ljungdahlii* has been shown to be tolerant of H_2S or COS in concentrations exceeding typical levels in synthesis gas.

ACKNOWLEDGMENT

Financial support for this research was provided by the U. S. Department of Energy, Pittsburgh Energy Technology Center, on contract DE-AC22-89PC898976.

LIST OF REFERENCES

1. Graboski, M. S. (1984), In *Catalytic Conversion of Synthesis Gas and Alcohols to Chemicals*, R. G. Herman (ed.) Plenum Press, New York, pp. 37-50.
2. Specks, R. and Klussmann, A. (1982), *Energy Progress*, 2, 60-65.
3. Dashekvicz, M. P. and Uffen, R. L. (1979), *J. Syst. Bacteriol.*, 29, 145-148.
4. Klasson, K. T., Lundbäck, L. M. O., Clausen, E. C., and Gaddy, J. L. (1992), "Kinetics of Light Limited Growth and Biological Hydrogen Production from Carbon Monoxide and Water by *Rhodospirillum rubrum*," submitted for publication, *J. Biotechnol.*
5. Lorowitz, W. H. and Bryant, M. P. (1984), *Appl. Environ. Microbiol.*, 47, 961-964.
6. Genthner, B. R. S. and Bryant, M. P. (1982), *Appl. Environ. Microbiol.*, 43, 70-74.
7. Grethlein, A. J., Worden, R. M., Jain, M. K., and Datta, R. (1990), *Appl. Biochem. Biotechnol.*, 24/25, 875-884.
8. Barik, S., Prieto, S., Harrison, S. B., Clausen, E. C., and Gaddy, J. L. (1988), *Appl. Biochem. Biotechnol.*, 18, 363-378.
9. Vega, J. L., Prieto, S., Elmore, B. B., Clausen, E. C., and Gaddy, J. L. (1989), *Appl. Biochem. Biotechnol.*, 20/21, 781-797.
10. Clausen, E. C., Ackerson, M. D., and Gaddy, J. L. (1991), "Biological Production of Ethanol from Coal," Quarterly Report 2-4-91, June-September, Contract No. DE-AC22-89PC89876.
11. Klasson, K. T., Ackerson, M. D., Clausen, E. C., and Gaddy, J. L. (1992), *Proceedings, American Chemical Society, Division of Fuel Chemistry*, 37, No. 1, 464.
12. Phillips, J. R., Klasson, K. T., Clausen, E. C., and Gaddy, J. L. (1992), "Biological Production of Ethanol from Coal Synthesis Gas: Medium Development Studies," presented at the 14th Symposium on Biotechnology for Fuels and Chemicals, Gatlinburg, TN.
13. Vega, J. L., Klasson, K. T., Kimmel, D. E., Clausen, E. C., and Gaddy, J. L. (1990), *Appl. Biochem. Biotechnol.*, 24/25, 329.
14. Smith, K. D., Klasson, K. T., Ackerson, M. D., Clausen, E. C., and Gaddy, J. L. (1991), *Appl. Biochem. Biotechnol.*, 28/29, 797.

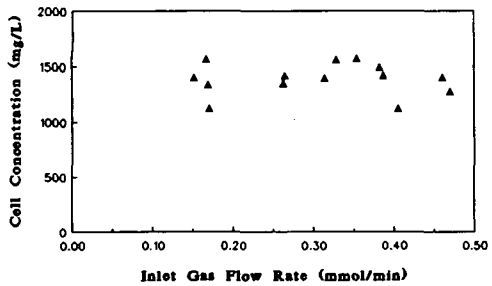

Figure 1. Cell Concentrations Obtained in the CSTR

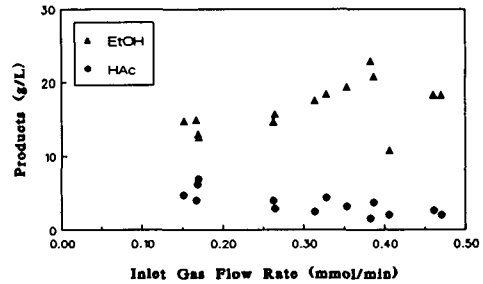

Figure 2. Product Concentrations Obtained in the CSTR

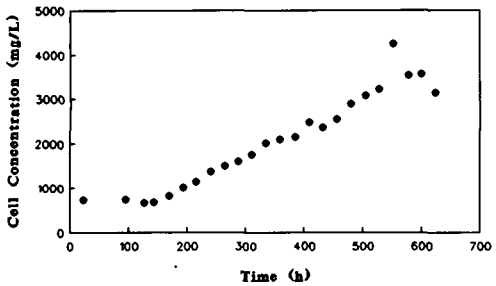

Figure 3. Cell Concentration Measurements in the CSTR with Cell Recycle

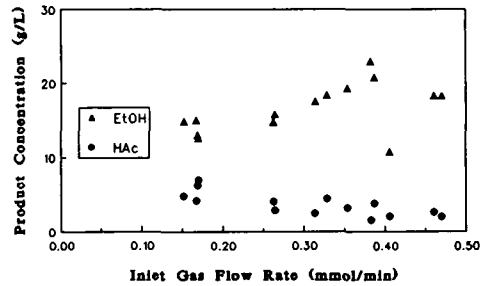

Figure 4. CO and H_2 Conversions in the CSTR with Cell Recycle

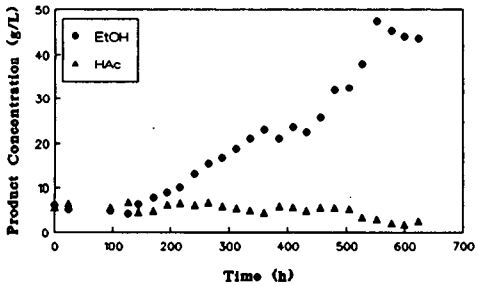

Figure 5. Product Concentration Measurements in the CSTR with Cell Recycle

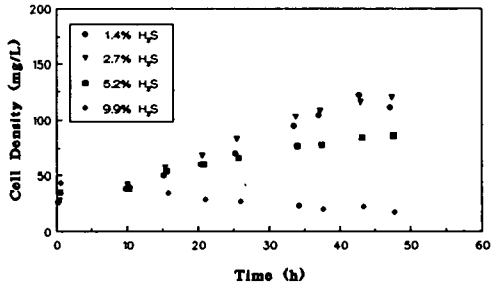

Figure 6. Effects of H_2S on the Growth of *C. ljungdahlii* in Batch Culture

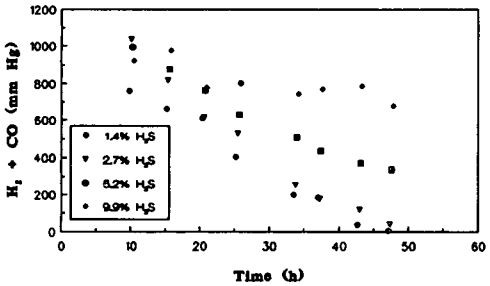

Figure 7. Effects of H_2S on CO and H_2 Uptake by *C. ljungdahlii* in Batch Culture

MINERAL LIBERATION OF ILLINOIS COALS

E.J. Hippo, M. Blankenship, S.C. Yen, B. Newton, C. Lia, H. Jao
Mechanical Engineering and Energy Processes
Southern Illinois University
CARBONDALE, IL. 62901

INTRODUCTION

Extensive studies of coal structure and utilization have been conducted on every known aspect of coal for many decades in an attempt to produce a more efficient and less polluting energy source. The first priority toward this energy goal is to deep clean coal prior to combustion, gasification, or liquefaction. Deep cleaning coal requires the liberation of pyrite and other minerals to facilitate high recovery of clean product. High recovery is necessary to make any cleaning process economically feasible. The high degree of liberation necessary for deep cleaning suggests that the physical properties of coal/mineral interaction be considered during comminution. Most grinding techniques use random fracture to reduce coal to roughly a cubic or spherical shape which simplifies the prediction of combustion rates in various types of furnaces[1]. This type of grinding does not significantly aid in exposing minerals for possible liberation. In particular, current grinding processes have never been able to effectively liberate microcrystalline pyrite from coal. Studies have shown that 60 to 80% of the mineral content in coal is located in the bedding planes[2]. These interfacial areas, separating relatively clean coal bands, are zones of weakness which contain porosity, fractures, and poorly bonded minerals[2][3].

This paper is a summary of research efforts to utilize bedding plane interfacial areas as a means to improve liberation of pyrite and other minerals in the final product. By cleaving large coal particles along the interfacial boundaries, relatively clean coal particles would be produced that have the majority of the mineral matter coating the exterior of each particle. Subsequent grinding would attrite the outer surface into ultrafine size distributions that allow separation of minerals and macerals particles. These particles would then be separated from the clean coal by sieving.

Over the past few years, low temperature studies have been conducted to determine the relationships between the fracture resistance of coal treated at low temperature and the effectiveness of coal grinding, to investigate the effect of cryogenic temperature treatment on the effectiveness of coal grinding and potential of selective pyrite liberation[4][5]. This work indicated that brittleness after rewarming increases with decreasing cryogenic treatment temperature. Experimental data has shown that the effect of cryogenic temperature does increase friability, mean particle size is significantly reduced, and pyrite/mineral liberation increased. This was the result of increased crack propagation and decreased microhardness[6][7]. Several methods of preconditioning are currently being investigated; thermal, mechanical, and chemical.

In thermal treatments, coals are being exposed to cyclic freezing and thawing at equilibrium moisture contents. The freeze/thaw cycling is bases on using the expansion property of freezing water to place pressure on fracture ends in the hope to expand and propagate cracking with the particle. In mechanical preconditioning, literature indicates that roll crushing yields particles that are plate-like or flakes and have a high aspect ratio[1][8]. Roll crushing and stage roll crushing of raw and cryogenic samples were examined to determine if this mechanical step would enhance liberation in subsequent ball milling. Solvent swelling of coal during mild extraction has been examined as a preconditioner. The reason is to enlarge pores during extraction and remove the soluble organic. The organic soluble phase may be responsible for the thermoplastic matrix of coal and reduced mineral liberation rates.

EXPERIMENTAL

The main coal used in this research is Illinois Basin Herrin #6 coal. This is do to its local economic importance and unique microdispersed pyrite particles. These microdispersed pyrite particles are the most difficult to liberate and separate of all the Illinois Basin coals. Wyodak and Pittsburgh coal is also currently being tested.

Knoop microhardness testing after rewarming was employed to examine brittleness of coal and the effect of cryogenic temperature on its microhardness[1][6][7]. An Automated Image Analyzer connected with an optical microscope was used to obtain pyrite liberation and particle size distributions for samples ground by a Fritsch centrifugal ball mill. Surface artifacts were examined by scanning electron microscopy (SEM) and optical microscopy.

The desired cryogenic temperatures were obtained using liquid nitrogen as a refrigerant to cool a flowing gaseous nitrogen stream which was in actual contact with the specimen. Detailed experimental setup and procedures for cryogenic treatment are given elsewhere[5][6].

Using the thermal expansion of water when frozen, coal samples were mixed with various weight percents of distilled water; 5, 10, and 20 grams. The samples were sealed into plastic freezer bags with all excess air removed. These samples were frozen and thawed for various cycles that range from 5 to 20 times.

Mechanical preconditioning of the coal was conducted using a roll crusher with its rollers set at staging widths of various increments; 0.1", 0.7", 0.5", and 0.3". Untreated and cryogenic coal samples were used in these experiments.

An evaluation of THF extraction as a means of preconditioning the unextractable residue is currently being conducted.

RESULTS AND DISCUSSION

Figure 1 includes information on three coals; Herrin Illinois #6, Wyodak, and Pittsburgh. Data from these samples of untreated and cryogenically treated coals are included. Rate of particle size reduction is greater for cryogenic coals. For a given grinding time, pyrite liberation is greater for cryogenically treated coals, but this is obtained by reduced particle size and not by enhanced selective liberation. The untreated coals give similar shape curves. The slope of liberation changes during treatment. During initial particle size reduction, the liberation is slow. When particle size distribution reaches 70 to 100 μm, a jump in liberation occurs. This is followed by a period in which coal becomes fine in size but liberation remains static. For the cryogenically treated coals, particle size reduction is faster and the initial slow period is not observed. A relatively high rate of liberation occurs as the mean particle size distribution is reduced from 90 to about 40 μm. The rate of liberation is relatively linear until the mean size approaches 10 to 12 μm and begins to level off as 100% liberation is approached. The earlier liberation is more selective for the untreated coals, but a maximum liberation level is observed. The liberation of cryogenically treated coals reaches a higher limit. Although the selectivity of untreated coals is higher, the extent of liberation is not sufficient to be of commercial interest. Even though the amount of pyrite and the particle size distribution of pyrite vary for the three untreated coals, the extent of liberation approaches the same limit (≈84%) and the same mean particle size of 20 μm. The untreated Pittsburgh coal has a larger pyrite size distribution than the Illinois coal which results in a higher rate and selectivity of pyrite liberation as expected[6]. Thus cryogenic treatments are helpful in increasing the ultimate liberation. This is probably due to two factors. One is enhanced cracking around pyrite. The second is enhanced fracture, flaw generation, in the coal matrix[6]. This allows for the coal to be reduced in size as compared to untreated coals. Even with cryogenic treatments, ultrafine particle sizes must be obtained to reach sufficient levels for deep cleaned coal.

Economic considerations of cryogenic treatments makes it a less than desirable method for liberation. For this reason freeze/thaw cycling was studied as an alternative. Figure 2 is a comparison of pyrite liberation to the mean particle size for untreated, cryogenically treated, and freeze/thaw treated Illinois coal samples after ball milling. The points of each plot represent a grinding time, from left to right, of 1, 3, 5, 7, and 10 minutes. As discussed in figure 1, the rate of liberation for the untreated coal is slow until a mean size of about 70 μm is reached. A large jump in liberation occurs until a mean size of about 50 μm is reached. At that time the liberation becomes nearly stationary. Freeze/thaw liberation appears to be a extension of the untreated plot and increases to about 84%. Rapid particle mean size reduction is very evident with the freeze/thaw treatment. Three minutes of ball milling of freeze/thaw sample yields about the same size distribution as ten minutes ball milling of the untreated sample. Freeze/thaw

cycling improves the upper level of liberation compared to the untreated. However, cryogenic treatment yields 93% pyrite liberation while freeze/thaw yields 84%.

Figure 3 compares freeze/thaw, cryogenic roll crushed, untreated, and untreated roll crushed Illinois coal samples after subsequent ball milling for pyrite liberation at various mean particle sizes. The points of each plot represent a grinding time, from left to right, of 1, 3, 5, 7, and 10 minutes. All three plots show significantly improved liberation compared to the untreated sample. The BG-CRYO is cryogenically treated for five minutes, compared to 10 minutes in Figure 2, and staged crushed from 0.1" to 0.05". At five minute exposure time, the cryogenic liberation does not approach the level attained by freeze/thaw. This would indicate that freeze/thaw results are better than 5 minute cryogenic exposure but falls short of 10 minute cryogenic exposure results. The freeze/thaw sample, was thermally cycled 10 times with 10% by weight distilled water added. This sample shows a nearly linear increase in liberation to about 87%. It may be concluded that the mechanical and thermal treatment increases liberation above that attainable by untreated samples ball ground in an identical manner.

Figure 4 is a comparison of single roll crushing and staged roll crushing of untreated, UNT-RC-0.1, and cryogenically treated, cryo-, coal followed by ball milling. The slope for all the samples is nearly the same. The rate of pyrite liberation of the untreated single roll crush sample, UNT-RC-0.1 is consistently less than the other roll crushed samples but much greater than the rate of liberation for the ball milled only sample. Single roll crushing was conducted at 0.07" gap on one cryogenic sample still at liquid nitrogen temperature, CRYO-C-RC-0.07, and another allowed to rewarm before roll crushing, CRYO-R-RC-0.07. The rewarmed sample maintained a consistently higher liberation rate throughout. Roll crushing at 0.1",CRYO-R-RC-0.1, has better liberation than roll crushing at 0.07", CRYO-C-RC-0.07. This is possibly due more force being applied to the 0.07" sample to the extent that the pyrite particles are embedded into the viscoelastic coal matrix. Both the rewarmed staged, CRYO-R-SC and single roll crushed samples had better results than both the untreated and cold roll crushed samples. Crack propagation may be improved upon thermal expansion after thermal contraction. If the stage crushed sample was ball ground for 10 minutes and the slope of this sample remains consistent with the other samples, a higher level of pyrite liberation should be obtained.

CONCLUSIONS

This study of preconditioning treatments indicates that both thermal and mechanical methods will improve pyrite liberation above that obtained for untreated samples. Freeze/thaw cycling improves liberation but not to the degree obtained by cryogenic treatment. Rewarming of cryogenically treated coal prior to comminution improves the overall pyrite liberation. Stage roll

crushing improves liberation. Enhanced liberation of pyrite by all the preconditioning methods presented is at the expense of smaller mean particle sizes.

REFERENCES

1. Durney, T.E., and Moley, T.P., "Particle Shape Effects Due to Crushing Method and Size", International Journal of Mineral Processing, Vol. 16, pp109-123, 1986.
2. Stach, E., Textbook of Coal Petrology, Pub. Gebruder Borntraeger, Berlin and Stutgart, Germany, 1982.
3. Ward, C.R., ed., Coal Geology and Coal Technology, Blackwell Scientific Publications, Ca., U.S.A., pp157, 1984.
4. Yen. S.C., and Hippo, E.J., "Comminution Employing Liquid Nitrogen Pretreatment", Final Report to PETC, August 31,1991.
5. Yen. S.C., and Hippo, E.J., "Enhanced Coal Cleaning Through Low Temperature Treatment of Coal", Final Report to The Center for Research of Sulfur in Coal, August 30 1990.
6. Blankenship, M., M.S. Thesis, Southern Illinois University at Carbondale, Carbondale, Il., 1991.
7. Jao, H., M.S. Thesis, Southern Illinois University at Carbondale, Carbondale, Il., 1991.
8. Mishra, S.K., and Klimpel, R.R., Fine Coal Processing, Noyes Publications, Park Ridge, N.J., U.S.A., pp 19-37, 1987.

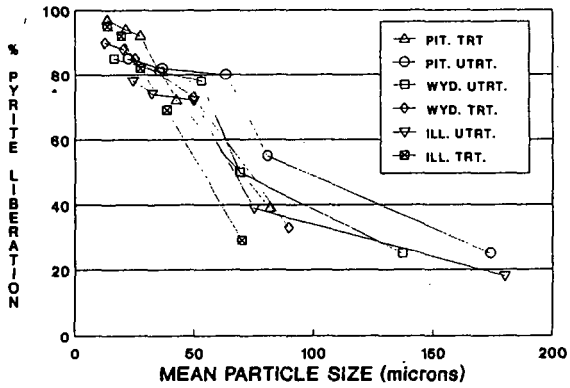

Figure 1. Comparison of Pyrite Liberation as a Function of Mean Particle Size for Pittsburgh, Wyodak, and Illinois No. 6 Coals. Both Cryogenically Treated and Untreated Samples Were Ball Milled for Various Times.

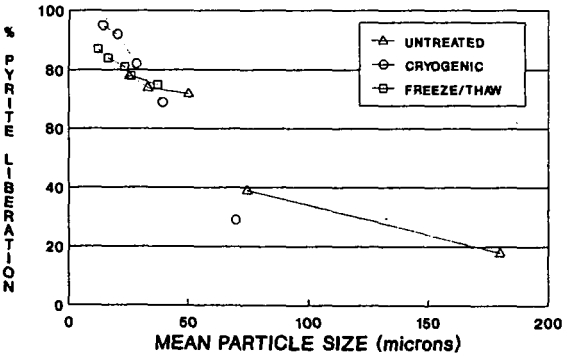

Figure 2. Comparison of Pyrite Liberation as a Function of Mean Particle Size for Illinois No. 6 Coals. Untreated, Cryogenic, and Freeze/Thaw Treatments Are Compared.

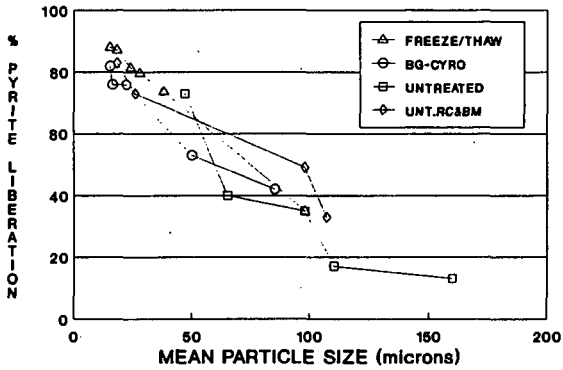

Figure 3. Comparison of Pyrite Liberation as a Function of Mean Particle Size for Illinois No. 6 Coals. Data Includes Roll Crushing, Freeze/Thaw, and Cryogenic Treatments.

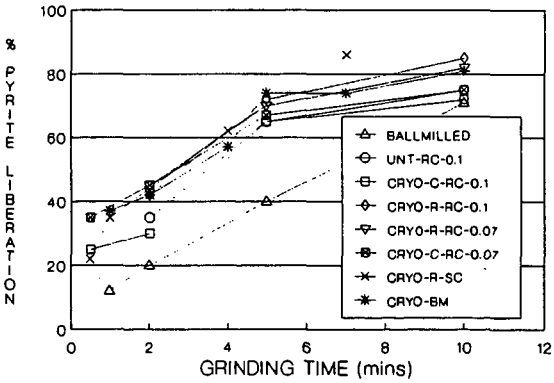

Figure 4. Pyrite Liberation as a Function of Grinding Time for Illinois No. 6 Coals with Various Mechanical and Thermal Pretreatments.

COAL FLOTATION WITH IBS/OIL FROTH

Edwin J. Hippo, Deepak Tandon, Michael E. Blankenship
and Seema Khan
Mechanical Engineering and Energy Processes
Southern Illinois University, Carbondale
Illinois 62901

INTRODUCTION

International coal markets are expected to grow in the near future [1]. U.S. has sufficient coal reserves that will last for centuries, but a major problem in coal utilization is sulfur. Fifty five to 80% of the sulfur in most coals is in the form of pyrite, and if this pyritic sulfur can be removed by advanced physical coal cleaning techniques, sulfur dioxide (SO_2) emissions in the U.S. could be cut by as much as 50% [2]. Presently, the alternative for the prevention of SO_2 emissions is post-combustion scrubbing, but is too costly and consumes as much as 5% of the power station's output (adding to CO_2 emissions). Therefore, incentives exists to explore pre-combustion cleaning. Coal has to be grounded to -325 mesh in order to liberate pyrite and other minerals from the organic components. At this fine particle size attractive forces between particles are much greater than the differences in the gravity forces exerted on the particles, and thus the gravity separation based conventional coal cleaning processes become inefficient [3].

Of the existing fine coal cleaning techniques froth flotation is most effective, but is inefficient in making good separation with ultrafine coal [4]. There is a wide range of chemicals that are required for coal preparation in these process, for improved process efficiencies and to meet stricter environmental standards [5]. This makes process control very complex. At ultrafine sizes, the small mass and momentum of clay particles, is the primary cause of their physical entrainment and transportation into the froth. This lowers the efficiency of the froth flotation process when excessive amounts of clay are present. The entrained ash can be washed from the froth by counter-current washing as in column flotation, but at the same time it may rupture the bubble and reduce the recovery.

Coal flotation by Intrinsic Bubble Separation has shown to circumvent surface phenomena which reduce the efficiencies of the conventional cleaning processes [3]. This process takes the advantage of the natural porosity of the organic fraction of the coal. In this approach bubbles are formed directly on the organic coal particles, eliminating the bubble-particle collision and attachment probabilities. The nonporous minerals do not form bubbles, assuring 100% bubble-particle contact. Thus, flotation can be highly selective. Since the bubbles form from the pore openings, this minimizes free bubble formation and enhances the cleaning of high ash coals.

Washability curves are the graphs showing the ash-density distribution. These curves are indicative of the maximum cleaning potential of any physical coal cleaning process for a particular coal sample. Washability curves were obtained for four coals from the Illinois Basin Coal Sample Program (IBC 101, 102, 104, and 106). Southern Illinois University at

Carbondale has developed a method for rapidly and accurately evaluating fine and ultrafine coal liberation using Density Gradient Centrifugation (DGC), Micro Sulfur and Thermogravimetric Analysis (TGA) methods to establish washability curves [3]. For the IBC 102 coal there was small difference in the liberation of minerals between -100 and -400 mesh material. The ash yields went through a minimum with increasing density, indicating that the inertinite and the liptinite macerals have higher inherent ash yields than the vitrinites. Washability curves for the IBC 101 and 106 coals were like the 102 Coal but had much higher ash yields which indicated that even at ultra-fine size there is substantial amount of unliberated minerals in these coals [6].Previous results on intrinsic bubble formation process showed that pressure, in general, increased the hydrophobicity of the organic portion of the coal. Except for Octanol, additives did not have any positive effect on the process. Lower pHs seem to favor the process. The process works effectively on weathered coals and pulp densities as high as 20% [2].

All the IBC coals at -32 mesh have been cleaned to their respective -100 mesh washability lines. Results from the high clay IBC 104 coal are the best thus far. For this coal substantial ash (> 90%) and sulfur rejection (> 80%)have been obtained. These results compare quite favorably with those of the Illinois State Geological Survey Aggregate Flotation process (Fig. 1) [6].

Recoveries and ash rejections with this process compared very favorably with other processes. Flotation kinetics are much faster. There were some problems with the wetting of coal at high pulp densities (> 20 wt.%) which were overcome by using a bigger mixing chamber and two 10,000 rpm mixing motors. This high mixing rate should help in breaking some of the mixed phase mineral/coal particles which caused problems in the early phases of this project.

EXPERIMENTAL PROCEDURES

The coals selected for use in this research were IBC 101, 102, 104 and 106 from the Illinois Basin Coal Sample Program (IBCSP) and a Herrin # 6 coal from the Monterey #2 mine located near St. Louis. The choice of these coals was made on the basis of their differing rank (reflectance), ash yields and pyrite/organic sulfur ratios (3). The particle sizes used for the IBC coal samples were -32, -100,-400 mesh and for the Monterey coal -400 mesh sample was used. The particle size distribution for -32 and -100 mesh were determined by wet sieving, and that for -400 mesh was performed using the Microtrack analyzer. Washability curves were plotted for -100 and -400 mesh samples. A schematic of the experimental setup used is shown in figure 2. Dried coal is fed into the lock hopper where it is pressurized using air. Water and the flotation media used are fed into the mixing chamber and are pressurized to the same pressure as the coal. Coal is then dumped in the mixing chamber, mixing starts simultaneously (two 10,000 rpm motors are used for mixing). A plug valve is used for slurry output at the bottom of the mixer and for depressurization control. The outlet pipe is immersed in a separation column with a water cushion. Coal slurry depressurizes through a nozzle in the separation column; float froth rises to the top and is collected in a trough attached to the separation column. The liquid left in the column is termed as the suspension and the solids settled at the bottom are called the sink. Recovery and ash values are determined on each of the collected fractions. Runs with good recovery and separation are subjected to additional analyses.

Initial runs, to study the effects of various conditions, were performed with IBC coals. Pressure variations were made ranging from 15 to 300 psig on the three mesh sizes of these coals. pH variations were made using NaOH and HCl. After the optimum pHs were determined, the effect of various gases (N_2, CO_2, and Air) on the process were studied. Runs were performed with various additives to assess their effect on recovery and separation. Also, the effect of mixing rate, mixing time, pulp density, and weathering (oxidation) on cleanability and recovery were studied [6].

Effects of additives (Octanol, Corn oil, Pentane, and various dispersants), pH (2.3 to 11.0) and pulp density on the Monterey coal were studied. These runs were performed at 60 psig and 5% pulp density (-400 mesh samples), in the new apparatus shown in Fig. : 2. Various loadings of additives were used to study the effect of the additive loadings.

RESULTS AND DISCUSSION

Ultrafine (8μm mean size) Monterey coal was subjected to sink float analysis by centrifuging at 34,000 rpm and specific gravity of 1.6. The float from this run had a recovery of 59 wt.% (5.4 wt.% ash) and the sink had a recovery of 41 wt.% (45.6 wt.% ash). This result showed that even at ultrafine size minerals are unliberated. Also, from the optical microscopy it is seen that there are a lot of mixed phase mineral/coal particles present at this fine particle size.

Increase in mixing rates and time have a positive effect on the process, though very high mixing time (> 30 min.) tend to wet the organic matter and caused a decrease in the recovery (Fig. : 3). With increased mixing rate the recoveries go up but the ash rejections tends to level off, this could be due to unliberated minerals or mixed phase mineral/coal particles. The problem of mixed phase is more evident at -400 mesh where the electrostatic charges are much stronger.

Additive loadings had mixed effect on the cleaning of ultrafine Monterey coal. With increased octanol loading there was a very small increase in the recovery but the ash yield in the float almost doubled (6.4 to 11.2 wt.%). Thus lower octanol loadings are favorable for the process. This in contradiction to results reported previously for -32 and -100 mesh fractions of IBC 104 coal and may be due to change in wetting angle, resulting in more particle bubble detachment in the case of ultrafine coal. Increased bubble detachment would be expected to entrain liberated ultrafine clay particles. In the case of larger particle size fractions the detached bubbles are not sufficient to float the larger sized clay particles.

Oil froth agglomerates generated with corn oil gave higher recovery and high ash yields, when the oil loading was increased there was a slight drop in recovery but the ash yields went down almost to half of that at lower loadings (7.4 from 12.5 wt.%). Since Ocatnol and corn oil had different effects on the process a run was performed with both octanol (at lower loading) and corn oil (at higher loading), this combination of additive gave a very high carbon recovery (> 90 wt.%) and an ash yield of 9.3 wt.%. Other additives had no positive effect on the process. In fact dispersants tend to give very low recovery. This is due to wetting of organic particles that results in less gas being trapped in the coal pores.

Effects of pH on the process were also studied. pH seems to depend on the additive. When corn oil was used higher pH (11.0) was optimum for the process and both the recovery and ash rejection increased with the increasing pH. Whereas, with pentane neutral pH favored the process and any change in pH resulted either in the lower recovery (with lower pH) or lower ash rejection (with an increase in pH). At higher pHs minerals were dispersed in the separation column(high clay content in the suspension), lower pH on the other hand tends to sink not only the minerals (clear suspension) but also the organic coal particles.

The process has been operated at pulp densities as high as 20 wt.%, after which wetting of coal and mineral entrainment in the froth becomes a problem. We think that this problem can be overcome when the process is scaled up to the pilot plant.

CONCLUSIONS

Fine and ultrafine coal cleaning by the IBS/Oil froths process is feasible. Coals have been cleaned to their washability limits by this process. Additive loadings have no systematic effect on the process and higher additive loadings work just as well as the lower additive loadings. Octanol gave very high ash rejections (> 90 wt.%), the carbon recoveries were depressed (50 wt.%). Corn oil/Octanol (neutral pH) and pentane at lower pH all cleaned Monterey coal to the washability limits. Organic particle flotation is almost instantaneous. Results thus far have shown that the process has much better recovery and ash rejection than the conventional flotation processes. Increased mixing rates have a positive effect on the efficiency. The process is limited by the unliberated minerals and especially by the interaction of coal and mineral particles. There is a need to find a dispersing agent that could break the phase of mineral/coal interactions without adversely affecting the wetting angle or a better grinding/liberation process is required. This would improve the effectiveness of the process for ultrafine coal cleaning.

REFERENCES

1. Kneller, W.A., Physico-Chemical Characterization of Coal and Coal Reactivity: A rewiew.

2. Hippo, E.J., Sarvela, D.P., and Tandon, D., Coal Flotation by Intrinsic Bubble Formation. Technical Report Prepared for CRSC 1990.

3. Tandon, D., "Coal Cleaning By Intrinsic Bubble Formation". Master's Thesis, Department of Mechanical Engineering and Energy Processes. Southern Illinois University at Carbondale. Sept. 1990.

4. Yoon, Roe-Hoan, Flotation of Coal using Micro-Bubbles and Inorganic Salts, Mining Congress Journal 68(12) 76-80, 1982.

5. Williams, K.P., Unlu, M., Coal Flotation in the Presence of Polymeric Flocculants. Coal Preparation, 1987, Vol.4, pp. 109-132.

6. Hippo, E.J., Tandon, D., and Sarvela, D.P., "Coal flotation by Intrinsic Bubble Formation. 1991 International Conference on Coal Science Proceedings. University of Newcastle-upon-Tyne, U.K. pp. 893-896.

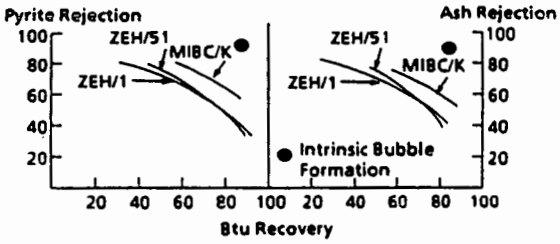

FIGURE : 1 Comparison of intrinsic bubble formation with aggregate flotation.

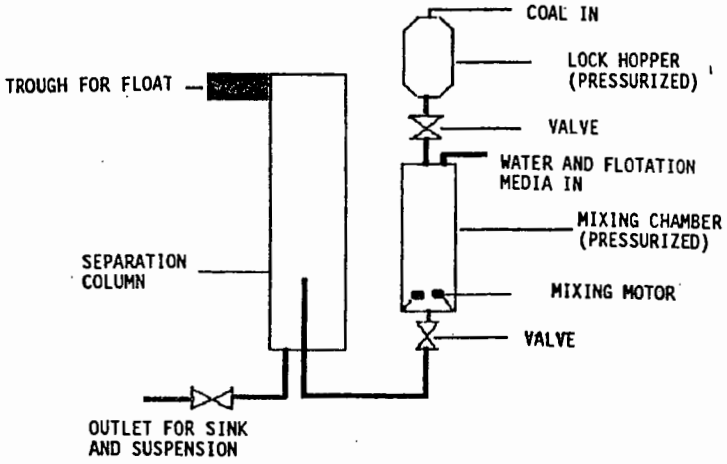

FIGURE : 2 SCHEMATIC OF FLOTATION APPARATUS

WASHABILITY CURVE FOR HERRIN #6 HIGH ASH COAL

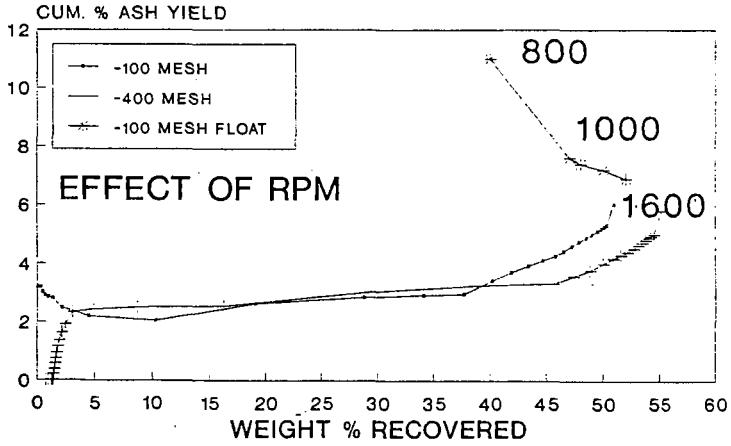

FIGURE : 3 EFFECT OF RPM ON THE RECOVERY AND ASH REJECTION OF IBC 104 (HERRIN # 6) COAL.

A NEW SOLUTION-BASED COAL-UPGRADING PROCESS

David L. Morgan
Division of Energy Technology: CSIR
P.O. Box 217, Pretoria, 0001, South Africa

Key words: coal, solvent extraction, upgrading

INTRODUCTION

The development of effective means of upgrading the organic part of coal by separating it from the inorganic part has long been the goal of coal chemists and engineers, with several processes having been studied in recent years. Amongst these are the removal of mineral components by hot-alkali dissolution [1,2], the removal of minerals and some organic sulphur by treatment with perchlorethylene [3], and the high-severity extraction of the organics by coal-derived and supercritical solvents [4]. Relatively milder extraction with refluxing N-methyl-pyrrolidone (NMP) has also enjoyed attention [5], although the degree of solubilization obtained has been less than 50%. The aim of these studies has been to develop processes suitable for the manufacture of clean fuels or, after carbonization, of electrode carbons. The low value of these products places great pressure on the economics of the process.

The development of a new purification process has been prompted by the observation that relatively small additions of sodium hydroxide allow very high solubilization of certain high-rank bituminous coals into relatively cheap N,N-dimethylformamide (DMF) and similar solvents. A patent has been granted in South Africa [6], allowed in the USA and applied for in a number of other countries. The purified dissolved organics may be recovered from solution as "Refcoal" but the coal solution itself may be exploited to prepare products of much greater value than fuel or electrodes.

EXPERIMENTAL

Small-scale extractions

The extractions were performed at room temperature in stainless-steel tubes (80 mℓ volume) fitted with screw caps and PTFE seals. Typically coal (7 g), solvent (70 g) and alkali were introduced together with a stainless-steel slug (1 cm by 1 cm diameter). Air was displaced by nitrogen and the tubes sealed. Up to 12 tubes were placed in a tumbling apparatus and rotated end-over-end at 60 r/min for 24 hours at room temperature. The extract was filtered through No. 3 sintered-glass filter, washed once with solvent (70 g), then exhaustively with water to remove residual solvent and dried under vacuum at 60 °C. The residue was weighed, the carbon content determined and the degree of carbon extraction calculated using the formula:

$$\% \text{ Carbon extraction} = \frac{(\text{wt coal extr. x \% C in coal - wt extr. residue x \% C in residue}) \times 100}{\text{wt. coal extr. x \% C in coal}}$$

The repeatability, particularly for high degrees of extraction, was high. The figures shown are averages of at least two determinations.

Bench-scale extractions

The extraction apparatus consisted of a jacketed stainless-steel reactor 240 mm x 81 mm I.D., fitted with internal baffles and a flat stirrer 40 x 40 mm driven by a variable-speed motor capable of 1 500 r/min. The extractions were conducted under an argon atmosphere. Oil or water from a thermostat was pumped through the jacket to provide temperature control. The reactor was

loaded with coal (70 g) and solvent (700 ml) and heated to operating temperature. Alkali was added and the extraction commenced. Samples of slurry were taken as required and the degree of extraction measured.

Monitoring the degree of extraction
Slurry samples (≈ 1 ml) were centrifuged at 3 000 r/min for 5 minutes, then 0,1 g of supernatant was weighed rapidly into a volumetric flask and diluted to 50 ml with solvent. The absorbance at 600 nm was measured on a Unicam SP 1700 spectrophotometer.

Minerals removal
Extracts were centrifuged at 6 000 r/min for 30 minutes in 1-ℓ buckets and the supernatant filtered under vacuum through polypropylene filter cloth. The removal of minerals was monitored by XRF analysis of recovered Refcoal.

Refcoal recovery and alkali removal
The bulk of the solvent was removed by vacuum distillation at 90 °C. The product was washed with boiling water to remove residual solvent and alkali, and then dried to give Refcoal.

RESULTS AND DISCUSSION

Small-scale extractions
The effect of adding potassium hydroxide (coal:solvent:KOH ratio 10:100:1,6) on the carbon extractabilities into NMP of various South African coals is shown in Table 1. Coals of higher and lower dry, ash-free carbon content showed much lower extractabilities. Clearly the vitrinite concentrates were much more soluble than the corresponding inertinites. Coal B - a flotation concentrate rich in vitrinite - showed a remarkably high extractibility considering the mild conditions employed.

The suite of Argonne Premium coal samples [7] was similarly extracted using the same coal: solvent:KOH ratio. The results are given in Table 2 where a similar rank effect is seen. It should be noted that southern African coals have experienced a very different history to those of North America and that direct comparisons based on particular rank parameters should be approached with caution.

The effectiveness of numerous solvents was examined using Coal A and potassium hydroxide in the same ratios as above. The results are given in Table 3. Amide solvents are seen to be generally effective, with dimethyl sulfoxide somewhat less so. Pyridine alone or with KOH was ineffective but the addition of the phase-transfer catalyst 18-crown-6 gave greatly increased extraction when five consecutive extractions were done. Hexamethyl phosphoric triamide was ineffective, even on addition of crown ether.

Various amine, ether, polyether and alcohol solvents showed no great increase in solubility on the addition of potassium hydroxide/crown ether.

Similar results in both NMP and DMF were found when an equivalent amount of sodium hydroxide was used in place of potassium hydroxide. Lithium hydroxide was very much less effective.

The most significant points arising from these results are:

(1) The organic part of a variety of coals can be very effectively solubilized.
(2) Relatively cheap and volatile DMF may be used.
(3) Relatively cheap sodium hydroxide may be used.

Bench-scale extractions

Numerous bench-scale experiments aimed at defining process conditions for the extraction of Coal B have been done using DMF and NMP. The extraction curves found show, in some cases after an induction period, a steadily decreasing rate of extraction until a final plateau is reached.

In summary the more significant observations are:

The effect of air. The extraction is severely affected, with approximately half the potential extraction being obtained.

The effect of temperature. The rate increases rapidly with temperature. In NMP the time to completion ranges from 10 minutes at 180 °C to 17 hours at 30 °C. In DMF the time ranges from 60 minutes at 150 °C to 24 hours at 30 °C. An induction period is seen at lower temperatures.

The effect of alkali. Potassium hydroxide, in equivalent amounts, gives marginally faster extraction.

The form of the sodium hydroxide is important. In NMP and DMF the extraction rate increases with the use of finer NaOH. The induction period becomes shorter. Sodium hydroxide solution gives rapid dissolution, but in DMF the final plateau of extraction is much lower than that found for solid. The addition of more NaOH solution leads to further extraction. Reaction of the base with the solvent must be occurring before the coal is fully solubilized.

The quantity of sodium hydroxide required for maximum extraction in both solvents is about 10% of the mass of the coal.

The effect of phase-transfer catalyst. The addition of as little as 0,7% (of the mass of coal) of polyethyleneglycol 400 increases the rate of extraction noticeably. The addition of 5% polyethyleneglycol 400 decreases the time to maximum extraction at 90 °C in DMF from 200 to 60 minutes. The catalyst clearly assists alkali mass transfer.

The effect of stirring rate. The extraction rate increases with the stirring rate, but plateaus in the bench apparatus at about 1500 r/min.

The effect of particle size. In both NMP and DMF there is a moderate effect at 30 °C and no difference at 90 °C when comparing coals -500 μm +212 μm and -160 μm in size.

Solution properties

The solutions are dark brown in colour. The DMF solution ranges in viscosity from 1,8 cp at 90 °C to 3,5 cp at 30 °C. Solutions in both solvents are unstable when exposed to atmospheric water and carbon dioxide. The NMP solutions have an indefinite stability when in closed containers, but the DMF solutions gel after a few weeks. The addition of acid or other solvents miscible with DMF and NMP leads to immediate precipitation of the coal-derived material.

Monitoring the degree of extraction

The absorbtion measured correlated extremely well with the degree of carbon extraction determined gravimetrically in a series of partial extractions done in the small-scale extraction apparatus on various coals. The absorbance per gram of coal dissolved remained constant, independent of the degree of extraction for each coal, but differed widely from coal to coal.

Minerals removal

The undissolved coal present in the extraction slurry is highly swollen with solvent and very sticky. Filtration is difficult. Centrifugation at 6000 r/min of the solution directly from the hot extraction vessel gave the best results. Table 4 compares the ash analyses of Coal B with those of a series of unwashed Refcoals prepared from a solution of this coal centrifuged at various speeds. Increased speed is clearly important.

Refcoal recovery and alkali removal

Vacuum distillation of DMF solutions proceeded smoothly at 10 mbar pressure and 90 °C bath temperature, but removal of NMP was difficult and slow. Complete removal of either solvent was not possible but, based on nitrogen analysis, can be brought down to about 10% for DMF and 16% for NMP. Hot-water washing brings these percentages down to < 1% and about 3% respectively. Sodium is also removed by water washing, from 3% in the vacuum-dried product to less than 100 ppm. The final product is a dry, free-flowing granular material. Analysis of Refcoal gave values very close to those found for the coal used in its preparation. Nitrogen increased 0,1 - 0,2%, representing 0,5 - 1,0% DMF, while sulphur was halved, representing removal of pyrite.

Exploitation

Several uses for coal solutions and Refcoal show promise. Refcoal would be a very clean fuel. The carbonization yield of Refcoal prepared from Coal B is 75% at 1100 °C making it an efficient carbon source. Some control of the degree of ordering of the carbon formed appears possible. The low viscosity of the solutions makes it attractive as an impregnation medium. Higher-valued uses are being investigated - fibres can be spun from suitably treated solution and the solution can be used as a source of carbon of high reactivity for the carbothermal preparation of metal carbides and nitrides.

LITERATURE CITED

1. Chriswell, C.D., Shah, N.D. and Markuszewska, R. Sept. Sci. and Tech. 1991 26(7) 961.

2. Waugh, A.B. and Bowling, K.M. EP 0302864/B1/ 1991.

3. Fullerton, K.L., Lee, S. and Kulik, C.J. Fuel Science and Eng. Int'l. 1991. 9(7) 873.

4. Pullen, J.R. in Coal Science, Vol. 2, p. 259 ed. McGorbaty, J.W. Larsen and I. Wender, Academic Press, 1983.

5. Renagnathan, K., Zondlo, J.W., Minty, F.A., Kneisl, P. and Stiller, A.H. Fuel Proc. Tech. 1988 18 273.

6. Morgan, D.L. SA Patent No. 90/7606, *Coal solubilization*, 1991, ENERKOM (Pty) Ltd.

7. Vorres, K.S. Energy and Fuels, 1990 4(5) 420.

ACKNOWLEDGEMENTS

The author wishes to thank:

The South African Department of Mineral and Energy Affairs for funding these studies.
Dr J Dekker for helpful discussions.
Charl Fourie, Stefanie McMenamin and Alpheus Bokaba for technical assistance.

TABLE 1: Extraction of South-African coals in N-methylpyrrolidone

COAL	% daf C	No additive % carbon extraction	KOH addition % carbon extraction
A	86.8	8.6	80.5
B	88.5	5.0	90.3
C	88.2		80.3
D1 vitrinite	86.8	20.7	47.7
D1 inertinite	86.2	5.4	13.4
D2 vitrinite	87.0	19.0	57.0
D2 inertinite	85.8	6.8	24.8
E1 vitrinite	86.0	10.5	40.0
E1 inertinite	86.3	5.7	16.1
E2 vitrinite	88.8	6.3	86.1
E2 inertinite	86.8	3.4	25.9

TABLE 2: Extraction of Argonne Premium coals into N-methylpyrrolidone/KOH

COAL	% dmmf C	% Carbon extrection
Wyodak-Anderson	76.04	6.0
Beulah Zap	76.05	6.4
Illinois #6	80.73	14.4
Blind Canyon	81.32	16.2
Lewiston-Stockton	85.47	17.5
Pittsburgh #8	84.95	25.3
Pocahantas #3	91.81	76.9
Upper Freeport	88.08	85.8

TABLE 3: Extraction of Coal A in various solvents
(Coal:solvent:KOH ratio 10:100:1,6)

SOLVENT	% CARBON EXTRACTION
N-methylpyrrolidinone	80.5
Dimethylformamide	82.5
Dimethylacetamide	79.4
Tetramethylurea	56.7
Dimethylimidazolidinone	83.1
Dimethyltetrahydropyrimidinone	63.8
Dimethylsulphoxide	62.2
Hexamethylphosphoric triamide	8
Pyridine	6.5 (5 consecutive extractions)
Pyridine + 18-crown-6 + KOH	16.9 (1 extraction)
(70 ml: 0.5 g:0.22 g)	84.5 (5 consecutive extractions)

TABLE 4: **A comparison of inorganic elements present in Refcoals prepared from solutions centrifuged at various speeds with their contents in the original coal.**

		CENTRIFUGE SPEED (r/min)		
OXIDE	COAL	2000	4000	6000
SiO_2	4.2%	0.14%	0.11%	0.10%
Al_2O_3	2.1	0.15	0.04	0.03
Fe_2O_3	0.43	0.006	0.01	0.005
CaO	0.28	0.004	-	-
K_2O	0.13	0.008	0.004	0.003
TiO_2	0.18	0.04	0.02	0.015
MgO	0.10	0.03	0.02	0.02
Total	7.4	0.38	0.20	0.17

PRE-OXIDATION AND PERCHLOROETHYLENE (PCE) DESULFURIZATION OF ILLINOIS COALS

M.-I. M. Chou, J.M. Lytle, R.R. Ruch, C.W. Kruse, and C. Chaven, Illinois State Geological Survey, Champaign, IL 61820; D.H. Buchanan, Dept. of Chemistry, Eastern Illinois University, Charleston, IL 61920

INTRODUCTION

A pre-combustion coal desulfurization process using perchloroethylene (PCE) at 120°C to remove up to 70% of the organic sulfur has been claimed by the Midwest Ore Processing Co. (MWOPC). The importance of oxidation and drying conditions as well as temperature control is stressed by the developers (Lee et al., 1991; Leehe and Sehgal, 1988). According to MWOPC, this process gives higher organic sulfur removal from Ohio and Indiana coals than from Illinois coals.

Over the past few years, the ISGS and Eastern Illinois University (EIU) have jointly developed analytical methods to measure forms of sulfur in PCE extracts of high-sulfur Illinois coals (Buchanan et al., 1990). Some elemental sulfur and limited amounts of organic sulfur have been removed from oxidized Illinois coals during these studies; however, these sulfur removals were much lower than those reported by MWOPC. Several hypotheses may explain these differences, but to date, limited data addressing these hypotheses have been reported. MWOPC postulated that the organic sulfur removed was mainly aliphatic, and that the organic sulfur in Illinois coals may contain less aliphatic sulfur than other coals tested. We have hypothesized that errors in interpreting data from American Society for Testing and Materials analysis methods (ASTM) may account for the higher organic sulfur removal reported by the MWOPC. For example, elemental sulfur extracted by the PCE can be derived from the pre-oxidation of pyrite, but this elemental sulfur will be erroneously reported as organic sulfur by the ASTM analysis. Furthermore, the high chlorine content in the PCE-treated material could decrease its suitability for combustion.

One goal of this study was to independently confirm the organic sulfur removal from high-sulfur Illinois coals with the PCE desulfurization process reported by the MWOPC. Another goal was to verify the forms-of-sulfur determination using the ASTM method for evaluation of the MWOPC process. The overall commercial value of this process also depends on removal of the chlorine from the PCE-treated coal residue. Chlorine up-take during PCE desulfurization, and techniques for removal of chlorine from the process residue, also were investigated.

EXPERIMENTAL

Samples - An oxidized Ohio 5/6 coal was provided by Mr. C. Kulik of Electric Power Research Institute. Coals identified as IBC-101, -102, -104, -106 were obtained from the Illinois Basin Coal Sample Program (Kruse, et al., 1991). Mineral pyrite was provided by Mr. R.H. Shiley, an ISGS staff member.

Procedures

Ambient oxidation (laboratory weathering) - During ambient oxidation, samples (IBC-104 coal and mineral pyrite) were stored in a container under room air at laboratory conditions for periods of both 2 weeks and greater than 5 years for coal and for more than 3 years for a pyrite sample.

PCE extraction of oxidized samples of coals IBC-104 and Ohio 5/6 - Azeotropic drying was conducted prior to each PCE extraction. This was accomplished by adding the sample to well-stirred PCE at 70 to 100°C in an open flask, heating the mixture until all of the water was removed and the temperature in the flask rose to 121°C. The temperature was maintained at 121°C for 30 minutes to complete the extraction. The residue coals from PCE extraction were isolated by hot filtration. The feeds and products from these operations were subjected to both ASTM and X-ray absorption near edge structure (XANES) analyses. The PCE extracts were analyzed for elemental sulfur by high performance liquid chromatography (HPLC).

Short-term air oxidation/PCE extraction - Oxidation in air in the presence of PCE was conducted by bubbling filtered air through a coal/PCE slurry with and without water at a specified temperature for a selected length of time. After oxidation, the temperature was increased to 121°C and maintained for 30 minutes. The extracts produced from PCE extraction were then isolated from the residues by hot filtration. After purification, the PCE extracts were analyzed by HPLC for elemental sulfur contents.

ASTM forms-of-sulfur analysis - In the ASTM D-2492 procedure (1991), the sample (-60 mesh) is first digested with a dilute HCl solution. The acidic solution is filtered and sulfatic sulfur is precipitated and quantified as $BaSO_4$. After washing with distilled water, the HCl-free residue is digested with dilute HNO_3. The solution is filtered and the volume adjusted for atomic absorption (AA) determination of iron, which is then calculated as pyritic sulfur. At this point, all the iron from pyrite (FeS_2) should have been removed and analyzed. To obtain total sulfur, a separate split of coal sample is combusted in a Leco model SC32 total sulfur analyzer equipped with an on-line IR detector which is used to monitor SO_2 production. Organic sulfur is obtained by taking the difference between total sulfur content and the sum of pyritic and sulfatic sulfur contents. Any elemental sulfur present appears as organic sulfur since it is not reported as pyritic or sulfatic sulfur.

Elemental sulfur determination - Elemental sulfur in the PCE extract was first purified by passing the solution through a Florisil column. Sulfur was then determined with a Perkin-Elmer Model LC65 HPLC with an ultraviolet - visible light (UV-VIS) detector.

X-ray absorption near-edge structure (XANES) analysis - This method has been developed (Huffman et al., 1991) for the quantitative determination of all major forms of sulfur in coal, both organic and inorganic. The method is based on a least-squares analysis of the X-ray absorption near-edge structure (XANES). This analysis produces a series of peaks that represent 1s → np photoelectron transitions. Because the major sulfur forms occurring in coal (pyrite, elemental sulfur, organic sulfide, thiophene, sulfoxide, sulfone, and sulfate) have characteristic s → p transition energies, the relative peak areas contributed to the XANES spectrum by each sulfur species can be determined. Aliphatic sulfur is represented by organic sulfide, aromatic compounds by thiophene, and oxidized organic sulfur species by sulfoxide and sulfone. These peak areas are converted to weight percentages of sulfur using calibration constants derived from XANES data from standard compound mixtures. Since XANES derives the signal from the bulk of the sample, detailed information concerning the aliphatic, aromatic, and oxidized forms of organic sulfur removed during PCE desulfurization can be obtained.

Dechlorination and chlorine analysis - Procedures for chlorine removal from the PCE-extracted coals were examined. An ISGS proprietary method was used to remove chlorine from the processed residues. The chlorine contents of the treated products were determined by a Leco CL350 chlorine analyzer.

RESULTS AND DISCUSSION

PCE desulfurization and sulfur analyses by ASTM and HPLC methods - PCE desulfurization was conducted on short-term (2 weeks) and long-term (>5 years) air-oxidized IBC-104 coal samples and an oxidized Ohio 5/6 coal sample. The results of the ASTM analyses of the desulfurization products and the HPLC analyses of the PCE extracts are shown in Table 1. Coal oxidation before PCE extraction produces more elemental sulfur to be extracted. The ASTM data also show a reduction in both total sulfur and organic sulfur after PCE extraction of the highly oxidized coal samples.

The sample from two weeks oxidation indicates no total sulfur reduction with an undetectable amount of elemental sulfur by HPLC analysis of the PCE extract. The increase in organic sulfur content of this sample as shown by ASTM analysis appears to be an error of the ASTM analysis. Considering the ASTM forms-of-sulfur determination (ASTM D-2492, 1991), the error in organic sulfur determination is associated with the errors from sulfate, pyrite, and total sulfur determinations. The changes in the two-week oxidized sample after PCE extraction may be too small to offset these errors. However, the sample from a long-term (>5 years) ambient oxidation shows a noticeable reduction in both total sulfur (20%) and organic sulfur (10%), and a noticeable amount of elemental sulfur (0.07%) obtained by PCE extraction. Similar reductions in sulfur content of the residues and increases in extracted elemental sulfur were obtained for the highly oxidized Ohio 5/6 sample. The reduction in total sulfur was 20% and in organic sulfur was 21%, and 0.10% elemental sulfur was obtained by PCE extraction.

PCE desulfurization and sulfur analyses by XANES and ASTM methods - Least-squares sulfur K-edge XANES analysis was utilized to resolve organic sulfur into aliphatic, aromatic, and oxidized forms. To take the most precise data on sulfur forms, the data from XANES analysis were combined with wt% pyritic sulfur in coal from the ASTM analysis. The results are listed in Table 2. The data show that two-week oxidation has little effect on elemental sulfur extraction, which is consistent with the HPLC analysis result. However, these data do not identify any form of organic sulfur reduction.

The five-year oxidized sample (Table 2) differs significantly from the two-week oxidized sample in that 35% of the pyritic sulfur has been oxidized to sulfate and to a small amount of elemental sulfur. In addition, the principal forms of organic sulfur appear to be 10% lower in the five-year oxidized sample than in the two-week oxidized sample, suggesting that organic sulfur has been oxidized to some extent. Oxidized organic sulfur (0.13%) observed by the XANES analysis supports the indication that organic sulfur has been partially oxidized during this long-term air oxidation. The XANES data also indicate that PCE treatment removes all the elemental sulfur and about half of the oxidized organic sulfur. The apparent difference in sulfate content before and after PCE extraction is attributed to water washing after the PCE treatment, which removes soluble sulfates.

The Ohio 5/6 sample behaves similarly to the IBC-104 coal in that the PCE treatment removes all the elemental sulfur and 71% of the oxidized organic sulfur. The treatment has little or no effect on other forms of sulfur. As was the case with the coal previously discussed, the large decline in sulfate content is attributed to aqueous washing after PCE extraction.

Overall, the results indicate that oxidation is important to subsequent PCE desulfurization.

The effects of process conditions (time, temperature, and oxidation) on the amounts of elemental sulfur obtained by PCE extraction - In addition to ambient oxidation, various short-term, air-oxidation effects (achieved by varying the amount of water, temperature, and time) were examined. As indicated in Table 3 for a partially oxidized coal O-IBC-101, bubbling air through a suspension of coal in hot PCE with water present produces more elemental sulfur (0.10%) in the extract than the run conducted under the same condition without water present (0.06%). Without water present, as seen in the two runs of O-IBC-101 coals, bubbling air at 90°C for two hours does not produce additional elemental sulfur. A similar trend is observed for a fresh sample of IBC-104 (F-IBC-104). The run that was conducted with water present (at 90°C bubbling air for two hours) shows a 2-fold increase in elemental sulfur production (0.02%), whereas, the run that was conducted without water present (at 24°C bubbling air for two hours) shows no change in elemental sulfur production. Among all the IBC-104 coal samples, the sample which underwent long-term ambient oxidation has the most elemental sulfur (0.07%).

The results of this investigation indicate that the presence of water during oxidation enhances elemental sulfur production. This implies that the oxidation process can be speeded up by maintaining moist conditions during oxidation.

Dechlorination - A steam-stripping technique has been reported to give a PCE residue from Illinois Herrin (No. 6) coal with a chlorine content of 0.9% (Atwood and Leehe, 1991). This level of chlorine in the treated coal would be considered unacceptable by coal users.

Various methods for chlorine removal from the PCE process residues were examined. The amount of chlorine remaining in the PCE-extracted coals was determined. Without any washing, a PCE-extracted coal had a chlorine content as high as 4.68%, as indicated in Table 4. An ISGS proprietary method was developed to remove excess PCE. This method can totally remove PCE and give PCE-extracted coal with a chlorine content as low as 0.03%.

ASTM forms of sulfur in fresh and oxidized coal samples - Four coals from the Illinois Basin Coal Sample Program (IBCSP) were oxidized under ambient conditions. The forms of sulfur in coals with and without oxidation were then analyzed by the ASTM method. The analyses were performed at the same time with the same instrumental calibration, and by the same operator. The results (Table 5) indicated that the oxidized samples show a noticeable decrease in pyritic sulfur, a noticeable increase in sulfatic sulfur, and a slight increase in "organic sulfur". Total sulfur content in the coals remains unchanged, but the decrease in the amount of pyritic sulfur appears to be equal to the sum of the increases in the amount of sulfatic and organic sulfur. This variation is consistent for all four coal samples analyzed.

In a separate study, a sample of oxidized pyrite (OPY) was extracted with PCE. The OPY was prepared by subjecting a pure sample of pyrite to ambient oxidation for more than three years. The oxidized sample was mixed with inert celite for the purpose of diluting the sample for analysis. The diluted sample was then used for PCE extraction. The ASTM analysis of the oxidized sample shows 0.28% "organic sulfur," 0.32% of sulfatic sulfur, and 3.53% of pyritic sulfur (Table 6). After PCE extraction, this ASTM "organic sulfur" disappears, and the PCE extract shows elemental sulfur (0.03%) from HPLC analysis. These data suggest that during oxidation, pyrite in the coal is oxidized. Part of the pyritic sulfur is converted to a sulfatic form and part to the elemental form. Perchloroethylene is known to be an efficient solvent for elemental sulfur extraction. Thus, the elemental sulfur removed by PCE extraction apparently originated with oxidation of pyrite. This elemental sulfur will be credited as

"organic sulfur" by the ASTM analysis. This explains why an increase in "organic sulfur" content was observed by ASTM analysis of the oxidized coal samples, and why over-estimation of "organic sulfur" removal by PCE desulfurization of highly oxidized coal samples could occur. Overall, the results of these oxidation studies confirm the hypothesis that oxidation produces elemental sulfur that complicates the interpretation of data on organic sulfur removal by PCE desulfurization obtained from ASTM forms-of-sulfur analyses.

CONCLUSIONS

Oxidation of coals was found to affect subsequent PCE desulfurization. Not only pyritic sulfur but also some of the organic sulfur in coal is oxidized. Elemental sulfur produced from pyrite oxidation and some oxidized forms of organic sulfur are amenable to removal by PCE desulfurization.

The uncertainty in an organic sulfur content calculated by the ASTM method includes the separate errors of the sulfate, pyrite, and total sulfur determinations. A high value for ASTM organic sulfur results from oxidation of coal. Air oxidation of pyrite in coal produces PCE-extractable elemental sulfur. This elemental sulfur is interpreted as "organic sulfur" using the ASTM method for forms-of-sulfur determination.

The data indicate that the ASTM-2492 analytical method for forms-of-sulfur determination is inadequate for interpreting "organic sulfur" removal by PCE desulfurization.

ACKNOWLEDGEMENT

This work has received direct financial support from the Illinois Department of Energy and Natural Resources (IDENR), through its Coal Development Board and the Center for Research on Sulfur in Coal (CRSC), and from the United States Department of Energy (DOE) through CRSC. However, any opinions, findings, conclusions or recommendations expressed herein are those of the author(s) and do not necessarily reflect the views of IDENR, CRSC, and DOE. The authors wish to acknowledge Dr. G.P. Huffman and Dr. F.E. Huggins, University of Kentucky, Lexington, KY, for XANES analysis.

REFERENCES

American Society for Testing and Materials, *Annual Book of ASTM Standards*, D-2492, Forms of Sulfur in Coal, 1991, p. 289-294.

Atwood, G., and H. Leehe. 1991. "Perchloroethylene Coal Cleaning," *J. Coal Preparation*. Vol. 11, p. 77-86.

Buchanan, D.H., C. Chaven, K. Puharich, L.C. Warfel, K.C. Hackley, C.W. Kruse, and K.K. Ho. 1990. "Organic Sulfur Removal from Illinois Coal," *Final Technical Report to the Center for Research on Sulfur in Coal*, September 1989 to August 1990.

Kruse, C.W., C. Chaven, L.B. Kohlenberger, H.P. Ehrlinger III, D.M. Rapp, J.M. Lytle, and K.S. Vorres. 1991. "Illinois Basin Coal Sample Program," *Annual Report to the Center for the Research on Sulfur in Coal*, September 1990 to August 1991.

Lee, S., K.L. Fullerton, S.K. Kesavan, E.A. Berthinee, and S.W. Watson. 1991. "Process Engineering Studies of the Perchloroethylene Coal Cleaning Process," *Proceedings: Sixteenth Annual Conference on Fuel Science and Conversion*, EPRI, Palo Alto, CA, May.

Leehe, H.H., and R.S. Sehgal. 1988. "Pyritic and Organic Sulfur Removal From Coal With Perchloroethylene," *Proceedings: 1987 Work Shop on Coal Structure*, Electric Power Research Institute, EPRI ER-6099-SR, pp. 8:1-18, November.

Huffman, G.P., S. Mitra, F.E. Huggins, N. Shah, S. Vaidya, and F. Lu. 1991. "Quantitative Analysis of All Major Forms of Sulfur in Coal by XAFS Spectroscopy," *Energy and Fuel*, 1991, Vol. 5, No. 4, p. 574-581.

Table 1. Elemental sulfur from PCE extraction and ASTM forms of sulfur in short-term and long-term air oxidized coals before and after PCE extraction.

	Wt %, moisture-free, whole-coal basis				
Sample	Sulfatic	Pyritic	Organic	Total	S°
IBC-104, un-oxidized	0.03	2.44	1.66	4.13	
IBC-104, 2 wks oxid, before PCE extract	0.12	2.17	1.68	3.97	
IBC-104, 2 wks oxid, after PCE extract and dechlorination	0.05	2.18	$1.75^{+4\%}$	$3.98^{+0.3\%}$	0.00
IBC-104, >5 yrs oxid, before PCE extract	0.87	1.40	1.84	4.11	
IBC-104, >5 yrs oxid, after PCE extract and dechlorination	0.25	1.40	$1.66^{-10\%}$	$3.31^{-20\%}$	0.07
Oxidized Ohio 5/6, before PCE extract	0.63	0.79	2.08	3.50	
Oxidized Ohio 5/6, after PCE extract and dechlorination	0.28	0.87	$1.64^{-21\%}$	$2.79^{-20\%}$	0.10

$^{-20\%}$, % of reduction in total sulfur or organic sulfur; S°, elemental sulfur in PCE extracts by HPLC analysis, in wt% on moisture-free, whole-coal basis.

Table 2. Analysis of sulfur forms by XANES in three oxidized coals before and after PCE desulfurization.

	Wt %, moisture-free, whole-coal basis					
Sample	Pyritic	S°	Sulfide	Thiophenic	Oxid	Sulfatic
IBC-104, 2 wks oxid, before PCE extraction	2.17	0.00	0.61	1.07	0.00	0.12
IBC-104, 2 wks oxid, after PCE extract and dechlorination	2.18	0.00	0.61	1.12	0.00	0.07
IBC-104, >5 yrs oxid, before PCE extract	1.40	0.17	0.54	0.86	0.13	1.01
IBC-104, >5 yrs oxid, after PCE extract and dechlorination	1.40	0.00	0.56	0.88	0.07	0.40
Oxidized Ohio 5/6, before PCE extract	0.79	0.26	0.50	1.00	0.14	0.81
Oxidized Ohio 5/6, after PCE extract and dechlorination	0.87	0.00	0.54	1.04	0.04	0.30

* All data were obtained from least-squares sulfur K-edge XANES analysis with the exception of pyritic sulfur which was obtained from the ASTM analysis; oxid., sulfoxide and sulfone.

Table 3. The effects of oxidation conditions on the amount of elemental sulfur removed by PCE extraction

Starting coal	PCE/H_2O (mL/mL)	Oxidation Method	Time	Temp.(°C)	S° %
F-IBC-104	100/0	none	-	-	0.01
F-IBC-104		long-term ambient-air oxidation	>5 yrs	Room	0.07
F-IBC-104	100/0	bubbling air, 20 mL/sec	2 hrs	24	0.01
F-IBC-104	100/20	bubbling air, 20 mL/sec	2 hrs	90	0.02
O-IBC-101	100/0	none	-	-	0.06
O-IBC-101	100/0	bubbling air, 20 mL/sec	2 hrs	90	0.06
O-IBC-101	100/20	bubbling air, 20 mL/sec	2 hrs	90	0.10

F-IBC-104, un-oxidized IBC-104 coal; O-IBC-101, slightly ambient-oxidized IBC-101 coal; S°, elemental sulfur by HPLC analysis of PCE extracts, in wt%, moisture-free, whole-coal basis.

Table 4. Results of chlorine removal from PCE-extracted residues of an un-oxidized (F-IBC-104-PCE) and an oxidized (O-IBC-104-PCE) coal.

Sample	Method of washing	Total Chlorine (%)
F-IBC-104		0.03
F-IBC-104-PCE	NONE	4.68
F-IBC-104-PCE	Water	2.96
F-IBC-104-PCE	Proprietary A	0.17
F-IBC-104-PCE	Proprietary B	0.03
O-IBC-104-PCE	Proprietary B	0.03
O-IBC-104-PCE	Proprietary B	0.03

Total chlorine contents are in weight percent, moisture-free, whole-coal basis.

Table 5. ASTM forms of sulfur in oxidized and un-oxidized IBCSP coal samples.

Coal Sample		ASTM forms of sulfur (weight %, moisture free, whole-coal basis)			
		Sulfatic	Pyritic	Organic	Total
IBC-101	A	0.05	1.20	3.10	4.35
	B	0.54	0.54	3.30	4.38
IBC-102	A	0.06	2.20	1.00	3.26
	B	1.12	0.81	1.34	3.27
IBC-104	A	0.03	2.40	1.70	4.13
	B	0.84	1.33	2.00	4.17
IBC-106	A	0.02	1.80	1.90	3.72
	B	0.57	1.00	2.25	3.82

A, un-oxidized, preserved under nitrogen; B, oxidized.

Table 6. Sulfur in an oxidized pyrite before and after PCE extraction.

Sample	ASTM forms of sulfur weight %, moisture-free, Celite-diluted sample				
	Sulfatic	Pyritic	Organic	Total	S°%
Oxidized pyrite*, before PCE extraction	0.32	3.53	0.28	4.13	na
Oxidized pyrite, after PCE extraction	0.35	3.68	0.01	4.04	0.03

* Long-term (> 3 years) ambient air oxidized pyrite, 10% in Celite (an inert additive for the purpose of diluting the sample for analysis); S°, elemental sulfur in PCE extracts by HPLC analysis, in wt% on moisture-free, celite diluted sample.

POZZOLANIC REACTIVITY AND COMPRESSIVE STRENGTH OF GASIFIED COAL SLAG ADDED WITH LIMESTONE FLUX

Yoshihiko Ninomiya*1, Mitsuho Hirato and Atsushi Sato*1
Department of Chemical Engineering
Tokyo University of Agriculture and Technology
Koganei, Tokyo 184 Japan

*1) Department of Industrial Chemistry
Chubu University
Kasugai, Aichi 487 Japan

INTRODUCTION

In recent years, an entrained flow gasification of coal, which has several advantages over other gasification processes including high throughput per reactor volume and flexibility in coal types, has attracted special interest in many countries. The gasifier involves wet ash removal. The liquid slag formed has suitable viscosity for tapping and is withdrawn at the bottom of the reactor without promoting the corrosion in the reactor insulation. To operate the gasifier stably and to maintain high gasification efficiency, it is necessary to control ash melting temperature by adding limestone which causes decrease in ash melting temperature and slag viscosity(1). The use of the slag/lime mixture as a partial replacement in slag portland cements is of interest, because of utilization of waste slag. Slag portland cements with higher slag contents are used for mass concrete because of their low heat evolution. And those with lower slag content are used as a substitute of portland cement. Japanese Industrial Standard (JIS) has permitted the addition of slag or other latent hydraulic or pozzolanic materials to the portland cements.

In this paper, characterization on coal gasification slag loaded with limestone additive obtained from a laboratory-scale entrained bed gasifier was performed in order to obtain the relation between the character of the glass phase, pozzolanic reactivity and compressive strength of the blending component.

EXPERIMENTAL

Two sorts of Blair Athol slag, gasified slag A and B, were obtained from a laboratory-scale entrained bed gasifier(2). Limestone was added to the coal as a flux to control operation temperature of the gasifier. The CaO content of the slag was relatively high and, therefore, the melting temperature of the slag was much lower than that of original slag. Important characters of the slag are shown in Table 1.

Infrared spectrum of ν_3 stretching vibration of Si-O bond in slag was measured by FT-IR method. 30% $Ca(OH)_2$ and 10% $CaSO_4 \cdot 2H_2O$ as activator were added to each slag. The slag was mixed with water solid ratio of 0.5 and cured at 313K for 1, 7 and 28 days. Hydration reactivity of the blending component was evaluated from its hydration degree, amount of combined water and reacted $Ca(OH)_2$. Hydration degree of the blending component was determined by XRD after heating and recrystallizing hydrated sample at 1273K for half an hour. Amount of combined water and reacted $Ca(OH)_2$ was measured by ignition loss and TG method, respectively(3). Compressive strengths of the blending component and the slag cements containing 25 to 75wt% of portland cement were measured in conformity to the JIS (Japanese Industry Standard) method.

RESULTS AND DISCUSSION

Condensation Degree of Silicate Ions in Glass Phase

Most slag and melted ash are more complex than vitreous SiO_2. Glass phase results from co-melting silicate with other oxides, some of which provide elements with coordination numbers generally of 3 or 4 (e.g. Al, Fe, etc.), which are capable of replacing Si in the polymeric network, known as network modifiers(4). As CaO is introduced into a silica melt, the resulting slag formed on quenching became increasingly depolymerized, relative to the parent coal slag.

The averaging phenomena for heterogeneous assemblages of melted glass phase containing CaO was observed by the FT-IR method. Typical infrared spectra of ash-CaO mixture slag showed a number of characteristic bands which are seen to vary with the origin of the slag, which can be compared with other similar mineral species. It is well known that ν_3 stretching vibration of Si-O bond makes strong absorption at $1100cm^{-1}$ in IR spectrum and this absorption peak shift towards high wave number as the condensation degree of silicate ions increases(5). The peak position each slag component by IR is shown in Figure 1. Gasified slag A and B and blast furnace slag had a peak at about 950 to $940cm^{-1}$. While Blair Athol slag and fly ash had a peak at about $1060cm^{-1}$. The condensation degree became larger in the order of high calcium slag.

Pozzolanic Reactivity of Slag

The amount of combined water and reacted $Ca(OH)_2$ and hydration degree are shown in Figure 2. Since the glass phase has higher level of free energy than the crystalline phase, the glass phase is corresponded with the reactivity of the blending component more deeply. Content of glass phase in slag was above 99%. Hydration degree and combined water of the gasified slag B were almost equal to those of the blast furnace slag at 28 days. Those of the gasified slag A with less than 1% crystalline phase, however, were small. The pozzolanic reactivity of slag is considered to correspond to CaO content and the condensation degree of silicate ions, i.e. a network with a lower degree of connectivity. On the other hand, amount of reacted $Ca(OH)_2$ could not estimated in case of slag rich in CaO.

Compressive Strength of Slag

Figure 3 shows the compressive strength of the blending component. As expected, blast furnace slag and gasified slag B gave the highest strength development after 28 days. However, gasified slag A resulted in significantly lower strength due to the low pozzolanic reactivity.

The effect of portland cement content on the compressive strength developed by the slag shows in figure 4 and 5. Blending cements containing 25wt% of the slag/ 75wt% portland cement show higher strength from 7 days onwards. The strengths of the gasified slag B cement were found to exceed the JIS value. The improved strengths are more likely to be due to the speeding up the pozzolanic reaction.

CONCLUSIONS

The pozzolanic reactivity of the slag was enhanced with increasing basicity and CaO content in slag and decreasing of the degree of condensation of silicate ion in the glass phase. Hydrated products from the slag cement were not basically different from those from blast furnace slag cement. The compressive strength of high calcium slag cement (gasified slag B) was almost equal to that of blast furnace slag.

REFERENCES

1) M.Hirato and Y.Ninomiya: Study of Fusibility of Coal Ash with Additives -Estimation of Ash Fusion Temperature and Fusion Behavior of Blending Coal Ashes-, J. of Fuel Society of Japan, 68, 5, 393-398 (1989)
2) S.-Y. Lin, S.Kameyama, Y.Ninomiya and M.Hirato: Study on Entrained Flow Gasification of Coal under Ash Fusion Controlling (I), J. of Fuel Society of Japan, 69, 3, 191-199 (1990)
3) M.Hirato and Y.Ninomiya: Fundamental Studies on the Cement Material of Coal Gasification Slag with Limestone Additive, J. of Japan Institute of Energy, 71, 3 , 181-188 (1992)
4) R.T.Hemmings and E.E.Berry: On the Glass in Coal fly Ashes -Recent Advances-, P.3-38, Symposium Proceedings 113, "Fly Ash and Coal Conversion By-Products: Characterization, Utilization and Disposal IV", ed. G.J. McCarthy et.al., Material Research Society (1988)
5) H.Uchikawa, S.Uchida and S.Hanehara: Effect of Character of Glass Phase in B lending Components on their Reactivity in Calcium Hydroxide Mixture, J. Research of Onoda Cement Company, Vol.116, (1987)

Table 1 Characteristics of slags used in this study

		Gasified slag A	Gasified slag B	Blast furnace slag	Fly ash
SiO_2	(%)	46.5	39.46	32.67	54.10
Al_2O_3	(%)	21.68	14.61	12.43	21.03
Fe_2O_3	(%)	2.12	2.94	0.56	4.71
CaO	(%)	17.34	35.56	44.50	10.41
MgO	(%)	0.24	0.32	5.56	1.24
ST	(K)	1610	1540	-	-
HT	(K)	1660	1580	-	-
FT	(K)	1700	1610	-	-
C/S		0.37	0.90	1.36	0.19
(C+M)/S		0.38	0.91	1.53	0.22
(C+M)/(S+A)		0.26	0.66	1.11	0.16
(C+M+A)/S		0.84	1.28	1.91	0.60
Content of glass phase (%)		0.99	0.99	0.99	0.70

A:Al_2O_3, C:CaO, M:MgO, S:SiO_2

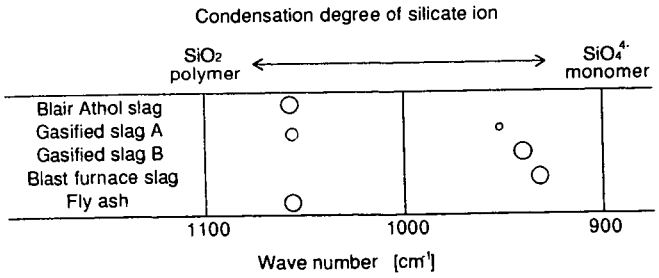

Figure 1 Peak position of infrared absorption spectrum of blending component

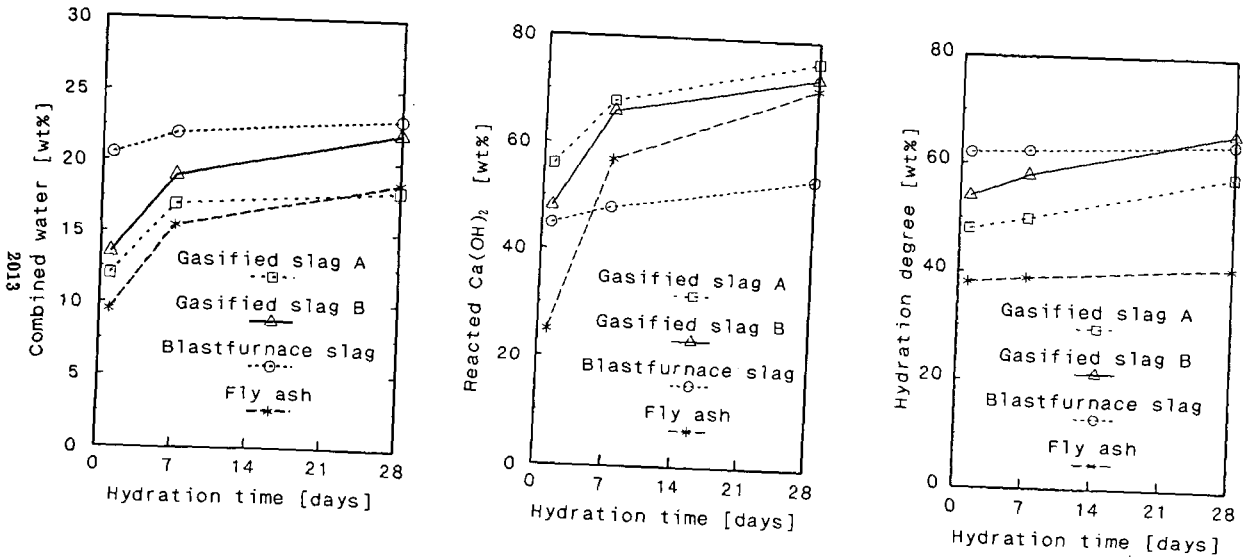

Figure 2 Amount of combined water, reacted $Ca(OH)_2$ and hydration degree of blending component with hydration time (313K)

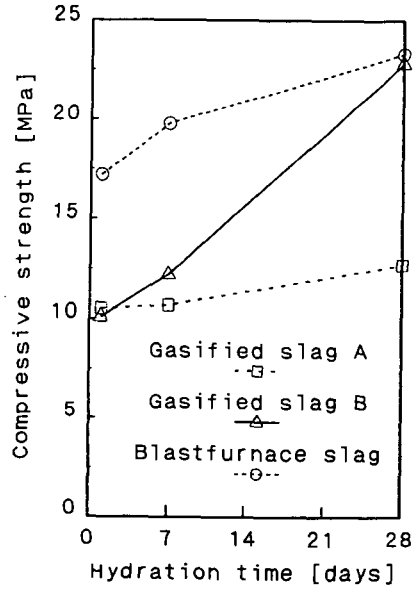

Figure 3 Compressive strength of blending component with hydration time

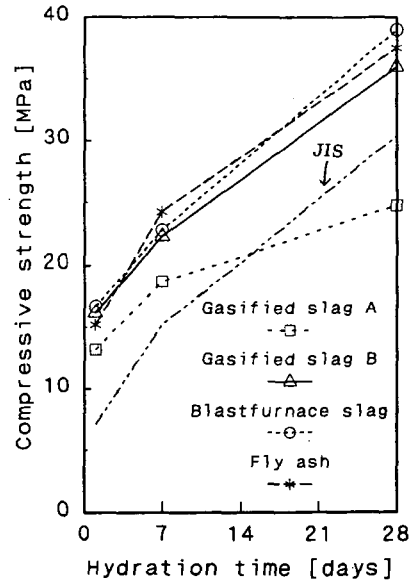

Figure 4 Compressive strength of slag cement containing 75wt% portland cement with hydration time

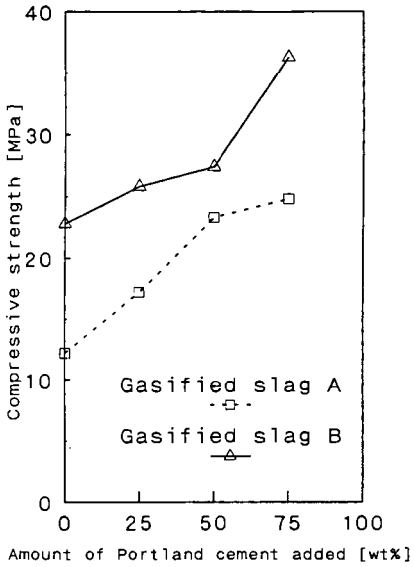

Figure 5 Effect of portland cement content on the compressive strength developed by the slag